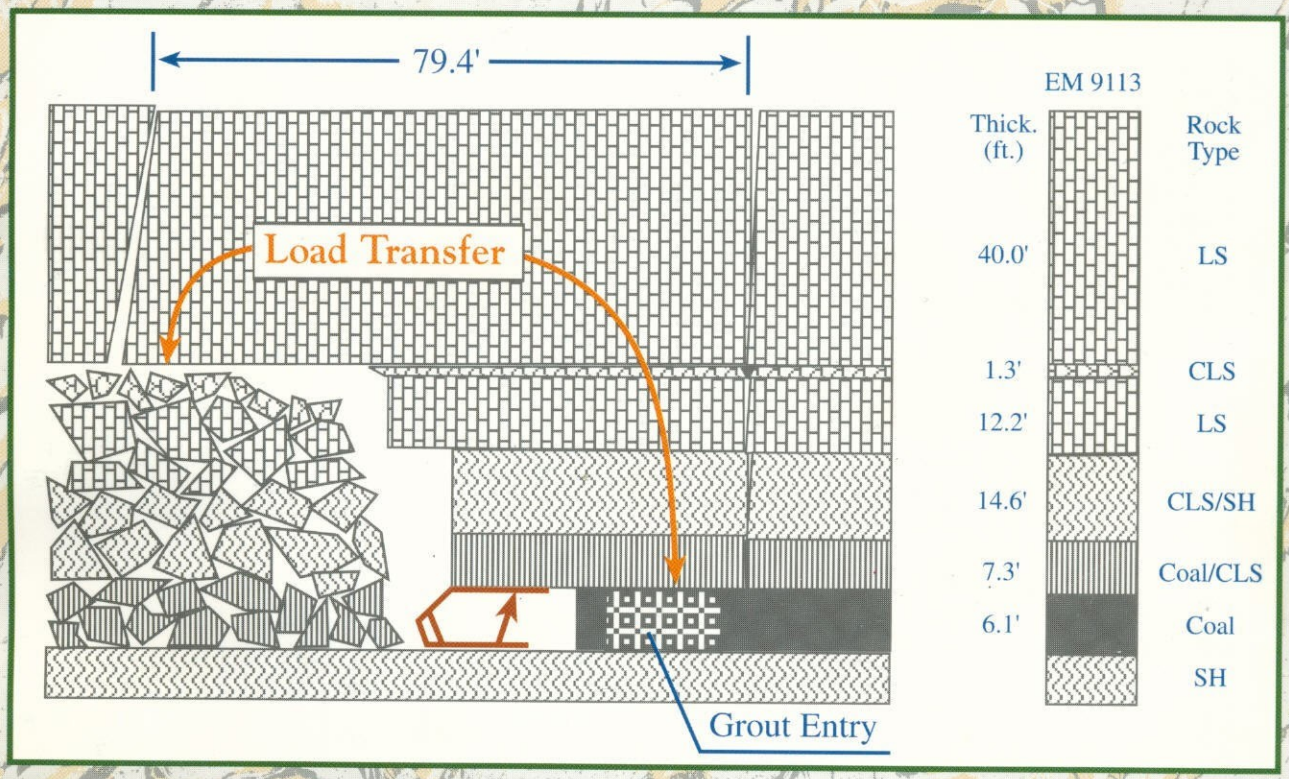
# 16th International Conference on

# Ground Control in Mining

## August 5-7, 1997




**Sponsors**

**U.S. National Institute for Occupational Safety and Health**
**U.S. Mine Safety and Health Administration**
**West Virginia Coal Association**
**West Virginia University**

FRANK CHASE



# *Proceedings*
# of
# 16th International Conference on Ground Control in Mining

**August 5-7, 1997**

**edited by**

**Syd S. Peng**
**Chairman and Charles T. Holland Professor**

**Department of Mining Engineering**
**College of Engineering and Mineral Resources**
**West Virginia University**
**P.O. Box 6070**
**Morgantown, WV 26506**
**U.S.A.**

**Tel: (304) 293-7680**
**FAX: (304) 293-5708**

**ISBN 0-939084-56-9**

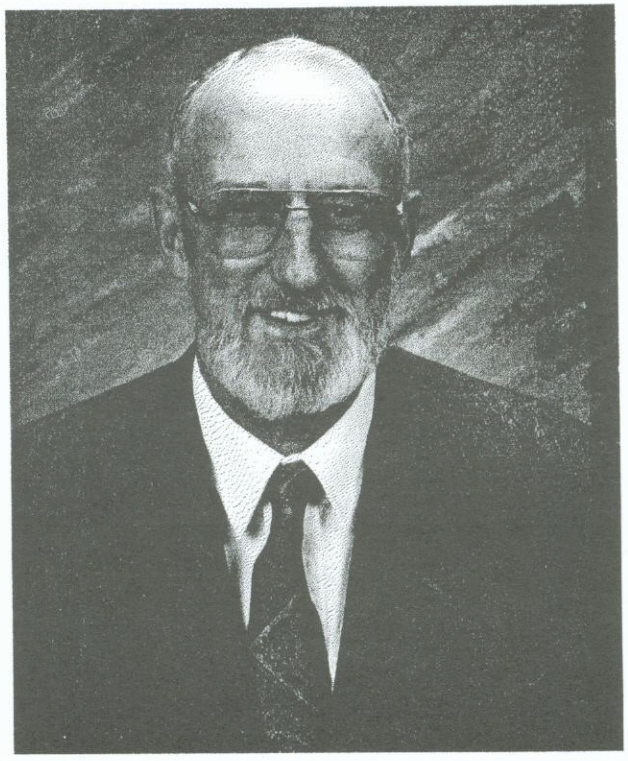


# 16th International Conference on Ground Control in Mining

## Organizing Committee

| | |
|---|---|
| **Syd S. Peng** | *Chairman, WVU* |
| **Mike Amick** | *Fosroc, Inc.* |
| **Naj I. Aziz** | *University of Wollongong, Australia* |
| **Tom Blevins** | *E.I. DuPont de Nemours & Co.* |
| **Ed Doney** | *Kerr-McGee Coal Corp.* |
| **Ian W. Farmer** | *I. W. Farmer & Partners, UK* |
| **Gerry Finfinger** | *NIOSH* |
| **Dick Gray** | *GAI Consultants* |
| **Chris Hamilton** | *WV Coal Association* |
| **Greg Hasenfus** | *CONSOL Inc.* |
| **Greg Hendon** | *Jim Walter Resources* |
| **John Hoelle** | *Archveyor Mining Services* |
| **Mike Karmis** | *VPI & SU* |
| **A. Wahab Khair** | *WVU* |
| **Rao Pothini** | *Glamorgan Coal Corp.* |
| **John Stankus** | *Jennmar Corp.* |
| **J. N. Van der Merwe** | *Itasca Africa, South Africa* |
| **Kelvin K. Wu** | *MSHA* |

# Dr. James J. (Jim) Scott (1928-1997)
## -A Tribute-



On Friday, April 11, 1997, the ground control community lost an advocate, researcher, teacher, inventor and developer, and most of all, a dear friend when his private airplane went down in dense fog near his home in Rolla, Missouri.

In July of 1981, Jim attended the First Annual Conference on Ground Control in Mining and, along with his son-in-law Brian Castle, presented a paper entitled, "A New Combination: Friction-Suspension Support Systems-Scott Cable Slings." Jim was a loyal supporter of this Conference and had attended many of these Conferences, where he was always an active participant, mixing rock mechanics theory with his own brand of practical "in the pit" experience.

Jim was born on April 22, 1928 near Platteville, Wisconsin. After completing his B.S. in mining engineering from Missouri School of Mines, he worked for seven years, from 1950 to 1957, for Bethlehem Steel Company as an engineer, shift foreman, and mine foreman. He then received his Ph.D. from the University of Wisconsin-Madison in 1962 and moved to Rolla in 1963. From 1970 to 1972, he served as the Assistant Director of Mining-Research with the U.S. Bureau of Mines while on leave from school. At the time of his death, Jim was Chairman of Scott Mine Technical Services, Managing Director of Jennmar/Scott Joint Venture, and Adjunct Professor to the Department of Mining Engineering of the School of Mines and Metallurgy, University of Missouri-Rolla.

Jim authored over 70 papers and publications. He was considered a leading authority on rock mechanics and ground control, and held 14 patents on roof support fixtures, the most important being the Split-Set Friction Rock Stabilizer. This particular innovation was considered to be a pioneering contribution to friction bolting in the mining industry. He received the Jackling Award from the Society of Mining Engineers in recognition of his development of the Split-Set patent.

All of us who had the opportunity to meet and work with Jim will remember him for his boundless enthusiasm, persistence, great sense of humor, infectious smile, and sense of commitment to his family, his profession and all those who worked in the mining industry. He credits many of his ideas to the miners he met in the mine. Jim dedicated his professional life to protecting those who work underground from ground falls. Through his teaching, innovations, and successful application of ground control techniques, Jim made the world a better place. Thank you, Jim. We are all going to miss you!





# TABLE OF CONTENTS

## *Longwall Mining and Surface Subsidence*


1. **Longwall Mining-Through the Back-filled In-panel Entries at Cyprus Emerald Mine,** *J. Chen and M. Mishra, Pennsylvania Services Corp., S. Cario, Cyprus Emerald Resources Corp., and J. DeMichiei, Cyprus Amax Coal Co., Waynesburg,* PA. . . . . 1

2. **Performance of Various Standing and Cribless Tailgate Support Configurations in a Large Eastern Mine,** *G.M. Molinda, D.R. Dolinar, and T.M. Barczak, NIOSH-PRC, Pittsburgh, PA and J. Hustus, Cyprus Cumberland Resources Corp., Waynesburg, PA.* . . . . . 9

3. **Measurement of Effects of Interaction and Influence on Mine Layout Design at Maltby Colliery,** *J.S. Oram, Rock Mechanics Technology Ltd. and C.G. Ponder, Maltby Colliery, RJB Mining (UK) Ltd., UK* . . . . . 16

4. **Effects of Longwall Mining on Streamflow in the Pittsburgh Seam Basin,** *K.L. Johnson, R&D, CONSOL Inc., Library, PA* . . . . . 25

5. **Longwall Surface Subsidence Prediction Through Numerical Modelling,** *N. Mohammad, P.W. Lloyd, and D.J. Reddish, University of Nottingham, UK.* . . . . . 33

6. **Long-term Subsidence and Its Effects on Surface Structures,** *Y. Luo, S.S. Peng, and H.J. Chen, West Virginia University, Morgantown, WV* . . . . . 43

7. **Subsidence Prediction Influence Assessment and Damage Control,** *Y. Luo and S. S. Peng, West Virginia University, Morgantown, WV* . . . . . 50

8. **Formation of Face Headings Using Stress Relief at Asfordby Mine,** *J. Cassie, Rock Mechanics Technology Ltd. and A. McLennan, Asfordby Mine, RJB Mining (UK) Ltd., UK* . . . . . 58

9. **Significant Weighting Events on the Longwalls in the Phalen Colliery,** *R.J. MacDonald, The Cape Breton Development Corp., Canada.* . . . . . 68

10. **Full-face Pressure Monitoring in Medium-Weak Roof Condition,** *S.S. Peng and H. Cheng, West Virginia University, Morgantown, WV* . . . . . 79

11. **Research on the Interaction Between Roof Strata and Shield Supports,** *Y. Shi and Q. Gu, Central Coal Mining Research Institute and C. Zhang and J. Li, Lu'an Coal Bureau, China* . . . . . 85

12. **Roof Instability of Longwall Face at Ikeshima Colliery,** *K. Matsui and H. Shimada, Kyushu University, Japan* . . . . . 91

13. **Gob Canopy Roof Support for Difficult Natural Conditions,** *J.H. Kelley, West Virginia University, Morgantown, WV* . . . . . 98

14. **Yielding Cement Roof Supports for Longwall Mining,** *A.A. Campoli, M.R. Amick, P.S. Mills and A.J. Rohaly, Fosroc, Inc., Georgetown, KY* . . . . . 105

15. **Management of the Dynamic Phenomena of Rock Pressure in Underground Mines,** *V.I. Klishin, Institute of Mining, Academy of Sciences Siberian Branch, Russia* . . . . . 110



## *Roof Bolting*

16. **Continuing Development of Innovative Cable Support Systems,** *J.G. Oldsen, J.C. Stankus, and S. Guo, Jennmar Corp., Pittsburgh, PA and A. W. Khair, West Virginia University, Morgantown, WV* . . . . . 117

17. **Extending the Limits of Strata Bolting by the Use of Flexible Strand Rockbolts,** *D.R. Barratt, Exchem Mining & Construction, UK* . . . . . 130

18. **Implementation and Evaluation of Roof Bolting in MICARE Mine II,** *G.H. Rico, R. Orea R., and R. Mendoza L., MICARE, Mexico and S. C. Tadolini, Excel Mining Systems, Golden, CO* . . . . . 139

19. **New Methods and Technologies of Roofbolting in Australia Coal Mines,** *M. Rataj, Ani Arnall and R. Thomas, Strata Engineering Australia, Australia* . . . . . 149

20. **New Design Criteria for Roof Bolt Systems,** *J.C. Stankus and S. Guo, Jennmar Corp., Pittsburgh, PA* . . . . . 158

21. **Control Mechanism of a Tensioned Bolt System in the Laminated Roof with a Large Horizontal Stress,** *S. Guo and J. C. Stankus, Jennmar Corp., Pittsburgh, PA* . . . . . 167

22. **A Study of the Performance of Glass Fibre Rock Reinforcement Components,** *J.P. Furniss and D.J. Reddish, University of Nottingham, and G. Adkins, MAI Systems UK Ltd., UK* . . . . . 173

23. **A Method for the Selection of Rock Support Based on Bolt Loading Measurements,** *S. P. Signer, D. Cox, and J. Johnston, NIOSH-SRC, Spokane, WA* . . . . . 183

24. **Strategies for the Application of Rockbolting Technology to Longwall Gateroads in Chinese Coal Mines,** *Z. Xiu and X. Wang, Beijing Research Institute of Coal Mining, and A. Wang, Daliuta Coal Mine, China* . 191

25. **A Troubleshooting Guide for Roof Support Systems,** *R.A. Mazzoni and J.E. Carpetta, MSHA-Pittsburgh Safety and Health Technology Center, Pittsburgh, PA* . . . . . 199

## *Retreat Mining*

26. **A Statistical Overview of Retreat Mining of Coal Pillars in the United States,** *C. Mark, F.E. McCall, and D.M. Pappas, NIOSH-PRC, Pittsburgh, PA* . . . . . 204

27. **Full-Scale Performance Evaluation of Mobile Roof Supports,** *T.M. Barczak, NIOSH-PRC and D.F. Gearhart, SSI Services, Inc., Pittsburgh, PA* . . . . . 211

## *Rock Salt*

28. **Effect of the Interchamber Pillar Yield on the Surface Strains in the Movement Trough Edges,** *M.P. Nesterov and N.F. Anikin, Institute of Halurgy, Russia* . . . . . 221

29. **Salt Pillar Design Equation,** *L.L. Van Sambeek, RE/SPEC Inc., Rapid City, SD* . . . . . 226

30. **Case Study of Conditions Observed During the Removal of a Highly Fractured Roof Beam in Bedded Halite,** *L.J. Terrill and J.D. VandeKraats, Westinghouse Electric Corp. Waste Isolation Division, Carlsbad, NM* . . . . . 235



31. **Case Study of the Effect of Stratigraphic Location on Roof Stability in Rock Salt,** *C.T. Francke, L.J. Terrill, and J.D. VandeKraats, Westinghouse Electric Corp. Waste Isolation Division, Carlsbad, NM* . . . . . 243

32. **Ground Control and the Inundation of the Retsof Mine,** *V.A. Scovazzo, John T. Boyd Co., Pittsburgh, PA* . . . . . 251

## *Coal Pillar and Rock Properties*

33. **Weatherability Test of Rocks for Underground Mines,** *K.F. Unrug, University of Kentucky, Lexington, KY* . 259

34. **Shear Strength Characteristics of Soft Rock Joints Based on Constant Normal Stiffness Testing,** *B. Indraratna, N. Aziz, and A. Haque, University of Wollongong, Australia* . . . . . 267

35. **Comparison of Pillar Strengths Calculated Using Empirical Equations and Finite Elements,** *A. de Arade Lima, T.R. Gopinath and M.E. de Alcantara, Federal University of Paraiba, Brazil* . . . . . 274

36. **Effects of In-seam and Near-seam Conditions and Asymmetric Pillar Loading on Coal Pillar Strength,** *D.W.H. Su and G. Hasenfus, R & D, CONSOL Inc., Library, PA* . . . . . 282

## *Roof and Ground Control*

37. **Ground Control Worker Safety During Extended Cut Mining,** *R.H. Grau, III and E.R. Bauer, NIOSH-PRC, Pittsburgh, PA* . . . . . 283

38. **Analysis of Extensometer Data from a Room Widening Experiment Designed to Induce a Roof Fall,** *D.R. Dolinar, D.C. Oyler, and C.S. Compton, NIOSH-PRC, Pittsburgh, PA* . . . . . 289

39. **Airbag Support for Ground Control in Thin Seam Coal Mining,** *S. Fan and L. Kang, Central Coal Mining Research Institute and K. Yu, Shangjing Coal Bureau and Z. Zhang, Lu'an Coal Bureau, China* . . . . . 296

40. **Development of a Statistical-Analytical Approach for Assessing Coal Bump Potential,** *H. Maleki, Maleki Technologies, Inc. and E. Zahl and J. Dunford, NIOSH-SRC, Spokane, WA* . . . . . 304

41. **Ground Control Criteria for Coal Reserve Optimization in Multiple-Seam Mines,** *E. Westman, J. Luo, C. Haycocks, and M. Karmis, Virginia Polytechnic Institute and State University, Blacksburg, VA* . . . . . 311

42. **Calcium Aluminate Binders in Hard Rock and Coal Mining,** *B. Woolley, Lafarge Calcium Aluminates, Chesapeake, VA* . . . . . 316

43. **Simplified Pre-and Post-Processing Technique for Performing Finite-element Analyses of Deep Underground Mines,** *M.T. Filigenzi, NIOSH-SRC, Spokane, WA* . . . . . 320

***Author's Index*** . . . . . 329



16th CONFERENCE ON GROUND CONTROL IN MINING

# Longwall Mining-Through the Backfilled In-Panel Entries at Cyprus Emerald Mine

*J. Chen,* Sr. Mining Engineer
*Mike Mishra*, Manager Technical Resources
Pennsylvania Services Corp., A Cyprus Amax Coal Company

*Sam Cario,* Manager Engineering
Cyprus Emerald Resources Corporation

*John DeMichiei,* Sr. VP of Longwall Operations
Cyprus Amax Coal Company
Waynesburg, PA

## ABSTRACT

In recent years, improvements made to the longwall system have accelerated at a faster pace than those made to the gate entry development system. As a consequence, unless planned years ahead of time, extending the panel length is nearly impossible without some innovative approach. At Cyprus Amax Coal's Emerald mine the G panel length was extended by 3,500 ft. by developing three entries across it to facilitate development of its headgate and tailgate entries simultaneously when the adjoining F panel was in operation. After evaluating alternative supporting methods and associated risks, determination was made to backfill these entries and crosscuts using a low strength flyash cement mixture prior to mining thru. Instrumentation was also used to monitor the stress change or front abutment stress in both the coal and the backfilled material ahead of the face. Longwall mining thru these three entries took about four eight-hour shifts and proved to be very successful. The designed flyash cement mixture provided adequate roof stability and caused no difficulty in the shearer's cutting while eliminating an in-panel longwall face move and minimizing the risk of roof or floor failure in the in-panel openings, or in the worst scenario loss of the face during the longwall cutting thru. This approach provided the intended result of extending G panel and recovered about one million tons of coal.

This paper summarizes the engineering design of the cutting-thru project and flyash cement mixture, front abutment stress changes within the longwall coal block, backfilled material, and coal pillars ahead of the longwall face, and our underground observations

## INTRODUCTION

The imbalance of longwall retreat and continuous miner development necessitates the addition of more development sections or idling the longwall production or extending the panel length. Unless planned years ahead the addition of development units does not give short term result. However, extending one panel does provide additional development time for subsequent panels, but is nearly impossible without some innovative approach. At Cyprus Amax Coal's Emerald mine the challenge was to increase the longwall panel lengths so as to keep the longwall production from the same panel for longer time which in turn would help the timing of the gate development of the next panel, and as a domino effect provide additional float time for subsequent panels. In addition the longer panels provide additional tonnage to offset the cost of panel setup such as the cost of cutting and installing the ventilation overcasts, belt transfer point, belt drive, longwall belt storage unit, bleeder setup, and the cost of the longwall face move.

The concept of cutting thru in-panel entries was discussed and evaluated as early as 1993 to be implemented at the B panel of Emerald Mine. During previous years 1991 thru 1993, Cyprus Emerald used the predeveloped and well supported 16 ft. wide recovery entries at its longwall panels designated as 6Gate, 22Right, 7Gate, and A+ panels. In addition to the primary roof bolts, these pre-developed recovery entries were meshed and supported with 12 ft. superbolts, trusses, donut cribs, and wood cribs. The secondary supports were instrumented to measure the stress level as the longwall face approached the recovery area. These recovery entries were fairly successful and uneventful, but some floor heave and the associated failure of some of the donut cribs did not provide enough confidence level to try the in panel entries at the back end of B panel. Consequently B panel, C panel, D panel, and E panel did not mine about 4,200 ft. of additional longwall coal each due to the fact that the longwall retreated much faster than the development of the next panel.

In 1995 the concept was again reevaluated to extend the longwall block at G panel by about 3,500 ft. long by developing three in-panel entries across the G panel to facilitate development of its headgate and tailgate entries simultaneously when the longwall was operating in the adjacent F panel (Fig. 1). During the evaluation of extending the G panel length, considerations were given to the stability of the support system, ease of mineability, cost and benefit of the alternatives, and the associated risk. The alternatives considered were: (1) in-panel move, (2) supporting but not backfilling the in-panel entries, and (3) backfilling the in-panel entries.

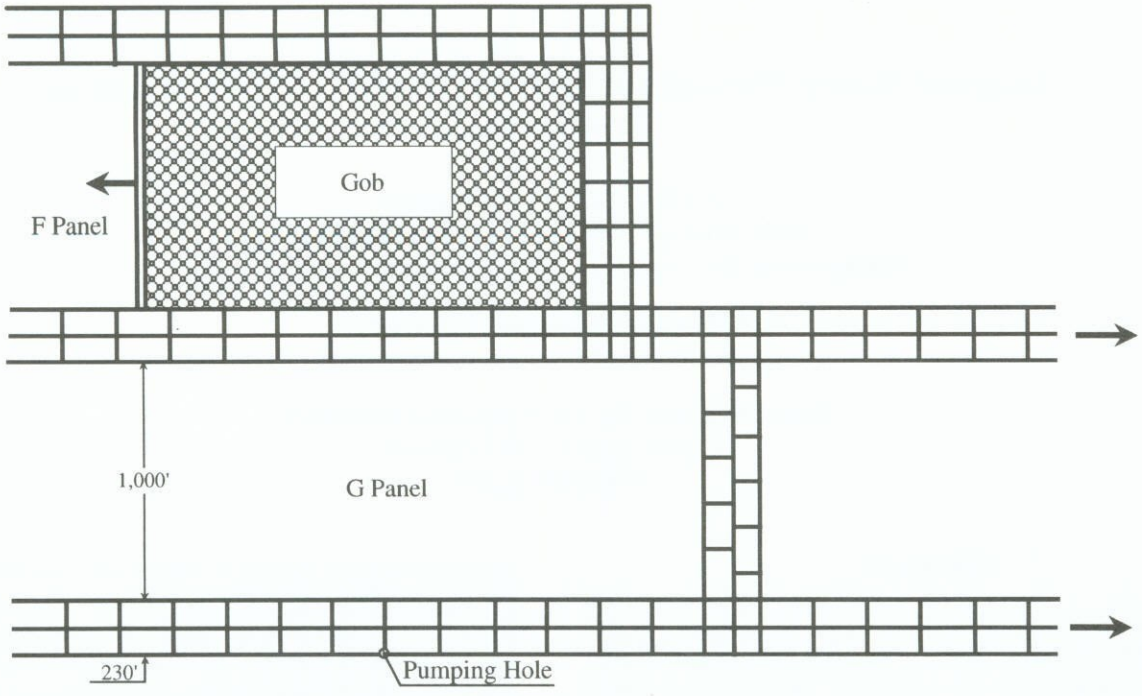



Fig. 1 Extending Plan of the G Panel at Cyprus Emerald Mine

After evaluating alternative supporting methods, costs and associated risks, a decision was made to backfill these entries and crosscuts using a low strength flyash cement mixture and then to mine thru with longwall. In designing the mixture strength, roof lithology and rock properties in the entry area were carefully examined and studied. The in-situ stress monitoring result indicated that the original design of the flyash mixture for this project was adequate to control the roof and compatible with the front abutment stress condition.

## THE LONGWALL CUT-THRU PROJECT

As illustrated in Fig. 1, to extend G panel to about 3,500 ft. inby the F panel's setup room when the F panel was still active, three in-panel entries had to be developed to support the ventilation and transportation of the tailgate entries inby. Three alternatives were considered to mine the G panel longwall block. They were: (1) in-panel face move; (2) supporting the entries by traditional supplementary supports and cutting thru the in-panel entries; and (3) backfilling the entire entries by flyash cement material and longwalling thru them.

For alternative one, in-panel face move, at least one barrier pillar has to be left inby the first in-panel or inby entry if the third in-panel or inby entry is widened as the setup room of the outby panel. In doing so the total cost due to production delays, coal reserve loss, consumptions of labors and materials during longwall face move, and loss of revenue was excessive.

For alternative two, supporting the entries by traditional supplementary supports and cutting thru the in-panel entries, the in-panel entries have to be supported by cable bolts, cable trusses, and several rows of either donut or wood cribs. For this alternative, the cost due to using these supplementary roof supports ranges from 10% of that of the in-panel face move. However, the risk of this alternative can be either production delays due to the shearer's cutting the standing supports, dealing with the floor heave and small scale roof falls, or the potential of loss of the face due to large scale roof falls during the cutting thru. Therefore, the total cost for this alternative including loss of revenue was estimated to be 35% of that of the in-panel face move.

For alternative three, backfilling the in-panel entries by flyash cement material, the entire entries are to be fully supported using flyash cement material prior to the cutting thru. For this alternative, the total cost due to materials, surface mobilization, and underground backfilling process is about 25% of that of the in-panel face move. However, it can be risk-free and thus causes no production delays if the strength of the backfilling material is properly designed.

Figures 2 and 3 illustrate the cutting-thru project and the roof and floor lithology nearby the cut-thru entries, respectively. It can be seen from Fig. 3 that the immediate roof consists of claystone, coal, laminated shale and sandyshale and is weak; the main roof is massive limestone; and the immediate floor is claystone and heave-prone. It is obvious that the potential of roof failure or floor heave are pretty high under the effect of the front abutment load as the face approaches the openings if the in-panel entries are

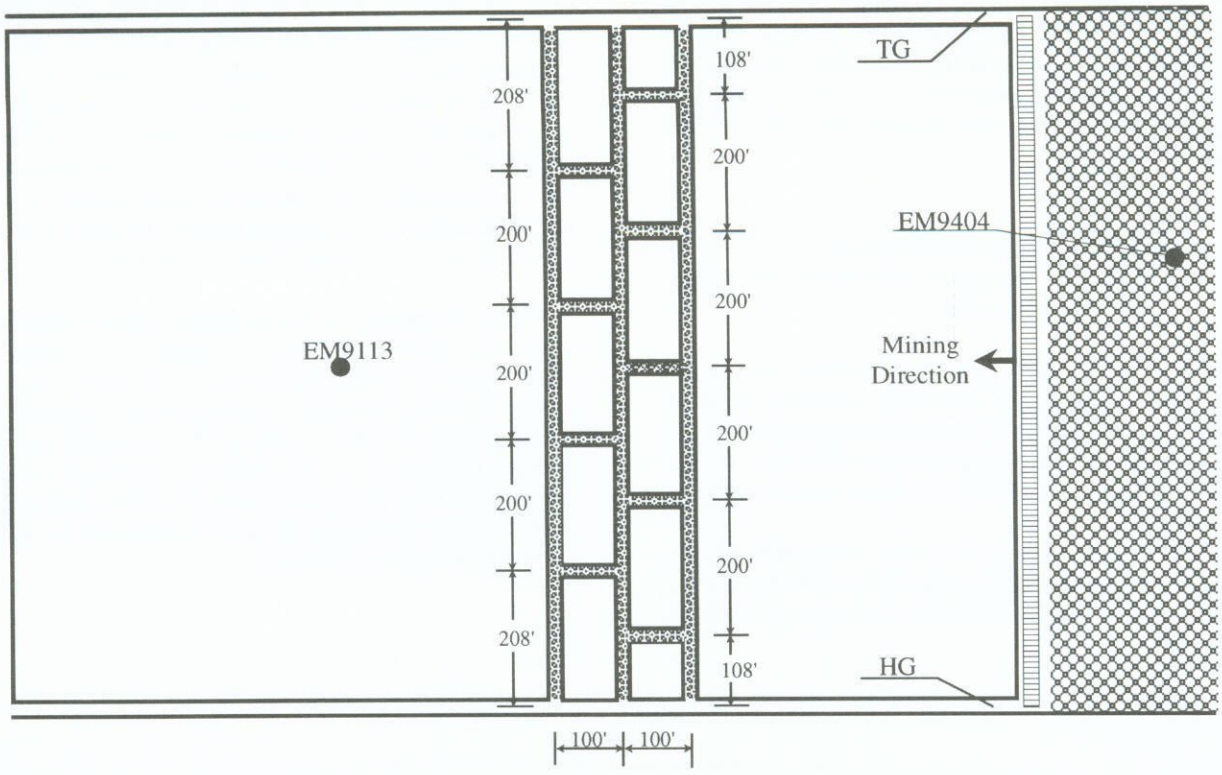



Fig. 2 Longwall Cut-Thru Project at Cyprus Emerald Mine

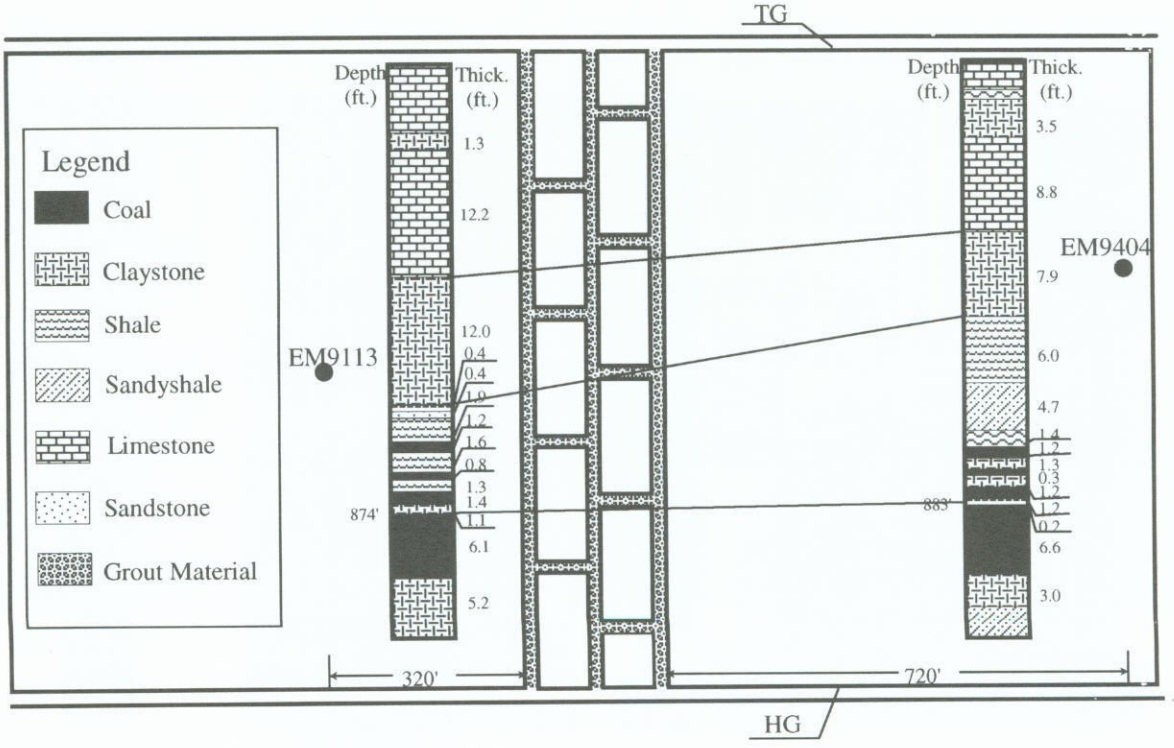



Fig. 3 Roof Condition Nearby the Three Cut-Thru Entries

supported by the conventional roof supports such as the combination of cable bolts, cable trusses, and standing cribs. In addition to the risk, cutting-thru the standing cribs could result in production delays. Therefore, a decision was made to backfill the in-panel entries with flyash cement material and to cut thru the backfilled in-panel entries.

## ENGINEERING DESIGN OF THE CUTTING-THRU PROJECT AND BACKFILLING MIXTURE

To ensure a smooth cutting-thru the backfilled entries and crosscuts, the strength of the backfilling materials must be designed in such a way that (1) it is strong enough to effectively control the roof and floor during the cutting thru and (2) it must be soft enough not to create difficulty in the shearer's cutting.

Based on the characteristic of strata movement above a longwall face, the roof load demand on the backfilling material was estimated in lieu of the roof lithology of Borehole EM9113 (Fig. 3), which is 320' away from the last grout entry. The required strength of the backfilling material was estimated by assuming that the roof strata broke immediately outby the grout entry (Fig. 4) when the face was still one web inby the grout entry; (2) the gob end of the top limestone block (40 ft. thick) was not supported by the rock fragments; and (3) shield resistance to the roof was ignored to provide an additional safety factor. Under this worst scenario, the material strength for this cut-thru project was designed to be 500 psi (Table 1 thru Table 3).

Since the strength of flyash cement mixture mainly depends upon the ratio of cement to flyash and curing time, a comprehensive testing program was conducted to determine the proper cement percentage. Testing results illustrated in Fig. 5 indicates that the Mix 4 with 22.5% of cement can meet the strength requirement for this project. Additional consideration was given to keep the flyash cement fill to have a specific gravity of greater than 1.6 so that the grout material can be separated out in the processing facilities.

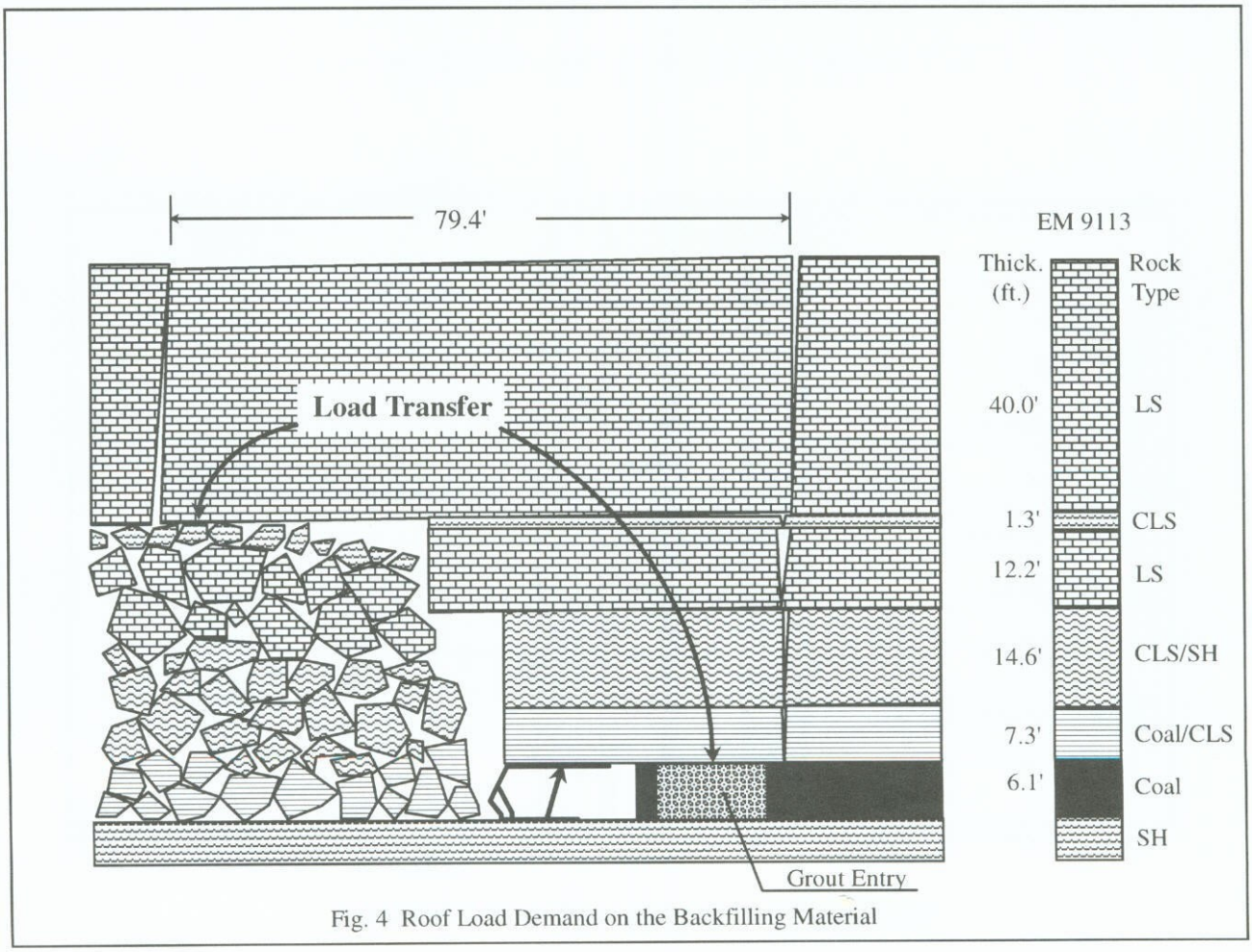



Fig. 4 Roof Load Demand on the Backfilling Material

Table 1 Minimum Control Length of the Immediate Roof

| Item | Unit (ft.) |
|---|---|
| Canopy length | 14.9 |
| Tip-to-face distance | 1.5 |
| One web depth (yield) | 3.0 |
| Entry width | 16.0 |
| Yield zone in the outby pillar | 3.0 |
| Minimum control length of the immediate roof | **38.4** |

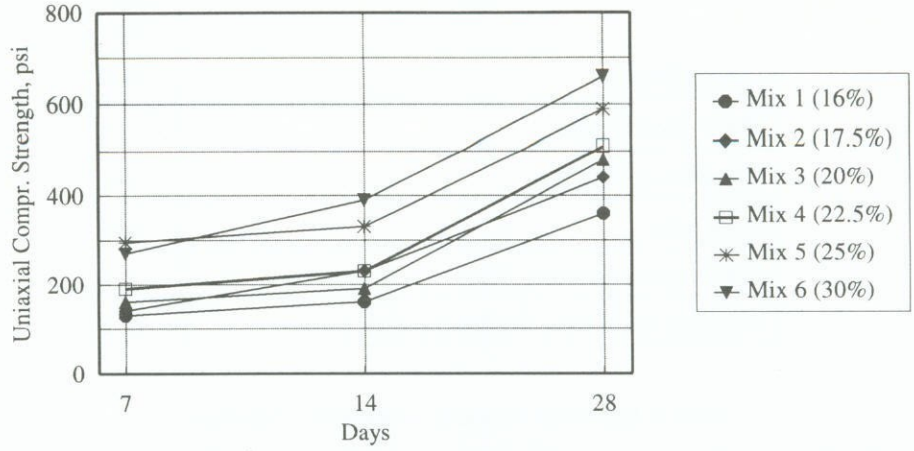
Table 2 Maximum Overhang of Each Rock Stratum

| Rock Layer | Rock Type | Thickness | Density | Tensile Strength | Unifom Load | Max. Overhang |
|---|---|---|---|---|---|---|
| | | (ft) | ($lb/ft^3$) | (psi) | ($lb/ft^2$) | (ft) |
| 0 | Coal | 6.1 | 82 | | | |
| 1 | Coal/clay | 7.3 | 124 | 84 | 908 | 15.4 |
| 2 | Shale | 1.9 | 160 | 105 | 296 | 7.6 |
| 3 | Sandstone | 0.4 | 172 | 757 | 60 | 8.6 |
| 4 | Shale | 0.4 | 160 | 105 | 56 | 3.3 |
| 5 | Claystone | 12.1 | 160 | 84 | 1,928 | 17.4 |
| 6 | Limestone | 12.2 | 171 | 561 | 2,086 | **43.8** |
| 7 | Claystone | 1.3 | 160 | 84 | 208 | 5.7 |
| 8 | Limestone | 40.0 | 171 | 561 | 6,840 | **79.4** |

Table 3 Required Strength of the Backfilling Material

| Item | Layer Thickness | Max. Control Length | Weight/ Shield Width | Comments |
|---|---|---|---|---|
| | (ft.) | (ft.) | (lb) | |
| Roof | | | | |
| Layer 1 | 7.3 | 38.4 | 174,093 | |
| Layers 2 to 5 | 14.6 | 38.4 | 448,512 | |
| Layer 6 | 12.2 | 43.8 | 457,191 | |
| Layer 7 | 1.3 | 43.8 | 45,583 | |
| Layer 8 | 40.0 | 79.4 | 2,714,112 | |
| Roof load demand | | | 3,839,491 | Ignore shield resist. |
| Front abutment stress (psi) | | | **333** | Fully grouted |
| Safety factor | | | 1.5 | |
| Required material strength (psi) | | | **500** | Ultimate strength |

Fig. 5 Strength Development of Various Mixtures of Cement and Flyash




## ACTUAL MATERIAL STRENGTH AND IN-SITU VERTICAL STRESS

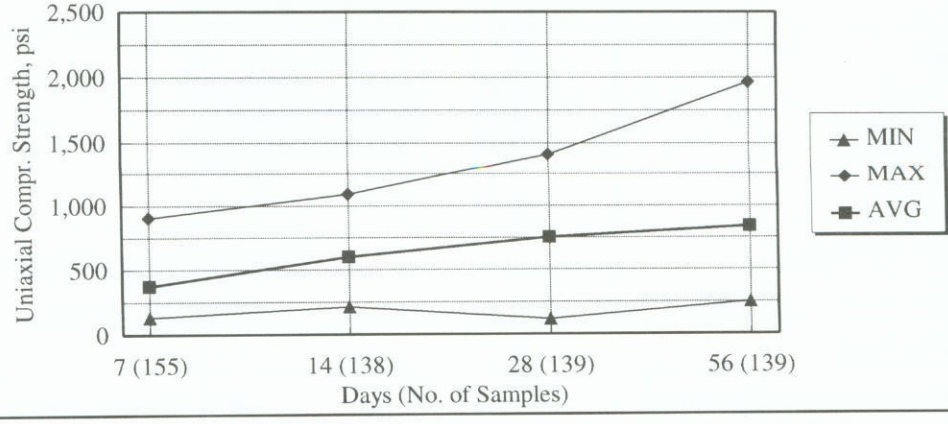
For the benefit of future use of this backfilling method, strength tests beyond 28 days were also conducted (Fig. 6). It can be seen from Fig. 6 that the average strength increases about 32, 11 and 3 psi/day for the period of 7th to 14th day, 14th to 28th day, and 28th to 56th day, respectively. Since suppliers usually take only the 28th day's strength as the design criterion, the ultimate strength of the backfilling material in the future application should include both the 28th day's strength and the strength increment for the targeting date. Therefore, the following equation can be used to determine the 28th day's strength for manufacturers.

$$S_{28} = S_d - (d*\Delta S) \quad (1)$$

where $S_{28}$ is the strength of flyash cement mixture on the 28th day, in psi; $S_d$ is the designed strength or ultimate strength, in psi; d is the number of days between the 28th day and the day when the material is cut, and $\Delta S$ is the strength increment between the 28th day and 56th day, in psi. It must be pointed out that these testing samples were directly taken from the batch plant on surface immediately before pumping.

The front abutment stress within the longwall coal block (7 ft. inby the first in-panel entry), the backfilled material (center of the first in-panel or inby entry), and the center of the first pillar ranged from 600 to 800 psi, 115 to 230 psi, and 1,500 to 3,000 psi, respectively. Obviously, the backfilled material took much less vertical load than the longwall coal block and pillars due to pre-softening of the entry roof after development, the compacting feature of the backfilled material during pumping, and the extended curing time.

Fig. 6 Actual Strength of the Backfilling Material



In our original design, the calculated roof load was 333 psi (see Table 3) before considering a safety factor of 1.5. If we consider both the shields (70% of its vertical yield capacity) and the grout wall resisting the roof load, the strength of the grout wall should be:

$$S = 333 - p_v = 333 - \frac{0.7\times700\cos20^o\times2{,}000}{14.9\times5\times144} = 247 \quad psi \quad (2)$$

where $p_v$ is the vertical pressure provided by a shield to the roof, in psi.

## BACKFILLING PROCESS AND FULL PANEL CUTTING THRU

The flyash cement mixture was pumped from the batch plant on surface 250 ft. to the vertical pumping hole, which was about 700 ft. deep, and then horizontally 1,200 ft. to the in-panel entries. The backfilling sequence began by filling the inby entry first from tailgate to headgate because the three entries dipped downwards from tailgate to headgate. Entries were segmented using solid concrete block bulkheads with two piers built into each wall. Design of the segment lengths depended mainly on elevation changes, roof profiles and ventilation. Witness pipes through the bulkheads were used to insure complete backfilling in higher roof elevations. The two remaining entries were filled by sequencing the pumping of material back and forth between the two entries while moving from the tailgate side of the panel to the headgate while paying particular care to proper ventilation.

Longwall mining thru these three in-panel entries took about four eight-hour shifts and proved to be very successful. The designed flyash cement mixture provided adequate roof and floor stability and caused no difficulty in the shearer's cutting while eliminating an in-panel face move and minimizing the risk of roof or floor failure at the longwall face.

### Underground Observations

In order to ensure a smooth cutting thru the grout entries, Cyprus engineering personnel monitored cautiously each shift's operation and provided on-site technical service for shearer's operators to control the cutting horizon during the mining-thru period. Based upon our observations, it can be summarized as follows:

(1). The backfilled material fully contacted the entry roof except in one crosscut.

(2). No roof deteriorations occurred above either the grout entries or crosscuts during the extraction of the grout material, but the roof inby and outby the grout entries and the roof around the crosscuts in the middle of the face tended to be slightly inferior due to coal pillar yielding at ribs or the porous concrete material's compacting, transferring additional load to those areas.

(3). The strength of the backfilled material caused no difficulty in the shearer's cutting and no extra bits were consumed.

(4). Heavier-than coal's density (about 100 lb/ft$^3$) and greater coefficient of friction between the backfilled material and the AFC made the face conveyor difficult being re-started in several occasions though the shearer's haulage speed was reduced from 40-45 ft./min for the coal cutting to 15-25 ft./min for the backfilled material cutting. On one middle night shift, it took about 45 min. to unload the backfilled material on the AFC.

(5). Materials, such as channels, witness and grout pipes were cut during longwalling caused the stageloader and face conveyor chain jam in several occasions.

(6). No obvious indicator in the backfilled material caused difficulty controlling the cutting horizon. Therefore, when the shearer cut into a point anchor bolt, it broke at the coupler and the lower half pulled out.

(7). More coal spalling near the top occurred when the face was about 10 to 15 ft. either inby or outby the grout entry.

(8). A roof fall between the canopy tip and faceline occurred from the face center to the tailgate side (shields #100 to #165) when the face was about 17 ft. outby the last grout entry.

It must be noted that the operational downtime during the cutting thru included the time delays caused by the handling of cable trusses at both the headgate and tailgate sides of the longwall. It is obvious that under a normal entry roof condition, the delay time due to loading and unloading the supplementary roof supports can be eliminated. Therefore, the total time required for the longwall face cutting thru the grout entries could have been reduced.

### Analysis of the Face Roof Fall at 17 ft. Outby the Last Grout Entry

A roof fall occurred near the center of the face toward the tailgate side (between #100 shield to #165 shield) on Nov. 16 when the face was about 17' outby the last grout entry. Actually, underground observations indicated that whenever the face was about 15' either inby or outby the three grout entries, roof spalling from the top portion of the face occurred and thus made the coal supporting line deeper into the coal face. This phenomenon in turn made the unsupported distance between the canopy tip and the actual faceline become greater and thus increased the potential of face roof failure due to tension. Since the coal block or pillar ribs yielded already after the entries and crosscuts were developed and before the back-filling, deflection of the entry or crosscut would shift the roof load above them and the yield zones at coal block or pillar ribs onto the deeper part of the coal block or pillars. As the longwall face approached, the front abutment load made this situation even worse. In order to answer the question why the roof fall did occur when the face was 17' away from the last grout entry and rarely occurred elsewhere, roof conditions around the grout entries were examined.

It can be seen from Fig. 3 that the immediate roof 320' outby the last grout entry (see Borehole EM9113) is much weaker than that 720' inby the first grout entry (see Borehole EM9404). If

roof falls occurs under both roof conditions, the roof fall at Borehole EM9404 may reach only the bottom of the sandyshale (6.8' from the roofline) and at Borehole EM9113 may reach the bottom of the first limestone (22.1' from the roofline). In reality, a roof fall with a height of 4' to 6' in the area between the canopy tip and the faceline may not result in a production delay at the face. However, a roof fall with a height of greater than 10' most likely cause production delays at the face. Actually, small roof falls were observed when the longwall face was in other areas but rarely resulted in production delays. Therefore, it can be concluded that both the shifted front abutment load and the local weak roof condition outby the last grout entry caused the face roof fall.

## FUTURE APPLICATION OF LONGWALL BACKFILLING TECHNIQUES

As longwall panels get longer and longer, due to the constraint of inproportional ratio of the current longwall retreat and CM development rates, and for the sakes of enhancing longwall production and reducing the potential of injuries resulted from longwall face move, backfilling entries, crosscuts, and recovery rooms may be the best approach in the future. If we do it again, the following measures should be taken:

(1). Use fully grouted bolts without steel channels to support the entry roof.

(2). Employ a metal detector to locate all tramp metal in the entries prior to backfilling.

(3). Use an indictor at the top portion of the grout wall or leave an 1.5' to 2' bottom coal during entry development as a indicator for horizon control during longwalling.

(4). Inject chemical grout into the fractured roof over pillar or panel ribs prior to backfilling if necessary.

(5). Use bagged concrete mixture rather than wood bridges to fill any holes created by and during CM development.

(6). Reduce the shearer's haulage speed whenever cutting thru backfilling material or use partial web cutting to keep the paneline from stalling.

(7). Use unidirectional cutting if necessary.

## CONCLUSIONS

The project of cutting-thru in-panel entries at Cyprus Emerald mine has been proved to be risk-free and very successful. This approach can be used for solving the problems resulted from the unparallel rate of face advance and entry development in longwall mining and may also be used for longwall recovery room to speed up longwall face move.

## ACKNOWLEDGMENTS

The authors would like to thank Wm. Mark Hart, President of Cyprus Australia Coal Co., and Scott Langley, Brian Shaffer, Ed Zeglen and Chuck Zabrosky and the entire working force at Cyprus Emerald mine, for their enthusiasm, advice, and assistance in this project. The authors would also like to thank members from both R. J. Johnson Co., Inc. and NIOSH for their assistance in this project.

## REFERENCES

E. Bauer, J Listak, M. Berdine, W. Bookshar, D. Raab, and T. Mucho, 1988, "Longwall Recovery Utilizing the Open Entry Method and Various Cement-Concrete Supports," *Proc. of the 7th Int. Conf. on Ground Control in Mining*, Morgantown, WV, pp. 30-42.

T. Wynne, J. C Stankus, S. Guo, and S. S. Peng, 1993, "Design, Monitoring and Evaluation of a Pre- Driven Longwall Recovery Room," *Proc. of the 12th Int. Conf. on Ground Control in Mining*, Morgantown, WV, pp. 205-216.

# Performance of Various Standing and Cribless Tailgate Support Configurations in a Large Eastern Coal Mine

*Gregory M. Molinda,* Geologist
*Dennis R. Dolinar,* Mining Engineer
*Thomas M. Barczak,* Research Physicist
National Institute for Occupational Safety and Health
Pittsburgh Research Center
Pittsburgh, PA

*Jason Hustus,* Mining Engineer
Cyprus Cumberland Resources
Waynesburg, PA

## ABSTRACT

Difficult mining conditions in deep western U.S. longwalls have necessitated the use of novel tailgate support systems. Extreme ground movement in these yielding gate systems has caused operators to utilize secondary support systems which match yield and strength characteristics with expected ground reaction. Other benefits include ventilation and safety gains, as well as lower costs. Recently, the use of novel support has been tried at longwall mines in other U.S. coal basins. One of the main considerations is the capability of the support to maintain an adequate airway for gob ventilation in gassy eastern coal mines. In one large Pennsylvania mine working the Pittsburgh seam, a number of support configurations were monitored over a 2,300 ft tailgate test area. The test included 4-pt wood cribs, Link-N-Lock cribs, Propsetter yieldable posts, cable trusses, and vertical cable bolts. Ground reaction, and thus support performance, was documented by roof sag and convergence instruments, ventilation measurements, and photographs. Various combinations of standing support and cable truss and vertical cable bolts provided adequate support for ventilation and safe escape. A cribless configuration consisting of only cable trusses and vertical cable bolts was inadequate to provide inby gob ventilation to the next open crosscut. Instrument ground movement data and visual documentation are presented.

## INTRODUCTION

A primary goal of National Institute for Occupational Safety and Health (NIOSH) at the Pittsburgh Research Center is to improve longwall safety by reducing the potential for methane explosions, blocked longwall escape, and materials handling injuries. In gassy mines it is critical to maintain a stable airway on the tailgate corner for the purpose of keeping gob gases from leaking out of the bleeder and onto the face and tailgate escapeway. Gob caving and sloughing adjacent to the shields and panline and even outby the face can cause a dangerous gas accumulation to shut down the longwall. From 1990-1995 in district 2 (10 longwall faces) MSHA investigated over 225 unintentional falls of roof (1). Of these falls, 68 occurred in gateroads. In recent years this number has been declining, but the introduction of unproven tailgate support could reverse this trend.

Most tailgates and bleeders are still supported with wood cribbing. Injuries resulting from materials handling in coal mines exceed injuries from all other sources. From 1992-1994, 55% of permanent disabling injuries in underground coal mining occurred from materials handling. During the same period over 7,000, or 35%, of non-fatal lost day accidents resulted from materials handling. This total exceeded all other categories including slips and falls, powered haulage, and machinery-related accidents (2). Recent trends in tailgate support require less handling of bulk materials and promise to reduce these injury totals.

Active research at the PRC has centered on evaluating the strength and stability capabilities of various tailgate support through testing in the Mine Roof Simulator (MRS). Equally important is the field evaluation of new supports through cooperation with mine operators. The poor performance and scarcity of wood in the west has caused operators to adopt alternative secondary tailgate support (3). These supports include various yieldable posts, cans, cribs, and cribless systems comprised of cable bolts and trusses. The benefits of these supports have motivated operators in eastern coal mines to consider alternative supports. Conditions common to eastern coalfields include gassy coalbeds, high insitu horizontal stresses, full abutment pillar gate roads, and weak roof. For these reasons test areas for new supports are desirable.

Rigid trusses have had mixed success in eastern applications, and cable trusses are currently being tested. Link-N-Lock cribs and Propsetter posts have found numerous applications in tailgates and bleeders. Cable bolt applications as tailgate support are rare outside the west, although there have been several eastern tests. MSHA is concerned about untensioned cable bolts allowing excessive roof sag in weak strata with high horizontal stresses. Additionally, shear failures of cable bolts have been a limiting factor in their application, especially in proximity to sandstone channels. There is also a concern of cable failure in a

domino fashion causing large tailgate falls. The use of mobile roof supports as secondary tailgate support has also been discussed, although none have yet been used in this application. NIOSH/PRC research is aimed at addressing these and other questions regarding tailgate support. The following report describes the results of a test of several alterative secondary supports in the tailgate of a large Pittsburgh seam coal mine.

## TEST SITE DESCRIPTION

The test area is 2,300 ft long with overburden ranging between 600-800 ft (figure 1). Surface relief is about 200 ft with mining occurring under two stream valleys. No significant entry damage was observed either from insitu horizontal stress or stream valley effects in the test area. The mine utilizes a three entry gate road with pillars on 140 ft centers and entry width of 16 ft. Crosscuts are angled approximately N40° east to minimize damage from the principal horizontal stress. Entries are mined with a miner-bolter system which installs two bolts and then a center bolter finishes the three bolt pattern. Two types of primary bolts were used as shown on figure 1. The first is an 8 ft 3/4 in grade 75 Jenmar Insta'l bolt, the second is a 6 ft fully grouted 3/4 in Birmingham torque tension bolt.

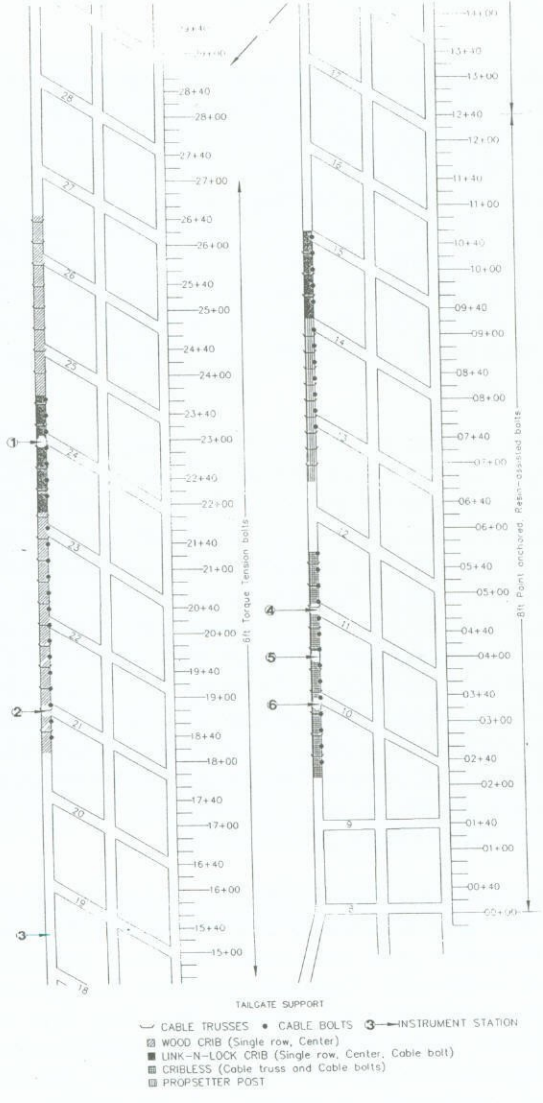



Figure 1. Tailgate test area.

The roof is typical Pittsburgh seam roof which is a sequence of alternating rider coals and weak shales with coal streaks (figure 2). The Coal Mine Roof Rating = 38.

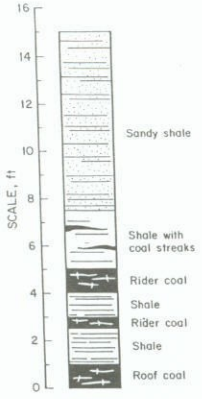



Figure 2. Roof lithology in the test area.

Regular tailgate supplemental support consists of two rows of fiber concrete block (6x8x16 in) cribs on 6 ft spacing. The mine has successfully extracted a number of panels with this tailgate support but, due to high cost and materials handling injuries, was testing alternative support. A number of different support types and combinations were installed and monitored. The tailgate test areas included the following (figure 1):

- Single row of 4 pt, 30 in long **wood cribs** on 6 ft centers with **cable trusses** on 8 ft centers and **no cable bolt** (26+50 to 23+70).

- Single row of 30 in **Link-N-Lock cribs** on 6 ft centers, **cable trusses** on 8 ft centers with 12 ft long **cable bolts** on 6 ft centers located 4 ft from the rib (23+70 to 21+90).

- Single row of 4 pt, 30 in long **wood cribs** on 6 ft centers with **cable trusses** on 8 ft centers and 12 ft long **cable bolts** on 6 ft centers located 4 ft from the rib (21+90 to 18+15).

- Single row of 10 in **Propsetter posts** on 6 ft centers, **cable trusses** on 8 ft centers, with 12 ft long **cable bolts** on 6 ft centers located 4 ft from the rib (9+25 to 6+70).

- Single row of 10 in **Propsetter posts** on 6 ft centers, **cable trusses** on 8 ft centers, **no cable bolts** (7+60 to 6+70).

- Jenmar **cable trusses** on 8 ft centers with a single row of 12 ft long **cable bolts** on 6 ft centers located 4 ft from the rib (5+60 to 2+10).

### Instrumentation

Roof instrumentation was limited to existing roof test holes which were drilled to depths of 12 and 15 feet and sporadically spaced along the test section. These holes were located on the panel side of the tailgate entry. This location prevented the collection of data inby the shields because the instruments were destroyed by gob.

Roof separation and sag was monitored by a BuMines-developed wire extensometer in six different locations (figure 1). Convergence was recorded automatically at these same locations

by roof to floor wire meters. Convergence was also periodically recorded manually by spring-loaded pogo sticks. Entry damage was documented by photographs, and by visual damage rating. Ventilation measurements were taken periodically to record gob ventilation and assess damage to air courses.

## SUPPORT PERFORMANCE

### Wood Cribs with Cable Truss and no Cable Bolt

The first test section consisted of a **single row of wood cribs** (6 ft centers), and **cable trusses** on 8 ft centers from 26+50 to 23+70 (figure 1). No cable bolts were placed on the rib side of the tailgate entry. As the face passed through this test area the airway on the chain pillar side of the crib generally remained open approximately one crosscut inby the face (figure 3). The entry on



Figure 4. Looking inby the face at the tailgate supported by a single row of Link-N-Lock cribs.

Figure 3. Looking inby the face at the tailgate supported by a single row of wood cribs.

the chain pillar side of the crib was estimated to be open 35% to the first inby crosscut. The row of cribs in the center of the entry was acting as a breaker line for the gob. The wood cribs were notched due to loading adjacent to the shield, but minimal loading was seen outby the face. The roof generally stayed intact and it was the gob flushing and rib sloughage which filled up the entry. The fact that there was no cable bolt on the rib side of the entry may have contributed to the inby rib sloughage by allowing the roof to sit down on the pillar and spall it out. A similar increase in rib sloughage was seen in the Propsetter test with no cable bolts on the rib side. One incident did occur in this test area. The longwall was gassed off four times in one shift due to gob flushing which knocked out several cribs and caused caving tight across the entry just behind the shields.

### Link-N-Lock Cribs with Cable Truss and Cable Bolt

The next test section is a **single row of Link-N-Lock cribs** on 6 ft centers with a 12 ft long cable bolt in the roof on 6 ft centers located approximately 4 ft from the rib ( 23+70 to 21+90). Cable trusses were placed on 8-ft centers. The entry stayed open at least 2 crosscuts inby the face with the entry condition better than in the previous section with wood cribs and no cable bolts. The cable bolts also noticeably improved the condition of the airway corner nearest the rib (open 100%), as well as reduced rib sloughage (figure 4). Link-N-Lock cribs show very little loading and were standing straight. Outby conditions were excellent. A

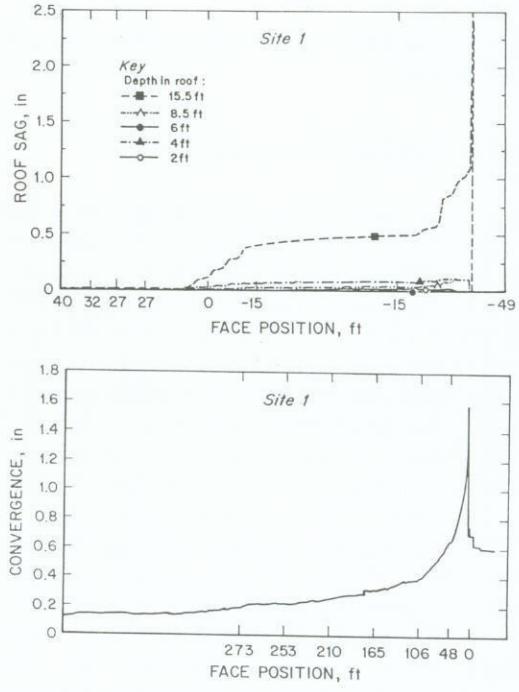



Figure 5. Convergence and roof sag at instrument station number 1.

differential sag station located at crosscut 24, showed bulk roof sag (total of 1.1 in.) ocurred between 8.5 and 15.5 ft. into the roof (figure 5). This movement began approximately 10 ft in advance of the face and continued until the shield passed the instrument approximately 30 ft after the face pass (figure 5). Most of the roof sag occurred above the bolt and truss anchorage.

This amount of movement could be critical if horizontal stress or roof discontinuities occur. Because of it's location, the immediate tailgate corner is critical to escape and ventilation. Movement above support anchorage should be noted. Automated convergence data show 7 days of gradual increase (up to 1.6 in) before mineby (figure 5). Only .5 in of the total convergence is floor heave. Since the floor is a soft underclay, high loads were not transferred through the support into the roof, and this amount of floor heave was not a problem.

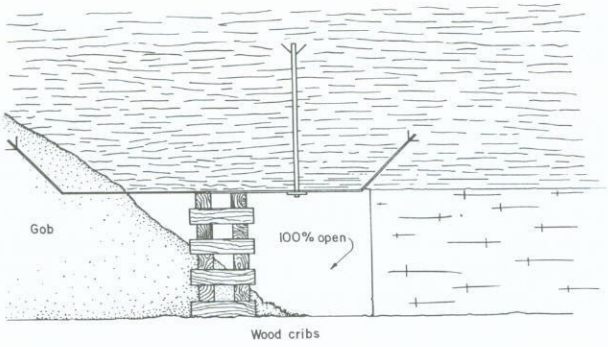



Figure 6. Condition of tailgate airway inby the face in wood crib test section.

Wood Crib with Cable Truss and Cable Bolt

The next test section was again a **single row of wood cribs** (6 ft centers) (21+90 to 18+15), with the cable truss on 6 ft spacing and with a 12 ft cable bolt (6 ft centers) added on the rib side of the tailgate entry. The inby airway remained 100% open on the rib side for at least 1.5 crosscuts behind the face (figure 6). The roof was intact on both sides of the crib and all slough was from the rib and gob. The cribs were standing straight with no buckling. The cable bolts were showing loading by plate bending. There were no incidents of gob flush kicking over the wood cribs, or methane incidents at the face. Primary support from 12+50 inby was Birmingham torque tension bolts, and plates have bent with some nut heads splitting. Outby conditions were excellent with no crib loading or entry damage. The rib side roof was undamaged outby the face, where a cutter had often formed in previous panels. This may be attributed to the additional support provided by the cable bolt. On all test sections, the cable trusses were undercut when the face passes and provide no entry support inby the shield line. Measurements showed a total of 1.7 in of convergence on the rib side of the entry (site No. 2, figure 1). The recording convergence station showed 1.25 in of convergence mostly occurring over the four days (264 ft) prior to mineby. This station was also located in the intersection. The roof sag instrument was damaged prior to mineby and, as a result, no usable data was recorded.

Propsetter Posts with Cable Truss and Cable Bolts

The next tailgate test section consisted of a **single row of 10 in diameter Propsetter yieldable posts on 6 ft centers** from 9+25 to 6+70. Cable trusses were set on 8 ft centers and 12 ft cable bolts were installed on 6 ft centers. The Propsetters were set 4 ft from the rib and intended to support roof which may be severed by a cutter. The first half of this test section was also supported by the 12 ft cable bolt on the rib side of the tailgate, but in the section from 7+60 to 6+70 the cable bolt was dropped. When the face passed, the gob was broken right at the Propsetter row with sloughage between the props. The posts were standing straight and kept the airway open 30-75% on the rib side (figure 7). The airway was open at least 1.5 crosscuts inby the



Figure 7. Looking inby the face at the tailgate airway supported by a single row of Propsetter posts.

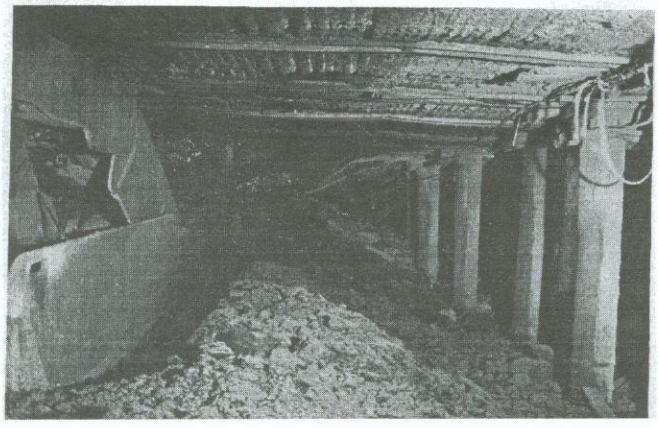


Figure 8. Looking inby the face at the tailgate supported by Propsetter posts showing weight at the base.

shields. The concern was that floor heave would cause the Propsetters to lean, but soft bottom flowed around the bottom of the posts and did not offset them. Additionally, no lateral movement of the roof occurred to offset the top of the post. Several posts were showing weight adjacent to the shields (figure 8). No loading was apparent outby the face on props, cable trusses, or cable bolts (figure 9).

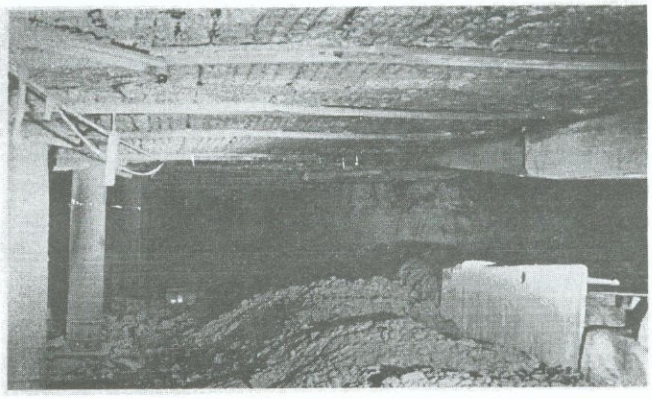


Figure 9. Looking outby the face at Propsetter test section.

From 7+60 to 6+70 the cable bolt was dropped and only the Propsetter remains. The rib sloughage was significantly worse in this section and continues approximately 30 ft outby the face. There also was a cutter in the roof. The cable appeared to be suspending the roof, and when it was removed the roof was allowed to sit on the pillar, loading it and causing more pillar slough and a fracturing of the cantilevered corner. The tailgate was open to 1.5 breaks inby the face. The airway was open 50%. Entry damage is generally less in the section with the cable bolt installed.

Cribless Test Area with Cable Truss and Cable Bolts

From 5+60 to 2+10 all standing support was removed and only the cable trusses on 8 ft centers and a single row of 12 ft cable bolts on 6 ft centers support the roof (figure 10). Intersections were supported with supplemental cable bolts. Now only the cable bolt remains to act as a breaker line for the gob. The cable bolt row breaks the gob but gob flush rolls right to the rib closing the airway to 25% (figure 11). There is no evidence of cable bolt failure.



Figure 10. Looking inby the face at the Cribless test section.



Figure 11. Looking inby the face at the Cribless ribside airway corner. It remains approximately 25% open.

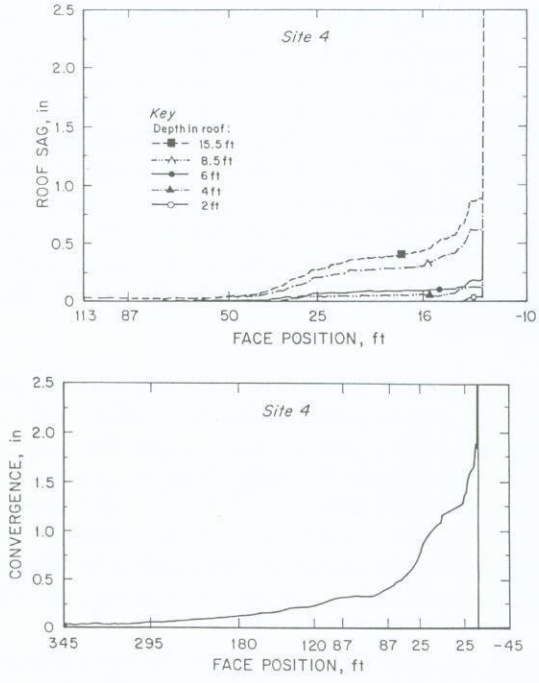



Figure 12. Convergence and roof sag at number 4 instrument station in the cribless test section.

There is minor damage due to outby loading or movement. Convergence measurements show outby movement up to 400 ft in advance of the face, but most of this early movement is floor heave (figure 12, convergence site No. 4). The inby-ribside airway remains marginally open through most of the pillar length (smoke release shows a small movement of air towards the gob). A 2 x 2 ft opening remains in the ribside corner of the entry at crosscut 11 when the face is at 3+65, but closes completely when the face reaches 3+30 (crosscut No.10) (figure 13). At this point no air movement was detected by smoke release at the first inby crosscut (No. 11). It appears that the airway can survive (barely) about 3/4 of a crosscut, but not the full crosscut. Foremans' records indicate "methane problems" all throughout day shift, and curtains were hung to direct air back through gob. The



Figure 13. Looking inby the face at the ribside airway corner in the Cribless test section showing complete closure.

cribless configuration does not provide an adequate gob airway, and some standing support or alterative cabling scheme is needed. Air measurements at the tailgate corner at 3+65 (a small airway 2 x 2 ft was still open) showed no movement. Air movement was detected at the first inby crosscut (No. 11). This indicates that air was moving behind the shields and the tailgate gob was being ventilated. When the face reached 3+30 no air movement was detected on the tailgate corner and no air was detected at the first inby crosscut (No. 11). The gob was not being ventilated through the tailgate. Air was moving down crosscut No. 10 and into the No. 2 bleeder, as directed by a regulator curtain.

Three extensometers with accompanying wire convergence meters were located in the cribless test section as shown on figure 1 (instrument station 4,5,6). Additional convergence measurements were taken manually at each site. Two instrument sites were in intersections (No. 10 and 11) and one was mid-pillar between them. At site No. 4 (4+70) a total of 1.85 in of convergence was measured on the panel side of the tailgate after mineby. Approximately 1 in of this movement was floor heave.

A roof sag meter was also located at the intersection of crosscut No. 11 (site No. 4). It shows approximately 0.25 in of movement between 8.5 and 15.5 ft into the roof, 0.45 in between 8.5 and 6 ft, 0.15 in between 2 and 4 ft, and negligible movement between 0 and 2 ft as the face passed the instrument (figure 12). Movement in an intersection above truss and bolt anchorage could be a problem, especially between the face and back of the shield. In this cribless tailgate, there is no standing support to break the cantilever, and this deflection could extend onto the rib side cable bolt. The roof sag began to occur approximately 50 ft in advance of the face. Roof sag occurred outby the face at instrument sites 1, 4, and 6. All these sites were in intersections. Total convergence was 1.85 in, with approximately 1.0 in of floor heave. Floor heave began to occur approximately 300 ft in advance of the face.

Another instrument site (No. 5) was located at mid-pillar between No. 10-11 crosscut. The recording convergence wire was buried by rib roll approximately 300 ft in advance of the face. Manually, 1.4 in of total convergence was measured at mid entry. Small amounts of convergence (<.1 in) began to occur several thousand feet in advance of the face. Over 90% of the total convergence occurred over the last 600 ft prior to mineby. The roof sag instrument was located mid pillar between crosscut No. 10-11 on the panel side. It showed no movement anywhere up hole prior to mineby. Therefore all of the entry convergence (1.4) can be considered floor heave. Roof separation and sag was not present at this mid pillar size as it was in the previous intersection. The inby airway on the rib side was only open to 20% at the time of instrument site mineby due to gob flush and rib roll.

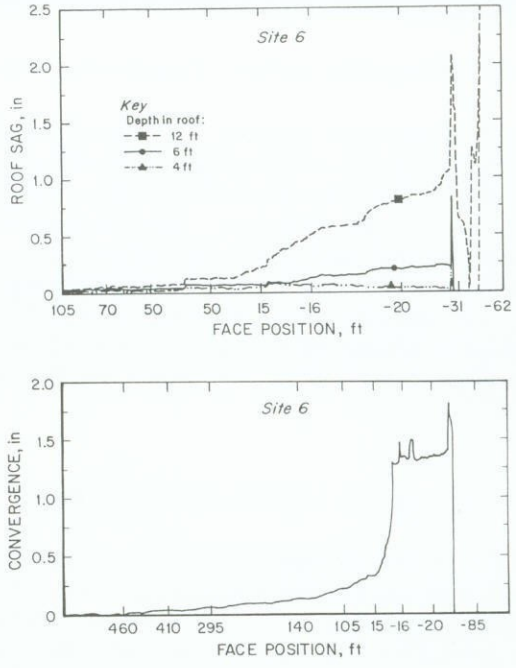



Figure 14. Convergence and roof sag at the number 6 instrument station in the Cribless test section.

The final instrument site (No. 6) was located in the tailgate intersection at crosscut No. 10. 1.75 in of convergence occurred beginning when the face was over 500 ft away up to mineby. Convergence accelerated when the face was 15 ft away (figure 14).

A roof sag instrument was located at 3+50 in the cribless section (Site No. 6). Roof sag began approximately 50 ft outby the face and measured a total of 1.1 in at mineby. 0.55 in of sag occurred between 12 ft and 6 ft in the roof, and the remaining 0.1 in occurred from 0-4 ft. (figure 14). Approximately .5 in of sag had occurred by the time of mineby, with the remainder (.6 in) occurring from mineby to gob forming behind the shield. Most of this sag likely occurs above truss and bolt anchorage (the anchor at 8 ft malfunctioned), again in or near an intersection. As in site 4 roof sag began to occur outby the face. Roof sag outby the face in the intersection of the tailgate escapeway above anchorage could become a problem. Ground loading outby the face was expressed in the form of increased pillar spall.

Table 1 summarizes the measured entry movement for each site. Floor heave was roughly equivalent whether at intersection or mid pillar, but there was more roof sag in intersections than mid pillar. Floor heave appears to have occurred over a period of days or weeks unrelated to face location, but roof separation and sag generally occurred within 1 day (100 ft) of mineby.

Table 1. Total Entry Deformation

| Instrument Site & Location | Total Convergence (in) | Roof Sag (in) | Floor Heave (in) |
|---|---|---|---|
| | | | |
| #1 Intersection #24 | 1.60 | 1.10 | .50 |
| #2 Intersection #21 | 1.70 | ? | 1.70 |
| #3 Mid Pillar #18-19 | 1.60 | 0 | 1.60 |
| #4 Intersection #11 | 1.85 | .85 | 1.00 |
| #5 Mid Pillar #10-11 | 1.40 | 0 | 1.40 |
| #6 Intersection #10 | 1.75 | 1.10 | .65 |

## DISCUSSION AND CONCLUSIONS

From the standpoint of escapeway safety, all of the test configurations provided adequate support on the tailgate corner and outby the face. Rib sloughage was worse 30-50 ft outby the face in the section with Propsetter posts and no cable bolts, but at no time were there any significant roof or rib falls which would impede escape. Up to 1.1 in of total roof sag occurred in the cribless test section between 6 and 12 ft up in the roof. Additionally, this movement began to occur up to 50 ft outby the face and above support anchorage. Roof sag was greater in the intersection than at mid pillar. Floor heave (up to 1.7 in) began days to weeks before face pass but was insignificant because of soft floor.

The support of the immediate tailgate corner and inby one crosscut is critical for gob ventilation in gassy mines. Standing support in the middle of the entry (Link-N-Lock cribs and 4 pt wood cribs provided a gob line breaker as well as a barrier to gob flushing. The Link-N-Lock cribs were very stable and did not experience rollout as happened with the 4 pt wood crib. The Link-N-Lock cribs provided a ribside airway at least 2 crosscuts into the gob. Propsetter posts also provided a gob line breaker and showed no signs of excessive loading or failure. In the test sections with 4 pt wood cribs and in the test section with the Propsetter posts, rib sloughage and cutter roof was improved by the addition of the vertical cable bolt near the rib. The inby tailgate airway was not maintained for the full pillar length between crosscuts in the cribless test section. While the roof remained intact it was gob flushing and rib slough which closed off the airway. The cable bolts acted as a gob line breaker, but gob flushing across the entry effectively closed off the airway. There was no evidence of cable bolt failure. The cable trusses were ineffective in maintaining the inby airway because falling gob as the face passed removed one anchor. It is difficult to estimate the outby roof control value of the cable trusses because they were used throughout the test area. They may serve to combat horizontal stresses activated on development or preserve the rib side corner as the front abutment stresses approach, but this could not be determined.

## REFERENCES

1. MSHA, District 2, personal communication. Available from G. Molinda.

2. Report of the Future focus Team: Mining Health and Safety Research at the Pittsburgh and Spokane-Research Centers, Dec. 10, 1996, CDC/NIOSH/PRC , pp. 6.

3. Barczak, T.M., and G.M. Molinda. Innovative Secondary Support technologies for Western Mines. Proceedings of the 15th International Conference on Ground Control in Mining, Golden, CO. August 13-15, 1996 , pp. 349.

# Measurement of Effects of Interaction and Influence on Mine Layout Design at Maltby Colliery

*J. S. Oram,* Geotechnical Engineer
Rock Mechanics Technology Ltd.
Burton-on-Trent
UNITED KINGDOM

*C. G. Ponder,* Mine Manager
Maltby Colliery
RJB Mining (UK) Ltd.
UNITED KINGDOM

## ABSTRACT

Maltby Colliery, operated by RJB Mining (UK) Ltd is successfully mining the Parkgate Seam in Yorkshire at a depth of 1000m using longwall retreat. Extraction in the Parkgate seam is influenced by interaction from previous workings in the Swallow Wood Seam 160m above.

The paper describes in-situ stress measurements and simple gate road convergence measurements carried out to assess the extent of the interactive influence.

The stress measurements, obtained using the stress relief overcore technique, were carried out from a maingate development roadway in an area where the stress redistribution under an overlying pillar and adjacent panel goaf could be measured. The measured vertical stress distribution confirmed a significant interactive influence with high imposed vertical stresses under the overlying panel edges.

Simple roadway convergence monitoring stations established in the gateroads of a retreating panel and in the development gateroads of the adjacent panel, confirmed higher rates of roadway deformation relating to overlying panel edges and pillars, particularly in the areas where a vertical stress window developed during panel retreat. In addition to highlighting a close relationship between closure rate and the measured vertical stresses, the convergence monitoring proved valuable in establishing characteristic deformation behaviour under specific interactive influences and also in defining the optimum location, extent and time of installation of additional roadway support and reinforcement.

The information from the measurement programme has enabled the Mine Management to gain a better understanding of the interactive influences on roadway behaviour and was instrumental in designing the layout of panels in an area of the North East district of the mine where previous experience had indicated the combined influence of high interactive stresses and weak roof lithology resulted in difficult strata conditions both at development and on panel retreat. The planned location of panels and gateroads took into account both mining operational considerations and the need to avoid potentially high risk interaction zones as highlighted from analysis of the monitoring results. To obtain additional data on parameters influencing roadway deformation, extended roadway convergence monitoring has been established.

## INTRODUCTION

Maltby colliery, operated by R.J.B. Mining (UK) Ltd is successfully mining the Parkgate seam in South Yorkshire, England at a depth of 1000m using longwall retreat. Early development work within the Parkgate seam highlighted extractions were influenced by interaction from previous workings in the Swallow Wood Seam, 160m above. The Swallow Wood workings extend over the Parkgate Seam such that potential interactive influences cannot be avoided over a substantial area of future development. It was important to obtain an early measurement of the magnitude and extent of the interactive effect and in late 1995 a suitable site became available for stress measurement in the maingate development of a panel in the North East district of the mine. At the same time convergence monitoring stations were installed in the gateroads of the adjacent panel to measure the deformational behaviour in an area where a vertical stress window effect would develop during panel retreat. The paper describes these measurements and highlights the implications of the results for gateroad location and panel layout.

## SITE DESCRIPTION

Figure 1 shows the layout of longwall panels and gateroads in the North East district of the Parkgate seam at Maltby colliery and the outline of the overlying Swallow Wood seam extractions. The seam dips gently in a northerly direction, the depth of cover increasing from 950m at T02's panel to 1010m over T12's panel. The interval to the

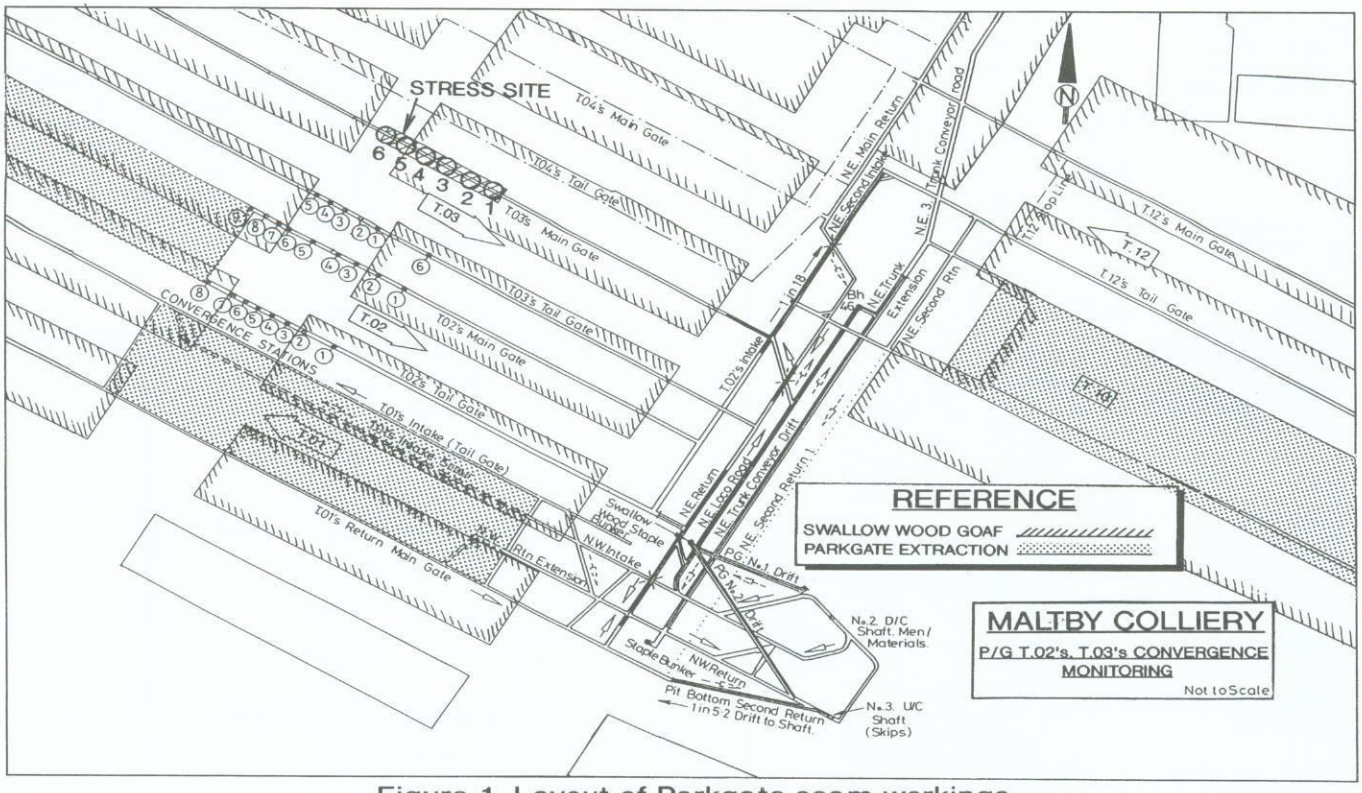



**Figure 1. Layout of Parkgate seam workings**

Swallow Wood Seam is in the range of 150 - 160m.

With the exception of T01's which was a longwall advancing panel, the layout consists of longwall retreat panels with a single entry gate at each side, separated from the adjacent panel by a large stable pillar. Figure 1 shows the Parkgate layout in the proximity of the underground measurement sites and in this area the panel widths are generally 200 - 220m and panel lengths 2000 - 2500m. The inter-panel pillars are 95 - 110m increasing with depth of cover. The panels are orientated at 297° parallel with the long edge of the overlying Swallow Wood panels. At the time of the measurements T01's and T10's panels had been extracted, T02's panel was retreating towards the monitoring stations in the area of the overlying Swallow Wood pillar and T03's and T12's panel development was complete.

The panel gateroads are rectangular in cross section, supported solely by systematic roof and rib bolt reinforcement and generally 2.8 - 3.0m high and 4.3 - 4.8m wide. As the seam thickness averages 1.5m, normally 0.6 - 0.8m of immediate roof strata and 0.5 - 0.7m of immediate floor strata is cut out during development. In anticipation of a vertical stress window developing as T02's panel retreated under Swallow Wood pillars, additional support was installed for 60m under the solid from the outbye overlying pillar edges in both gate roads. In the maingate the additional support consisted of 6m long roof cables and 5m long rib cables and in the tailgate stiff concrete block pillars were installed over a similar area, the remaining area under the Swallow Wood pillar being timber cribbed throughout prior to any influence from the panel retreat.

Table 1 shows a 5m roof core assessment which is typical of the strata encountered in the block to the west of the N.E. Trunk Roadways. The strata consists mainly of competent siltstones and sandstones. The immediate roof above the seam consists of weaker mudstone and silty mudstone which is generally cut out to a competent siltstone top. Variation in the immediate roof lithology due to sandstone channel activity does however occur and in an area around the pit bottom and on the eastern side of the N.E. trunk roadways, the immediate roof consists of weak mudstones up to 10m thick. The immediate floor strata below the seam consists of a thin layer of seatearth mudstone (removed during development) underlain by mudstone and siltstone layers of varying thickness. In the areas of the measurement sites the characteristic strata deformation was rib movement on distinct bedding planes at or near roof horizon and floor heave, sometimes as failed slabs where stiffer strata layers were present. In interaction zones both these features became more pronounced. The competent siltstone roof remained intact with very little movement occurring in most circumstances.

In-situ virgin stress measurement undertaken in the N.E. Main Return indicated a maximum horizontal stress of 17.3MPa at an orientation of 342°. In conjunction with visual observations this confirmed that T02's and T03's maingates would be horizontally stress notched gates on panel retreat. In T02's tailgate it was anticipated there could be additional interaction adjacent to T01's extracted panel.

Colliery: Maltby
Seam: Parkgate
District: T03's M/G

Metre Mark: 1118m
Date: 29/3/95
Cored by: RMT

| LITHOLOGICAL DESCRIPTION | Height into Roof (m) | Core Log | Compressive Strength (S) (MPa) | Modulus of Elasticity (E) (GPa) | Ratio (S/E) |
|---|---|---|---|---|---|
| | 6m | | | | |
| SANDSTONE Fine. x laminated,occasional carbonaceous/micaceous partings | 5m | | 113.6 | 14.5 | 7.83 |
| SANDSTONE-SILTSTONE | | | | | |
| SILTSTONE Dark grey,coarse, massive. | | | 95.3 | 15.8 | 6.03 |
| SANDSTONE-SILTSTONE Finely interlaminated Ferruginous bands | 4m | | 96.4 | 18.6 | 5.18 |
| | | | 105.7 | 12.9 | 8.19 |
| | | | 108.1 | 18.4 | 5.87 |
| | 3m | | 121.0 | 11.4 | 10.6 |
| SANDSTONE Medium. x laminated,silty carbonaceous partings | | | 124.0 | 15.4 | 8.05 |
| SILTSTONE Dark grey, massive. | | | 107.6 | 24.6 | 4.37 |
| | 2m | | 105.7 | 19.1 | 5.53 |
| SANDSTONE-SILTSTONE Fine interlaminated,carbonaceous micaceous partings common | | | | | |
| SILTSTONE Dark grey,carbonaceous,coarse and sst.fine laminae. Rare weak carbonaceous/micaceous partings | | | 110.6 | 23.7 | 4.66 |
| | 1m | | 115.9 | 10.9 | 10.6 |
| SILTSTONE coarse, massive. | | | 107.8 | 25.6 | 4.21 |
| | | | 101.5 | 26.7 | 3.80 |
| | | | 116.6 | 15.3 | 7.62 |
| SILTSTONE Medium, massive. | 0m | | 110.6 | 14.0 | 7.90 |
| Start of Core | | | | | |

ZONE OF STRESS CELL INSTALLATION

**Table 1. Roof Strata Assessment**

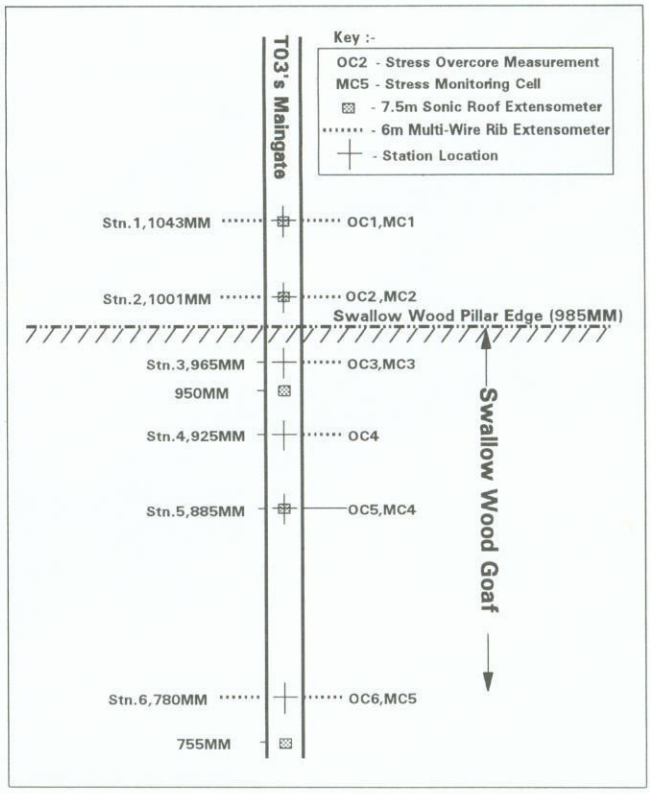



**Figure 2. Location of Measurement and Monitoring Instrumentation**

## MEASUREMENT AND MONITORING INSTRUMENTATION

### Stress Measurement and Monitoring

The general location of the stress measurement site in T03's maingate is indicated on figure 1. The detailed layout of the measurement and monitoring instrumentation in relation to the overlying Swallow Wood pillar edge is indicated on figure 2. Six stress measurements were carried out at the locations indicated using the stress relief overcoring technique. The instruments used were CSIRO, 12 gauge, thin walled, hollow illusion (HI) stress cells and the measurement procedure conformed closely to ISRM suggestions and the manufacturers handbook (1,2). The object of the stress measurement was to determine the extent of the stress redistribution in the Parkgate Seam due to overlying Swallow Wood extraction. The overcore tests were carried out under Swallow Wood goaf and solid close to a panel end where a sandstone washout had resulted in a remnant 118m wide pillar. The approximate test locations relative to the outbye pillar edge were under the pillar centre, 20m from the pillar edge and 20m, 60m, 100m and 200m under goaf. Table 1 shows the rock strata properties obtained from a 5m roof core close to the test site. It confirms the stress tests at 1.7m - 2.4m on the core log, were carried out in a strong stiff test rock, a requirement for successful application of the measurement technique. In general the access holes were drilled to a depth of 8.4m - 9.7m on a rising angle of 18° - 20° over the right hand rib locating the tests under the centre of the overlying panel. To monitor the stress changes occurring when T03's panel retreated through the potential vertical stress window area under the pillar and out under goaf, five CSIRO HI stress monitoring cells were installed in the same access holes at the locations indicated on figure 2. A summary of the hole geometry, overcore test location and monitoring cell location is given in Table 2.

### Gateroad Deformation Monitoring

Simple convergence monitoring stations consisting of rib to rib and roof to floor closure points were installed in T02's gateroads and T03's tailgate in pillar interaction zones at the locations indicated on figure 1. The monitoring stations were located to measure the extent of the Swallow Wood interaction and any vertical stress window effect, the effectiveness of the additional gateroad support and reinforcement and the influence of adjacent panel extraction as T02's panel retreated through the interaction area.

In T03's maingate convergence monitoring stations were installed at the six stress test locations. In addition 7.5m long sonic roof extensometers and 6m long multi-wire rib extensometers, were installed at the locations indicated on figure 2. Results from this monitoring would highlight any relationship between the measured stress and gateroad deformation.

a) Overcore Tests

| Station no. and Location | Overcore Test No. | Hole Length (m) | Hole Dip (Degrees) | Hole Bearing (Degrees) | Depth Into Rib (m) | Height Above Seam (m) |
|---|---|---|---|---|---|---|
| 1 1043MM | OC1 | 9.07 | -18 | 33 | 8.65 | 2.65 |
| 2 1001MM | OC2 | 9.11 | -18 | 27 | 8.70 | 2.75 |
| 3 965MM | OC3 | 8.65 | -19 | 29 | 8.20 | 2.60 |
| 4 925MM | OC4 | 8.36 | -20 | 32 | 7.90 | 2.60 |
| 5 885MM | OC5 | 8.42 | -19.5 | 25 | 7.95 | 2.80 |
| 6 780MM | OC6 | 8.61 | -19 | 18 | 8.10 | 2.70 |

b) Monitoring Cells

| Station no. and Location | Monitoring Cell No. | Hole Length (m) | Hole Dip (Degrees) | Hole Bearing (Degrees) | Depth Into Rib (m) | Height Above Seam (m) |
|---|---|---|---|---|---|---|
| 1 1043MM | MC1 | 9.71 | -18 | 33 | 9.25 | 2.90 |
| 2 1001MM | MC2 | 9.60 | -18 | 27 | 9.20 | 2.90 |
| 3 965MM | MC3 | 9.49 | -19 | 29 | 9.0 | 2.90 |
| 5 885MM | MC4 | 9.15 | -19.5 | 25 | 8.65 | 3.05 |
| 6 780MM | MC5 | 9.30 | -19 | 18 | 8.80 | 2.95 |

**Table 2 - Location,Length and Orientation of Test Holes**

| Test No. | Elastic Modulus (MPa) | Poissons Ratio | Stress Components (MPa) | | | | | |
|---|---|---|---|---|---|---|---|---|
| | | | N-S/N-S | E-W/E-W | Vrt/Vrt | N-S/E-W | N-S/Vrt | E-W/Vrt |
| OC1 | 21456 | 0.30 | 20.36 | 17.28 | 32.76 | -3.40 | 7.48 | 4.12 |
| OC2 | 22000 | 0.33 | 17.35 | 18.28 | 39.28 | -5.50 | 3.74 | 4.74 |
| OC3 | 25185 | 0.32 | 21.83 | 20.19 | 27.34 | -3.66 | -1.47 | 1.89 |
| OC4 | 21332 | 0.34 | 18.88 | 17.65 | 20.48 | -3.72 | -0.06 | -0.18 |
| OC5 | 17000 | 0.25 | 19.57 | 17.84 | 17.59 | -2.42 | -0.09 | -0.09 |
| OC6 | 21678 | 0.34 | 19.60 | 14.06 | 22.89 | -2.47 | 0.71 | -0.23 |

| Test No. | Principal Stresses | | | | | | | | |
|---|---|---|---|---|---|---|---|---|---|
| | Major | | | Intermediate | | | Minor | | |
| | Value MPa | Bearing | Dip | Value MPa | Bearing | Dip | Value MPa | Bearing | Dip |
| OC1 | 36.57 | 18 | 66 | 21.72 | 134 | 11 | 12.12 | 48 | -21 |
| OC2 | 40.59 | 57 | 78 | 23.29 | 134 | -3 | 11.03 | 44 | -12 |
| OC3 | 28.73 | 317 | -60 | 23.41 | 144 | -30 | 17.23 | 52 | -3 |
| OC4 | 22.04 | 320 | 3 | 20.48 | 172 | 87 | 14.49 | 50 | 2 |
| OC5 | 21.28 | 325 | 0 | 17.60 | 240 | 85 | 16.13 | 55 | 5 |
| OC6 | 23.11 | 340 | 74 | 20.32 | 159 | 16 | 13.12 | 69 | 0 |

| Test No. | Secondary Principal Stresses | | | | | | | | |
|---|---|---|---|---|---|---|---|---|---|
| | In The Horizontal Plane | | | Vertical Plane Normal to T03's M/G | | | Vertical Plane Parallel to T03's M/G | | |
| | Max.(MPa) | Bearing | Min.(MPa) | Max.(MPa) | Dip | Min.(MPa) | Max.(MPa) | Dip | Min.(MPa) |
| OC1 | 22.6 | 327 | 15.1 | 36.5 | 66.5 | 13.3 | 32.8 | 88.6 | 20.7 |
| OC2 | 23.3 | 313 | 12.3 | 40.4 | 78.6 | 12.0 | 39.7 | 81.7 | 22.1 |
| OC3 | 24.8 | 321 | 17.3 | 27.3 | -86.8 | 18.5 | 28.5 | 64.2 | 22.3 |
| OC4 | 22.0 | 320 | 14.5 | 20.5 | -88.8 | 15.6 | 20.9 | 76.7 | 20.5 |
| OC5 | 21.3 | 325 | 16.1 | 17.6 | -80.0 | 17.3 | 20.2 | -89.0 | 17.6 |
| OC6 | 20.5 | 339 | 13.1 | 22.9 | 85.6 | 16.5 | 22.9 | -85.0 | 17.2 |

**Table 3. Summary of Overcore Results - T03's Maingate**

## RESULTS

### Stress Measurements

The overcore tests were analysed using an isotropic solution and the elastic properties of the host rock determined by biaxial testing of the recovered rock core. The results of the stress measurements are summarised in table 3.

Figure 3 indicates the magnitude and direction of the secondary principal stresses in the horizontal plane. The major horizontal stresses are in the range 20.5 - 24.8 MPa at an orientation of 310° to 339° (13° to 42° to the line of T03's maingate).Under goaf close to the overlying Swallow Wood pillar edge and under the pillar where the vertical stresses are higher, the major horizontal stresses are highest (22.6 - 24.8 MPa). The measurement 200m from the pillar edge, under goaf and remote from potential interaction indicated a major horizontal stress of 20.5 MPa at 339° and this may represent more closely the magnitude and direction of the virgin horizontal stress field. The minor horizontal stress was 13.1 MPa at this location, giving a horizontal stress ratio of 1.56. With the exception of the result from station 2 (20m under the overlying pillar), the horizontal stress ratios were in the range 1.3 - 1.6. Close to the pillar edge the major horizontal stress is rotated more normal to the line of it in the range 310° to 321° (13° to 24° to T03's Maingate). The horizontal stress component normal to T03's maingate was in the range 15.6 - 18.5 MPa with the exception of station 2 where a lower stress component of 8.6 MPa was measured.

Figure 4 shows the secondary principal stresses in the vertical plane parallel to T03's maingate highlighting the overlying pillar influence on the orientation and magnitude of the stresses. The major stress is shown near vertical under the pillar and under goaf well away from the pillar

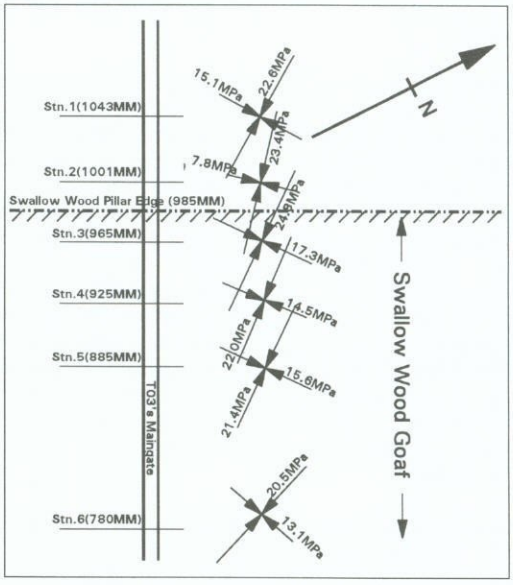



**Figure 3. Principal Stresses in the Horizontal Plane**

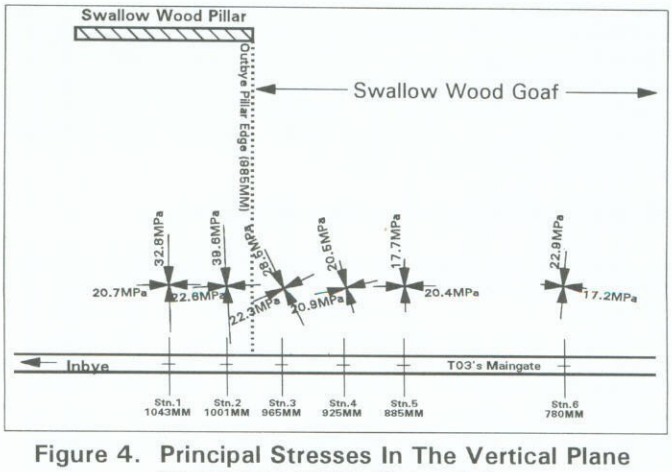



**Figure 4. Principal Stresses In The Vertical Plane (Parallel to T03's Maingate)**

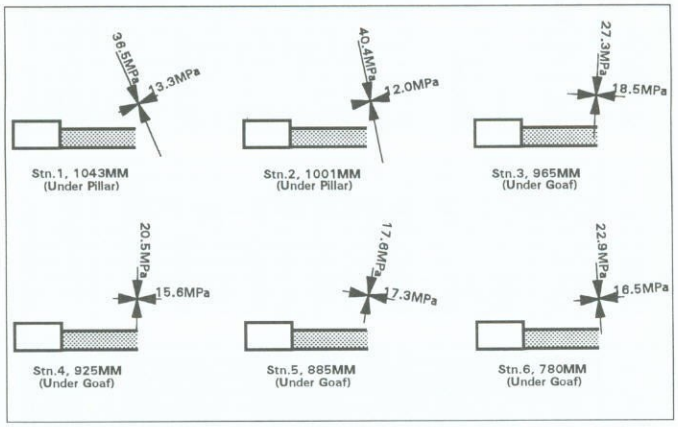



**Figure 5. Principal Stresses In The Vertical Plane (Normal to T03's Maingate)**

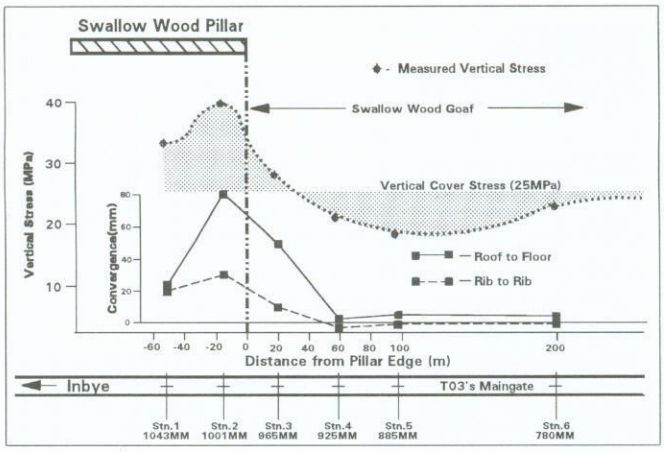



**Figure 6. Vertical Stress Distribution and Related Strata Deformation.**

edge. As the pillar edge is approached the major stress becomes more inclined towards the overlying panel edge.

Figure 5 shows the secondary principal stresses in the vertical plane normal to T03's maingate. The measurements under Swallow Wood goaf indicate the stress components are orientated approximately vertical and horizontal suggesting they were unaffected by T03's maingate. The measurements under the pillar, however, indicate a major stress inclined over T03's maingate suggesting the measurements at 9m into the ribside were not outside of the zone of stress redistribution around the maingate in this high stress interaction zone. Further evidence that these measurements are within the yield zone around T03's maingate are the low minor stress components (7.3 and 13.3MPa) suggesting a measure of stress relief into the maingate opening.

Figure 6 shows the distribution of the measured vertical stress component in relation to the position of the overlying Swallow Wood pillar. The distribution indicates high vertical stress under the pillar as anticipated, the highest stress (39.6 MPa) measured 20m from the pillar edge. The influence of the overlying pillar extends beyond the pillar edge, the vertical stress returning to cover load (25MPa) some 30m from the pillar edge under goaf. The vertical stress reduces to 17.8MPa at 100m before building back towards cover load 200m from the pillar edge.

**Gateroad Deformation - T03's Maingate**

Figure 6 shows the background convergence in T03's maingate at the six monitoring stations in relation to the vertical stress distribution obtained from the stress measurement. The graphs show a close correlation between the vertical stress distribution and the vertical and horizontal convergence which developed over a period of 75 days following the stress measurement. The highest closure rates were measured under the pillar extending beyond the pillar edge in a similar pattern to the stress distribution. Minimal convergence was measured at the outbye stations under goaf. Continued monitoring over a longer period has confirmed this to be a consistent pattern of behaviour.

The multi-wire rib extensometers indicated a similar pattern to total rib displacement. Under the goaf the high strains were confined to the immediate 1m from the ribside compared with 3m in the pillar interaction zone. The left hand rib (face side) showed greater rib movement generally which could be due to the orientation of the main cleat and the major horizontal stress relative to the direction of development drivage. The sonic roof extensometers measured no significant movement, a consistent feature of the competent roof lithology of the district and vertical convergence thus almost entirely represents floor heave.

**Gateroad Deformation - T02's panel**

Figure 7 summarises the results obtained from eight monitoring stations in both T02's tailgate and maingate. The figure shows the influence of T02's face retreat on gateroad convergence from 400m in front of the face and compares behaviour in the potential stress window zone under the pillar with that under goaf remote from the interactive influence. The results indicate higher background convergence rates and a greater magnitude of convergence in the interaction zone, the main influence from the face extending for 120 - 130m. Within 100m of the face the convergence increased at a much greater rate in the maingate resulting in the steep curves and greater magnitude of convergence indicated. Under goaf the background convergence rates were very low and the face influence extended only 60 - 80m. In T02's tailgate, for example, the background vertical convergence rate outside the influence of panel retreat was typically 0.3mm/day in the interaction zone compared to 0.03mm/day under goaf. The pattern of behaviour of the rib to rib closure was similar but the rate and magnitude was 30 - 50% of the vertical convergence and in the interaction zone the face influence extended only 80 - 100m.

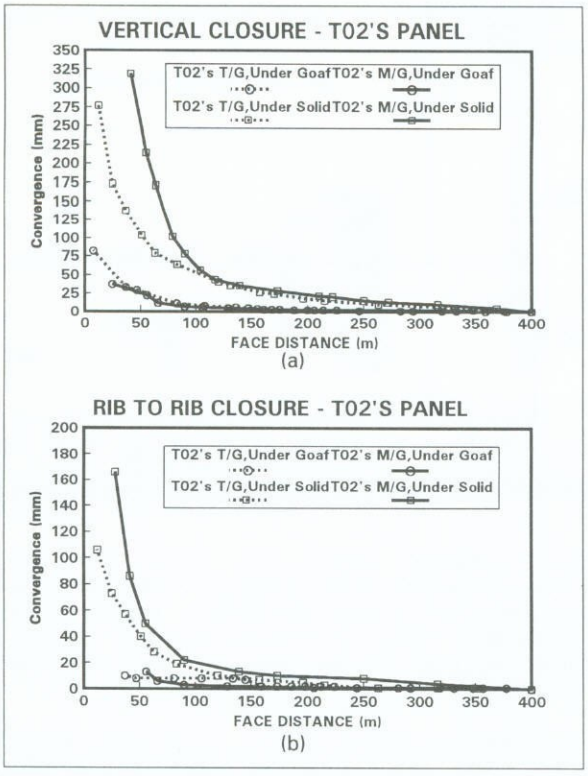



Figure 7. Face Influence on Gateroad Convergence

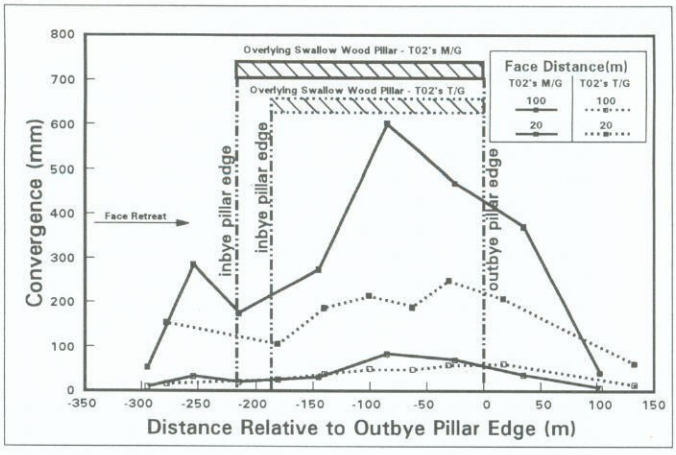



Figure 8. Vertical Closure - Comparison of T02's Gates

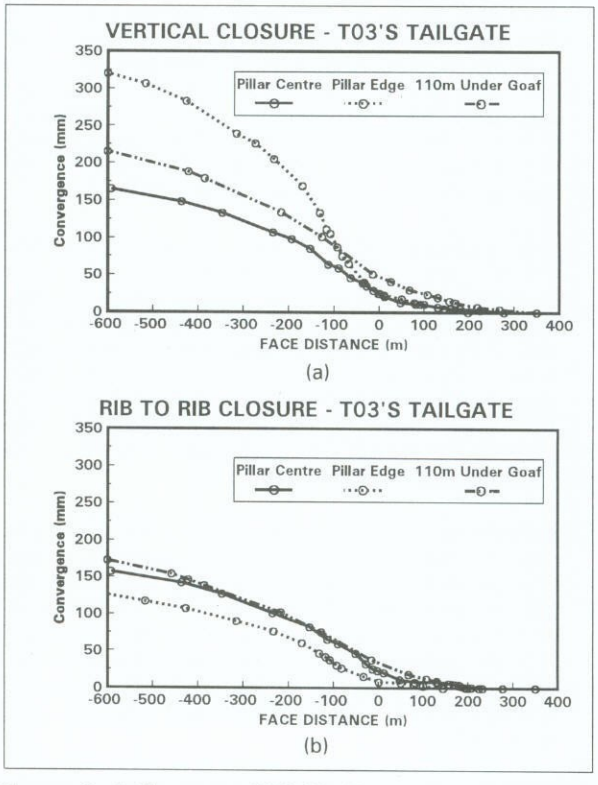



Figure 9. Influence of T02's Retreat on T03's T/G

The distribution of convergence through the interaction zones in T02's gateroads relative to the outbye overlying pillar edge is shown in figure 8 which compares the magnitude of vertical closure in the two gateroads when the retreating panel was 100m and 20m from the monitoring locations. The figure highlights within 100m of the face, a significant stress window effect developed in T02's maingate under the outbye half of the overlying pillar which caused considerable floor heave. Through this zone a 0.4 - 0.5m floor dint was taken 30m in front of the face to maintain clearance for the face end equipment. However from the closure trends it is estimated 600 - 800mm of floor heave would have developed up to the face. In the tailgate the window effect was less noticeable, and the equivalent floor heave in the interaction zone was 300 - 450mm. Figure 8 also highlights the interactive influence of the overlying pillar extended at least 30m beyond the outbye pillar edge.

**T03's Tailgate**

Figure 9 shows the vertical and horizontal convergence in T03's tailgate in relation to T02's panel retreat. Three monitoring stations have been selected to indicate the range of behaviour measured under the centre and edge of the 215mm wide Swallow Wood pillar and 110m from the pillar edge under goaf. The passage of T02's panel (separated from T03's tailgate by a 95m wide pillar) caused an increase in the convergence rates the major effect developing when the face was adjacent until 200 - 300m past the monitoring station. The convergence rate continued to slow down towards a background level 600m behind the faceline. No vertical stress window effect was measured but the additional vertical convergence due to T02's extraction was greater under the Swallow Wood pillar than under goaf, particularly towards the pillar edges. The influence of T02's extraction on horizontal closure was similar at all monitoring locations and largely independent of Swallow Wood interaction.

## CONCLUSIONS

### General Conclusions from Measurements

1. The stress measurements confirmed extraction in the Swallow Wood seam had a significant influence on stress magnitudes, directions and distribution in the Parkgate seam 160m below. In particular an area of high vertical stress exists under the edges of the overlying panels which generates high convergence rates in gateroads at development and during panel retreat. The zone of high stress extends beyond the panel edges which is reflected in high convergence for 30m from the panel edge under goaf.

2. Roadway deformation measurements confirmed vertical stress window effects developed on retreat which resulted in substantial vertical convergence. The additional support and reinforcement installed in the stress window zone maintained effective gateroad stability and good production levels were achieved through the pillar interaction area. The combination of competent siltstone roof and additional cable reinforcement prevented any significant roof failure or deformation developing. In weaker roof lithology a greater density of roof reinforcement might be necessary to maintain effective roof stability in such interaction areas.

3. The measured horizontal stresses confirmed T02's and T03's maingates would be horizontally stress notched on panel retreat. The increased horizontal stress combined with the vertical stress window effect resulted in more pronounced floor heave in T02's maingate. A higher gateroad initially may have avoided the subsequent floor dint necessary to maintain clearance through the interaction zone.

4. Gateroads experience a significant influence due to the extraction of an adjacent panel. The main influence occurs as a trailing wave up to 300m behind the adjacent faceline and apart from higher convergence under overlying pillar edges affects the whole roadway in a similar manner. The effect may be accumulative as additional panels are extracted.

5. Due to the apparent correlation between imposed stress levels and roadway deformation valuable comparative data relating to overlying and adjacent interaction would be obtained by extending the roadway deformation programme to development areas with different interaction geometry.

### Implications for Panel Layout - Parkgate Seam

The measured vertical stress distribution was used to give a comparative estimate of the imposed vertical stress levels on roadways in different locations as indicated on figure 10. On this basis, roadway 1, 60m under goaf would have a

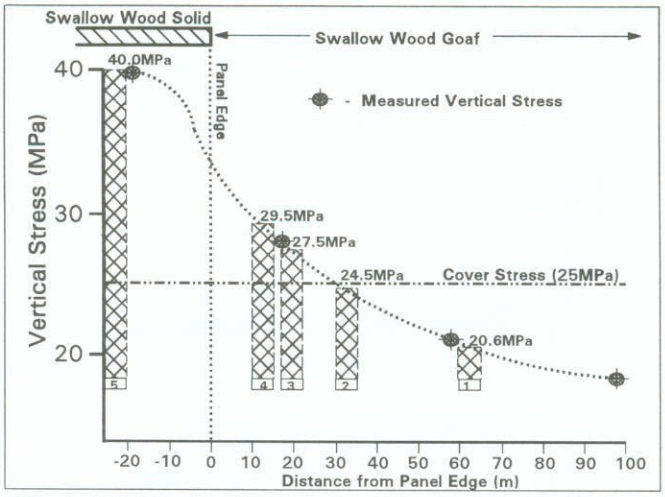



**Figure 10. Comparative Levels of Imposed Vertical Stress**

vertical imposed stress 20% below cover load (20.6MPa) compared with roadway 4, 10m under goaf at 20% above cover load (29.5MPa). Roadway 5, 20m under Swallow Wood solid would be in a very high imposed vertical stress zone possibly 60% above cover load.

Confirmation of the need to avoid high vertical stress zones was obtained from T14's panel developments. T14's tailgate, 35 m under solid, (figure 11) experienced excessive floor heave 8 - 10 times that recorded in T14's maingate, 16 m under Swallow Wood goaf. Based on the potential stress distribution determined from an approach developed by Wilson (3) and extrapolation from the stress measurements, it was estimated T14's tailgate would have an imposed vertical stress of 35 MPa (40% above cover) compared with 27.5 MPa (10% above cover) in T14's maingate.

The response of a roadway to increased vertical stress will be governed by a number of different parameters eg roadway geometry, immediate lithology, geological features, adjacent panel interaction, etc. The influence of a zone of thick weak mudstone roof lithology combined with high imposed vertical stresses was observed further inbye in T14's tailgate. In this area substantial additional roof and rib reinforcement was unable to generate long term stability under the combined interactive influences.

Figure 11 illustrates how the existing data on the extent of vertical stress interaction zones and weak roof lithology areas has been used to generate a composite plan highlighting the most potentially vulnerable zones of combined interaction in the T16's - T20's block. The stress magnitudes and areal extent of these zones are based on stress measurements and vertical roof cores and as such are estimates upon which a comparative risk assessment has been carried out. The dark shading highlights the most vulnerable zones, one of which coincides with the area where difficult strata conditions developed in T14's tailgate. The proposed layout of panels in this block as indicated on figure 11, took into a account the

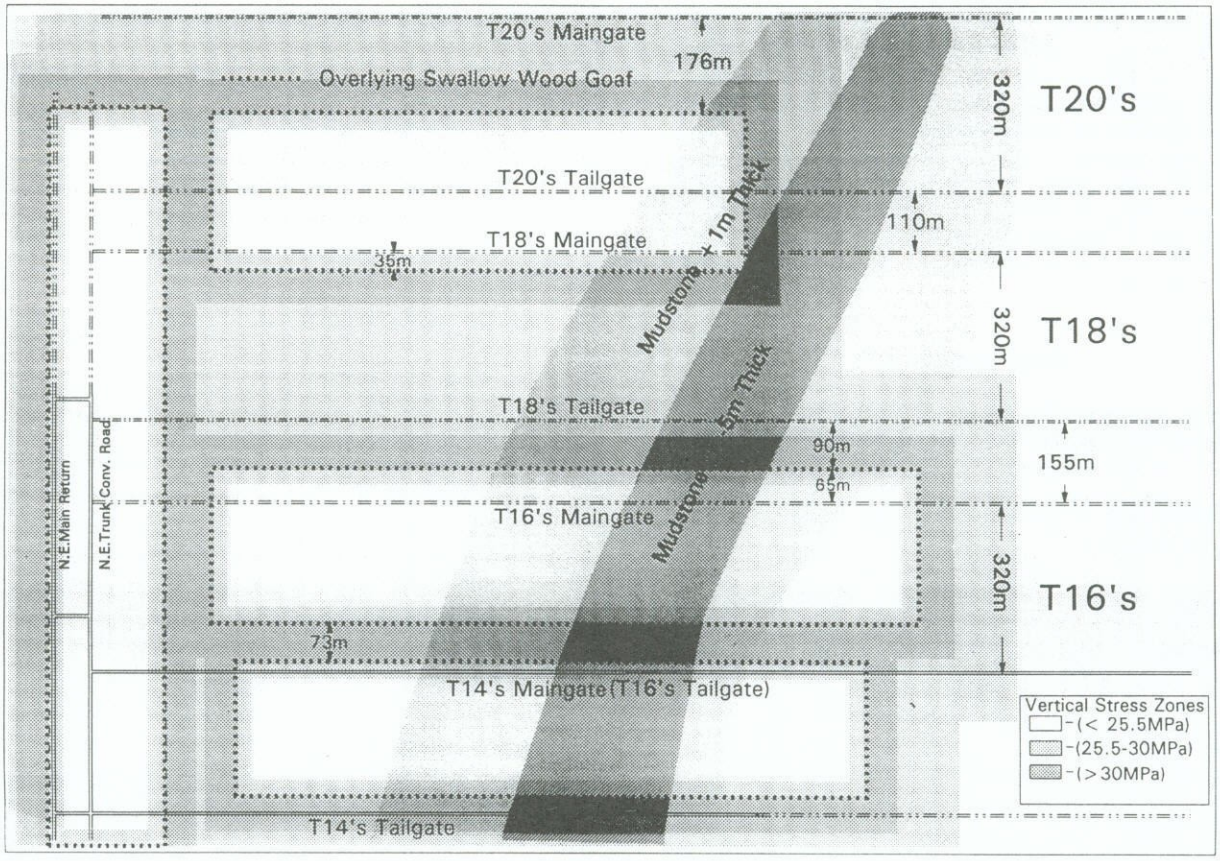



**Figure 11. Combined Vertical Stress and Lithological Interaction**

requirement to avoid the high risk interaction areas in conjunction with mining operational considerations. This particular layout was selected for the operational advantages of maximum and consistent panel widths and reduced development drivage compared to alternative layouts. To minimise interaction influences gateroads were located a minimum distance of 30m under goaf and 90m under solid in relation to overlying Swallow Wood panel edges. It was not possible however to totally avoid areas of combined interactive influence in this block as figure 11 indicates and a support strategy will have to be developed for the most critical areas.

**Implications for Future Mine Planning**

The information from this work has enabled the Mine Management to gain a better understanding of the extent and magnitude of Swallow Wood interaction on the Parkgate seam workings and has been instrumental in the development of the gateroad support strategy in interaction zones and in designing the layout of panels to minimise combined interactive influences. As a result of information from measurements and operational experience the following strategy has now been adopted as standard practice for interaction zones in development roadways:-

1. Maingates - Additional roof and rib cable reinforcement installed for 60m from outbye overlying panel edges under solid and extended at least 20m under goaf. Under narrow pillars additional reinforcement is installed the full width of the pillar.

2. Tailgates - Early installation of timber cribs prior to influence from the retreating panel.

3. Increased height of extraction through interaction zones to minimise dinting operations in front of the retreating panel.

Also, an on going programme of roadway deformation monitoring using simple convergence stations has been established in both existing roadways and new developments to obtain additional data on the various parameters influencing roadway deformation during development and panel retreat. This results in increased understanding and awareness of the physical processes going on and the basis behind associated developments in support and design strategy which in turn assists mine personnel to make a more effective and timely assessment of potential risks in the work place.



ACKNOWLEDGEMENTS

The authors would like to thank Mr W Rowell, Managing Director, (Deep Mines), RJB Mining (UK) Ltd, for his permission to publish this paper. They would also like to thank their colleagues at Maltby Colliery and Rock Mechanics Technology Ltd for their assistance with the work described. The contents of the paper reflect the views of the authors and not necessarily those of RJB Mining (UK) Ltd or Rock Mechanics Technology Ltd. Some of the work reported was funded by the European Coal and Steel Community.

REFERENCES

1. ISRM "Suggested methods for rock stress determination" Int. J. Rock Mech. 1987, vol 24, 1, 55 - 73.

2. MINDATA LTD, 1986, "CSIRO HI stress cell, Field Manual"

3. Wilson, A. H. "The stability of underground workings in the soft rocks of the Coal Measures," Int. J. Min. Eng., 1983, vol. 1, July, 91 - 187.

# Effects of Longwall Mining on Streamflow in the Pittsburgh Seam Basin

*Kenneth L. Johnson,* Senior Research Hydrologist
CONSOL Inc.
Research and Development
Library, PA

## ABSTRACT

The effects of underground longwall coal mining on flow in perennial streams within the Pittsburgh seam basin were evaluated. Four streams above four different longwall mines were studied. Overburden depths at the study sites ranged from 500 to 600 feet. At all four locations, premining streamflow measurements were made to establish baseline flow conditions. Measurements were then repeated at each location after the longwall face passed beneath the stream. At one location, in which the longwall panel axis was roughly parallel to the stream, the streamflow was monitored as the longwall face advanced. Measurements at this location showed that temporary flow reduction occurred as the face advanced underneath; however, after the tensile portion of the traveling subsidence profile passed, this effect was lessened. At two of the sites in which the stream was roughly perpendicular to the panel axis, postmining streamflow increased across the panel and decreased over the development headings, such that the net lateral change in streamflow across the fully subsided panel and associated development headings was small compared to the measured flow.

## OBJECTIVES AND METHODOLOGY

This paper evaluates the effects of longwall coal mining on streamflow in northern Appalachia, including northern West Virginia and southwestern Pennsylvania. Other investigators[1,2,3] have conducted similar evaluations, but their studies do not present both premining and postmining data for the same streams, and assume that any reduction in flow over a portion of the stream is due to underground mining. In contrast, this paper presents premining and postmining streamflow data for the same portions of four streams over four different longwall mines in northern Appalachia.

The depth of cover at the four study sites ranges from 500 to 600 feet. The overburden between the stream and the mine consists of typical Lower Permian and Upper Pennsylvanian coal measure strata - alternating layers of shale, siltstone, sandstone, limestone, and coal. In all cases, the Pittsburgh seam was mined.

Most streamflow measurements were taken at a series of weirs temporarily installed in the stream, and spanning the longwall panel or panels. However, where bedrock outcropped in the stream channel or where flow was high, a velocity profile across the natural channel was used to estimate flow. Based on experience with both weir and natural channel flow measurements, the accuracy of the weir method is estimated to be 5%-10%, and that of the natural channel flow method is estimated to be 15%-20%. At each study site, a minimum of one set of premining measurements and one set of postmining measurements were taken across a defined section of the stream. However, at most of the sites, several premining and postmining flow measurements were taken.

Results from monitoring premining and postmining streamflow at two of the four study sites are also discussed in Johnson, 1991.[4]

## DESCRIPTION OF STUDY SITES

### Site A

At Site A, the study stream is located over a single longwall panel, the fourth panel in a block of seventeen panels. The stream crosses the panel edge at roughly a 45° angle and then flows roughly parallel to the panel to its discharge point into a larger regional stream (Figure 1). Streamflow was measured at Points 1, 2, and 3 (Figure 1) on several dates both before and after the study panel was mined. The overburden strata are comprised mostly of shale

and limestone, with the majority of the massive limestone beds occurring at depths between 250 and 500 feet. The overburden thickness between the stream and the mine is approximately 500 feet.

Exposed sandstone bedrock in the stream channel and relatively large stream size prevented effective use of weirs at this site. Therefore, velocity profiles were taken across the channel at the three locations. Flow was estimated by multiplying the velocity (at 0.6 times the depth of flow) by the width and depth of flow measured at regular intervals across the channel.

The study panel was mined from west to east. A block of solid coal was left within the panel, as shown in Figure 1. Therefore, it is likely that a portion of the stream above and adjacent to the coal block remains in tension.

Site B

Site B also is located over a single longwall panel, the last in a block of seven panels. The study stream over the panel flows roughly parallel to the longwall face advance direction from west to east (Figure 2). Streamflow was measured at Points 1, 2, and 3 on several dates before, during and after the stream was undermined. The overburden consists mostly of shales and limestones. As at Site A, the majority of massive limestone beds occur at depths between 300 and 550 feet. The overburden thickness between the stream and the mine is approximately 550 feet.

At Station 1, the upstream flow monitoring point, no weir could be installed because of exposed bedrock in the channel. At Stations 2 and 3, weirs were installed in the softer streambed. Flow measurements were taken in a similar fashion at all three stations. Average velocity, depth, and width of flow were measured at the three locations. At Station 1, the natural channel was utilized, whereas at Stations 2 and 3, the rectangular weir opening was utilized.

Site C

Site C is located along a stream which flows over several successive longwall panels where the approximate depth of cover is 600 feet (Figure 3). The study panels were the second and third panels within a block of eight. The panels were mined from west to east. The overburden consists predominately of shale, sandstone and limestone, with more abundant sandstone than at either Site A or Site B. The stream flows across the panels at approximately a 75° angle. Streamflow was measured before and after mining using temporary weirs at a total of 20 stations spanning both panels.

Site D

Site D is located along a stream which flows over several successive longwall panels (Figure 4). The study stream is formed by two streams which merge over Panel 7, and flows at approximately a 90° angle to Panel 6. The depth of cover at Site D is approximately 550 feet. The panels were mined from west to east. The overburden consists predominately of shale and limestone with lesser amounts of sandstone, claystone and coal. Flow was measured before and after undermining by taking velocity, depth, and width measurements across the natural channel. Weirs were deemed impractical because of the large channel and high flows. Four streamflow measurement stations were used at this site (Figure 4).

## RESULTS AND DISCUSSION

To clearly illustrate average spatial changes in streamflow, flow data are presented graphically as normalized flow as a function of distance along the stream. The assigned normalized flow rate at the extreme upstream station of each site represents the average flow rate measured at each site during the monitoring period. For example, if flow at a particular site ranged from 100 gpm to 1000 gpm at the upstream station during the monitoring period, the normalized flow at the upstream station might be, say, 500 gpm. Downstream flow rates were calculated from the percent change in flow between each station.

Site A

Based on premining streamflow measurements taken at the three stations on November 29, 1988 and January 27, 1989, Site A showed an average gain in flow downstream between Stations 1 and 2 of 17% and an average gain between Stations 2 and 3 of 10%. Based on postmining measurements made on April 20, 1989, March 6, 1990 and August 14, 1990, Site A showed an average gain between Stations 1 and 2 of 59% and an average loss between Stations 2 and 3 of 15%.

The postmining increase in flow between Stations 1 and 2 is not fully understood, but it could be attributed to increased contribution from two tributaries (flows not measured), and/or increased groundwater discharge to the stream. The postmining decrease in flow between Stations 2 and 3 could be due to high surface strain which is typical over the gateroads. Figure 5 shows premining and postmining streamflow data normalized to 950 gpm (average

measured flow for this stream at Station 1), and demonstrates that the net effect of longwall mining on streamflow across the entire panel and associated development can be considered negligible.

Site B

Based on premining flow measurements taken on July 8, 1992 and July 10, 1992. Site B showed an average gain in flow downstream between Stations 1 and 2 of 8% and an average gain between Stations 2 and 3 of 8%.

While the stream was being undermined by the longwall face, flow measurements were taken on August 10, 1992 and August 11, 1992. These measurements showed an average 30% flow reduction between Stations 1 and 2 and an average 15% flow reduction between Stations 2 and 3.

After completion of the panel, flow measurements were taken on September 24 and 25, 1992, and May 18 and 19, 1993 at all three stations. The data collected in September 1992 showed an average 26% flow reduction between Stations 1 and 2, and an average 12% gain between Stations 2 and 3 (short-term postmining). The data collected in May 1993 showed an average 16% flow reduction between Stations 1 and 2, and an average 17% gain between Stations 2 and 3 (long-term postmining). Premining, during mining, and postmining normalized streamflows as a function of distance are shown graphically in Figure 6, using an average flow of 500 gpm at Station 1. There appears to have been "healing" of the streambed with time, particularly between Stations 2 and 3. The sustained flow reduction between Stations 1 and 2 is attributed to sandstone bedrock outcrops in the stream near Station 1 combined with the surface tension zone associated with the beginning of the panel.

Site C

A total of 20 flow stations established across the two adjacent longwall panels at Site C provides a detailed picture of lateral changes in streamflow before and after longwall mining. Premining flows were measured at all 20 stations. However, because of postmining deepening of the stream near the center panel, flow could be measured at only 14 of the stations. An average flow of 2500 gpm at the upstream station was used to normalize the data.

Prior to mining Panel 3, the first of the two study panels, flow measurements were taken on November 8, 9, and 14, 1988 over the panel and development headings. These data indicate a 22% gain in flow across the panel and adjacent development headings, although localized flow reduction was measured near panel edge and panel center. After Panel 3 undermined the stream, flow measurements were taken on July 18 and 19, 1989. These data indicate that flow over the headgate and panel were unchanged. Over the tailgate, however, some streamflow was diverted to the subsurface for a short distance, and then re-emerged. This local flow reduction did not prevent an overall postmining gain of approximately 4% across the panel and associated development headings (Figure 7).

Prior to mining Panel 4, flow measurements were taken on November 15 and 20, 1989, and showed no net gain or loss in flow in the study stream from headgate to tailgate (Figure 7). Lateral changes in flow prior to mining were considered less than measurement error. After mining Panel 4, flow measurements taken on July 25 and 26, 1990 showed there was a measurable flow reduction over both the headgate and tailgate development, but a significant gain over the panel area. Although lateral changes in flow after mining were greater than those measured before mining of Panel 4, there was no measurable change in total flow from headgate to tailgate.

Postmining flow reductions over the gateroads of both panels can be attributed to high surface strain. The significant gain in flow over Panel 4 could not be attributed to increased visible inflow to the stream. Perhaps drainage of shallow groundwater toward panel center resulted in increased groundwater inflow to the stream after mining.

Site D

Premining streamflow measurements at Site D were taken on April 22, 1994 over Panel 6 and on October 13, 1994 over Panel 7. There was a 10% gain in flow prior to mining over Panel 6 and zero gain or loss over Panel 7.

Postmining streamflow measurements were taken on May 3, 1994, May 23, 1994, and November 4, 1994 over Panel 6, and on November 4, 1994 over Panel 7. These measurements showed an average 2% flow reduction over Panel 6 and no gain or loss over Panel 7 after mining. Premining and postmining normalized flow as a function of lateral distance over Panels 6 and 7 is illustrated in Figure 8.

The effect of longwall mining on the study stream at Site D was considered negligible because any lateral change in streamflow over either panel was within the accuracy of the measurements.

## SUMMARY AND CONCLUSIONS

Streamflow was measured in four streams both before and after longwall undermining within the Pittsburgh seam. Where streamflow was relatively low, the channel was narrow, and no massive bedrock outcrop was present, temporary weirs were constructed upstream and downstream of (and, in some cases, several points in between) the study panels. In larger streams, or where massive bedrock outcrops were present in the stream, flow in the natural channel was measured by velocity/cross-sectional area profiling.

The following conclusions made from this study apply to Pittsburgh seam mining at depths of 500 to 600 feet.

1. During active undermining by longwall, streamflow reduction related to the traveling subsidence tensile wave may occur temporarily. After the tensile wave has passed, streamflow usually rebounds such that the net effect on streamflow is small. The type of near-surface strata may affect the magnitude and longevity of streamflow changes.

2. Flow reduction may occur over the development headings where postmining surface strain tends to be high, but flow gains over the subsided panel tend to offset these localized reductions.

3. At some locations, a measurable change in streamflow after longwall undermining may not occur. Where a measurable reduction in flow did occur after longwall mining, it was small in comparison to measured flow rates.

## REFERENCES

1. Dixon, D. Y. and Rauch, H. W. The Impact of Three Longwall Coal Mines on Streamflow in the Appalachian Coal Field. Proceedings of the Ninth International Conference on Ground Control in Mining. West Virginia University. Morgantown. West Virginia. 1990. pp. 169-182.

2. Tieman, G. E., Rauch, H. W., and Carver, L. S. Study of Dewatering Effects at a Longwall Mine in Northern West Virginia. Proceedings of the Third Workshop on Surface Subsidence Due to Underground Mining. West Virginia University. Morgantown. West Virginia. 1992. pp. 214-221.

3. Carver, L. S. Hydrogeologic Effects of Subsidence at a Longwall Mine in the Pittsburgh Coal Seam. Masters Thesis. West Virginia University Department of Geology and Geography. 1994. 225 p.

4. Johnson, K. L. Effects of Longwall Coal Mining on the Hydrology of Two Appalachian Stream Valleys. Proceedings of the Fifth National Outdoor Action Conference on Aquifer Restoration, Ground Water Monitoring and Geophysical Methods. Las Vegas. Nevada. 1991. pp. 1111-1125.

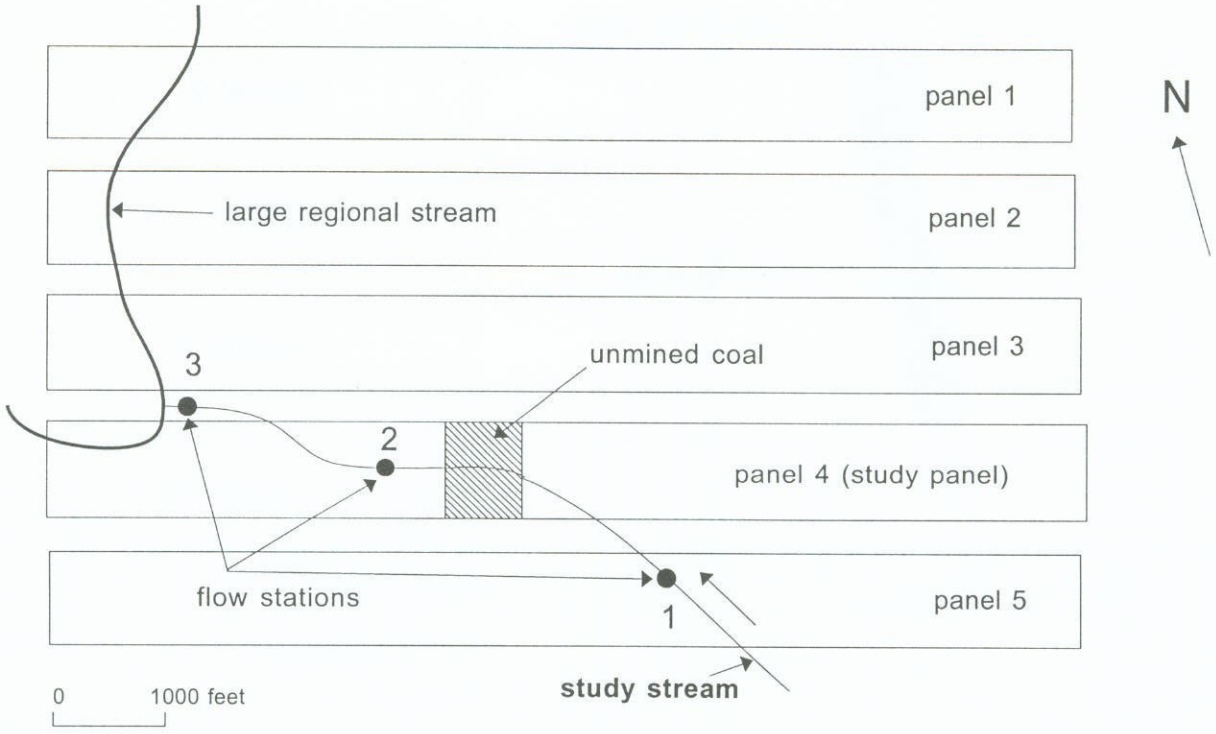



Figure 1. Layout of Site A.

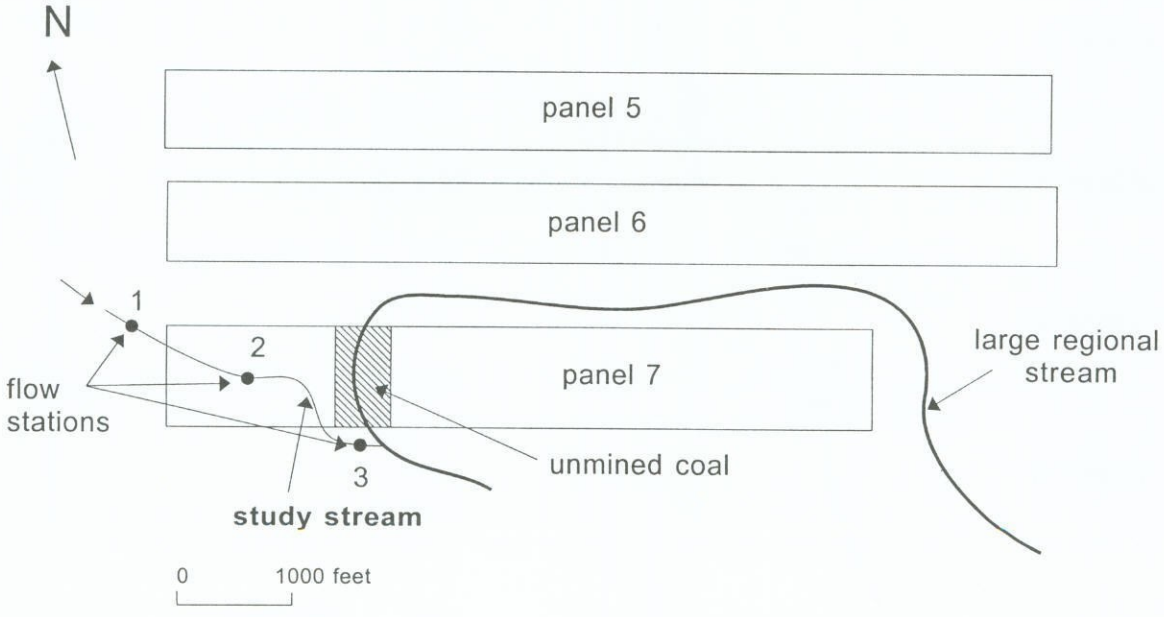



Figure 2. Layout of Site B.

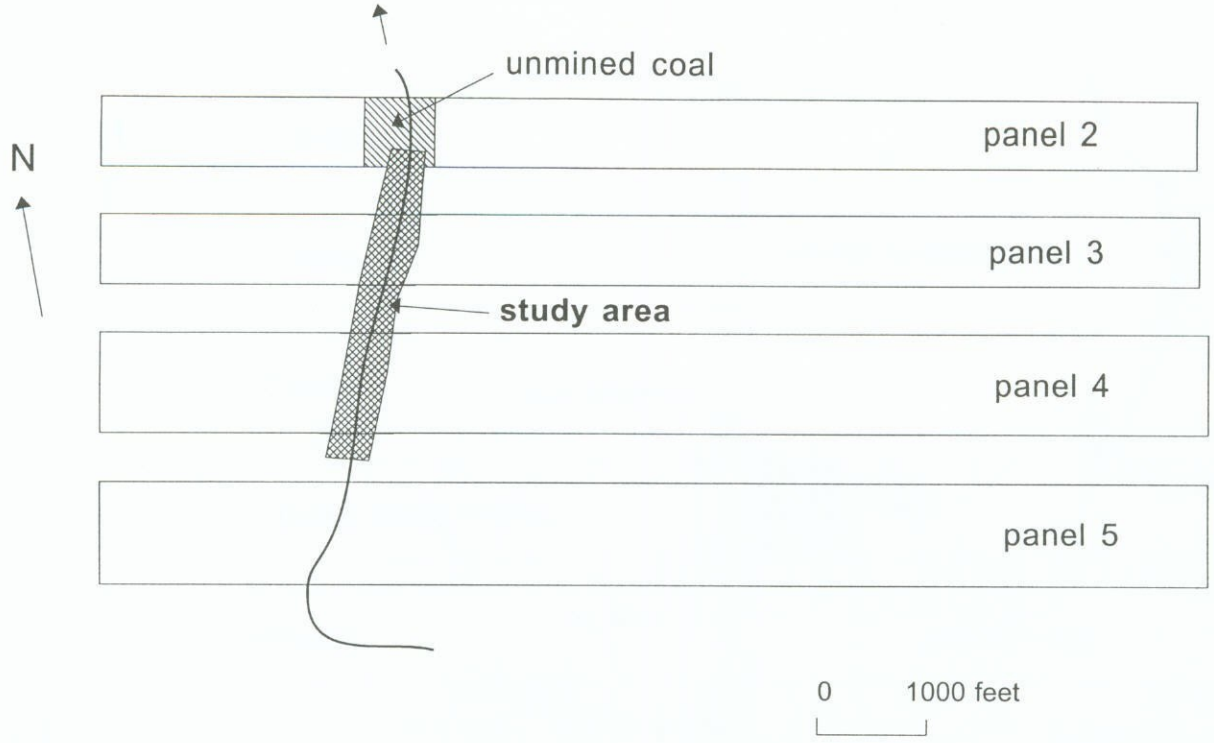



Figure 3. Layout of Site C.

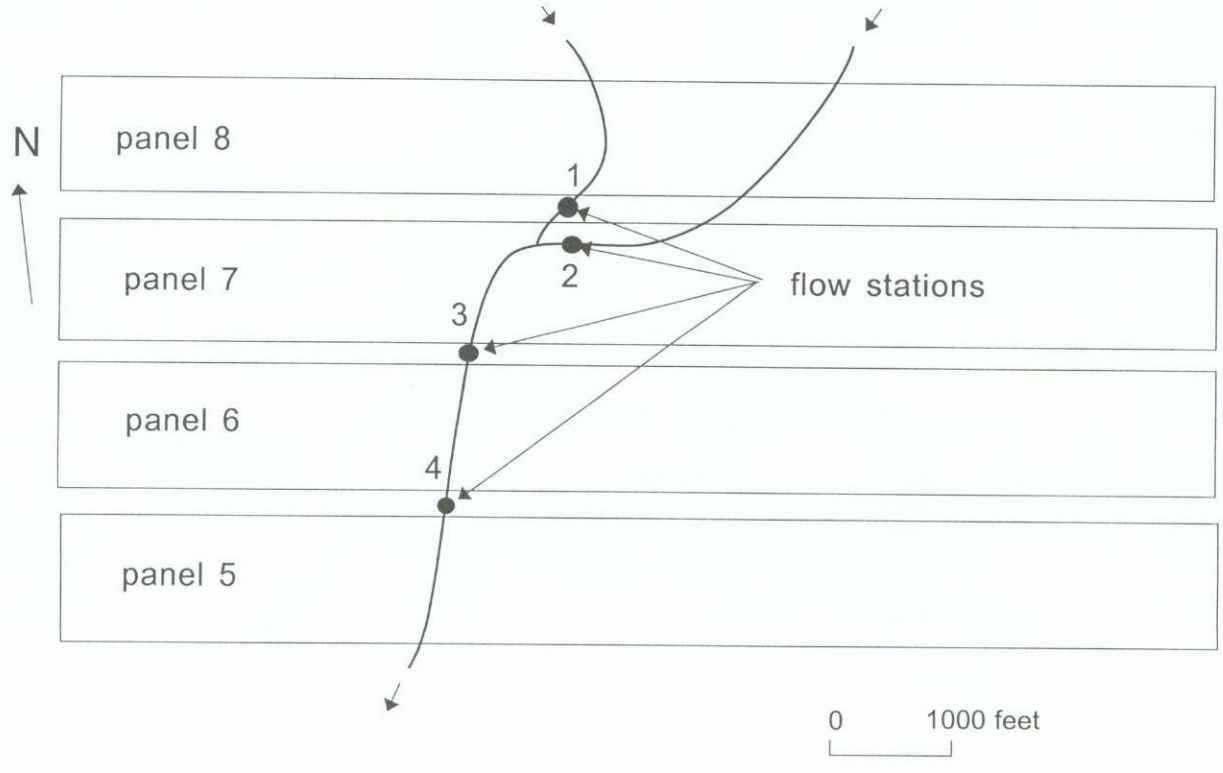



Figure 4. Layout of Site D.

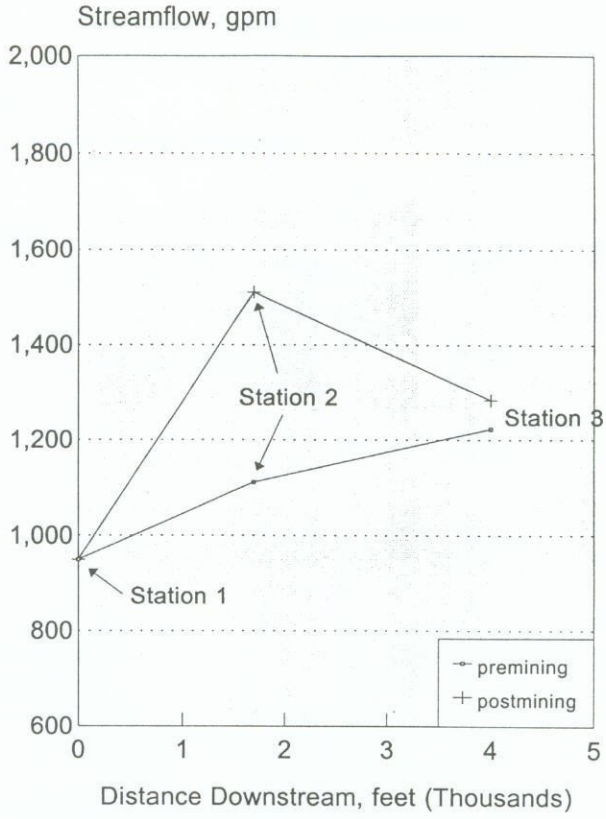



Figure 5. Normalized streamflow for Site A.

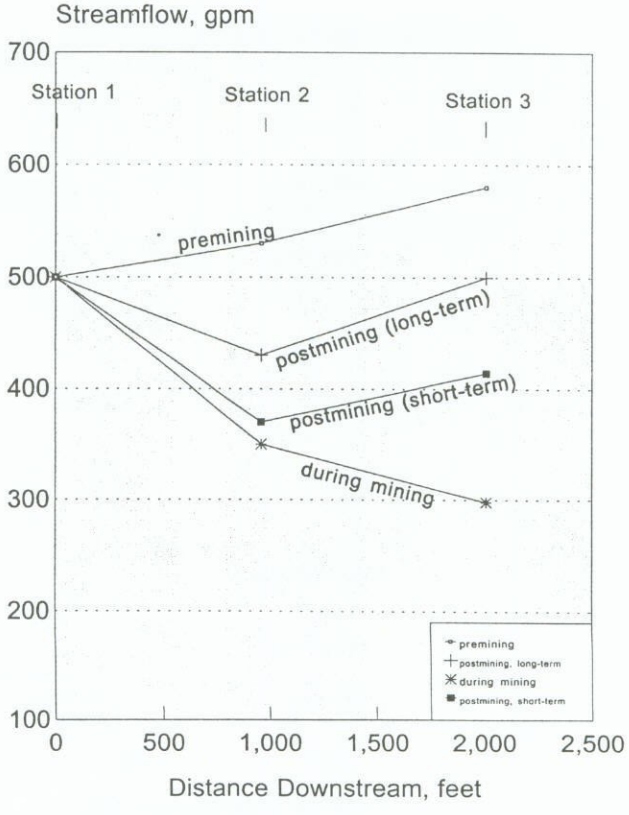



Figure 6. Normalized streamflow at Site B.

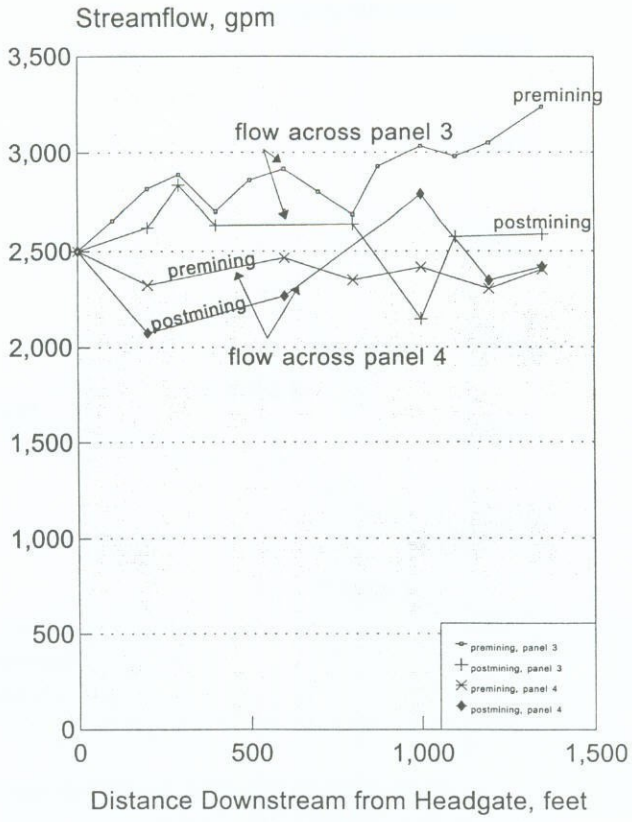



Figure 7. Normalized streamflow at Site C.

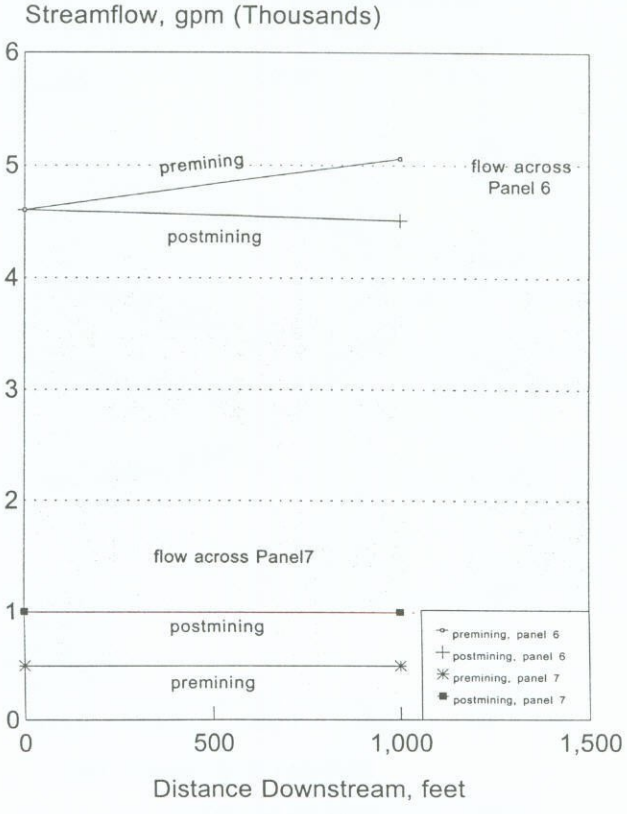



Figure 8. Normalized streamflow at Site D.

# Longwall Surface Subsidence Prediction Through Numerical Modelling

*Noor Mohammad,* Postgraduate Student
*Philip W. Lloyd,* Research Fellow
*David J. Reddish,* Lecturer
Department of Mineral Resources Engineering
University of Nottingham
UNITED KINGDOM

## ABSTRACT

Comprehensive numerical modelling of the subsidence associated with longwall mining in UK Coal Measures strata has been conducted and validated against UK data. The Rock Mass Classification System (RMR) was used as the main basis to derive representative in-situ rock mass properties for stiffness and strength parameters for the numerical modelling input. A Finite Difference Method, Fast Lagrangian Analysis of Continua (*FLAC*) has been used to design a suitable non-linear model and simulate the behaviour of the caved zone with a unique modification of the post failure properties within the zone of influence. The established model was validated for different configurations, varying depth, panel width and extraction thickness, in a sensible and realistic range. The Subsidence Engineers Handbook (SEH) and a stress abutment model were used as a validation tool in this respect. The approach developed will be modified for application to a number of different International Coalfields with different geological environments.

## INTRODUCTION

The extraction of longwall coal face panels induces overburden strata movements. The overburden undergoes various degree of displacement from coal seam to ground surface and the overlying damaged strata can be divided into a caved zone, fractured zone and continuous deformation zone (Peng 1992). An important feature that results from coal face extraction below Coal Measure rocks is the degree of subsidence produced at the surface. Therefore accurate simulation of the surface subsidence profile is of particular importance to help minimise or eliminate any damage to surface structures and to optimise the mining method design. Significant research has already been carried out in this complicated field at Nottingham in order to establish design tools which can be used to predict the amount and extent of any displacement at the surface using empirical, physical, and numerical modelling methods. (Reddish 1984, Yao 1992, Benbia 1996).

During this research programme a series of numerical models have been established, to simulate a 200m wide longwall panel at a wide range of depths between 100m and 800m below ground with a 2m extraction thickness. Model input parameters for strength and stiffness first considered to be typical of UK Coal Measure rock masses were used (Yao et al. 1993). A Finite Difference Method, Fast Lagrangian Analysis of Continua (*FLAC*) *Version 3.3* with a wide range of constitutive models was used in the initial analyses (ITASCA 1995). The Subsidence Engineer's Handbook (SEH) method was used as a reference to validate the surface subsidence results obtained from the numerical model (NCB 1975). The SEH empirical method is considered to be the most acceptable validation tool for subsidence caused due to mining in UK Coal Measure rocks by some researchers who have carried out significant investigations in this field. (Dunham et al. 1995).

## MODELLING METHODOLOGY

### Model Configuration

A numerical modelling programme was carried out using axi-symmetrical Finite Difference grids of 100m to 800m depth by 800m in width. The width of 800m was found to be sufficient to model the full surface subsidence profile for one half of the 200m panel for the whole range of depths. The model grids contained some 10,000 elements. A roller boundary was assumed along the sides and bottom of the grid.

### Stress Conditions

Gravitational loading conditions were assumed to generate the virgin stress conditions (Terzaghi and Richart 1952). The vertical stress $\sigma_v$ throughout the grid was determined as $\rho gh$, (Bigby et al. 1992).

where $\rho$ = density of the rock mass = 2350 kg/m$^3$
(Yao et al. 1993)
g = acceleration due to gravity = 9.81 m/sec$^2$
h = depth

The horizontal stresses $\sigma_h$ were determined as $\sigma_v$ times $\nu/(1-\nu)$.
where $\nu$= Poisson's Ratio of the rock mass was assumed to be 0.2 (Yao et al. 1993)

## MECHANICAL PROPERTIES OF UK COAL MEASURES ROCK MASS

The elastic rock mass stiffness properties for the modelling programme using *FLAC* are specified as Bulk (K) and Shear (G) Moduli derived using the following relationships:

$$K = \frac{E}{3(1-2\nu)} \quad \text{(GPa)} \qquad (1)$$

$$G = \frac{E}{2(1+\nu)} \quad \text{(GPa)} \qquad (2)$$

where E = Young's Modulus of rock (GPa)

In order to determine representative rock mass mechanical properties, laboratory test results on intact specimens of rock must be reduced for in-situ condition (Bieniawski 1978, Serafim and Pereira 1983, Nicholson and Bieniawski 1990, Afrouz 1992, Mitri et al. 1994).

Generally there are two widely used methods:
1. A reduction to laboratory intact rock modulus by a specified value to consider the effect of scale and the presence of discontinuities in the rock mass.
2. The use of rock mass classification techniques to classify rock mass environments and use expressions developed from a wide range of measured data to determine rock mass modulus.

Initial Modelling

The base model at the first stage of the modelling programme used a reduction factor methodology based on previous work by Yao et al. (1993). The following input properties were initially used:

$E_{rm}$ = 1200 MPa
$\nu$ = 0.2
$UCS_{rm}$ = $E_{rm}/300$ = 4 MPa
$UTS_{rm}$ = $UCS_{rm}/10$ = 0.4 MPa

where $E_{rm}$ = Modulus of Elasticity of Rock Mass
$UCS_{rm}$ = Uniaxial Compressive Strength of Rock Mass
$UTS_{rm}$ = Uniaxial Tensile Strength of Rock Mass

Model input strength parameters of Cohesion (c) and Angle of Internal Friction ($\phi$) were determined from the inferred $UCS_{rm}$ and $UTS_{rm}$.

The base model analyses were carried out using the above mentioned mechanical properties in the standard constitutive relations within *FLAC*:
1. Elastic, Isotropic
2. Elastic, Transversely Isotropic
3. Non-Linear, Mohr-Coulomb Model
4. Non-Linear, Ubiquitous Joint Model
5. Non-Linear, Strain Softening Model

Figure 1 presents a typical example of the modelled surface subsidence results, compared to that predicted by the SEH method for the 400m depth case. Although the modelled maximum subsidence at the centre of the 200m wide longwall panel was relatively close to that predicted by the SEH method, serious anomalies occurred in the profile towards the model boundary.

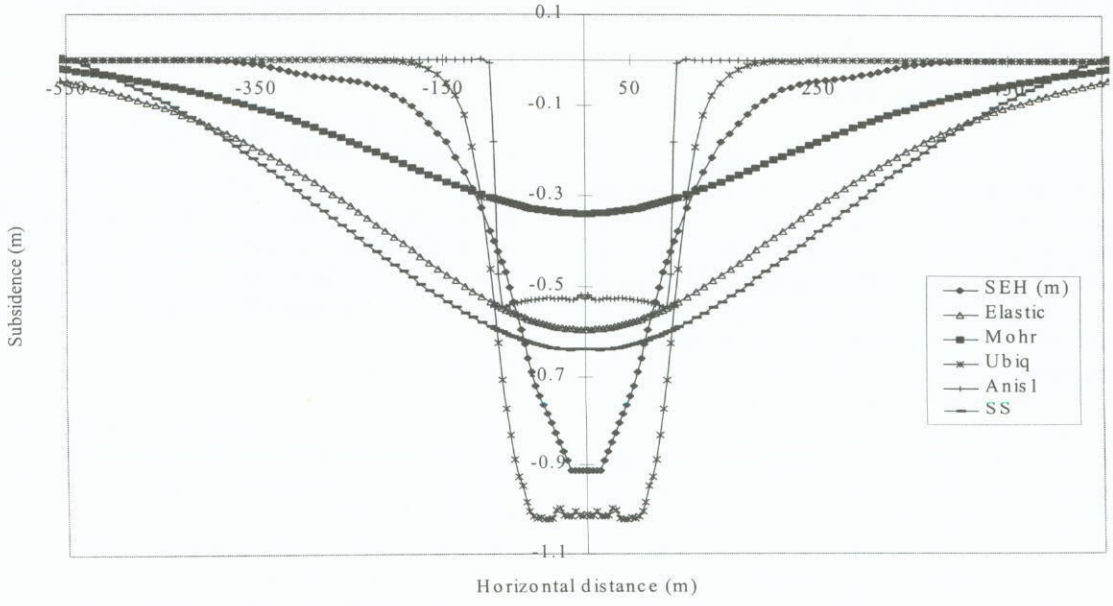



Fig 1: Subsidence predicted by standard *FLAC* models (400m) compared with SEH.

Where this end effect was eventually eliminated by input parameter adjustment, the subsidence profiles simulated in the models did not accurately represent the predicted subsidence trough. It is possible to have a variation of maximum surface subsidence and displacement profile from the actual monitored data when different numerical modelling codes are used to simulate surface subsidence (Kay et al. 1991). However, after a large number of systematic adjustments to the mechanical properties and stresses input into the models it was concluded that the constitutive relations within *FLAC* could not accurately simulate surface subsidence magnitude or model the subsidence profile predicted by the SEH method. It was concluded that the modelling package is sensitive to subtle changes in stiffness and strength parameters and therefore a detailed parametric study to determine accurate pre and post failure stiffness was essential for successful large scale modelling.

## DEVELOPMENT OF MODELLING INPUT PARAMETERS BASED ON ROCK MASS CLASSIFICATION

A wide ranging literature search was conducted to assess and evaluate the methodologies used to fine tune mechanical properties for input within numerical models applied to sub-surface rock engineering to accurately represent rock mass conditions (Mohammad et al. 1997).

Out of the hundreds of publications examined it was found that approximately 120 articles clearly stated the origin of their mechanical properties and where applied, the methodology utilised to fine tune their input parameters to represent the rock mass scale. It was significant that some 60% of the numerical modellers did not mention the methodologies they adopted or used laboratory test results on small intact rock specimens within their models and applied no reduction to the stiffness or strength parameters to represent scale effects, the presence of discontinuities and the influence of mining in the third dimension. The other 40% of the numerical modellers however introduced reductions to their input parameters by the use of either a straight reduction to the stiffness and strength determined from laboratory tests on intact rock specimens or by utilising a rock mass classification within expressions based on in-situ measurement and empirical failure criteria (Mohammad et al. 1997). The review conducted studied case histories and back analysed the input parameters separating the rock mass stiffness properties from the strength data. The model stiffness properties indicated interesting differences in the respective average reduction factors adopted by various researchers. Figure 2 presents the Young's Modulus results for laboratory rock tests plotted against the reduced values used in a wide range of rock mass environments (Mohammad et al. 1997). The stiffness values fine tuned to represent in-situ conditions by the numerical modellers varied considerably when compared in Figure 2 to intact stiffness for typical UK Coal Measure strata (10,000 MPa to 25,000 MPa). Some researchers reduced stiffness for model input marginally from intact laboratory test results.

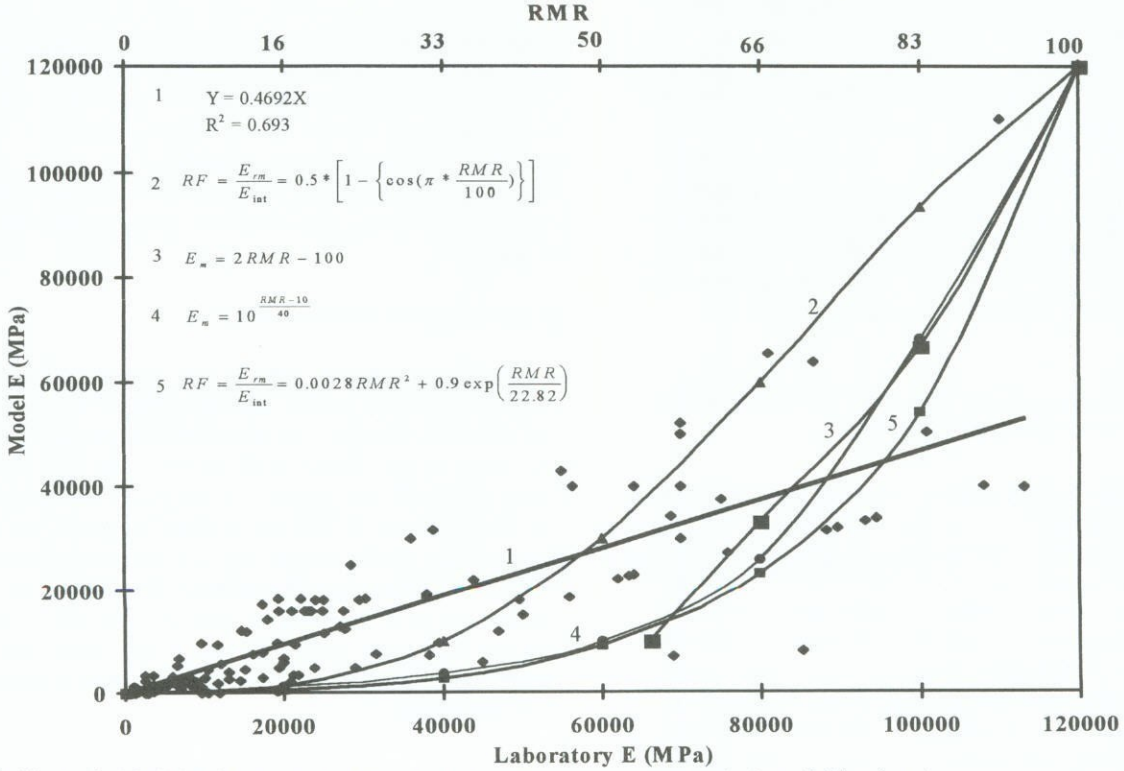



Figure 2 : Young's Modulus from case histories for laboratory tests and numerical modelling input (Mohammad et al 1997)

Hence the average in-situ stiffness illustrated in Figure 2 may be increased by this bias in the data. From the results of a numerical modelling sensitivity analyses it was concluded that much lower in-situ stiffnesses than the average stiffness derived in Figure 2 was necessary for accurate simulation of UK Coal Measure rocks. The expressions that have been derived from in-situ measurement of deformation modulus and related to rock mass classification ratings suggest a much lower in-situ deformation modulus for UK Coal Measures (Figure 2). After an extensive parametric study Serafim and Pereira's (1983) expression was found to derive the best in-situ deformation modulus of UK Coal Measure rocks for the large scale subsidence modelling:

$$E = 10^{\frac{RMR-10}{40}} \quad \text{(GPa)} \qquad (3)$$

This expression was modified during the research to take into account the anomaly in the original expression that suggested a rock mass with a zero rock mass rating had a significant in-situ modulus. The modified relationship was used within the analyses and is presented below:

$$E = 10^{\frac{RMR-10}{40}} - 0.562 \quad \text{(GPa)} \qquad (4)$$

During the simulation of the 200m wide longwall panel with a 2m extraction thickness the input parameters for bulk and shear moduli were determined from equations (1) and (2) utilising the rock mass deformation modulus obtained from modified Serafim and Pereira's relationship (equation 4). A sensitivity analysis was conducted by varying the Poisson's Ratio in the determination of these in-situ stiffnesses for model input. A Poisson's Ratio of 0.2 was found to provide the optimum results in terms of the simulation of deformation processes that were reasonably valid when compared to reality for the full range of depths. Within the numerical models, the deformation processes and surface subsidence induced by mining the 200m longwall panel at 2m extraction thickness at a depth range of 100m to 800m was determined by adjustment of the RMR value as a control for determining the pre and post failure stiffness properties (Table 1).

## MODELLING OF PANEL EXTRACTION AND CAVED WASTE PROPAGATION

In order to better control surface subsidence, the height of mining induced displacement in the overburden must be determined (Peng 1992). To simulate the propagation of a caved waste the model must be constructed to allow the development of an extensive yield and failure zone that can be considered representative of reality. However to literally imitate the actual deformation processes of a caved waste propagation and yield zone development would be unrealistic, therefore a simplification of practice is essential when using numerical modelling techniques in these circumstances (Starfield and Cundall 1988).

Although complex this could be achieved by defining a strain-stiffening caved zone and reduced input properties within the zone of influence above the extracted panel (Lloyd 1995). A valid alternative that was adopted, was to extract the 2m high, 200m wide panel within the model allowing the roof and floor strata to converge (Reddish 1989). The introduction of post failure stiffness parameters would then be governed by yield and failure of the elements within the model. This methodology provided better results for subsidence prediction and displacement distribution within the models. Post failure stiffness properties were incorporated within the simulations as a straight reduction of the initial pre failure stiffness that was determined using RMR. After extensive evaluation the optimum reduction factor of 1/10th the pre-failure stiffnesses were specified within elements that had undergone varying degrees of yield and plasticity.

Table 1: Summary of the stiffness parameters.

| Depth (m) | RMR | $E^*$ (GPa) Pre Failure | $E^*$ (GPa) Post Failure |
|---|---|---|---|
| 400 | 40 | 5.0611 | 0.50611 |

$E^*$ is calculated according to the modified Serafim and Pereira expression (equation 4)

## MODEL STRENGTH CRITERION

After a systematic series of Numerical Model runs, it was clear that the strain softening constitutive model provided an accurate balance between stiffness and strength. The stress-strain relationship was controlled by the elastic and plastic strain increment for the strain softening relation. Plasticity propagation was considered reasonably accurate when the failure mechanisms were assessed and evaluated using the authors monitoring experience of actual in-situ deformation processes.

### Strain-Softening Model in *FLAC*

The strain-softening (SS) model uses the Mohr-Coulomb failure criterion to detect material failure. It is possible that the cohesion, friction, and dilation may harden or soften after the onset of the plastic yield. In the Mohr-Coulomb Model these properties are assumed to remain as constant, whereas, the SS behaviour is simulated in FLAC by specifying values of strength parameters that change as a function of plastic strain. Major and minor principal stresses $\sigma 1$ and $\sigma 3$ are used in equation 5 to calculate shear yield ($f^s$) throughout the entire domain during the computer run. The failure envelope is defined from point A to point B by the Mohr-Coulomb yield function (Figure 3).

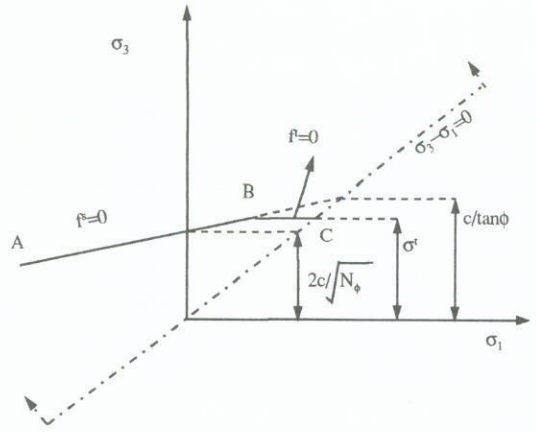



Figure 3: Mohr-Coulomb failure criterion in *FLAC*.

$$f^s = \sigma_1 - \sigma_3 N_\phi + 2c\sqrt{N_\phi} \qquad (5)$$

where $N_\phi = \frac{1+\sin\phi}{1-\sin\phi}$

The physical values of strength parameters evaluated and assigned in the data file to a corresponding strain are updated according to the following procedure:

1. The material behaves in an elastic manner until the shear yield function $f^s$ is exceeded
2. When the model detects $f^s<0$ for any zone during the computer run plastic flow is allowed to occur in order to restore the condition $f^s = 0$
3. The values of strength parameters to that zone are then modified in the following time step according to the degree of plastic flow calculated in step 2.

Strain-Softening Parameters

The initial input properties for strength were determined using a modified coal measure rock mass failure criterion related to actual intact rock test data for UK Coal Measure rocks, fine tuned for UK coal mine in-situ conditions using a rock mass classification rating (Stace and Lloyd 1996). During the analyses it was further concluded that the strain increment specified was significant with respect to the full propagation of yield and failure within the model (Itasca 1995). A thorough evaluation of the influence of the specified strain increment on model results was considered to be important by previous modellers (Raffield 1993, Trueman et al. 1992). Fine tuned strain softening parameters and strain increments were therefore evaluated and are presented in Table 2.

Table 2: Final strength parameters used in SS model with detuned strain increments.

| Strain | Cohesion C (MPa) | Dilation d (deg) | Fric. Angle ϕ (deg) |
|---|---|---|---|
| 0 | 0.8 | 10 | 35 |
| 0.005 | 0.5 | 5 | 30 |
| 0.0075 | 0.4 | 5 | 25 |
| 0.01 | 0.2 | 5 | 20 |
| 0.05 | 0.1 | 5 | 20 |

## RESULTS

Validation of Model Depth Sequence

When the depth sequence was run for a particular RMR based input parameter set, the results displayed a specific pattern. When a low RMR was used good results could be obtained for shallower situations but deeper models gave a poor fit. Conversely, when a high RMR was used the deep models produced a good fit but the shallower models underestimated. Fine adjustments in the stiffness to strength balance could not at first overcome this fairly fundamental trend. As a result it was felt that RMR and hence stiffness and strength must in some way change in the models with depth. Essentially deeper buried rocks of the same type appeared to be stiffer. An alternative explanation would be that the gravitational stress field assumptions made were incorrect and vertical stress at depth is considerably reduced from that assumed. Some trials with increased horizontal stress also proved ineffective. The authors felt that the stiffening of rocks under higher stress and compaction was relatively logical and chose to investigate it further. Models were run at each depth and RMR and its associated properties adjusted until the best subsidence fit to the SEH validation model was obtained. The *FLAC* models were run for the full range of depths and were compared with results from the SEH surface subsidence prediction method (Table 3). The RMR to determine the stiffness was the controlling parameter and was adjusted with depth until the subsidence profile simulated that predicted by SEH in terms of limb profile and maximum subsidence magnitude. An error band of ± 20% was considered reasonable for maximum subsidence (Whittaker and Reddish 1989, NCB 1975). It must be noted that the fine tuned Rock Mass Classification Ratings are presented in Table 3, since even relatively minor subtle changes in the RMR produced major differences in the maximum subsidence and subsidence profile shape. Sensitivity analysis is furthered to see the affect of reducing and increasing stiffness by variation of the RMR between 35 and 50 for the 400m depth case. The results suggested that relatively low variation in RMR (stiffness) produced significant differences in modelled maximum subsidence and subsidence profile shape.

Table 3: Summary of the FLAC and SEH results.

| Depth (m) | RMR | $S_{max}$ SEH (m) | $S_{max}$ FLAC(m) | Error % | $E^*$ (GPa) |
|---|---|---|---|---|---|
| 100 | 8 | 1.78 | 1.805 | 1.4 | 0.329 |
| 200 | 20 | 1.647 | 1.580 | -4.07 | 1.216 |
| 300 | 28 | 1.291 | 1.372 | 6.27 | 2.256 |
| 400 | 41 | 0.913 | 0.932 | 2.08 | 5.394 |
| 500 | 47 | 0.678 | 0.679 | 0.15 | 7.852 |
| 600 | 54 | 0.4876 | 0.476 | -2.38 | 12.027 |
| 700 | 57 | 0.371 | 0.349 | -5.93 | 14.4 |
| 800 | 63 | 0.313 | 0.2928 | -6.45 | 20.573 |

$E^*$ is calculated according to the modified Serafim and Pereira expression (equation 4)

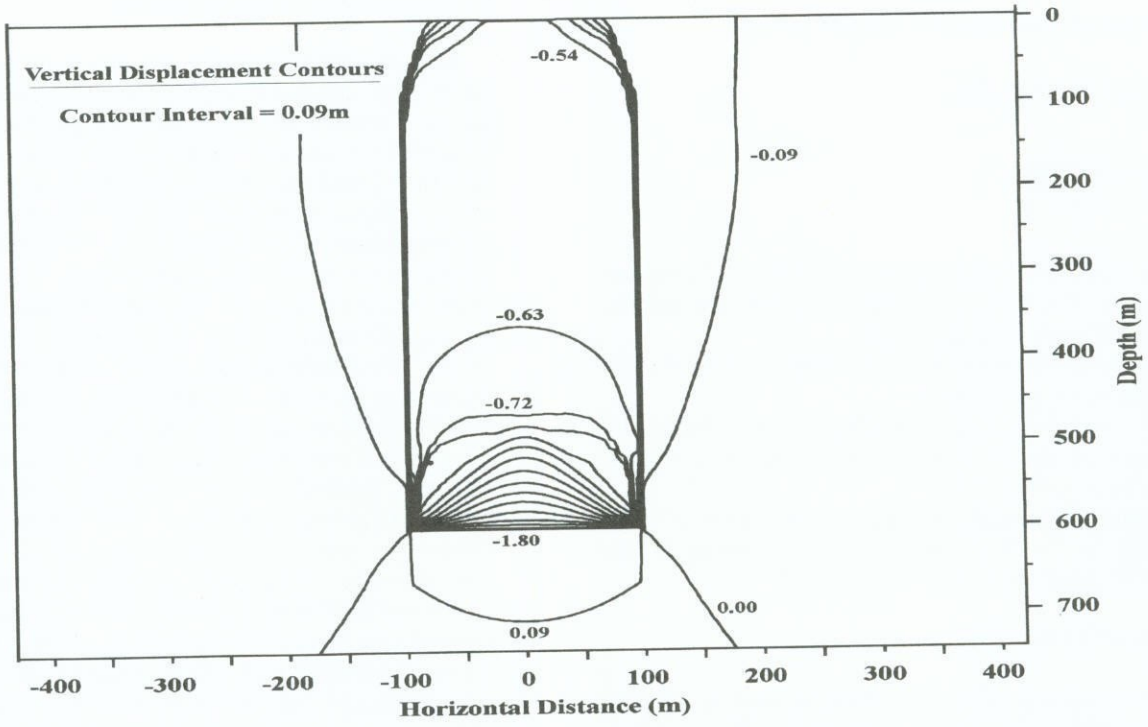



Figure 4: Distribution of vertical displacement around a 200m wide longwall panel at 600m depth

Vertical Displacement Distribution Around a Longwall Panel

The distribution of vertical displacement around a 200m wide longwall panel at 600m depth is presented in Figure 4. It was observed that the roof sagged by an amount of 1.84m, i-e 92% of the extraction thickness of 2m, while the floor heave was 0.16m which was 8% of the extraction of thickness. From the vertical displacement contours with contour intervals of 0.09m it was observed that in the highly fractured zone its magnitude was maximum. With the propagation of caved waste vertical displacement gradually decreasing resulting in maximum surface subsidence of 0.55m at the centre of longwall panel. However, a narrow band of contour interval closely spaced directly over the edge of the longwall panel indicating a zone of shear failure was observed.

ANALYSIS OF RESULTS

Depth Below Surface Variation

From the full range of model results displayed in Table 3, it was evident that the stiffness parameters of the rock mass appeared to increase with depth.

Consequently the rock mass classification rating (RMR) increased with depth. Figure 5 illustrates this relationship (equation 6) and is represented by the following expression:

$$RMR = 27.213 Ln (D) - 121.65 \quad (6)$$

where D = Depth of seam below surface (m)

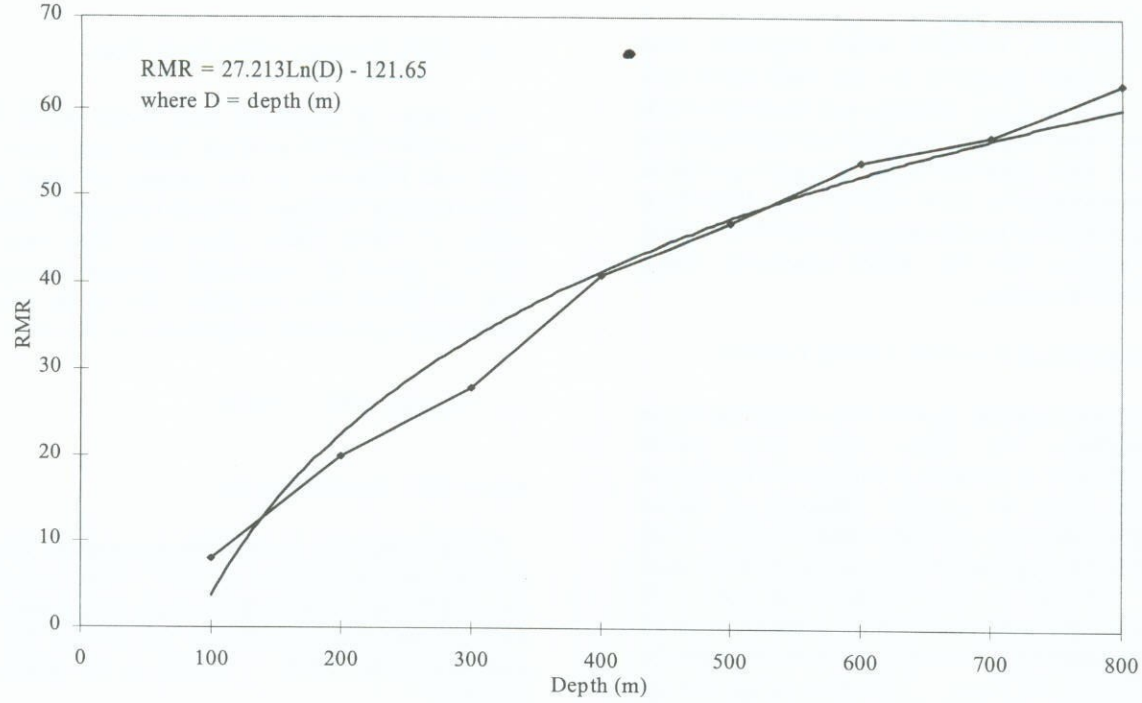



Fig 5: Model relationship between depth and RMR

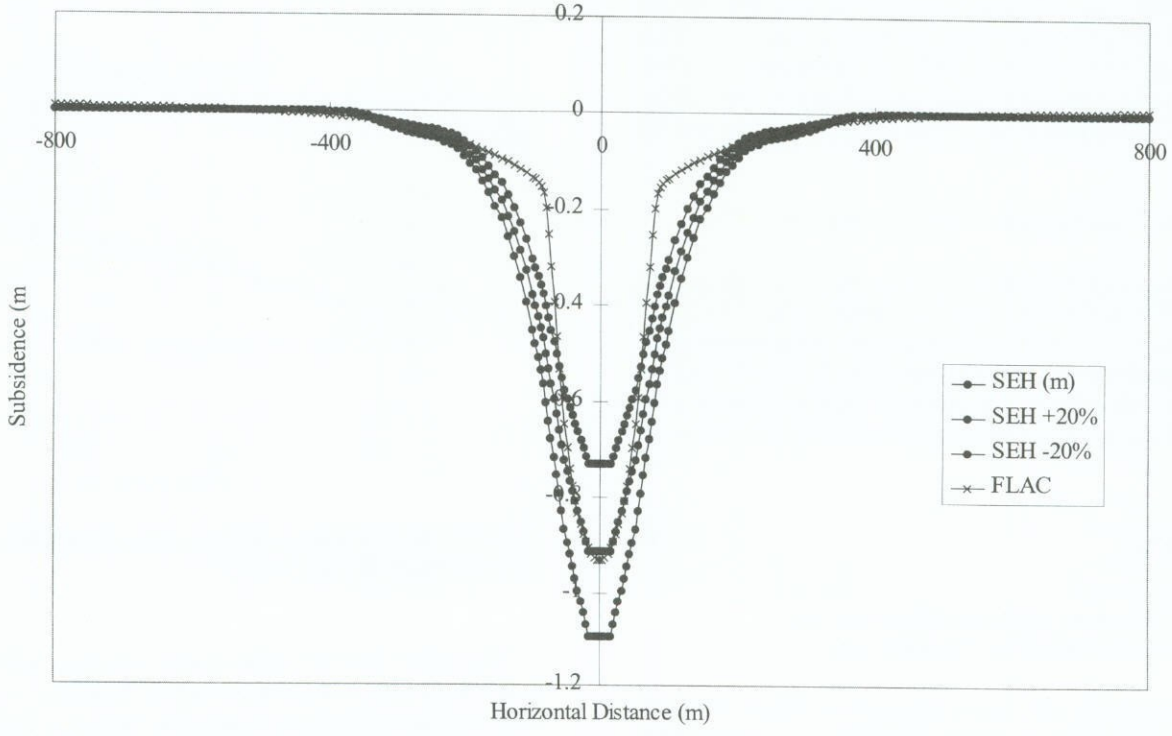



Fig 6: Modelled surface subsidence compared to SEH prediction for 200m longwall panel at 400m depth.

Figure 6 shows the modelled surface subsidence when compared to the SEH prediction for the 400m depth case. The displacement distribution modelled was found to be valid throughout from seam level to the surface and additionally the redistribution of flank abutment stresses seemed reasonable. The horizontal displacement at the surface of the 400m depth case determined from the model compared with SEH method. The results indicate that the model reasonably closely simulates the SEH prediction.

Seam Extraction Thickness and Panel Width Variation

The modelling methodology derived from simulating the 2m extraction thickness and 200m panel width proved insufficiently sensitive to variation in extraction thickness and panel width in terms of accurate prediction of surface subsidence. Manual control on the development of the caving or yielding zone was required to sensitise the model to these parameters. Manual iteration of the model had to be introduced with a limitation placed on the propagation of the yield and failure zone above the extracted panel to produce a universal modelling technique. The relationship between RMR and depth was used to determine stiffness parameters as in the analyses previously discussed. A series of numerical models were established that examined the sensitivity of the methodology developed when simulating the surface subsidence predicted by the SEH method for varying coal seam extraction thicknesses and panel widths. From the modelling results it was found that the extent of the yield and failure zone around the longwall panel significantly influenced the magnitude of maximum subsidence and the surface subsidence trough profile shape when compared to the SEH method (Alejano Monge et al. 1995). For the purpose of this publication the sensitivity study carried out for the 400m depth case was selected for further analysis and is presented below.

Seam Extraction Thickness Variation (400m Depth Case)

Seam extraction thicknesses of 1m, 1.5m, 2m, 2.5m and 3m were specified within the numerical model for the 400m depth case, and run. The fine tuned properties remained the same and the following expression (equation 7) was derived to provide an indication of the extent of yield and failure zone around a longwall panel for a specified extraction thickness, Figure 7:

$$\frac{Y}{X} = 37.435e^{0.415X} \qquad (7)$$

where Y = Extent of yield and failure zone (m)
X = Seam Extraction Thickness (m)

From evaluating the results displayed in Figure 8 it was noted that when seam extraction thickness was varied within the 400m depth case, then the extent of the zone influenced by the longwall panel required to be significantly increased.

Panel Width Variation (400m Depth Case)

The results of varying the panel width for the 400m depth case indicated that the yield and failure zone above a longwall panel was influenced by the variation of panel width while seam extraction thickness remained constant. Longwall panel widths of 150m, 200m 250m and 300m were specified. Figure 8 shows the relationship between the extent of the yield and failure zone and panel width in the models. The relationship is presented in equation 8 as follows:

$$\frac{Y}{X} = 89.596Ln(PW) - 394.59 \qquad (8)$$

where PW = Panel Width (m)

Further sensitivity analyses were conducted where the full variation of panel widths of 150m, 200m and 250m were specified for the 400m to 800m depth range, seam extraction thickness remained constant at 2m as did the properties determined from RMR. Details of the analyses will be published.

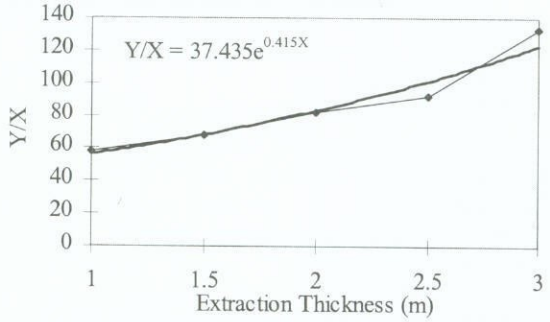



Figure 7: Extent of the failure zone for varying extraction thickness.

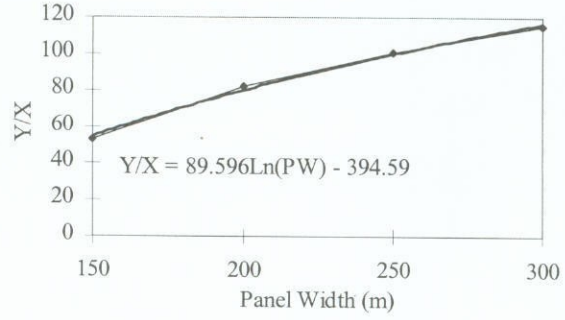



Figure 8: Relationship between extent of the failure zone for different longwall panel widths.

The results from the panel width variation models for the 400m depth case with a 2m extraction thickness, were plotted with maximum subsidence/extraction thickness ratio ($S_{max}/t$) against panel width/depth ratio (W/H) and compared to the same configuration predicted by the SEH Method (Figure 9).

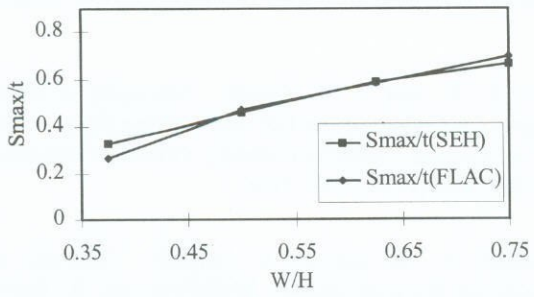



Figure 9: $S_{max}/t$ vs W/H for depth= 400m.

The results of the models were found to be in close agreement with the predictive methods results. The results for the full series of modelled depths were evaluated in terms of ($S_{max}/t$) vs (W/H) for the 200m panel with 2m extraction thickness and compared with the SEH method prediction. The full range of numerical models was further validated when compared with the predicted results (Figure 10).

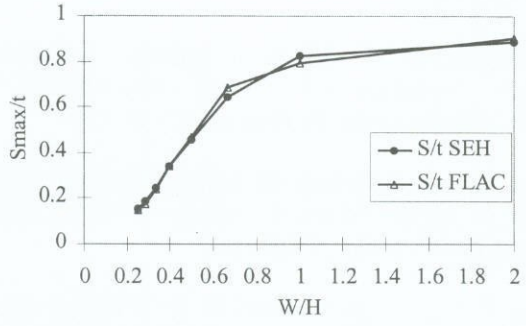



Figure 10: $S_{max}/t$ vs W/H for depth= 100m - 800m.

Strain Softening Sensitivity Analyses

When strain-softening constitutive relations are used in numerical modelling, results may be sensitive to element size and shape (Trueman et al. 1992). In the grid specified for the modelling series symmetrical elements were utilised and the width to height aspect ratio between adjacent elements were kept well within tolerances suggested by *FLAC* (Itasca 1995). A sensitivity analysis was conducted for the 400m depth case where a much more dense grid with smaller symmetrical elements was utilised. A model with a total of 36,000 elements as opposed to the usual 10,000 elements was specified and run. The maximum modelled subsidence was within 3% of the original run with a near perfect subsidence profile simulated. This condition occurred when the post failure property zone was specified to propagate to the same extent as in the model with the smaller grid.

## CONCLUSIONS

A valid but complex methodology for simulating surface subsidence for UK Coal Measures has been developed, applicable to a comprehensive range of depths between 100m to 800m. A relationship between RMR and depth for pre and post failure stiffness determination was derived. The use of Rock Mass Classification principles to more accurately characterise UK Coal Measure rocks would be useful for fine tuned in-situ strength and stiffness determination. The modelling technique developed is sensitive to extraction thickness variation and longwall panel width variation when the propagation of the zone of influence above the panel is finite.

## FUTURE WORK

Research is currently ongoing into interactive yield and failure propagation control within the model, as well as extending the subsidence modelling technique for use in international coalfields. The existing methodology will be modified to simulate surface subsidence in the Australian, Appalachian and Indian mining environments where the coal measure conditions are significantly different from each other and from UK Coalfields.

## REFERENCES

1. Afrouz, A. A. Practical Handbook of Rock Mass Classification Systems and Modes of Ground Failure, CRC Press Inc. 191 pp. 1992.

2. Alejano Monge, L. R., P. R. Oyanguren and R. De La Fuente. A Method to Predict Final Subsidence Basins by Means of a Finite Difference Computer Code, Land Subsidence (Proc. of the Fifth International Symposium on Land Subsidence, Fissols-95), The Hague, Germany, October. IAHS Publ. No. 234, pp 251-258. 1995.

3. Benbia, A. Ground Movement Associated with Longwall Mining Extraction, Ph.D. Thesis, University of Nottingham, UK. 272 pp. 1996.

4. Bieniawski, Z. T. Determination of Rock Mass Deformability: Experience from Case Histories, Int. J. of Rock Mech. Min. Sci. and Geomech. Abstr., Vol. 15, pp 237-247. 1978.

5. Bigby, D. N., J. C. Cassie and A. R. Ledger. Absolute Stress and Stress Change Measurements in British Coal Measures, Proc. of ISRM Symp. Eurock 92, British Geotechnical Society, London, pp 390-395. 1992.



6. Dunham, R. K, D. J. Reddish, X. L. Yao and B. H. Roberts. A Review of Mining Subsidence Prediction Systems, Final Report for British Gas Research and Technology, University of Nottingham, UK. 130 pp. 1995.

7. Itasca. Fast Lagrangian Analysis of Continua, FLAC, Version 3.3, Volume 1-4, Itasca Consulting Group Inc., Minneapolis, Minnesota 55415 USA. 1995.

8. Kay, D. R., K. E. McNabb and J. P. Carter. Numerical Modelling of Mine Subsidence at Angus Place Colliery, Proceedings of Computer Methods and Advances in Geomechanics, Beer, Booker and Carter (eds) Balkema, Rotterdam. pp 999 - 1004. 1991.

9. Lloyd, P. W. An Investigation of the Influence of Mining Method Upon Rock Mass Behaviour in Stratified Deposits, Ph.D. Thesis, University of Wales. 378 pp. 1995.

10. Mitri, H. S., R. Edrissi and J. Henning. Finite Element Modelling of Cable-Bolted Stopes in Hard Rock Underground Mines, Presented at the SME Annual Meeting Albuquerque, New Mexico / February 14-17, Preprint Number 94-116. 1994.

11. Mohammad, N., D. J. Reddish and L. R. Stace. The Relationship Between In-Situ and Laboratory Rock Properties used in Numerical Modelling, Int. Jr. of Rock Mech. Mining Sc. and Geo. Abstracts, Vol. 34, No. 2 pp 289-297. 1997.

12. NCB, SEH, Subsidence Engineers Handbook, National Coal Board, Mining Department, London. 111 pp. 1975.

13. Nicholson, G. A. and Z. T. Bieniawski. An Empirical Constitutive Relationship for Rock Mass, Rock Mechanics: Key to Energy Production, Proc. of the 27th U. S. Symposium on Rock Mechanics, H. L. Hartman (ed), SME, pp 898-905. 1986.

14. Peng, S. S. Surface Subsidence Engineering, Society for Mining, Metallurgy and Exploration, Inc. Littleton, Colorado. 161 pp. 1992.

15. Raffield, M. P. Stability Investigations Associated with Shaft Reef Excavation in a Deep Level Gold Mine, Ph.D. Thesis, University of Wales. 224 pp. 1993.

16. Reddish, D. J. Study of Ground Strain in Relation to Mining Subsidence, Ph.D. Thesis, University of Nottingham, UK. 364 pp. 1984.

17. Reddish, D. J. The Modelling of Rock Mass Behaviour Over Large Excavations Using Non-Linear Finite Element Techniques, Mining Department Magazine, Vol. No. XLI, pp 93-105. 1989.

18. Serafim, L. J. and P. J. Pereira Consideration on the Geomechanical Classification of Bieniawski, Proc. of the International Symposium on Engineering Geology and Underground Construction, Lisbon, Portugal, V2 pp 33-42. 1983.

19. Stace, L. R. and P. W. Lloyd. Managing a New Technology - An Update of the UK Rockbolting Story, 15th Int. Conf. on Ground Control in Mining, Golden, Colorado, (August 13th-15th), pp 333-347. 1996.

20. Starfield, A. M. and P. A. Cundall. Towards a Methodology for Rock Mechanics Modelling, Int. Jr. Rock Mech. Min. Sci. and Geomech. Abstr., Vol. 25, No. 3, pp 99-106. 1988.

21. Terzaghi, K. and F. E. Richart. Stresses in Rock about Cavities, Geotechnique, Vol. 3, pp 57-90. 1952.

22. Trueman, R., I. G. T. Thin and D. B. Tyler. Rock Mass Classification as an Aid to Estimating the Strength of Coal Pillars, Proc. of the 11th International Conference on Ground Control in Mining, Wollongong, N. I. Aziz and S. S. Peng (eds), pp 22-29. 1992.

23. Whittaker, B. N. and D. J. Reddish. Subsidence Occurrence, Prediction and Control. Developments in Geotechnical Engineering, 56, Elsevier. 528 pp. 1989.

24. Yao, X. L. Modelling of Mining Subsidence with Reference to Surface Structure Behaviour, Ph.D. Thesis, University of Nottingham. 275 pp. 1992.

25. Yao, X. L., D. J. Reddish and B. N. Whittaker. Non-linear Finite Element Analysis of Surface Subsidence Arising from Inclined Seam Extraction, Int. J. of Rock Mech. Min. Sci. and Geomech. Abstr., Vol. 30, No. 4, pp 431-441. 1993.

# Long-term Subsidence Over Longwall Chain Pillar Systems and Its Effects on Surface Structures

*Yi Luo,* Research Assistant Professor
*Syd S. Peng,* Chairman and Charles T. Holland Professor
*H.J. Chen,* Graduate Student
Department of Mining Engineering
College of Engineering and Mineral Resources
West Virginia University
Morgantown, WV

## ABSTRACT

A research has been conducted to study the long-term subsidence and its possible effects on surface structures. In this research, the surface movements in areas where potential for developing long-term subsidence is high have been monitored over an extended period of time. Long-term subsidence data have also been collected from other sources. The available data from this on-going research have been analyzed and the results is presented in this paper.

## INTRODUCTION

Under the influence of underground longwall mining, the movement at a surface point initiates, accelerates, decelerates and practically stops within a normal subsidence duration which could range from about 10 days to one months in US mining conditions. Considerable efforts have been made by the senior authors in the last decade to study the dynamic subsidence process. A number of mathematical models have been proposed to predict the different phases of the dynamic subsidence process associated with longwall mining operation (Luo and Peng, 1992). However, it has been suggested that a slow surface movement process might follow this normal subsidence duration (Mehnert et al., 1992). If this subsidence process does indeed exist, it is called the long-term subsidence process. Thus far, very little research has been conducted to address the issue of long-term subsidence. Due to the relatively unknown nature, there is often a great public concern on the long-term subsidence and its potential effects on surface structures.

An effort has been made to study the issue of long-term subsidence process. The subsidence data collected from a number of selected longwall subsidence sites over extended periods after mining, including a site still being monitored by the authors, have been analyzed. The selected sites for this study were located in the areas over longwall chain pillars where the long-term subsidence is most likely to occur. The emphasis of this study is placed on: (1) existence of long-term subsidence process and the necessary condition for its occurrence, (2) the characteristics of the development process, and (3) the possible effects of long-term subsidence process on surface structures. This paper presents some results of this on-going research on the long-term subsidence.

## NORMAL SUBSIDENCE DURATION

As stated previously, the long-term subsidence process occurs after a normal subsidence duration. Therefore, the characteristics of the normal subsidence process associated with longwall mining should be understood first.

### Normal Dynamic Subsidence Process

There are the following three distinguishable phases in the dynamic subsidence process associated with longwall mining operation (Luo and Peng, 1992): (1) subsidence initiation phase in a short period at the beginning of mining a longwall panel, (2) normal dynamic subsidence phase as the longwall face advances in the remaining length of the panel, and (3) the residual subsidence phase after mining in the panel stops. Phases 1 and 3 of the dynamic subsidence process only affect small surface areas near the panel setup and recovery entries, respectively. The major portion of the subsidence basin over a longwall panel will experience the normal dynamic subsidence phase. In the normal dynamic subsidence process, a surface point does not begin to subside until the advancing longwall face has reached a certain distance inby the point. This distance is called the offset of subsidence initiation point ($l_1$). Then the subsidence process accelerates and the subsidence velocity reaches its peak when the longwall face has passed the surface point a distance called the offset of subsidence velocity peak, $l$. A deceleration process is followed afterwards and the subsidence process practically stops or reaches its quasi-stable state after a period of time. Figure 1 shows a subsidence development curve derived from the collected data over a longwall panel mining in the Pittsburgh seam. The overburden depth over this panel was about 680 ft and mining height was 6.5 ft. The average face advance rate was about 62 ft/day

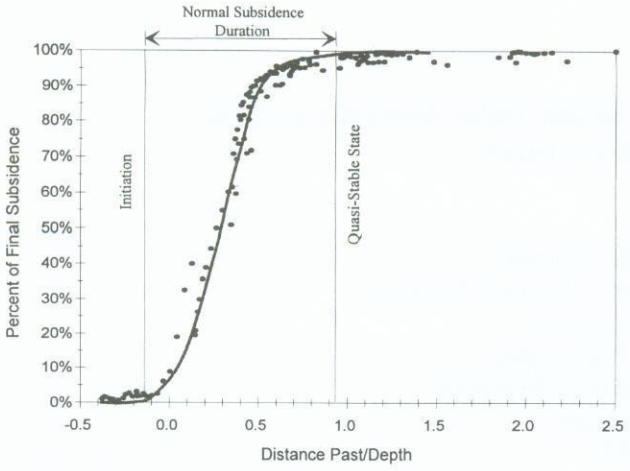



**Fig. 1 Development Curve for Normal Dynamic Subsidence Process of a Longwall Operation**

while the monitoring site was affected by the subsidence process. In deriving the subsidence development curve, the ratio of the measured subsidence on a given day to the final subsidence at a surface point is plotted against the ratio of the distance between the advancing face and the surface point to the overburden depth ($L/h$ ratio). It shows that surface began to subside when the $L/h$ ratio was about -0.15 (the face was still about 100 ft inby the surface point or $l_1$ = 100 ft). About 50% of the final subsidence was reached when the $L/h$ ratio was 0.31 (the face was 210 ft outby the point or $l$ = 210 ft). It should be pointed out that the subsidence velocity at this point of time is also the highest. The surface appeared to become stable (referred as the quasi-stable state) when the face is about 0.93 times of the overburden depth passed the point. Near symmetry between the first and the second halves of the subsidence development curve over the point of the 50% of final subsidence is observed in the figure. Therefore, the offset of subsidence initiation point ($l_1$) and offset of subsidence velocity peak ($l$) are two important parameters to define the normal dynamic subsidence development curve. Based on the longwall dynamic subsidence data collected for Pittsburgh seam and for Herrin coal seams, the updated empirical formulae for these two dynamic subsidence parameters are:

$$l = (0.2102 + 0.0171\sqrt{v})h \qquad (1)$$

$$l_1 = \frac{0.0383h}{1-0.0796\sqrt{v}} \qquad (2)$$

where: $v$ - average face advance rate, ft/day
$h$ - overburden depth, ft

**Normal Subsidence Duration**

Using Eqs. 1 and 2, a graph for determining the normal subsidence duration for longwall mining operations is derived as shown in Fig. 2. Three lines are plotted in this figure. The first line is for the determination of the offset of subsidence initiation point and the second one for the distance between the longwall face and the point where quasi-stable state is reached. The third is the total distance for a surface point to experience the normal dynamic subsidence process. For the range of average face advance rate from 20 to 70 ft/day, the normal subsidence duration varies from 0.76 to 1.04 times of the overburden depth. The subsidence process at a surface point reaches its quasi-stable state when the longwall face has passed this point a distance between 0.70 and 0.94 times of the overburden depth based on this figure. It should be pointed out that most of the collected and published *final* subsidence data for longwall operations should be considered as the subsidence at quasi-stable state because most of the monitoring programs ended after a relatively short duration.

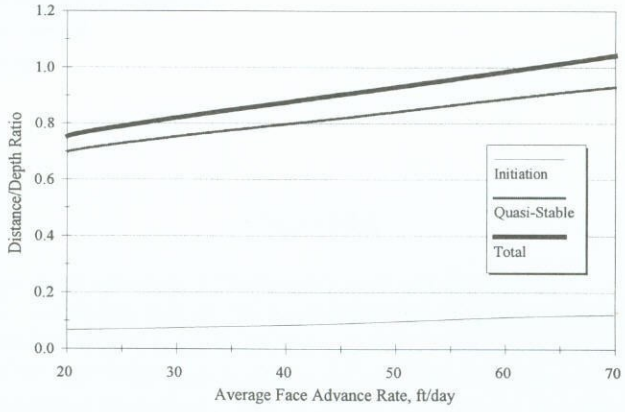



**Fig. 2 NormalLongwall Subsidence Duration Based on Data Collected from Pittsburgh Seam and Illinois Coal Basin**

## LONG-TERM SUBSIDENCE

After the quasi-stable state of the normal dynamic subsidence process is reached, long-term subsidence could also develop over an extended period of time. The maximum long-term subsidence at a surface point is defined to be the difference between the ultimate final subsidence ($S_u$) and the subsidence measured when the quasi-stable state is reached (quasi-final subsidence, $S_q$) at this point. The two possible sources for inducing the long-term subsidence for underground longwall mining operations are:

- Re-compaction in the overburden strata which has been disturbed during the normal dynamic subsidence process. Re-compaction is most likely to cause long-term subsidence over the central portion of the longwall panels due to the presence of caving and fracture zones there.
- Creep deformation of the chain pillar system and its floor strata located between two successive longwall panels. The long-term subsidence caused by the creep deformation is most likely in the area over and near the chain pillar system.

In a number of longwall subsidence cases in which the collected data appear to substantiate the existence of long-term subsidence, the measured long-term subsidence occurred over the chain pillars is generally much larger than that over the cen-

tral portion of longwall panels. This indicates that creep deformation of the chain pillar system contributes more to the long-term subsidence process than re-compaction of the overburden strata in these cases. In addition, the surface deformations (i.e., slope, strain and curvature) and their potential to cause structural damages in the area near the chain pillar system are normally much higher than those over the central portion of the panels. Therefore, long-term subsidence occurring in the area near the chain pillar system and its possible effects on surface structures will be subjected to more scrutinies than those in other areas over a longwall panel. For these two reasons, the emphasis of this study is currently placed on the long-term subsidence over and near the chain pillar system.

## Long-Term Subsidence Cases

In order to study the long-term subsidence, eight sets of subsidence data measured over and near the longwall chain pillar systems have been collected thus far. The general information (i.e., coal seam mined, overburden depth, panel width, the total width of chain pillar system and mining height) for each of the collected cases is listed in Table 1. Longwall mining in four of the cases was conducted in the Pittsburgh seam and another four in Herrin #6 seam in the Illinois coal basin.

The subsidence data in cases 1, 3 and 4 have been measured over three chain pillar systems left between four successive longwall panels. The measured subsidence profiles for these three cases are shown in Fig. 3. Panel P-1 was mined first and P-4 the last. Therefore, the chain pillar system between panels P-3 and P-4 (case No. 1) has been affected by mining for the shortest duration and that in case No. 4 has been exposed for the longest time among the three. The numbers shown in the figure legends are the days after the subsidence monument line over each chain pillar system has been undermined by the longwall face for the first time. The subsidence monument lines of cases 1, 3 and 4 were undermined again by the longwall face in the subsequent panel 210, 227 and 271 days afterwards, respectively. For the surface area over a chain pillar system, the quasi-stable state of the normal subsidence process is reached when the longwall face in the second adjacent panel has passed the location a normal subsidence duration (Fig. 2). For cases 1, 3 and 4, the normal subsidence durations are about 19, 18 and 14 days, respectively. The incremental subsidence after this period is considered to be the long-term subsidence.

Figure 3a does not show any significant long-term subsidence understandably due to a very short time elapsed (the last survey was conducted only 10 days after the quasi-stable state had been reached). However, notable amount of long-term subsidence can be found in cases 3 and 4 where the last survey was performed 206 and 426 days after the quasi-stable state, respectively. The quasi-final subsidence and the subsidence measured in the last survey at the middle point of the chain pillar system for the each of the three cases are also listed in Table 1 along with the elapsed time after the quasi-stable state.

Figure 4 shows the measured subsidence profiles in case No. 8. Although the last survey was performed 286 days after the quasi-stable state, the incremental subsidence is still considered very small.

## Development of Long-Term Subsidence

The long-term subsidence development curves at four surface points in case No. 4 (points A, B, C and D in Fig. 3c) are plotted in Fig. 5. In this figure, the measured subsidence is plotted against the time elapsed after the quasi-stable state has been reached. All the four points show that the subsidence velocity was higher initially and decreased afterward. Similar development patterns can also be observed in the other cases. Based on these observations, it is reasonable to assume that the subsidence velocity at a surface point and at a given time in the long-term subsidence process is proportional to the difference between the ultimate final subsidence ($S_u$) and the current subsidence at the point. This assumption can be expressed in the following ordinary differential equation:

$$V(t) = \frac{dS(t)}{dt} = c[S_u - S(t)] \qquad (3)$$

where: $t$ - time elapsed after the quasi-stable state is reached

$V(t)$ - subsidence velocity at time $t$

$c$ - a coefficient characterizing the long-term subsidence process

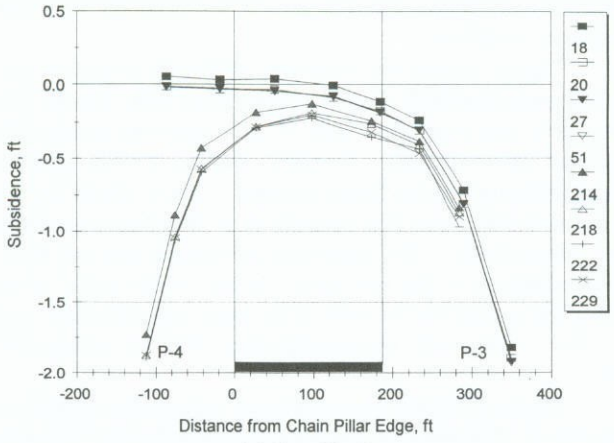
**Table 1 General Information of the Collected Long-Term Subsidence Cases and Subsidence Development at Middle Point over Chain Pillar System**

| Case No. | Coal Seam | Mining Depth | Panel Width* | CPS** Width | Mining Height | ALPS SF | Subsidence, ft | | | Percent Increment | Time*** Elapsed |
|---|---|---|---|---|---|---|---|---|---|---|---|
| | | | | | | | Time 0 | Last | Increment | | |
| 1 | Pittsburgh | 675 | 940 | 185 | 6.50 | 2.22 | -0.19 | -0.20 | 0.01 | 4.2% | 10 |
| 2 | Pittsburgh | 859 | 940 | 182 | 6.50 | 1.53 | -0.52 | -0.66 | 0.14 | 26.9% | 45 |
| 3 | Pittsburgh | 677 | 940 | 185 | 6.50 | 2.21 | -0.39 | -0.79 | 0.40 | 102.8% | 206 |
| 4 | Pittsburgh | 680 | 895 | 185 | 6.50 | 2.20 | -0.25 | -0.68 | 0.43 | 170.0% | 426 |
| 5 | Herrin #6 | 725 | 600 | 200 | 9.90 | 1.62 | -0.50 | -1.44 | 0.94 | 188.0% | 1044 |
| 6 | Herrin #6 | 384 | 645 | 130 | 6.29 | 3.14 | -0.24 | -0.32 | 0.08 | 33.3% | 33 |
| 7 | Herrin #6 | 356 | 645 | 130 | 6.95 | 3.24 | -0.29 | -0.42 | 0.13 | 44.8% | 91 |
| 8 | Herrin #6 | 362 | 645 | 130 | 6.17 | 3.48 | -0.23 | -0.31 | 0.08 | 34.8% | 286 |

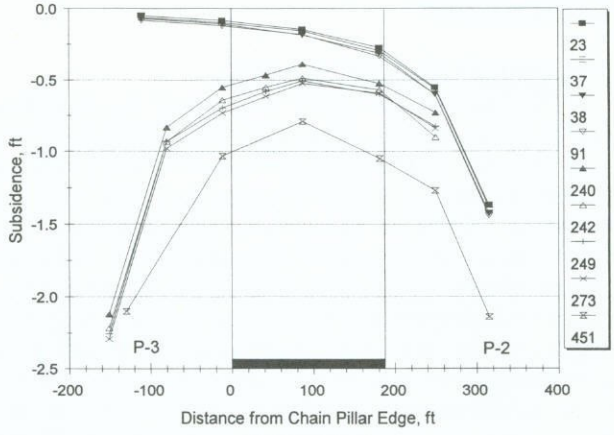
* Average width of the two adjacent longwall panels

** CPS - Chain pillar system between two adjacent longwall panels

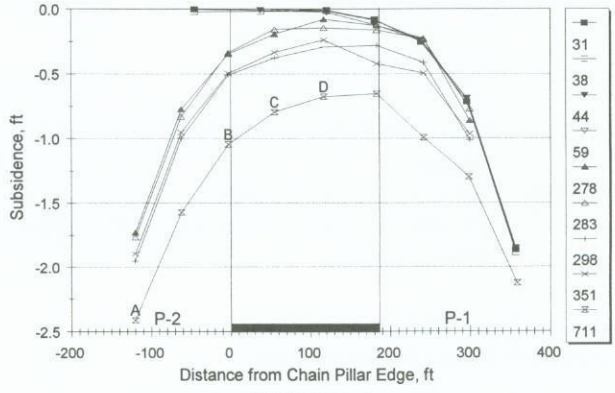
*** Time Elapsed - Days after quasi-stable state is reached after the second panel has been mined




(a) Case No. 1




(b) Case No. 3




(c) Case No. 4

**Fig. 3 Measured Subsidence Profiles over Three Chain Pillar Systems Between Four Successive Longwall Panels in the Pittsburgh Seam. Panel P-1 was Mined First and P-4 the Last.**

$S_u$ - ultimate final subsidence
$S(t)$ - subsidence at time $t$

By solving the differential equation with the initial condition of $S(0) = S_q$ ($S_q$ is the quasi-final subsidence at the point), the mathematical expression for subsidence at a surface point and at time $t$ can be obtained as the following:

$$S(t) = S_u - (S_u - S_q)e^{-ct} \qquad (4)$$

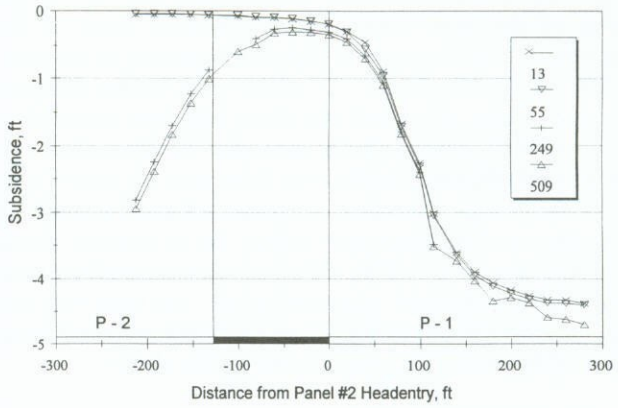



**Fig. 4 Measured Subsidence Profiles over the Chain Pillar System Between Two Longwall Panels in Herrin #6 Seam (Case No. 8)**

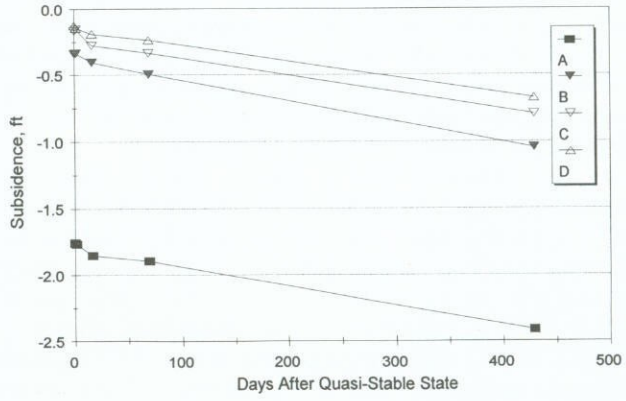



**Fig. 5 Long-term Subsidence Development Curves at Four Points for Case No. 4**

In this equation, $S_u$ and $c$, and sometimes $S_q$, are unknown terms but can be back-calculated from a measured development curve of the long-term subsidence process as those shown in Fig. 5. Mathematically, only three data points are required to define the development curve. However, since the change in subsidence during the process is normally small, the measurement errors, which could be very significant compared to the magnitude of the long-term subsidence, could make the determination using back-calculation method very unreliable. Redundancy in data points are needed in order to produce a reliable relation using non-linear regression technique.

## Chain Pillar Stability Factor vs. Long-Term Subsidence

The data presented in Figs. 3 and 4 and in Table 1 show that a significant long-term subsidence can be observed in some cases while in other cases its existence is doubtful in terms of the absolute increments. In search for the possible causes for such uncertainty, the stability factor for each of the longwall chain systems for the collected cases is calculated using the ALPS method (Mark, 1992). The determined ALPS stability factors ($SF$) as listed in Table 1 range from 1.53 to 3.48. The ALPS stability factor is an indicator for the loading intensity to which the chain pillar system is subjected. The smaller the stability factor is, the more intensely the chain pillar is loaded.

The measured long-term subsidence at the middle point of the chain pillar system for each of the cases is also normalized by the measured quasi-final subsidence and shown in Table 1. The normalized long-term subsidence (i.e., $\frac{S(t)-S_q}{S_q}$ ) is plotted against the elapsed time after the quasi-stable state in Fig. 6. It is interesting to note that there is no discernible distribution pattern and the long-term subsidence is insignificant for the three cases with APLS *SF* larger than 3. However, those cases with ALPS *SF* less than 3 (**Caution**: do not regard *SF* = 3 as a critical value for causing long-term subsidence) show a much clear distribution pattern as the dashed line in the figure suggests. This phenomena agree well with the creep deformation characteristics in rock mechanics. The larger is the applied load, the higher will be the creep rate and the faster could be the long-term subsidence process.

The shape of the suggested curve in Fig. 6 also agrees well with the following transferred form of Eq. 4, an exponential decaying function:

$$\frac{S(t)-S_q}{S_q} = \frac{S_u-S_q}{S_q}(1-e^{-ct}) \qquad (4a)$$

This agreement indicates that Eq. 4 can be used to represent the long-term subsidence development process once the unknowns, $c$ and $S_u$, in the equation can be reliably determined. The coefficient $c$ is most possible a function of the ALPS stability factor. However, due to the limited amount of data collected so far, a reliable relationship between $c$ and ALPS stability factor can not be established, yet.

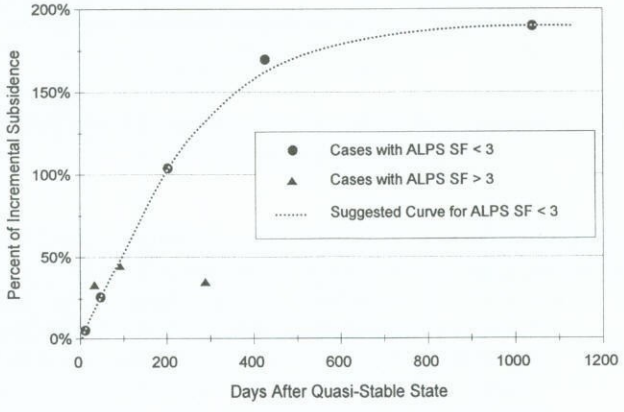



**Fig. 6 Percent of Incremental Subsidence vs. Elasped Time After the Quasi-Stable State is Reached**

## EFFECTS OF LONG-TERM SUBSIDENCE ON SURFACE STRUCTURES

It has been a well known fact that uniform surface movements (i.e., subsidence and horizontal displacement) will not cause problems to most surface structures. The integrity, stability and functionality problems developed on most of the subsidence influenced structures are caused by surface deformations (i.e., slope, strain and curvature). This section will assess the possible effects of long-term subsidence on existing and structures constructed after mining of the longwall panels. Deformations derived from the measured subsidence data in case No. 4 are used in this assessment. This case is chosen because a fairly long time has elapsed after mining and the relative increase in subsidence is the maximum among the cases. The largest changes in surface deformations are expected in this case.

### Surface Slope

Three derived surface slope profiles are shown in Fig. 7 for the following three time stages: (1) subsidence process due to mining of panel P-1 has reached quasi-stable state, (2) subsidence process due to mining of panel P-2 has reached quasi-stable state, and (3) last survey which was conducted 426 days after stage 2. The difference in surface slope between stages 2 and 3 is caused by the long-term subsidence.

Figure 7 shows varying amount of reduction of the surface slope from stage 2 to stage 3 along this entire monument line. Therefore, the long-term subsidence process actually reduces the slope on an existing structure located in this area. The maximum reduction in slope is about 0.2%. For a structure constructed after stage 2, this structure will experience a surface slope equal to the difference between stages 2 and 3 with the maximum being about 0.2%. A slope less than 1% would have no effect on the living condition of any residential structures and has very little influence on the other types of structures. Therefore, effects of the slope caused by the long-term subsidence process on new structures will be very minor, if any.

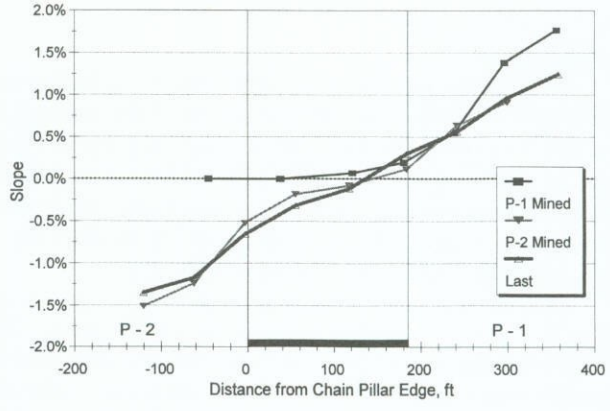



**Fig. 7 Measured Surface Slope at Different Time Stages in Case No. 4**

### Surface Curvature

The derived surface curvature profiles for the same three time stages are shown in Fig. 8. A positive curvature indicates that the surface is in convex bending. Figure 8 shows that the peak curvatures at stage 2 are $6.8\times10^{-5}$ and $9.0\times10^{-5}$ 1/ft on panels P-1 and P-2 sides, respectively. Since the measured surface curvatures near the edges of the chain pillar system at stage 2 are larger than the critical value of $6\times10^{-5}$ 1/ft (Luo and Peng, 1991), the surface curvature has potential to cause problems to residential structures located around these

locations at that time. However, due to the development of long-term subsidence, the surface curvatures at the same two locations have decreased to $5.8x10^{-5}$ and $7.3x10^{-3}$ 1/ft, respectively. Although the surface curvature near the tailentry of panel P-2 is still capable of causing problems to structures, the magnitudes of curvature has reduced as a result of development of long-term subsidence. Figure 8 also shows an increase in surface curvature from stage 2 to stage 3 over the middle portion of the chain pillar system. The maximum increase is about $3.1x10^{-5}$ 1/ft. Such amount of curvature will not produce any noticeable effects on new structures constructed there after stage 2.

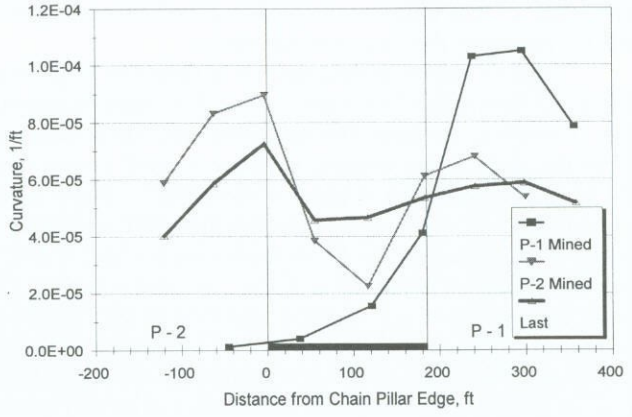



**Fig. 8 Measured Surface Curvature at Different Time Stages in Case No. 4**

## Surface Strain

Among the three types of deformations, surface strain, particularly the tensile strain, is often the No. 1 cause for problems developed on most structures or structural parts that have direct contact with ground. Previous studies on subsidence effects on residential structures (Luo and Peng, 1991) have shown that critical strain for brick or block house walls is $2x10^{-3}$ ft/ft while that for stone walls is $3x10^{-3}$ ft/ft.

The derived surface strain profiles for case No. 4 are shown in Fig. 9. A positive value is for tensile strain. The strain profiles for stages 1 and 2 indicate that structures located near the strain peaks could be seriously impacted. After the development of long-term subsidence, though the surface strain is still capable of causing problems to structures, the severity could be reduced significantly. For a structure built over the chain pillar system after stage 2, it could experience the differential strain between stages 2 and 3 as shown in Fig. 10. It shows that the strain caused by long-term subsidence process is insufficient to influence most structures to any noticeable degree.

## CONCLUSIONS

Eight sets of subsidence data measured over and near chain pillar systems between longwall panels for extended periods after mining have been studied for long-term subsidence. The following conclusions can be made from this study:

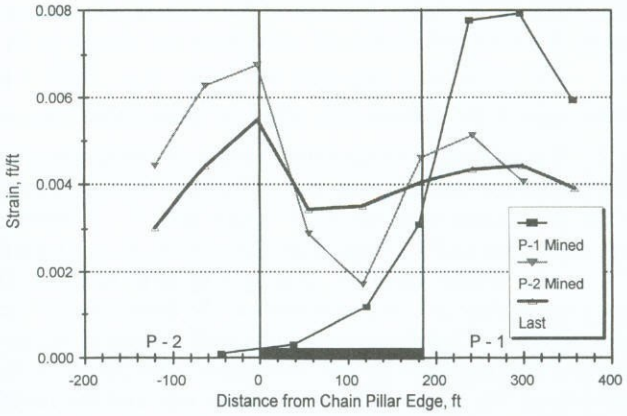



**Fig. 9 Measured Surface Strain at Different Time Stages in Case No. 4**

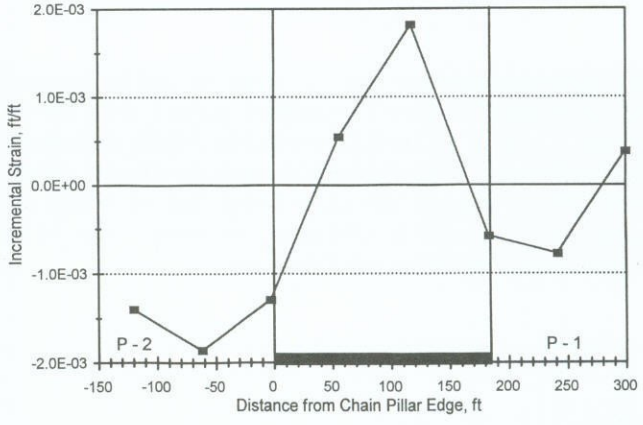



**Fig. 10 Incremental Surface Strain Caused by Long-Term Subsidence Process in Case No. 4**

- Long-term subsidence process appears to exist based on the collected cases. Some of the cases showed significant amount of long-term subsidence while other cases indicated very minor amount. Possible factors contributing to long-term subsidence include seam depth, pillar width, coal strength and overburden strata property, floor bearing capacity, etc.
- Assuming all other factors being equal, the magnitude and development process of the long-term subsidence appear to be heavily dependent on the loading intensity on the chain pillar system which is expressed by the ALPS stability factor. For those cases with low ALPS stability factors, the long-term subsidence is apparent and the development process agrees with the proposed exponential decaying function well.
- The development of long-term subsidence generally reduces the magnitudes of the deformations (i.e.,

slope, strain and curvature) to be experienced by existing structures located over and near the chain pillar system. Therefore, the severity of subsidence influences on these structures will be gradually lessened. The deformations induced by the long-term subsidence process alone are very unlikely to cause problems to structures built after mining due to their relatively small magnitudes.

- Continued research efforts should be made to collect more field data under varying conditions so that a reliable predictive method for long-term subsidence process can be developed.

## REFERENCES

Luo, Y. and S.S. Peng, 1991, "Protecting a Subsidence Affected House -- A Case Study," *Proc. of VIII Congress of the International Society for Mine Surveying (ISM)*, Ed. R.W. DeVore, University of Kentucky, Lexington, KY, pp. 297-300.

Luo, Y. and S.S. Peng, 1992, "A Comprehensive Dynamic Subsidence Prediction Model for Longwall Operations", *Proc. 11th International Conference on Ground Control in Mining*, Ed. N.I. Aziz and S.S. Peng, University of Woolongong, Woolongong, Australia, pp. 511-516.

Mark, C., 1992, "Analysis of Longwall Pillar Stability (ALPS) -- An Update," *Proc. Workshop on Coal Pillar Mechanics and Design*, USBM, pp. 238-249.

Mehnert, B.B, D.J. Van Roosendaal and R.A. Bauer, 1992, "Long-term Subsidence Monitoring over a Longwall Coal Mine in Southern Illinois," *Proc. Third Workshop on Surface Subsidence Due to Underground Mining*, Ed. S.S. Peng, West Virginia University, pp. 311-316.

# Subsidence Prediction Influence Assessment and Damage Control

*Yi Luo,* Research Assistant Professor
*Syd S. Peng,* Chairman and Charles T. Holland Professor
Department of Mining Engineering
College of Engineering and Mineral Resources
West Virginia University
Morgantown, WV

## ABSTRACT

An extensive subsidence research program conducted by the authors has greatly improved the accuracy and the capabilities of subsidence prediction under complicated mining and surface conditions. The techniques developed for assessing and mitigating subsidence influences on various surface structures have been applied in numerous cases with a very good record of success.

## INTRODUCTION

Total extraction of a coal seam using longwall mining or room-and-pillar mining with pillar extraction tends to disturb the overburden strata and causes immediate surface subsidence. Depending on various factors, such subsidence events may or may not have the potential to cause problems to surface structures. Surface subsidence research conducted by the authors has demonstrated that in order to effectively and efficiently minimize the subsidence influences on surface structures, the following techniques should be applied systematically:

- *Methods for accurately predicting surface subsidence under varying mining and surface conditions.* Success in dealing with the issues of subsidence depends primarily on the accurate prediction of the magnitude, distribution and timing of surface subsidence. By studying the subsidence basins produced by different mining plans, the possible subsidence effects on surface structures can be greatly reduced.
- *Techniques for assessing the subsidence influences on surface structures.* The probability and severity of subsidence influences on a structure of interest need to be assessed before it is undermined. Due to the large differences in types, design, material and construction of the structures as well as variations of movements and deformations to be experienced by the structures, the different assessment techniques are required.
- *Techniques for mitigating subsidence influences.* If the assessment indicates that the subsidence influences on a structure exceed the structure's tolerable level in terms of its integrity, stability and functionality, proper mitigation techniques should be designed and implemented to reduce the subsidence influences on the structure.

This paper describe the efforts and results of a subsidence research program conducted by the authors.

## SUBSIDENCE PREDICTION

Accurate prediction of surface subsidence caused by underground mining is required for assessment of the subsidence influences and is the basis for the design of effective and efficient mitigation measures. In the past a great majority of subsidence research have been concentrated on the prediction of final subsidence over a single longwall panel with a relatively flat surface. The prediction models produced by those researches have limited value for practical applications because of varying and complicated mining, geological and topographical conditions. In order to improve the prediction accuracy, the authors have collected more than 200 longwall subsidence cases all over the US coal fields through an intensive subsidence monitoring program and from various other sources. These data were used to continuously refine and improve a PC-based program package, CISPM (Comprehensive and Integrated Subsidence Prediction Model) developed previously by the authors (Peng and Luo, 1992). This program package has a unique and rich set of capabilities for meeting nearly all of the subsidence prediction requirements in underground coal mining employing high or total extraction methods in the US. It is very user-friendly requiring neither particular skills in computer operations nor in-depth knowledge of subsidence theory. It has been proven fairly accurate according to the feedback from its domestic and international users and according to our own

subsidence monitoring data. The following important findings from our subsidence research program have been incorporated into the current version of CISPM program package:

- *Dynamic subsidence process associated with longwall mining operations.* As underground mining progresses, a surface point will experience a fairly complicated dynamic subsidence process before it becomes stable again. During the dynamic subsidence process, the magnitudes, natures and directions of the subsidence movements and deformations at the surface point change with time and their influences to structures are also time dependent. Very often the dynamic subsidence process plays a more important role in assessing and mitigating subsidence influences than final subsidence. Mathematical models have been developed to predict the entire dynamic subsidence process associated with longwall mining operations (Luo and Peng, 1992).
- *Final subsidence basin over a single and multiple longwall panels.* Most of the subsidence prediction methods have been developed for mining of a single panel only. They are unsuitable for the prediction of subsidence over multiple panels such as the longwall panels separated by chain pillar systems as normally practiced in the US. A mathematical model has been developed to predict the final subsidence basin over multiple longwall panels (Luo and Peng, 1990, 1991). This model is based on the finding that the convergence of the chain pillar systems between the longwall panels could contribute a very significant amount of subsidence in the area over and near the chain pillars.
- *Final subsidence caused by high extraction room-and-pillar mining method.* If the recovery ratio in a room-and-pillar panel is 70% or higher by partially or fully extracting the pillars in a room-and-pillar panel, immediate surface subsidence (versus the unpredictable subsidence events over low extraction room-and-pillar mines often seen as the abandoned mine subsidence) will be induced. The existing methods which have been derived from subsidence data collected over longwall panels are not suitable for subsidence prediction over high extraction room-and-pillar mines. Based on the available subsidence data collected over room-and-pillar panels, a method has been developed for the prediction of the final subsidence basin over high extraction room-and-pillar panels (Luo and Peng, 1993).
- *Studies of subsidence parameters.* The two basic components of a subsidence prediction method are the chosen mathematical models and the parameters involved in the mathematical model. The subsidence parameters often play a very important role in the prediction accuracy. However, the reported subsidence parameters often vary in very large ranges which are of little values in practical applications. Such large variations are often resulted from the use of inconsistent definitions of the subsidence parameters and inadequate determination methods. A great effort has been made in collecting subsidence data in the US coal fields, standardizing the definitions of and determining the subsidence parameters (Peng et al., 1995). Based on this study, the ranges of a number of commonly used final subsidence parameters have been greatly narrowed.

In additional to prediction of surface subsidence, tools are provided and self improvement mechanism is built in CISPM. They include data processing for subsidence survey, determination of subsidence parameters based on mining and geological information and deduction of parameters from collected subsidence data

Numerous field observations have demonstrated that complicated surface topography and steep surface slope in hilly regions have a profound impact on the ground subsidence process, often resulting in very different characteristics of subsidence basin from that on a relatively flat surface. Effort has been made to study the surface topography effects on ground subsidence process. A method has been developed for the prediction of final subsidence basin in hilly regions (Luo and Peng, 1990). Figure 1 shows a comparison of the calculated final horizontal displacement profiles with and without considerations of the surface topography. The surface elevation is also plotted at the top for reference. A much better agreement with the measured horizontal displacement in the steepest portion of the subsidence monument line has achieved when surface natural slope was considered. It should be noted that horizontal displacement often plays a much more important role in causing damages to surface structures than subsidence (i.e., vertical settlement).

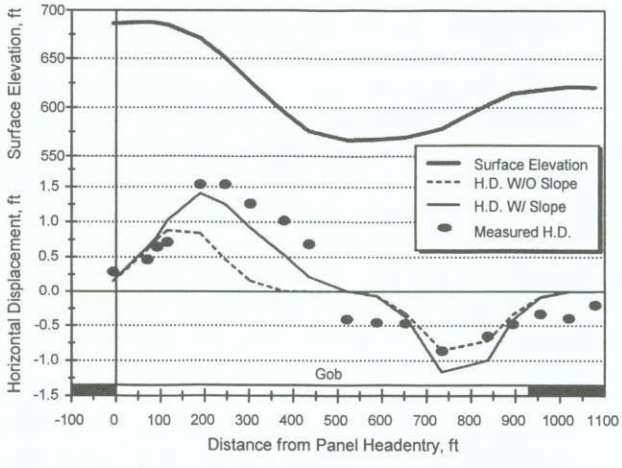



**Fig. 1 Measured vs. calculated final horizontal displacement (H.D.) profiles along a cross-section over a longwall panel with relatively steep surface slope**

## TECHNIQUES FOR ASSESSMENT OF SUBSIDENCE INFLUENCES

Research emphasis has also been placed on monitoring the interaction between the subsiding surface and various surface structures. Based on the collected data, critical deformation values for various relatively simple structures have been

established, techniques for assessing subsidence influences on those structures of large dimension and/or complexity have been developed.

A number of critical deformation values for typical residential structures (wood frame or brick super-structure on stone or concrete-block basement or foundation) in the northern Appalachian coal fields have been established. High surface tension and compression are generally responsible for cracks and buckling on the lower portion of the residential structures, respectively. High surface bending could causes problems to the super-structures such as sticky doors and windows, fissures on dry walls, peeling of old wall papers and paint. It is also found that a large tilting on floor could cause some inconveniences to the residents.

Ground cracks and bumps are caused by high surface tension and compression, respectively. Ground cracks as wide as 4 ft, though very rare, have been observed in certain locations over a few longwall panels. Generally ground cracks cause more problems (e.g., dewatering of surface streams or ponds) than the bumps. Criteria for initiating ground cracks on various ground surface have also been established.

For those structures of large dimensions and/or complicated design and construction, a more comprehensive and detailed assessment should be performed. However, due to the large variation of type, material, construction, dimension and functions of the structures, the techniques for assessing the subsidence influences on these types of structures vary considerably. Basic analysis should be performed to determine the nature and severity of the following three types of potential problems:

- *Structural integrity*: This is an indicator of mechanical failure of a structure of interest under the influence of subsidence. Ideally, the stress or strain field on the structures should be evaluated. The peak stress or strain are then compared to the permissible values of the structural material to determine the possibility of structural failure. For instance, a method has been proposed and successfully applied to assess the stress distribution on buried pipeline affected by subsidence (Peng and Luo, 1988). In cases where stress/strain fields are difficult or impossible to determine, the weakest components of the structure should be identified and empirical values are used to determine their integrity under the influence of surface subsidence.
- *Structural stability*: For those tall structures with small bases, the subsidence-induced slope could make them potentially unstable during or after subsidence process. Both the short and long term stability of the structure should be assessed. If the subsidence-induced slope could move the center of gravity of a structure out of its base, the structure is said to have lost its short-term stability. A structure loses its long-term stability if the strongest wind blowing in the direction of maximum slope caused by subsidence will be able to topple the structure.
- *Structural functionality*: The ability and level for the structures to perform their intended functions during and after subsidence may be affected by ground subsidence process. For example, subsidence could change the grade of a railroad well above its permissible grade. A conveyor belt could be rendered inoperable due to vertical and lateral alignment problems caused by the subsidence process.

The authors have applied the established criteria and the developed assessment techniques in various projects in assessing subsidence influences on various surface structures. Some examples of applying these assessment techniques are shown in Table 1.

## TECHNIQUES FOR SUBSIDENCE MITIGATION

If the assessment indicates that a structure will be adversely affected, effective and efficient mitigation measures should be designed and implemented. The following three approaches can be used to design the mitigation measures: (1) reducing surface movements and deformations in the area of concern to an acceptable level by modifying the mining plan (e.g., leaving a support area under the structure), (2) reducing transmission of movements and deformations from ground to the structure of interest (e.g., trenching and plan-fitting), and (3) reinforcing the structure so that it can tolerate higher

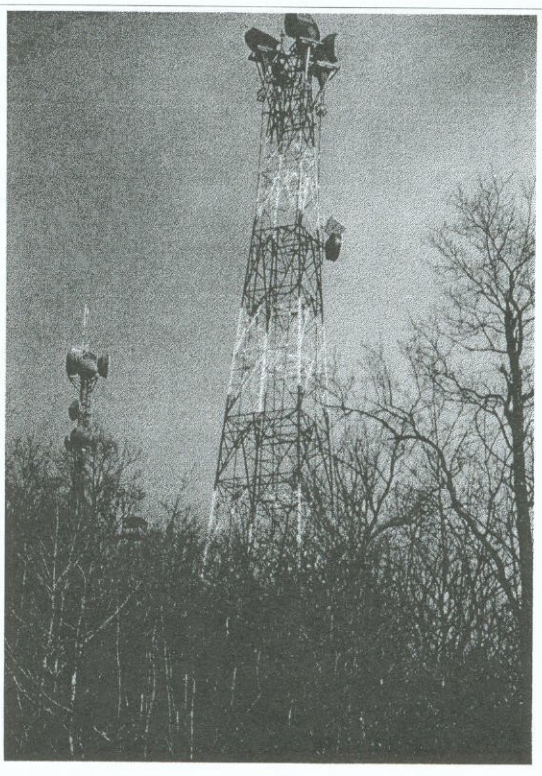


**Fig. 2 This telecommunication transmission tower, about 200 ft tall, was located on a steep slope of a mountain peak. It was undermined by a longwall panel. In order to protect this tower, trench was dug around one of its legs and reinforcement beams were installed at the base. Despite of ground cracks observed nearby, there was no damage on thestructure and its service was kept open all time.**

Table 1 Some Examples of Subsidence Influence Assessments and Results

| Structure or Feature | Descriptions | Major Concerns | Conculsions and Recommendations | Results |
|---|---|---|---|---|
| Residential Structures | More than 50 houses over or near longwall panels | Structural integrity and functionality | Verying damage potentials and mitigation measures recommended for about 30 structures | Accurate assessments and successful protection |
| Oil pipeline | Buried oil pipeline over 7 longwall panels | Structural integrity | Damage potential high. Mitigation measures recommended. | Feedback not available |
| Concrete water pipeline | Main transmission pipeline over 3 longwall panels | Structural integrity and functionality | Damage potential high. Mitigation measures and alternatives recommended | Alternative plan adopted |
| Cast iron water pipeline | Two pipelines over 2 longwall panels | Structural integrity and functionality | Damage potential moderate. Mitigations recommended. | Not yet undermined |
| Steel water pipeline | Main water supply line over 4 longwall panels | Structural integrity and functionality | Damage potential high. Mitigation measures recommended. | Protection successful |
| Plastic and steel gas pipeline | Low pressure distribution line over 3 longwall panels | Structural integrity and functionality | Damage potential for the steel pipe portions. Mitigation recomeended. | Mining in progress |
| Lake | A large lake over 11 planned longwall panels | Land area to be submerged by water after subsidence | About 400 acres of land will be submerged or ponded | Successfully undermined |
| Water ponds | 2 water ponds over 2 longwall panels | Stream dewatering, potential underground mine workings flooding | Possibility of dewatering is low | Accurate assessment |
| Streams | 3 streams over 7 longwall panels | Stream dewatering, potential underground mine workings flooding | Varying potential of stream dewatering | Accurate assessment |
| Mine refuse facility | Over 3 longwall panels with high embankment | Feasibility of longwall mining under | Support area recommended under the embankment, feasible to mine under pond | Successfully undermined |
| Mine refuse facility | Over 3 longwall panels previously mined | Feasibility of building the facility over the mined panels, long-term subsidence | Effects of long-term subsidence is very minor. Construction is feasible. | Feedback not available |
| Mine refuse facility | Over 3 planned longwall panels with very shallow overburden | Feasibility of longwall mining under | Safety questionable. Alternative mining plans suggested. | Not yet undermined |
| Railroad and bridge | A railroad over 4 longwall panels | Subsidence influences and operation safety | Influences could be strong. Monitoring and Mitigations recommended | Successfully protected |
| Power transmission system | 3 towers (80 to 120 ft tall) and one substation over two longwall panels | Integrity, stability, functionality and operation safety | Anticipated structural problem on one tower and stability problem on another | Accurate assessment |
| Telecommunication transmission tower | 200-ft tall tower located over a longwall panels (Fig. 2) | Integrity, stability, functionality | Strong influences. Mitigation measures recommeneded and implemented | Accurate assessment and successful protection |
| Highway and bridge | Highway across the end areas of 3 longwall panels | Subsidence influences | Very minor influence on highway. Questionable on bridge | Accurate assessment |
| Primary and secondary roads | Four roads over 8 lonwall panels | Subsidence influences | Varying degrees of influences. mitigations recommended for 2 roads | Accurate assessment |

movements and deformations without being damaged (e.g., tension cable method). Mitigation measures for various structures affected by subsidence have been developed and tested in field conditions. Table 2 shows some of the structures that have been successfully protected with direct involvement of the authors.

## Design of Support Area

By leaving an adequate area of coal unmined or partially mined under the structure to be protected, the surface movements and deformations in the area of the structure can be kept below the permissible level of the structure. The Pennsylvania method for designing support area is one example of applying this concept. However, the PA method over-designs the support area when mining depth is more than 350 ft. Based on a large number of collected longwall subsidence cases, a new method for designing support area has been proposed as shown in Fig. 3 (Peng and Luo, 1993) and successfully applied for two large structures (Table 2).

## Mitigation Techniques for Residential Structures

A number of simple but effective mitigation measures have been frequently applied by the authors in protection of nearly 30 residential structures (Table 2). Among them, *com-*

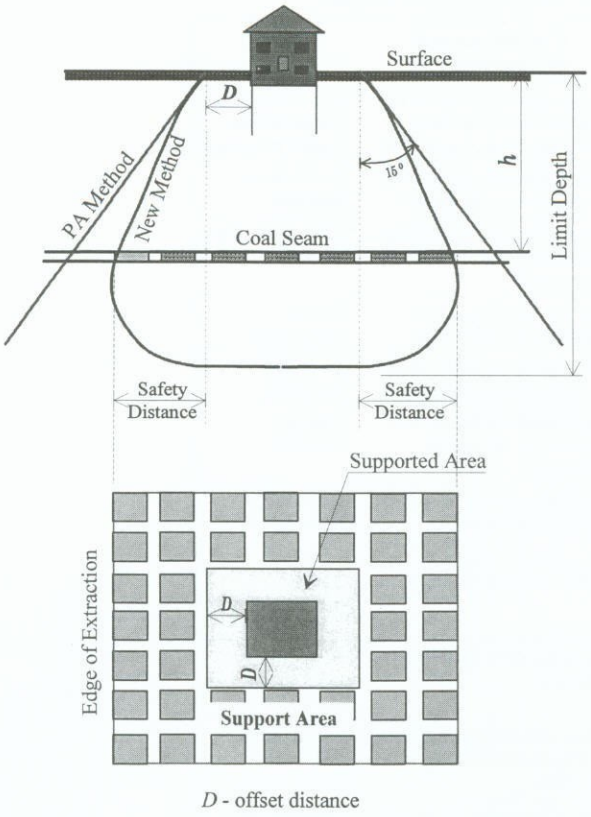



**Fig. 3 A method to design support area for surface structure has been developed based on the analysis of a large number of longwall subsidence cases. The support area designed using this method is usually smaller than that using PA method**

*pensation trench method* is used to absorb surface tension or compression that could be transmitted to the structure from its surrounding ground. This method has been proven effective to reduce problems on the structural parts that have direct contact with the subsiding ground, such as basement and foundations. *Plane-fitting method* is to protect the super-structure of a house from being damaged by the bending and twisting actions associated with subsidence process. During the implementation of this method, the house super-structure is placed on a time-dependent inclined plane so that the super-structure is free of stress while the required amount of adjustments are kept minimized. *Tension cable method* is used to strengthen the structures so that they can tolerate higher surface tension and bending. Figure 4 shows a brick house that were successfully protected using a compensation trench and two tension cables.

## Mitigation Measures for Buried Pipelines

Ground subsidence process often has the potential to cause damages to buried pipelines. Assessments of subsidence influences on various buried pipelines have indicated that the strain transmitted from the surrounding soil to the pipeline is always the No. 1 source of stress on the pipeline (Luo et al., 1997). Therefore, reduction of the strain transmission is the most effective method in the protection of buried pipelines. Uncovering pipeline only in the sections where the estimated stress is higher than the permissible stress of the pipeline material can greatly reduce the pipeline stress contributed by the ground strain. Such partial uncovering method has been successfully applied in the protection of a 7,800-ft section of water supply pipeline undermined by four longwall panels (Table 2).

## Mitigation Measures for Railroad

Ground subsidence is capable of causing serious problems to railroads if proper cautions are not taken. A partial

**Table 2 Some Examples of Successfully Protected Structures**

| Structures Protected | Descriptions | Mitigation Measures Employed | Results | Monitoring Performed |
|---|---|---|---|---|
| Residential Structures | 25 houses, 2 garages and 1 swimming pool over 19 longwall panels | plane-fitting, compensation trench, tension cable, external bracing | Very good rate of success. Figure 4 is one of the examples | Subsidence |
| Railroad | About 11,000 ft long over 4 longwall panels | Partial lifting | It was kept operating during subsidence. Great saving in material and labor costs | Subsidence |
| Railroad bridge | 130 ft, three sections | A 440x510 $ft^2$ support area under the bridge | Bridge not affected at all | Subsidence |
| Water pipeline | About 7,800 ft long 12-inch steel pipeline over 4 longwall panels | Partial uncovering | Service has never been intrrupted | Subsidence, strain |
| Overland conveyor belt system | About 1,400 ft long erected between 16 and 50 ft above ground level with a 300-ton transfer tower over a longwall panel | Uncovering support bases, loosening bolts at the bases, lateral stabilization | Despite of large surface movement, it required only some minor repairs before being put into operation again | Subsidence, strain, tilting |
| Telecommunication transmission tower | About 200 ft high located on the top of high mountain and between two longwall panels | Compensation trench, strengthening tower base | Despite of ground cracks observed nearby, no damage observed on the structure and service not interrupted | Visual observation |
| Coal refuse disposal facility | Large slurry pond with an embankment nearly 200 ft high. | A 1,300x1,930 $ft^2$ support area under the embankment only | The integrity, stability and functionality of the facility not affected | Subsidence |

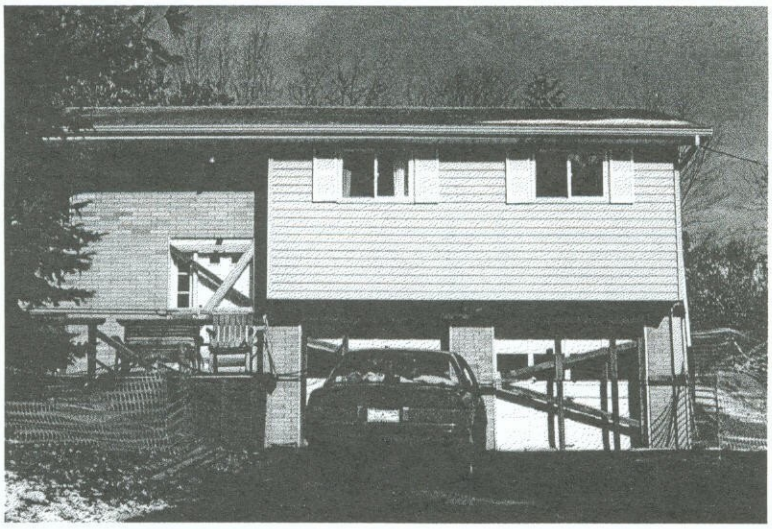


**Fig. 4 This brick house was successfully protected by a compensation trench and two tension cables. The placements of the trench and cables and the required tension in the cables were determined by subsidence simulations.**

lifting method has been developed. The original elevation profile of the railroad, the predicted final subsidence profile and the permissible railroad grade are considered in determining the required adjustment along the section of railroad to be affected. This method has been applied to protect a section of railroad about 11,000 ft long undermined by four longwall panels (Table 2). The maximum subsidence at the site was about 4.5 ft. Adjustment on the railroad was only recommended in some sections much shorter than the total length of the railroad affected by subsidence with the maximum adjustment being about 2.5 ft only. As a result of implementing the partial lifting method, the subsided and adjusted railroad was kept smooth for safe railroad operation while the required adjustment was kept to a minimum.

## A CASE STUDY

This section shows a case of the protection of a railroad over a longwall panel. The longwall panel was 930 ft wide mining a coal seam of about 6.5 ft thick. The overburden depth at the site was about 680 ft. The layout of the railroad over the longwall panel is shown in Fig. 5. The predicted final subsidence at the site is also plotted in this figure with the maximum subsidence being about 4.2 ft which matched very well with the measurements. The elevation profile of this section of railroad before subsidence is shown in Fig. 6. Based on the predicted final subsidence, original elevation and the permissible grade of 0.7%, the final railroad profile requiring the minimum amount of vertical adjustment was determined before it was undermined. In preparation, a large proportion of the required amount of gravel to raise the railroad was shipped to the site and spread in the sections needing the most amount of adjustment. During the active subsidence period, the railroad was monitored and vertical adjustment was made accordingly. A temporary speed limit of 5 mph was also posted as a precaution. Figure 6 shows one set of recommended adjustment during the active subsidence period and the elevation profiles of the railroad before and after the implementation of the recommended adjustment. By implementing the recommended adjustment, the maximum railroad grade was reduced from about 1.0% to the permissible 0.7% (Fig. 7). The railroad service was never interrupted during the entire subsidence process. Figure 8 shows a fully loaded coal train was passing the section of subsiding and adjusted railroad.

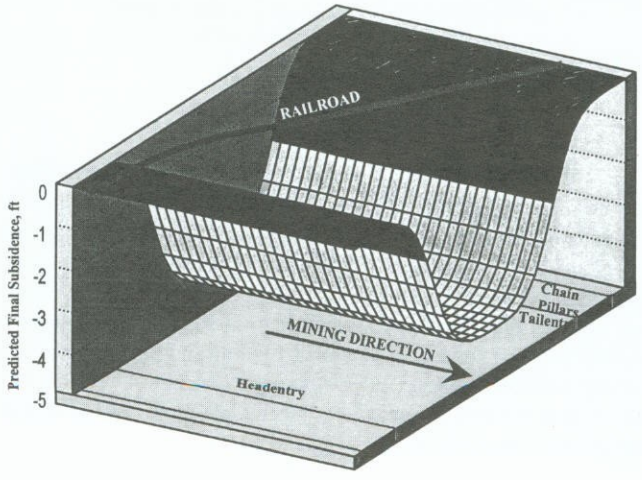



**Fig. 5 Layout of the railroad over the longwall panel and predicted final surface subsidence at the site**

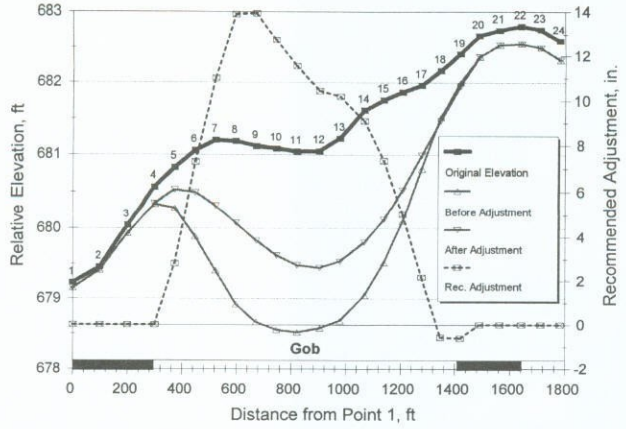



**Fig. 6 Elevation profiles of the railroad and one set of recommended vertical adjustment during the active subsidence period. Using the partial lifting method, the required adjustment was kept to a minimum while the railroad was smooth.**

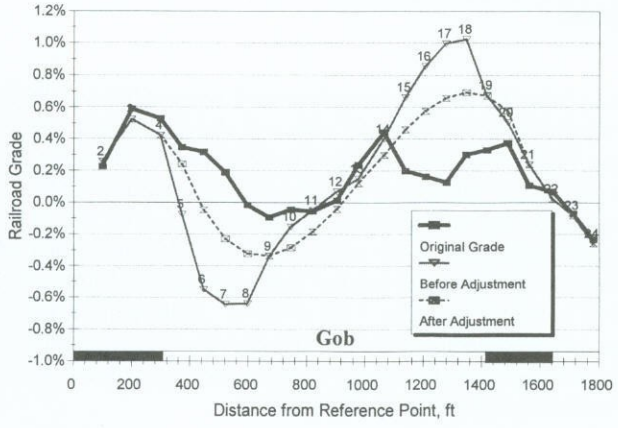



**Fig. 7 Grade profiles of the subsiding railroad before and after implementing the recommended adjustement. The maximum grade of the adjusted railroad was kept within the permissible grade of 0.7%**

## SUMMARY

Subsidence prediction, influence assessment and damage control have come a long way. A systematic subsidence research program coupled with intensive field monitoring and extensive data collection during the past twenty years have produced vast amount of quality data and knowledge. Numerous case studies have demonstrated that using these research results, surface subsidence caused by full and high extraction mining methods and its effects can be predicted with confidence, and mitigation measures can be selected, designed and implemented successfully.

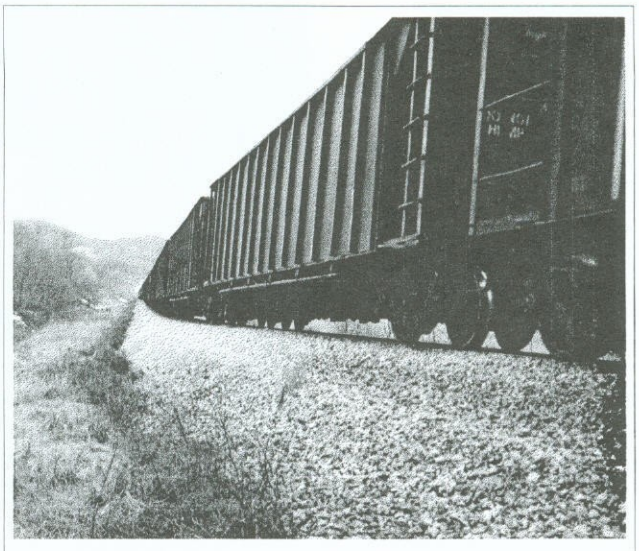


**Fig. 8 This loaded coal train was passing through a section of subsiding railroad. The railroad was successfully protected using the partial lifting method.**

## REFERENCES

Luo, Y. and S.S. Peng, 1990, "A Mathematical Model for Predicting Final Subsidence Basin in Hilly Regions," *Proc. AEG National Symposium on Mine Subsidence -- Prediction and Control*, Ed. C.D. Elifrits, Association of Engineering Geologists, pp. 223-231 (Republished in AEG Bulletins).

Luo, Y. and S.S. Peng, 1990, "A Mathematical Model for Predicting Subsidence over Chain Pillars Between Mined-out Longwall Panels," *Proc. AEG National Symposium on Mine Subsidence -- Prediction and Control*, Ed. C.D. Elifrits, Association of Engineering Geologists, pp. 247-257 (Republished in AEG Bulletins).

Luo, Y. and S.S. Peng, 1991, "Some New Findings from Surface Subsidence Monitoring over Longwall Panels," *Mining Engineering*, SME, Littleton CO, 1991 (10), pp. 1261-1264.

Luo, Y. and S.S. Peng, 1992, "A Comprehensive Dynamic Subsidence Prediction Model for Longwall Operations", *Proc. 11th International Conference on Ground Control in Mining*, Ed. N.I. Aziz and S.S. Peng, University of Woolongong, Woolongong, Australia, pp. 511-516.

Luo, Y. and S.S. Peng, 1993, "Using Influence Function Method to Predict Surface Subsidence caused by High Extraction Room and Pillar Mining", *Proc. 7th International FIG Symposium on Deformation Measurement*, Ed. W.F. Teskey, University of Calgary, Calgary, Alberta, Canada, pp 342-353.

Peng, S.S. and Y. Luo, 1988, "Determination of Stress Field in Buried Thin Pipelines Resulting from Ground Subsidence due to Longwall Mining," Mining Science and Technolgy, Vol. 6, pp. 205-216.

Peng, S.S. and Y. Luo, 1992, "Comprehensive and Integrated Subsidence Prediction Model - CISPM (V2.0)," *Proc. 3rd Workshop on Surface Subsidence Due to Underground Mining*, Ed. S.S. Peng, West Virginia University, Morgantown, WV, pp. 22-31.

Peng, S.S. and Y. Luo, 1993, "A New Method for Designing Support Area to Protect Surface Structures over Underground Coal Mining Areas," *AIME-SME 1993 Transactions*, Vol. 294, pp. 1927-1932.

Peng, S.S., Y. Luo and Z.M. Zhang, 1995, "Subsidence Parameters -- Their Definitions and Determination," a paper presented at 95 AIME-SME annual meeting, Denver, CO, 7 pp. (to be published in *Mining Engineering*)

# Formation of Face Headings Using Stress Relief at Asfordby Mine

*John Cassie,* Geotechnical Engineer
Rock Mechanics Technology Ltd.
Burton-on-Trent
UNITED KINGDOM

*Andy McLennan,* Rock Bolting Engineer
Asfordby Mine
RJB Mining (UK) Ltd.
UNITED KINGDOM

## ABSTRACT

The condition of roadways in the Deep Main seam at Asfordby Mine, operated by RJB Mining (UK) Ltd, is strongly dependant on drivage direction relative to the maximum horizontal stress. The mine is laid out with gate roads driven approximately parallel to the maximum horizontal stress giving favourable drivage conditions. This has led to particulary difficult conditions for face installation headings which have to be driven to an increased width and at a high angle to the horizontal stress.

A solution to the formation of face headings is described making use of stress relief with the face heading being driven in the zone of reduced stress surrounding a previous heading. In implementing this solution use was made of results from computer modelling and detailed monitoring of roadway behaviour. High reinforcement densities including cable bolts were used in supporting the headings.

The experience provides an example of a traditional technique being applied more scientifically. The results obtained demonstrate the effect of stress relief and reinforcement methods in altering drivage conditions and suggest possible alternative strategies for the formation of future face headings in these conditions.

## INTRODUCTION

Asfordby mine is located in North-East Leicestershire, England. It lies some 20 Kilometres to the South East of Nottingham and 3 kilometres from Melton Mowbray. Site preparation began in 1984 and by 1989 underground roadways were being developed. Two shafts access the workable coal seams which are the Deep Main at a depth of approximately 520 m below the surface and the Parkgate some 25 m lower. The initial planning, shaft sinking and development was completed by British Coal and the mine was brought into longwall production just prior to the privatisation of the British coal mining industry when it was sold to RJB Mining (UK) Ltd.

Following shaft sinking there was an extended period of underground development. It was found that roadway conditions were strongly dependant on drivage direction as a result of non-uniform horizontal stress magnitudes and the sensitivity of roadway behaviour to them. In order to maximise the length of drivage in the preferred direction, the mine was laid out, as far as possible, with gate roads driven approximately parallel to the direction of the maximum horizontal stress. As a result face headings have to be driven in an unfavourable direction.

The first purpose driven face heading at the mine, for 102's district, encountered sufficiently poor conditions for it to be abandoned. A strategy involving the use of stress relief was adopted to redevelop the face heading. A change in planned face length from 250 m to 60 m resulted in four headings being driven in close proximity to each other. The wide range of conditions obtained demonstrate the effect that stress relief and reinforcement methods can have in modifying drivage conditions.

## GEOLOGICAL CONDITIONS

The general geological structure of the mine and the in-situ stress conditions were established by an extensive programme of surface boreholes and seismic surveys, together with the use of in-seam seismic during development. The main features are that the seams incrop into the Permo-Trias aquifer to the South and West of the take and that the predominant fault trend is NE-SW, figure 1.

### Lithology

The Deep main seam which is currently being worked has an average thickness of 2.5 m. It is underlain by a particularly weak mudstone seatearth, generally 3 m thick or more. The immediate roof consists of approximately 0.8 m of weak mudstone

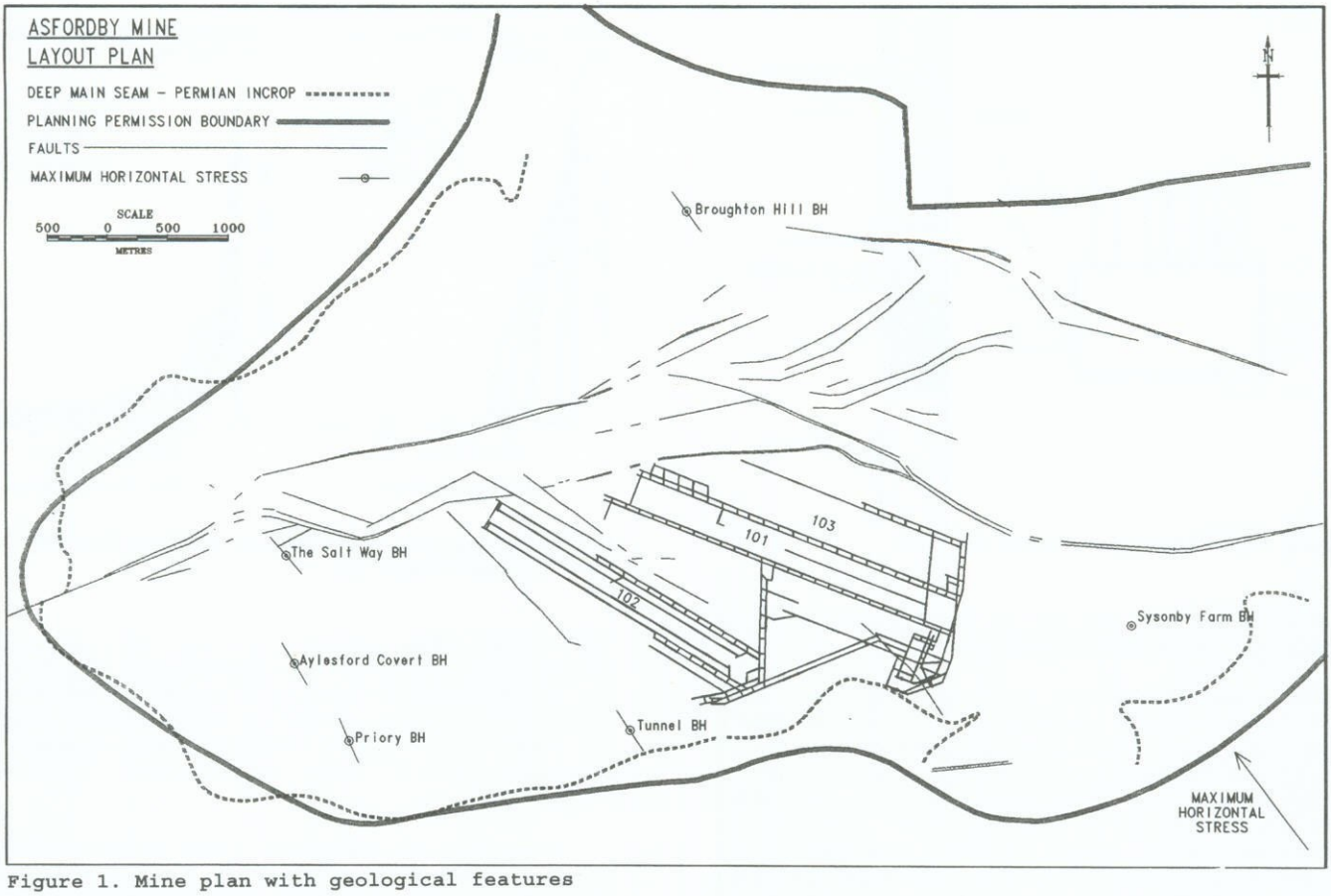



**Figure 1. Mine plan with geological features**

(termed clod) followed by more competent mudstones/siltstones and fine sandstones providing two or more clearly defined parting planes. A strata section together with the profile of gate road drivages relative to the seam is shown in figure 2. The clod is cut down on drivage to a parting which provides a good horizon for the installation of roof bolts and a clear plane of movement for decoupled ribs. Floor coal is initially left which provides a good running surface for the heading machinery which has difficulties on the seatearth particularly when water is present. In most roadways the remaining coal is removed during subsequent dinting.

Laboratory tests on samples obtained close to the face headings gave uniaxial compressive strengths of 35-50 MPa and elastic moduli of 6-11 GPa for the siltstones and sandstones in the roof with occasional stiffer and stronger sandstone samples. The friable nature of the clod and seatearth have prevented intact specimens being obtained for testing but they are considered to be significantly weaker.

### In-situ stress

Data on in-situ stresses has been obtained from hydraulic fracture testing in surface boreholes (1). The results in table 1 show a ratio of 1.75-1.93 between maximum and minimum horizontal stress components with the maximum lying on a bearing of 319°-327° azimuth. The magnitude of the maximum horizontal component ranges between 12.7-21.0 MPa with evidence of increasing values in the northern area of the mine.

**Table 1. Measured in-situ horizontal stresses**

| Borehole | Maximum horizontal | Minimum horizontal | Stress ratio | Bearing of maximum |
|---|---|---|---|---|
| Aylesford Covert | 13.7 | 7.3 | 1.88 | 324 |
| Broughton Hill | 21.0 | 10.9 | 1.93 | 325 |
| Sysonby Farm | 13.9 | 7.7 | 1.80 | - |
| The Priory | 12.7 | 7.2 | 1.75 | 326 |
| The Saltway | 16.6 | 8.8 | 1.89 | 319 |
| Tunnel | 14.3 | 7.7 | 1.86 | 327 |

## MINING METHODS AND CONDITIONS

### Drivage methods and support

The majority of the mine roadways are driven by continuous miners feeding a shuttle car which delivers onto a belt-end. When the shuttle distance becomes excessive the initial floor heave is dinted using the miner then the conveyor is extended. Roof bolts are installed by hand held pneumatic leg type machines, the mine also operates a bolter miner with hydraulic drill rigs. Average

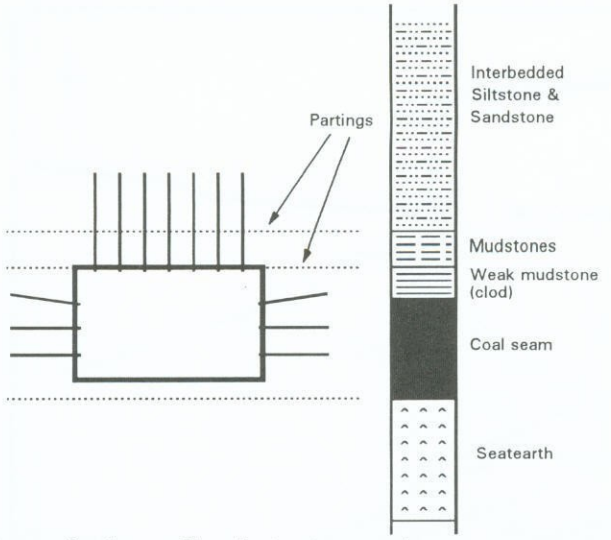



**Figure 2. Generalised strata section**

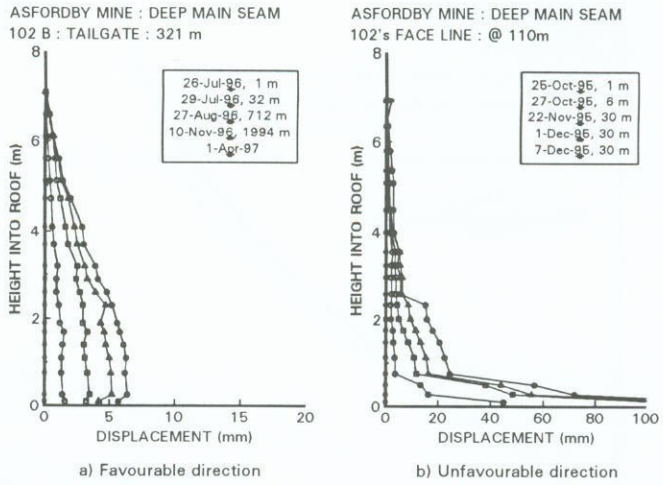



**Figure 3. Typical extensometer results for good and bad drivage directions.**

advance per week is 100 m using hand operated borers and 150 m with the bolter miner.

Gate roads are driven 4.7 m wide by 2.8 m high with 7x2.4 m high strength, full column resin bonded roof bolts installed each metre of advance giving a boltdensity of 1.49 bolts/$m^2$. Ribs are reinforced by 3x1.8 m bolts per cycle on each side with cuttable bolts on the face side. The roof is monitored using "dual height telltales" at intervals of 20 m, extensometers which provide more detailed information are placed at 200 m intervals. The roofbolting consumables and monitoring currently used in the UK are described in several publications, e.g. Bigby and Egan (2).

Drivage conditions

Considerable experience has been gained in driving roadways at various angles to the maximum horizontal stress. Typically roadways within 50° of the favourable direction will maintain a smooth parting at the chosen roof horizon. Initial roof deformations are relatively low, subsequently roof extensometers record gradual time dependant movement distributed throughout the monitored height (figure 3).

Roadways driven at greater than 50° to the maximum stress exhibit several effects including strap buckling, plate deformation and overbreak on the more highly stressed side of the heading. Even with additional bolts installed during drivage large deformations are likely within the bolted height. Failure may progress further into the roof requiring cable bolting (figure 3).

Where roadways have to be driven at a high angle to the maximum stress direction bolt densities are increased and the roadway is generally driven to a higher horizon to obtain a more competent roof.

Layout

The mine is laid out to place gate roads in a favourable direction relative to the stress regime.

The first three longwall panels were partially blocked out prior to face production starting on 101's 250 m retreat unit. Due to severe weightings accompanied by the inflow of considerable volumes of water, the mining strategy was changed to shortwall faces which have proved extremely successful.

The change to shortwall faces was made during the development of the face line for 102's district leading to a change from a single longwall face to two shortwall faces. The final layout of 102's district is shown in figure 4.

**FACELINE DRIVAGE**

The faceline for the first longwall at the mine (101's) was originally driven as an air connection at 4.7 m wide. Deteriorating conditions resulted in the roof horizon being some 2 m above the seam. When the roadway was eventually required as a face line considerable expense was incurred in additional support prior to widening out to the 6.2 m required for installing the powered supports. Initial production was delayed as the face graded down to the correct horizon.

The requirement for 102's longwall faceline was for a final width of 6.2 m with its roof and floor as close as possible to the face production horizon. The lowest practicable roof horizon was 0.8 m above the seam and the initial cut width was limited in view of the expected poor conditions. After some 150 m of drivage of the initial 250 m longwall face heading it was abandoned due to unacceptable roof conditions. It was decided to use the abandoned heading to provide stress relief for a new face line. To obtain stress relief for the full length of the face line a "sacrificial" heading was driven from the opposite end. At this point the mine plan was changed from longwalls to shortwalls and two shortwall facelines were driven in the stress relieved zone of the initial headings. The sequence of drivage was as follows:

102C Heading 1
- Planned as 250 m faceline, abandoned after some 150 m.

102B Heading 1
- Driven to complete stress relief for new 250 m faceline.

102C Heading 2
- Driven as 60 m face line alongside 102C Heading 1.

102B Heading 2
- Driven as 60 m face line alongside 102B Heading 1.

Further details of each heading are given in tables 2 and 3.

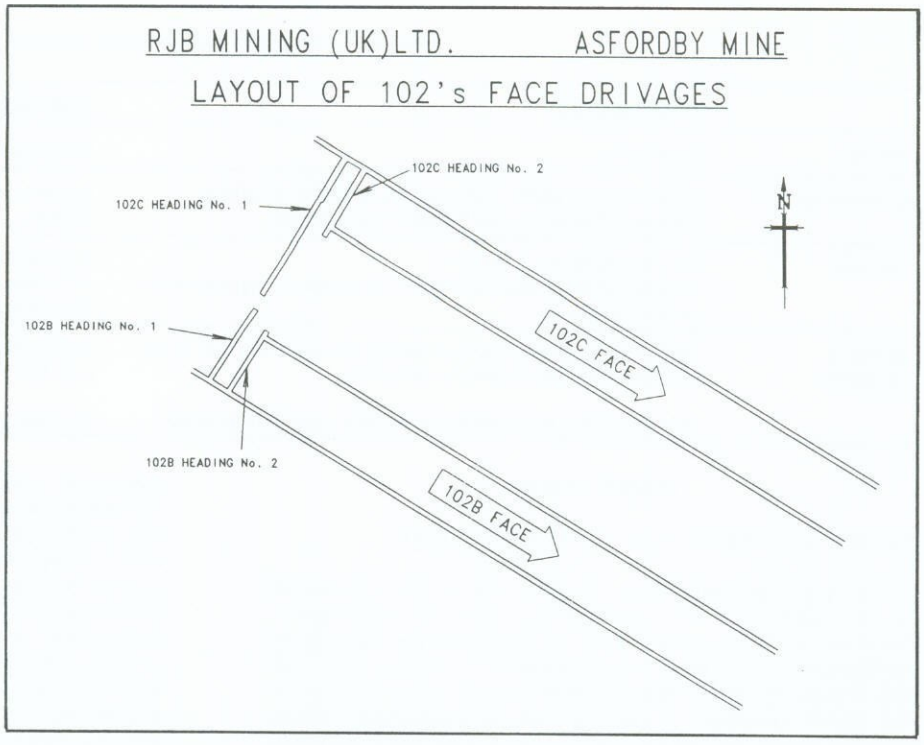



Figure 4 Plan of 102's district.

Table 2. Summary of first driven headings

| | 102C Heading 1 | 102B Heading 1 |
|---|---|---|
| Machine | Bolter miner | Continuous miner with hand held borers |
| Cutting sequence | Drive stub 12 m long x 4.7 m on right hand (gob) side. Take 6 m long x 1.5 m wide breasting on left hand (face) side. Advance the right then left hand cuts in 6 m stages. | Driven to 4.7 m width. |
| Support | 2.4 m roof bolts at 1.6 bolts/$m^2$, increased to in excess of 2.5 bolts/$m^2$ after spot bolting. 8 m double bird-caged cables at 0.65 cables/$m^2$, installed within 50 m of head end. | 2.4 m roofbolts at 2.77 bolts/$m^2$, installed as close to head end as practicable. 12 m double bird-caged cables at 0.85 cables/$m^2$, installed within 20 m of head end. |
| Outcome/ comments | Progressively worsening overbreak in right hand stub heading, left hand cut maintaining smooth parting. Ongoing movement within bolted height requiring spot bolting. Heading stood at 50 m mark with 2.5 m overbreak.<br><br>Cable bolts installed to head end and cavity secured to recover planned roof horizon. Decision taken to drive right hand stub only and to bolt using hand held machine to control overbreak, cables to be installed close to head end.<br><br>Right hand stub driven to 93 m mark. Floor heave dinted. Right hand stub driven to 155 m mark. 12 m cables being installed.<br><br>Machine removed from heading with extensometers registering accelerating roof lowering up to 8 mm/day, extending up to 7 m into roof. Ribs starting to fail. Roof failure starting to spread back towards start junction.<br><br>Face line abandoned. Junction protected by cribs along entrance to heading. Decision taken to drive Heading 2 in anticipated reduced stress. | Supports installed to high standards with heading teams aware of conditions in 102C Heading 1.<br><br>Overbreak on drivage up to 0.6 m but well contained. Movement confined to within bolted height. Heading driven to within 5 m of thirling with 102C Heading 1, dinted to give final height of 4.3 m.<br><br>Monitoring indicted limited roof deformation compared to 102C Heading 1. Remote reading intruments installed in case access to heading lost.<br><br>Heading widened by combination of cutting and firing coal rib to a depth of 1.5 m. Rate of movement still low.<br><br>Decision taken to delay drivage of Heading 2 due to limited stress relief and change in planned mine production schedule. Roof deformations monitored and stresses measured.<br><br>Heading 2 started after delay of 4 months with monitoring indicating suitable degree of stress relief obtained. |



Table 3. Summary of second driven headings

| | 102C Heading 2 | 102B Heading 2 |
|---|---|---|
| Machine | Bolter miner | Continuous miner with hand held borers |
| Cutting sequence | Driven to 4.7 m width. Subsequently breasted to produce required 6.2 m width, then dinted to base of seam. | Driven to required width of 6.2 m. Subsequently dinted to base of seam. |
| Support | 2.4 m roofbolts at 1.7 bolts/$m^2$.<br>12 m double bird-caged cables at 0.32 cables/$m^2$, installed within 10 m of head end. | 2.4 m roofbolts at 3.1 bolts/$m^2$.<br>12 m double bird-caged cables at 0.48 cables/$m^2$, installed within 10 m of head end. |
| Outcome/ comments | Roof horizon formed to smooth parting. No overbreak with small roof deformations recorded by monitoring.<br><br>No deterioration in conditions before face equipment installed. | Roof horizon formed to smooth parting. No overbreak with small roof deformations recorded by monitoring.<br><br>No deterioration in conditions before face equipment installed. |

## STRESS RELIEF

### Concept and application of stress relief

If particularly poor conditions are encountered in a heading, the potential for a subsequent heading driven alongside to experience improved conditions is well recognised. This can be explained by the redistribution of stress around the first heading. The failed or softened strata surrounding the heading will only transmit reduced levels of stress producing a zone of lower stress immediately adjacent to the first heading within which the subsequent heading can be driven.

The technique of driving a sacrificial roadway, the roof of which is expected or induced to fail, in order to provide improved conditions in a subsequent roadway is commonly used in Australian mines. In particular it is used for the formation of face installation roadways subject to high lateral stress levels. Gale (3) reports that lateral stress can be redistributed about softened roadways to provide stress relief up to 30-40 m adjacent. The effect and extent of the stress relief is dependent upon rock mass properties and the magnitude of in-situ stresses.

An example of its use in the USA involving the use of an initial arched entry to reduce cutter roof failure in subsequent adjacent entries is described by Aggson and Mouyard (4). In this case measurements indicated significantly reduced stresses in the roof at 36 ft from the arched entry compared to those at 80 ft. The technique was apparently effective in eliminating cutter roof failure in entries driven 30 ft (9.1 m) from the arched entry.

Several sites in the UK at which stress relief effects have been employed are documented (5-7). The majority of these were face headings and not pre-planned, i.e. the decision to drive a second heading was only taken after unacceptably poor conditions were encountered in the initial heading. Pillar widths of up to 9 m were utilised between the headings with improved conditions being encountered in the second headings. In other instances the application of stress relief was planned, i.e. poor conditions were anticipated in the first heading and it was intended to drive a subsequent heading at the outset. In these cases improved conditions were obtained in the second driven headings but not to a sufficient extent for the technique to be adopted for continued use. The difficulty would seem to be ensuring sufficient stress relief is obtained prior to the subsequent headings being driven. In addition to the strata properties at the site, the extent to which stress relief can be ensured will be dependant on the degree to which controlled roof failure and softening can be engineered in the first heading and on the techniques available and accepted to achieve this.

The initial decision to employ stress relief for these face headings at Asfordby Mine was taken after unacceptable conditions were encountered in the original face heading for 102C's panel (102C's Heading 1).

For the second panel (102B's) however, it was intended to employ stress relief and drive two headings from the outset. The effectiveness of the technique will be dependent on the amount of stress relief obtained and the extent to which conditions are determined by the horizontal stress magnitudes. The established sensitivity of roadways at the mine to horizontal stress suggested that stress relief was likely to be effective.

### Computer modelling of stress relief

Following the decision being taken to abandon the initial face installation heading (102C's Heading 1) an investigation into the behaviour and stability of the headings using computer modelling techniques was initiated. This was conducted concurrently with the drivage of the subsequent headings. Results obtained from the modelling investigation were used to assist in the interpretation of data obtained from strata monitoring and in deciding on appropriate courses of action at several stages during the development of the new facelines.

The degree of horizontal stress relief and the corresponding roof deformation developed in the computer simulations are shown in figure 5. The roof deformations are presented in the form of extensometer results relative to a reference anchor at 8 m into the roof. As would be expected stress relief also develops in the seam and floor. The relief generated by the model in the coal seam is

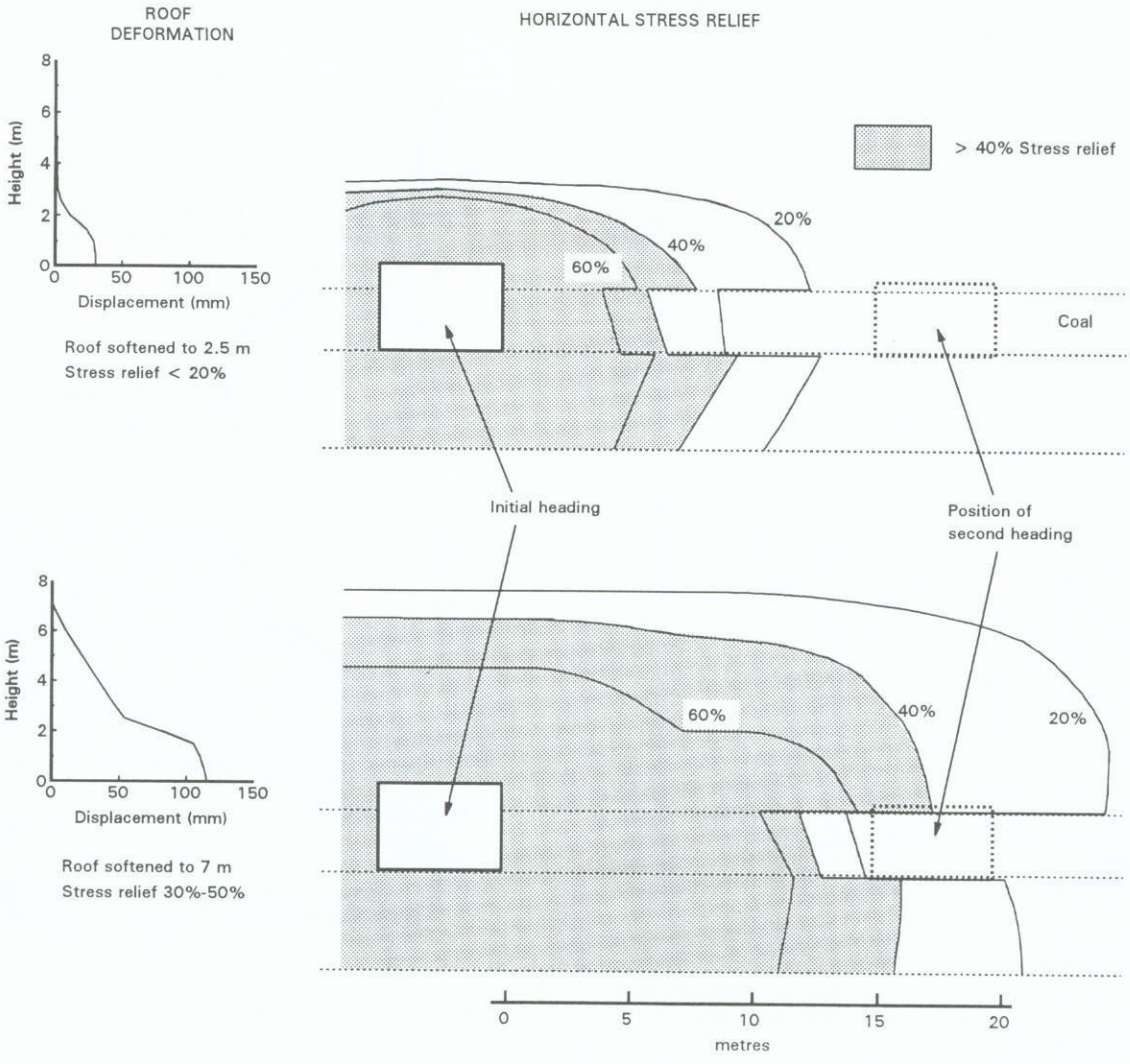



**Figure 5 Stress relief from computer modelling.**

less than in the surrounding strata, this is associated with the contrast in stiffness between the materials. The extent of stress relief obtained in the roof is strongly dependant on the degree of failure or softening generated by the first roadway. As softening and the zone of reduced stress spreads further into the roof of the first roadway the distance at which significant stress relief is obtained increases. This is associated with an increase in the magnitude of the roof deformations and the height to which they are occurring. It is important to have a method of assessing the extent of roof softening and hence the degree of stress relief likely to be obtained. Monitoring of roof deformation with extensometers provides a means of doing this.

Although it can be expected that the extent of stress relief may vary from site to site dependant on the strata properties, the degree of relief indicated by the results presented in figure 5 with the roof deforming up to 7 m is similar to that suggested by Gale (3).

Stress relief for 102's face headings

A 15 m pillar was left between the first and second driven roadways. This was wider than isoften used when applying this technique to face headings where long-term stability is not required. The pillar width was decided taking into account the nature of the seam with the underlying seatearth and known weak pillar characteristics.

In the case of the first pair of roadways (102C's Headings 1 and 2), at the time the decision was made to drive a replacement heading, significant deformations extended up to 7 m or more into the roof of Heading 1. With the roof softened up to 7 m above the first roadway the model simulations indicate a 30%-50% reduction in horizontal stress in the roof from the original magnitude at the position of the second heading. It was expected that this degree of reduction would be sufficient to produce a significant improvement in conditions. Heading 2 was driven in good conditions with an initial width of 4.7 m then breasted out to the final width of 6.2 m.

In the case of the second planned faceline drivages (102B's Headings 1 and 2) the initial deformations were mostly confined to within the immediate 2 m of roof for reasons discussed below. With softening above the first roadway limited to the immediate roof the model simulations indicate a reduction in stress of less than 20%. There was concern that the degree of stress relief achieved at this point would be insufficient to promote good conditions in the second heading. The heading was dinted and widened in places in an attempt to initiate further failure in the roof. Fortunately an alteration in the production schedule allowed the formation of the second heading to be delayed. Because of the known time-dependant characteristics of the seam it was expected that this would increase the degree of stress relief as conditions in the first heading deteriorated.

An overcore stress test was obtained at 4.0 m into the roof and 15.2 m from the ribside of the existing heading. This gave a magnitude of 10 MPa for the vertical component (compared to an estimated overburden stress of 13 MPa) and 11 MPa for the maximum horizontal component in rock with an elastic modulus of 7.2 GPa. The measured horizontal stress magnitude was lower than measured in-situ values, however the measured elastic modulus of the rock was also low which could have accounted for the lower horizontal stress. Additional overcoring tests to give in-situ stresses in similar strata would be required to give a definite indication of the degree of stress relief obtained. Time constraints and the drilling distances involved prevented these being obtained.

When drivage of the second heading was commenced significant deformations had spread towards the top of the extensometers at 7 m into the roof of the first heading. The second heading was driven at its full width in the expectation that sufficient stress relief had been developed to allow this.

In both cases conditions in the second driven headings were greatly improved producing stable headings for face installation. The effectiveness of the technique in improving roof control at this site is demonstrated by the contrast between roof deformations measured in the first and second driven headings, figure 6. Although not measured it was also noted that the amount of floor deformation in the second driven headings was considerably reduced.

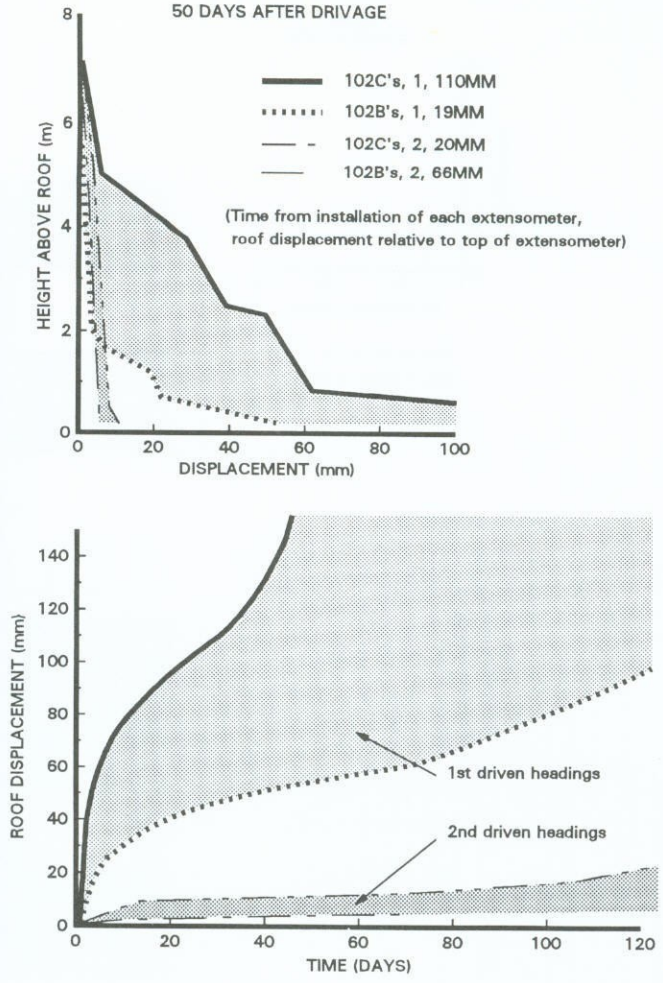



**Figure 6 Effect of stress relief.**

## INFLUENCE OF REINFORCEMENT PROCEDURE

As already noted there were considerable variations in behaviour along the length of and between the two first driven headings. For the first heading driven (102C's, Heading 1) significant roof failure was evident soon after drivage was started and the heading was delayed by a roof cavity which formed after 50 m of drivage. Once significant roof deformations started to develop further into the roof they spread rapidly along the rest of the heading with a marked deterioration in conditions and increase in the rate of roof movement. This coincided with a dint being taken through the heading.

In the case of 102B's Heading 1, although there was some overbreak, the heading was not stopped by any significant cavities. The initial deformations were mostly confined to within the immediate 2 m of roof. Despite dinting and firing the ribs the onset of deformations higher in the roof was delayed and, once they did develop, the rate of roof movement remained lower indicating improved control of the roof in comparison to 102C's Heading 1.

The overall roof displacements measured by the roof extensometers are plotted against the elapsed time from installation of the first extensometer for each of the headings in figure 7. This illustrates the extent to which the displacement rates accelerated and conditions deteriorated simultaneously along the length of 102C's Heading 1 in contrast to the slower displacement rate in 102B's Heading 1.

These headings were driven in close proximity to each other in apparently identical strata and in-situ stresses. It appears likely that the method of drivage and reinforcement were the cause of the difference in roof behaviour. As described above the reinforcement procedure adopted for 102B's Heading 1 resulted in the reinforcement being installed at an earlier stage than for 102C's

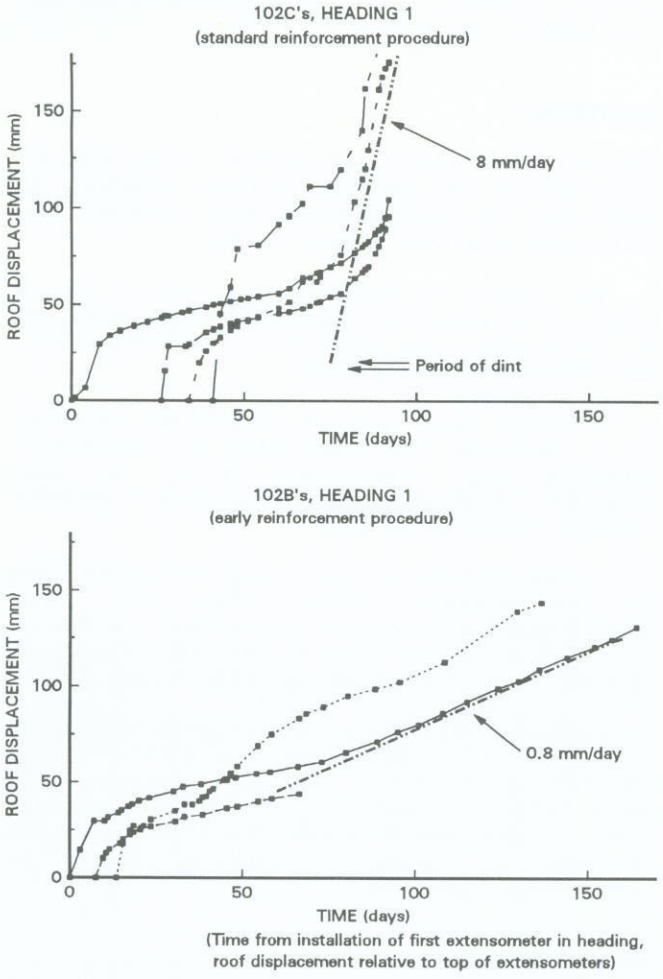



**Figure 7 Effect of reinforcement procedure.**

Heading 2. The primary reinforcement pattern of roofbolts was installed closer to the newly exposed face and the secondary reinforcement with cable bolts was installed systematically soon after, rather than post drivage as a remedial measure in response to excessive deformation in the roof.

The computer modelling techniques used to assess the degree of stress relief were also used to investigate the feasibility of the timing of reinforcement influencing conditions in this manner. Because of the 2-dimensional nature of the model used this could not be directly represented. The effect was approximated by simulating extracting the material in the heading then allowing the strata to start relaxing and some failure to initiate prior to installing the reinforcement. The model results indicated that delayed reinforcement could lead to significantly worse conditions.

The maximum roof lowering rate recorded in 102B's Heading 1 was approximately 0.8 mm/day compared to 8 mm/day in 102C's Heading 1. This contrast was obtained using the same reinforcement materials and with a similar final reinforcement density in both headings. Despite the widely differing rates of roof movement between these two headings there was

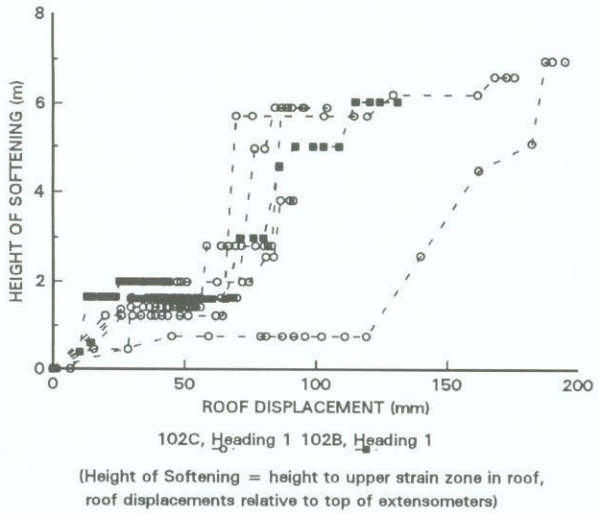



**Figure 8. Characteristic roof behaviour.**

a broadly consistent relationship between the total amount of movement and the height into the roof to which deformation was extending, figure 8. In the case of 102B's Heading 1, with the improved reinforcement procedure, the progression of softening into the roof was delayed along with the rate of roof movement.

The comparison between the two headings indicates the extent to which, in these circumstances, it can be more efficient to install additional reinforcement such as cables early on prior to excessive failure or softening of the strata. This may limit additional softening by providing additional reinforcement at an early stage. It is also possible that better installation standards and bond strengths are achieved by placing the cables in relatively unfractured strata.

Although it can result in slower drivage rates the experience with these two headings demonstrates the potential for the adoption of a tighter reinforcement procedure to produce a considerable improvement in roadway conditions. In turn this suggests the potential for future development of reinforcement products that can utilise these advantages.

## SUMMARY AND FUTURE FACE HEADINGS

The condition of roadways in the Deep Main Seam at Asfordby Mine is strongly dependant on drivage direction. This is the result of differing horizontal stress magnitudes and the sensitivity of roadway behaviour to them. In order to maximise the length of drivage in the preferred direction, the mine has been laid out, as far as possible, with gate roads driven parallel to the direction of the maximum horizontal stress. As a result face installation headings have to be driven approximately perpendicular to the maximum horizontal stress. Since they also have to be driven wider than standard headings to accommodate face equipment it could be expected that the would give difficult drivage conditions.

This was the case during the drivage of the first heading intended as a face installation roadway. Even when the drivage width was reduced, large deformations developed extending high into the roof with an accelerating rate of roof movement. The conditions encountered raised the question of the feasibility of forming such headings at a high angle to the maximum horizontal stress with the required width and supporting them using reinforcement with roof and cable bolts. If this could not be achieved the most obvious alternative would be to adopt standing support using steel sets. Given the conditions these would need to be heavy duty. The cost and risks of injury involved in handling such supports makes this an unattractive option.

Another option which was considered was that of driving the heading at a reduced width and adopting a procedure to install the face supports at the same time as widening out. Because of the operational constraints at the mine this was not considered a feasible option. In fact conditions in 102C's Heading 1 remained poor even at a reduced width. In other circumstances however this may be a feasible option.

The development of 102B's and 102C's headings demonstrated that stress relief provided an effective method which would allow the formation and support of face headings using roof reinforcement techniques. The experience with these headings was not ideal. In the case of 102B's the relatively slow deterioration of the first driven heading meant a considerable delay before the final face heading could be driven. For 102C's conditions during drivage of the first heading were considered too poor to be generally acceptable. It may be difficult to establish sufficient control of roof behaviour to ensure a suitable compromise between these two cases from the outset. In Australian mines measures such as widening out or shotfiring the roof have been used to overcome this difficulty. It remains the case that utilising stress relief provides a viable strategy should the first heading fail.

Although the slow deterioration in 102B Heading 1 was not desirable from the point of view of obtaining stress relief, it demonstrated the potential for tighter reinforcement procedures to produce a marked improvement in roof control. This suggested an alternative strategy for the formation of face headings. The results indicated that initially driving at a standard width with improved reinforcement, as for 102B's Heading 1, sufficient control could be established over the roof to allow the heading to be widened and face supports installed prior to the development of excessive deformations and strata softening higher in the roof. Monitoring using roof extensometers would establish whether the roof was responding in the required manner similar to 102B's or was deteriorating more rapidly as for 102C's.

This second strategy is still not ideal in that the intensive reinforcement entails slow development rates, nonetheless it involves less delay and is preferable to driving two headings as for stress relief. This strategy has since been adopted successfully for the formation of the next face heading at the mine.

## CONCLUSIONS

The particular conclusions relevant to the mine are contained in the previous section. However, the experience in driving these four headings does illustrate some more general points.

1. The extent to which stress relief can be effective in producing improved drivage conditions at sites where the conditions are sensitive to horizontal stress magnitudes.

2. If stress relief is to be adopted as a strategy it is important that monitoring is available to determine that significant relief is being obtained. Roof extensometers provide a suitable means of achieving this.

3. Drivage methods and the timing and installation of reinforcement, rather than just final reinforcement density, can significantly influence drivage conditions. This is relevant to ordinary headings as well as those employing stress relief.

4. Computer modelling in conjunction with detailed monitoring of underground conditions allows improved interpretation of these conditions and hence choice of appropriate strategies to deal with them. In this manner it provides a tool which can be used in conjunction with a "design by measurement" approach.

## ACKNOWLEDGEMENTS

The authors would like to thank Mr A Galloway, Director of Mining, RJB Mining (UK) Ltd for permission to publish this paper. They would also like to acknowledge the assistance of colleagues at Asfordby Mine and Rock Mechanics Technology Ltd. The contents of the paper reflect the views of the authors and not necessarily those of RJB Mining (UK) or Rock Mechanics Technology Ltd. The investigative work reported was funded by RJB Mining (UK) Ltd and the European Coal and Steel Community.

## REFERENCES

1. Investigation into the effects of lithology on the magnitude and ratio of in-situ stress in coal measures. Report on ECSC Research Project 7220-AF/854

2. Bigby, D. Egan, J. Harworth Colliery: Rockbolted support in weak roof at depth. Proceedings of 15th International Conference on Ground Control in Mining, Golden, Colorado, USA, Aug. 13-15, 1996, pp 543-557

3. Gale, W.J. Strata control utilising rock reinforcement techniques and stress control methods, in Australian coal mines, 1991, v.150, pp 247-253

4. Aggson, J.R. and Mouyard, D.P. Geomechanical evaluation of a coal mine arched entry, International Journal of Mining and Geological Engineering, 1988, v.6, pp 185-193

5. Lateral stress relief for longwall access and trunk roadways. Report on ECSC Research Project 7220-AB/834

6. Pugh, W.L. Strata control and roof bolting in Western Area. Mining Engineer, 1988, v.147, pp 584-594

7. Siddall, R.G. and Gale, W.J. Strata control - a new science for an old problem. Mining Engineer, 1992, v.150, pp 341-356

# Significant Weighting Events on the Longwalls in the Phalen Colliery

*Bob J. MacDonald,* Operations Planning Manager
Phalen Colliery
Cape Breton Development Corporation
New Waterford, NS, CANADA

## ABSTRACT

The Cape Breton Development Corporation is a federally owned Crown corporation in Canada that operates two coal mines the Prince and Phalen Colliery in the Province of Nova Scotia. Retreat longwall mining was first introduced to the shallower workings (180m) of Prince Colliery in the early 1980's. Phalen Colliery started longwall retreating in 1987 and since that time has extracted twelve panels.

In 1993 there had been a total of eight longwalls varying in widths from 140-230m mined in Phalen Colliery that is on the Phalen Seam. Up to this point there were only minor ground control problems on the faces except for one of the earlier longwalls that was mining a split seam. There is some interaction on Phalen workings from remnant structures in the overlying Lingan and No. 26 Collieries which worked the Harbour Seam. Induced abutments loads along pillar edges have been observed and resulted in poor face conditions when mining the Phalen Seam.

The ninth panel, 6 East was the first panel to suffer a major roof fall from the *First Major Weighting.* This was also the first panel to undermine a paleo sandstone river channel named the Lower Sandstone Unit (LSU). For the first time in Phalen's history subsequent longwalls began to experience periodic weighting events. The 6 East panel suffered a number of periodic weightings and on two occasions had to use foam cement to fill the cavities that resulted. On the next east side panel, 7 East, there were numerous periodic weighting events, but interestingly there was no significant *First Major Weighting.* 7 East was the first 260m wide panel and all others were 230m or less. This longwall was 3,400m long and began producing in December of 1994 and was still cutting coal in May of 1997. There were five significant roof fall events on this panel, three of which required foam cement to fill the cavities. Of these three the interruption to production varied from four days to seven months.

There were definite precursors to each of the weightings including: 1) an increase in audible noise (termed bumping) on the face, 2) supports went rapidly into yield, 3) roof convergence increased, 4) water percolated from the face roof strata, and 5) severe spalling of the coal occurred resulting in increased tip to face distance.

Longwall face weightings are a result of geomechanical factors and cannot be avoided. However, the loss of roof control is a different matter and highly subjective to operational procedures. The causes of weightings, their magnitude and impact on the mining at Phalen have been investigated. The following factors have been identified as relevant to these occurrences.

1. The influence of pillars in the overlying Harbour Seam workings.
2. Location of the LSU relative to the Phalen Seam.
3. Thickness of the LSU.
4. Pressure arch effect from the adjacent gobs.
5. Poor operational practices on the longwall including:
   a) slow rate of retreat;
   b) inadequate supply of pump pressure to the hydraulic supports;
   c) premature yielding of the yield valves; and
   d) poor face alignment practices.

This paper will review the events that took place on the 7 East longwall and show that the Lower Sandstone Unit is the primary cause of the weightings. However, other factors contributed to the loss of roof control and the formation of the roof cavities.

## INTRODUCTION

Coal is extracted in the Sydney Coalfield by the Cape Breton Development Corporation (CBDC) which is a federally owned crown corporation. There are two mines, Phalen Colliery and Prince Colliery, extracting coal from beneath the Atlantic Ocean at depths ranging from 200 -700m below sea level. Phalen Colliery underlies flooded workings located approximately 140m above in the Harbour Seam. Both mines use the retreat longwall method to extract the coal with two single entries driven and connected some 3,000m inbye to form the setup entry (wallface). Ground control on the longwalls at Phalen Colliery that is mining the Phalen Seam has become a major issue following the

subsequent flooding of the old workings above and the undermining of a paleo sandstone river channel now referred to as the Lower Sandstone Unit (LSU). Weightings have become evident on the longwall face and the conditions have reached a point where there have been extensive roof falls and subsequent interruptions in operation for up to seven months.

The undermining of the overlying flooded No.26 Colliery workings in 1992 by 5 East longwall in Phalen Colliery resulted in the breach of a barrier pillar (+360m wide) which brought water at the rate of 4,000 USgpm into the then operating Lingan Colliery. Lingan Colliery workings were lost along with two complete sets of longwall equipment and from this point onward ground control on Phalen's longwalls became a very important issue.

Almost a year later 6 East longwall experienced its first major weighting that resulted in an extensive roof fall that shut down the longwall for 3 weeks and required the first application of foam cement to fill the cavity. Subsequent roof control problems and the formation of other cavities strongly suggested that the LSU was the source of the problem. A detailed core drilling program was initiated to establish the extent of this body of sandstone. Data from earlier boreholes was colated to generate a fence diagram with representation of the strata between the Harbour and Phalen Seams (Fig.1)

Prior to the mining of 5 East and 6 East longwalls which were both 230m wide, the Corporation made a decision to increase longwall widths to 260m because of the inability of development to keep up with retreating longwalls. The development of 7 East panel was more than 50% complete when the Corporation confirmed with the assistance of outside strata mechanics consultants, that weighing events were associated with the LSU and could be more severe on the wider longwall faces.

Production on 7 East longwall began on December 4, 1994. More than two years later the longwall has experienced more than 50 recorded periodic weighting events of intervals ranging from 16m to 74m. A periodic weighting event can be best described as ***the alternating phases of low and high pressure build-up on longwall face supports (following support setting) and the resulting low and high rates of roof convergence***. There were a number of major roof falls which interrupted face production for periods ranging from four days to seven months.

There were definite precursors to each of the weightings and these including 1) an increase in audible noise (termed bumping) on the face, 2) supports went rapidly into yield, 3) roof convergence increased, 4) water percolated from exposed roof strata and 5) severe spalling of the coal occurred resulting in increased tip to face distance.

Longwall face weighting is a result of geomechanical factors and cannot be avoided. However, the loss of roof control is a different matter and highly subjective to operational procedures. Causes of the weighting, their magnitude and impact on mining at Phalen have been investigated. The following factors have been identified as being relevant to these occurrences.

1. The influence of pillars in the overlying Harbour Seam workings.
2. Location of LSU relative to the Phalen Seam.
3. Thickness of LSU.
4. Pressure arch effect from adjacent longwalls.
5. Poor operational practices on the longwall including:
   (a) slow rate of retreat;
   (b) inadequate supply of pump pressure to hydraulic supports;
   (c) premature yielding of yield valves; and
   (d) poor face alignment practices.

This paper will explain that the Lower Sandstone Unit is the primary cause of the periodic weightings on 7 East longwall. Other factors contributed to the loss of roof control and the formation of the roof cavities.

## PRECURSORS TO ROOF WEIGHTING

The weighting events at Phalen Colliery began on 6 East panel. However, their documentation was somewhat limited and it was really the beginning of serious roof control conditions on the longwalls. Two major events occurred on this longwall. These were roof falls associated with the first major weighting and a second roof fall that occurred following a three week shutdown of the face. Both these incidents resulted in the cessation of production and the need to fill the cavities with foam cement. As a result, management became increasingly aware that something different was occurring on the longwalls. Of particular concern was the width of 7 East panel ( 30m wider) and extensive development of the Lower Sandstone Unit over the panel. 6 East experience taught us valuable lessons about proper operational procedures for longwalls working under a strong main roof.

Consultants were solicited to help the Corporation understand the true magnitude of the effects of a strong main roof and to make recommendations on the support capacity for 7 East longwall. It was decided that the center portion of 7 East would require a higher support density since the face was in effect 30m longer than any retreat longwall panel previously mined in the Sydney Coalfield. Hence, the face was equipped with 550 tonne supports from the headgate (bottom level) to No. 58 then, from No. 59 to 109 the supports were rated at 700 tonne and the remainder of the face from No. 110 to 175 the capacity was 550 tonne. Pump set pressure was 315 bars and yield was 390 and 410 bars respectively on the 550 and 700 tonne supports. This gave a set to yield ratio of .77 to .81. The face would operate on a gradient ranging from 26% inbye to 14% outbye. This means that the headgate must stay ahead of the tailgate by up to 12m to keep the wall equipment from moving down hill.

The following is an analysis of 48 periodic weighting event (Table 1) on the 7 East panel and the precursor events associated with each of the weightings. The average interval for all weightings was 37.4m given a range from 16m to 74m. Hence, many variables can be considered as controlling the weightings on 7 East. The precursor events for most weightings included 1) an increase in

audible noise on the face, 2) supports went rapidly to yield , 3) roof convergence increased, 4) water percolated from exposed roof strata and 5) severe spalling of the coal occurred resulting in increased tip to face distance.

Increased Audible Noise

The workers on the face termed this observation ***bumping*** and it was basically the noise associated with coal and surrounding strata attempting to accommodate the stresses induced by the longwall and more specifically the cantilever of the LSU. Usually when this occurred there was significant coal spalling, sometimes violently both ahead and behind the shearer drum. This may be localized to one or two supports or affect a significantly larger areas of the face.

Supports Went Rapidly to Yield

Following the setting of supports during a weighting event, the supports would yield within 10 to 15 minutes. This was also the case, except the time frame was longer, in nonweighting periods where the supports were set at low pressures (less than 260 bars). As a result of this frequent cycling the yield valves were completely changed out more than four times during the life of the panel. This situation meant that the supports were operating with a set-to-yield ratio of 0.65, which is definitely too low for a longwall experiencing periodic weightings.

Roof Convergence Increased

The Insite Pressure Monitoring system indicated that during the weighting events there would be as much as 100mm of convergence between cuts on the face. Shift reports from the section supervisor indicated a roof lowering at the face of 50-100mm.

Water Percolated from the Roof Strata

The Lower Sandstone Unit porosity is saturated with super saline (up to 40,000 ppm sodium) water and as this unit begins to fracture during a weighting event the saline water begins to appear along roof between supports Nos. 30-130. If the magnitude of the event is great then the fracture zone height will increase (Fig.2) to penetrate two coal seams (Bouthillier and Back Pit) above and water stored in the interburden between these seams and the flooded Harbour Seam workings above will begin to pour onto the longwall face. When this occurs the term used for this phenomenon is flushing. This water usually disappears into the gob following 4 - 7 m of retreat. The flow itself will usually decrease from the gob following an additional 4 - 7 m of retreat.

Severe Coal Spalling

During the weighting event the coal may spall and in some instances violently blow off the cut face causing the canopy tip to face distance to increase by as much as 0.5 to 1.0m. As a consequence, the support resistance to load would decrease because of the larger exposed roof area to support. The result of this was supports rapidly yielding and an increase in roof convergence in this area and consequently tensile fracturing of the immediate roof. Roof cavities began to form along the length of the face.

## HIGHLIGHTS OF WEIGHTING EVENTS

It is best to describe the weighting events as they pertain to different zones throughout the life of the panel (Fig. 3). Prior to undermining the barrier pillar in the overlying Harbour Seam, there was no noticeable weighting events for the first 975m of wall retreat. During the first 430m, the wall averaged 3,200 tonnes per day (4m retreat). For most of this area the LSU was more than 7.5m above the seam and its' thickness ranged from 6.1m at the tailgate (top level) to 12.4 m at the headgate (bottom level). During this period the wall stood idle for up to one week on four separate occasions due to cable belt problems and roof convergence in the headgate and during these incidents the wall stayed in good condition. There was no noticeable first major weighting for this wall. The remaining 545m of this zone retreat averaged 6,500 tonnes/day (7.6m retreat). During the last 150m the LSU increased in thickness to 20.1m at the tailgate and 19.2m on the headgate. It took a retreat distance of 260m for the thicker sandstone to cantilever and develop the first weighting event. This was also 90m past the west side of the pillar edge in the Harbour Seam above.

Zone A Weightings

There were thirteen weighting events over a distance of 323m retreat (Table 1). The wall averaged 6,200 tonnes per day (7.5m retreat). The events were well defined by the precursors mentioned earlier. Intervals ranged from 18-44m with most being 24.5m on average. Coincidentally, the first weighting event occurred when the wall was approximately 35m past the beginning of the 6 East Wall gob (Fig. 4). Event number 13 was the most significant event on 7 East that resulted in a seven month rehabilitation program for the longwall. The supports sustained some damage to the stabilizer rams and severe damage to the electrohydraulics due to blasting practices and saline waters corroding the contacts and solenoids. The LSU ranged from 20.1 to 23.4m thick at the tailgate and 9.5 to 15.8m at the headgate. Its location above the seam ranged from 1.5 to 5.0m and 7.0 to 7.8m at the tailgate and headgate respectively. One interesting observation was that the water percolation from the saturated strata beneath the Harbour Seam was now up to 280 US gpm. Prior to the undermining of the pillar there was virtually no water inflow from the roof on the face. There was no real pattern to the inflows because they occurred where the LSU was from 1.5 to 5.0m above the seam and where the periodic weighting interval ranged from 18m to 41m. Also, as with the first weighting event, this one occurred when the wall was 30 meters past the 5 East gob (Fig. 4) now giving two adjacent gobs to the high side of the 7 East Wall.

Zone B Weightings

This zone constitutes the remaining 445 meters of mining beneath the barrier pillar. It experienced eight noted periodic weightings.



It also marks the beginning of production following a seven month shutdown. What's interesting about this area is that the interval has increased to 50 to 74m with the exception of two events. The LSU has thickened up to 25.5m, but remains between 1.6 to 4.0m above the seam at the tailgate and 6.2 to 9.5m at the headgate. What is also unusual is that production was averaging 5,000 tonnes per day (6.1m retreat). During the initial start up of the wall there were meetings held with the crews to explain the perceived reasons for the weighting events and how important it would be to maintain pump capacity along the wall and practice good face alignment. The objective was to keep the three pumps (Hauhinco 125 - delivering 52 US gpm) running and not to shut them down between shifts as was done in the past. This may account for the improved roof control and the increase in the periodic weighting interval. However, on September 16, 1996 following a weekend, the wall experienced a major weighting event and a roof fall that took five weeks to rehabilitate. This event also brought the highest inflow of water; 350 US gpm. This event was located directly under the east pillar edge of the barrier pillar in the overlying Harbour Seam.

Zone C Weightings

This area retreated for 280m following the five week rehabilitation period mentioned above. There were nine recorded periodic weighting events in this zone and the intervals had dropped to 18 to 28m with three above that interval. There was no significant change in the LSU thickness or it's location above the seam as compared to Zone B. It was interesting to note that the water inflows were 100 US gpm or less with no barrier pillar above. Production was poor during this period with around 3,500 tonnes per day (4.3m retreat). From mid December through to January, 1997 there was a roof cavity on the face (up to 2.0m in height) extending over a length of approximately 25 meters along the face. Because of our inability to stabilize this cavity over a four week period, roof control was lost and a significant weighting occurred on January 13, 1997. This event caused the supports to converge more than one meter in less than four hours. Fifteen support canopies crushed the AFC spill plates. It took two weeks to recover the face and fill the cavity with foam cement.

Zone D Weightings

The length of retreat in this zone was only 80 meters and the wall experienced four periodic weighting events. This zone was characterized by a failure of the surface rotary breaker main beams that resulted in a modified side chute and P120 AFC conveyor being set up to dump the coal on the ground. Given this situation it was necessary to minimize production from the wall so as not to overload the make shift load out. The daily production was limited to 4,000 tonnes (4.8m retreat). Again the weighting intervals remained in the 16 to 28m range. Water inflows reduced to 60 US gpm or less. The LSU condition remained similar to Zone B and C.

Zone E Weightings

In this zone the wall has retreated 670m with a total of fourteen periodic weighting events. There were a number of changes in the LSU in the zone. There was also a major improvement in longwall supervision with the introduction of longwall coordinator to oversee the day to day operation of the wall. A preventive maintenance program was initiated on the day shift. During the preventive maintenance the wall was shut down and the cable belt stopped for two to four hours. Also, during this period, other operation jobs were done so that the wall could produce the next 20 to 22 hours. Strict adherence to wall alignment was introduced. As a result, the average daily production increased to 7,500 tonnes (9m retreat) with many days exceeding 8,500 tonnes (10.2m retreat).

The weighting intervals increased to 52 to 73 meters for the first five events and thereafter back down to 22m to 29m and up again to 34m to 50m. Interestingly for the first five events the LSU was thinning from 21.0m at the beginning to 9.4m at event No. 29. Its height above the seam increased from 2.5m to 12.6m. However, as the LSU came down again and began to thicken slightly, the interval length decreased. Finally with the LSU now up to 15m thick again and within 3.4 to 7.5m of the Seam the weighting interval increases to 34 to 50m.

## FACTORS CONTRIBUTING TO PERIODIC WEIGHTINGS

There have been a large number of variables that can be attributed to the weighting events on the longwalls at Phalen Colliery. The precursors mentioned earlier were for the most part present for each of the weighting events on 7 East. It is believed that there are a number of possible causes for the weightings on 7 East panels. These are noted as follows:

1. The influence of pillars in the overlying Harbour Seam workings.
2. Location of the LSU relative to the Phalen Seam.
3. Thickness of the LSU.
4. Pressure arch effect from adjacent gobs.
5. Poor operational practices on the longwall including:
   a) slow rate of retreat;
   b) inadequate supply of pump pressure to the hydraulic supports;
   c) premature yielding of the yield valves; and
   d) poor face alignment practices.

The Influence of Pillars in the Overlying Harbour Seam Workings

Pervious walls mined at Phalen Colliery beneath remnant pillars above experienced roof control and face spalling problems beneath these pillars. Further evidence of roadways driven in the main slope experienced bumping and roof control problems during excavation beneath the edges of the pillars above in the Harbour Seam. Also, a directional drilling program lost a drill motor that became stuck while drilling the coal in the Phalen Seam beneath a remnant pillar above. All of these incidents along with the severe weighting condition and water inflow along and beneath the barrier pillar above are all strong indications that these workings 140 meters above do have an effect on the Phalen workings.

Location of the LSU Relative to the Phalen Seam

This is only relevant if the LSU is greater than 9.5m in thickness and contains no localize layers of clasts. If the immediate roof was greater than 7.5m thick and the LSU less than 9.5m thick then there were no noticeable weightings. At the same time, if the LSU began to thicken, but contained layers of clasts, these layers began to separate and act like bulking with the immediate roof to minimize weightings effects. One exception was in Zone E where the LSU thinned to less than 9.5m with 9 to 12m of weaker immediate roof, but weighting events were present. This was probably due to few core holes in the area to define the exact thickness of the LSU. All other locations where the LSU was greater than 9.5m with less than 7.5m of weak immediate roof experienced periodic weighting events.

Thickness of LSU

As mentioned earlier, once the LSU becomes massive and is greater than 9.5m in thickness then it will cause periodic weighting events to exist on the longwall.

Pressure Arch Effects from Adjacent Gobs

The first weighting event took place as 7 East Face was 35m past 6 East gob and the most significant event No. 13 resulting in a seven month shut down took place as the 7 East Face was 30m past the 5 East gob. It's possible that the pressure arches were surcharged by the barrier pillar or the thick Upper Sandstone Unit (USU), some 25 to 30m thick and 30m below the overlying Harbour Seam. Fig. 4 shows the geometry of the 7 east panel in relation to the 5 East and 6 East gobs.

Poor Operational Practices on the Longwall

1. Slow Rate of Retreat

This condition is sometimes difficult to quantify since there are situations when the wall was producing on average 7,500 tonnes per day. The weighting intervals varied from 22 to 73m (Zone E) while at the same time when the wall was averaging 5,000 tonnes per day the interval was between 26 to 74m (Zone B). Also, in Zone C where the average daily output was 3,500 tonnes, the interval was 19 to 68m. It can be said however, that when the wall was retreating at 7,500 tonnes per day or more there was very little roof stone falling and on many occasions no interruptions to production during a weighting. In other words the shift would cut 6 to 8 slices of coal, thereby mining through the event in one shift.

2. Inadequate Pump Pressure to the Hydraulic Supports

During the first twelve months of wall operation from December 1994 to December 1995, it was not uncommon for the wall to be operating with only two pumps (PK125 at 52 US gpm). Also there was no booster pump from the tank to the main high pressure pumps, hence they were starving for fluid. A common practice at the mine was to shut down the pumps between shifts or on non-productive shifts. These practices, along with a one inch ring main and one inch inter-chock hose with only three crossovers resulted in poor distribution to the supports. This was further sacrificed when in a weighting situation supports were being advanced over the shearer body and two groups behind the shearer, hence three to four supports being activated at once plus ten to fifteen on ram push. System pressures during these movements were measured from a pressure gauge of the ring main at no. 167 support 350m from the pumps to be around 200 bar.

3. Premature Yielding of the Yield Valves

Given the fact that the system pressure was always so low, especially during a weighting, the support resistance being applied to the roof was also very low (less than 65% of design). Consequently the effects of the weighting overcame the supports, causing them to cycle in and out of yield up to three times before the shearer return during poor production times. This meant mechanical seals wore prematurely causing supports to yield at lower pressures and the yield valves were changed out at least four complete times along the length of the face. Also, if the supports were yielding at lower pressure when the guarantee set was initiated, it pumped the fluid out the yield valve.

4. Poor Face Alignment Practices

Due to mechanical problems in the push rams with some of the supports on the face, it was not uncommon to see the center of the face behind in the gob up to 2.4m (8 feet). When a weighting occurred then the crew would cut out the middle of the face to try to catch the roof. This was measured on many occasions to be up to 5m (16.4 feet) ahead. Usually at this point up to 1.5m of roof began to come in and this got progressively worse with each cut.

## CONCLUSIONS

Phalen's 7 East panel was initially scheduled to extract its reserve over a period of 18 months. However, due to problems experienced with weightings, the actual time required to extract this panel was over 30 months. Management had expected some delays due to the effects of weightings because they had been experienced on previous east side longwalls. The weighting events are a result of geomechanical factors and the problems Phalen Colliery encountered were more a result of operational and design conditions.

From an analysis of the weighting events data and the monitoring of conditions on the longwall along with pressure and convergence data from the Insite Pressure Monitoring System, it was quite obvious that each event displayed similar precursor characteristics. These precursors were consistent throughout the mining of the panel but their relative magnitudes changed with the thickness and height of the LSU above the seam. For example, when there was more than 6-8m of weak immediate roof rock the inflow of percolated saline sandstone strata water was at a minimum. also, the severity of the coal face spalling seemed to lessen as the thickness of the weak immediate roof increased.



The weighting intervals were not consistently spaced throughout the various zones and did not appear to follow any defined pattern relative to the thickness and height of the LSU. However, if the LSU was located more than 7.5m above the seam and maintained a thickness of 12.4m or less, the effects of periodic weightings were not evident. This was recognized in the first 975m of retreat on the 7 East panel.

Patterns relating to production or rate of retreat of the longwall seem to indicate that in Zone E (where the longwall consistently produced more than 7,500 tonnes (9m retreat) daily ) there were few cases where roof control was lost. It should be noted that while working in this zone the control of the roof was such that the Corporation was able to ship directly to the customer more than 75% of the ROM product. During the mining of this zone close attention was paid to the control of face alignment. Surveys were done twice weekly and remedial cuts were taken within hours of analyzing the survey data. For the most part corrective action to re-align the face was not frequently required.

Pump pressures were not sufficient to accommodate movement of more than three supports at once and the initiation of more than ten supports on line push at the same time. The monitoring system and the gauge of the ring main clearly indicated that the pumps could not maintain the required 310 bar set pressure and a set-to-yield ratio of 0.80. When in a weighting situation, where many supports were being advanced forward to stabilize the tip to face distance, the support density was not sufficient to control the convergence effectively resulting in premature yielding of the leg cylinders.

Many lessons have been learned during the mining of 7 East longwall and many changes are being implemented for future longwalls at Phalen Colliery. These include the continued use of survey control for face alignment, installation of four high pressure pumps instead of three (if one breaks down the spare unit is turned on), upgrading the hose sizes to 1-1/2" pressure and 2" return, modification of the Insite Pressure Monitoring System to improve its availability, and replacement of the electro-hydraulic controls to a rotary-compac valve to minimize lost of controls function due to the saline water corrosion of the solenoid contacts.

## REFERENCES

1. CBDC, 1994, Risk Assessment Report, Vol. 1 & 2
2. Farmer, I. W., 1994, Weighting and inflow during longwall working
3. Farmer, I. W., 1994, Water inflows and Weightings at Phalen Colliery
4. Peng, S. S., 1993, Review of Ground Control Program at Phalen Colliery
5. Zou, D. and H. Steve, 1996, Longwall Caving Mechanisms and Periodic Weighting at Phalen Colliery

Table 1. 7 **EAST PERIODIC WEIGHTINGS**

| Zone | Event No. | Event Date | Interval (m) | Water (USgpm) | Ht. to LSU Top Level (m) | Thickness Top Level (m) | Ht. to LSU Btm.Level (m) | Thickness Btm Level (m) | Cavity |
|---|---|---|---|---|---|---|---|---|---|
| A | 1 | 95-09-21 | | 50 | 4.5 | 19.0 | 7.0 | 11.5 | moderate |
| | 2 | 95-09-27 | 28 | 200 | 4.3 | 19.2 | 7.0 | 10.5 | minor |
| | 3 | 95-10-02 | 25 | *yes-l | 4.1 | 19.7 | 7.0 | 9.8 | moderate |
| | 4 | 95-10-05 | 20 | **yes-h | 3.9 | 20.0 | 7.0 | 9.5 | |
| | 5 | 95-10-07 | 22 | yes-l | 3.5 | 20.5 | 7.1 | 9.6 | |
| | 6 | 96-10-10 | 25 | yes-h | 2.7 | 21.5 | 7.2 | 10.5 | |
| | 7 | 95-10-13 | 21 | 200 | 2.2 | 22.2 | 7.3 | 11.5 | |
| | 8 | 95-10-17 | 27 | 175 | 1.5 | 23.1 | 7.2 | 12.8 | |
| | 9 | 95-10-20 | 28 | 220 | 1.6 | 23.4 | 7.4 | 13.9 | severe |
| | 10 | 95-10-27 | 24 | yes-l | 2.5 | 22.5 | 7.5 | 14.5 | |
| | 11 | 95-11-03 | 44 | yes-l | 4.2 | 20.7 | 7.7 | 15.0 | |
| | 12 | 95-11-09 | 41 | 250 | 4.7 | 20.5 | 7.8 | 15.4 | moderate |
| | 13 | 95-11-13 | 18 | 280 | 5.0 | 20.3 | 7.7 | 15.8 | foam |
| B | 14 | 96-06-24 | 50 | yes-l | 4.0 | 25.5 | 7.2 | 17.0 | |
| | 15 | 96-06-29 | 70 | yes-l | 3.2 | 22.6 | 6.5 | 18.0 | |
| | 16 | 96-07-16 | 74 | yes-h | 2.5 | 23.6 | 6.2 | 19.0 | |
| | 17 | 96-07-29 | 63 | yes-l | 2.0 | 24.5 | 7.5 | 18.0 | |
| | 18 | 96-08-18 | 72 | 50 | 1.6 | 25.0 | 9.0 | 16.7 | minor |
| | 19 | 96-08-27 | 37 | yes-h | 1.7 | 25.0 | 9.5 | 16.5 | |
| | 20 | 96-09-10 | 52 | yes-h | 2.4 | 24.5 | 9.1 | 17.0 | minor |
| | 21 | 96-09-16 | 26 | 350 | 2.4 | 25.0 | 8.6 | 17.5 | foam |
| C | 22 | 96-10-28 | 25 | 250 | 2.5 | 24.7 | 8.0 | 18.0 | minor |
| | 23 | 96-11-11 | 68 | yes-l | 2.2 | 25.0 | 7.8 | 19.0 | minor |
| | 24 | 96-11-14 | 19 | 60 | 2.0 | 25.0 | 6.8 | 19.4 | minor |
| | 25 | 96-11-18 | 21 | yes-l | 2.2 | 25.0 | 6.5 | 19.5 | minor |
| | 26 | 96-11-26 | 25 | 20 | 1.5 | 25.5 | 6.0 | 20.0 | minor |
| | 27 | 96-11-30 | 18 | yes-l | 1.0 | 26.0 | 5.7 | 20.1 | moderate |
| | 28 | 96-12-14 | 42 | 100 | 0.4 | 26.3 | 5.0 | 20.9 | moderate |
| | 29 | 96-12-29 | 34 | 40 | 1.5 | 25.0 | 4.5 | 21.2 | moderate |
| | 30 | 97-01-13 | 28 | 50 | 2.8 | 23.5 | 4.0 | 22.5 | foam |
| D | 31 | 97-02-05 | 16 | 60 | 3.2 | 23.0 | 3.5 | 21.5 | moderate |
| | 32 | 97-02-10 | 28 | 50 | 3.3 | 22.5 | 3.3 | 21.5 | moderate |
| | 33 | 97-02-14 | 18 | yes-l | 3.5 | 22.0 | 3.0 | 21.5 | minor |
| | 34 | 97-02-18 | 18 | yes-l | 3.9 | 21.5 | 3.0 | 21.5 | moderate |
| E | 35 | 97-03-01 | 73 | yes-h | 5.5 | 19.0 | 2.5 | 20.7 | minor |
| | 36 | 97-03-10 | 71 | 200 | 8.5 | 15.0 | 2.7 | 20.0 | severe |
| | 37 | 97-03-19 | 64 | yes-h | 11.5 | 11.5 | 5.5 | 16.5 | moderate |
| | 38 | 97-03-26 | 71 | yes-l | 12.6 | 15.2 | 8.6 | 13.0 | moderate |
| | 39 | 97-04-05 | 52 | yes-h | 11.5 | 14.0 | 9.0 | 12.5 | minor |
| | 40 | 97-04-13 | 26 | yes-h | 10.6 | 15.2 | 9.0 | 12.8 | moderate |
| | 41 | 97-04-16 | 22 | yes-l | 9.8 | 15.2 | 8.5 | 13.0 | minor |
| | 42 | 97-04-21 | 29 | yes-l | 8.8 | 15.0 | 8.2 | 13.5 | minor |
| | 43 | 97-04-27 | 50 | yes-l | 6.5 | 12.5 | 7.5 | 14.3 | minor |
| | 44 | 97-05-02 | 42 | yes-l | 3.6 | 10.8 | 6.7 | 15.0 | minor |
| | 45 | 97-05-07 | 34 | no | 3.4 | 10.0 | 5.7 | 15.5 | minor |
| | 46 | 97-05-14 | 44 | yes-l | 3.4 | 10.0 | 4.5 | 16.4 | minor |
| | 47 | 97-05-16 | 38 | 100 | 5.0 | 9.5 | 3.0 | 17.9 | moderate |
| | 48 | 97-05-22 | 54 | yes-h | 4.5 | 9.3 | 2.0 | 17.5 | moderate |

* water flow from roof 20 - 30 USgpm

** water flow from roof 30 - 60 USgpm

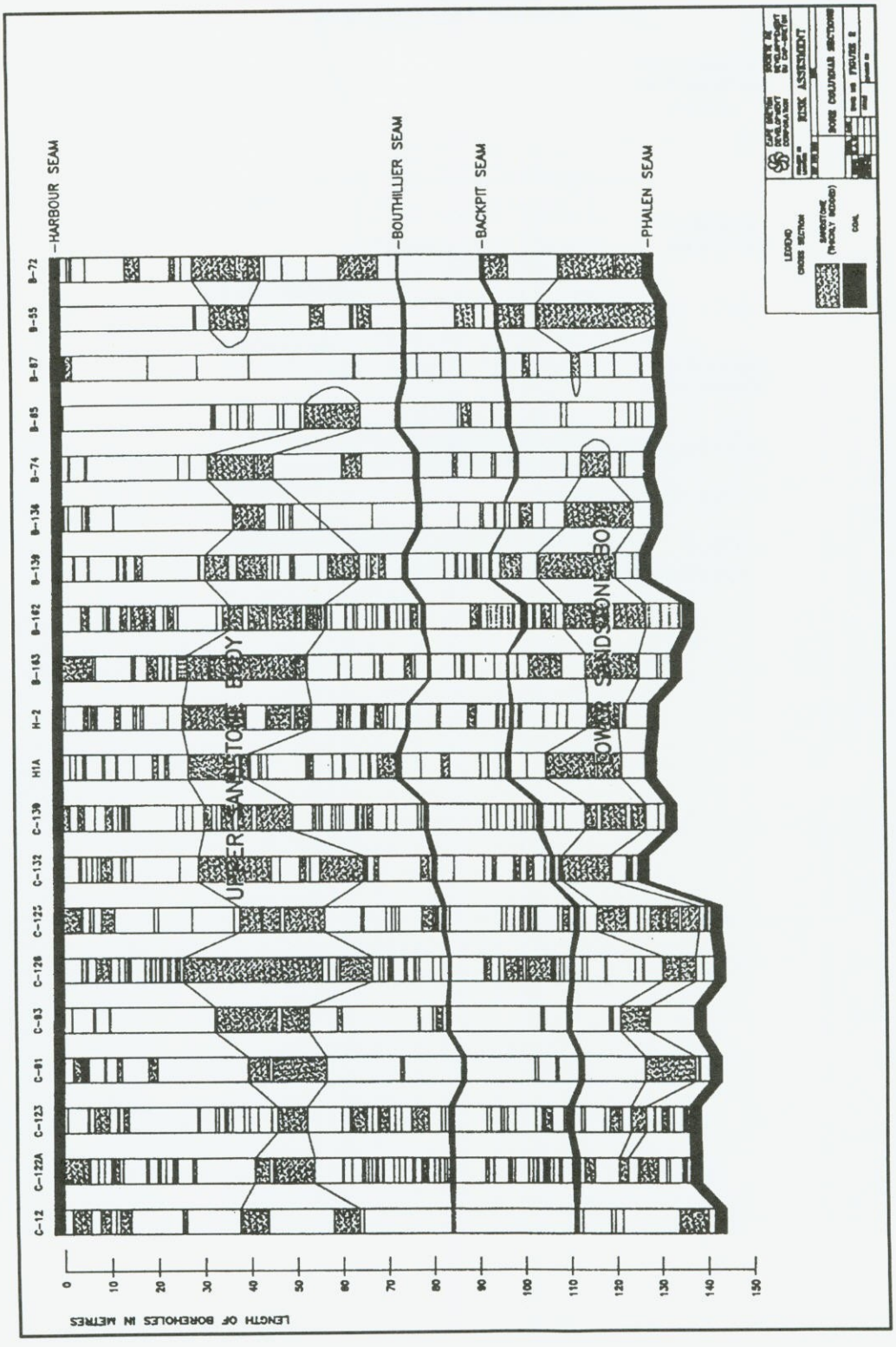



**Fig. 1 Interim Roof Strata of Phalen Seam (from CBDC)**

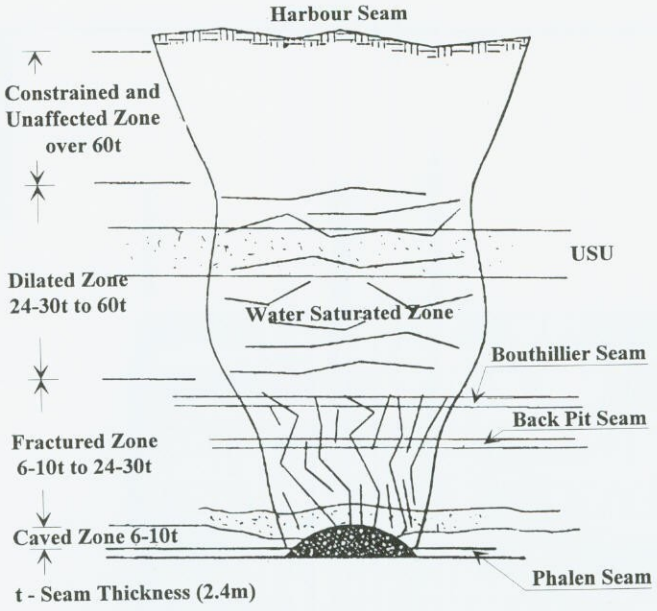



**Fig. 2 Schematic Showing Zones of Disturbed Overburden(Interburden) for a Longwall Panel**

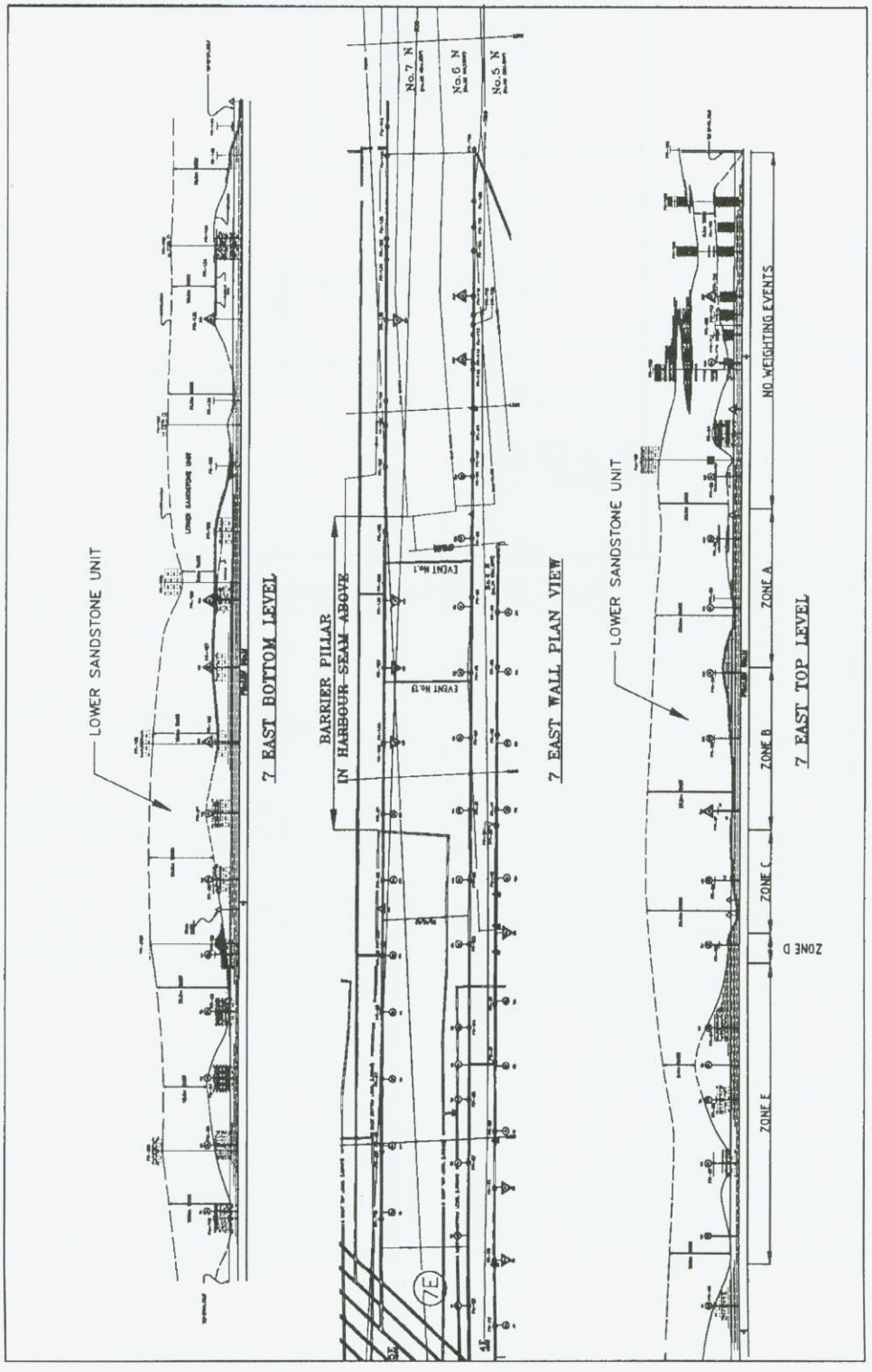



**Fig. 3 7 East Wall Layout**

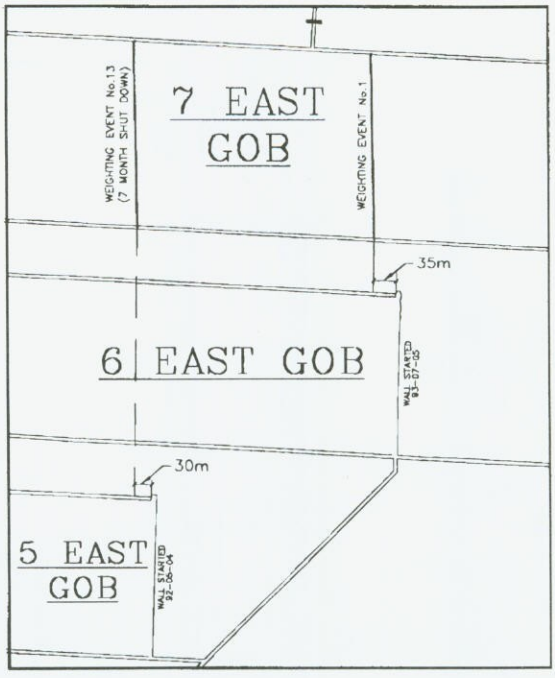



**Fig. 4 Abutment Gobs to 7E Panel**

# Full-Face Shield Pressure Monitoring in Medium-Weak Roof Condition

*Syd S. Peng,* Chairman and Charles T. Holland Professor
*H. Cheng,* Graduate Student
Department of Mining Engineering
College of Engineering and Mineral Resources
West Virginia University
Morgantown, WV

## Abstract

Full-face shield leg pressures in a longwall panel for a three-month period were collected and analyzed. The pressure data were presented in the following forms: full-panel full-face shield pressure, individual shield pressure, full-face shield pressure, full-panel time-weighted-average pressure, and relationships among setting pressure, final pressure and pressure increment. Although shield pressure varies from shield to shield and from cycle to cycle, the setting pressure and face advance rate do control the final pressure and time-weighted average pressure.

## Introduction

In recent years all shields are equipped with pressure sensors ( Harris, 1993; Park et al., 1996; Hart et al., 1996 ) such that shield leg pressures for the whole face can be monitored in real time thereby making face automation feasible. To take advantage of these massive data, researchers have been analyzing these pressure data and correlating it with roof condition at the longwall faces ( Park et al., 1996; Hart et al., 1996 ). In previous studies ( Hanna and Haramy, 1991; Peng and Chiang, 1984 ) where pressure data were analyzed systematically, shield pressures were monitored and restricted to a few selected shields located strategically across the face. The interpretation of these data could be bias without the benefits of the whole face shield pressure distribution. But recent study shows that interaction between roof, shield and floor is rather complicated. For one thing the contact between roof/floor and shield varies not only from shields to shields but also from cycle to cycle for the same shield. In other words the pressure history as recorded for each shield varies from shield to shield and from cycle to cycle. Obviously there are many factors that could contribute to the leg pressures as measured by the pressure sensor in each leg.

This paper attempts to evaluate the characteristics of full-face shield pressure and their variation for a significant period of time.

## Shield Pressure Data

The longwall panel monitored was 815 ft wide by 6460 ft long. This panel was the second panel in a new section. Therefore on the tailside the previous panel had been mined out while on the headside it was solid coal. The overburden in this panel varied from 500 to 800 ft and coal thickness averaged 6.2 ft. There were 180 units of 2-leg shields along the whole face. It had a rated yield pressure of 440 bars ( or yield load 700 tons ) and a rated setting pressure of 250 bars ( or setting load 400 tons ). Each shield was 5 ft wide. The cutting web width was 3 ft. Fig. 1 is the geological column for the section of the panel where shield pressure data were analyzed.

The original raw data consist of the following eight items: shield number, time, maximum and minimum pressures of left and right legs, and maximum and minimum strokes of DA ram in every minute. Normally one-day's data occupy a storage size of 8 megabytes in the form of text files and consist of 260,640 lines or 4,344 pages when print out. The data were converted into database tables and analyzed with SQL queries, database navigation models and other computer programs. Subsequently the database results were further processed by spread sheet and graphic tools.

## Full-panel Full-face Shield Pressure

Figure 2 shows the full-face shield pressure distribution in one-day period while Fig. 3 is an exploded view of area A as shown in Fig. 2. Fig. 2 can be extended to cover the full panel. Fig. 4 shows the full-face shield pressure distribution at selected points of time.

A detailed analysis of these three figures show that, in

**Figure 1. Geological column**

| Depth Min.-Max. / Average (ft) | Scale : 1"=20' | Thickness Min.-Max. / Average (ft) | Rock Type |
|---|---|---|---|
| 563.6 | | 28.6 | Limestone |
| 572.1 | | 8.5 | Clayshale |
| 483~697 / 590.6 | | 14.40~22.60 / 18.50 | Sandy Shale, Limy Shale |
| 498~713 / 605.73 | | 14.60~15.66 / 15.13 | Clayshale, Rider Coal, Shale |
| 504~720 / 612.07 | | 6.10~6.58 / 6.34 | Coal seam |
| | | | |

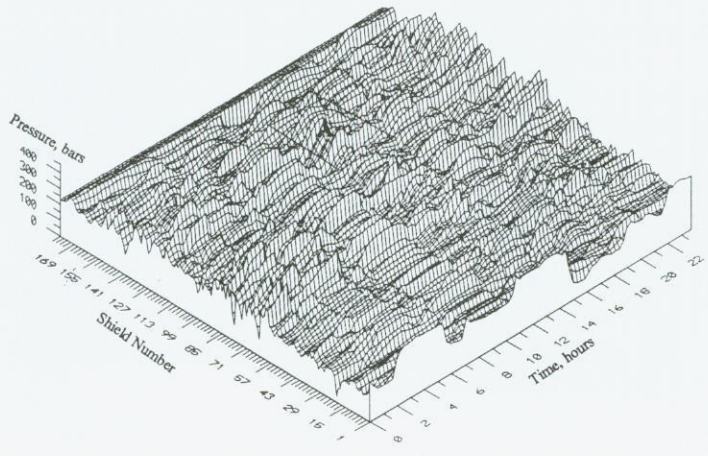



Figure 2. Full-face Shield Pressure Distribution on May 3rd

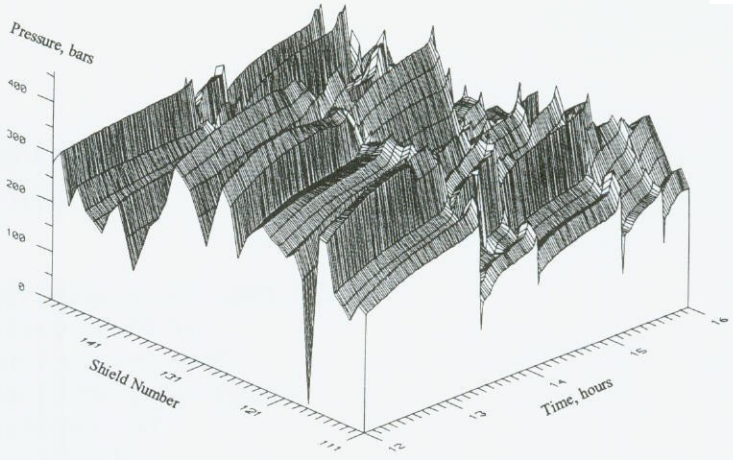



Figure 3. Detailed Shield Pressure Distribution in Area A of Figure 2

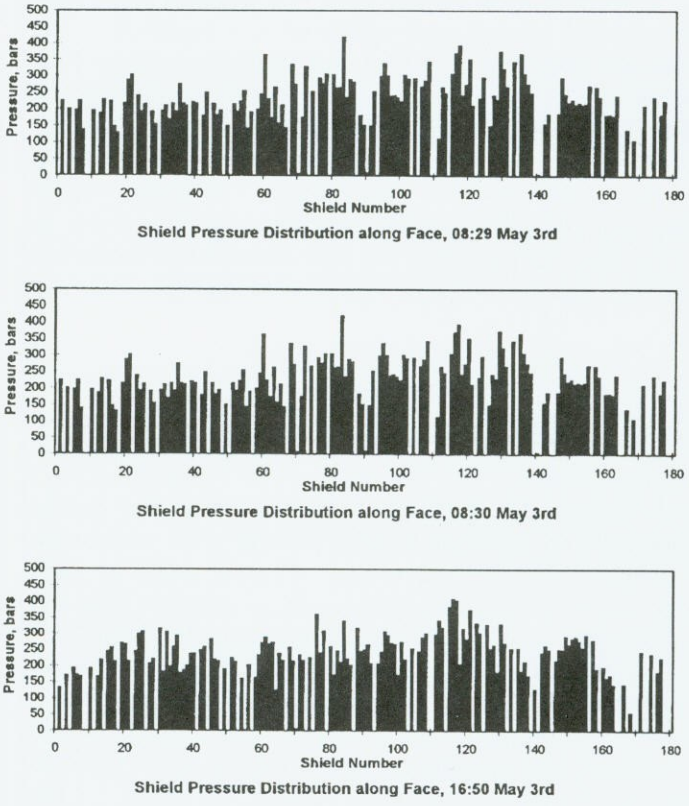



**Figure 4. Full-face Shield Pressure Distribution at Selected Points of Time**

addition to the change within a mining cycle, shield pressure varies from shield to shield and from cycle to cycle.

In order to show the nature of the potential trends, if exist, the values of various groupings of shields for various periods of time were examined. Figs. 5 and 6 show two types of average pressure in one-day period while Fig. 7 shows the full-face one-day average pressure in three weeks. In Fig. 5 when the one-day average shield pressure is computed for every shield across the face, the standard deviation of each shield from the average shield pressure of each shield varies from 6 to 32 %. In Fig. 6, when full-face average shield pressure is computed for every minute in a day, the standard deviation at each minute from the full-face average shield pressure at that particular time ranges from 19 to 34 %. In Fig. 7 when the full-face one-day average shield pressure is computed for a three-week period, the standard deviation for all shields in one day from the full-face one-day average shield pressure ranges from 31 to 40 %.

Figure 5. One-day Average Shield Pressure & Its Standard Deviation for Every Shield on May 3rd

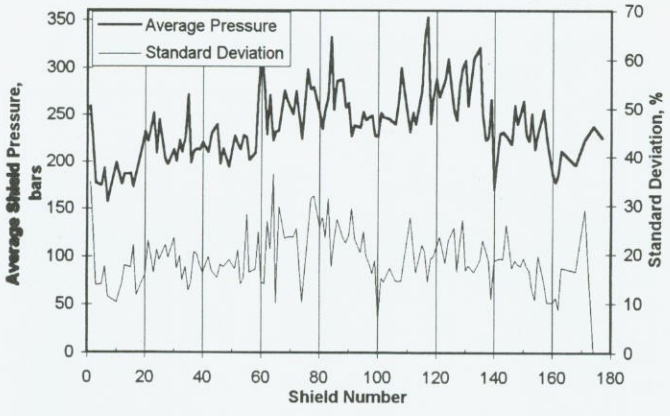



Figure 6. Full-face Average Shield Pressure & Its Standard Deviation in Every Minute, May 3rd

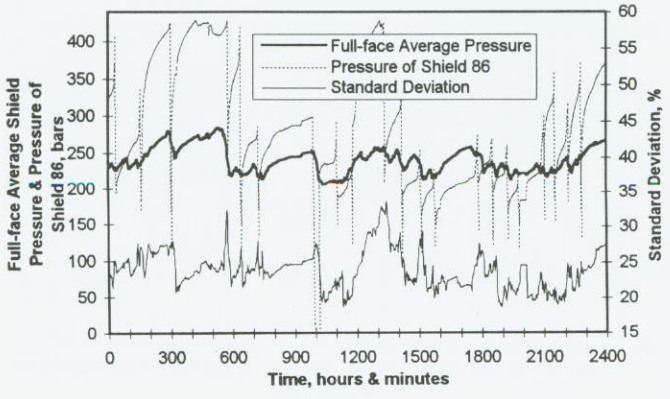
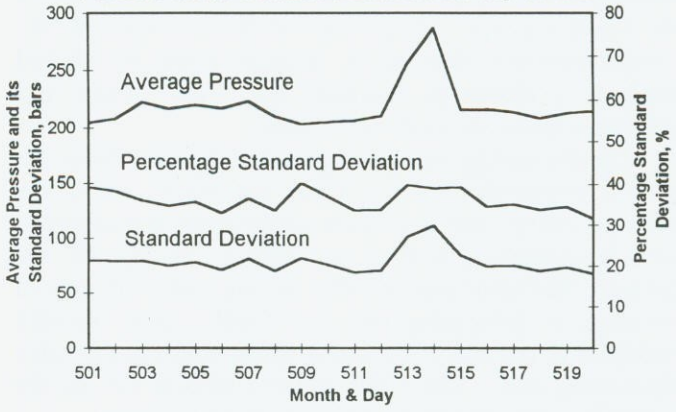



Figure 7. Variation of Full-face One-day Average Shield Pressure and its Standard Deviation from May 1st to 20




In summery the shield pressure varies along both the face transverse and face advance directions, with the pressure variance in the face transverse direction somewhat larger than that in the face advance direction in terms of standard deviation.

## Individual Shield Pressure

The leg pressure analysis of individual shields is the traditional method in this research field and here it is used to establish relationships between the pressure characteristics of individual shields and all the shields in the longwall face.

The pressure changes within a mining cycles can be divided into three types: increasing, steady and decreasing types based on whether the leg pressure, after setting, increases substantially, stay more or less the same, and decreases substantially, respectively. The following criteria of pressure changes were used:

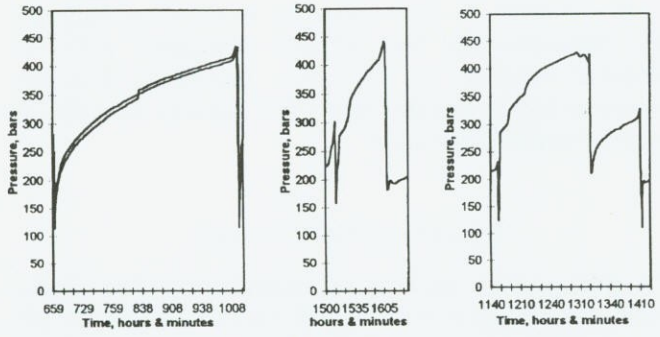
Increasing type : 80 bars < pressure change
Steady type : -20 bars < pressure change < 80 bars
Decreasing type : pressure change < -20 bars

Figure 8 shows examples of these three types of pressure changes in a mining cycle. The increasing type ( Fig. 8A ) receives the largest load increment. This type of pressure curve can be divided into three segments according to its rate of pressure change. The first segment is the initial rapid increasing segment and usually lasts less than 10 minutes just after setting. The second segment is the relatively steady increase segment after the initial rapid increase and takes most of the cycle time. The curve in the first and second segments is convexed. The third segment is the final rapid increase segment and occurs usually within 5 minutes just before shield unloading or the end of the mining cycle. The increasing type denotes a relatively intensive roof loading.

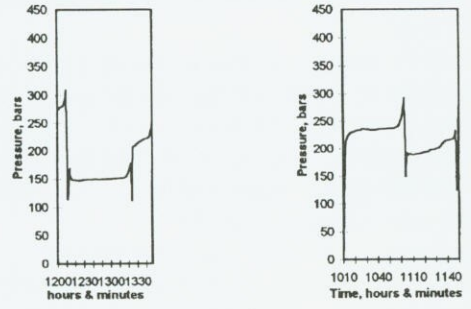
Shields with the steady type of pressure curves ( Fig. 8B ) receive less load than those with the increasing type.

The cycle curve can also be divided into three segments, but the first two segments are quite different from those of the increasing type. The pressure in the first segment may remain constant, decrease or increase while the second segment is always or normally flat. The steady type denotes a relatively weak roof loading.

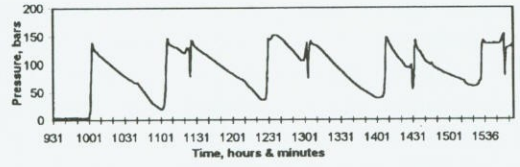
The decreasing type pressure curve denotes either the roof is extremely weak or it has too much roof debris between canopy and roof strata and/or under the baseplate or a leg leakage ( Hart et al., 1996 ). In Fig. 8C the pressure decreases rapidly after setting and continues to decrease at decreasing rate and finally some increase suddenly at the end of the cycle others finish at the same decreasing rate. Since this process repeats for all the cycles in a day, it is most likely a hydraulic leakage.




A Increasing Type




B Steady Type




C Decreasing Type

**Figure 8. Three Types of Pressure Changes in A Mining Cycle**

Although the final load in the increasing type is larger than either the steady or decreasing type, the frequency of the steady type is much larger, followed by the increasing type and finally the decreasing type ( Table 1 ).

**Table 1 Frequency Distribution of Three Types of Cycles**

| Cycle Type | Frequency, % | Number of Cycles |
|---|---|---|
| Increasing | 27.1 | 638 |
| Steady | 70.2 | 1,653 |
| Decreasing | 2.7 | 63 |
| Total | 100.0 | 2,354 |

## Full-face Shield Pressure

Figures 9 and 10 show the one-day average shield pressure and setting pressure for every shield in three consecutive days respectively. Note for clarity in these two figures the actual pressure is used for the first day and 50 bars and 100 bars are added to those in the second and third days, respectively. Again when examined in fine details the pressure varies from shield to shield and day to day. But a general trend or pattern exist as shown in Fig. 11. Pressures at both panel ends were smaller than the center. This is especially true for the pressure increment. This trend was also observed by Harris ( 1993 ) who attributed it to the effects of chain pillars on both ends.

**Figure 9. One-day Average Shield Pressure for Every Shield on May 1 ~ 3**

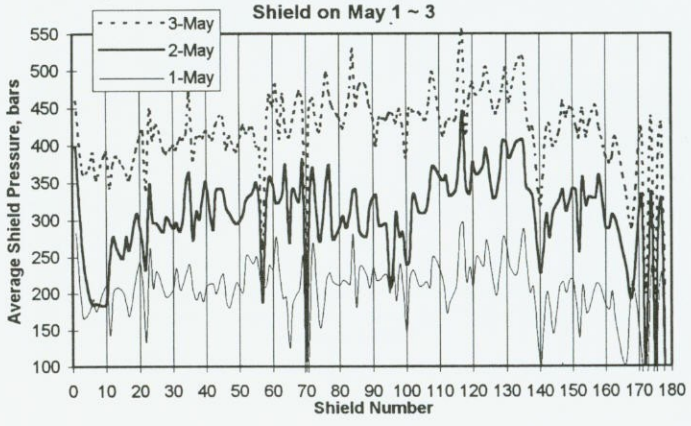



**Figure 10. One-day Average Setting Pressures for Every Shield on May 1 ~ 3**

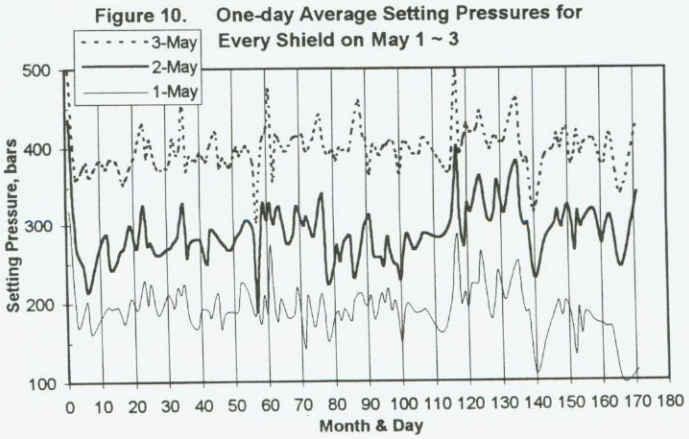


Figure 11. One-day Average Shield Pressures for Every Sheld May 3

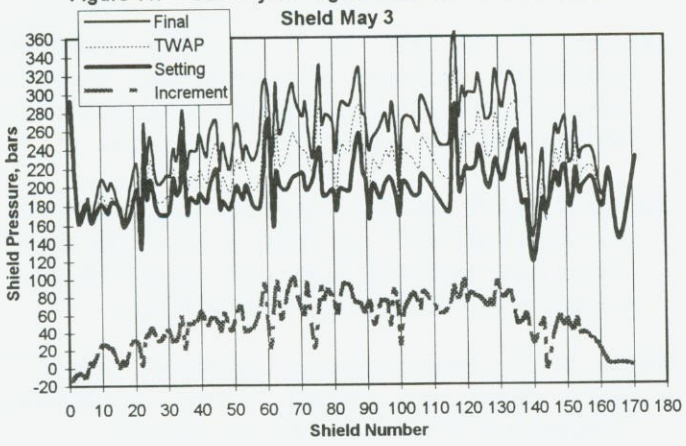



Figure 11 shows that the one-day average shield pressure patterns in final pressure, TWAP ( Time-weighted Average Pressure ), and setting pressure for every shield across the face appear to be similar. Therefore the setting pressure controls the final pressure ( and thus the pressure increment ) and TWAP.

Table 2 shows the frequency distribution of setting pressure for all cycles in a three-week period. There are many factors that could contribute to the wide ranging distribution of setting pressure even though the hydraulic pressure was set at 250 bars and positive setting was activated in this case. These factors include hydraulic distribution system, roof/floor condition, leg mechanics ( Barczak and Gearhart, 1997 ), positive ( or guarantee ) setting algorithm, valve integrity, hydraulic fluid, etc.

## Periodic Weighting

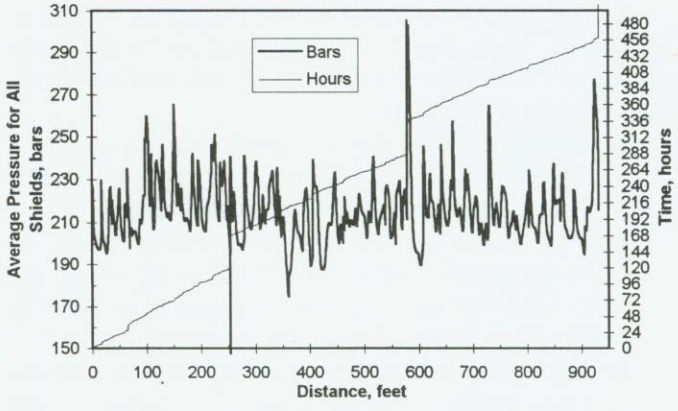
Figure 12 shows the full-face one-hour average shield pressure and time vs. distance for 22 days period. There are alternating peaks and valleys in pressure. The conventional method is to relate the peak pressures to weighting caused by various roof strata right before their breakage. Based on this concept the periodic weighting interval is 30 ~ 40 ft. Similarly the exploded view in Fig. 6 indicates that the peak pressure period consists of 2 ~ 3 cycles and the low pressure period consists of 2 ~7 cycles. It must also be noted that when the cycle time is long, the pressure is high and conversely when the cycle time is short the pressure is low. In other words when the face stops for a period of time, the pressure is increased to a higher value. The low pressure periods correspond to mostly normal face advance rate and in lesser parts to slower face advance rate and/or shorter face stops. Therefore roof loading on shield is controlled by the face advance rate and the time location in a mining cycle.

Table 2 Setting Pressure Distribution for 3 Weeks

| Setting Pressure* bars | Frequency % | Cycles |
|---|---|---|
| 0~20 | 1.24 | 493 |
| 20~40 | 0.93 | 370 |
| 40~60 | 0.74 | 295 |
| 60~80 | 0.55 | 218 |
| 80~100 | 0.56 | 223 |
| 100~120 | 0.93 | 369 |
| 120~140 | 2.87 | 1,138 |
| 140~160 | 9.25 | 3,669 |
| 160~180 | 18.55 | 7,357 |
| 180~200 | 23.30 | 9,243 |
| 200~220 | 15.74 | 6,246 |
| 220~240 | 9.87 | 3,917 |
| 240~260 | 7.34 | 2,911 |
| 260~280 | 4.25 | 1,687 |
| 280~300 | 1.96 | 778 |
| 300~320 | 0.76 | 303 |
| 320~340 | 0.53 | 210 |
| 340~360 | 0.32 | 128 |
| 360~380 | 0.22 | 88 |
| 380~400 | 0.04 | 14 |
| 400~420 | 0.03 | 10 |
| 420~440 | 0.01 | 3 |
| 460~480 | 0.00 | 1 |
| Total | 100.00 | 39,671 |

* the rated setting pressure is 250 bars

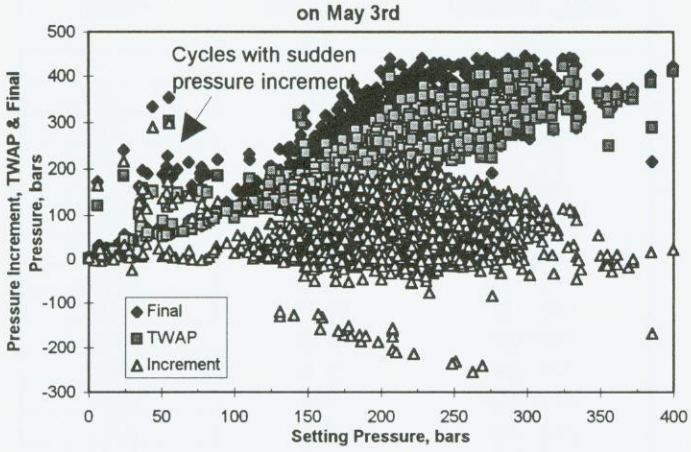
Figure 12. Full-face One-hour Average Pressure & Time vs Distance for 22 days




## Setting Pressure, Final Pressure and Pressure Increment

Each day there were more than 3,000 mining cycles for the 180 shields on the face. Those data were analyzed to show the relationship, if any, between setting pressure, final pressure and pressure increment ( Peng et al., 1987 ). Fig. 13 shows a representative total data presentation for May 3rd. Note, in a mining cycle of the increasing type, a sudden pressure increment occasionally occurs and these

Figure 13. Final Pressure, TWAP & Pressure Increment vs Setting Pressure for Every Individual Shield and Cycle on May 3rd




pressure increments most likely occur when the setting pressure is low.

Regression analysis shows the following relationships exist and confirmed the previous conclusion ( Peng et al., 1987 ).

$$P_f = 3.063 + 1.136 * P_s + 0.001231 * P_s^2 - 4.893 * 10^{-6} * P_s^3$$

$$P_i = 3.063 + 0.136 * P_s + 0.001231 * P_s^2 - 4.893 * 10^{-6} * P_s^3$$

where $P_f$, $P_s$ and $P_i$ are final pressure, setting pressure and pressure increment, respectively.

## Summary

Quantitatively, the shield pressure varies from cycle to cycle and from shield to shield and are multi-factor controlled. However for the medium-weak roof condition, the following trends exist:

1. Individual shield pressure pattern can be classified into three types: increasing, steady and decreasing. The steady type is by far the most common.
2. Even under positive setting operation mode the setting pressure varies considerably and mainly due to manufacturer's positive ( or guarantee ) setting algorithm, leg mechanics, valve integrity, etc.
3. Setting pressure controls the final pressure and the time-weighted average pressure, because they appear to have similar patterns in full-face shield pressure distribution.
4. In most cases the final pressure in a mining cycle or the maximum pressure imposed on a shield is proportional to the length of cycle time, and face stoppage, but inversely proportional to face advance rate.
5. The shield pressure is higher at the panel center and lower at/near both ends.

## References

Barczak, T. M. and D. F. Gearhart, Full-scale Performance Evaluation of Mobile Roof Supports, Proc. 16th Int'l Conf. on Ground Control in Mining, Morgantown, WV, August 1997, pp . 211-220.

Hanna, K. and K. Haramy, Automated Longwall Mining For Improved Health and Safety at the Foidel Creek Mine, paper presented at the SME Annual Meeting, Denver, Feb. 1991, preprint No. 91-165, 8 pp.

Harris, R. G., Longwall Support Monitoring, proc. 12th Int'l Conf. On Ground Control in Mining, Morgantown, WV, August 1993, pp. 143-151.

Hart, W. M., S. S. Peng, Q. H. Shen and J. S. Chen, Development of a Longwall Management System, Mining Engineering, 1996, 48 (9), pp. 67-72.

Park, D. W., D. Deb, Y. M. Jiang and R. L. Sanford, Monitoring and Prediction of Longwall Instability Using Artificial Intelligence Techniques, SME, Trans. T300, 1996, pp. 34-38.

Peng, S. S. and H. S. Chiang, Longwall Mining, Wiley, 1984, 709 pp.

Peng, S. S., S. M. Hsiung and J. M. Jiang, Method of Determining the Rational Load Capacity of Shield Supports at Longwall Faces, the Mining Engineer, Oct. 1987, 147 (313), pp. 161-167.

# Research on the Interaction Between Roof Strata and Shield Supports

*Shi Yuanwei*, Professor
*Gu Quanzhong*, Mining Engineer
Central Coal Mining Research Institute
P.R. CHINA

*Zhang Changgen*, Chief Engineer
*Li Jeanping*, Mining Engineer
Wangzhang Mine of Lu'an Coal Bureau
P.R. CHINA

## ABSTRACT

This paper discusses the results of research on the interaction between roof strata and shield supports including the active and passive supporting functions of the shield supports which prevents roof strata separation; pressure distribution on the canopy and under the base plate as measured in the laboratory and underground; comparison between various shield structures regarding their effectiveness on roof and floor control; and determination of optimum support capacity under given geological and mining conditions including hard-to-cave roof.

## INTRODUCTION

Research on the interaction between roof strata and shield supports produces the scientific results on which the criteria for selection of support type and parameters and the development of roof control measures are based. In recent years, we have not only completed underground and laboratory measurements of support loading behavior, we also engage in the theoretical analysis of the interaction between roof strata and shield supports. The major results are discussed in this paper.

## LABORATORY AND UNDERGROUND STUDY OF THE CONTACT SURFACE BETWEEN SHIELD AND IMMEDIATE ROOF SURFACE

### 1. *Active supporting function along mining direction*

Equilibrium conditions between a 2-leg shield and roof strata show that a shield has two supporting functions against the roof strata. The first one is the active supporting force during setting. It is determined by

$$P_{x1} = P_a(\delta_3 \cos\beta_a - \delta_4 \cos\beta_a) \qquad (1)$$

where $P_{x1}$ = pushing force of the shield support
$P_a$ = setting load of the tilt cylinder
$\beta_a$ = tilt cylinder's angle of inclination from the horizontal
$\delta_3, \delta_4$ = geometrical constants related to tilt cylinder and caving shield

$$\delta_3 = \frac{c + l_o \sin\beta_a}{h_2}$$

$$\delta_4 = \frac{\ell_o \cos\beta_a}{h_2}$$

$\ell$ = length of caving shield
$h_2$ = canopy thickness
c = length of tilt cylinder

Equation 1 shows that the push force of the shield increases with that of the tilt cylinder. It can prevent the roof movement toward the gob, thereby improving the roof especially the unstable roof.

The second active supporting function is created while the shield support is being loaded. When the external load does not pass through the shield's center of gravity, shield will rotate forward creating an active horizontal force against the roof. Loading tests in the CCRI full-scale powered support test show that during loading shield canopy moves toward the coal face horizontally which creates a horizontal force against the roof. The reverse is true during unloading, i.e. the canopy horizontally moves rearward toward the gob. (Figs. 1 & 2).

The active horizontal force mentioned above pertains to the 2-leg shield. This is one of the reasons that 2-leg shields are superior to the 4-leg shields. It is also one of the reasons why 2-leg shields are popular in China.

### 2. *Passive horizontal force along mining direction*

Theoretical analysis and underground load measurements (using the loading measurement pins) of shield components showed that a 2-leg shield creates a passive horizontal force along the mining direction. It can be calculated by

$$R_{x2} = \frac{f_1[P_1 \cos\beta_1 (1 - \frac{h_o}{b\tan\beta_1} - P_a \frac{c}{b}]}{1 - f_1 \frac{h_1}{b}} \qquad (2)$$

where $f_1$ = coefficient of friction between roof and canopy
$h_1$ = vertical distance between the upper surface of the canopy and the instantaneous center of intersection of the lemniscate links
b = horizontal distance between the joint where canopy and caving shield intersect and the instantaneous center of intersection of the lemniscate links
c = vertical distance from tilt cylinder to the joint between canopy and caving shield
$P_1$ = total load of the two hydraulic legs
Pa = pushing force of the tilt cylinder
$\beta_1$ = angle of inclination of the hydraulic legs from the horizontal

The characteristics of the passive horizontal forces observed underground for several models of shields are shown in Table 1.

Table 1 shows roof movement creates a horizontal force against the shield support, 80% toward the gob and in only a few face the roof exerts a horizontal force toward the face, probably only occurring during periodic weighting. The ratio of horizontal-to-vertical force ranges from 0.1 to 0.4.

It should be pointed out that both 2-leg and 4-leg shields create a passive horizontal force against the roof.

## CANOPY LOAD DISTRIBUTION

Canopy load distribution is an important factor in improving roof control. Laboratory and underground experiments conducted so far produce the following results.

### A. *Statistical distribution of canopy loading*

By nature, the roof is not flat and the contact between canopy and roof is restricted to a few small areas, normally three points of contact. Research shows that the points of contact are random and that loads at those points of contact follows the equilibrium conditions of moments about the joint between canopy and caving shield. Figure 3 shows the statistical canopy load distribution measured at Yima Coal Bureau for 2-leg shield ZY-1.

From Figure 3 it can be seen that the statistical canopy load distribution is not linear, but wavy. During periodic weighting it increases sharply. The common feature is that the resultant roof load also acts at or near the connection point between canopy and hydraulic legs. This point is located approximately at the center of moments of the canopy. An important conclusion is that the canopy load distribution can be simulated by the Unequal Contact Probability model developed by the senior author. A comparison between those calculated by the model and actual underground measurements is shown in Figure 4.

Through regression, we obtain

$$R_1/R_y = (5.5 \frac{L_2}{L_1} - 0.2)\% \qquad (3)$$

where $R_1$ = segment load on canopy (the canopy is divided into 12 segments)
$R_y$ = total load on canopy
$L_1$, $L_2$ = length of the front and rear end of canopy, respectively, as divided by the connection point between canopy and hydraulic legs

Equation 3 indicates that canopy load distribution can be changed by changing the ratio of $L_2$ to $L_1$.

In general most users adopt the linear load distribution that simplifies the determination of pressure distribution under a base plate (Fig. 5) in order to compare various types of shields.

### *B. Pressure Distribution Under the Baseplate*

The pressure distribution under baseplate can be determined by a specially-designed pressure sensor. Experiments show that the pressure decreases from the toe to the rear end following the negative exponential function (Fig. 6).

$$q_y = R_y \frac{A}{B_o} e^{-bx} \qquad (4)$$

where A, b = constants related to shield structures

$A = b[1 - 4.5 \exp. (-L_o/X_o)]$

$b = \frac{1 - B_o}{x_o}$

$B_o$ = shield spacing (ctr-to-ctr)

$L_o$ = length of the base plate

$x_o$ = distance from the toe to the point of application of the resultant load on the base plate

Figure 7 shows the pressure distribution for two different coefficients of friction (f = 0.2 and f = 0) for QY-320 shields at mining height of 3 m.

From Figs. 6 and 7, it can be seen that the maximum pressure under the base plate occurs near the toe and decreases rapidly away from it. Therefore the following factors must be considered in support design and selection:

(1) The maximum pressure is determined by shield's yield load capacity. Therefore for soft floor the shield load capacity must not be too large in order to avoid its toe being sunk into the floor.

(2) The maximum pressure is controlled simultaneously by shield support structure, working height, and coefficient of friction. They all affect the location of the resultant force on the base plate. In general pressure distribution for 4-leg powered supports is better than that of 2-leg shields.

## COMPARISON AMONG VARIOUS TYPES OF POWERED SUPPORTS

According to the analysis mentioned above, Table 2 summarizes the comparison between various shields and chock shields considering the advantages of support-roof strata interaction, moments of support, pressure distribution on canopy and under the base plate, etc.

## DETERMINATION OF POWERED SUPPORT CAPACITY

The required capacity of the powered support is determined in accordance with the mechanics and movement of the immediate and main roofs. It includes the rotation trends of the shear-fractured immediate roof and main roof movement characteristics. The fractured blocks in the immediate roof can be divided into two categories: those that rotate toward the face ($R_2$ & $R_4$) and those that rotate toward the gob ($R_3$) (Fig. 8). In $R_2$, the angle of fracture $\alpha = 90°$ while in $R_4$, $\alpha > 90°$. In $R_3$ $\alpha < 90°$. In the former case the support exerts a resistive force toward the face whereas in the latter case it is toward the gob.

The required support capacity is determined by the following equations:

For the first case

$$R_{y2} = \gamma h \ell_s \frac{\frac{1 + k_d(1 + \tan\delta)}{\tan(\alpha - \delta)}}{1 + \frac{f_d}{\tan(\alpha - \delta)}} \quad kN/m \qquad (5)$$

For the second case

$$R_{y2} = \gamma h \ell_s \frac{\frac{1 + k_d(1 + \tan\delta)}{\tan(\alpha - \delta)}}{1 - \frac{f_d}{\tan(\alpha - \delta)}} \quad kN/m \qquad (6)$$

r = rock weight per unit volume

h = height of immediate roof

$l_s$ = length of roof beam

$\alpha$ = angle of fracture in the immediate roof

$f_d$ = coefficient of friction between fractural rock blocks

$\delta = \tan^{-1}(f_d)$ = angle of friction between fractured rock blocks

$k_d$ = constant due to passive or weighting load by the main roof. Normally $k_d$ = 1.2-1.8 as determined by the force equilibrium condition

Figure 9 shows the required support capacity varies with immediate roof thickness and the angle of fractured rock blocks. It can be seen that the required support capacity increases with the thickness of the immediate roof but decreases with the increase in the

angle of fractured rock blocks, which means the harder the rock strata (the larger the angle of fractures) the larger the required support capacity.

## DETERMINATION OF REQUIRED SUPPORT CAPACITY IN HARD ROOF

Under this condition there are special features in roof movement. When the face has advanced for a certain distance the roof breaks suddenly above the supported area in the face and rotates toward the gob. Finally it rests on the rock blocks laying on the floor of the gob and reaches equilibrium after forming a semi-arch. Under this condition, the required support capacity is

$$R_y = \gamma h_1 \frac{C_y}{D_y} \qquad (7)$$

where $C_y$, $D_y$ = coefficient of load transfer and

$$C_y = 0.5 \left[L_p + \frac{h_2}{\tan\alpha} - 0.5 (Z-A) \tan (\alpha_1 - \delta)\right]$$

$$D_y = fd \frac{Z+A\sin(\alpha_1-\delta)}{2\sin(\alpha_1-\delta)} - 0.5 (Z-A) \tan (\alpha_1 - \delta)$$

$$\alpha_1 = \delta - \tan \left[\frac{M-h_1 (K_c-1)}{L_p}\right]$$

$h_1$ = thickness of immediate roof
$h_2$ = thickness of main roof
$K_c$ = bulking factor of immediate roof
$L_p$ = periodic weighting interval
$\alpha_1$ = angle of fractured rock blocks
$\delta$ = angle of friction between rock blocks
A = distance between the surface of the rock block and the contact point between adjoining rocks

$$Z = (h_2 - A) \sin (\alpha_1 - \delta_2) + [L_p + (h_2 - A) \cot\alpha] \cos (\alpha_2 - \delta_2)$$

From equation 7, the periodic weighting interval can be determined by

$$L_p = 0.41 L_{ob}$$

$$L_{ob} = \frac{b}{2} \sqrt{\frac{b^2 - \sqrt{b^4 - 2.56 h_2^2 R_t^2 C_1}}{\gamma h_2 R_{tC_1}}} \qquad (8)$$

where b = panel width
$h_2$ = thickness of main roof
$R_t$ = tensile strength of main roof
$C_1$ = strength reduction factor

The strength reduction factor can be determined by correlating the measured values with those calculated for equation 8. Equation 8 has been applied to and proven in, case studies in Datong Coal Bureau in which the measured and calculated values were very close.

## CONCLUSIONS

1. The 2-leg shields can generate active and passive horizontal forces against the immediate roof and improve roof control. This is one of the major reasons why the 2-leg shields are so popular.
2. Shields and chock-shields differ in the interaction with the surrounding strata. Final selection of support type depends on the classification category of immediate and main roof, canopy and base pressure distribution and other-structural features of the support.
3. Formulas for determining the required support capacity have been presented including for those hard roof which has been proven in practice.

## REFERENCES

1. Y. W. Shi and S. J. Chen, Selection of Support Capacity and Basic Structure of Powered Supports in Application of Rock Mechanics to Planning and Design Prior to Mining, A. A. Balkema Publishers, 1984.
2. Y. W. Shi and S. J. Chen, Floor Control in Longwall Faces, Coal Industry Publication Co., 1993 (in Chinese).
3. Y. W. Shi, Dynamic Interaction Between Roof and Powered Supports and Determination of Support Capacity, *Proc. of 2nd Sym. of Mining Sciences and Technology*, China University of Mining and Technology, 1991.
4. Q. H. Gu, Relationship Between Support and the Surrounding Strata in Sublevel Coal Faces, MS Thesis, 1995.

**Table 1. Characteristics of passive horizontal forces**

| Shield model | Ratio of horizontal to vertical force $R_x/R_y$ | Frequency of force direction % | |
|---|---|---|---|
| | | Toward gob | Toward face |
| G-320 | 0.225 | 82.8 | 17.2 |
| QY-1 | 0.323 | 90.2 | 9.8 |
| QY | 0.430 | 85.5 | 14.3 |
| YZ-1 | 0.133 | 98.2 | 18.2 |
| WS1.7 | 0.220 | 94.8 | 5.2 |
| ZY35 | 0.124 | 90.2 | 9.8 |
| X-4 leg | 0.070 | 80.6 | 19.4 |

**Table 2. Characteristics of Powered Supports**

| Type | | Structure | Mechanics | Adaptability to surrounding strata |
|---|---|---|---|---|
| shield | leg to caving shield | 2 legs to caving shield | support capacity smaller, uniform base pressure distribution, active horizontal force large | immediate roof I & II; main roof I & II combined |
| | leg to canopy | 2 legs to canopy | support capacity large, good stability, base toe pressure high, active horizontal force large | suitable for immediate roof, I, II, & III; main roof I, II & III; floor II or higher |
| | | 3 legs to canopy | support capacity larger, larger adjustable range for resultant force | |
| chock-shield | leg to canopy and caving shield | 4 legs to canopy & caving shield | good stability, poor anti-horizontal force, uniform base pressure, large adjustable range of resultant force, lower efficiencies use of support capacity | mainly suitable for immediate roof II & III; main roof II & III |
| | leg to canopy | 4-leg X type | large adjustable range of canopy resultant load, large ratio of maximum to collapse height, large support capacity | mainly suitable for thin seams |
| | | 4-leg chock shield | large support capacity, large adjustable range of resultant load, uniform base pressure | mainly suitable for immediate roof II & III; main roof II, III, & IV; no restriction on floor |

**Table 3. The ratio of required support capacity to immediate roof weight for different angles of fractures**

| Angle of fracture (degree) | 50 | 60 | 70 | 80 | 90 | 100 | 110 |
|---|---|---|---|---|---|---|---|
| Ratio | 7.30 | 4.80 | 3.64 | 2.73 | 2.14<br>1.77* | 1.49 | 1.24 |

* when the angle of fracture = 90° there are two likely movement trends for the immediate roof: rotating toward the face or toward the gob. Obviously the required support capacity for the latter case is larger than the former (2.14:1.77).

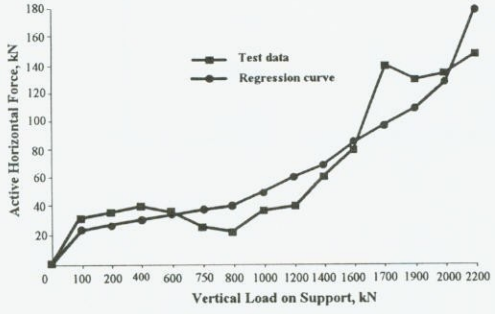



**Fig. 1 Horizontal Force of Shield Canopy Resulted from the Loading Test**

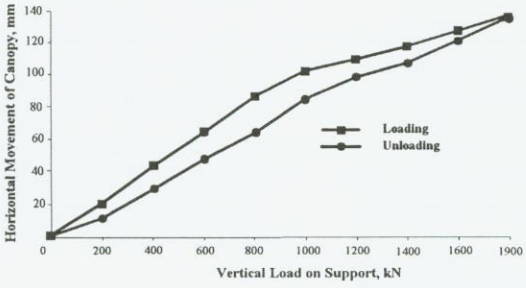
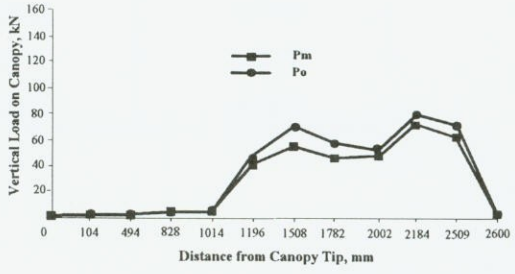
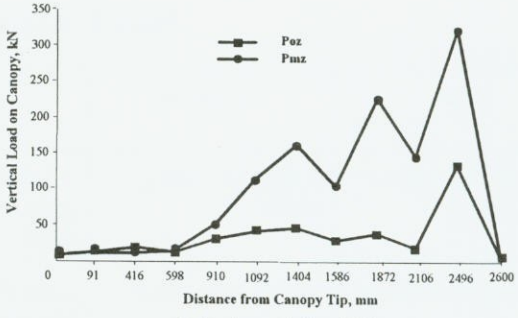



**Fig. 2 Horizontal Movement of Shield Caused by Loading Process**




**(a) During normal face advance**




**(b) During periodic weighting**

**Fig. 3 The Statistical Distributions of Load on Canopy for Shield ZYZ-1**

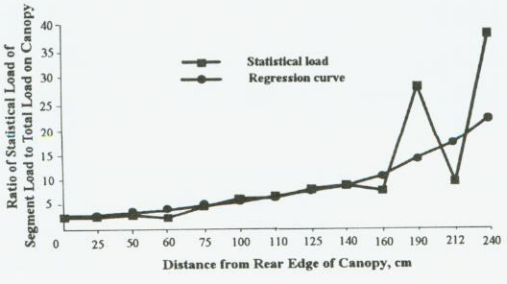



**Fig. 4 Comparison of Calculated and Measured Load**

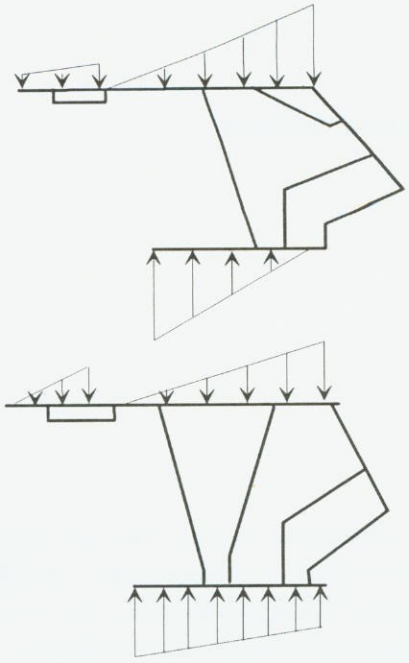


Fig. 5 Linear Load Distributions for Two-and four-legs Shields

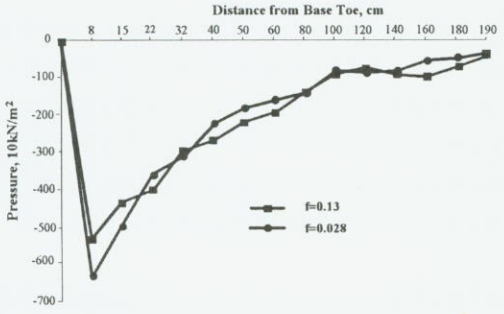



Fig. 6 Pressure Distribution under Base of Shield G-320

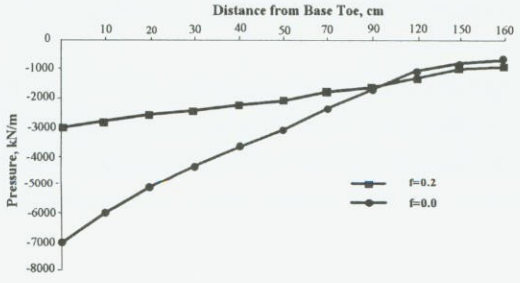



Fig. 7 The Calculated Base Pressure Distribution for Different Frictions Between Surrounding Rock and Supports

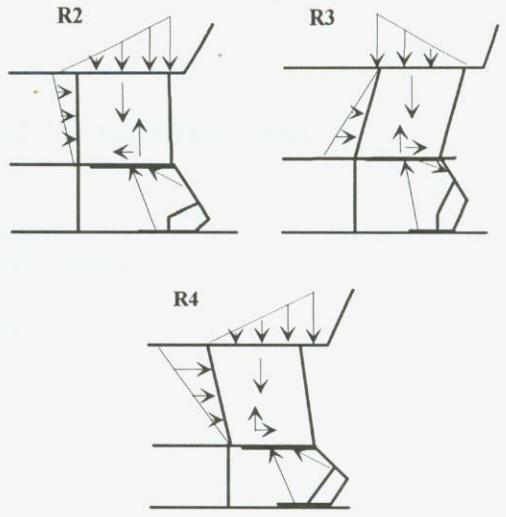



Fig. 8 Rotational Trends of Roof Blocks R2, R3, and R4

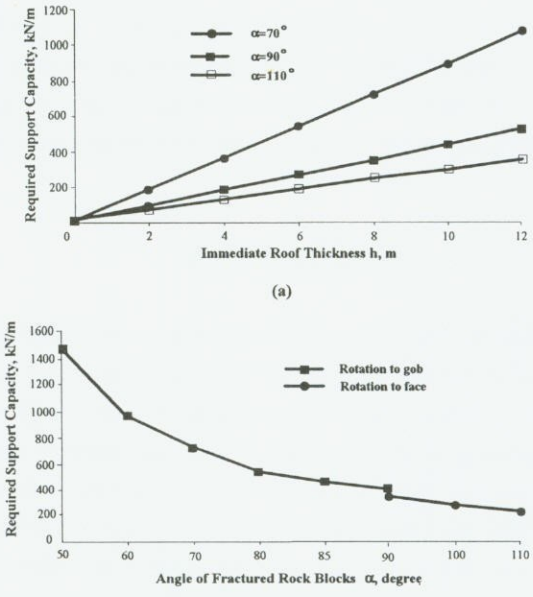



Fig. 9 The Required Load Capacity of Support as a Function of Immediate Roof Thickness (a) and of Fractured Rock Blocks (b)

# Roof Instability of Longwall Face at Ikeshima Colliery

*Kikuo Matsui,* Professor
*Hideki Shimada,* Associate Professor
Department of Mining Engineering
Kyushu University
Fukuoka, JAPAN

## ABSTRACT

Longwall mining is more productive in comparison to other methods but requires particular conditions for its effective use. This paper relates to longwall roof instability at Ikeshima Colliery. In order to make clear the cause of the longwall roof instability, scientific investigation in terms of geomechanical factors and longwall support system was planned and carried out.

## INTRODUCTION

Longwall mining method is used under a wide variety of geological conditions and is the most productive and safest underground mining system that is used worldwide. It is also the most promising mining method for thick and multiple seams. The introduction of the shield support improved the stability of longwall face remarkably. However, there are still two things to improve. One is the roof failure in the exposed immediate roof between the faceline and the tip of the canopy, and the other is spalling at the coal face. Instability of longwall face have a direct effect on the productivity, safety, and economy of longwall mining.

This paper describes longwall roof instability at Ikeshima Colliery in terms of why the roof fall is occurring and also the various measures available that may be used to prevent further occurrences. Some investigation visits were made to the face to examine the roof instability of the longwall face. Several roof boreholes were drilled in the roof to inspect the detailed roof lithology for the concerned area. Laboratory tests with the drilled cores of the roof were carried out. Another visit from the manufacturer of the shield supports was also made to check the support control system in the longwall face. The information gained from each of these investigations has been used to understand and solve the problems being experienced.

## FACE ROOF INSTABILITY

The concerned longwall panel is LW-West#4 and its panel size is 125m wide and 600m long. The working depth is around 540m below sea level. The working height is about 2.6-2.7m. The face is supported by 113 × 1.1m wide four-leg shield supports at the 125m wide face area. Figure 1 shows the design and some technical data of the four-leg shield support called IS (Ikeshima Support)-9 of Mitsui Miike Machinery Co. Ltd.

Observed roof falls and cavities occurred mainly in the central part of the faceline during the extraction of LW-West#4 panel as shown in Figure 2. The shaded portions and the solid lines show the roof fall area and the position of the faceline at the stage after the daily production, respectively. The distance between the lines means the daily advance of the longwall face.

The height of the cavities varies from 0.5m to 2.0m and the cavities extended back over the canopies of supports. From discussions with staff and face crews, the cavities tend to enlarge with both time and face advance unless any remedial action is taken.

Roof remedial measure was taken by using wood cribs that were set up on the shield canopy to prevent enlargement of the roof cavities and to ensure a normal working condition for the

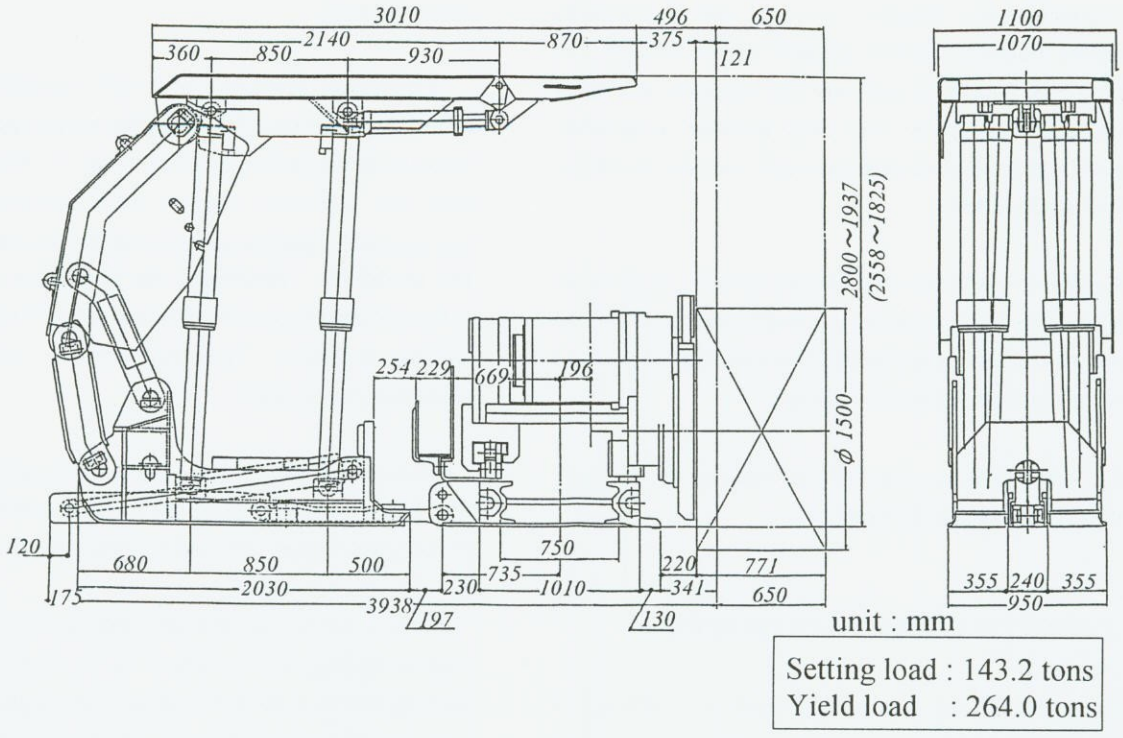



Figure 1 Four-leg shield support.

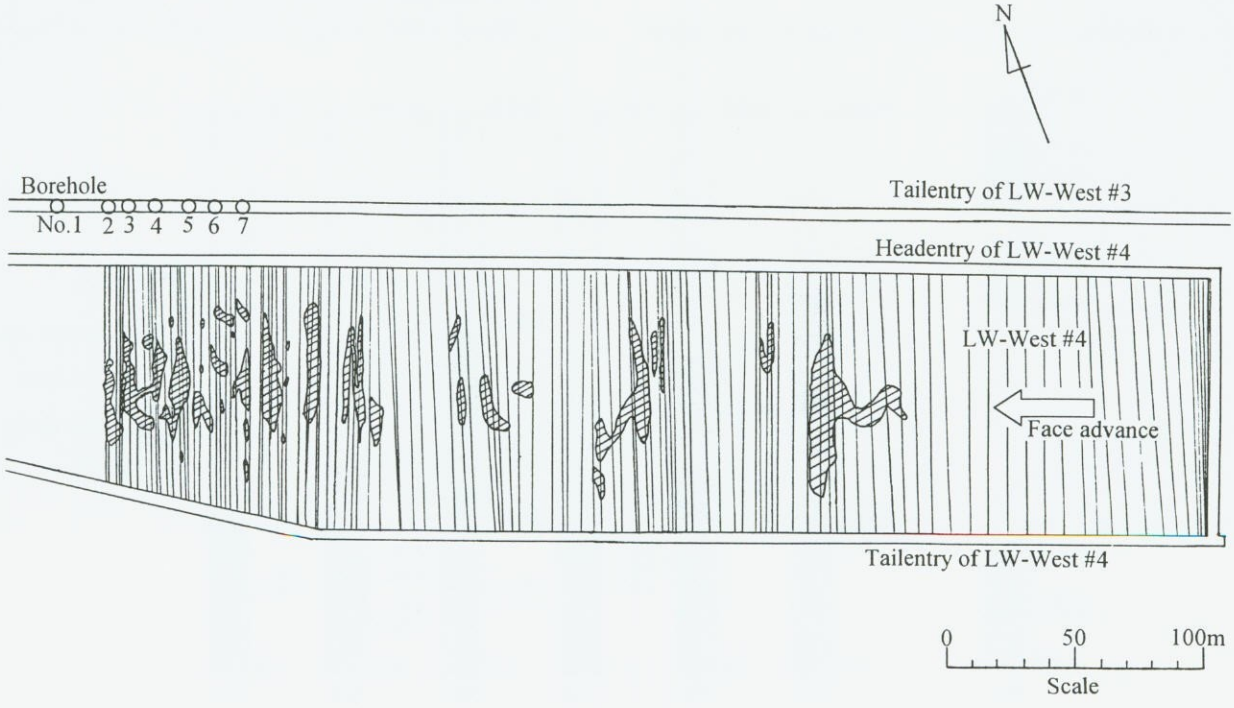



Figure 2 Roof fall during LW-West#4 panel extraction.

shield supports.

From examining the cavities, it is clear that they contain mining induced fractures running parallel to the faceline and hading back toward the gob and over the canopies at a steep angle. These fractures can be very close together in sections, delineating thin slices of immediate roof rock that tend to fall out quite ready if unsupported.

Coal face failure was observed with face advance, at times the face standing well along the entire face length, and at others, the central portion spalling quite readily thus exposing more roof than cut by the double ranging drum shearer.

Ground water conditions were damp and wet in the face. Water flow was not seen in the panel.

## GEOMECHANICAL INVESTIGATION

The behavior of mine roof is extremely sensitive to changes in roof geology. Seven boreholes (one is 39m long and six others are 10m long) were drilled and borecores were recovered to check the lithology and the geomechanical properties of the roof along the tailentry of the adjacent panel as shown in Figure 2.

Figure 3 is the lithology of the roof. Vertical and horizontal changes in lithology are clearly seen in the roof. A distinct massive sandstone unit of over 10m thick is present some 3-6m above the seam.

Mechanical properties and slake durability were estimated from laboratory tests by using the borecores. Table 1 lists the mechanical properties obtained from the laboratory tests. The shale and sandyshale showed weak strength properties under wet conditions and low slake durability as compared to those of the sandstone. Especially the immediate roof shale shows extremely poor properties. The main roof is relatively strong and massive sandstone. The floor rock is weak shale that is weakened due to water.

As mentioned before, ground water conditions were damp or wet in the concerned panel. So the in-situ mechanical properties of the rocks seemed to be deteriorated greatly.

Except for abrupt and abnormal geological structure areas such as faulting zones, there were no roof instabilities in other sections where a thick and weak immediate roof shale existed over 10m distance in the roof. Of course, there was not a thick and massive sandstone as a main roof.

It is necessary to understand well enough the mechanism of roof fall and the relation between the instability of the roof, and the thickness and strength of the immediate and main roof for

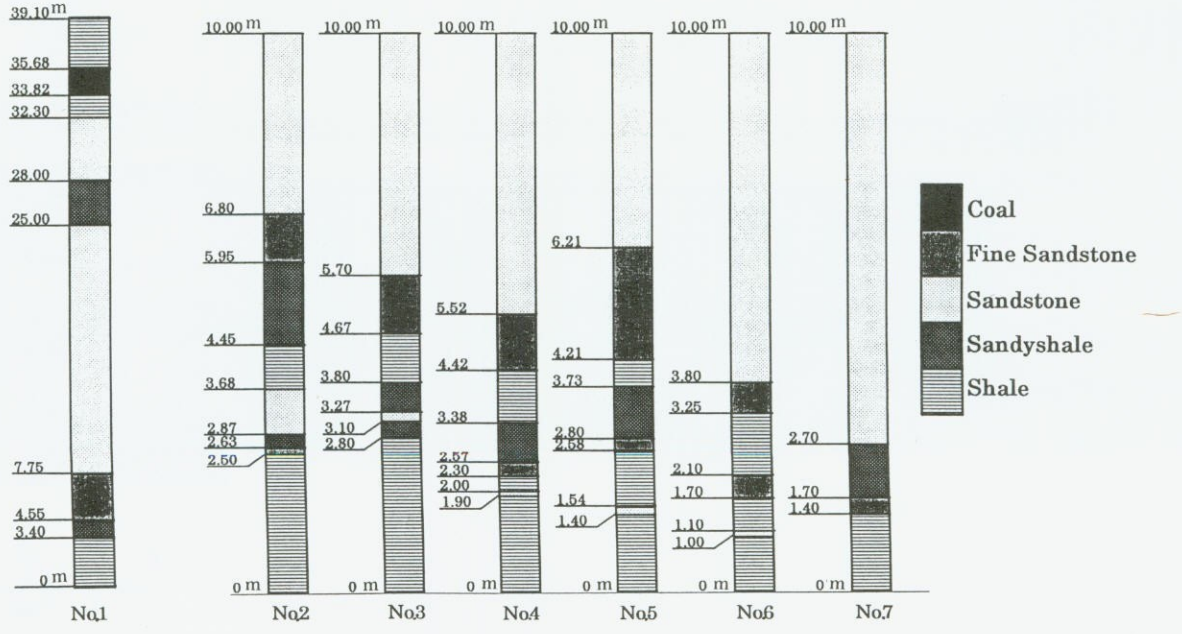



Figure 3 Lithology of the roof.

Table 1 Mechanical properties of roof, coal, and floor rocks in LW-West area.

| | | $Is_{(50)}$(MPa) | Sc(MPa) | $E_{50}$(GPa) |
|---|---|---|---|---|
| Roof | Shale(room) | 0.6 | 12.2 | 1.1 |
| | Sandstone(room) | 1.4 | 30.3 | 2.8 |
| | Fine Sandstone(room) | 2.9 | 63.0 | 5.7 |
| | Sandstone(room) | 3.6 | 78.2 | 7.1 |
| | Coal(room) | 1.4 | 11.5 | 1.8 |
| Floor | Shale(room) | 1.2 | 27.2 | 2.5 |

$Is_{(50)}$ : Point Load Index
Sc : Uniaxial Compressive Strength
$E_{50}$ : Tangent Young's Modulus at 50% of Peak Stress

achieving the roof stability.

## CONDITIONS OF SHIELD SUPPORTS

Shield support capacities have generally increased throughout the history of longwall mining. Nowadays, over 800tons capacity supports have been introduced to cope with difficult ground control problems (Barczak, 1992). In Australia, a 1000-ton four-leg shield support is now used (ACIRL: Australian Coal Industry Research Laboratories Ltd., 1994). However, the capacity of the IS-9 support is only 264tons. Despite this light duty support, it is true that the stability of longwall face has been achieved under most kinds of strata conditions at Ikeshima Colliery.

It is important to make clear the effect of the shield support system on the roof instability during mining cycles. Investigation visits from the support manufacturer were made to check the support system conditions. From examining the conditions, it was pointed out the following problems in terms of the support system:

1) Most supports were set at less setting load than the prescribed load of 143.2tons.
2) There were some leakage of hydraulic fluid from the legs and the control valves.
3) Lateral tilting of the support was occurring in some supports due to poor floor conditions.

These three problems inevitably affect the required setting load to control the immediate roof.

Four-leg shield supports have been traditionally used in Japan. In 1996, Kushiro Colliery first introduced a 738-ton two-leg shield support that is made in Germany. This capacity is the biggest in Japan.

Differences in two-leg and four-leg shield support provide for different strata interactions. The primary difference is the ability of the two-leg shield support to provide an active horizontal force. Since the leg in two-leg shield support is inclined toward the coal face, horizontal components of the leg force push the canopy toward the coal face. This induces a force into the immediate roof that tends to maintain the roof in a state of compression. On the other hand, a four-leg shield support do not produce an active horizontal force. Therefore, two-leg shield supports are more effective in controlling highly fractured or friable immediate roof.

## ROOF FAILURE MECHANISM

In this section, roof failure mechanism will be discussed by using the results that were obtained from the field observations and laboratory tests. The facts that the roof falls are confined almost entirely to the central part of the face and the falls occur after a certain interval of face advance suggest that the importance of the behavior of the roof strata or the periodic weighting of the overburden be taken into consideration. The periodic weighting is that the energy in the overburden is periodically stored during longwall mining cycles and released as the face advances.

The face roof fall mechanism that is related to the periodic weighting was discussed by ACIRL (Frith, et al., 1992). The

inferred mechanism of load storage and release that is associated with the periodic weighting is shown in Figure 4, whereby a massive strata unit is of sufficient thickness and strength by which it has the ability to form a significant cantilever as the face advances and stores the loading of the overburden. Under this condition, the loading is thrown ahead of the face and distributed over a large area, hence a light face loading condition occurs. At some point, the cantilever will break as its length increases and it will fracture in tension at its fixed end. As a result, the distributed load is concentrated on the immediate few meters of coal and the shield supports. The thinner the immediate roof is, the greater the load concentration is.

The behavior of the main roof is irresistible in terms of any shield support capacity that conceivably could be provided. Hence, it is concluded that the support has no influence on main roof behavior. Therefore, setting pressure should be about 60% of the yield pressure to maximize the available support capacity to absorb the load concentrations that is developed from the periodic weighting (Barzak, 1992).

The next issue is why the central part of the faceline is always affected. Figure 5 is an example of the redistributed vertical stress along the faceline. A higher front abutment stress is occurring at the central part of the faceline. This is the reason why the cavities and the coal face failures are created predominantly in the center of the face. The presence of solid ribs/pillars on either side of the panel gives protection to the face ends from the effects of longwall mining.

Time effect cannot be disregarded. Under certain conditions, time can play an important role in roof stability. Although longwall faces are stood for extended periods, the ground conditions do not deteriorate significantly as a result. However, in some cases, roof falls have occurred after a face has been stood for only one day, and even for a few hours.

It is concluded that stopping the longwall will have a varying effect on the local ground conditions due to the existence of a massive sandstone in close proximity to the seam and the periodic weighting.

The final issue is the existence of ground water. Water weakens certain rocks. Especially, shale or sandyshale deteriorates and loses almost all its mechanical properties by slaking or cracking with water (Matsui, et al, 1990). Under wet conditions, it will be greatly difficult to control the immediate roof and floor, and also the shield supports.

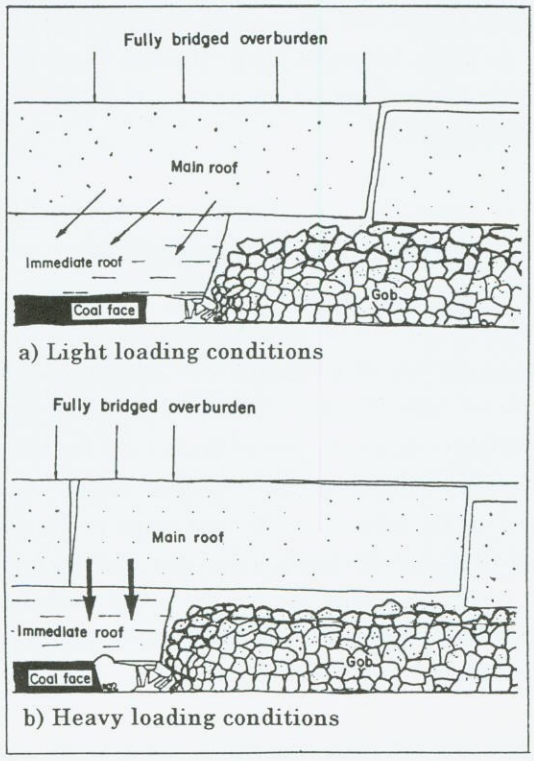



Figure 4 Periodic weighting.

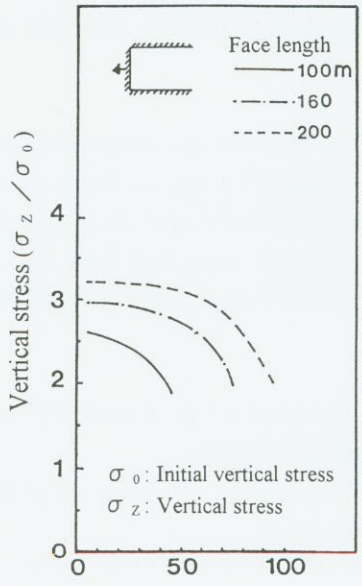



Figure 5 Vertical stress distribution along the faceline.

## CONCLUSION AND RECOMMENDATIONS

In conclusion, this paper describes the longwall roof instability at Ikeshima Colliery. Some investigation visits were made to the face in order to check the roof instability and the shield support system. Geomechanical investigation was also performed by using borecores. From these investigations, it is clarified that the roof instability mainly results from the face support conditions, and the periodic weighting that relates to the existence of the relatively thin and weak immediate roof shale, and the strong and massive main roof sandstone.

It is suggested that the following measures be taken to control the roof more effectively:

1) The shield supports should be set at about 60% of the yield pressure.
2) The shield supports should be checked, maintained, and repaired periodically to secure the performance.
3) A thin coal septum should be left in the roof to control the weak and prone-to fractured shale above.
4) Roof bolts should be installed at the longwall roof locally.
5) Two-leg shield supports should be introduced instead of four-leg shield supports, if possible.

After being taken the first two measures above, the roof instability is improving very well.

Knowing the geological conditions is extremely important for mining layout. It is possible to know overall geological conditions roughly, but extremely difficult in detail. Under the complicated and ever-changing geological conditions in Japanese underground coal mines, various geological structures often occur in the same section or panel. Therefore, it is likely that a stable roof will change partially into an unstable one.

## ACKNOWLEDGMENTS

The authors would like to thank the staff of Ikeshima Colliery and the staff of Mitsui Miike Machinery Co. Ltd. for their help and cooperation in providing relevant information in the preparation of this paper.

Any opinions stated in this paper are those of the authors themselves and are not necessarily those of the colliery or the maker.

## REFERENCES

1. ACIRL, 1994, Australia's Longwalls.
2. Frith, R.G., A.M. Stewart and D. Price, 1992, Australian Longwall Geomechanics - A Recent Study, Proc. 11th International Conference on Ground Control in Mining, Wollongong, N.S.W., Australia: 131-139.
3. Barczak, T.M., 1992, Examination of Design and Operation Practices for Longwall Shields, U.S. Bureau of Mines Information Circular, IC 9320 14 pp.
4. Matsui, K., M. Ichinose and H. Shimada, 1990, Characteristics of Mechanical Properties of Coal Measure Rocks and Coal and Their Application to Mining, Proc. 8th Japan Symposium on Rock Mechanics, Tokyo, Japan: 375-380,(in Japanese).

# Gob Canopy Roof Support for Difficult Natural Conditions

*Jay Hilary Kelley,* Distinguished Professor Emeritus
Department of Mining Engineering
College of Engineering and Mineral Resources
West Virginia University
Morgantown, WV

## ABSTRACT

This paper proposes a modification of longwall roof support to meet new difficult mining conditions that are anticipated in the future. A gob canopy is a movable appendage attached on the rear of a longwall shield to counterbalance the troublesome forward downward force couple (FDFC). The gob canopy can be swung in both vertical and horizontal directions, powered by hydraulic cylinders. Several functions and applications are described

## INTRODUCTION

As we move into the next decade of longwall mining, improvements and advancements will have to be made in the design, function, and fabrication of the roof supports. Assuming that the preferred design of longwall roof support will continue to be the two or four legged shield, the shields themselves will require a number of modifications in order to remain a critical component of the evolving system. While one could conger up several design improvements for longwall roof supports, this paper focuses on one: the gob canopy. The gob canopy can improve the productivity, the environmental aspects, and the resource recovery potential of the mining operation. Indeed, some of the improvements are even applicable for current longwall operations. Current problems such as the digging in of the front toe of the base plate of the shield and/or the misalignment of the shields could be remedied by the adoption of the gob canopy modification.

## PREVIOUS ROOF SUPPORT DESIGNS

In the history of mechanical roof support development, there have been many designs ranging from manually installed chocks to the modern shield. Previous designs include special purpose mobile shields for pillar recovery, for entry driving, and for sublevel stoping in very thick mineral deposits. Some of these roof support designs are similar to the gob canopy modification on shields, described herein. At least 25 patents have been awarded to inventors in the U.S., United Kingdom, France, and Eastern Europe for hydraulic support designs. However, none of these directly address the defects that are addressed by the gob canopy concept. Early types of longwall chocks did not have caving shields but had chain bars on the gob side of the chocks to prevent the incursion of the caved gob into the inside of the chock area. In sub level stoping type of mining, various roof supports have been designed which were less directional than longwall roof supports in coal mining. However none of these devices were specifically designed to perform the three functions that are addressed by the gob canopy additions to the longwall roof support described herein.

### Current Longwall Mining Conditions and Problems

The acceptable configuration of the machinery in a longwall face and the system of extracting and transporting the coal at the face renders it nearly impossible to avoid a differential bearing pressure on the roof support base. A force diagram of a typical longwall roof support demonstrates that if a uniform loading is placed on the total length of the canopy there will be a differential force placed upon the base. Because the area of the main canopy extends forward beyond the area of the base plate, with the centerline of it also forward of the centerline of the base plate, typically 50 inches or more, it is easily seen that there will be a differential pressure on the base and not uniformly loaded.



Current Practice to Meet the Dilemma

Measures have evolved to offset the differential pressures on the base of the roof support. Understanding the tendency for the toe to sink into the bottom, most designs of roof support now incorporate:

- a sloping skid type of toe which tends to restore the base plate to the level of the mine floor as it is pulled forward by a hydraulic ram.
- The kinematic angle of the ram system or lifting jack which raises the toe of the base.
- loading the main canopy non-uniformly, i.e. heavily on the rear and by lightening the setting pressure on the tip of the canopy.
- roof support design in which the base plate centerline is no greater than four feet rearward of the main canopy centerline.

Frictional force between the main canopy and the roof surface plays a role in current roof support. Given heavy setting and yield loads on the canopy, some elastic stress and strain could offset the tendency to the forward force couple.

Caved roof from the gob also adds weight on the caving shield helping to offset the FDFC. Moreover, many successful longwall operations rely on favorable natural conditions. These conditions are:

- stable roof over the extracted web;
- dry shale or slate bottom.
- roof not caving on any part of the canopy.

Anticipation of Future Mining Conditions

One can safely predict that future longwall mining methods will encounter:

- more difficult natural conditions,
- continued harassment from opponents of surface subsidence, and
- economic demand for yet higher productivity.

One can also expect that there will be a merging of the speed of face advance and the better control of subsidence. One can then conclude that longwalls will operate in worse mining conditions because of lesser choices of coal seams and be designed for much higher face advance speeds, i.e. much wider webs. One should also expect that due to the need to reduce respirable dust that even greater amounts of water sprays will be utilized and that seams of coals will be encountered where the bottom consists of soft clays.

## EQUIPMENT DESIGNS FOR FUTURE LONGWALLS

The history of mining technology has always been the joint innovative efforts by machinery designer and manufacturers and mine operators. The reasonable expectation is for this concept to continue.

Description of the Gob Canopy

Figures 1A and 1B shows a typical two-legged shield, and Figure 2 shows how a gob canopy would be attached to it. The Gob Canopy modification of a typical longwall roof support, whether a two or four legged shield, is attached to the caving shield with a horizontal pivot and through a mating plate of the gob canopy system. The arrangement is shown in Figure 3, and in Figure 4. The gob canopy replaces some of the function of the caving shield, but the caving shield maintains the essential function of the lemniscate structure. Oriented toward the gob, the gob canopy can swing right, left, and vertically up and down.

In the up position, the gob canopy engages the solid roof or fractured roof in the gob and applies as much force as necessary to restore a uniform pressure density to the base-floor interface. When advancing the shield, the gob canopy can pivot rightward or leftward, interacting with debris, fractured roof, etc. in the gob to impart a force that steers the shield as it advances thus realizing tilted and out of line shields. The movement of the gob canopy is actuated by hydraulic cylinders in various arrangements.

Figure 2 is a simple version of the Gob Canopy. It swings vertically on a horizontal pivot actuated by a single hydraulic cylinder connected between the rear of the base plate and the gob canopy. The more advanced version pivots both vertically and horizontally and is actuated by hydraulic cylinders for both types of movements. An opening in the caving shield of the roof support allows for access to the gob canopy for its control. Horizontal movements can be achieved either by the differential extension of the two hydraulic cylinders angled from the sides of the base plate to a center point on the gob canopy. These two cylinders also raise and lower the gob canopy. An alternate arrangement for horizontal movement is the placement of a hydraulic cylinder within the two plates of the gob canopy as shown in Figures 5A and 5B.

Functions of the Gob Canopy.

The Gob Canopy has 3 functions:



1. It counterbalances the forward-downward force couple (FDFC) imposed by loading the main canopy. Longer forward canopies would be used for shortwall mining using continuous mining machines. A shortwall system would require also a much longer gob canopy probably with a detachable extension.
2. It can steer the direction of advance of the roof support.
3. It can provide an area of the gob immediately behind the roof support for collecting, gathering and distributing debris for packing and backfilling.

Benefits of the Gob Canopy at the Future Longwall Face

The use of a rearward extending gob canopy into the gob counteracts the forward downward force couple (FDFC) caused by the off-center loading of the roof strata on the main canopy of the shield. The gob canopy establishes a counteracting couple as it engages any solid resistance in the gob, be it remaining strata of fallen rock or debris. The couple would maintain a level base even in a very soft bottom or otherwise restore the pressure density on the base of the roof support and to offset the additional downward force couple when it is desired to increase the web distance.

There are two reasons for anticipating a wider web distance The one is to increase productivity at the face which one should expect to occur over the next decade. Already having increased from a very short web of the six inch plow to 30 inches and now in some cases to 42 inches, one should expect web distances to increase to five, six and seven feet once the cutting equipment is developed. An increase in web width would clearly be an essential feature for increased productivity when one considers the savings in turn around and setup times.

The argument could be made that wider webs could be treated in much the same way the mal-distribution of loading is now handled, i.e. by loading the rear end of the shield supports plus other measures previously discussed, including friction on the roof surface. But this is unlikely, because there is a limit to what yield loads can be feasibly installed. Yield pressures of hydraulic fluids and metal strengths are limited by the physical space available for the larger hydraulic cylinders to support the enormous weights. Moreover, future designers will have to expect less favorable mining conditions.

Gate Entry Support

Longer canopies are even now needed at the gate entries, especially in the head gate entry where there is usually considerable congestion of equipment and where roof action is often severe. The gate entries would preferably require long supporting canopies beyond the T-section. While the tailgate entry is less of a problem, the headgate entry is today a problem and will remain a problem unless better solutions are found for supporting the roof in this critical area of the longwall. To begin with, the roof strata stresses encountered in the headgate entries are particularly severe especially as the face advances.

The ideal support for the headgate entry as a whole has not been realized after many decades of research and development and manufacturing experimentation. Although the longwall roof support is not intended to provide support throughout the total length of the headgate entry, an improved longwall roof support would go a long way to alleviate the problem at least at the T-section. It would be desirable to extend the canopies for the three or four roof supports that span the headgate entry at the T-section. Extended forward canopies would be feasible if those supports were equipped with gob canopies. The headgate entry support is a special case where the gob canopy can counter balance the heavy loading of the entry roof. To offset the long main canopy or canopy extensions, a rear canopy can also be extended by the use of H-beams or box beams temporarily attached through a bolting or clamping fastening scheme and then could also be released as a disposable appendage. There are occasions when the roof will not cave behind the roof support and such cases there would be no fixed or restraining anchor for the gob canopy to interact with and in some cases, if that situation could occur, the gob canopy could be raised even into the vertical position. But less likely if there were a disposable extension on the canopy. Then the angle that the gob canopy would have to be raised to contact the restraining force would be minimal

Directional Control of Shield Supports

Moreover, one should also expect that longwall mining will encounter more and more inclined coal seams by which longwall roof supports will be more difficult to maintain in good alignment. Tilting shields is often a problem also. Maintaining alignment of the supports is labor intensive and is a chore the mines could do without. A much easier way of adjusting the alignment of the roof supports is using the rearwardly extending gob canopy. It can steer roof support as it advances toward the face by thrusting the rearward facing canopy to the opposite side of the desired direction. In this way a misaligned roof support can be redirected along side of the adjacent roof supports and correcting its tilt. This function is applicable in sloping seams and undulating surfaces.



Optional Debris Gathering and Distribution

While it is not known at this time what the future will hold for the requirements for mining companies to use pack walls and back filling to counteract the surface subsidence due to mining; or in another aspect, using the underground excavations as a disposal for the surface produced environmental wastes. In either case the use of an auger or slusher type or chain conveyer type device could be placed under the gob canopy and be protected by it from the falling rock. In either case the rear of the longwall roof supports could be used either for the distribution of surface materials or the gathering of smaller pieces of crushed rock for the use in pack walling and back filling.

The gob canopy concept lends itself to the use of the gob side of the roof support for environmental ends. For example, the rearward canopies could be shaped in the form of grizzly bars for the recovery of fragmented rock pieces. The debris and rock fragments could then be transported using a slusher or other type of conveyance at the gob side of the roof support for potential use in pack walls in the case of advancing longwall or in the better control of surface subsidence. Subsidence control could become one of the economic determinants considering that much longwall mining is conducted underneath residential and industrial structures.

## PATENT STATUS AND CONCLUSION

The Gob Canopy concept was patented in 1984. but was never put into the market or even promoted to the industry. It is probably of more interest now that longwall mining is dominate as an underground production method and the problem of longwall support will be regarded as a necessity.

## REFERENCES

Peng, S.S. and Chiang, H.S. Longwall Mining. John Wiley & Sons. New York, 1984.

Peng, S.S. and Chen, J.S. "Determination of floor pressure under the base plate of powered support"The Mining Engineer, March 1993. London,

Kelley, J.H. "Gob Canopy for a Mine Roof Support" U.S.Patent #4,480,946.Washington, DC Nov. 1984

Sanzotti, M.J. and Bise, C.J. "Concomitant backstowing: Potential for alleviating concerns associated with high-production longwall mining." Mining Engineering October 1996. SME/AIME.

Koehler, J.R.,Demarco, M.J.,and Wuest, W.J. "Critical pillar concept in yield-pillar-based longwall gate-road design." Mining Engineering August 1996. SME/AIME.

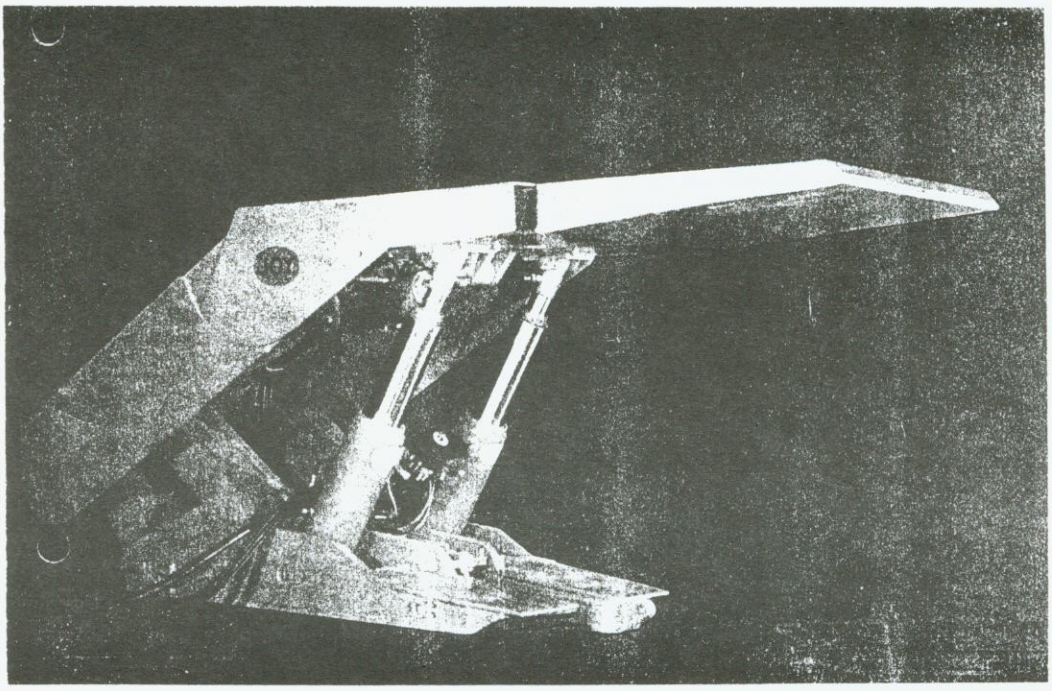


FIGURE 1A. PHOTO OF A TYPICAL 2-LEGGED LONGWALL SHIELD BY JOY MFG. CO.

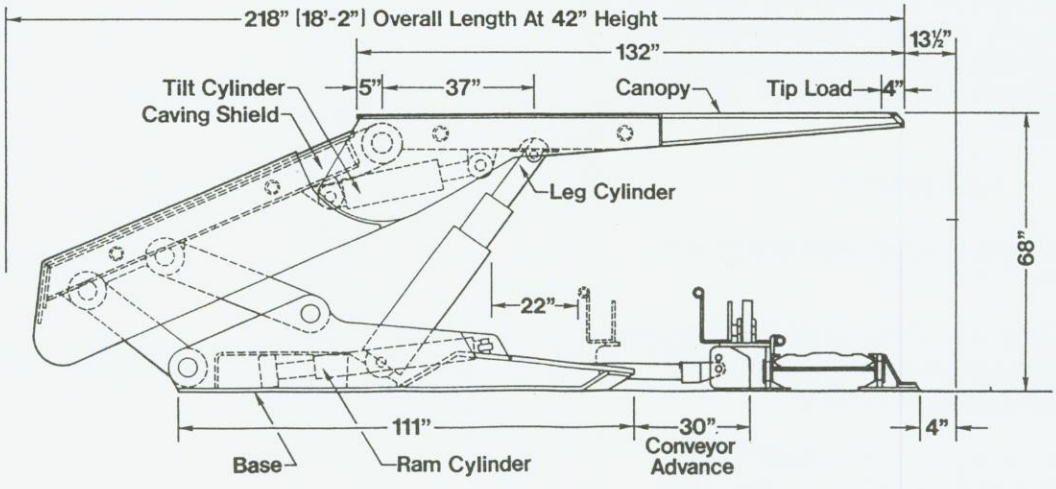



FIGURE 1B X-SECTION OF A 2-LEGGED LONGWALL SHIELD

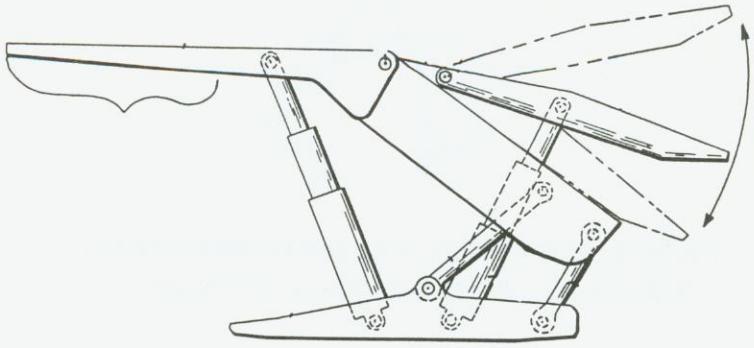


FIGURE 2 2-LEGGED LONGWALL SHIELD MODIFIED WITH GOB CANOPY ATTACHMENT WITH A SINGLE OPERATING CYLINDER

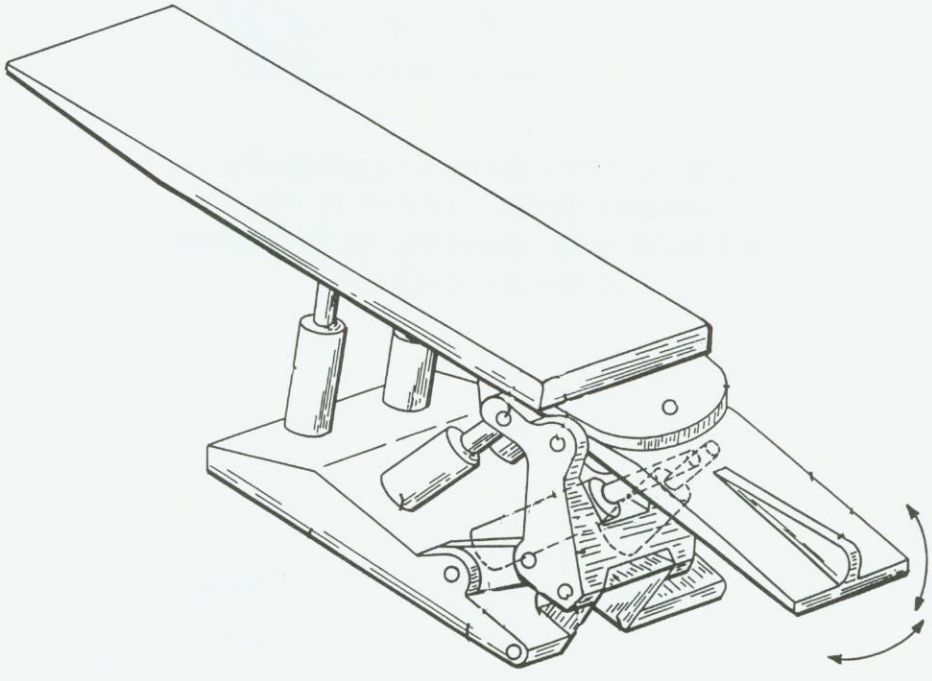


FIGURE 3. ISOMETRIC VIEW OF A 4-LEGGED SHIELD WITH DUAL GOB CANOPY OPERATING CYLINDERS

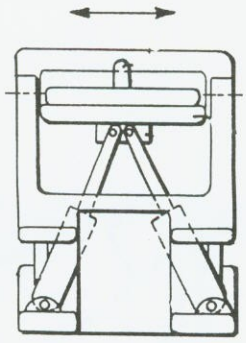


FIGURE 4. END VIEW OF A 4-LEGGED SHIELD WITH DUAL GOB CANOPY OPERATING CYLINDERS.

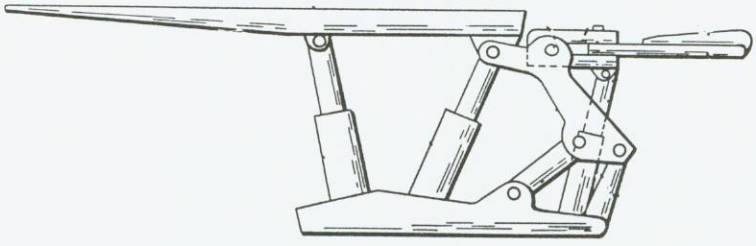


FIGURE 5A. SIDE VIEW OF A 4-LEGGED SHIELD MODIFIED WITH A GOB CANOPY WITH HORIZONTAL SWING POWERED BY AN INTERNAL HYDRAULIC CYLINDER

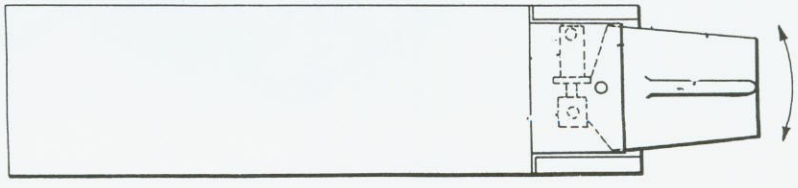


FIGURE 5B. TOP VIEW SHOWING THE HORIZONTAL THRUST CYLINDER OF FIGURE 5A.

# Yielding Cement Roof Supports for Longwall Mining

*Alan A. Campoli,* Business Development Manager
*Mike R. Amick,* Divisional Marketing Manager
*Peter S. Mills,* Technology Manager
*A. J. Rohaly,* Product Development Engineer
Fosroc Inc.
Georgetown, KY

## ABSTRACT

Fosroc continues as a leader in the development of cementitious technology for the mining industry. The considerable expertise accumulated in the development of the Fosroc cement line has been employed in the development of two pumpable, supplemental roof support systems. The Tekprop system is a unique combination of steel and concrete, specifically designed as a viable alternative to conventional wooden supplemental support. The second system is the Fosroc mineable crib which is a cost competitive variable yield system designed to support longwall ventilation and pre-driven recovery room entries. Two, separate, ongoing, full scale applications of these systems will be discussed during the conference presentation.

## INTRODUCTION

Traditional longwall secondary and supplemental roof support consists of wooden posts and cribs. The deformation characteristics of wood allow the design and construction of roof support compatible with the coal roof, floor and pillars. However, the remarkable production rates of modern longwall retreat sections require very rapid installation of secondary and supplemental roof support. These same supports must provide ever increasing reliability to protect the massive capital invested in longwall mining equipment. Further, the high strength and low cost wood necessary for longwall roof support is in increasingly short supply. In reaction to these trends a number of products have been developed to replace traditional wood supports.

Fosroc has led the development of pumpable cement products for longwall roof support. In 1993, the Southern Ohio Coal Company employed Fosroc's Tekcrib to support gateroad entries at the Meigs No. 31 Mine. The Tekcrib supplemental support consists of foamed cement pumped into tubular bags. Due to the difficult to access location, in this case the cement was mixed on the surface and pumped down a borehole. These efforts resulted in a successful solution to a critical longwall supplemental support problem where limited access, speed of installation and support resistance were primary concerns (Amick, et al., 1993).

In 1995, the Cyprus Coal Company employed Fosroc foamed cement to reinforce a severely deteriorating tailgate at the Cyprus Shoshone mine. Approximately 6,000 ft of tailgate, containing wooden cribbing, had to be supported. The initial wood crib support system left a 6 ft wide walkway for access and construction of additional support. Access was further reduced as the roof loaded and deformed the wood cribs.
Thus mechanized material handling was not feasible and all materials were forced to be hand delivered along the 6,000 ft tailgate. An additional 500 tons of support capacity was placed along the tailgate by filling the wooden cribs with Tekseal® (Woomer and Stewart, 1995).

The Tekseal® was pumped down 900 ft long surface boreholes drilled on 2,000 ft centers and up to 1,800 ft horizontally underground. Shoshone Mine reduced downtime due to tailgate ground control problems by approximately 70 percent in comparison with previous longwall panels.

The purpose of this paper is too discuss the Fosroc cement line, hightlighting two exciting value added systems which employ Fosroc cements in longwall roof support technology. The first system is Tekprop, a combination steel and concrete support designed for longwall gateroad support. The second is the Fosroc mineable crib, desinged to support longwall ventilation and pre-driven recovery room entries.

## FOSROC CEMENTS

Fosroc continues as a leader in the development and utilization of pumpable cement grouts for mining applications. Our product line includes a range of cementitious based products for use in ventilation seals, tailgate support, cavity filling, and underground construction projects. (Table 1).

## TEKPROP

The considerable expertise accumulated in the development of the Fosroc cement line has been employed in the development of a pumpable, supplemental roof support system. The Tekprop roof support system is specifically designed as a

viable alternative to conventional wooden supplemental support. It is an incombustible, simple, and innovative system, which incorporates superb stiffness, appreciable yield, and ease of installation. A telescopic tube is extended between the mine roof and floor, then filled with a single component, pumpable cement. To maximize Tekprop efficiency, the aspect ratio (tube diameter divided by the entry height) should be five or less. The cement is similar to the above discussed Tekgrout. A dual batch mixing/pumping unit enables an effectively continuous pumping cycle and maximizes mix accuracy. The 2.5:1 water to solids mix begins to gel within minutes of discharge and provides a +100 ton capacity, twice the capacity of a standard four point crib.

Advantages

The advantages of the patent pending Tekprop system include:

Ease of Use - Simple design enables substantially reduced material handling and quick installation.

Engineered Performance - Tekprop supports +100tons within the first ¼ to ½ inch of deformation and maintains that full load over 10 inches of deformation.

Variable Strength - The grout strength can be easily varied by adjusting the water/solids ratio.

Full Surface Contact - The top and bottom of Tekprop consist of rubber bladders that conform to the irregularities of the roof and floor, and are not effected by the point loading forces that damage wooden and fiber cribs.

Installation Speed - Dependent on pumping and entry height considerations, over 60 units per shift can be installed.

Consistent Performance - The steel and cement Tekprop provides repeatable load and deformation performance, while conventional post and crib performance varies with wood quality.

Laboratory Test Results

The function of supplemental roof support systems is to prevent the delamination of the roof beam and to support the weight of the strata which becomes separated from stable roof structures. It is important to realize that, in areas of active mining, the closure of the mine opening is largely irresistible in terms of capacity of the supplemental support. Assuming a passive support that develops load only through the closure of the mine opening, the ideal roof support would be initially stiff and then yield indefinitely without loss of load capacity or support stability. This somewhat paradoxical requirement for an ideal support is shown in figure 1, together with the load-displacement behavior of a conventional wood crib. It is seen from figure 1 that wood cribs provide a support behavior similar to the ideal support requirements, except a wood crib is considerably less stiff prior to reaching its yield load capacity than the ideal support (Barczak and Gearheart, 1993).

The ideal support referred to by Barczak and Gearheart in 1993 has been largely produced by Fosroc in the form of Tekprop.

Full scale Tekprop testing to failure has been conducted at the National Institute of Occupational Safety and Health, Strategic Structures Testing Laboratory, Pittsburgh, Pennsylvania. Tekprops, up to 10 feet high, have produced very encouraging results. Figures 2 and 3 demonstrate that Tekprop units, with aspect ratios of 5 or less, provide over 100 tons of support at 6 and 10 feet high, respectively.

The implementation of Tekprop is especially attractive to mines with challenging logistics and/or limited labor availability. Geologic conditions and mining method selection can make underground material handling of traditional wooden cribbing very difficult. Mining in a deep shaft only access coal mine, such as the Virginia Pocahontas No. 3 Coalbed longwall mines, present much greater supply challenge than a drift mine in the Pittsburgh Coalbed. The addition of a second face to an existing retreat longwall coal mine doubles the tailgate entry support requirements. As of the writing of this paper, MSHA has approved a Tekprop tailgate test section in mine conducting retreat longwall mining of the Pocahontas No. 3 Coalbed.

## CUTABLE CEMENT CRIBBING

The development of increasingly more sophisticated and powerful retreat longwall equipment has led to ever wider and longer longwall panels. Panels in excess of 10,000 feet long and 1,200 feet wide are not uncommon. As gateroads become longer, the pressure necessary to ventilate the longwall workings increases. In an effort to reduce these ventilation pressures, longwall operators cut ventilation entries across the longwall panels in advance of the face. These entries must be supported with mineable supports to prevent falls of immediate roof in advance of the face. Historically, ventilation entries and pre-driven recovery rooms entries were filled with expensive yielding cement pillars or fully hydraulically backfilled (Bauer, et al., 1987).

Fosroc has developed an efficient, yielding, multiple component, cement crib to support longwall panel ventilation entries and pre-driven recovery rooms. The Fosroc mineable crib combines inexpensive flyash cement pillars with a yielding bag filled with the previously discussed Tekset formulation. The four foot diameter flyash cement pillar is poured in a bag, within a temporary metal form. The form is moved to a subsequent pillar location after the initial hardening of the flyash pillar. The remaining entry height between the mine roof and the top of the flyash cement pillar is filled with the specially designed bag filled with Tekset. The thickness of the Tekset is determined by the expected closure of the mine entry, under longwall front abutment loading.

The flyash cement will be pumped from the surface and the Tekset will be mixed and pumped underground. As of the writing of this paper, a retreat mine in the Pittsburgh Coalbed is reviewing the proposed support of mine ventilation entries with the Fosroc mineable crib system.

## SUMMARY

The considerable expertise accumulated in the development of the Fosroc cement line has been employed in the development of two pumpable, supplemental roof support systems. The Tekprop roof support system is specifically designed as a viable alternative to conventional wooden supplemental support. It is an incombustible, simple, and innovative system, which incorporates superb stiffness, appreciable yield, and ease of installation. A telescopic tube is extended between the mine roof and floor, then filled with a single component, pumpable cement. The second system is the Fosroc mineable crib which is a cost effective methodology to support longwall ventilation and pre-driven recovery rooms. The Fosroc mineable crib combines inexpensive flyash cement pillars with a custom designed yielding bag filled with the previously discussed Tekset formulation.


## REFERENCES


1. Amick, M., J. Mazzoca, and D. Vosefski, The Use of Foamed Cement Cribs at American Electric Power Fuel Supply Meigs Division, 12th Conference on Ground Control in Mining, Morgantown, WV, August 1993.

2. Woomer, C. C. and C. Stewart, Innovative Tailgate Support for Heavy Ground: 11 Left longwall Panel, Cyprus Shoshone Mine, 14th Conference on Ground Control in Mining, Morgantown, WV, August 1995.

3. Barczak, T. M. and D. F. Gearhart, assessment of Wood and Alternative Materials for Supplemental Roof Support Construction, 12th Conference on Ground Control in Mining, Morgantown, WV, August 1993.

4. Bauer, E., J. Listak, M. Berdine, W. Bookshar, D. Raab, and T. Mucho, Longwall Recovery Utilizing the open Entry Method and Various Cement-Concrete Supports, 7th Conference on Ground Control in Mining, Morgantown, WV, August 1987.


Table 1. Fosroc Pumpable Cement Line

| Product | Use | Characteristics |
|---|---|---|
| Tekseal | Pumpable permanent ventilation seal | Air entrained cement, yields to 60 % of original height MSHA/USBM approved |
| Tekfoam | Cavity filling and backfilling | Air entrained cement, only four bags yield a $yd^3$ |
| Tekrok | Underground construction projects | 3,000 psi strength, non-shrinking, durable |
| Tekgrout | Strata consolidation water sealing and mud solidification | Variable strength and viscosity, very short gel times |
| Tekset | Blocking and wedging cribs and posts | Conforms to irregular roof, sets in 10 to 15 minutes, improves support performance |
| Ultracem and Terracem | Foundation consolidation, sealing flowing water | Low viscosity, minimal bleed, sulfate resistant, ultra-fine |
| Celroc P | Rock anchoring and stand pipe installation | Thixotropic, controlled expansion, high speed |
| Preco Plug | Stops fast flowing water in cracks and small holes | Very fast setting and high strength |

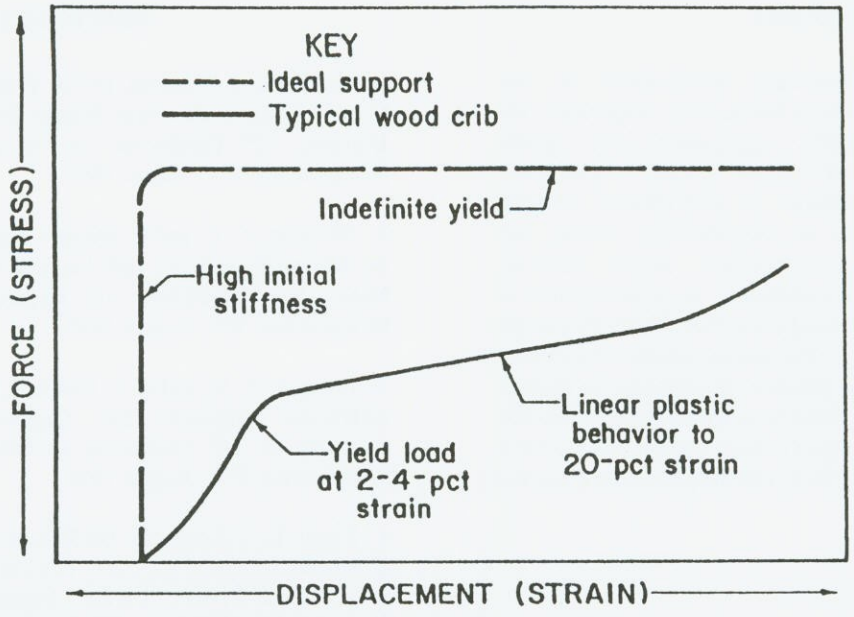



Figure 1. Performance of ideal passive roof support and comparison to conventional wood crib behavior. (Barczak and Gearhart, 1993)

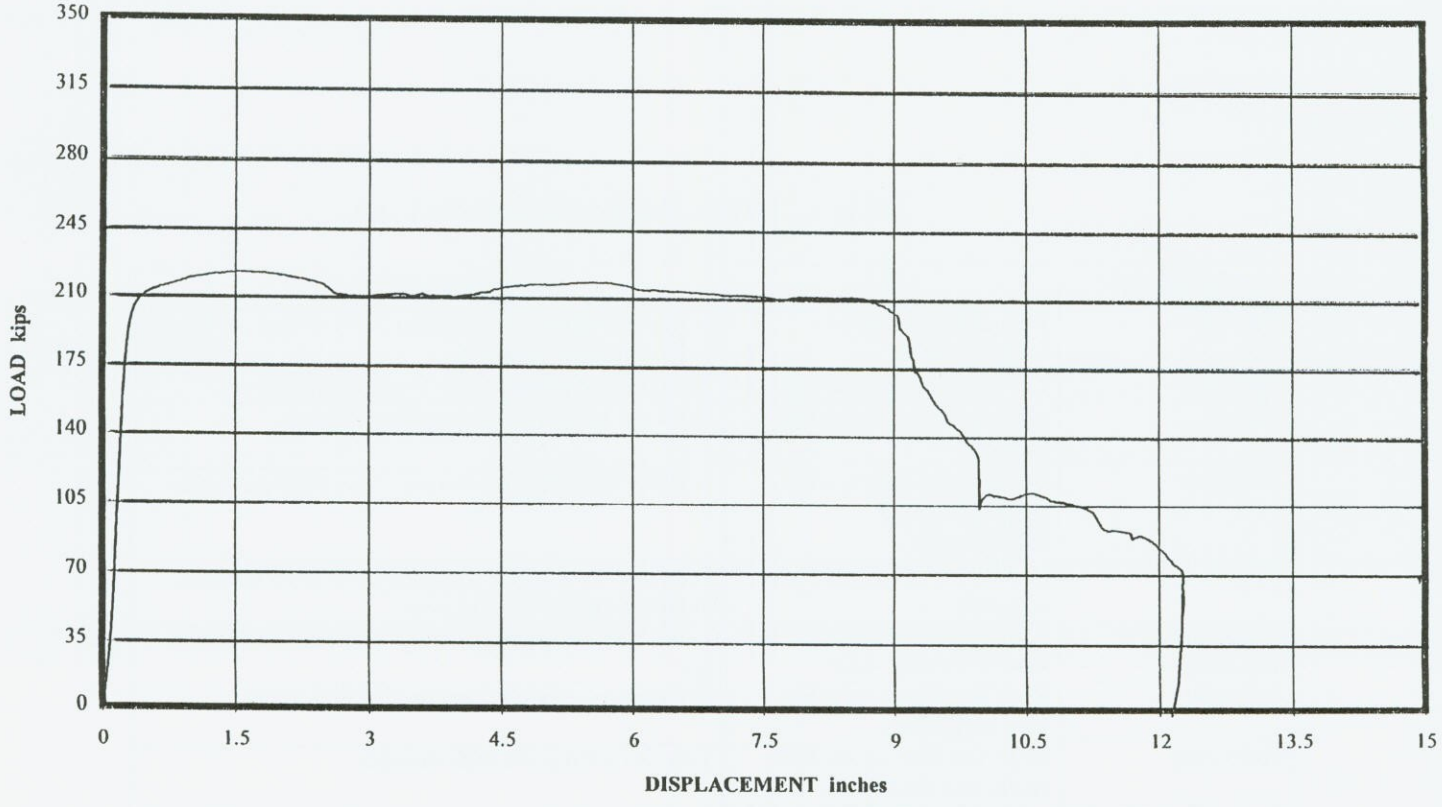



Figure 2. Load -vs- displacement behavior of 6 ft. high 18 inch diameter Tekprop.

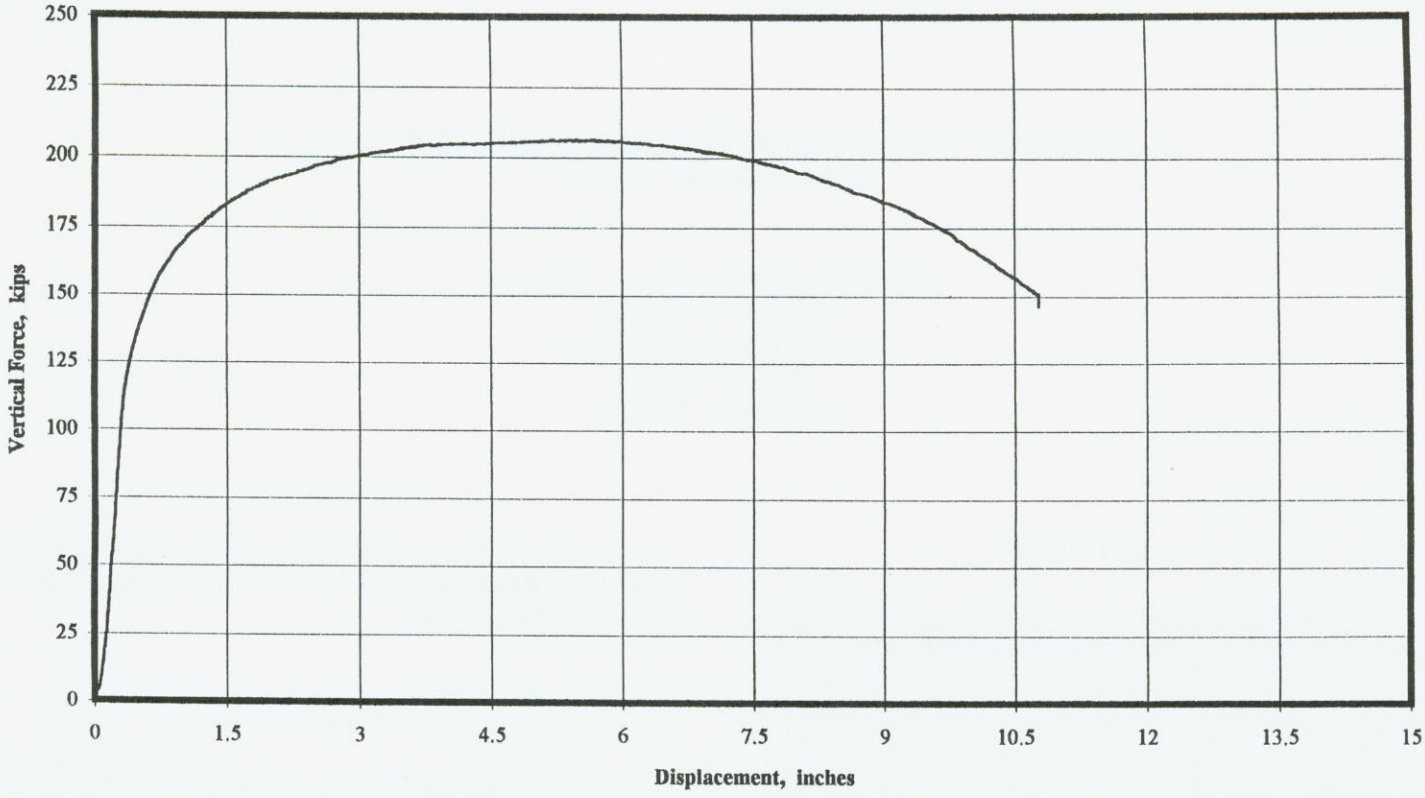



Figure 3: Load -vs- displacement behavior of 10 ft. high, 24 inch diameter Tekprop.



# Management of the Dynamic Phenomena of Rock Pressure in Underground Mines

*Vladimir I. Klishin,* Mining Engineer
Institute of Mining
Russian Academy of Sciences
Siberian Branch
Novosibirsk, RUSSIA

## ABSTRACT

Complex method of ruling of rock pressure is considered in conditions of rapid roof subsidence. The purpose of this method is elaboration of emergency devices into hydraulic props. Also method of unloading of solid roofs is worked out. An analysis of means of protecting hydraulic props of powered supports from dynamic loads made it possible to divide them into four classes according to principle of operation: emergency, operating from an increase of pressure; emergency damping; emergency, operating according to the "plastic element" principle; inertial emergency, operating from dynamic loads. It was established that the overwhelming majority of designs of the first three classes of emergency devices (EDs) are based on traditional approaches, which exhausted their possibilities of high-speed response. Delay on their opening is caused mainly by inertia of the moving locking parts. In our opinion, the most prospective are EDs using the inertia of the moving locking parts for depressurizing the piston cavity of the hydraulic prop with a minimum delay (inertial EDs). The essence of the designs of EDs having an inertial principle of action is that into the hydraulic prop containing movable and immovable elements is additionally introduced a spring-operated contracting support, which is installed on the movable element. Under dynamic loading of such a hydraulic prop from the roof, the support moves relative to the movable element, performing the role of an inertial mass, which leads to instantaneous depressurization of the piston cavity of the hydraulic prop. Technological measures for unloading of solid roofs consists in creating of long oriented cracks in rock massif. Description of method for creating cracks, demanding equipment and means for control the progress of splits are included. Also technological schemes for realization of the method of saving underground mines and rock mass are included. The results of experimental realization of this method on the Kuzbass and Poland coal mines are also included.

## INTRODUCTION

Great importance is attached to dynamic phenomenon in underground conditions. Most of foreign researchers consider them as brief impact, and while collapsing of the solid roof into mine. However, Russian specialists divide the conception of mine impact and sudden collapsing of roof. Don't fixing your attention on analysis of different points of view, we note, that we suggested typical classes of dynamic displays of underground pressure as follows : underground impacts; a rapid throwing of coal and rock; fast setting down of the roof, including the block failure; seismic oscillations of rock from technical sources. In suggested report the complex method of lowering of dynamic loads of rock pressure in underground mine is considered. The essence of this method is that the hydraulic prop with emergency devices from dynamic loads is created and the roof is unloaded by means of creating a long oriented cracks in rock mass.

## CREATION OF NEW TYPES OF EMERGENCY DEVICES TO PROTECTING THE HYDRAULIC PROPS FROM DYNAMIC LOADS

An analysis of means of protecting hydraulic props of powered supports from dynamic loads carried out in [1, 2] made it possible to divide them into four classes according to principle of operation: emergency, operating from an increase of pressure; emergency damping; emergency according to the "plastic element" principle;

inertial emergency, operating from dynamic loads.

It was established that the overwhelming majority of designs of the first three classes of emergency devices (EDs) are based on traditional approaches, which exhausted their possibilities of high-speed response. Delay of their opening is caused mainly by inertia of the moving locking parts. In our opinion, the most prospective are EDs using the inertia of the moving locking parts for depressurizing the piston cavity of the hydraulic prop with a minimum delay (inertial EDs).

The essence of the designs of EDs having an inertial principle of action proposed by Institute of Mining, Siberian Branch, Russian Academy of Sciences, and State Design and Experimental Institute of Coal Machinery (Giprouglemash) is that into the hydraulic prop containing movable and immovable elements is additionally introduced a spring-operated contracting support, which is installed on the movable element. In the support is a cavity which is constantly connected to the piston cavity of the hydraulic prop. The area of this cavity under the support exceeds the area of the cylinder, which leads to the formation of an uncompensated area. The pressure of the fluid on the uncompensated area creates a force constantly separating the support and movable element; the latter makes it possible to seal the cavity of the hydraulic prop. Under underground conditions the hydraulic props of the powered supports are loaded by lowering the roof, and therefore depending on the placement of the hydraulic props (with the rod or cylinder upward), the role of the movable element can be played either by the rod or cylinder. Under dynamic loading of such a hydraulic prop from the roof, the support moves relative to the movable element, performing the role of an inertial mass, which leads to instantaneous depressurization of the piston cavity of the hydraulic prop.

Figure 1 shows design variants of such a hydraulic prop with an inertial ED. The hydraulic prop includes a piston pair made in the form of movable and immovable elements containing a cylinder 1 with a hollow rod with piston 3 installed in the cylinder with the possibility of axial movement, which form the cavity 4 of the hydraulic prop filled with the working fluid and connected to safety valve 5 which provides nominal resistance of the hydraulic prop. The role of the movable element is played either by hollow rod 2 with piston 3 (Fig. 1a, b) or cylinder 1 (Fig. 1c-e). The means of protection from dynamic loads is the support and ED mounted in one assembly 6. On the movable elements of the piston pair is fastened a protection 7 providing force interaction with assembly 6 and sealing cavity 4 of the hydraulic prop. Preliminary pressing of assembly 6 against projection 7 is provided by spring 8. Channels with the possibility of communication of cavity 4 of the hydraulic prop with the atmosphere are made between assembly 6 and projection 7 (see Fig. 1b).

When a pressure is created in the hydraulic prop by the pumping station, the fluid fills cavity 4 of the hydraulic prop and enters under assembly 6 hermetically pressed against projection 7 by spring 8 (see Fig. 1a, c). Their further constant pressing is provided by the pressure acting on area $S_1$ and creating the closing force of the ED pushing apart the support with the movable element. The opening force counteracting it, trying to draw together assembly 6 relative to the movable element (or rod 2 with piston 3, or cylinder 1) is less than the closing force, since the area of the support in the end part of the assembly contacting the working medium is greater than area $S_2$ of cylinder 1.

During static loading the relationship of the forces of opening and closing cavity 4 is preserved and the hydraulic prop remains sealed for any degree of its separation. When a pressure providing nominal resistance, for example, 40 MPa, is reached in the hydraulic prop, safety valve 5 operates.

During dynamic loading of the hydraulic prop from any initial pressure in it, assembly 6, through which the impact is transmitted, almost instantaneously acquires a speed equal to the rate of loading and moves downward relative to projection 7 fastened on the movable element, which, in turn, owing to their large mass, do not have time to acquire an instantaneous speed and, hang up, lagging behind the movement of assembly 6. Loss of the seal occurs at this time, and the working fluid in a short time interval into the atmosphere from cavity 4 of the hydraulic prop through channels 9 (see Fig. 1b, where movement of assembly 6 is shown by a dashed line).

In the case of a brief impact the hydraulic prop, as though "screening", leaves the load without triggering the safety valve 5. After instantaneous ejection of the fluid into the atmosphere through the ED, the movable element with the projection installed on it, owing to spring 8 and the residual pressure acting on the uncompensated area ($DS = S_1 - S_2$), follows the movement of assembly 6 and covers cavity 4, and the hydraulic prop again restores its bearing capacity.

Design variants of the hydraulic prop with modified assembly 6 and projection7 are possible. Figure 1d shows a variant of an ED representing assembly 6, the force interaction of which with projection 7 is realized by axle 10 fastened on it, in which are made channels 11 with the possibility of connecting cavity 4 with the atmosphere, and the projection are made through holes 12. Figure 1e shows a diagram of a hydraulic prop in which the force interaction of assembly 6 with projection 7 is realized through axle 13 fastened on the projection.

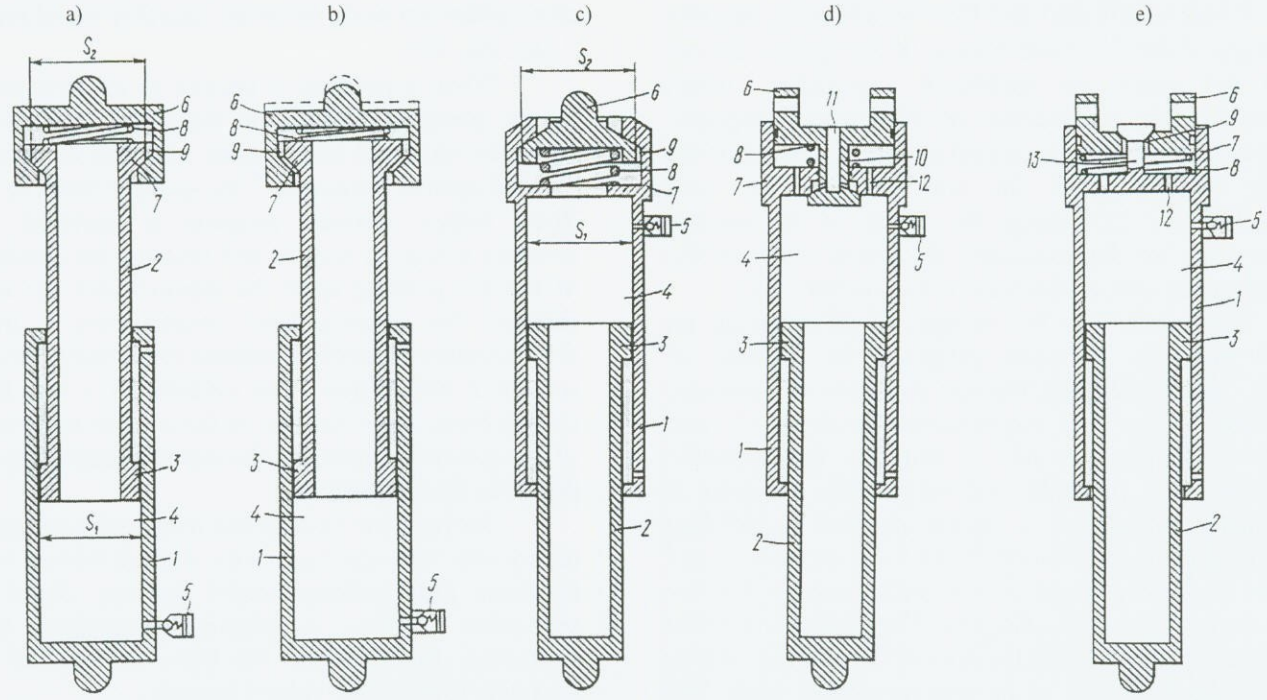



Figure1. Structural schemes of hydraulic props with emergency inertial valves (EIV) : a - EIV installed on rod (in static); b - same in dynamics; c - EIV installed on cylinder; d - EIV is placed on central axis, which is fixed on the support and has a canals; e - EIV is placed on central axis, which is fixed on the support, but canals are made into support.

In such a design of the hydraulic prop the working medium enters under the end surface of assembly 6 through the through holes 12. The structural elements and operation of the variants of the hydraulic prop given in Fig. 1d, e are analogous to the aforementioned.

An analysis of the data obtained indicates that the mass of the movable element m, the initial pressure in the hydraulic prop $P_0$ , size of uncompensated area DS, and loading rate u affect the pressure in the hydraulic prop during its dynamic loading. A decrease of the initial thrust and size of the uncompensated cavity and increase of the mass of the movable element (inertial loads) lead to an increase of sensitivity of the ED to dynamic loads and to depressurization of the piston cavity of the hydraulic prop. An increase of the falling mass with a constant loading rate has almost no effect on the sensitivity of the ED, but an increase of the loading rate with a constant mass of the falling load increases the sensitivity of the ED. Furthermore, the sensitivity of the ED to impact increases with decrease of the height of the fluid column in the hydraulic prop. Closing of the ED occurs within 5 msec, and at that moment a proportional increase of the fluid pressure occurs with a constant character of loading the hydraulic prop. The rate of a proportional increase of pressure increases for a greater loading rate and smaller height of the fluid column.

According to the scheme 1d the full-size models of hydraulic props No. 1 with inner diameter 220 mm and maximum hydraulic height 800 mm has been developed. Uncompensated cavity, connected with canals to the piston cavity, managed the work of ED. Force of spring between support and movable element (cylinder) has 5 kN, dimensions of uncompensated cavity (DS) was 9 and 15 sm. During changing of the pressure into hydraulic prop from 20 till 40 MPa the force of pressing of concentrating section changed accordingly : while DS = 9 $sm^2$ - from 18 till 36 kN; while DS = 15 $sm^2$ - from 30 till 60 kN. According to the scheme 1a, the models of hydraulic props No. 2 with inner diameter 100 mm and hydraulic height till 310 mm has been developed. Dimensions of uncompensated area was 4.8 and 9.7 $sm^2$.

Both type of fluid columns have been tested on dynamic stand at AO "Giprouglemash" which permits dynamic loads till 2,400 kN and with maximum energy till 440 kDj with velocity till 2 m/sec [4]. Moreover fluid column No. 2 have been tested with the mass of falling weight 7 kN and height of throwing 1.5 m. Tests showed the high efficiency of ED's work, which also closed in time and provided necessary remaining pressure into fluid column. Fluctuation of pressure into piston cavity does not exceed 20 % from the primary value of safety valve. During dynamic loading of fluid column No. 2 with a force of 1,000 kN the intensity of pressure increasing

into piston cavity was 7,000 mPa/s, but at the same time effectively of ED's operating have been placed. The examples of the record of the pressure alteration into piston cavity of hydraulic prop are shown on figure 2. The further improving of the construction of fluid column with ED's, having an inertial principle of action, is provided by dividing the functions of support and ED. Taking into consideration, that while ejection of the fluid into the atmosphere there occurs a high-speed flowing of fluid through the sealing valves with sealing with movable sealing elements has been suggested and developed.

## THE METHOD OF UNLOADING THE ROCK WITH ORIENTED LONG CRACKS

Nowadays except the improving of design of the prop's fluid columns special measures are designed for unloading the roofs. The analysis of known ways of roof unloading certificates that all of these methods possesses, except particular, common deficiency - unevenness and uncontrolness of unloading. Prof. Chernov from IGD SO RAN have suggested a new method of roof unloading, which has been named as method of hydrodynamic roof stratification (HRS) [5,6].

The essence of the HRS method is accomplished in the following way. The initiating disk-shaped slit with a given shape and dimension, normally oriented to the hole, is drilled into the wall of blast hole (blast hole), that concentrate the pressure. Then slit is hermetically sealed and a fluid-flowing substance is forced under pressure into the initiating slit. By means of brittle gap the increasing of the slit in the given direction is happens and artificial long cracks create in the rock mass. During the hydrobreakage of roof by the HRS method, rock failure renders the minimum resistance by means the following reason : the duration of rock on breakage as a rule ten times less than duration on compressing, and energy, essential for failure, is proportional to the square of critical effort; if gap is carried out inside the layered area, then tensile strength of the rock mass along the surface of layer is usually less then strength of monolithic massif.

The GDS method of roof is carried out in two regimes: preliminary (prophylactic) unloading and operative unloading which includes the elements of compulsory roof failure on the free surface (fig. 3).

Preliminary (prophylactic) unloading of the roof could be used for lowering of the initial and following collapsing the roof and also while cutting out the mass [7]. Operational unloading of the roof can be provide in the area of underground mine. Under these conditions crack arrives on free surface, mass loses cohesion and

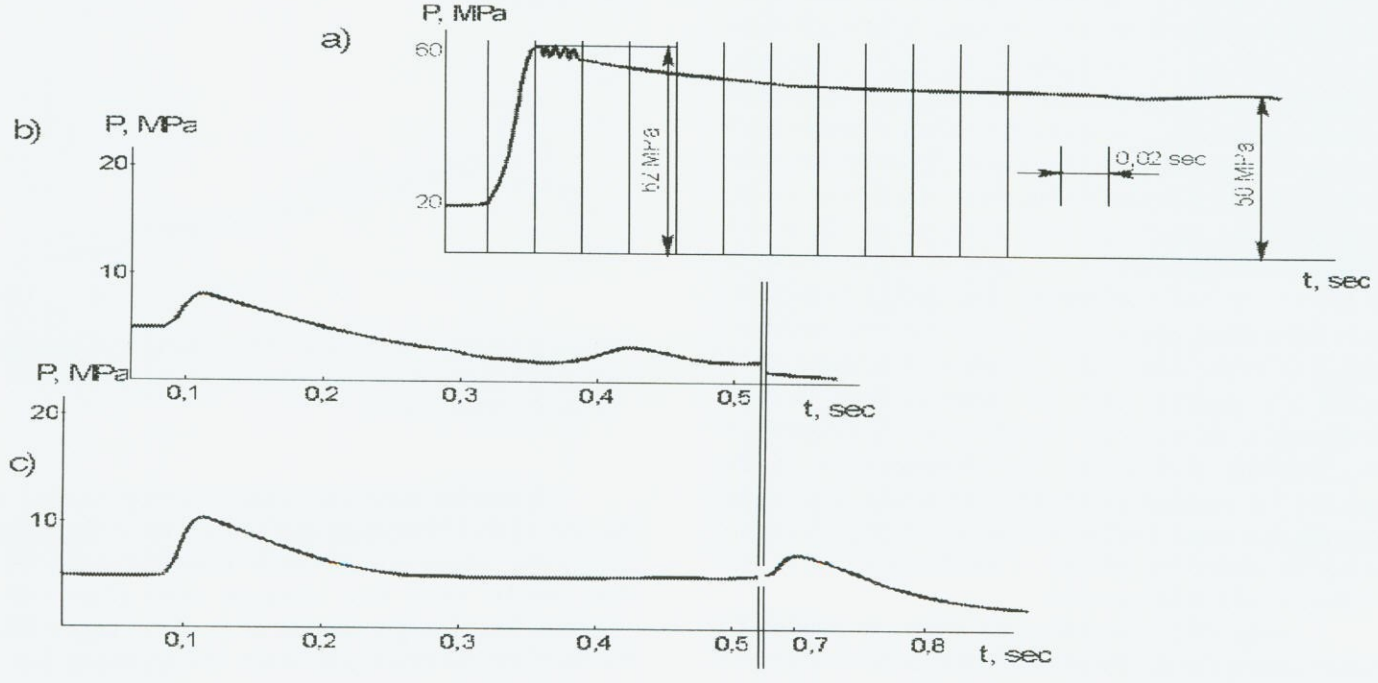



Figure 2.Oscilloggramma of loading of the fluid column № 1 ($\Delta S = 15$ sm$^2$) with a force of 2,400 kN (a) and fluid column №2 with emergency device (b) and without emergency device (c)

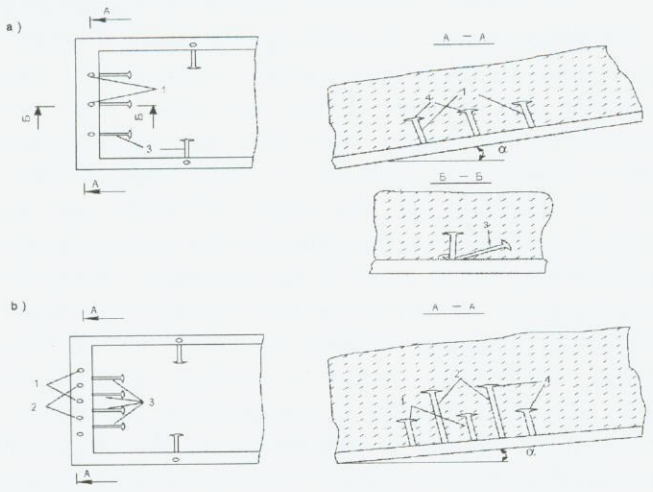


Figure 3. The scheme of placement of stratification hole for initial setting of the roof : a - during the creation of hydrobreakages on one level; b - during the creation of hydrobreakages on two levels (1 - stratification holes of the first level; 2 - stratification holes of the second level; 3 - cutting holes; 4 - initial slits)

compulsory mass collapsing is provided by means of pressure of fluid into crack.

The HRS method does not require various of equipment, but its necessary to have equipment for cutting an initiating disk-shaped slit into the wall of the blast hole for realization of this method. Initiating slits can be cut with aid of mechanical, (), high - pressured hydraulic and other apparatus. For realization of oriented hydrobreakage into coal mines the various mechanical slit making devices has been developed. These devices have individual constructural peculiarities, depending on the size of holes, depth, on which the initial slit is cut, strength of the rock and other. Initial slit has been created is need to re-roof with packer. The special hermetisers have been developed applying to the concrete conditions (diameter of the hole, width, the place of arrangement of initial slit, pressure and the temp of fluid forcing). Important work has been carried out for investigation of the methods and means for determination of the geometrical parameters of slits and cracks, developing into the rock mass. Drilling a holes and cutting a slits on it walls are carried out with aid of serial equipment, as well as feed a fluid under pressure.

Using HRS into rock mass allows to receive it's failure during the stratification of the roof behind the () of the hydraulic prop. The engineering method for calculation of the power of layer with single width has suggested.

$$h^3 - \frac{3l^2h^2\gamma}{4[\sigma]} + \frac{3Pl}{[\sigma]} - \frac{3P^2}{\gamma[\sigma]} = 0$$

where $h$ -- a power of stratification layer, m;

$\gamma$ -- a volume of weight of rock mass, T/m$^3$;

$l$ - place of applying the prop's reaction $P$, m;

$P$ - prop's reaction, t;

$[\sigma]$ - limit of crook strength of the roof, T/m$^2$.

Calculations demonstrated, that layer's capacity depends on resistance value of the prop and limit of crook strength of the layer.

Results of mine investigation of HRS method during experimental and industrial inculcation into different technological schemes on given mines at Kuzbass and one mine at Poland, are particularly generalized in table 1. Hydrobreakage is carried out both layered and perpendicularly through the blast holes with a diameter to 45 mm and holes with a diameter 93 mm. For the first time the character of changing of the pressure by hydrobreakage and hydrobreaking up of rock mass has been instrumentally fixed and presented as an example on Fig 4. The process of hydrobreakage is characterized by rapid speed (to 1 min), the time of achievement the maximum pressure forms not greater then 5 sec. During the temps of forcing the fluid from 35 to 90 liters/min and achievements the max. pressure, the rapid falling of pressure occurs, which indicates on formation of man-made crack in rock.

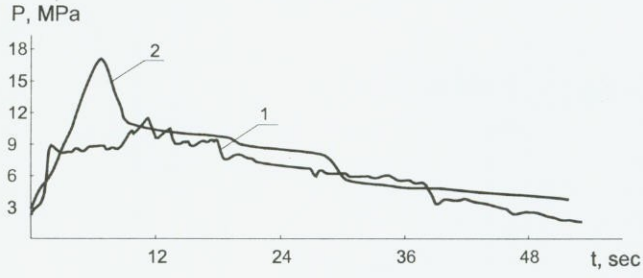



Figure 4. Changing of pressure of fluid during roof breakage into langwalls 3-6-13 of mine «Raspadskaya» (1) and 4-1-8 of mine «Tomskaya» (2)

During the maximum temp of forcing the fluid, the process of hydrobreakage has some noticeable splashes of pressure, which indicate the development of the crack,. And besides every next breakage takes place with a pressure, less then previous because of the bigger filling the fluid into the developing crack and according that for increasing the sum pressure, in force on stones of slit. During insufficient rate of fluid pumping into the running crack, only one jump is revealed, that is characterizes the beginning of hydrobreakage.

Oriented hydrobreakages, obtained from blast holes, considerably decreases difficulty of work and enlarge the field for applying HRS method, allowing to carry out work under constrained underground conditions, including (). Creating filled under pressure with fluid long cracks in massif, hanging over empty space, provides sudden increasing of force, acting on layered massif to the side of empty space and promotes to the rock failure. The process of hydrobreakage is characterized with smooth pressure increasing, which is sufficient for cracks development and stays constant during analogous rate of fluid pumping.

Experimentally obtained, that while oriented hydrobreakage of the roof with HRS method, the development of main crack is happens, which parameters has been fixed by means of the control blast holes method. The effectively of hydrobreakage has been provided with parameters of initial slits and degree of its hermetiaition.

**Realization of complex method of management the dynamic manifestation of loads into underground conditions promotes to increasing the effective and safety of underground works.**

## REFERENCES


1. Klishin V.I. "Analysis of operating principle of means of protecting powered supports from dynamic loads," Psh.Gur., 45, No. 1 (1989)
2. Klishin V.I., Shcherbakov "Substantiation of the operating principle of means of protecting powered supports from dynamic loads," Fiz.-Tekh. Probl. Razrab. Polezn Iskop., No. 3 (1990)
3. Klishin V.I. "Inertial means of protecting powered supports from dynamic loads," Fiz.-Tekh. Probl. Razrab. Polezn Iskop., No. 4 (1994)
4. Shevchenko G.E., Hazanov H.I. "Tests of equipment of underground devices," Moscow, "Nedra" (1988)
5. Cherrnov O.I. "Hydrodynamic stratification of strong monolithic rocks as a method of controlling difficult-to-form roofs," Fiz.-Tekh. Probl. Razrab. Polezn Iskop., No. 2 (1992)
6. Chernov O.I. and Kyu N.G. "Fluid rupturing of rock masses," Fiz.-Tekh. Probl. Razrab. Polezn Iskop., No. 6 (1988)
7. Kocminov E.A., Klishin V.I., Matvietz U.V. "Method of saving of the second time using underground mines," Ugol, No. 6 (1996)

Table 1 Results of investigation of HRS method during experimental and industrial inculcation on mines

| Demonstrations | m.«Raspadskaya» longwall 3-6-13 | m.«Tomskaya» longwall 4-1-8 | m.«Yubileynaya» block №6 | m. «Dalnye Gory» longwall 56 | | | 60 years of USSR (Alarda) longwall 6-1-4 | | | m. «Komsomoletz» (cutting holes) longwall 1896 | | | | | | m. «Pokyi» (Poland) assemblinjg camera | | |
|---|---|---|---|---|---|---|---|---|---|---|---|---|---|---|---|---|---|---|
| Depth of mine work, m | 140...150 | 150...190 | 450 | 100...180 | | | 220...260 | | | 190...240 | | | | | | 700 | | |
| Power of layer, m | 3,8 | 9...9,8 | 2,3 | 2,4 | | | 8,5 | | | 2,20...2,35 | | | | | | 1,9 | | |
| Angle of inclination of layer, degr. | 6...8 | 9...11 | 8...10 | 3...20 | | | 3...10 | | | 6 | | | | | | 7...10 | | |
| Height of longwall, m | 105 | 106 | - | - | | | - | | | 90 | | | | | | 200 | | |
| Power of roof, m: direct | 1,5 | 1,6 | 2,25 | - | | | 1,9 | | | 0,3...3,0 | | | | | | - | | |
| main | 40 | 17 | 25 | 18 | | | 15...18 | | | 6...14 | | | | | | 10 | | |
| Strength of roof, Mpa direct | 50...60 | 120...130 | 40...45 | - | | | - | | | 42 | | | | | | - | | |
| main | 80...90 | 100...120 | 50...85 | 55...75 | | | 85...87 | | | 73 | | | | | | 120 | | |
| Hydraulic prop | 4M130 | 2УКП | - | KM-81 | | | KM-130 | | | Glinik | | | | | | - | | |
| Resistance of prop, $kN/m^2$ | 720 | 1250 | - | 435 | | | - | | | - | | | | | | - | | |
| Height of slit placement, m | 6,5 | 7,9 | 5,8 | 11 | 8,2 | 7 | 7,9 | 9,4 | 9,2 | 12 | 6 | 8,5 | 12,5 | 12 | 6 | 4,5 | 7,0 | 7,0 |
| Maximum pressure of fluid during rock breakage, MPa | 12,5 | 17,5 | 28,5 | 13 | 12,5 | 20 | 13,5 | 16,5 | 15 | 27 | 25 | 21 | 21 | 32 | 24,5 | 27,5 | 23 | 31,5 |
| Working pressure of fluid forcing, Mpa | 4,5 | 4,8 | 17,5 | 9 | 8 | 9 | 3,5 | 6,5 | 6 | 16,5 | 17,5 | 14,5 | 12,5 | 21,5 | 21 | 13,5 | 14 | 12,5 |
| Time of beginning the breakage ($T_1$), sec | 10,8 | 6,8 | 12 | 2 | 4 | 2,5 | 2 | 2 | 3 | 6 | 17 | 2 | 6 | 5 | 10 | 8 | 8 | 6 |
| Duration of breakage ($T_2$), sec | 52 | 120 | 90 | 45 | 52 | 30 | 10 | 55 | 35 | 50 | 40 | 10 | 20 | 18 | 35 | 60 | 60 | 20 |
| Fixed radius of fluid spreading, m | 15 | 30 | 56 | 14 | 18 | 6 | 12 | 40 | 20 | - | 27 | - | 15 | - | 15 | - | - | - |
| Temp of forcing, $m^3/sec$ | $1{,}17 \times 10^{-3}$ | $1{,}5 \times 10^{-3}$ | $1{,}8 \times 10^{-3}$ | $5{,}8 \times 10^{-4}$ | | | $5{,}8 \times 10^{-4}$ | | | $5{,}8 \times 10^{-4}$ | | | | | | $1{,}0 \times 10^{-3}$ | | |

# Continuing Development of Innovative Cable Support Systems

*John G. Oldsen,* Assistant VP-Sales
*John Stankus*, Vice President-Engineering
*Song Guo,* Assistant VP-Engineering
Jennmar Corporation
Pittsburgh, PA

*A. Wahab Khair,* Professor
Department of Mining Engineering
College of Engineering and Mineral Resources
West Virginia University
Morgantown, WV

## ABSTRACT

Passive cable bolting and active cable trusses have been used in roof support for more than two years. Excellent roof control has been experienced by many coal operations.

This paper covers the new and innovative developments in cable support systems and their application in mines. Multiple cable bolts, tensioned cable bolts, coal rib wrapping, and other cable applications will be covered.

## INTRODUCTION

Since the expanded trial tests by Stankus et al., (1994) cribless tailgates supported by roof trusses have been utilized in the Pittsburgh #8 coal seam. Up until recently, the roof trusses utilized have been high capacity, tensioned rod trusses. Generally, these trusses have done an adequate job in controlling roof and floor performance in tailgates. With the present ventilation requirements and the trend of longer and wider panels, the concept of removing cribs as full tailgate supplemental support is very attractive to mines. The economic impact on costs, improved ventilation, and elimination of a source of many job injuries are all positive benefits.

It was proven that tensioned trusses could be successfully utilized to provide effective supplemental support in tailgates. However, our research has shown that, under certain conditions, the combination of in-situ and mining induced areas of high horizontal shear stress affects the rigid angle bolt. The recently introduced JMS Cable Truss has a design which is not affected by horizontal stress induced shear. A project was proposed for both four entry and three entry development panels, Figure 1 and Figure 2, utilizing cable trusses as supplemental support.

## ROOF CONTROL PLAN

Based on the success of the support plans originally used in cribless tailgate design, cable trusses were installed between the rows of primary bolts, as shown in Figure 3. Primary support consisted of point anchor, INSTáL II Compress'ion roof bolt, grade 75, 7/8-inch J-Bar in 8-foot lengths with two equivalent feet of resin, donut embossed channel plate and T-5 roof channel on 4 foot spacing. The JMS Cable Truss, as shown in Figure 4, is produced with 0.6" seven strand, grade 270, cable having a nominal break strength of 58,600 pounds. The cable truss consists of two angle bolts, a horizontal member, two splice tube assemblies to couple the angle bolts to the horizontal member, and two cable truss plates, 6" x 16", to provide load transfer at the angle borehole collar or suitable stress point. The angle bolts are constructed with three nutted birdcage anchor units, which enhance resin mixing and provide the anchorage point in the cured resin, and a "cup and compactor" unit which provides resin retention and compression in the borehole for full anchorage encapsulation.

Several unique features that make the JMS Cable Truss user friendly, need to be pointed out. First, the cable is relatively flexible. This flexibility allows for installation without regard to the level or degree of bearing surface provided by the immediate roof. Also, the exact borehole drill angle is of less concern, since the cable flexibility compensates for changes in drill angle and the borehole can be close coupled to the ribline. In extreme instances in supplemental headgate support by stageloaders, installation angles approaching 90 degrees have been used with success. Figure 5 shows the installed angle bolt. A special wrench is used to drive the angle bolt into the borehole and rotate the bolt to mix the resin. The splice tube assembly may be attached to the angle bolt at installation or just prior to tensioning. As shown in Figure 6, a tensioner powered by bolt machine hydraulics, provides cable takeup and applies up to 16,000 pounds of preload. Figure 7 shows the finished JMS Cable Truss installation.

## MINE TEST DATA ANALYSIS

Based upon previous research conducted at this mine, the most critical roof condition occurs when the longwall face is 30' inby the intersection. At that time, due to the panel orientation and major in-situ horizontal stress direction (in Figures 1 & 2), the mining-induced frontal abutment pressure and horizontal stress interact causing a very high stress concentration in the intersection. Therefore, to facilitate measuring maximum loading, the strain-gaged cable trusses were located approximately 15' inby the intersection.

During the first test in the four-entry panel, Figure 1, one of the cable strain gages failed prematurely. The second gage did function properly and provided sufficient data. Shown in Figure 8 is the change in truss loading of the instrumented trusses as a function of longwall face distance. The maximum increase in truss loading outby the face measured 6,000 pounds and occurred when the face was 3' inby. Total truss load would be the initial 12,000 lbs plus the maximum recorded increase or 18,000 pounds. A photographic record was made of conditions in the tailgate during the test period. Observations made during the test indicated uniform caving behind the shields with the roof "hanging up" 12-16' before setting down. At the T-junction, pressure was minimal and there were no adverse conditions (Figure 9). On the pillar side of the tailgate, significant cutter roof did develop as shown in Figure 10. Due to the high stress concentration at the intersection, several primary bolts had incurred shear failure leaving the ends of the T-5 channel hanging down as shown in Figures 11 and 12. Throughout the entire test area, no cable trusses failed. Significant rib sloughage occurred on the pillar rib (Figure 13). Due to the loading condition, truss horizontal members remained in tight contact with the immediate roof. (Figure 14).

The second test was conducted in a three-entry panel. Shown in Figure 15 is the change in truss loading of the instrumented trusses as a function of longwall face distance. The maximum load increase for Truss No.1 and No. 2 measured 4,200 and 4,700 lbs respectively(4,450 lbs average). Installed tension was again 12,000 lbs equating to a total maximum load of 16,450 lbs. After cable truss installation and before the tailgate was subjected to the mining-induced frontal abutment pressure from the second panel, cutter roof developed in both the cable trussed section of the tailgate and in the cribbed area both inby and outby the cable trussed area. Observations and measurements taken in each area show that the cutter development in the trussed area was much less than the cribbed area (Figure 16). Average width and height of cutter development in the truss area was 18.1" and 14.4" respectively. In the cribbed area it was 25.0" and 15.4". When the area became influenced by the mining-induced frontal abutment pressure from the second panel, the roof cutter at the face/tailgate T-junction in the cribbed area became very severe. The average width and depth of the cutter in the cribbed area increased to 30" and 20" respectively, while in the trussed area it remained unchanged. As compared to the 4-entry configuration, more floor heave occurred. With the larger pillar next to the tailgate, this would be expected because mining induced horizontal stress would be larger. A reduction in the size of the pillar next to the tailgate would reduce the floor heave effect because it would help relieve the horizontal stress. Floor heave in both the cribbed and trussed area was the same (approximately 2'). However, this amount of floor heave did not cause any operational problems when mining through.

In both test areas, no cable angle bolts or horizontal members failed even under the influence of high horizontal stress induced shear. Previous failures with the 7/8" rod truss always initiated with horizontal stress induced shear failure of the angle bolt. The truss plan better controlled cutter distribution than the cribs. The cable truss plan, as implemented, controlled both the in-situ and mining-induced horizontal stresses.

## LABORATORY TEST DATA ANALYSIS

The JMS Cable Truss is an active truss in that a high installed load is applied at installation to generate upward loading into the roof. This loading results in compression of the immediate roof since force vectors are directed inward at the plate load transfer points. However, the design of the truss allows communication of any loading on the truss to both resin anchored angle bolts deep over the rib.

It was theorized that the ability to communicate loads should result in a truss capacity greater than the absolute strength of the cable component. To investigate this theory, a truss testing fixture (Figure 17) was built at the Jennmar R & D facility. This fixture allowed assembly of the JMS Cable Truss with a 45 degree angle bolt installation. Hydraulic rams were used to measure and apply cable loads and plate loads.

Figure 18 displays a normal tensioning cycle, cycle 1 to cycle 2, followed by roof loading applied evenly to both left and right roof plates. This loading represents roof shear failure occurring at both ribs and total dead weight support evenly distributed on the truss. As can be seen, tensioning the horizontal member to 16,000 pounds results in a bolt load of 12,000 pounds and a plate loading of 10,000 pounds. As the plate loading is applied the load on the horizontal member falls below that on the angle bolts and the plates. Extrapolating this data to a bolt loading of 50,000 pounds, both plates would have 45,000 pounds loading which means that in this configuration, the JMS Cable Truss employing a 0.6" cable nominally rated at 56,800 pounds would support a load of 90,000 pounds.

Figure 19 displays loading applied evenly to both angle bolts. This loading represents horizontal induced shear stress and was conducted to insure that load transfer to the horizontal member did not exceed that applied to both angle bolts.

Figure 20 displays cyclic loading applied to the horizontal member. This test was performed to determine the uniformity of load transfer to each angle bolt through several loading cycles. Also, this loading represents pure center tensile roof failure applying the total load to the horizontal member and transferring the load to both angle bolts. Again, extrapolating a horizontal loading to 50,000 pounds, each bolt would have a load of 38,000 pounds. This means that in this loading condition, a load of 76,000 pounds could be supported by the JMS Cable Truss.

Figure 21 displays cyclic loading applied to the left angle bolt. This test was performed to determine the uniformity of load transfer to each angle bolt through several loading cycles. Also, this loading represents horizontal stress induced shear failure on one side of the entry and applied to only one angle bolt. Again, extrapolating the bolt loading to 50,000 pounds, the opposite bolt would have a load of 33,000 pounds. This represents a loading capacity of 83,000 pounds.

The theoretical load capacity of the JMS Cable Truss in the three different loading conditions, are at the nominal yield load of the 0.6", grade 270, seven strand cable. If the cable tensile value was used, the capacity in all loading conditions would be over 40 tons.

## SUMMARY/CONCLUSION

The dynamic JMS Cable Truss system has demonstrated success in tailgate support of Pittsburgh #8 seam coal mines. It has also shown success at many other mines in different seams. It should be pointed out that the trusses in the mine tests were installed several months after initial entry development. Better roof stability can be obtained by installing roof trusses on cycle during development so that interaction between primary and supplemental systems occur as soon as possible. Based on these test results, plans are now being made to implement this truss plan in lieu of cribbing for tailgate support.

The laboratory tests demonstrate the unique design features of this truss system. The design allows for load transfer to the anchorage points over each rib. Since angle bolt installation can be accomplished at the roof/rib corner, maximum utilization of the angle bolt length over the rib can be accomplished. This feature will reduce any rib sloughage effect by allowing load transfer to occur farther into the coal pillar. The effect on floor heave is also mitigated by allowing load transfer farther into the coal pillar. Also, the truss capacity, by design, exceeds that of its individual components and thus provides an economic alternative to rod truss systems.

## REFERENCES:

Stankus, J. C., J. J. McCaffrey, S. Guo, S. Peng, 1994, "Innovative Concept in Tailgate Entry Support: Elimination of Crib Blocks Through Utilization of New High Capacity Roof Truss Systems," *Proc. 13th International Conference on Ground Control in Mining*, edited by S. S. Peng, West Virginia University, pp. 166 - 174.

Stankus, J. C., S. Guo, S. Peng, 1995, "Truss Systems for Longwall Tailgate Support-Update," *Proc. 14th International Conference on Ground Control in Mining*, edited by S. S. Peng, West Virginia University, pp. 1 - 8.

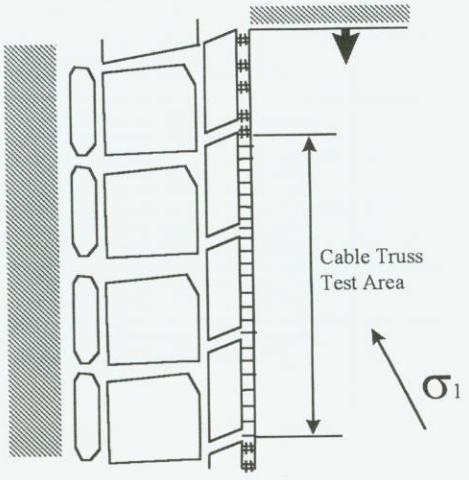



Figure No. 1 4-Entry System

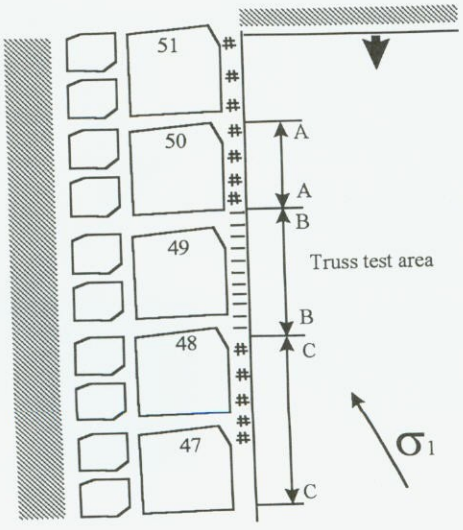



Figure No. 2 3-Entry system

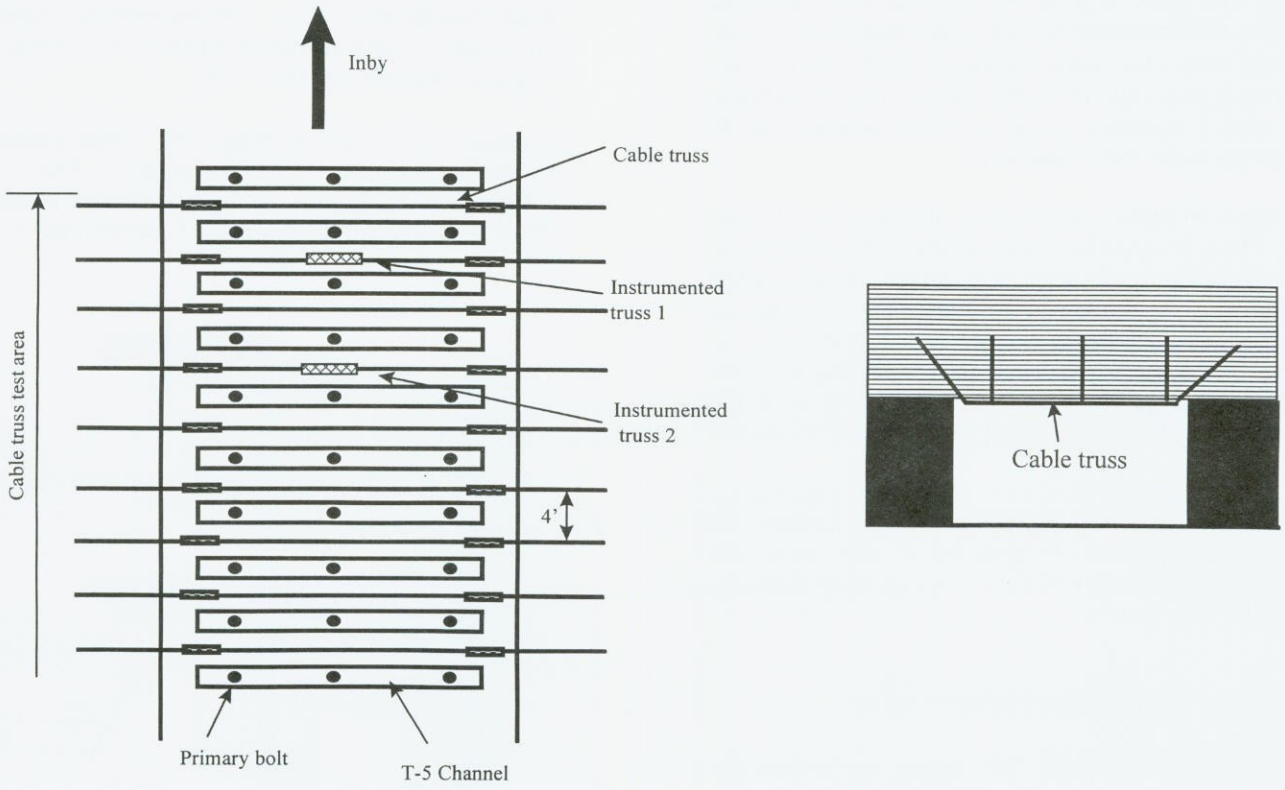



Figure No. 3 - Cable Truss Installation in the Test Area

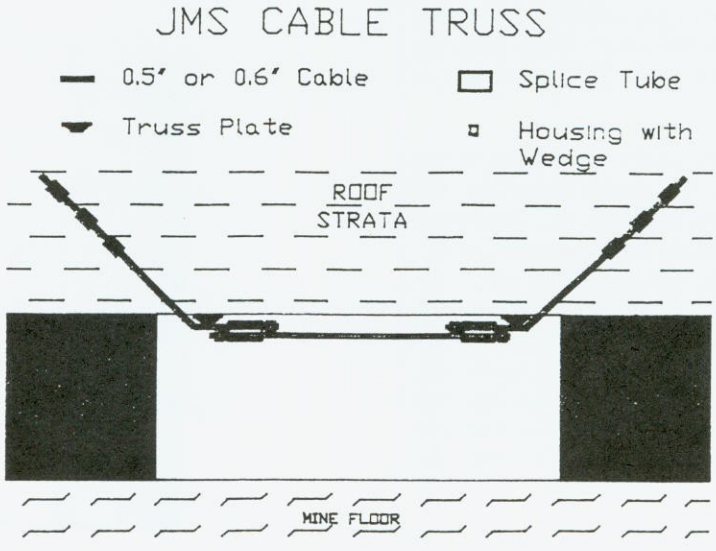



Figure No. 4

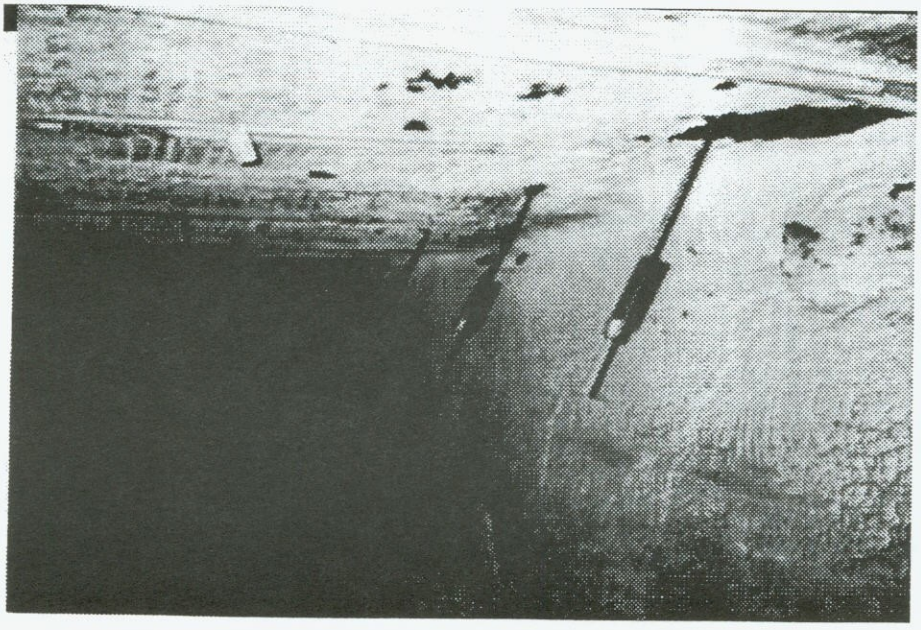


Figure No. 5

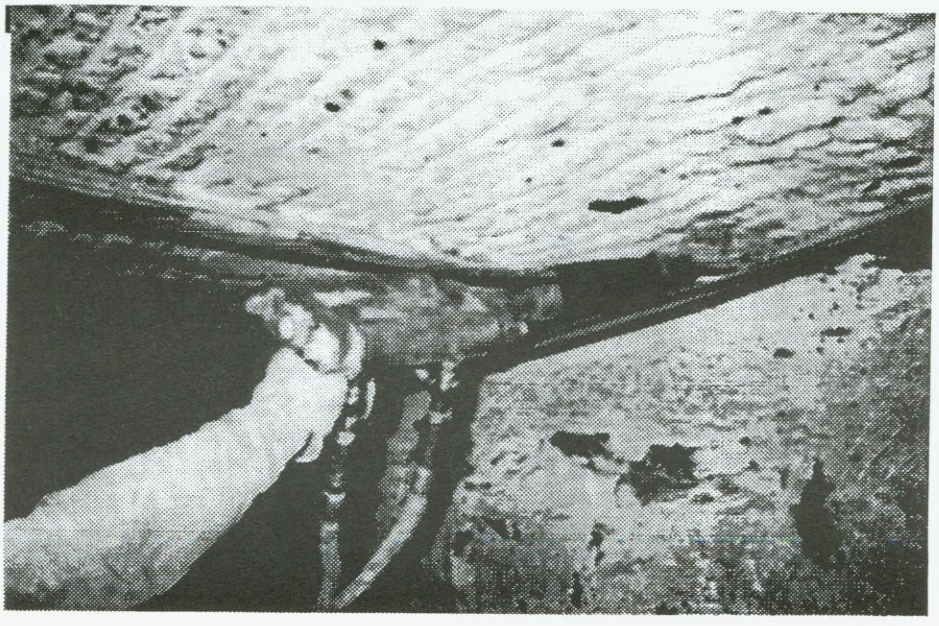


Figure No. 6

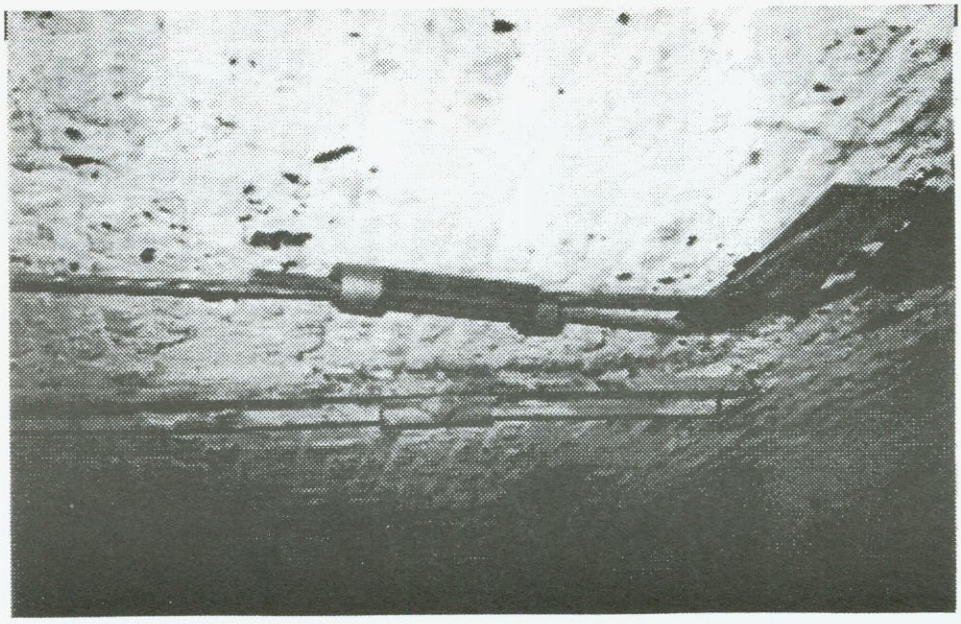


Figure No. 7

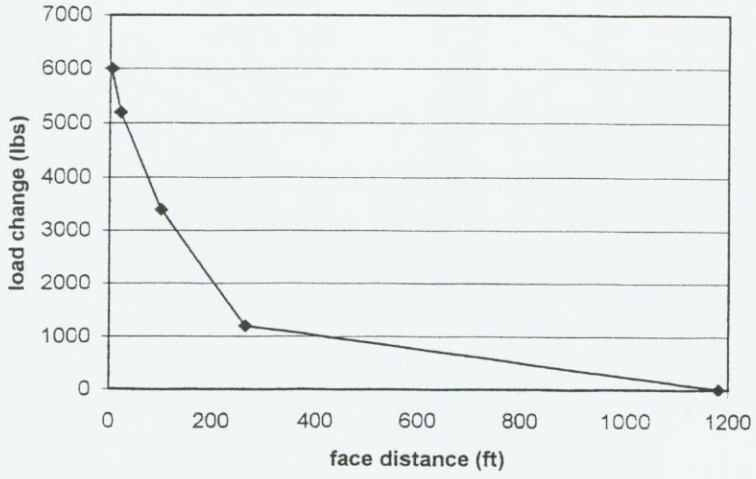



Figure No. 8 - Load change as a function of face distance in cable truss test area for a 4-entry system

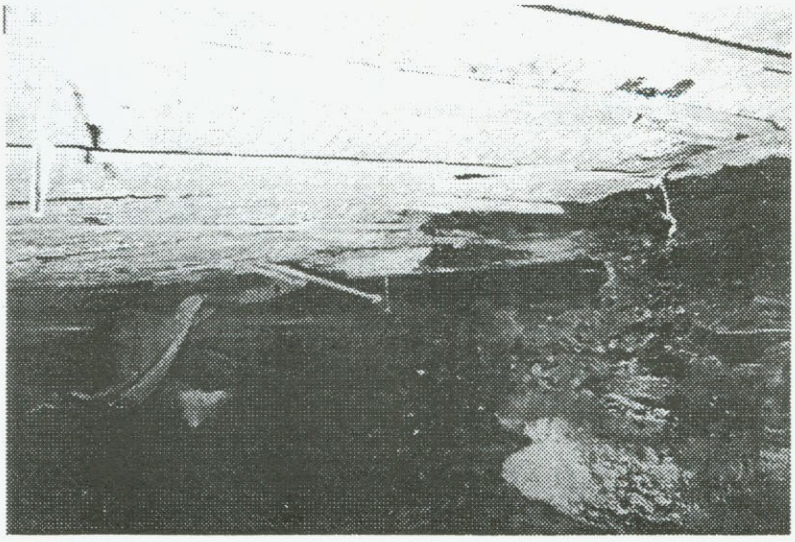


Figure No. 9

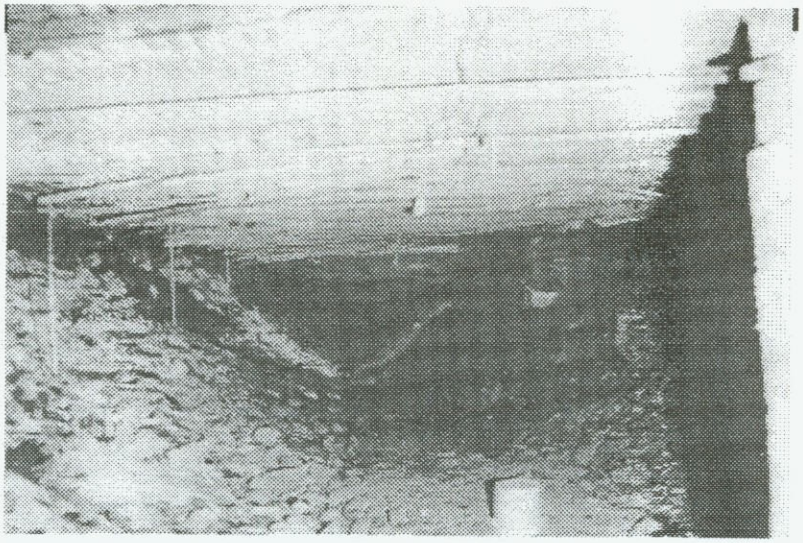


Figure No. 10

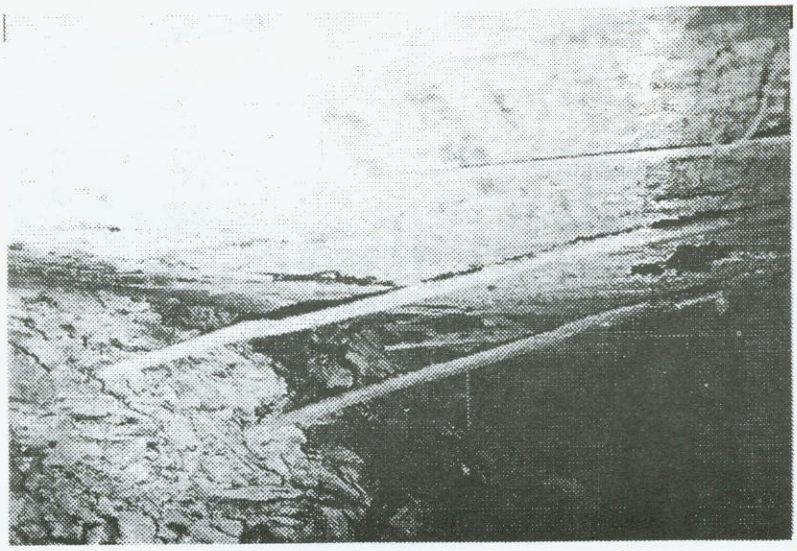


Figure No. 11

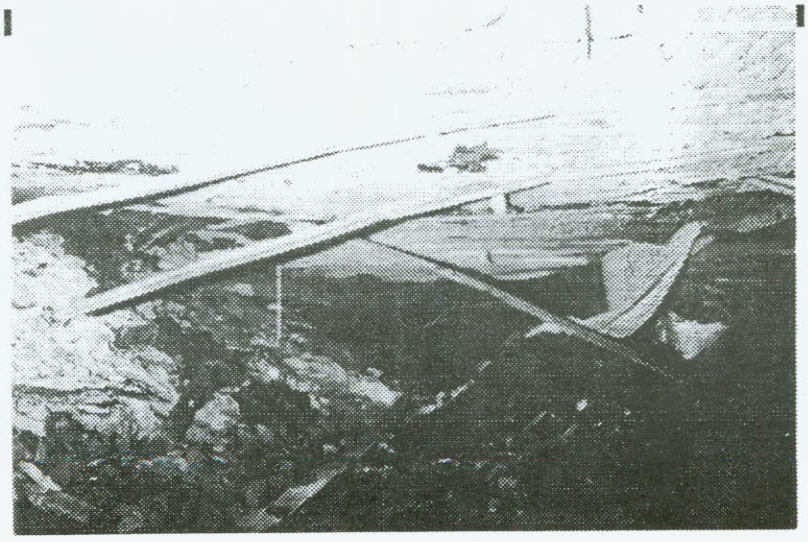


Figure No. 12

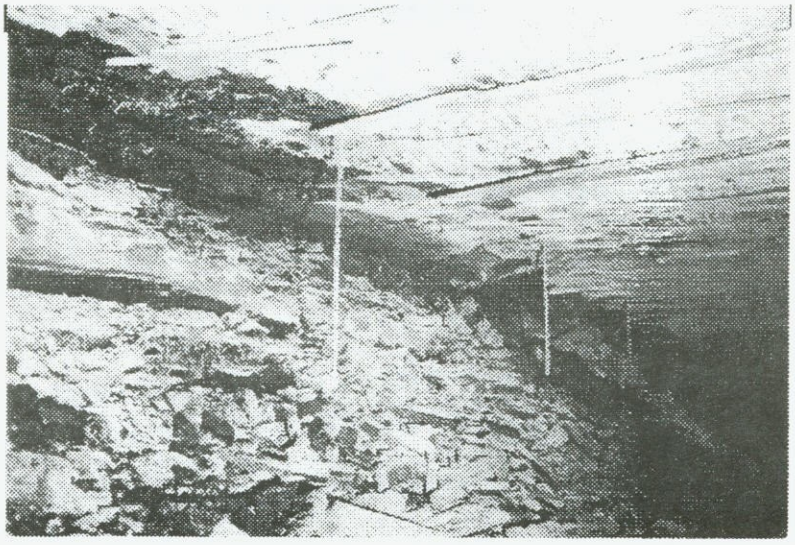


Figure No. 13



Figure No. 14

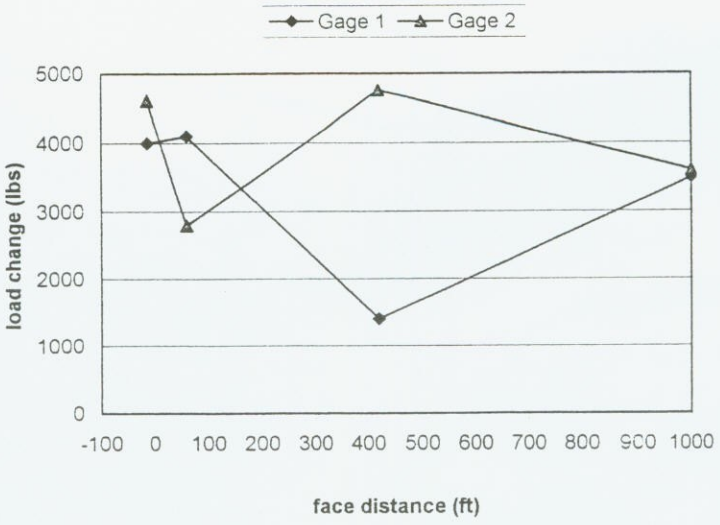



Figure No. 15 - Load change as a function of face distance in cable truss test area for 3-entry system (+ outby, - inby)

Table 1 Cutter Distribution in Tailgate Entry

| | | | | | | | | |
|---|---|---|---|---|---|---|---|---|
| Cable Test Area B-B | L (ft.) | 1+60 | 1+50 | 1+40 | 1+30 | 0+80 | 0+40 | 0+20 |
| | W (in.) | 18 | 21 | 22 | 16 | 16 | 18 | 16 |
| | H (in.) | 11 | 15 | 16 | 17 | 19 | 10 | 13 |
| Crib Area B-B | L (ft.) | 0+20 | 0+40 | 0+60 | 0+80 | 1+00 | | |
| | W (in.) | 21 | 26 | 28 | 24 | 26 | | |
| | H (in.) | 11 | 15 | 18 | 16 | 17 | | |

Notes: L - Observation location; W - Width of cutter; H - height of cutter

Figure No. 16

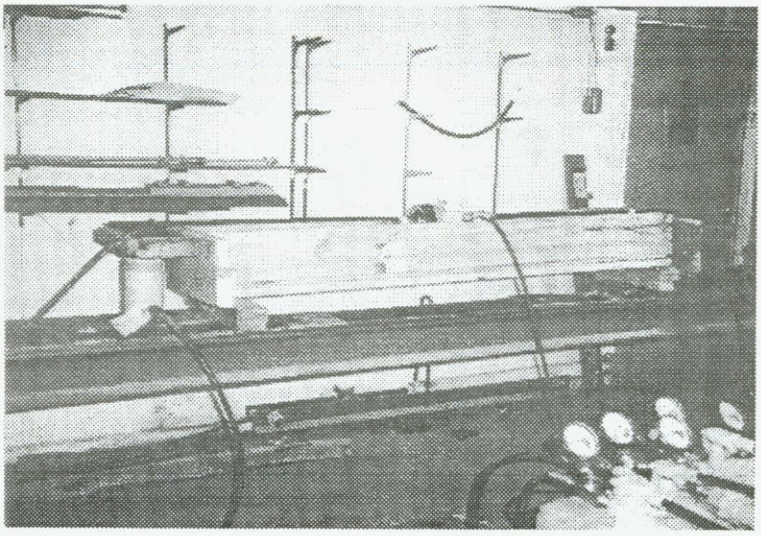


Figure No. 17

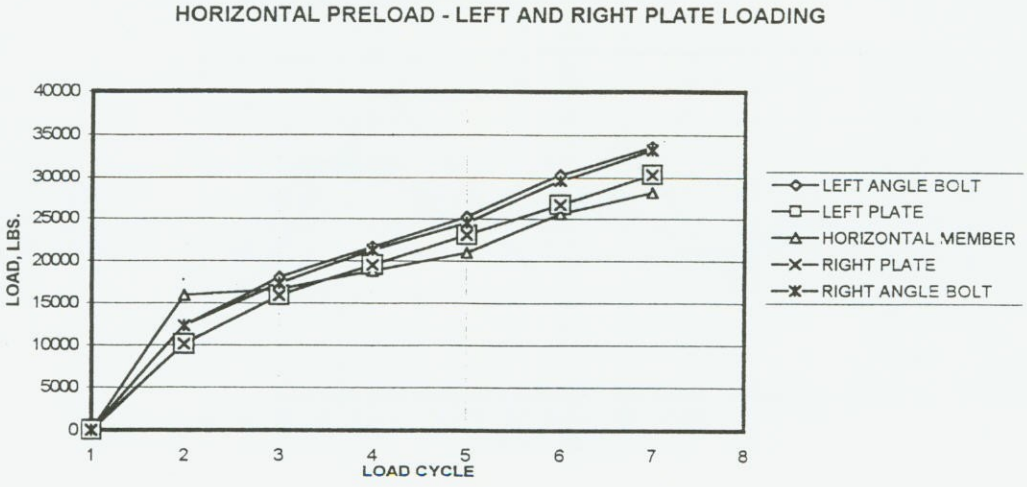



Figure No. 18

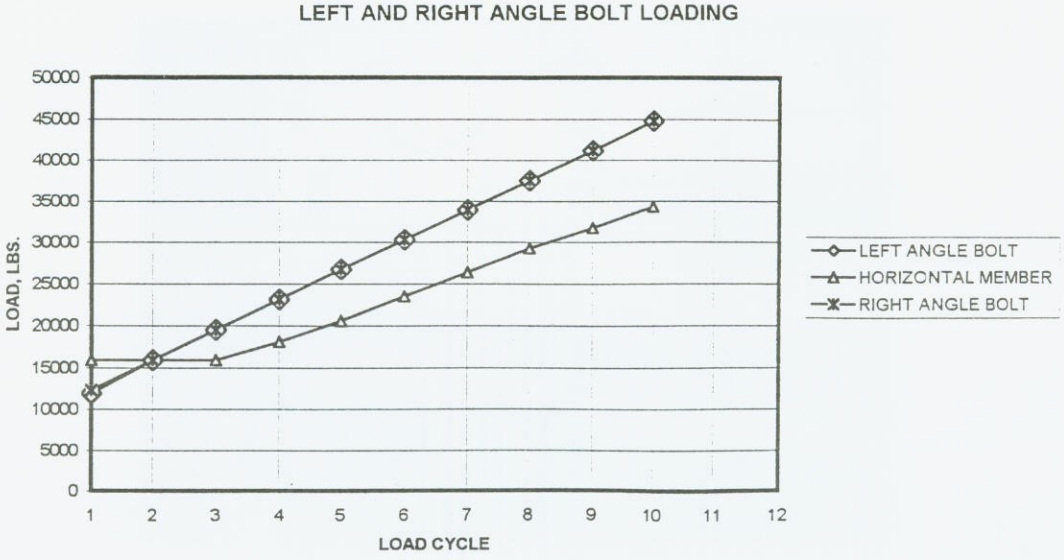



Figure No. 19

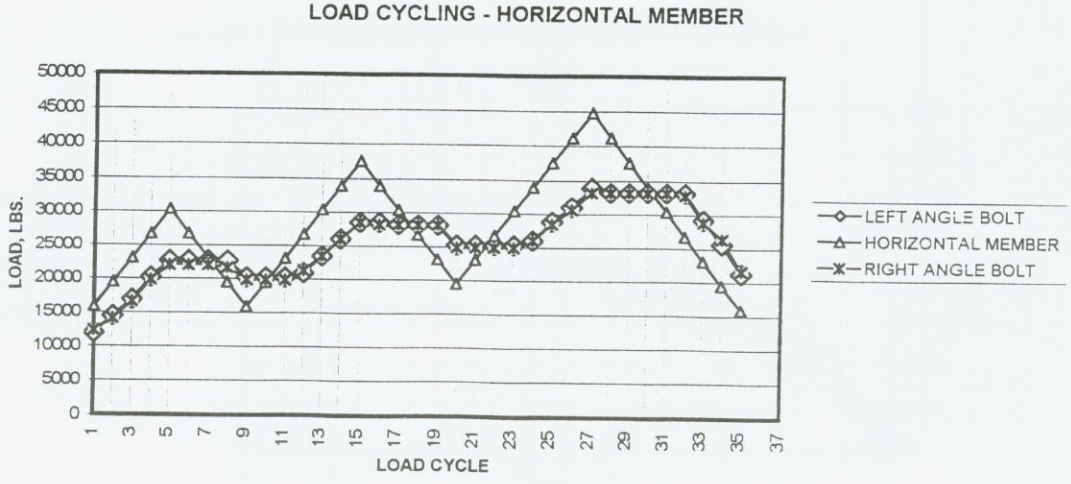



Figure No. 20

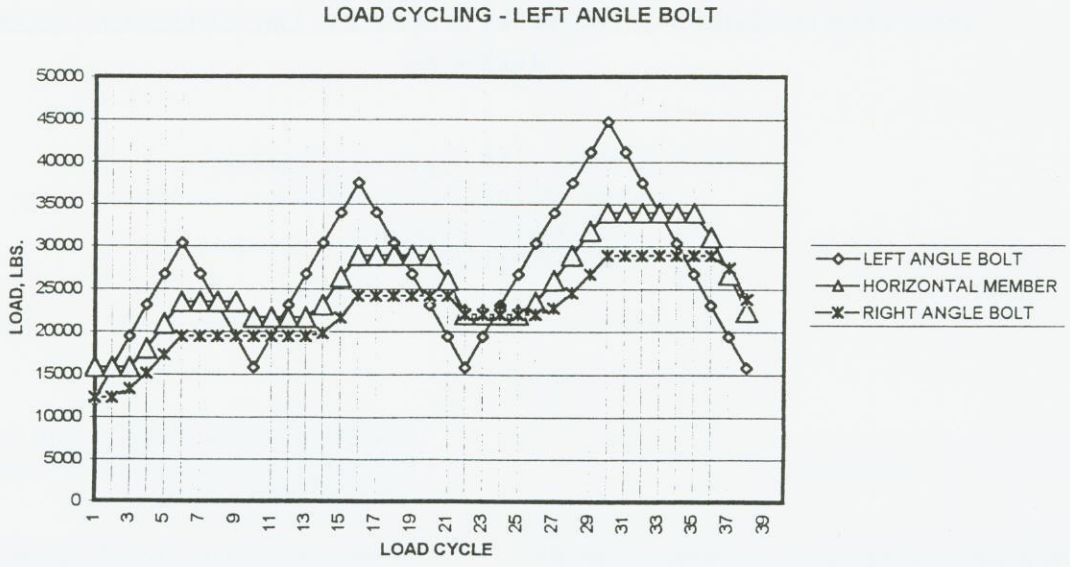

LOAD CYCLING - LEFT ANGLE BOLT
LOAD, LBS.
50000
45000
40000
35000
30000
25000
20000
15000
10000
5000
0
1
3
5
7
9
11
13
15
17
19
21
23
25
27
29
31
33
35
37
39
LOAD CYCLE
LEFT ANGLE BOLT
HORIZONTAL MEMBER
RIGHT ANGLE BOLT

Figure No. 21

# Extending the Limits of Strata Bolting by the Use of Flexible Strand Rockbolts

*Dennis R. Barratt,* Mining Systems Engineer
Exchem Mining & Construction
Derbyshire, England
UNITED KINGDOM

## ABSTRACT

Rockbolting is now used extensively as a method of primary support in UK coalmines. Over the past fifteen years an optimum bolting system has evolved, based on a high grade steel bolt and a very strong stiff resin. Where necessary, cablebolts are used in conjunction with rockbolts as a supplementary means of support.

The rockbolting system, as currently used, is based on a maximum bolt length of 2.4 m whilst cablebolts are generally 6 or 8 m long. Based on the UK experience, there are situations where it is necessary to extend the bolted horizon above that normally achieved with a 2.4 m long rockbolt. Until recently the only options available were coupled rockbolts or cablebolts, both of which have inherent problems in terms of installation.

Flexible Strand Rockbolts (FSR), in lengths of 4 to 6 m, provide the means of being able to extend the normal bolted horizon. Other advantages include increased strength characteristics (tensile and shear), able to be installed in the UK standard hole size (26-28 mm), encapsulation using resin capsules, thus offering immediate support, high bond strength compared to conventional strand, and able to be installed using existing drilling and bolting equipment.

The FSR is considered to be a new concept in terms of strata control and one that compliments the rockbolting system currently in use.

## INTRODUCTION

Within the field of strata control, the development of rockbolting system components and the introduction of such systems as a method of primary support in UK coalmines, is recognised as one of the main achievements of the UK coal industry over the past ten years. The reduced cost of rockbolting systems compared with the use of conventional steel arches, has been a major contributory factor in reducing overall production costs.

Having accepted that the full column resin bonded bolting techniques developed in Australia were most suitable for the UK mining conditions, the concept was first introduced in the mid 1980's on a trial basis. It was soon realised that improvements in product and system performance could be achieved. Hence, with the co-operation of materials and component manufacturers, British Coal Rock Mechanics Department and H M Mines Inspectorate, a high strength bolting system has now evolved, based on a high grade steel bolt and a very strong, stiff, resin. The decision to standardise on a 22 mm diameter bolt installed in a 27 mm diameter hole, and using 24 mm diameter resin capsules has also helped to ensure the successful introduction of the "AT" system at most UK operating mines.

Essentially, the "AT" system provides good bond strength together with high resistance to shear. These qualities provide a high degree of confinement to the roof, which in turn increases the shear strength of the overlying strata. However whilst rockbolts may be effective within the bolted height, they are not always sufficient to maintain roof stability. Where roof softening develops above the bolted height, cablebolts are generally installed in order to provide reinforcement at a higher level. Generally, fully grouted double birdcaged cablebolts are used, having a 60 tonne capacity and in the range 6 to 10 m long. An alternative means of achieving reinforcement beyond the normal bolted height would be the use of coupled rockbolts, but these have not proved popular, mainly due to the problem of achieving a resin bond below the coupled joint.

Due to the method of installation and the use of cementitious grout, with all the necessary mixing and pumping equipment, in a roadway drivage situation cablebolts are generally installed outbye of the heading, and are consequently used as a supplementary means of support. However, there are situations where it would be advantageous to instal rockbolts

of a length longer than the normal 2.4 m, but not necessarily up to the length of a 6 m cablebolt, and where with the use of a resin grout, immediate support could be achieved. The Flexible Strand Rockbolt (FSR) is able to achieve these criteria, whilst offering other features which are considered to be advantageous.

The development of the current "AT" rockbolting system and cablebolting techniques has been an evolutionary process, and having developed what are now considered to be the optimum forms of this type of strata reinforcement, further development of such systems and techniques can only be in the form of fine tuning. However, the development of the FSR is considered to be a new concept, which compliments the existing forms of strata reinforcement, whilst offering a number of distinct advantages and range of applications.

## DEVELOPMENT OF THE FLEXIBLE STRAND ROCKBOLT

The FSR has been developed by Exchem Mining & Construction in conjunction with Bridon Ropes Ltd., either for application as part of a primary support system together with AT rockbolts or as a secondary support system where either AT rockbolts or standing steel supports are used. There are also a number of specific applications where it is considered that the use of the FSR would be advantageous.

The FSR consists of a steel strand made up of nineteen wires, having a 9/9/1 construction and left hand lay, which is compatible with the clockwise rotation of the drilling machine when the bolt is being inserted into the strata.

Each wire has a tensile strength of 1770 N/mm², giving the bolt a minimum breaking load of 50 tonnes and an outside diameter of 22.9 mm. The outer wires of the strand are indented in order to give adequate bonding between the bolt and the resin, thus utilising the maximum strength of the bolt.

The lengths of the bolts can be made to suit, but are normally 3 to 5 m long. At the inner end of the bolt the wires are fused and tapered to allow for ease of penetration through the resin capsule and to ensure adequate mixing and shredding of the capsule. The outer end is fitted with an octagonal steel ferrule (38 mm A/F x 140 mm long), see Fig.1., which is pressed on to the strand and with the aid of a spinning adaptor is used to instal the bolt into the strata. The relatively long end termination, ensures a positive location with the spinning adaptor and helps to overcome the potential for "whipping" of the free strand when installing the FSR. This type of end termination has a proven history and is commonly used within the rope industry in a number of applications. The ferrule is designed to withstand a minimum end loading of 40 tonnes. However, having been subjected to an end loading sufficient to cause the ferrule to begin slipping off the strand, the bolt will continue to support load, but over a period of time continual loading will cause the ferrule to gradually slip off the strand in a controlled manner. The FSR is suitable for use

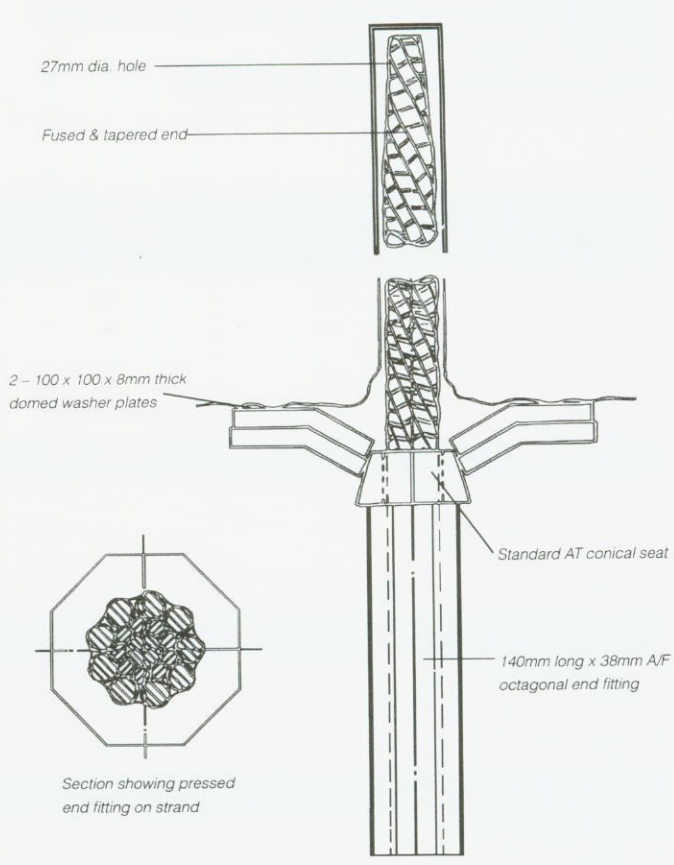



**Figure 1 – Flexible Strand Rockbolt**

with a standard "AT" conical seat, which allows the bolt to be used with conventional "AT" domed washer plates. Tests have shown that the use of two 8 mm thick washer plates will begin to flatten at approximately 35 tonnes, and allow the FSR to pull through at approximately 38 tonnes. The use of such plates therefore will give an indication of the on-set of maximum loading on the bolt.

## LABORATORY TESTING AND EVALUATION

A full series of laboratory tests have been carried out both on the strand alone and as part of a bolt/resin system, in order that an evaluation may be made with a view to receiving full approval for underground use.

The laboratory tests included the following:-

- Tensile test on the strand
- Tensile test on the end fittings
- Load/Extension test on the strand
- Short Encapsulation pull test on the bolt/resin system
- Shear test on the bolt/resin system

A summary of the physical parameters and technical characteristics of the FSR, based on the results of the laboratory tests are given in Table No.1.

## Comparison of Technical Parameters of 'AT' Type Rockbolt and Flexible Strand Rockbolt

Table 1

| | PARAMETER | 'AT' ROCKBOLT | FLEXIBLE STRAND ROCKBOLT |
|---|---|---|---|
| 1 | Bolt Diameter (mm) | 21.7 | 22.9 |
| 2 | Hole Diameter (mm) | 27.0 | 27.0 |
| 3 | Effective Cross-sectional Area of Bolt ($mm^2$) | 370 | 346 |
| 4 | Thread Size | M24 | Pressed End Fitting |
| **Tensile Properties (Body)** | | | |
| 5 | Yield Strength (tonne) | 25.7 | 44.1 |
| 6 | Max Force (tonne) | 34.7 | 55.1 |
| 7 | Effective Elongation of Free Length (mm/T/M) | 0.125 | 0.235 |
| **Tensile Properties (End Fitting)** | | | |
| 8 | Max. Force (tonne) | 30.0 | 40.0 (Min) |
| 9 | Shear Strength (tonne) | 26.4 | 36.6 |
| **Short Encapsulation Pull Test** | | | |
| 10 | Average Stiffness (kN/mm) | 60 | 69 |
| 11 | Average Peak Bond Strength (kN) | 183 | 197 |

Although it is not envisaged that the FSR will replace the standard "AT" rockbolt, it is relevant to make comparisons between the two systems, particularly in terms of the advantages and disadvantages. These can be summarised as follows:-

Advantages of the FSR

- increased tensile strength for equivalent bolt diameter
- increased shear strength
- equivalent bond strength with AT rebar
- flexibility, allowing longer bolts to be installed in low height roadways
- compatible with existing drilling technology
- suitable for use with "AT" type resin capsules
- compatible with existing washer plates, conical seats, etc.

Whilst there are no real disadvantages with the FSR, there are two factors which should be assessed when considering their use, these being the cost and installation in terms of the physical limitations of the site, length of bolt, type of drilling machine, etc.

The cost of the FSR has to be judged in terms of what it is achieving and the alternatives that are available. For example, whilst the cost of a 4 m long FSR including the resin capsules is comparable with a 4 m long double birdcaged cable including cementitious grout, the cost of a 4 m long coupled "AT" bolt would be approximately half such costs. However, when considering cablebolts, the extra cost of drilling a 55 mm hole, the time taken to instal and grout the cable, together with the fact that immediate support is not achievable, all have to be taken into account. Similarly, the extra cost of the FSR compared with the coupled "AT" bolt, has to be judged against the increased strength and flexibility of the FSR, and the difficulties usually encountered when installing coupled bolts.

Whilst the FSR offers a degree of flexibility in terms of being able to instal longer bolts in low height roadways, there are limitations as described in the installation procedures, and such limitations may also determine whether or not a full column resin bond can be achieved.
Evaluation reports on the FSR have been carried out by Dr L R Stace of Cerebus (Mining Acceptance Services) Ltd[1] and by Dr G Daws of Graham Daws Associates[2], both of whom assess the FSR in terms of its use as secondary support.

### TYPICAL APPLICATIONS FOR FLEXIBLE STRAND ROCKBOLTS

It is envisaged that in most applications the FSR will be used in conjunction with standard "AT" rockbolts, typically where it is necessary to extend the bolting horizon; where high "AT" bolt densities are required; or where problems are being experienced with installing "AT" bolts in low height roadways. However, there are a number of specific applications which are worth considering and these are described below.

Roadway drivage with high stress conditions

Due to their ease of installation, FSR's can realistically be installed in conjunction with the primary roadway support system, and have been shown to be particularly advantageous where high stress conditions are being experienced. In some roadways the application of FSR's in conjunction with AT bolts may obviate the need for cablebolts or free standing steel supports.

Remedial work

Where strata monitoring indicates progressive failure of the primary system, i.e. excessive strata deformation extending above the original bolted height, immediate roof flaking or sagging, FSR's can be installed as a means of offering additional confinement following the initial and continued movement of the strata.

Distressed situations to prevent falling strata blocks

Situations may arise where "AT" rockbolts or cablebolts become fractured by high shear stresses. In such cases when the confining stresses are released, as at a longwall "T" junction, there is the potential for roof blocks to become dislodged. The use of FSR's with their high end load

capability and high shear strength, installed at the appropriate time in the mining cycle, could address such a situation in a controlled and systematic manner.

Rib bolting

In areas of high stress, resulting in excessive strata deformation, it is important to maintain the integrity of the ribs. This may involve the use of long tendons and FSR's are considered ideally suitable for such applications.

Special applications

Junctions or large excavations (e.g. drive houses, substations, etc.,)
Faulted areas with potentially loose roof blocks
Longwall face drivage or salvage
Anchoring of steel girders or supporting roof girders at "T" junctions.

## INSTALLATION PROCEDURES

As with the standard "AT" bolting system, the application and installation of FSR's in UK coal mines should be carried out in accordance with the Health & Safety Commission document. "Guidance on the use of rockbolts to support roadways in coal mines".[3] Sites should be assessed to determine their suitability for the application of FSR's taking into account any relevant information such as strata types, monitoring results, drilling trials (indications of breaks and their location) and installation tests to determine resin bond lengths that can be achieved.

It is recommended that FSR's are installed in holes having a nominal diameter of 27 mm, and are used in conjunction with Exchem's Celtite AT 24 mm diameter resin capsules. It has been demonstrated that both the drilling of the longer holes and the installation of the FSR's can be achieved using compressed air operated leg type drilling machines. Machine mounted, hydraulic drilling rigs have also been used. In either case it is important that the drilling machine has sufficient thrust and torque available, to cope with both the longer hole required, and also for installation of the FSR through the resin. It is also recommended that 22 mm hexagonal drill rods are used, designed for quick coupling and release.

The holes should be drilled to approximately the free strand length of the FSR being installed, in order to ensure that the washer plate(s) can be thrust tight to the roof. Resin capsules can then be inserted into the hole in the normal way using capsule insertion tubes, with the plastic capsule retainer behind the last capsule. The length and types of capsule used (Fast and Slow or Slow only) should be chosen to suit the particular application, with the aim of endeavouring to achieve as long an encapsulation length as possible. Exchem have now developed a 2 m long slow set capsule, which when used with a 4 m long FSR can give full encapsulation. As part of an installation package Exchem are also able to offer a three stage compressed air operated drilling/bolting machine, which has a closed height of only 1 m, and together with a specially designed two stage spinning adaptor this will allow a 4 m long FSR to be installed in a roadway having a minimum height of 2.74 m. As shown in Fig.2, in practice it is the combination of bolt length, roadway height and drilling machine configuration, which govern the allowable capsule length and hence the amount of encapsulation. It should be noted that whilst full encapsulation is desirable, since the FSR has different performance characteristics to the AT bolt, underground monitoring has shown that the FSR gives improved roadway stability even with less than full encapsulation.

Having inserted the resin capsule or capsules, the FSR is then entered into the hole and can be used to push the resin to the back of the hole before entering the ferrule into the spinning adaptor located in the drilling machine.

The FSR should then be rotated at a steady speed and fed slowly into the hole, taking care not to over thrust and so cause excessive bending of the bolt. As with a conventional AT bolt, as the FSR enters further into the hole, penetrating the resin, the thrust can be gradually increased. The rigidity of the exposed length of the bolt increases as the exposed length reduces.

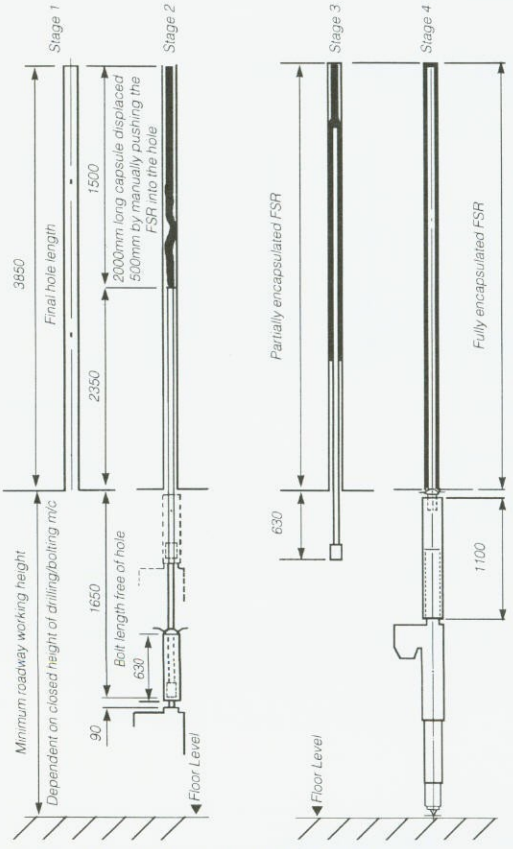



**Figure 2 – Drilling/Installation Details**

Maximum thrust should be applied when the plate hits the roof, and rotation at full revs should be continued for 3-5 secs. The bolt should then be held to the roof on full thrust until the resin has gained sufficient strength to support the bolt (typically 10 secs). The drilling machine can then be lowered, leaving the bolt completed. Since there is no tensioning mechanism built into the FSR, no torquing-up of the bolt is required.

## CASE STUDY

Daw Mill Colliery

Site details: 203's Tail Gate. Warwickshire Thick Seam
Roadway size: 5 m wide x 3 m high
Type of support: Steel 150 x 125 section supports together with rockbolts as secondary support
Rockbolts: Roof 8 x 2.4 m at 0.7 m spacing
Ribs 3 x 1.8 m at 0.7 m spacing
FSR's See Fig 3
Initially 3 x 4 m long at 0.7 m spacing
Reduced to 2 x 4 m long at 0.7 m spacing

203's tailgate was driven adjacent to the workings of 202's, which had been fully worked. Due to the 15 m slim pillar between 203's tail gate and 202's waste area, and a compaction zone, which was known to cross the planned extraction, high stress conditions were expected particularly between the 600 and 800 m mark.

**Daw Mill Colliery 203's TG**

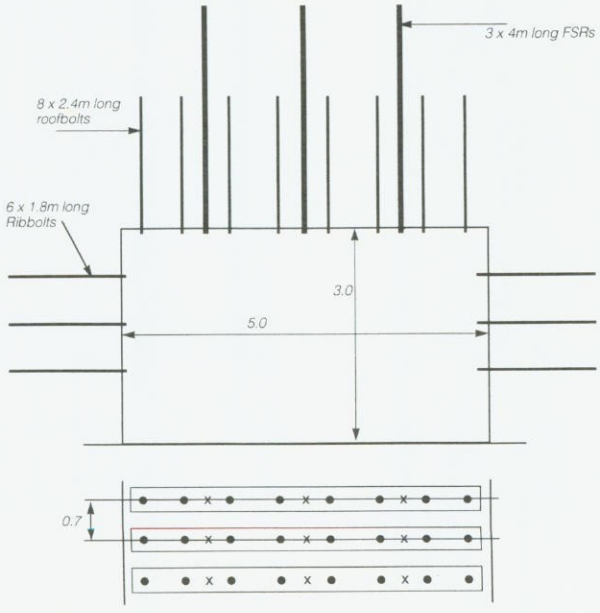



**Figure 3 – Bolting Plan**

The roadway was driven from both ends and rapid roof movements were soon evident in both headings resulting in bending of the RSJ sections of the standing supports, despite a high roofbolt density. Previously, cablebolting had been employed in such conditions and it was again envisaged that a full cablebolting exercise would be required throughout 203's tail gate, particularly in the region of the compaction zone. Cablebolting was therefore commenced in both of the tail gate drivages. High roof deformation was now occurring very quickly in the outbye drivage before cablebolts could be effectively installed and FSR's were introduced at the 410 m mark in an attempt to reduce this.

The FSR's were installed at the front of the heading and their use continued until the roadway thurled at the 800 m mark. Initially, three 4 m long FSR's were installed at every 0.7 m along the roadway, but this was subsequently reduced to two every 0.7 m. The FSR's were used with AT resin capsules and approximately 55% encapsulation was achieved. Installation was carried out using a compressed air operated leg type drilling machine.

The results from this section of the roadway were immediately encouraging, and due to their success it was decided to include the FSR's as part of the outbye drivage support cycle, starting at the 990 m mark (210 m from the start of the outbye drivage).

The results of the monitoring throughout 203's tailgate is shown graphically in Fig 4. It can be seen that the introduction of FSR's significantly reduced the roadway deformation, even through the area of high stress compaction which showed up in the previous monitoring of 202's gate roads. In the sections of roadway where cablebolting was carried out, on either side of the 600 m length of roadway reinforced with FSR's, total roof displacement levels up to 240 mm were recorded. Whereas the maximum level of displacement recorded throughout the FSR section was 140 mm. It was also noted that the strata displacement levels above the bolted height, i.e. 2.4 m, were significantly lower throughout the FSR section than they were on either side where cablebolts had had to be installed.

The results were immediate and dramatic, and in addition to the monitoring, the visual evidence also confirmed the considerably improved roadway stability, with little or no bending of the RSJ section supports and virtual elimination of floor lift. Further cablebolting of the roadway was not necessary and the face has now retreated back successfully.

Whilst the particular study at Daw Mill has been highlighted, underground trials at other collieries have also been carried out, and the effectiveness of the FSR has been highlighted at a number of sites. FSR's are also being installed on a regular basis at Boulby potash mine and here they have also been used as anchors, as part of a truss bolting system.

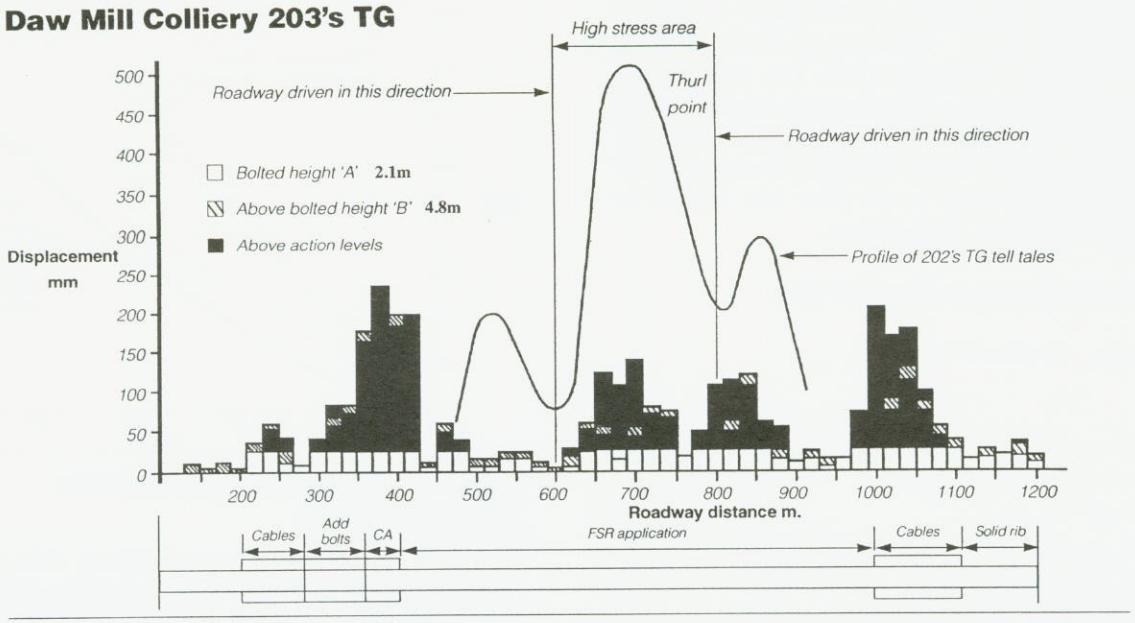



**Figure 4 – Graphic Representation of Monitoring Results**

## SHORT ENCAPSULATION PULL TESTS

As with the use of AT bolts, and as described in the HSE document "Guidance on the use of rockbolts to support roadways in coal mines", prior to the use of FSR's short encapsulation pull tests need to be carried out in all new sites, and when major changes in roof strata take place.

The short encapsulation pull test is used to measure the performance of the FSR/resin/rock system in terms of the bond strength, which is defined as the force applied to the bolt at which the slope of the applied force versus bond displacement graph falls below 20kN/mm. Fig.5 shows a typical arrangement of the short encapsulation pull test, which has a bond length of 300 mm, and tests are required to be carried out at different horizons over the length of the installed bolts.

Fig.6 shows a typical applied force v bond displacement graph for the FSR at a 2.0 m horizon and this is compared with the AT bolt at a similar horizon.

A full series of short encapsulation pull tests have been carried out at a number of collieries, including Daw Mill and Maltby. Whilst this test is recognised as giving valuable information relating to the performance of the bolt, it is a very site specific test and it can be difficult to obtain consistent results due to a number of variables, including variation in strata, condition of the hole and achieving a known encapsulation length.

With the FSR also, the free length of the bolt does not exhibit the same characteristics as the AT bolt. In theory, since both the FSR and the AT bolt are made of steel, the elastic modulus for both types of bolt should be the same. In practice the elastic modulus for the FSR has a lower value due to:-

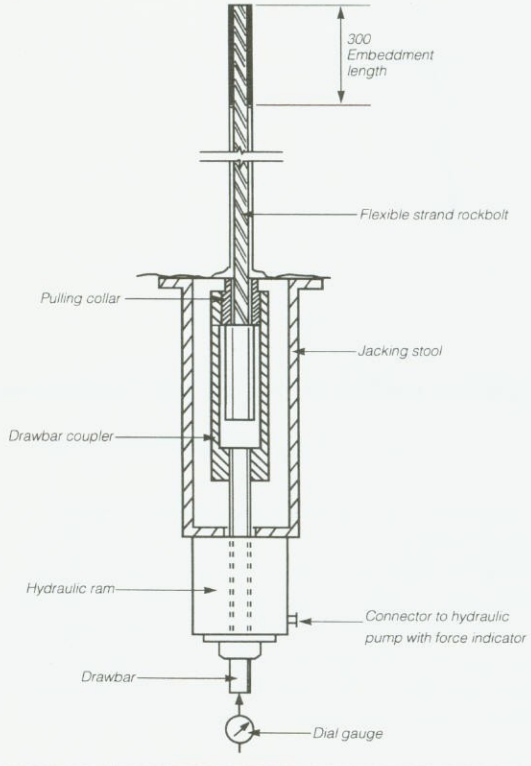



**Figure 5 – Arrangement of Short Encapsulation Pull Test**

i the helical effect, which means that load applied to the bolt has an angular path, being inclined to the axis of the bolt.

ii bedding down of the wires during loading, which can lead to some permanent stretch.

iii a fill factor of 79.2%, which is the ratio of the actual steel area to the circumscribing area.

The overall effect of these factors on the elastic modulus is shown graphically in Fig.7. Based on an elastic modulus value of 128 GPa, the elongation of the free strand under load, can be expressed in terms of an Extension Factor, having a value of 0.235 mm/m/tonne. When assessing the results of the short encapsulation pull tests therefore, the extension of the free length of FSR needs to be taken into account in determining the actual bond displacement.

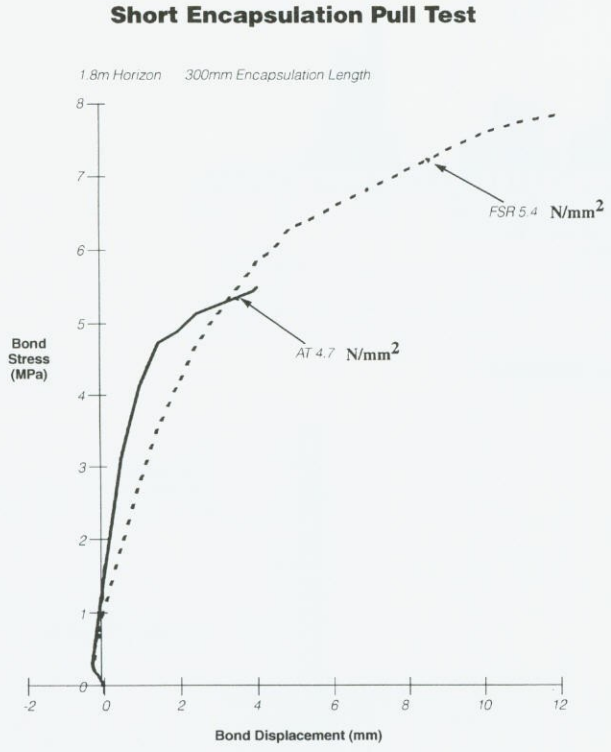



**Figure 6 – Applied Force v. Bond Displacement**

## ENCAPSULATION OF THE FSR

As explained, as part of the installation procedures, there are practical restraints which dictate the length of encapsulation that can be achieved with a particular length of FSR. Whilst it is desirable to fully encapsulate the bolts, as has been proved with the Daw Mill trial, and has been demonstrated at other sites, less than full encapsulation when using a high strength strand can still offer significant benefits in terms of strata control, over and above anything else that is currently available.

For a particular roadway height, the two main factors which govern the length of encapsulation that can be achieved are the free length of the strand exposed from the roof and the closed height of the drilling machine being used to instal the FSR's.

Any system of strata reinforcement using rockbolts relies on the transfer of ground stresses into each bolt, which can be in the form of both tensile and shear stresses. Induced tension in the bolt generates confinement of the strata which produces a much stronger roof beam and increases its shear strength.

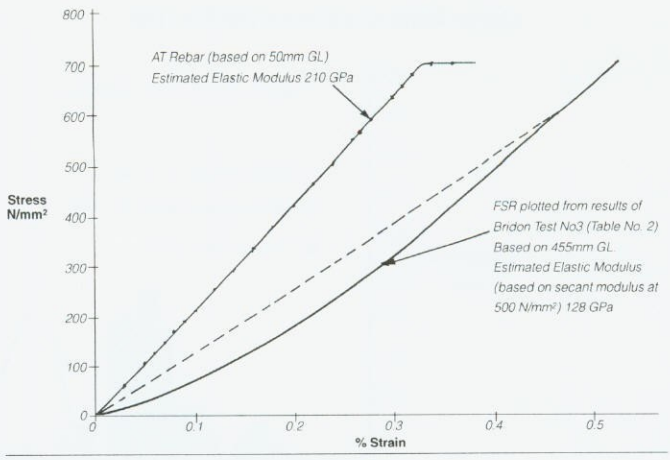



**Figure 7 – Graphs Showing Variation in Stress v. Strain**

If the FSR is only partially encapsulated, then a typical bolt load characteristic, expressed as a function of bolt load and height, would be as shown in Fig.8. Along the encapsulated section the ground stresses cause the bolt to be discretely loaded at intervals corresponding to the dilation of the individual layers of rock. The mechanical properties of the different layers determine the stress profile in the roof and consequently the stresses along the bolt. The length of FSR which is not encapsulated effectively acts as a point anchor system, where the stresses are not confined to individual sections of the bolt. The stress in each of the strata layers acts throughout the free length of the bolt, and so the stresses become cumulative.

As shown in Fig.8, although the lower section of the FSR may not be encapsulated it is still capable of providing confinement

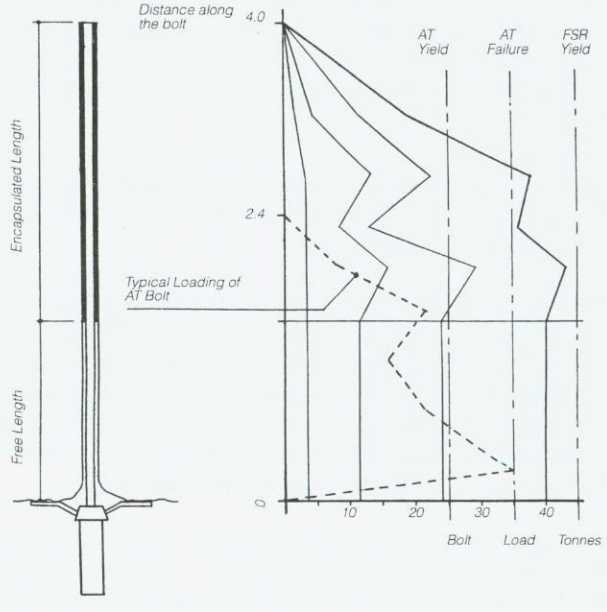



**Figure 8 – Graphical representation of the loading of Flexible Strand Rockbolt**

to the immediate roof strata and will accept a cumulative load up to the rating of the end fitting, i.e. 40 tonnes minimum.

One of the main advantages of the FSR is the high shear strength and although the benefit of this is maximised when the bolt is fully encapsulated, with the diameter of the FSR being 22.9 mm, leaving only a 2.05 mm annulus, very little lateral strata movement is required before the bolt becomes resistant to shear.

The use of the FSR, having a nominal length of say 4 m, allows the bolted height to be extended, beyond that normally achieved with AT bolts, and it is in this region where the FSR is considered to be most effective, particularly if it is encapsulated with resin grout.

## ROLE OF THE FSR AS A SECONDARY REINFORCEMENT SYSTEM

As indicated previously, it is envisaged that the main application of the FSR will be as a secondary reinforcement system, and in order to appreciate this role it is necessary to understand the rock failure mechanism around an excavation and the action of the primary support system.

When an excavation is driven a redistribution of the initial state of stress takes place, and stress concentrations occur around the excavation, which can lead to rock failure and subsequent deformation of the strata.

Fig.9 shows a hypothetical load deformation curve for a rock mass with respect to the roof of an excavation only. The extent of the elastic deformation varies with the rock type, and in coal measures strata it will be small before the onset of dilation.

If the roof of an excavation is left unsupported, failure will occur after a given period of time. This period is known as the stand-up time. However, if a support system is installed within the stand-up time, at say point A in Fig.9, then as the strata relaxes, the support system is loaded and follows the line A-B. If the primary support system is in the form of fully encapsulated AT rockbolts, and if it is adequate for the conditions then ground movement is arrested at the point indicated in Fig.9.

If high stress conditions occur and the primary support system proves to be inadequate, then the scenario shown in Fig.10 applies. The primary support system provides some support but cannot control the deformation. A secondary support system is therefore required, which may be in the form of additional rockbolts. However, since these would have the same stiffness as the primary support, the loading would be along the same support reaction line. If FSR's are used as the secondary system and installed at the same time as the primary system, since the two systems have different stiffness, then each system could provide sufficient support pressure to limit this as shown in Fig.10. The FSR's may also be used as a remedial support system and still generate sufficient pressure

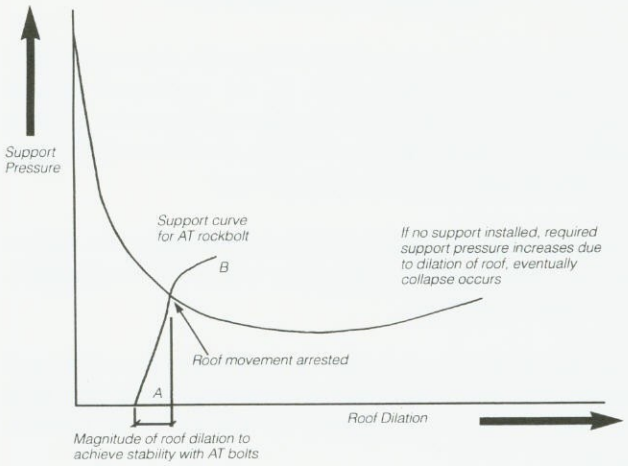



**Figure 9 – Load v. Deformation Curve for a Typical Mine Roof**

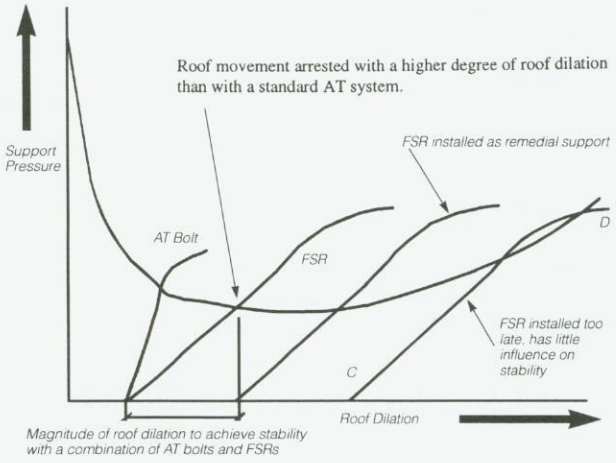



**Figure 10 – Load v. Deformation Curve Showing use of FSR**

to arrest roof movement. However, if installed too far outbye of the drivage, then sufficient support pressure may not be generated to arrest the movement, as indicated by the line C-D, Fig.10.

It should be noted that if FSR's and AT rockbolts are used as indicated in Fig.10, then although satisfactory roof control may result, the total roof dilation will be greater than that associated with satisfactory roof control using AT rockbolts alone.

## OVERSEAS EXPERIENCE

Currently, both the Australian[4,5] and the American[6] coal industries are conducting trials on the application of steel strand type bolts, together with resin capsules as the grouting medium and in fact a number of mines are now using this type of reinforcement system on a regular basis.

However, there are significant differences between the various systems with regard to strengths, length of encapsulation, resin bond strength, etc.

It is interesting to note that for both the Australian and American industries, the aims in using steel strand type bolts are in-line with those required by the UK coal industry, namely:-

- the system to be compatible with existing technology and parameters, i.e. hole size, drilling equipment, etc.,
- bolts to have higher tensile and shear strength
- supplementary support possibly leading to primary support
- able to be installed at the face of the heading
- to provide reinforcement above the normal bolted height
- increase roadway stability, particularly in areas of high deformation
- reduction in standard bolt density
- complimentary to other support systems

The benefits that have been realised from the introduction of steel strand type bolts, particularly based on the UK experience, can be summarised as follows:-

- reduced roadway deformation in highly stressed conditions
- increased resistance to lateral shear
- reduced deformation above the normal bolted height
- reduced deformation in the immediate roof strata
- reduced floor lift
- reduction in standard bolt density
- reduction in the need for long tendon reinforcement

## CONCLUSIONS

Whilst it is not envisaged that the FSR will replace the standard "AT" rockbolt, it is considered to be complementary to it, and will offer the facility for extending the bolting horizon beyond the normal 2.4 m, and will in certain circumstances obviate the need for installing cable bolts.

The high shear strength of the FSR is considered to offer major benefits, particularly in sites where the roof is subject to high shear stress.

Being able to use the FSR in conjunction with AT resin capsules provides the facility for achieving immediate support, without the need to provide extra equipment to that normally used with AT rockbolts.

Whilst it may not be possible to achieve full encapsulation, since the FSR combines high tensile strength with high end load rating, then it is still able to provide confinement to the immediate roof strata, in excess of that offered by an AT rockbolt.

The applications where FSR's have been used to date, both in the UK and abroad have demonstrated that they could have a significant role to play in achieving effective strata control in conditions where AT rockbolts alone have proved to be inadequate.

## REFERENCES

1. L R Stace. Assessment report on the Exchem Flexible Strand Rockbolt. Cerberus (Mining Acceptance Services) Ltd. 1995

2. G Daws. An evaluation of the Exchem Flexible Strand Rockbolt. Graham Daws Associates. 1996

3. Health & Safety Commission. Guidance on the use of rockbolts to support roadways in coal mines. Deep Mines Coal Industry Advisory Committee. 1996.

4. B McCowan. New Roof and Rib Support Technology a Major Breakthrough for Ellalong Colliery. Australian Roadway Development Workshop. 1994

5. R Butcher. Experience with Flexibolts at Angus Place. Australian Roadway Development Workshop. 1994

6. J P McDonnell, S C Tadolini, P E Digrado. Field Evaluation of Cable Bolts for coalmine roof support. Report No. RI9533. USBM 1995

16th CONFERENCE ON GROUND CONTROL IN MINING

# Implementation and Evaluation of Roof Bolting in MICARE Mine II

*Gustavo Herrera Rico,* Rock Mechanics Engineer
*Rafael Orea R.,* Senior Mine Geologist
*Rafael Mendoza L.,* Mine Planning Engineer
Minera Carbonifera Rio Escondido
S.A. de C.V. (MICARE)
Coahuila, MEXICO

*Stephen C. Tadolini,* Manager of Technical Services
Excel Mining Systems, Inc.
Golden, CO

ABSTRACT

As part of a general effort to increase safety, efficiency, and profitability of its mining operations, MICARE personnel with the support of NorWest Mine Services, Inc. determined that the key to improving development mining was the implementation of roof bolting as the means of primary roof support for both main entry and longwall gate road development. Until mid-1994, MICARE had relied exclusively upon primary roof support systems composed of heavy steel beams and wooden posts. Support systems were designed, implemented, and evaluated that were successful in controlling the mine roof under extreme geological conditions. This paper describes the geological challenges, support selection criteria, and presents the instrumentation and mine measurements made to assess the bolting performance during the development and retreat mining process of longwall mining.

## BACKGROUND

Minera Carbonifera Rio Escondido, S.A. de C.V. (MICARE) operates a complex of underground and surface coal mines in the state of Coahuila, Mexico which supply thermal coal to two nearby electric power stations that have a combined generating capacity of approximately 2,600 MW. The surface mines extract coal by means of both truck-shovel and dragline-based operations, and the underground mines employ fully-mechanized longwall faces along with continuous mining units for main entry and longwall development.

In 1996, MICARE obtained certification on their quality control system under the International norm ISO 9002. This system consists of regulation, specifications, and methods for the purpose of guaranteeing the fulfillment of the external quality control of the product. MICARE determined that such a system was necessary to establish, document, and maintain effective quality control that would assure clients that the company can meet their quality needs. The ISO 9002 eliminates non-conformance products in their production stages and if such products exist, will detect and identify them, adequately implementing the necessary corrective actions. This system was strictly adhered to during this investigation.

As part of its general effort to increase the safety, efficiency, and profitability of its mining operations, MICARE contracted the services of NorWest Mine Services, Inc. (NorWest), an international consulting firm specializing in both engineering and operations in the coal industry, to provide technical assistance at its underground mines. A critical element of the technical assistance effort has been the improvement of the safety and efficiency of MICARE's development mining operations, the key to improving development mining was the implementation of roof bolting as the means of primary roof support for both main entry and longwall gateroad development. Until mid-1994, MICARE had relied exclusively upon a primary roof support system composed of heavy steel beams (with a mass of approximately 200 kg each (440 lb)) placed on 1 m (3.3 ft) centers and supported by 20 cm (7.9 in) diameter wooden posts; this system has a relatively low support capacity, is physically difficult to handle and install (thus limiting the development advance rate), and requires considerable post-installation maintenance due to yield-deformation of the beams and deterioration of the posts. A typical beam installation is shown in figure 1.

MICARE acquired several complete sets of development equipment for its underground mines; each set of equipment includes a Joy continuous mining unit, a pair of Joy shuttle cars, a Fletcher twin-boom bolter, a Stamler feeder-breaker, and a Line Power electrical supply unit. With this newly acquired equipment, MICARE began a gradual implementation of modern place-mining techniques and roof bolting for primary roof



Figure 1. Typical posts and beam installation with additional beams placed after realized abutment loading.

support. Early results in the roof-bolting program were mixed; roof-bolted areas in Mine I showed evidence of being well-supported, whereas the roof in some areas in Mine II deteriorated considerably, and rapidly, following development and support with bolts. It appears that the initial areas in Mine II that were supported by bolts were subjected to relatively heavy water influx within the immediate roof strata, combined with a poor inherent rock quality. The inconclusive nature of the initial roof-bolting results, combined with a natural physchological reluctancy among the miners to adopt this new technology, served to keep the implementation effort at a very conservative pace.

It was determined that a significant effort would be applied to utilize roof bolting as the primary means of roof support for the new West Mains which would serve as the ventilation and transportation backbone for the remainder of the mine's life. A general plan for Mine II showing the location of the West Mains is provided in figure 2. After an extensive preliminary evaluation program, to design adequate support systems and patterns, a final program was implemented. From March 1996 thru November 1996 the patterns designed to be tested during the on cycle development of the West Mains were installed and evaluated; it was during this period that each of the various bolting patterns were installed and monitored for a sufficient span of time to evaluate their short and medium term effectiveness.

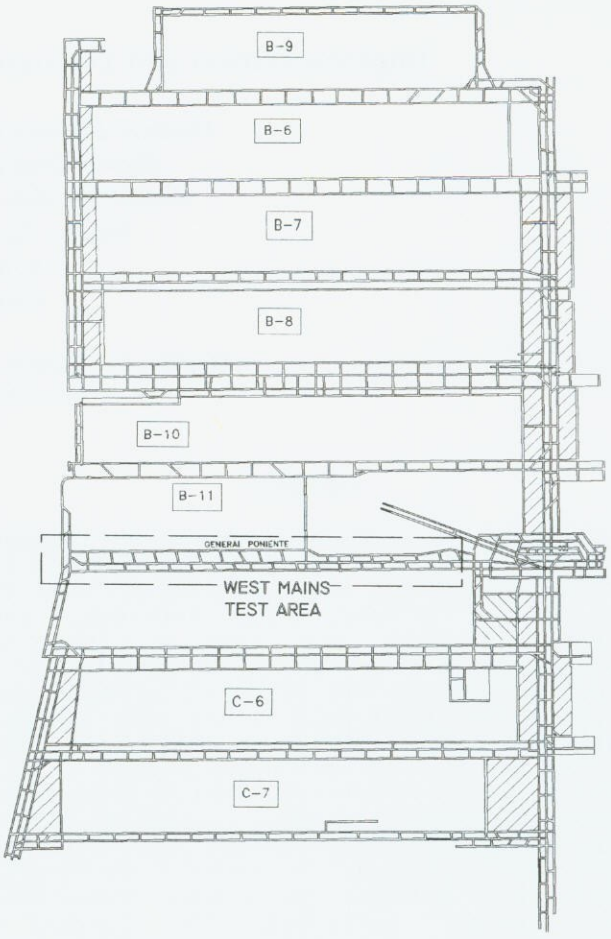



Figure 2. General mine plan for Mine II and test area location.

## PHYSICAL SETTING

### General Geology

All mining at MICARE's Mine II occurs within a single coal seam which averages 1.4 to 2.8 m (4.6 to 9.2 ft) in thickness in the planned mine area, and which dips gently to the East at approximately $2^{o}$ to $3^{o}$. Average depth of the coal seam in Mine II is approximately 125 m (410 ft). The strata overlying the coal seam are composed primarily of shales, mudstones, and siltstones, with occasional lenses or channels of sandstone. The main coal seam is sometimes found in conjunction with smaller overlying sub-seams; these sub-seams have been known to be occasionally good conductors of groundwater.

Structurally, the Mine II reserve is characterized by frequent medium to high angle faults that are depositional in origin; these faults generally trend NE-SW and vary greatly in their continuity and displacement. Faults of tectonic origin also exist in the vicinity of Mine II and usually serve to define major reserve blocks. There is no evidence that suggests a horizontal stress field in the Mine II area that is greater in magnitude than would be produced by the overburden elasticity effect.

The coal seam exploited in Mine II is relatively hard and strong, though very little physical strength testing has been performed to date; one analysis from an outside laboratory indicated an unconfined compressive strength of up to 31 MPa (4,500 psi) though this value is considered to be anomalous and a lab-scale strength of 7 to 14 MPa (1,000 to 2,000 psi) is probably more realistic based on in-mine observations of the coal seam's behavior.

The most common rock type in the immediate roof of Mine II is a clayey shale or mudstone; definitive strength testing results for this rock type are not available but experience in the mine indicates that it is notably weaker than the coal seam and for design purposes should be considered to have an unconfined lab-scale compressive strength in the 4 to 8 MPa (500 to 1,000 psi) range. The clayey shale or mudstone has also been observed to deteriorate rapidly in the presence of water. Rock types with a sandier composition (siltstone, sandy siltstone, and sandstone) have demonstrated a physical competence that increases proportionally with sand content.

The immediate roof rock lithology of the West Mains is illustrated in Figure 3. As the figure shows, the roof in the first half of the test area (cross-cuts 1 to 21) is composed partially of mudstone and partially of siltstone or sandy siltstone. The coal sub-seam(s) generally remain at a distance above the roof line that will not interfere (should they be water-bearing) with bolt installation. An analysis by MICARE geologic and rock mechanics personnel indicated that the roof rock quality as expressed by the Coal Mine Roof Rating (CMRR) for the West Mains ranges from 36 to 60 with an average of 50; a CMRR value 50 indicates a "moderate" roof quality. Based on general observations in Mine II the rock quality levels from these specific boreholes are above the average for the mine, the immediate roof horizon is generally categorized as weak. The floor consists of a massive sandstone and has a CMRR value of 90 or a "strong" rating (see Molinda & Mark, 1994 and Molinda & Mark, 1996).

### Mine Design

The entries and cross-cuts driven for the West Mains range in width from 4.0 to 5.0 m (13.1 to 16.4 ft), with 4.5 m (14.8 ft) being average. The entry height varies from 2.0 to 2.5 m (6.6 to 8.2 ft), with approximately 20 to 30 cm (7.8 to 11.8 in) of coal left in the roof as an essential part of the roof support system. Wherever possible, cross-cut intersections are designed as 3-way in order to minimize the effective roof span in the intersections.

Pillar sizes in the West Mains range from 15 m x 50 m (50 ft x 165 ft) to 30 m x 55 m (100 ft x 180 ft). The variation in pillar dimensions is due to the intended service life of the entry openings; the larger pillars (30 m x 55 m) are employed adjacent to the entry that will be used as the headgate entry of the B-11 longwall panel.

## PRE-DESIGN TESTING

A number of preliminary tests were conducted prior to design and implementation of the roof control testing program in the West Mains; these include the drilling test, anchorage capacity testing, and materials testing for locally made bolting supplies. The preliminary tests are summarized as follows.

### Drilling Tests

One of the first technical questions that needed to be answered was whether the roof in Mine II could be physically drilled for the installation of roof bolts; there were diverse opinions on this subject in the early stages of the program. Drilling trials were conducted in the South Mains with dry-vacuum and wet-pressure cuttings removal. The overall conclusion was that the Mine II roof can be drilled in a reasonable amount of time for the installation of an internal roof support system, using a wet-head system in wet roof and a vacuum-head in drier conditions.

### Anchorage Capacity Testing

Anchorage capacity tests were performed on 6 potential bolt options for roof support in Mine II, including: 1.82 m (6 ft) and 2.13 m (7 ft) full-column resin-grouted rebar bolts; 1.82 m double-lock bolts with 0.91 m (3 ft) of resin anchorage; 1.82 m double-bail expansion anchor (mechanical) bolts; 4.27 m (14 ft) cable bolts with 1.52 m (5 ft) of resin; and, 4.27 m 2-piece coupled rebar bolts with 1.52 m of resin (see ISRM, 1974). The first tests were performed in an area of wet and fractured

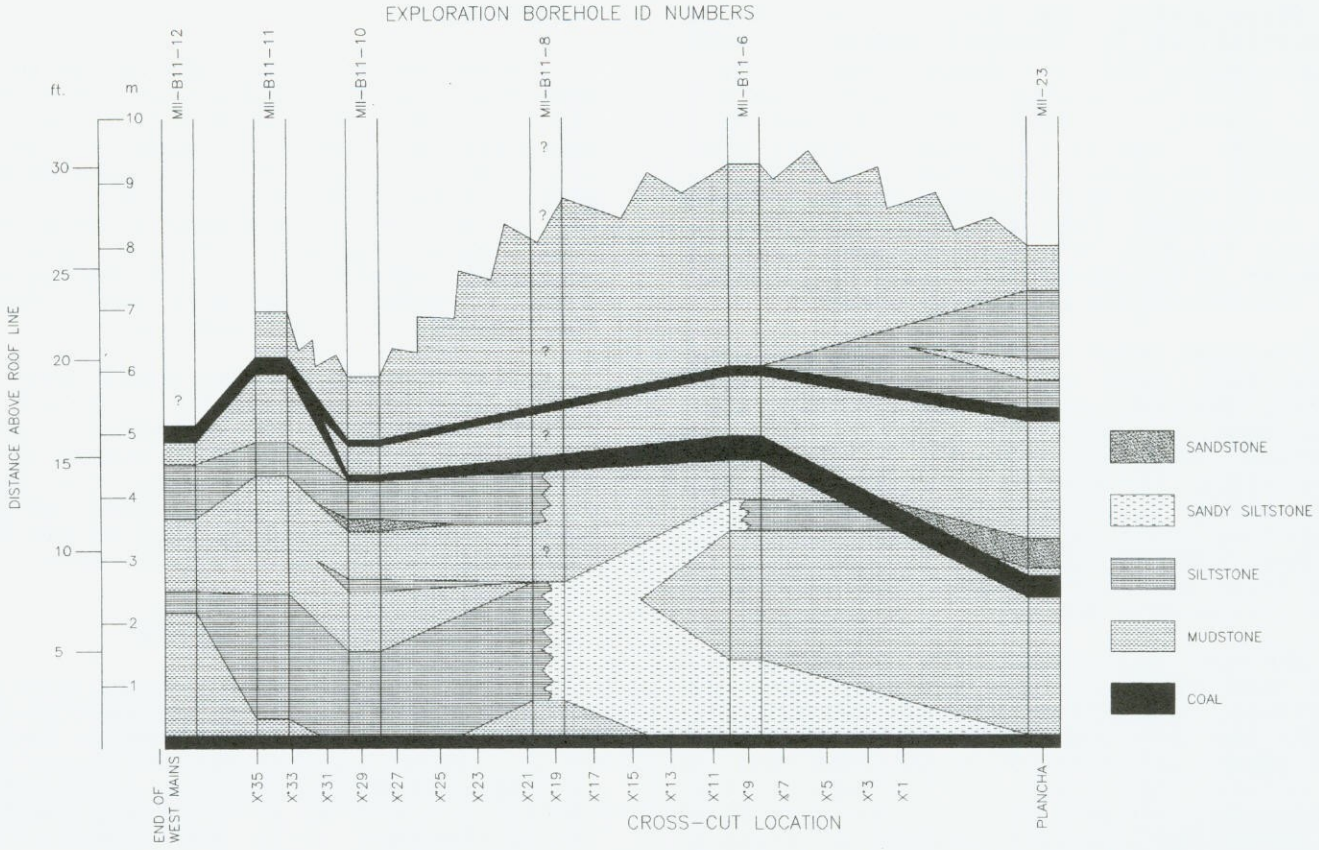



Figure 3. West Mains roof lithology and exploration borehole locations with respect to cross-cut locations.

| Drill Core | Coal Seam Thickness | m | ft | Roof Type | C.M.R.R. | Floor Type | C.M.R.R. | Coal Mine Roof Rating | |
|---|---|---|---|---|---|---|---|---|---|
| | | | | | | | | Roof | Floor |
| MII-23 | 2.30 m | 1.83 | 6 | Shale | 36 | Sandstone | 90 | Weak | Strong |
| | | 2.44 | 8 | Shale | 36 | | | Weak | |
| | | 4.88 | 16 | Shale-Sandstone | 45 | | | Moderate | |
| MII B11-6 | 2.30 m | 1.83 | 6 | Siltstone | 59 | Sandstone | 90 | Moderate | Strong |
| | | 2.44 | 8 | Siltstone | 53 | | | Moderate | |
| | | 4.88 | 16 | Siltstone | 50 | | | Moderate | |
| MII B11-8 | 2.30 m | 1.83 | 6 | Siltstone | 55 | Sandstone | 90 | Moderate | Strong |
| | | 2.44 | 8 | Siltstone | 58 | | | Moderate | |
| | | 4.88 | 16 | Shale-Siltstone-Shale | 46 | | | Moderate | |
| MII B11-10 | 2.38 m | 1.83 | 6 | Siltstone | 57 | Sandstone | 90 | Moderate | Strong |
| | | 2.44 | 8 | Siltstone | 53 | | | Moderate | |
| | | 4.88 | 16 | Siltstone | 51 | | | Moderate | |
| MII B11-11 | 2.40 m | 1.83 | 6 | Siltstone | 60 | Sandstone | 90 | Moderate | Strong |
| | | 2.44 | 8 | Siltstone | 60 | | | Moderate | |
| | | 4.88 | 16 | Siltstone | 50 | | | Moderate | |
| MII B11-12 | 2.23 m | 1.83 | 6 | Shale | 36 | Sandstone | 90 | Weak | Strong |
| | | 2.44 | 8 | Shale-Siltstone | 41 | | | Weak | |
| | | 4.88 | 16 | Shale-Siltstone | 45 | | | Weak | |

roof rock (which had been mined approximately 8 months earlier) and with mixed results. Tests performed in less-disturbed ground yielded acceptable results, though it was determined that the wet-drilled holes probably liberated a type of mud which diminished the performance of the resin. There was also evidence that some of the resin used in the tests may have been damaged prior to use due to the way it had been stored. The combined data from 26 individual tests indicated that an anchorage capacity of 142 kN (16 tons force) to 178 kN (20 tons force) can be used for support design calculations. The best anchorage results were obtained by the full-column resin-grouted units, with acceptable results by the cable and 2-piece combination units. The mechanically-anchored units did not function satisfactorily in this type of roof rock. (see Karabin & Hoch, 1980)

Material Testing

Cost and importation logistics provide incentives to utilize Mexican-made materials as much as possible for roof support systems. To ensure that locally available materials met minimum strength requirements, three locally-made rebar bolts and three bolt bearing plates were tested for strength and performance in accordance with the ASTM F432-91 Standard Specification for Roof and Rock Bolts and Accessories. The testing indicated that the strength demonstrated by bolts exceeds the requirements for ASTM Grade 75 steel by large margins. The bearing plates were found to have sufficient strength to be used in combination with No. 6 or No. 7 rebar bolts, but did not have sufficient strength or stiffness to be used with stronger rebar or cable bolts. Plates that met the Grade 6 criteria were substituted for the cables installed in the test areas.

## PRIMARY ROOF SUPPORT SYSTEMS

Consideration of support design strategies began with an on-site evaluation and review of the past performance of roof control systems used in Mine II. The general observations of this evaluation were:

- The main challenges to roof control in Mine II include: an apparent low horizontal stress field; the presence of low-strength mudstones in immediate roof which are frequently disrupted by structural discontinuities of apparent depositional origin; the strength of the mudstone is negatively impacted by the introduction of water and also may be negatively impacted by drying when introduced to mine air; water-bearing rider seams in the roof which could cause problems if penetrated during roof bolting or fractured by roof deformation.
- Any roof control system must include leaving a cap layer of coal at least 30 cm (11.8 in) in thickness in order to insulate the shale from the mine atmosphere and to help distribute the load carried by the support system.
- Suspension of a dead load should form the design basis for a roof control system; the height of the potential zone of material to be suspended may range from 2 m (6.6 ft) (based on observations of roof failures in Mine II) up to a height equal to the width of the entry.
- Roof support designs should incorporate angled bolts placed over the pillars and should include some type of stiff member that mechanically links the elements of the support system.

A series of primary roof support designs were prepared for testing in the West Mains of Mine II. Generally, the designs involve a progression from a more to less conservative basis. The designs and their basis are briefly described and summarized as follows:

NorWest Pattern #1

The first element of this pattern, shown in figure 4, consists of rows of 4-1.82 m (6 ft) fully resin-grouted rebar bolts placed on 1.22 m (4 ft) row centers, installed through a special roof channel which is considerably stiffer than the standard bolting strap, plus 2-2.13 m (7 ft) fully resin-grouted rebar end bolts in each row which are angled over the ribs at an inclination of at least 30° from the vertical. The second element of this pattern consists of rows of 4-4.27 m (14 ft) cable bolts anchored with 1.52 m (5 ft) of resin placed

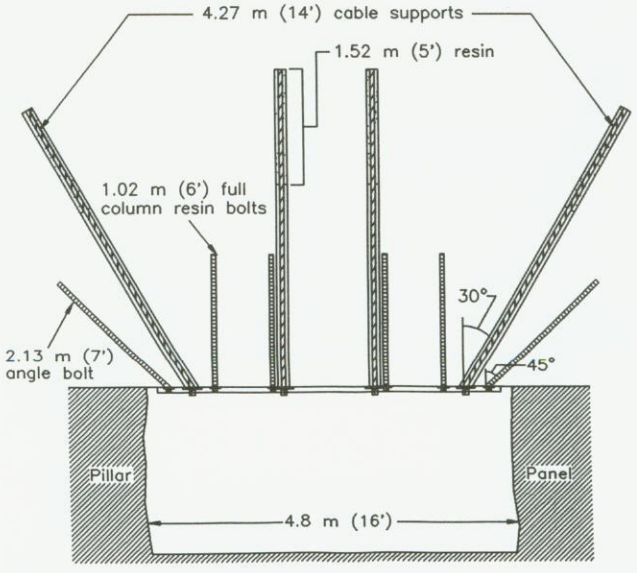



Figure 4. NorWest roof support pattern #1.

on 1.2 m (4 ft) centers (between the rows of conventional rebar bolts) and installed through oversized (20 x 20 cm or 8 x 8 in) bearing plates (see Tadolini & Koch, 1993); the end cable bolts in each row are angled over the ribs at an inclination of at least 30° from the vertical. Both elements of this bolt pattern are installed in conjunction with welded-wire roof mesh with a nominal aperture of 10 cm (4 in).

NorWest Pattern #2

This support pattern, shown in figure 5, retains all components and specifications of the NorWest #1 pattern except that the number of 1.82 m (6 ft) conventional rebar bolts in each row of the first element of the pattern is reduced from 4 to 2.

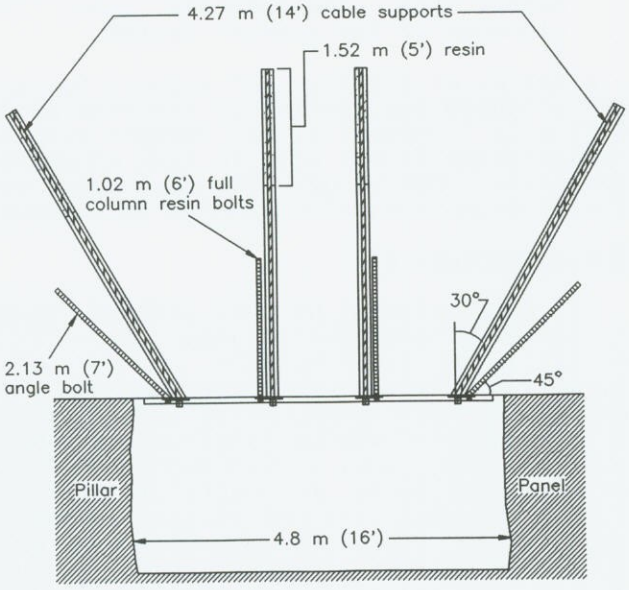



Figure 5. Norwest roof support pattern #2.

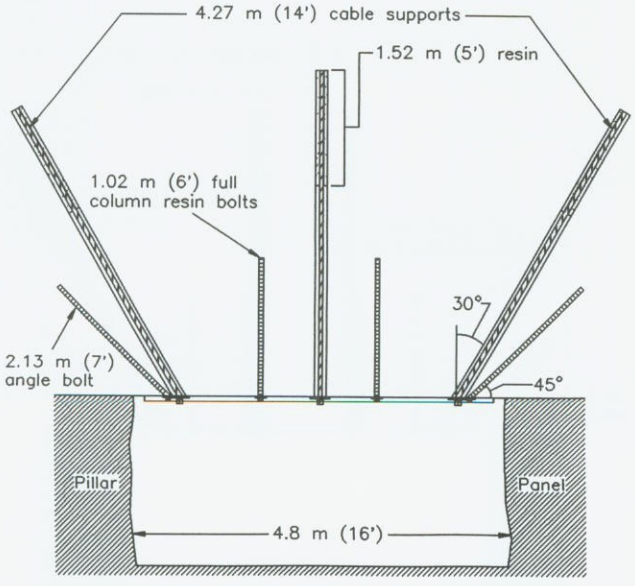



Figure 6. NorWest roof support pattern #3.

NorWest Pattern #3

This pattern, shown in figure 6, retains all the components and specifications of the NorWest #2 pattern except that number of 4.27 m (14 ft) cable bolts in each row of the second element of the pattern is reduced from 4 to 3.

MICARE "Regular" Pattern

The first element of this pattern, shown in figure 7, consists of rows of 5-2.44 m (8 ft) fully resin-grouted rebar bolts placed on 0.75 m (2.5 ft) row centers, installed through a standard bolting strap; no specification is made for inclination of the end bolts, though in practice some degree of inclination is generally achieved. The second element of this pattern is for use as additional support in intersections and consists of rows of 3-3.66 m (12 ft) coupled bolts anchored with 2.44 m (8 ft) of resin placed on 0.75 m (2.5 ft) centers (between the rows of conventional rebar bolts) and installed without bolt straps; no specification is made for inclination of the end bolts. There is no specification made for installation of roof mesh, but in practice it is usually installed if available.

MICARE "Fast" Pattern

This support pattern retains all components and specifications of the "Regular" pattern except that: the number of 2.44 m (8 ft) conventional rebar bolts in each row of the first element of the pattern is reduced from 5 to 4; the row spacing for the first element of the pattern is reduced from 0.75 m to 0.60 m (2.5 ft to 2.0 ft); the number of 3.66 m (12 ft) coupled bolts in

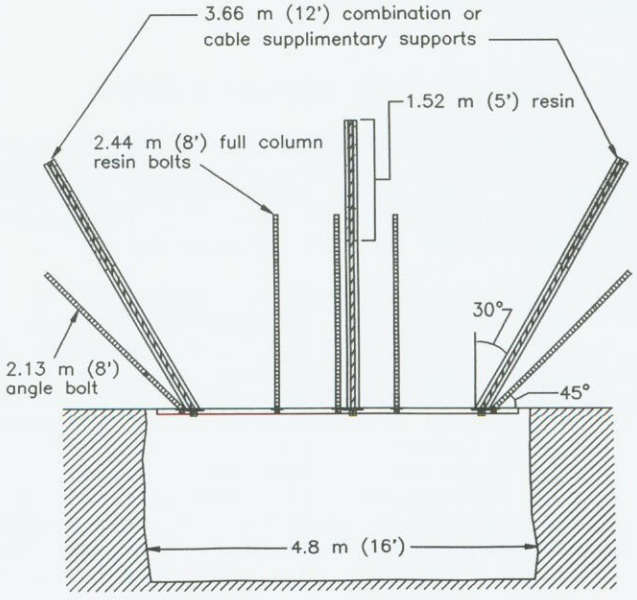



Figure 7. MICARE "regular" roof support pattern.

each row of the second element of the pattern (for intersections) is increased from 3 to 4; and, the row spacing for the second element of the pattern is reduced from 0.75 m to 0.60 m (2.5 ft to 2.0 ft). The pattern is shown in figure 8.

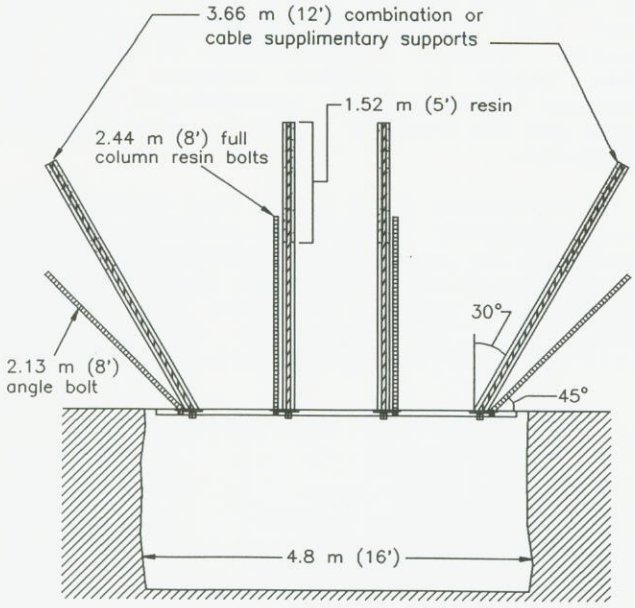



Figure 8. MICARE "Fast" roof support pattern.

## IMPLEMENTATION AND ANALYSIS OF MONITORING DATA

The testing of roof bolting as the primary means of roof support in the West Mains commenced shortly after the drivage of the West Mains was initiated from the slope-bottom area. After advancing the first 300 m (984 ft) with the various test patterns, operation elected to use the MICARE fast pattern for the remaining portion of the gate road. This was based on an examination of the preliminary data and observational techniques.

### Monitoring Method

The objective of the monitoring program in the test areas was to collect sufficient data to enable an assessment of the effectiveness of the installed primary and secondary support systems. The monitoring plan included specifications for multi-point extensometer stations in the intersections and approximately mid-span in the entries. These readings were coupled with visual monitoring techniques.

The extensometer stations are comprised of two or three point-anchored lengths of plastic water pipe which are placed in separately drilled holes in the roof of the entry as close together as possible. In general, one unit was anchored at a depth of 2.4 m (7.9 ft) and the other was anchored at a depth of 3.6 m (11.8 ft). This would capture roof separations within the primary and secondary support system horizons. Displacement readings are taken using a hand-held measurement tape which is checked against a reference point located on the roof. Displacement readings were taken at least on a daily basis during the first month following installation and then at appropriate intervals based on movements but generally not exceeding one week between readings.

### Failure Criteria

An independently established failure criteria was developed for the West Mains utilizing bolting as primary support. The failure criteria specifies the magnitude of allowable deformation of the roof strata before installation of the secondary support is required.

Based on field and laboratory data it was determined that strain levels exceeding 2 to 3 percent in any of the immediate roof layers would warrant the installation of secondary support. Additionally, this criteria was coupled with the accepted standard practice utilized in all of MICARE's underground mines. If an average deformation rate of 1.0 mm/day (0.039 in/day) sustained for at least 30 days, or a total of 70.0 mm (2.76 in) cumulative deformation at any time would warrant the installation of secondary support. The depth at which these deformations are measured is not specified and an acknowledged weakness of this criterion.

## GENERAL DISCUSSION AND OBSERVATIONS

The recommended operations for the West Mains suggested a development cut of 4.0 m (13.1 ft). The management of the cut depth is the foundation of a dynamic roof control program. If the miner operator sees that the roof is beginning to break and fall into the entry, the cut can be shortened. Likewise, if the cut is going well and the roof remains intact, the length of the cut can be extended to the desired depth. Four and six meter cuts have been routine and 1 to 2 m (3.3 to 6.6 ft) cuts have been necessary in poor conditions.

Difficulties were initially encountered during the evaluation of various anchorage systems; resin, mechanical, and combinations of these systems were tested. It was determined that the best option for adequate anchorage was a resin-grouted system in combination with a thrust-bolting technique in order to achieve a degree of immediate tension (see Tadolini & Dolinar). Because of the drilling problems experienced with moist, highly plastic roof rock it was determined that the optimum diameter for the

bolts should be 22 mm (7/8 in) installed in a 35 mm (1-3/8 in) diameter hole. This system provided the easiest drilling, superior anchorage between the resin/rock interface, and helped minimize downward roof movements in the immediate roof. Additionally, based on previous testing and the inherent weakness of the main roof, it was determined that longer bolts should be installed to suspend the mine roof should a separation occur above the primary support systems.

Surface Control

From the beginning of the testing program, based on previous experience and underground observations, it was felt that surface control was imperative to help the roof become self supporting, to minimize the effects of sloughage with respect to progressive type failures, and to eliminate the hazards associated with material falling from the immediate roof. To accomplish surface control wire mesh, roof bolt mats, and channels were used at various places and with different combinations throughout the test area. The roof mats and mesh are already proving that they are required to meet the stated objective of surface control. The mesh has helped control failed areas and where omitted the negative effects of progressive failures and the associated hazards can be seen. The roof channels have provided the required surface control but have not indicated that they are required to resist larger downward roof movements, not justifying the increased costs.

## MONITORING RESULTS

To evaluate the effectiveness of the tested roof control systems, monitoring data was taken for a maximum of 9 months and a minimum of 1 month for the stations located near the back of the development section. A total of 81 extensometer stations have sufficient data to be considered in this analysis. Displacement and strain plots were created for all of the extensometers. An example of the deformation and strain plots is shown in figure 9. This specific figure is from an intersection and shows the amount of roof movement measured at the 2.4 and 4.6 m (7.8 and 15 ft) locations. The roof strains are calculated for each station. The strain estimate between the station anchors, which is useful in isolating where the greatest stratigraphic separation is occurring, is called the "Upper Zone." The accuracy of this estimate depends on the assumption that there is no independence of movement between the components of the system. There is a potential for getting erroneous results if the two extensometers happen to be installed in two blocks of rock moving independently of each other.

The displacement/strain plots indicated that only 14 out of 81 extensometer stations showed strains greater than 1% and only 4 stations show strains of 2% or higher. The average cumulative strain for all of 153 measured roof intervals was 0.43%. In over 4,000 m (13,125 ft) of development drivage in the West Mains, there was not a single roof fall of ground supported with roof bolts. Visual observations of plate and bolt loads in general suggest that the current loading is not substantial in magnitude and the current support capacity may be excessive.

In instances where large roof deformations were observed, stability problems are attributed to significant structural discontinuities in the immediate vicinity of the measurement point; in these site specific situations, virtually any support system will have difficulty maintaining complete

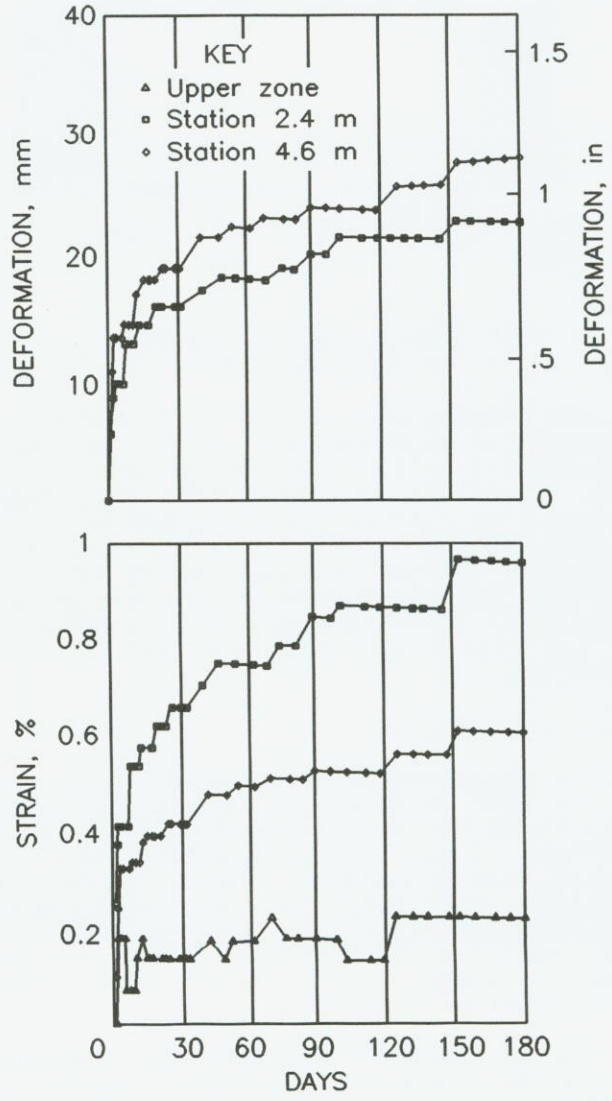



Figure 9. Deformation and strain plots from differential sag station located in an intersection.

control. The installation of secondary support in unstable areas was effective in preventing complete roof failure.

## CONCLUSIONS AND RECOMMENDATIONS

Based on the evaluation of the monitoring data and visual inspections of the areas included in the roof bolting test areas, the following conclusions are offered.

In generally dry and occasionally damp roof conditions, the roof can be physically vacuum drilled and roof bolts can be installed that achieve an adequate anchorage capacity.

Roof bolts can be successfully used as primary roof support. The lower roof horizon should be supported by fully-grouted resin rebar bolts with a length of at least 2.13 m (7 ft). Angled, fully-grouted resin rebar bolts should be installed at both ends of primary support bolt rows. These bolts should be a minimum of 2.13 m (7 ft) and should be angled at 30 to 45 degrees from vertical over the ribs.

The upper roof horizon should always be supported in intersections, utilizing cables or combination bolts of at least 3.66 to 4.27 m (12 to 14 ft) in length and be anchored with a minimum of 1.52 m (5 ft) of resin.

Welded-wire mesh should be installed in all bolted areas of the roof to help distribute the bolt loading over a large area, to eliminate or minimize the possibility of progressive roof failures, and to enhance the overall safety of bolted roof areas.

The implementation of roof bolting in conjunction with the use of a continuous miner and shuttle cars has been a major contributing factor to the dramatic improvement in development rates. The average per-shift development rate increased from 5 m (16.4 ft) per shift to 13 m (42.6 ft) per shift. Preliminary observations and geomechanical performance of the headgate entry of the longwall panel indicates that roof bolting can make a significant improvement in gate road stability compared to the use of wooden posts and beams as primary roof support. Photographs in figure 10 and 11 show the support conditions before and after the implementation of the roof bolting program.

The physical response of the mine roof, substantiated by the actual data, indicate that support patterns can become less conservative in areas that have similar roof conditions to those examined. Increases in row spacings are slated for testing that can reduce the bolting cycle time, which is currently causing production delays. MICARE personnel, with the assistance of NorWest Mine Services, Inc., are continuing to examine the effectiveness of roof bolting under a wide range of geological conditions. The ultimate goal of these investigations is to provide engineered and economically feasible support designs that will provide safe working conditions under diverse and hazardous ground control conditions.

## ACKNOWLEDGEMENTS

The authors would like to thank Richard Jones and Thelma Herrera, NorWest Mine Services, Inc., for their help in the preparation of this paper and the entire work force and management at MICARE Mine II for their continued support, enthusiasm, and assistance during this investigation.



Figure 10. Gate road support with traditional wooden posts and steel beams.



Figure 11. Transition from posts and beams to a support combination of resin-grouted bolts and cables.



REFERENCES

1. International Society for Rock Mechanics (Commission on Standardization of Laboratory and Field Test, Committee on Field Tests). Suggested Methods for Rockbolt Testing. No. 2, March 1974, pp. 1-16.

2. Karabin, G. J., and M. T. Hoch. Contemporary Roof Support Systems Provide a Diversified Approach to Modern Ground Control. Paper in Proceedings, Annual Institute on Coal Mine Health and Safety Meeting. VA Polytech. Inst., 1980, pp. 249-268.

3. Molinda, G. M. and C. Mark. Coal Mine Roof Rating (CMRR): A Practical Rock Mass Classification for Coal Mines. USBM Information Circular 9387, 1994, 83 pp.

4. Molinda, G. M. and C. Mark. Rating Coal Mine Roof Strength from Exploratory Drill Core. Paper in Proceedings, 16th International Conference on Ground Control in Mining (Golden, CO, August 13-15, 1996). Colorado School of Mines, 1996, pp. 415-428.

5. Tadolini, S. C. and D. R. Dolinar. Thrust Bolting: A New Innovation in Coal Mine Roof Support. Paper in Proceedings of 10th International Conference on Ground Control in Mining (Morgantown, WV, June 10-12, 1991). Dept. of Min. Eng., WV Univ., 1991, pp. 76-84.

6. Tadolini, S. C. and R. L. Koch. Cable Supports for Improved Longwall Gateroad Stability. Paper in Proceedings of 12th International Conference on Ground Control in Mining (Morgantown, WV, Aug 3-5, 1993). Dept. of Min. Eng., WV Univ., 1993, pp.9-15.

# New Methods and Technologies of Roofbolting in Australian Coal Mines

*Mietek Rataj,* R & D Manager
ANI Arnall
Newcastle, AUSTRALIA

*Rob Thomas,* Principal
Strata Engineering Australia
Newcastle, AUSTRALIA

## ABSTRACT

Methods of rock reinforcement in Australian coal mines are being advanced progressively through the better understanding of rock failure mechanisms around roadways and the development of improved bolting hardware and installation techniques. It has been recognised that to improve the performance of rock reinforcement systems, the stiffness of the system as a whole has to be improved. New style bolts and accessories together with high pre-tensioned roof and cable bolts are being developed as a result. A number of the new techniques used to stabilise the roof, especially in weak roof/high horizontal stress areas have been site proven and are now currently used on a routine basis as a means of improving development rates and gate road stability during longwall retreat.

## INTRODUCTION

It has long been acknowledged in the Australian coal industry that development rates need to be increased if longwall continuity problems are to be eliminated and that despite the use of high roof and cable bolting densities, roof control problems in longwall gate roads often eventuate up to and during face retreat.

Therefore, in order to improve roof control and minimise bolting densities it was recognised that each roof and cable bolt had to be made more effective than was currently the case. With this general philosophy in mind a number of projects have recently been commissioned to directly address the above dilemmas facing the Australian coal industry, more specifically;

- the use of less roof bolts to assist with continuous miner efficiency without compounding roof stability problems during roadway development and,
- the more effective management of roadway stability during longwall retreat without resorting to ever increasing densities of secondary reinforcement.

## EARLY DEVELOPMENT OF ALTERNATIVE MORE EFFECTIVE BOLT REINFORCEMENT

Pre-tensioned roof bolts were originally introduced into underground coal mines in Australia more than 20 years ago (Clark and Filipofski, 1984). At that time, all roof bolts were point-anchored and the level of pre-load on the bolts was increased through torque multiplication. However, with the advent of fully-encapsulated roof and cable bolting techniques in the 1980's, the Australian coal industry changed its focus to one of maximising the strength and stiffness of the rock-to-bolt load transfer system.

Accepting that some nominal pre-load was induced on the bolt upon installation, the reinforcing ability of the fully-encapsulated bolting system was essentially passive and hence, relied primarily upon displacement and therefore delamination and/or shear failure within the rock mass to develop any significant loading on the bolts. Therefore, in view of the number of geomechanical limitations inherent in such a "soft" bolting system, it was decided "to turn the clock back" and re-assess the comparative benefits of stiffer pre-tensioned roof and cable bolting systems.

Accepting that typical pre-load values on roofbolts varied from any new pre-tensioning technique had to generate a substantial increase in pre-load on roof bolts (ie, 10 to 50 kN off 135-270 Nm stall torques) and cable bolts (ie typical pre-load values on bolts varied from cable 0 on standard cables to 30 kN on Flexibolts), it is also worth noting that any new developments in pre-tensioning hardware had to also consider any impact the pre-loading operation would have upon the productivity of the existing mining system.

With these issues in mind, ACIRL (Australian Coal Industry Research Laboratories) developed a low friction thrust bearing which was fixed between the drive nut and the dome washer on the head of the roof bolt assembly. The pre-loading ability of the bearing was however limited, as at approximately 80 to 85 kN the bearing seized as the roller balls started to punch through the outer casing.

The initial underground trials with the thrust bearing measured pre-loads of between 65 and 85 kN. The trials concluded that by increasing the pre-load applied to a roof bolt (fully-encapsulated with two speed resin), the added confinement induced in the roof and the increased stiffness of the bolting system limited the generation of rock failure and hence, aided the retention of competent beam behaviour in the immediate roof (Frith and Thomas, 1994). It was consequently argued that providing beam behaviour could be retained in the immediate roof, the associated retention of intact rock strength and high levels of *in-situ* stress across the roof dramatically reduced the potential for a roof fall, as for any fall of ground to occur the dead weight of the roof material must have to overcome the vertical shear strength of the immediate roof (see Figure 1).

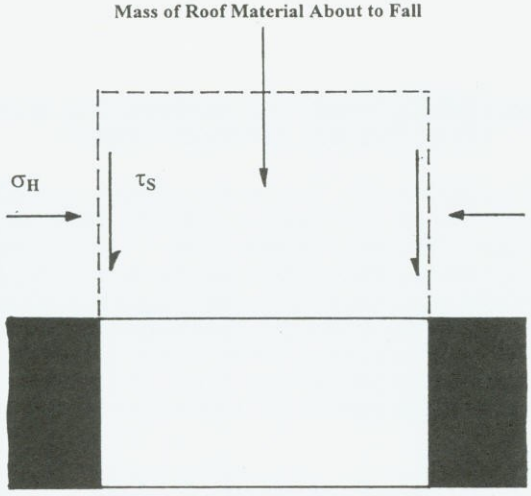



**Figure 1 Schematic Illustration of Roof Fall Conditions**

As a result of the success of the initial pre-tensioned roof bolting trials, additional research also focused on the application of higher pre-loads on cable bolts. The original pre-tensioned cable trials were undertaken by BFP (Barrett, Fuller & Partners).

The cable was tensioned hydraulically and at a pre-determined load, the applied tension was locked into the cable. In line with the industry standard, the majority of cables in the initial trials were point-anchored into the roof. For this purpose 4 to 8m ANI Arnall Flexibolts were used as the host cable. Flexibolt cables are 23.5 mm in diameter, are threaded at the termination to allow low level torque tensioning and although the bar itself will maintain loads in excess of 550 kN, the threaded portion of the cable limits the strength of the head assembly to a nominal 420 kN. Each Flexibolt was installed vertically in the centre of the roof and pre-tensioned to 250 kN, the tensioning operation taking typically no more than 10 minutes to complete.

Underground trialing demonstrated that following the application of the increased pre-load to the Flexibolt roof displacement was either immediately arrested or, as in the case of longwall retreat, any abutment related surcharge in displacement was reduced and delayed until only a few metres outbye of the face. Again, it was argued that in addition to the added confinement induced in the roof and the increased stiffness of the bolting system, one of the main mechanisms behind the measured improvement in pre-tensioned cable reinforcement was the retention of competent beam behaviour in the immediate roof and the ability of a stiff vertical cable to utilise the mechanical advantage inherent in a buckling beam.

## IMPACT OF STIFFER PRE-TENSIONED BOLTING SYSTEMS ON ROOF BEHAVIOUR

Strata Engineering's roof stability model is essentially based on the geomechanical and operational significance of buckling and non-buckling behaviour in the immediate roof, the stability of which is primarily a function of stress magnitude, beam thickness and roof structure.

Within the guidelines of the roof stability model it is considered imperative that the reinforcement design maintains either static non-buckling or stable buckling behaviour in the immediate roof. In both cases the strength and self-supporting ability of the rock mass is used to its maximum effect and as a result, the behaviour of the roof, both on development and longwall retreat, becomes more predictable and therefore manageable.

Conversely, if the rock mass is allowed to fracture and lose its self-supporting ability, underground monitoring and mine site statistics have demonstrated that not only does the level of reinforcement required increase but more significantly, the behaviour of the roof becomes inherently more complex and therefore difficult to manage.

Several collieries in Australia have now used pre-tensioned roof and cable bolting to great effect and with the aid of Strata Engineering's roof behaviour model, both the issue of improved development rates and gate road stability up to and during longwall retreat have been successfully addressed.

A number of case histories are summarised below:

### Teralba Colliery

The Young Wallsend seam at Teralba Colliery lies approx. 300 to 400m below surface. The immediate roof consists of either a 1.5m bed of tuff or thick coal. In view of the restricting influence of neighbouring dykes and faults, the longwall gate roads are aligned near perpendicular to the major horizontal stress and parallel to the main joint sets. All gate roads are reinforced on 6 roof bolts every 0.8 to 1m.

During the development of LW13, the roof in the gate roads experienced severe deformation immediately outbye of the continuous miner. Extensometry measured up to 300mm of displacement, excessive heights of softening and unpredictable displacement rates (see Figures 2 and 3). After several weeks some areas had visibly displaced up to 800mm. The measured data and the observed incidence of up to 1m of guttering, indicated that the roof was susceptible to excessive buckling type failure and as a result, the development unit was repeatedly stood-down to enable 8m cable bolts to be installed up to the back of the continuous miner. Several outbye areas also required on-going remedial reinforcement including timber props, cable slings and PUR injection.

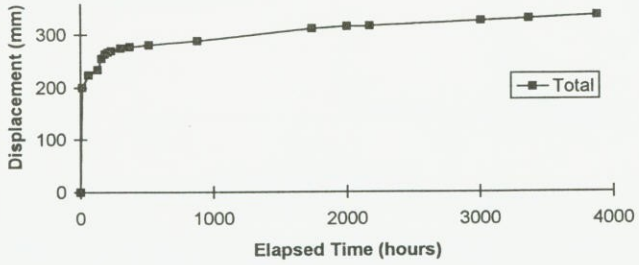



**Figure 2 Low-tensioned Roof Bolts - Roof Displacement (Teralba Colliery)**

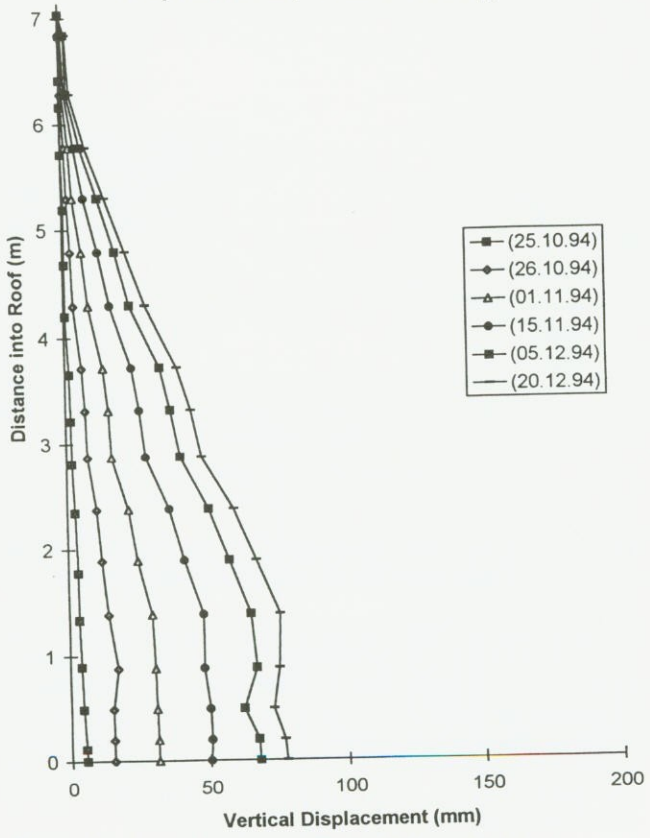



**Figure 3 Low-tensioned Roof bolts - Roof Displacement (Teralba Colliery) Note: Exto installed after 300mm of prior displacement**

In an effort to maximise the stability of the roof and hence the efficiency (and safety) of the development operation thrust bearing type pre-tensioned roof bolts were trialed (Coull and Thomas, 1997). The roof bolts were installed at the same density as per the low-tensioned bolts. Extensometry installed as part of the trial demonstrated that following the commencement of pre-tensioned bolting the roof displacement started to conform to a more controlled stable buckling signature and the incidence of guttering was either eliminated or reduced in severity (see Figures 4 and 5).

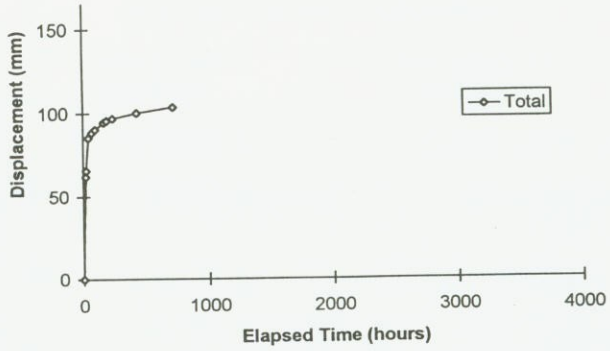



**Figure 4 Pre-tensioned Roof Bolts - Roof Displacement (Teralba Colliery)**

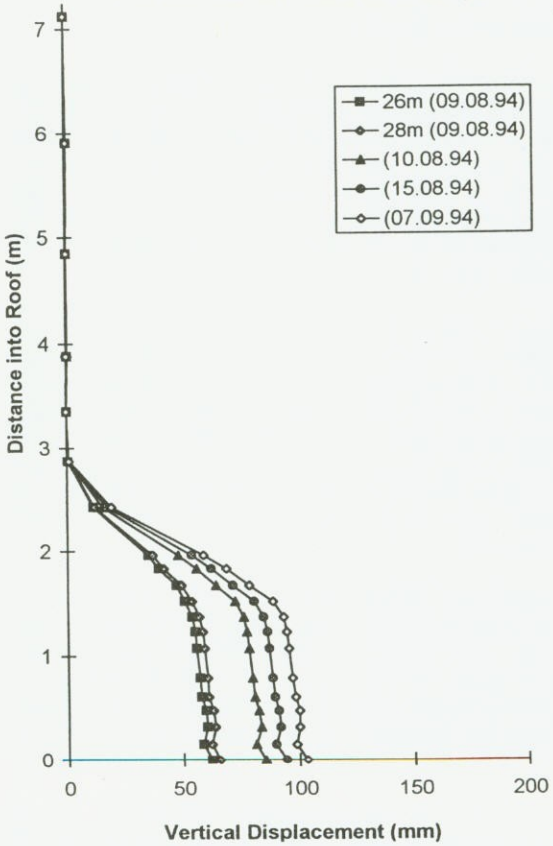



**Figure 5 Pre-tensioned Roof Bolts - Roof Displacement (Teralba Colliery)**

In order to fully illustrate the measured improvement in roof behaviour, a secondary reinforcement audit of the low and pre-tensioned sections of the panel was conducted. The data, outlined in Table 1, clearly demonstrates that following the introduction of pre-tensioned roof bolts the amount of secondary reinforcement required diminished considerably however, what the data does not show is that in the pre-tensioned section the continuous miner was never stopped

**Table 1 Teralba Colliery - Secondary Reinforcement Audit (Coal Roof)**

| Low-tensioned Roof Bolts | | Pre-tensioned Roof Bolts | |
|---|---|---|---|
| | | | |
| No. of Intersections | 12 | No. of Intersections | 14 |
| | | | |
| *% Cable Bolted* | *42%* | *% Cable Bolted* | *29%* |
| *% PUR'd* | 8% | *% PUR'd* | *0%* |
| | | | |
| Length of Gate Road - 900m | | Length of Gate Road - 900m | |
| | | | |
| *% Cable Bolted* | *29%* | *% Cable Bolted* | *0%* |
| *% PUR'd* | *6%* | *% PUR'd* | *0%* |
| *% Timber Propped* | *29%* | *% Timber Propped* | *0%* |

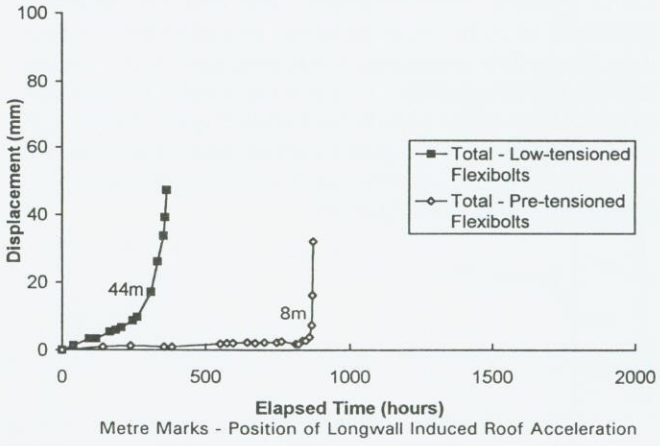
**West Wallsend Colliery**

The Borehole seam at West Wallsend Colliery lies approx. 200 to 300m below surface. Around LW511 to 13, the immediate roof consisted of an interbedded sequence of slickensided shales and thin coal seams. In view of the restricting influence of neighbouring dykes and faults, the longwall gate roads were aligned near perpendicular to the major horizontal stress and parallel to the major joint set.

Initially all roadways in West Wallsend were driven on 4 roof bolts every 1m. Following several roof falls on standard low-tensioned bolts the roof bolting density was increased to 6 bolts per metre. However, as a result of on-going deterioration in roof strength due to changing geological conditions and the measured incidence of buckling type failure, West Wallsend incorporated the thrust bearing on all roof bolts in an effort to increase the level of pre-load.

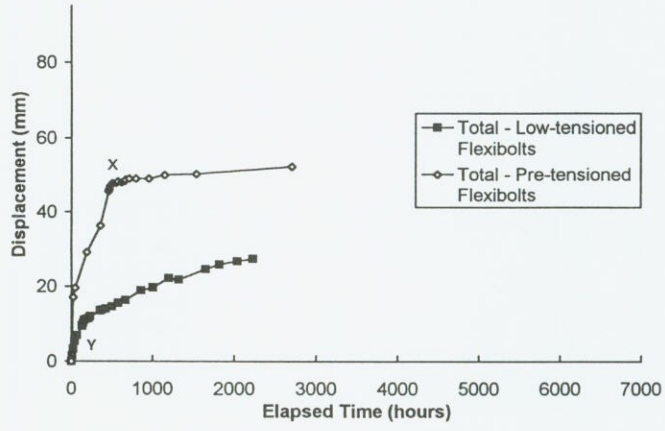
Following the introduction of pre-tensioned roof bolts, the bolting density was maintained at 6 bolts per metre and stable conditions were maintained on development. During longwall retreat the roof was reinforced with 6m low-tensioned point-anchored Flexibolts. The Flexibolts were installed vertically in the centre of the roof at a density of one cable every 2m.

In the most geologically aggressive areas, 6m pre-tensioned Flexibolts were installed as a preference to the low-tensioned Flexibolts, again at a density of 1 cable every 2 m. The time-dependent plots illustrated in Figures 6 and 7 demonstrate the effectiveness of pre-tensioned Flexibolts both around the gate end intersection of the longwall face and in an outbye section of roadway. As shown in Figures 6 and 7 on low-tensioned flexibolts the roof was more susceptable to the deteriorating affects of the longwall abutment and creep deformation.




Metre Marks - Position of Longwall Induced Roof Acceleration

**Figure 6 Low and Pre-tensioned Flexibolts - Roof Displacement During Longwall Retreat (West Wallsend Colliery)**




X - Installation of Pre-tensioned Flexibolts
Y - Installation of Low-tensioned Flexibolts

**Figure 7 Low and Pre-tensioned Flexibolts - Roof Displacement (West Wallsend Colliery)**

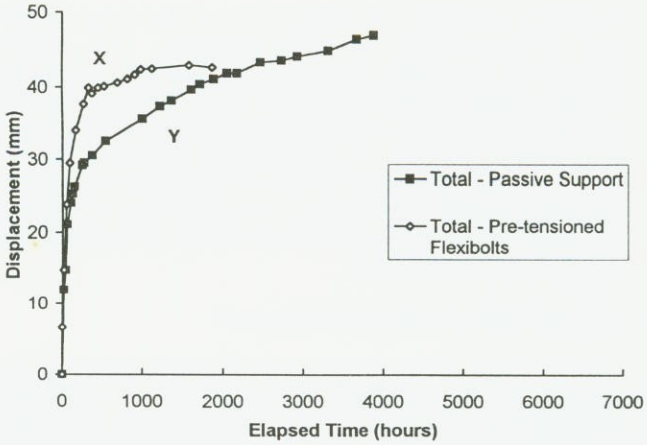
Following the introduction of pre-tensioned roof bolts at West Wallsend, roof falls were completely eliminated both on development and longwall retreat and moreover, several pillar lengths of gate road were also driven on a reduced density of 4 bolts per metre, a similar low-tensioned design had previously resulted in the unexpected failure of a 70m length of gate road one or two pillar lengths behind the continuous miner.

### Newstan Colliery

The West Borehole seam at Newstan Colliery lies approx. 70 to 170m below surface. The immediate roof consists of thick coal and claystone. In view of the restricting influence of neighbouring dykes and faults, the longwall gate roads are aligned sub-parallel to the major joint set. All gate roads are driven with a cut & flit technique and depending on the geological environment, are typically reinforced on 4 to 6 x 2.1 to 2.4 m roof bolts every 1m.

In view of the need to increase the rate of panel advance in the new TG the dual-entry panel was switched to a single-entry system. However, after the unexpected non-buckling type failure of an intersection in an outbye area of the dual-entry the reinforcement system had to be re-evaluated. After due consideration to the geomechanical environment and the new development system, the installation of soft, low-tensioned point-anchored Flexibolts or fully grouted cable bolts as a means of secondary reinforcement in the single-entry was deemed inappropriate. It was therefore decided that in order to maximise the development rate, the primary roof bolting density would remain on 6 x 2.1m bolts every metre on the proviso that the torque on the mobile bolter was maintained at a minimum of 350 Nm and that additional 6m pre-tensioned Flexibolts were installed outbye of the development face on down shifts. The Flexibolts were installed vertically in the centre of the roof at a density of one cable every two metres.

Even though the in bye area of the single-entry was adversely affected by large-scale structural disturbances, the non-buckling behaviour was controlled and as a result, the rate of panel advance was maximised and stable conditions retained up to and during longwall retreat. It is also interesting to note that the only section of the TG affected by roof instability during longwall retreat was outbye of the single-entry in an area reinforced on low tensioned roofbolts and passive support. See Figure 8 which compares the immediate confining affect of pre-tensioned Flexibolts to passive timber and FRC type support - note the on-going creep in the latter roof.




X - Installation of Pre-tensioned Flexibolts
Y - Installation of Passive Support

**Figure 8 Passive Support and Pre-tensioned Flexibolts - Roof Displacement (Newstan Colliery)**

## PRODUCT DEVELOPMENT FOR STIFFER SUPPORT

In order to provide the mining industry in Australia with products which will ensure stiffer and hence, more effective rock reinforcement, a number of ANI Arnall's internal research projects have focused on the development of high pre-tensioning hardware for roof bolts and cable bolts, as well as the development of products and materials with stiffer behavioural characteristics.

### Pre-Tensioned Roof Bolt Development

It has long been understood that in order to increase the level of pre-load induced along a bolt from a given torque, the friction between the nut and the washer has to be reduced hence, the thrust bearing. Only recently however it was recognised that the friction between the threads of nut and the bolt is far more critical in the torque/tension relationship. Furthermore it was discovered that when the immediate roof is relatively compressible, as the nut has to travel a greater distance under a high load, the friction between the nut and the bolt increases dramatically during nut tightening. The reason for the increased friction in such conditions was gulling. Based on these findings the special high performance Oz nut (HP Oz nut) was developed.

The HP Oz Nut is a modified ANI Arnall standard Oz nut. The standard Oz nut consists of a steel dish which is crimped into the nut (outside its thread). The resistance of the crimped plate allows for resin mixing on installation of the bolt and at a specified torque, the crimped plate breaks, enabling the nut to rise up the thread and tension the bolt. The modifications made to the HP Oz nut have resulted in an improvement in two critical areas ie, mechanical advantage and friction. Firstly, to improve the mechanical advantage of the nut/bolt system, the nut thread form was modified.

Secondly, to reduce the friction, the nut has been coated with a high pressure resistant lubricant. The coating eliminates the gulling completely. In effect, a roof bolt which is installed off a hydraulic bolter having a typical torque output of 300 Nm can be pre-tensioned to a load of 100 kN to 140 kN. In contrast, the standard Oz nut, allows for only 30 kN to 50 kN of load to be induced in the bolt from the same torque. An additional advantage of the HP Oz nut is its cost, which is only a fraction of the cost of the thrust bearing.

**Pre-Tensioned Cable Development**

The Flexibolt is a high strength (580 kN) resin grouted strand bolt. Since its diameter is 23.5 mm it is typically installed in a 28 mm bore hole. Even though Flexibolts have a threaded end, high torque tensioning through the nut is not possible, as the bolt is furnished with a cone and collar on the head assembly and that secondly, (Figure 9 ) due to the high coefficient of friction on the threads the free length of the cable twists under high torque. To alleviate some of these problems, the cone has been furnished with a rim (shown in Figure 9) which delays the wedging action of the barrel and cone until 50 kN of load in the cable has been achieved. At 50 kN the rim is then sheared by the collar.

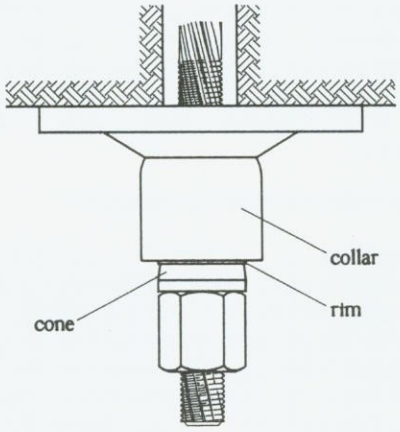



**Figure 9 Standard Flexibolt cone and collar**

Recent development has also focused on the pre-tensioning of Flexibolts to higher loads, typically 250 kN. The original BFP pre-tensioning system allows the bolt head assembly on the bolt to be pulled away from the roof. The tension is then locked in the bolt by extending a spacer (locker) between the plate and collar on the bolt. The locker consists of a threaded hollow bar and a supporting nut as shown on Figure 10.

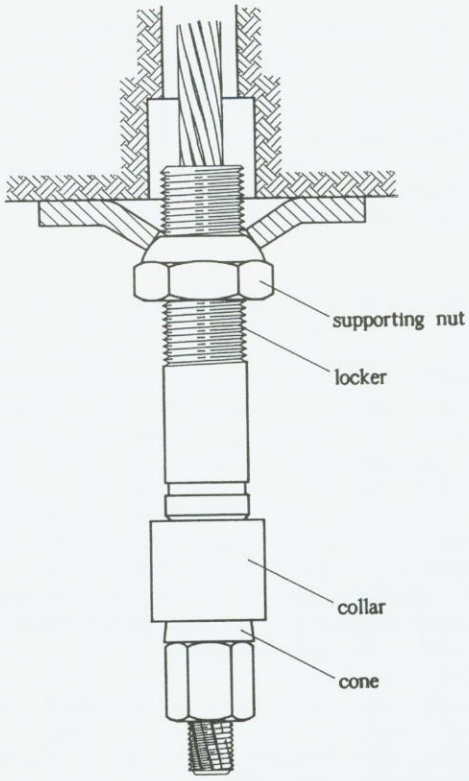



**Figure 10 Pre-tension Flexibolt Tension Locker (BFP System)**

The BFP system was developed by an industry funded project to determine the effect of high pre-tensioned cable bolts on roof behaviour. However, in spite of a number of down-sides, the BFP tension-locker has been accepted at a number of mines as a production unit. Some of the down-sides include the high cost of the locker, the length of the bolt tail protruding from the roof (approximately 300 mm) and the relatively cumbersome application of the tensioning jack.

In view of the above limitation inherent in the BFP system an alternative Flexibolt tensioning system has been developed by ANI Arnall. This system is currently being evaluated in a series of underground trials. The make-up of the system is illustrated in Figure 11, the main difference from the BFP system being the barrel and cone tension locking device and the location of an additional flat cone on the end of the cable.

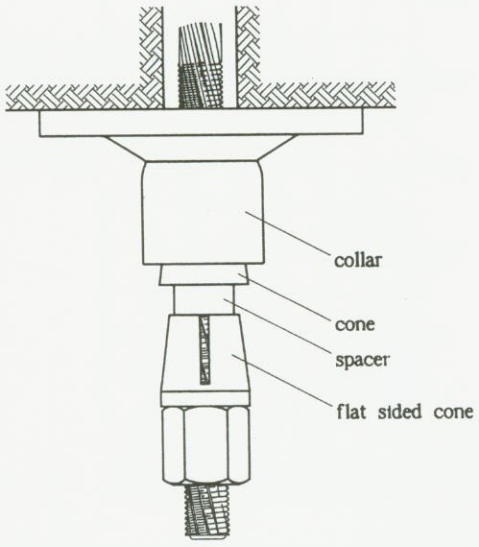



**Figure 11 ANI Arnall Flexibolt Pre-tensioning System**

The flat cone at the end of the cable allows for an easy connection with a double hydraulic ram tensioning unit on tensioning the ram unit pulls the end of the cable away from the roof and at the same time, pushes the cone and collar against the roof plate. Once the required load has been achieved the pressure in the jacks is released, the cone and collar wedges itself on the cable and the tension is thereby locked into the system. (In order to compensate for any bleed off in tension). Since the design of the cone limits any displacement between the cone and collar during the wedging process, the system only requires approximately 20-30 kN of over tensioning The design of this system allows for a reasonably fast application, (approximately 5 minutes) a reduced tail length and is relatively inexpensive.

## STIFFER ROCK REINFORCEMENT HARDWARE

In view of the high deformation environments commonly encountered in Australian coal mines, the yield strength and a post yield stiffness of a roof bolt is considered very important. A bolt loaded above its yield strength reduces its diameter and debonds itself from the resin and as a result, a progressively longer section of the bar is thus exposed to the high load. The longer the loaded section of the bar, the softer the bolt and therefore the larger its elongation. Since in practice, up to 60% of the bolt's total length may be debonded from the resin, excessive bolt elongation may therefore allow for larger roof displacement.

In order to increase bolt stiffness, ANI Arnall have developed a number of high strength/high stiffness grades of steel bolts. Typically, bolt yields now vary from as little as 100 kN to as much as 260 kN. The latest bolt types developed by ANI Arnall provide even higher yield strength.

### AVH Bolt Type

The AVH bolt has the strongest material among the solid bolts. The material yield stress is as high as 770 MPa and is achieved by cold working high grade steel. The bolt is produced out of a round bar which passes through a set of dies which form transverse deformations on the bar. A blank section of the bar is always left for thread rolling. The yield strength of the AVH bolt is 260 kN. This bolt has successfully replaced the "softer" AH type bolt. The mechanical characteristics of these two bolts are compared in Figure 12.

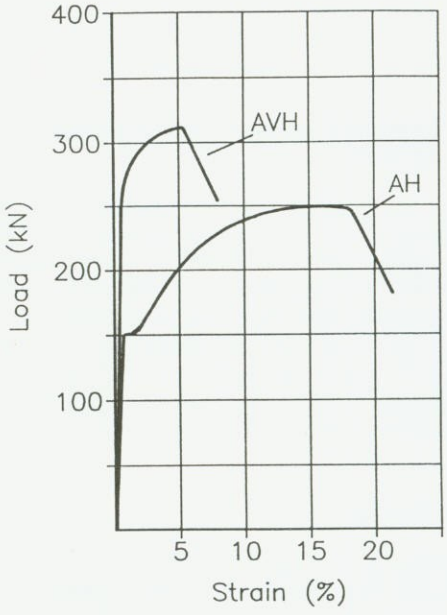



**Figure 12 Loading characteristics of AVH and AH Bolt**

### Flexibolts

As discussed earlier the implementation of Flexibolts has allowed for a significant increase in reinforcement stiffness. This was achieved by both the pre-tensioning of the bolts and the very high yield strength of the cable. The yield strength of Flexibolt strand is about 400 kN and is shown in Figure 13. Its behavioural characteristics are much stiffer than even the strongest solid bolt used in Australia ie, the AX type of which the ultimate strength is 340 kN.

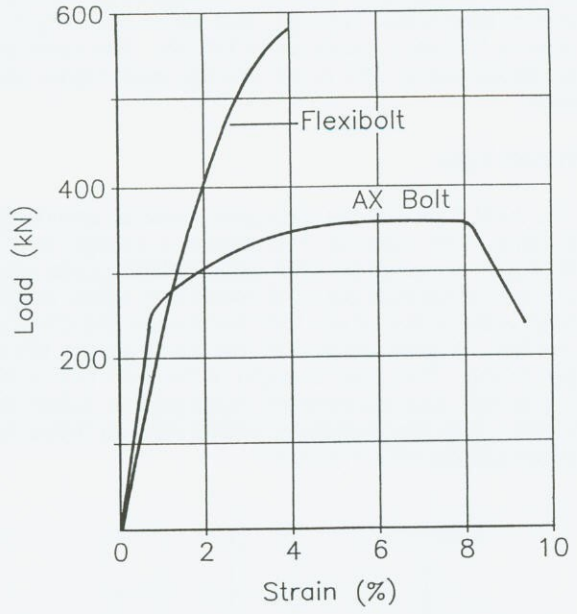



**Figure 13 Loading Characteristics of Flexibolt and AX Bolt**

Although the majority of long tendon Flexibolts in Australia are point-anchored, the stiffness of such bolts has been further increased by a recently developed method of full encapsulation. The new installation method involves a specially designed bolter which has the ability to spin and push the cable into the hole at the same time. By using up to 4 metres of extra slow set resin cartridges, 6m Flexibolts have been successfully fully encapsulated and in one colliery, pre-tensioned to 250 kN.

### Face Plate Design

The stiffness of the roof plate is also considered very important as in high deformation areas plates are often heavily loaded, even though the bolts are fully encapsulated. The stiffness of the reinforcement system was therefore also increased by the introduction of a new type of roof plate called a Turtle Plate. These plates have been formed in such a way that their stiffness is significantly higher when compared to conventional domed plates.

Figure 14 compares the behavioural characteristics of the conventional 100 x 100 mm x 8 mm thick domed plate and the much stiffer Turtle plate, which is circular in form, 4 mm thick and 100 mm diameter.

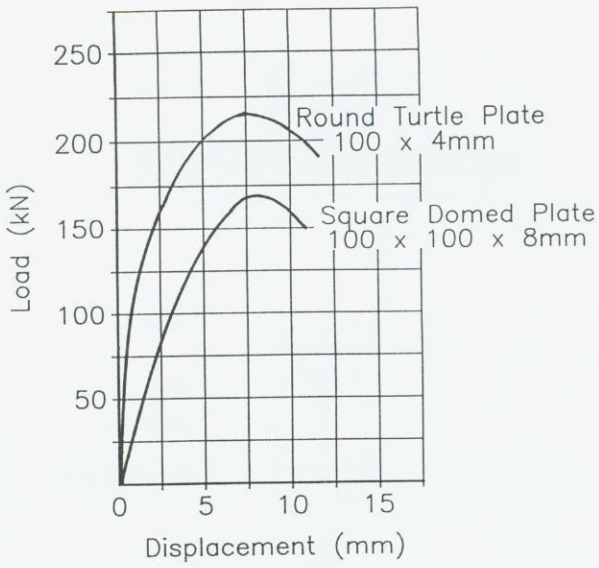



**Figure 14 Loading Characteristics of Domed and Turtle Roof Plates**

## CONCLUSIONS AND RECOMMENDATIONS

The documented improvements made to reinforcement system stiffness, through increased pre-tensions and stiffer material characteristics, has been site proven to be an efficient means of improving the effectiveness of each roof and cable bolt.

Some successful developments include the HP Oz nut, pre-tensioned Flexibolt, the AVH bolt and the Turtle Plate.

The resulting improvements in reinforcement design have made roof behaviour more stable and predictable and consequently, through the development of a site based roof behaviour model, have enabled several collieries in Australia to directly and successfully address both the issues of improved development rates and gate road stability during longwall retreat.

As a result of the measured success of the work to date, both ANI Arnall and Strata Engineering are actively involved in several research projects which will focus on (a) the optimisation of existing technology to the particular mining conditions and needs of each colliery and (b) the further improvement in the design and application of stiffer/pre-tensioned hardware.




## ACKNOWLEDGEMENTS

The authors wish to thank the management of Oceanic Coal and Powercoal for their kind support and permission to publish this paper. The views expressed are those of the Authors and not necessarily those of ANI Arnall or Strata Engineering Australia.


## REFERENCES


1. Clark D. and Filipofski
"An *in-situ* Investigation of the Correlation Between Underground Roadway Stability and Roof Support Intensity."
Australian Tunnelling Conference, Sydney. (1984)

2. Frith, R.C. and Thomas R.
"Roofbolt Pre-tensioning and its Effect on Roof Stability."
ACARP Underground Roadway Development Workshop, Brisbane. (1994)

3. Coull, M. and Thomas R.
"The Geotechnical Factors Influencing Teralba Colliery's Longwall 13 Gateroad Development and the Lessons Learnt."
Coal International. (1997)

# New Design Criteria for Roof Bolt Systems

*John C. Stankus,* Vice President-Engineering
*Song Guo,* Asst. VP-Engineering
Jennmar Corporation
Pittsburgh, PA

## ABSTRACT

From research started six years ago, a new design criteria has been developed for mine roof bolt systems. This design criteria precisely and quantitatively determines parameters such as bolt length, installed tension, and spacing that will produce the Optimum Beaming Effect (OBE). OBE, a new roof control term, is defined as the roof beam that has no separation above and within the bolted range with the shortest bolt possible. Utilization of this design criteria has shown that in many cases shorter roof bolts with higher installed tension can produce a much stronger beaming effect (Stankus, 1995). This paper will first present a brief description of how the design criteria was formulated. From there, actual case studies where the design criteria was utilized will be discussed. In conclusion, current and future research efforts will be presented.

## INTRODUCTION

Roof bolting is the primary method of roof support in today's modern mine. However, despite all the advances made in mine roof control through the utilization of roof bolts, a precise and quantitative design criteria to determine such parameters as bolt length, installed tension required (if any), spacing, etc. has yet to be formulated. Part of the problem has been the lack of a quantitative method to accurately analyze stresses (in-situ and mining induced), bed separations, and friction between strata bedding planes. With the advent of new computer finite element modeling techniques (Stankus and Guo, 1996) these parameters can now be addressed.

Developments of recent years has shown that the point anchor, fully tensioned resin assisted roof bolt has greatly improved mine roof control. These particular bolts are installed at high tensions in the mine roof as soon as possible after mining. In bedded and laminated strata, where beam building is the primary mechanism, these bolting systems have been very effective.

One particular longwall mine in the Pittsburgh No. 8 seam has virtually eliminated roof falls through implementation of this type of bolting system. However, is the length of bolt and amount of installed tension correct? This mine was utilized to collect the necessary data to formulate the design criteria.

## METHODOLOGY

### Objectives

The objectives of the project were as follows:

- Implement instrumented test areas in an active longwall gateroad section during development.
- Monitor the test areas as long as physically possible after the longwall mines outby.
- Analyze data and validate same through computer modeling.
- Formulate the design criteria.

### Basic Test Plan

One longwall gate entry development section was selected for the mine test. The entry chosen for the test site was the entry adjacent to the headgate entry. This entry was chosen for several reasons. First, because of the yield pillar size (35' wide), this entry would be subjected to the abutment loading when the longwall passes through this area. Secondly, this entry would provide easy access to each test site as the longwall face approaches and subsequently mines through this area.

The entire test area included sites with three different bolt lengths: L1 (11'), L2 (8'), and L3 (5'). Bolts were installed at three different tensions: T1 (15,000 lbs.), T2 (20,000 lbs.) and T3 (25,000 lbs.). This combination of lengths and tensions required nine sub-test areas within the main test area.

Refer to Figures 1 and 2 for overall section and test area layout respectively. It should be noted that these bolts were not installed supplemental to the primary plan, but installed in cycle, as the primary plan in normal pattern as shown in Figure 3. The entire test area consisted of 72 rows of bolts with 3 bolts per row or 216 total bolts. Note that intersections are not included in the test.

It was crucial that a uniform installed load be maintained in each subtest area. Further, it would be impractical to adjust machine torque output for each sub-test. Therefore, to achieve this without hindering production and maintaining the same machine torque, three different configurations of anti-friction washers were used on the test bolts. Prior to the test, to ensure that the anti-friction washers would produce the desired bolt tensions, extensive underground load cell testing was conducted.

Once the test site was installed, the entire test area was monitored through extensive instrumentation. Since the key parameters to evaluate roof stability with respect to beam building are roof deflection, strata separation, and bolt loading, the instrumentation for each sub-test consisted of the following:

- Strain gaged bolts,
- Sonic probe extensometers,
- Convergence stations,
- Stratascope boreholes.

A 12' rock core was taken from the roof at mid-pillar in each of the three bolt length test areas. The core was subsequently tested for uniaxial compressive strength, Young's modulus, and Poisson's ratio.

Monitoring and collection of data began upon initial installation of the test sites. Subsequent readings were taken as the retreating longwall approached and mined through the test area. Final readings were taken when the longwall face was approximately 1000' outby the test area. Deteriorating conditions in the test area physically prevented further access.

**Analysis of Test Data**

The term beam deflection as used in this research is defined as a collective term for change in strata thickness of the beam consisting of the roof layers that are concerned. The change could be due to a bedding plane separation, fractures, or pure elastic deformation, which all can cause a change in roof thickness. When the longwall was 300-350' outby, the deflection was significantly less for the 5' bolts as shown in Figure 4.

Roof sag and floor heave was determined by correlating the sonic probe and convergence data. Floor heave was seen before roof sag in all the sub-test areas when the longwall was 100' inby or less. At this point, the test area would have been subjected to the frontal abutment pressure. Once the longwall was outby the sub-test areas, the heave continued reaching a maximum average of 3-4". Roof sag began when the face was 300-350' outby, with the minimum amount occurring in the 5' bolt sub-test area.

As far as bolt loading for bolts installed at the same tension, when the longwall was 400-500' outby, more loading was seen in the longer bolt as shown in Figure 5.

Based upon the test data analysis the following conclusions were made:

- The longer the bolt, the larger the beam deflection. Alternatively, the shorter the bolt, the smaller the deflection and the stronger the beam.
- For the same length of bolt, the larger the installed tension, the smaller the beam deflection. In other words, a stronger beam can be built with the same bolt by utilizing a larger installed tension.
- The bolt with higher installed tension induced a smaller beam deflection within the bolting range. The smaller deflection within the bolted range results in a smaller deflection higher up in the roof above the bolting range.
- The longer the bolt, a larger load will be induced in the bolt as the result of in-situ or mining related stresses.

**Validation of Test Data**

Computer modeling was utilized to validate the test data and conclusions drawn. In this project, ANSYS (v 5.1) was used because of its capability of modeling bedding planes and bed separation, automated features, and ease of inter-facing with other software. The program can also take into account horizontal stress induced lateral movement. It is also worthy to mention that most previous research on roof bolting modeling has been completely restricted to an elastic, continuous medium.

A two dimensional plane strain finite element analysis has been conducted. The rock domain was modeled by 4-node isoparametric elements. The bedding plane was modeled by placing a series of gap elements characterized by the most critical parameter, q, the friction coefficient. The bolt was modeled as one 1-dimensional truss element with the installed load simulated by two concentrated point loads applied at two anchorage points.

A coarse model (Figure 6) has been designed which include the gob, pillars, roof and floor. The fine model (Figure 7) has been designed to concentrate on the immediate roof and parts of the rib only. The fine model may be considered as a sub-model of the coarse model. In the sub-model, a much finer mesh with equal size is enforced with the addition of gap elements at every 1' interval and the bolt. The

boundary condition for the sub-model comes from the output data at the cut boundaries from the coarse model.

To confirm the working mechanism of the reduced bolt with higher installed tension, three models were run with bolt lengths of 5', 8', and 11' and 25,000 lbs tension. The vertical stress distributions for each model are shown in Figures 8. It can be seen that each bolt presents its own distinct influence zone (compression zone). As the bolt gets shorter, the two zones tend to overlap inducing compression within the bolted range.

The actual validation process mainly consisted of comparing roof sag and beam deflection measurements from the field with the data from the computer modeling. Roof sag and beam deflection is calculated from the computer modeling data output, the same as with the field measurements. Since the bolt loading is proportional to beam deflection, no bolt loading is compared.

Initially, nine models were run to consider nine different rib in the sub-test areas. Due to the fact that all materials are assumed to behave elastically, there is no significant difference among these nine models in terms of the boundary conditions at the cut boundary that will be applied to the submodels. Therefore, for consistency and comparison of the data, only one rib condition is used and assumed to be uniform with Young's modulus of $1 \times 10^5$ psi.

A total of 18 models were run with installed tension values ranging from 0 - 25,000 lbs. It should be noted that the models were designed to model the initial stage of roof failure which occurred in the test areas when the longwall face was 300' outby. After that point, the roof was classified as in an unstable state. A summary of the output data showing the relationship between these two parameters is shown in Figure 9. It can be seen that when the installed tension reaches 10,000 lbs., the roof sag is significantly reduced. Shown in Figure 10 is the beam deflection when the three bolt lengths are installed at 25,000 lbs. tension significantly less deflection is seen with the 5' bolt.

The computer modeling results indicates the relationship among installed tension, bolt length, roof sag, and beam deflection concurs with the field test data. In should be noted that in magnitude, some of the computer results differ from the field measurements. However, the trend between the actual and computer modeling data is the same.

**Formulation of Design Criteria**

The design criteria is formulated based upon the validated models. Shown in Figures 11 and 12 are the coarse model and submodel respectively in which a single entry is modeled with the applied vertical and horizontal stresses. The problem domain in the submodel is confined within the immediate roof and its adjacent area since the focus of this research is the beam building mechanism.

The following domain for design parameters are:

- Bolt length
- Roof, coal, and floor Young's modulus
- Loading values - both vertical and horizontal stress in psi.
- Friction coefficient for gap elements: 0.2-0.7, which represent weak and strong bedding plane interface.

Homogeneous, elastic, and isotropic material for the roof is assumed. However, the gap elements behave in a non-linear fashion. The default row spacing is 4'. Since the bolt load (including installed tension) is averaged over the row spacing, if the required installed load is too large, then bolt row spacing is reduced accordingly. The Boolean variable (q) is used to determine the status of the gap: q=0 indicates the roof layer does not separate, q=1 indicates roof layer separation.

The methodology used in the bolting criteria formulation is described as follows:

Based on the established reduced length bolt theory and realizing that increasing bolt tension as opposed to length is more economical, the 5' bolt is used first. Strata separation will be checked at every gap horizon. If a separation is found within the bolted range, then bolt tension will be increased in 5,000 lb. increments until no separation is found. At this point, the gap status above the bolted range is checked. If no separation is found, then the required installed tension is found. If a separation develops above the bolted range, then bolt length is increased in 3' increments. The flow chart showing this methodology is shown in Figure 13. From this perspective, the term Optimum Beaming Effect (OBE) is defined as the beam that has no separation above or within the bolted range with the shortest bolt possible.

A computer program has been written that stores all the data from the computer modeling in a database file. The program is designed with user friendly interface and searching capability. The user provides the input parameters which are mine site specific. The program automatically generates a model based on the parameters entered. Subsequently, a model is generated when either an increase in bolt installed tension or length is made. An additional model is run for each loop in the flow chart until the Boolean variable (q) equals zero for the area within or above the bolted range. The main output of the program is bolt length, installed tension (if any), and spacing.

## CASE STUDIES

Since the design criteria was formulated in late 1995, it has been utilized for bolt design at numerous operations under a wide variety of ground conditions. A few case

studies have been chosen for comparison of different mine site specific parameters and the resultant bolt design formulation.

**Case Study Mine #1**

The immediate roof at this mine consists of laminated, medium to dark grey shales with some silty sandstone. Primary support originally consisted of a fully grouted, non-tensioned, headed #6 (3/4") rebar x 6'. Horizontal stress is a factor at this mine and with the headed rebar numerous cutter roof type falls occurred. Keeping bolt diameter and length the same, the mine switched to a fully tensioned, resin assisted point anchor system. Installed bolt tension averaged 15,000 lbs. Conditions greatly improved and the number of falls was significantly reduced. However, minor roof cutter persisted necessitating additional supplemental bolting with longer bolts particularly in intersections.

The design criteria was applied utilizing the following mine site parameters:

Young's modulus for shales: $1.2 \times 10^6$ psi
Young's modulus for silty sandstone: $1.5 \times 10^6$ psi
Young's modulus for coal: $1.0 \times 10^5$ psi
Entry width: 20'
Entry height: 6'
In-situ vertical stress: 770 psi
In-situ horizontal stress: 900 psi

The modeling output data indicated that a reduction of bolt length to 4' and increasing installed tension to 20,000 lbs. would produce the OBE. This change was implemented and to date cutter roof has not occurred. Supplemental support for gateroad intersections was eliminated. For long term entries such as mains and sub-mains, even though no roof cutter occurred, intersection supplemental support was continued but in the form of high capacity cable bolts.

**Case Study Mine #2**

The immediate roof in this mine consists of a fine grained sandstone with some shale with average overburden depth of 600'. Primary support consisted of a 6' x 7/8" torque/tension system fully encapsulated with a fast and slow set resin. The bolt was installed on a 4' x 4' pattern with four per row. Average installed tension was 12,000 lbs. No roof control problems were incurred with this system.

The design criteria was applied utilizing the following mine site parameters:

Young's modulus of sandstone: $1 \times 10^6$ psi
Young's modulus of shale: $8 \times 10^5$ psi
Young's modulus of coal: $2 \times 10^5$ psi
Entry width: 16'
Entry height: 9'
In-situ vertical stress: 720 psi
In-situ horizontal stress: 1200 psi

In this case the modeling data indicated that no installed tension was needed and that bolt length could be reduced to 5'. A headed #7 x 5' J-Bar, fully encapsulated, and non-tensioned bolt was implemented as primary support. No roof control problems have been reported and costs were reduced.

**Case Study Mine #3**

The immediate roof in this mine consists of finely laminated shales and sandy shales. Overburden ranges from 750-1200' and horizontal stress, both in-situ and mining induced, is a factor. The primary support consisted of a fully tensioned, point anchor system, 7/8" x 8'. This bolt was installed with two ft. of resin in conjunction with a T-5 steel roof channel. Three bolts per row were utilized installed at an average tension of 18,000 lbs. Supplemental bolts in the form of a 7/8" x 12' fully tensioned system were used in every intersection.

The design criteria was utilized with the following mine site parameters:

Young's modulus of shale: $2 \times 10^6$ psi
Young's modulus of sandy shales: $3.2 \times 10^6$ psi
Young's modulus of coal: $1 \times 10^5$ psi
Entry width: 16'
Entry height: 7'
In-situ vertical stress: 1400 psi
In-situ horizontal stress: 3200 psi

The output data indicated that a 5' bolt with installed tension increased to 25,000 lbs. would provide the OBE. Because of the interaction of the in-situ and mining induced horizontal stress, this change was implemented in one section and monitored very closely. The entries and crosscuts remained in good condition. However, cutter roof that initiated in the crosscuts propagated into the intersections. Cable bolts were installed to supplement the primary support in the intersections and the roof cutter was controlled. Overall conditions were greatly improved over the previous primary support system with reduced costs.

## CONCLUSION

Current and future research efforts are and will be focused on:

- Determination of the amount of allowable bed separation. Setting the Boolean variable (q) to zero is acceptable for the computer modeling process. However, from real practice we know there can be some bed separation while still maintaining stable roof.

- As far as supplemental support for intersections, vertical cable bolts utilized with the proper positioning is improving the OBE beaming effect. It is felt that instead of relying on the suspension mechanism, OBE can achieve better roof control with a smaller number of bolts required. Identify the stress condition and its effect on a particular intersection configuration appears to be the key. Additional three dimensional models with large amounts of elements are being used to further refine intersection support plans.

- As for the computer modeling itself, element crashing/crushing capability will be incorporated to further address the horizontal induced cutter roof as well as its effect on bolt installed tension and length. More three dimensional modeling is being conducted. Upgrading to ANSYS (v 5.2) will enable computer time to be reduced.

- Applying the design criteria to more mines with different conditions.

This design criteria has provided the ground control engineer a tool to accurately determine stresses for any given mine layout. The appropriate support system can be designed that will be cost effective while improving ground stability and overall mine safety.

## REFERENCES

ANSYS 5.1 Theory Manual, SWANSON, Inc., 1995.

Stankus, J. C., 1995, Design Criteria for Tensioned Point Anchored Resin Assisted Roof Bolt Systems, Ph.D. dissertation, West Virginia University, December, 126 pp.

Stankus, J. C. and Guo, S., 1996, Computer Automated Finite Element Analysis - A Powerful Tool for Fast Mine Design and Ground Control Problem Diagnosis and Solving," *Proc. 5th Conference on the Use of Computers in the Coal Industry*, edited by S. D. Thompson, R. L. Grayson, Y. J. Wang, West Virginia University, pp. 108-155.

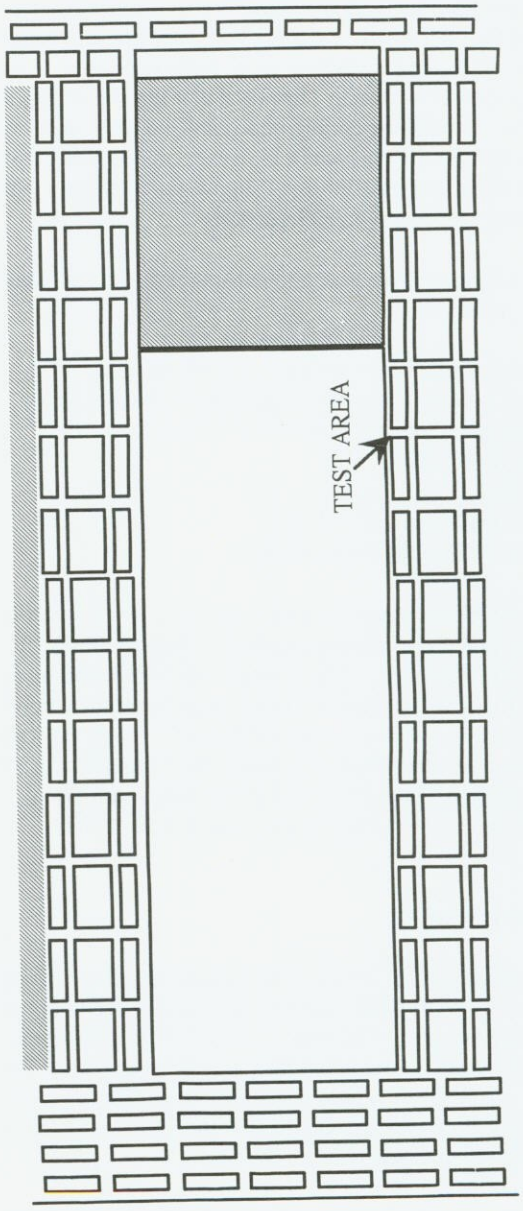



Fig. 1 Longwall Panel Layout

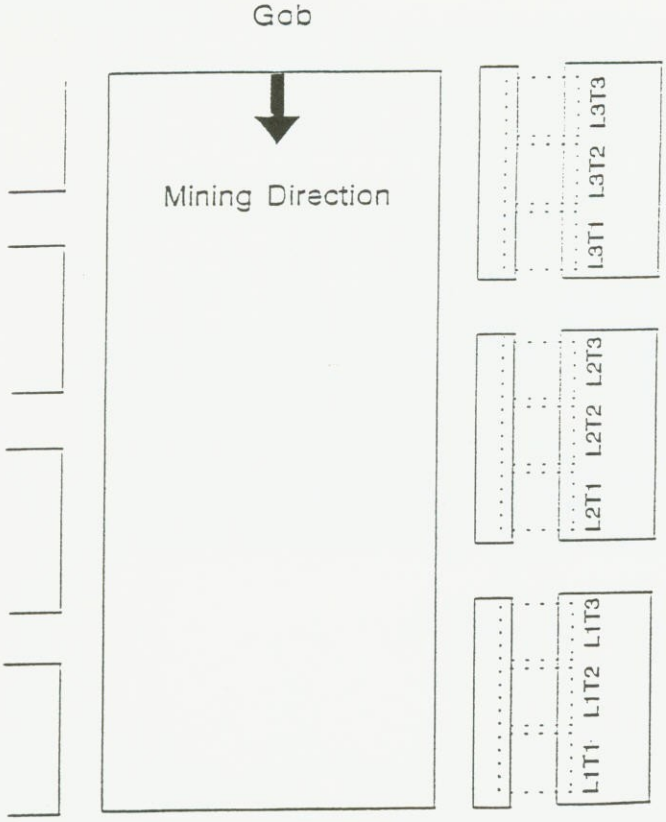



Fig. 2 Overall Test Plan

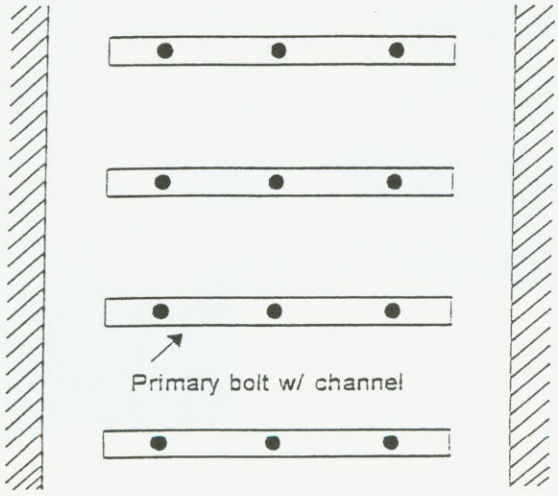



Fig. 3

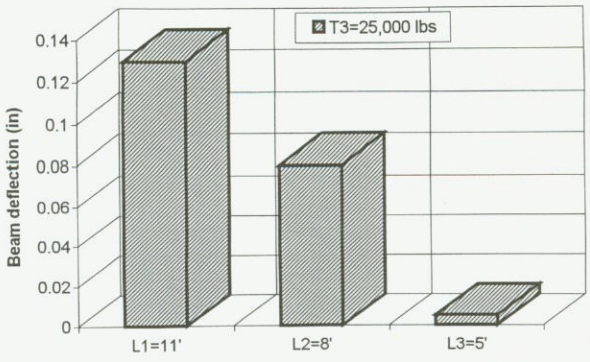
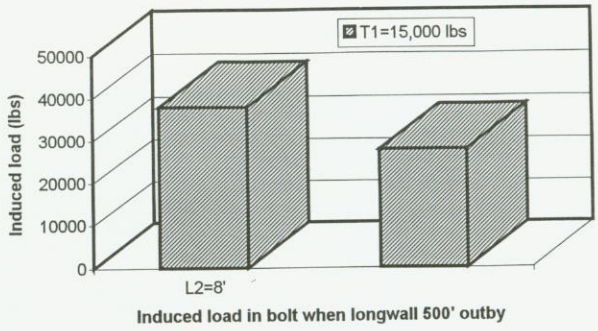



Fig. 4 Beam Deflection Within Bolting Range when Longwall is 300-350' Outby for T3=25,000 lbs.



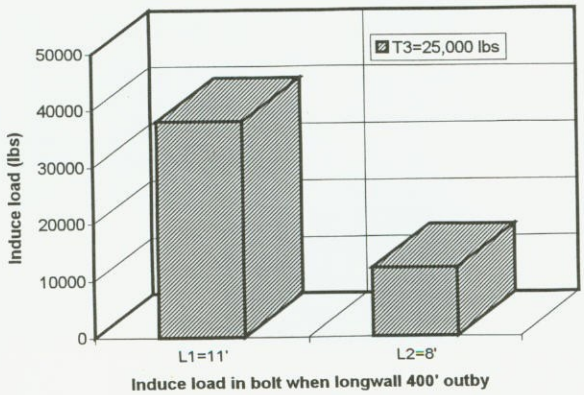




Fig. 5

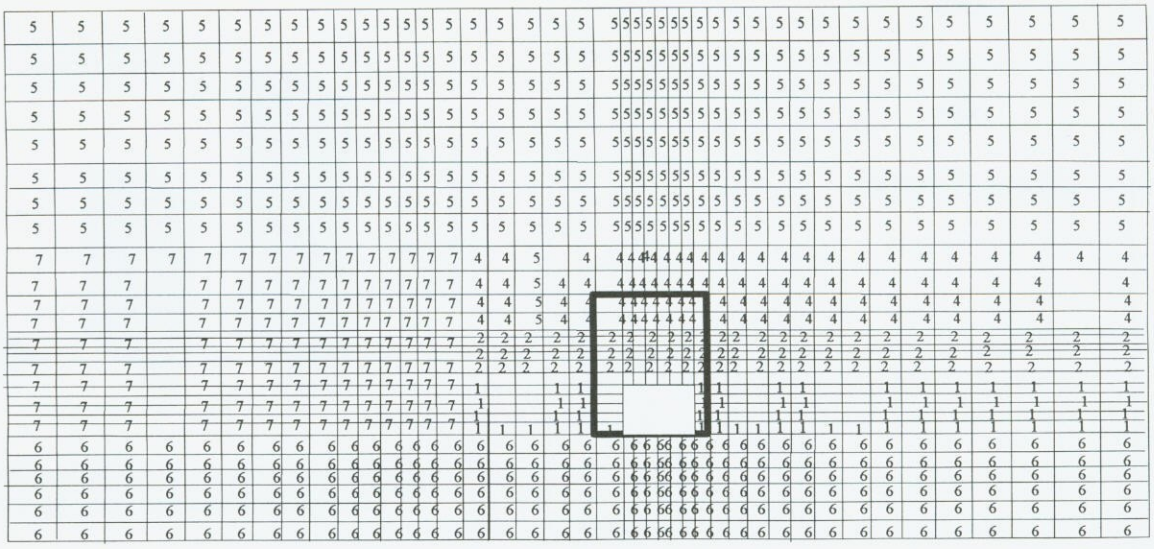


Fig. 6 **Coarse** Model: Gob, Pillars, Roof and Floor
(Sub-Model Outlined)

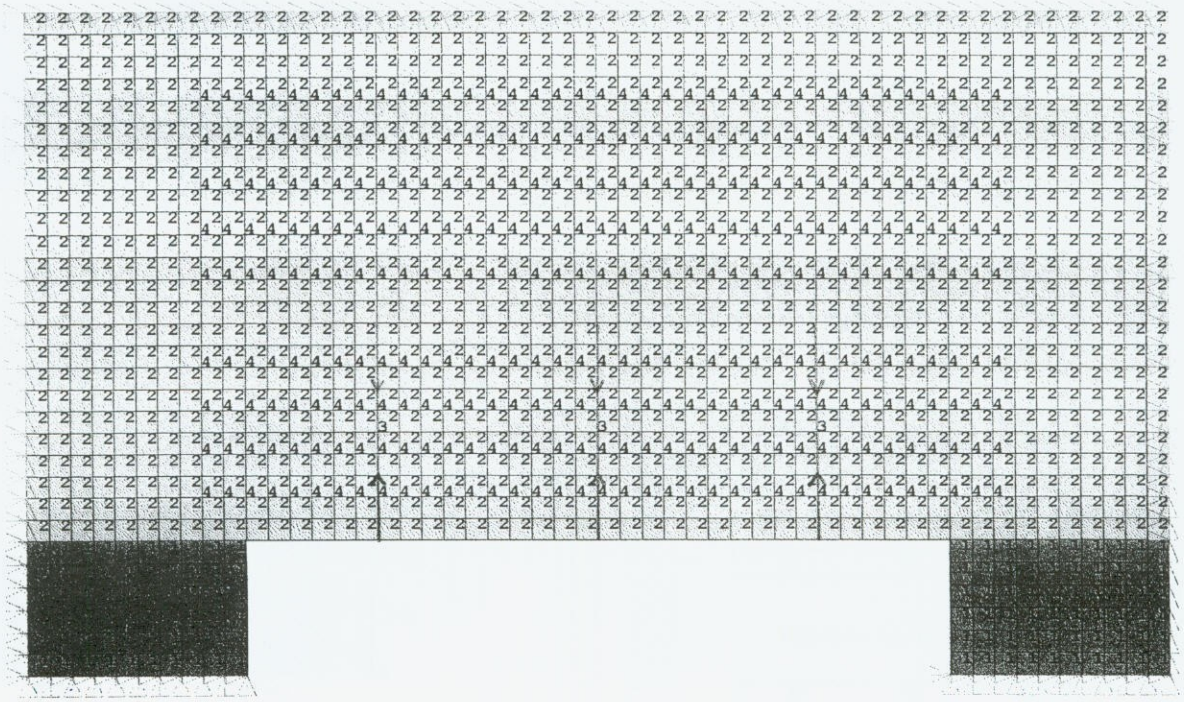
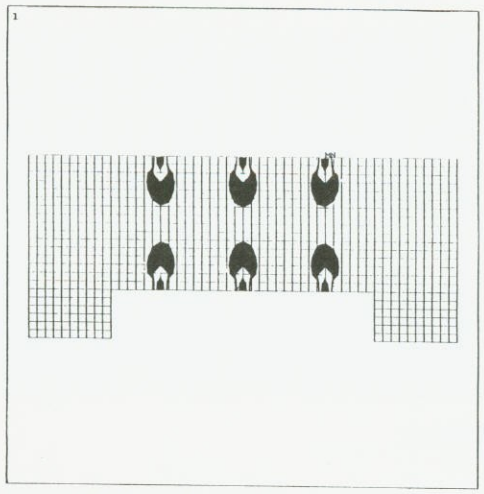
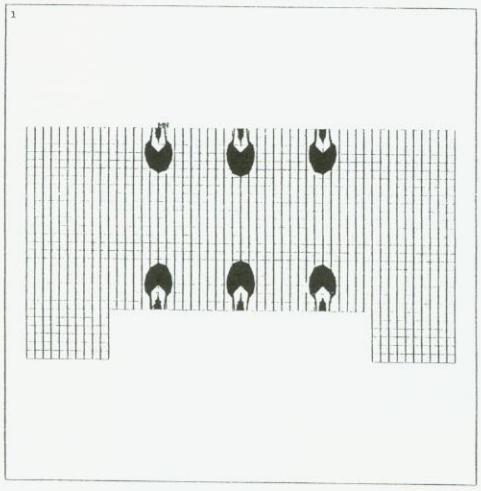


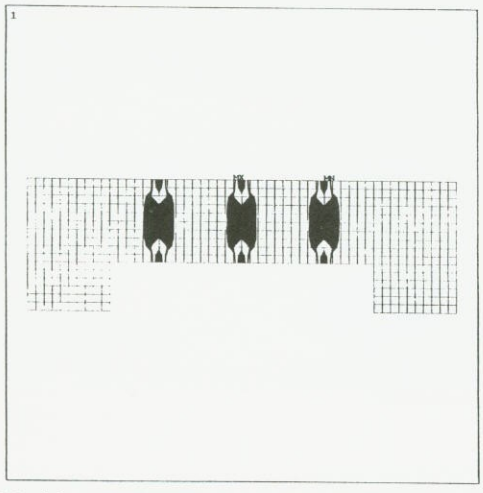
Fig. 7 Sub-Model



Model: 8' Bolt Influence Zone at T3 (25,000 lbs.)



Model: 11' Bolt Influence Zone at T3 (25,000 lbs.)



Model: 5' Bolt Influence Zone at T3 (25,000 lbs.)

Fig. 8

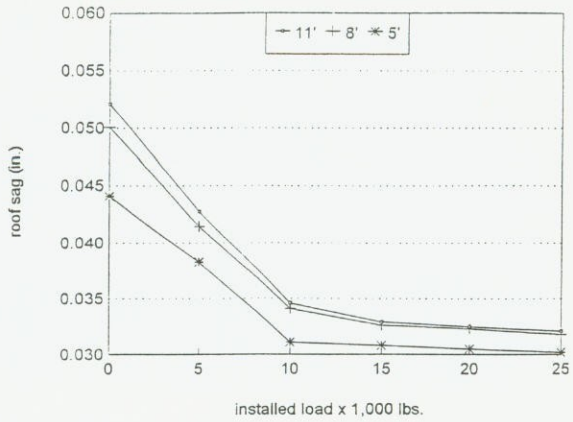



Fig. 9 Relationship of Installed Load and Roof Sag for L1 (11'), L2 (8'), L3 (5')

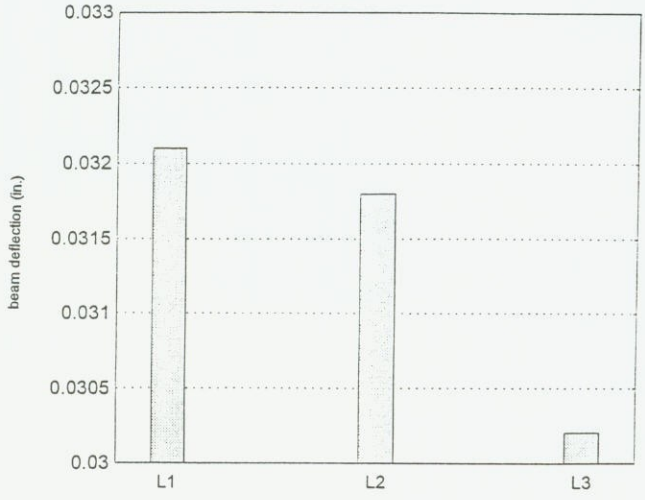



Fig. 10 Relationship of L1 (11'), L2 (8') and L3 (5') at T3 (25,000 lbs.)

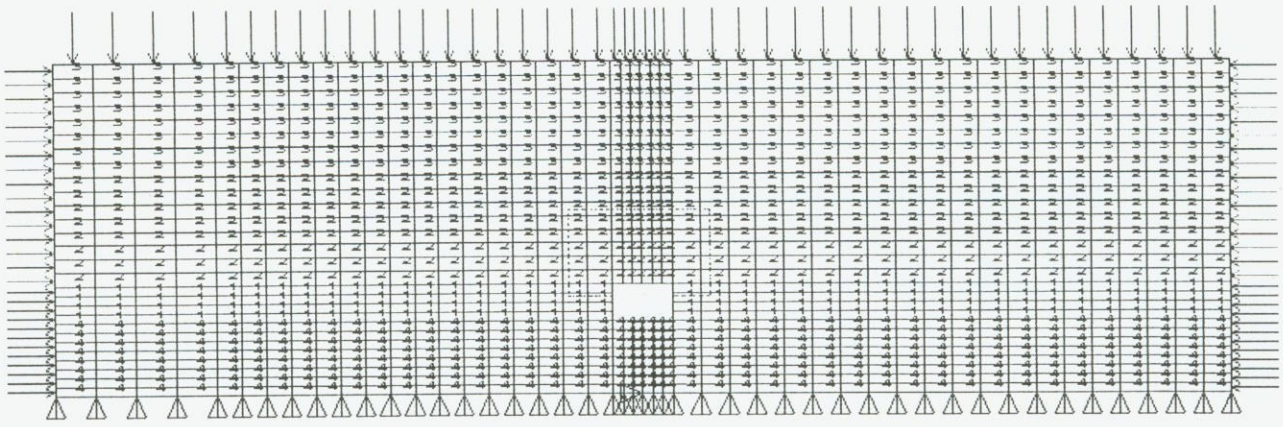


Fig. 11 Coarse Model: Single Entry
(Sub-Model Outlined)



Fig. 12 Sub-Model: Single Entry

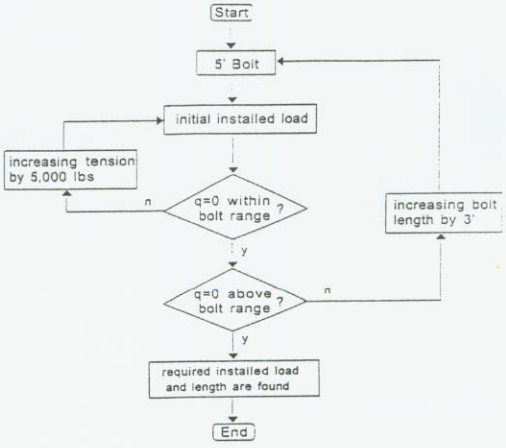



Fig. 13 Design Criteria Methodology Flow Chart

16th CONFERENCE ON GROUND CONTROL IN MINING

# Control Mechanism of a Tensioned Bolt System in the Laminated Roof with a Large Horizontal Stress

*Song Guo,* Asst. VP-Engineering
*John C. Stankus,* Vice President-Engineering
Jennmar Corporation
Pittsburgh, PA

## ABSTRACT

This paper will present the roof bolting finite element model developed at Jennmar Corporation used to study the control mechanism of the tensioned bolt system in the laminated roof with a large horizontal stress. In addition, it will discuss general support concepts pertaining to the tensioned bolt system which are derived from a series of studies in conjunction with the authors' working experience and extensive research efforts over the years.

## INTRODUCTION

The tensioned bolt system has been widely used in underground coal mines to effectively control thinly-laminated roof strata such as shale, sandy shale, and/or sandstone. This bolt system is an active type support in contrast to the passive bolt system such as non-tensioned, fully grouted rebar. It not only provides a high installed load, but also a high stiffness, and a quick interaction with the mine roof once it has a tendency to separate within the bolting range.

Over the last few years, extensive field research projects with instrumentation studying the mechanics of this bolt system have been conducted. Also, in conjunction with the field testing, a computer model has been developed using the finite element method permitting further investigation of the control mechanism of this bolt system.

### Horizontal Stress

Horizontal stress can be classified into two categories:

1. Low Horizontal Stress

In this case, the roof will fail in the form of tensile failure in the entry center or in the form of vertical shearing at the roof/rib corner. Normally, these types of failure are associated with noticeable roof sagging and separation. Within a certain limit, the larger the horizontal stress, the stronger the strength of the bolted roof will be in terms of reducing tensile stress (tensile failure) in the center of the entry and shear stress (vertical shearing failure) at the entry corner.

2. High Horizontal Stress

High horizontal stress can cause two major types of roof failure. The first type is cutter roof either at the entry corner or shear fracture in the middle portion of the entry.

Finite element analyses always indicate that the maximum horizontal stress concentration occurs at the entry corner in the roof surface, specifically, 1'-2' from the ribline when the high horizontal stress is oriented perpendicular to the entry direction in 2-dimensional modeling, and perpendicular to (or close to perpendicular) in 3-dimensional modeling. It is believed that if this concentrated horizontal stress exceeds the lateral compressive strength of the roof, cutter roof (horizontal shearing failure) will occur. The study of post-failure process of cutter roof is beyond the scope of this paper.

The second type of roof failure is the delamination or bed separation of the roof strata and lateral shift due to low installed load or delay in installation of the bolt. The roof sags in the entry center, inducing tensile failure.

### Roof Separation

Under the low horizontal stress condition, the bed separation in the thinly-laminated strata implies that each laminae behave independently in accordance with the classic beam theory. The function of the roof bolt is to form the multiple laminae into a monolithic beam that is more resistant to the tensile stress developed at the bottom of the beam and

shear stress at the center line of the beam (Fig. 1).

When a high horizontal stress condition exists, each laminae would be subjected to compressive stress only, except when tensile stress is developed associated with excessive roof sag. As a result of lateral shift at the interface between each laminae, the horizontal stress concentration would occur in the bottom side of each laminae at the entry corner (Fig. 2). Once bed separation initiates and propagates across the entry width, the stress state in the roof at the horizon where the bed separation occurs would be the same as that in the roof surface at the entry corner. Therefore, if the bolt is used to prevent any bed separation, it will allow each laminae to react to each other and provide vertical confining pressure, thus increasing the shear strength.

Two types of separation are defined in terms of roof control:

- separation within bolting range ($\delta_1$)
- separation above bolting range ($\delta_2$)

## Roof Bolting Model

Recently at Jennmar Corporation, a family of generic 2 and 3-dimensional finite element models for typical mine layouts (room and pillar, as well as longwall mining with up to 4-entry gateroad system) have been developed (Stankus and Guo, 1996). All these models will serve as coarse models. Other models (2 and 3-dimensional), called submodels, are constructed based on the coarse model output. In these coarse models, the number of layers, material properties, and mine geometry can be specified. The domain of the submodel is the area of concern that is cut out from the coarse models. In the submodels, a much finer mesh can be enforced while incorporating the gap and bolt element. The submodels are designed to be generic, where the input for the gap element, bolt system parameters, and element size can be arbitrarily specified. The boundary condition applied at the cut-out boundary is automatically applied with input coming from the coarse model at the same boundary. This is based on the assumption that the domain for the submodel is large enough to overcome the boundary effect, since the effect of delamination and the bolt is limited in area. Therefore, the boundary at a certain distance from the entry in the submodels will be identical to the boundary condition without considering bolt and gap elements in the coarse models. The same element size is maintained in the submodels for all the elements in the domain in order to make unique input values for normal and shear stiffness. Further, it is more convenient to base the adjustment of stiffness values on different element size. The input parameter for the bolt element is size, length, bolt stiffness, and installed load. The bolting pattern (bolt spacing and row spacing) can be specified.

The coarse and submodel for 2-dimensional modeling is illustrated in Fig. 3. Gap elements are utilized to model the bedding plane between each lamination. The bolts are modeled using 1-dimensional bar elements with initial installed load modeled by concentrated loads at two extreme ends of the bolt. The characteristic curve of the gap element is shown in Fig. 4. Three parameters unique to the gap element are normal stiffness, shear stiffness, and the coefficient of friction. Installed load and bolt length have been identified as the most important parameters in bolt design. Bolt design criteria can be centered around the optimum selection of these two parameters.

## Installed Load

It has been proven through the roof bolting models described above, that for any given roof property and in-situ stress condition (both vertical and horizontal), increasing the installed load of the bolt, without being subjected to any limitation, will prevent separation within and above the bolted range for any given bolt length. This is conceptually shown in Fig. 5. This concept is, in principle, equivalent to restoring initial confining pressure in the roof being released at the roof surface due to mining.

With increased installed load, the horizon where the large horizontal stress concentration at the corner occuring due to lateral shift along the lamination planes, is reduced.

A. Under High Horizontal Stress Condition

Under a high horizontal stress condition, the relationship between the installed load and total bed separation is depicted in Fig. 6.

In this condition, when the installed load is low, the bed separation occurs within and above the bolt range and can reach a high horizon in the roof. As the installed load increases, both $\delta_1$ and $\delta_2$ become smaller. When the installed load reaches the point where $\delta_1$ is zero, the bed separation ($\delta_2$) reaches zero. Further, sometimes $\delta_2$ can reach zero before $\delta_1$.

Ensuring no separation within the bolt range can ensure no separation above the bolt range (Fig. 6). This can be expressed as:

$$P_0 = P_{\delta 1 = 0}$$

To satisfy this condition, it is more practical and economical to shorten bolt length without being detrimental to roof stability.

B. Under Low Horizontal Stress Condition

Under the low horizontal stress condition, the relationship between the installed load and total bed separation is depicted in Fig. 7.

It can be seen that when the installed load increases to

$P_{\delta 1 = 0}$, bed separation within the bolting range is eliminated. However, bed separation ($\delta_2$) above the bolting range still remains. In other words, the installed load that ensures no separation within bolt range cannot guarantee no separation above the bolt range. This is especially true when the bedding plane is weak and the roof material is soft. By continuing to increase the installed load, $\delta_2$ will tend to reach zero.

The optimum installed load can be expressed as:

$$P_0 = P_{\delta 2 = 0}$$

## BOLT LENGTH

In certain situations, the optimum installed load to prevent $\delta$ from occurring may be too high to be practically achieved. In this case, focus can be given to adjustments in the bolt length. Increasing the bolt length has been proven to be more feasible and cost effective when the horizontal stress is low. However, increasing length must also be accompanied by a larger installed load.

There is a chance that increasing bolt length still may not be able to eliminate separation within the bolted range. The longer the bolt, it may be more difficult for the bolt to clamp the thick beam tightly.

## EFFECT OF FRICTIONAL COEFFICIENT

The frictional coefficient ($\mu$) between bedding planes has been identified as one of the most important factors that affect the optimum installed load. The relationship between the friction coefficient and optimum installed load is depicted in Fig. 8.

The scenario in which the optimum installed load might be too high is when the friction coefficient is too low. As $\mu$ increases, the optimum installed load would reduce considerably.

Also, when the friction coefficient is low, the roof horizon where the horizontal stress concentration at the corner occurs due to lateral shift is high. As the frictional coefficient increases, high horizontal stress concentration will be reduced to a lower roof horizon.

## SUMMARY

The magnitude of the horizontal stress dictates the control mechanism of the tensioned bolt system. Under a low horizontal stress condition, the tensioned bolt system builds a composite beam. Under a high horizontal stress, it allows each laminae to react to each other so that the vertical confining pressure is maintained at the lamination plane, thus increasing the shear strength of the roof.

The developed roof bolting model takes into account various factors such as in-situ stresses, material properties, mine geometry, and bolt parameters. Modeling of lamination plane through the use of the gap elements is a key in analyzing the thinly laminated roof strata condition. Currently, this model is being utilized for actual mine roof bolting design.

## REFERENCES

ANSYS 5.1 Theory Manual, SWANSON Inc. 1995

Stankus, J. C., and S. Guo, 1996, "Computer Automated Finite Element Analysis - A Powerful Tool for Fast Mine Design and Ground Control Problem Diagnosis and Solving," *Proc. 5th Conference on the Use of Comptuers in the Coal Industry*, edited by S. D. Thompson, R. L. Grayson, and Y. J. Wang, West Virginia University, pp. 108-115.

Snyder, V. W., 1983, "Analysis of Beam Building Using Fully Grouted Roof Bolts," *Proc. of the International Symposium on Rock Bolting*, edited by O. Stephansson, Abisko.

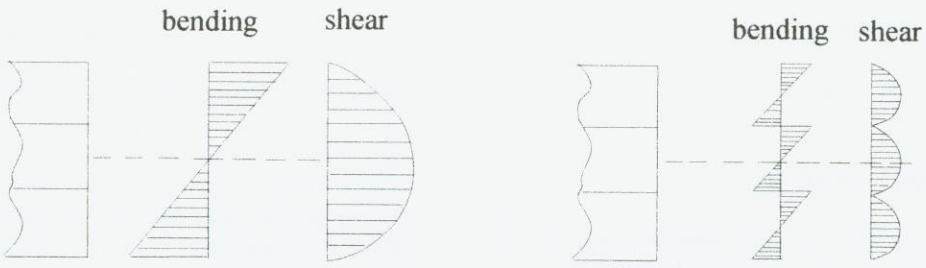



Fig. 1 Stress Distribution in Beam (Snyder, 1983)

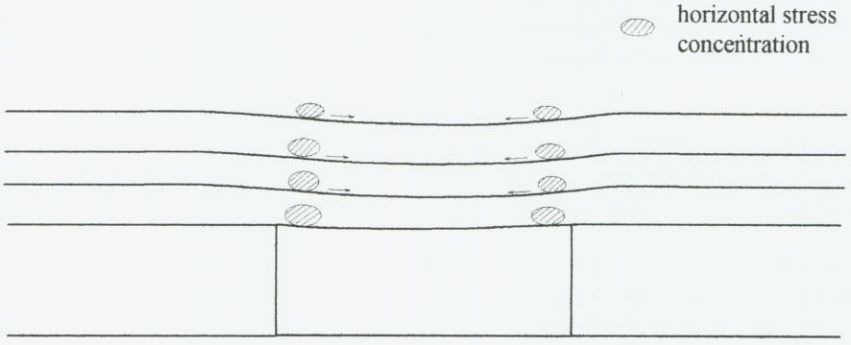



Fig. 2 High Horizontal Stress Concentration Due to Lateral Shift

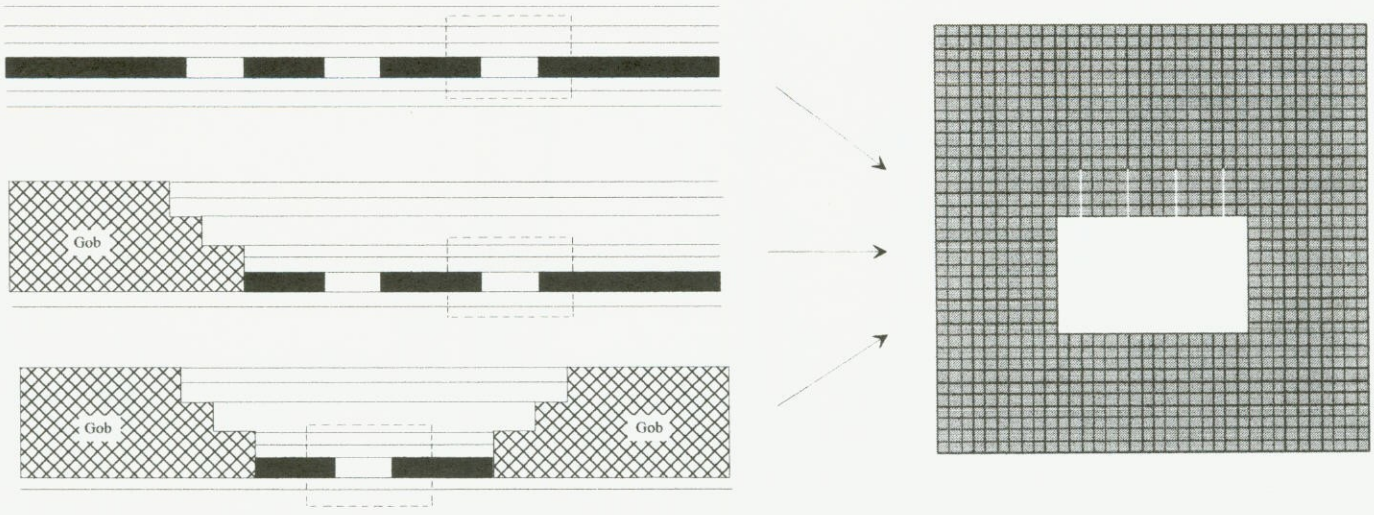



Fig. 3 Coarse Model and Submodel

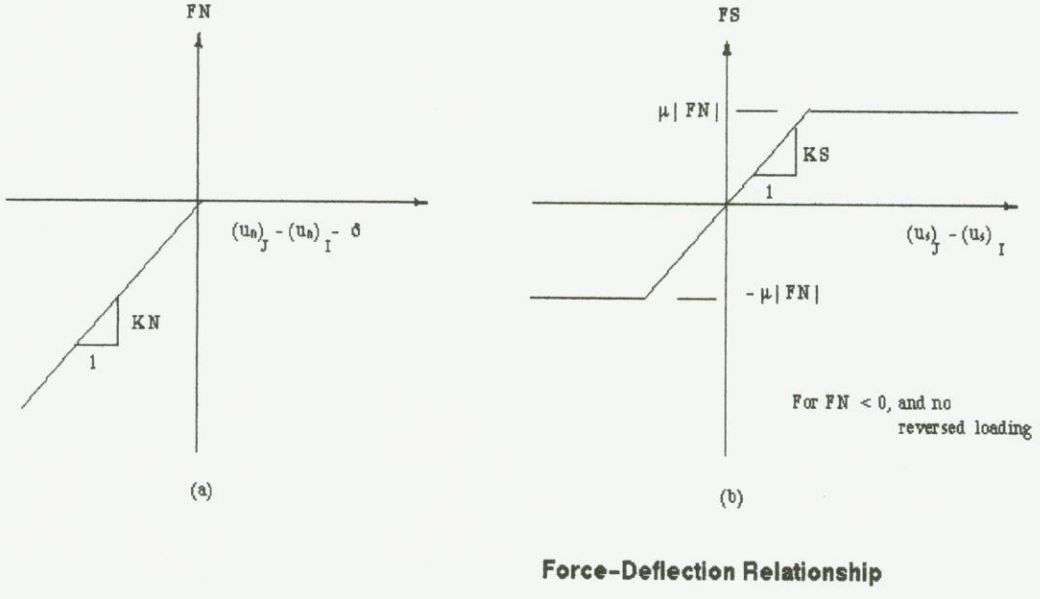



Fig. 4 Force-Deflection Relationship for Gap Element

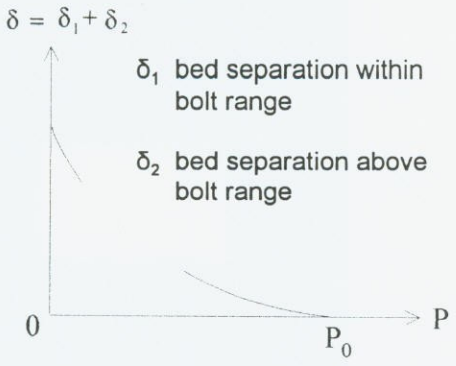



Fig. 5 General Relationship Between Optimum Installed Load and Total Separation

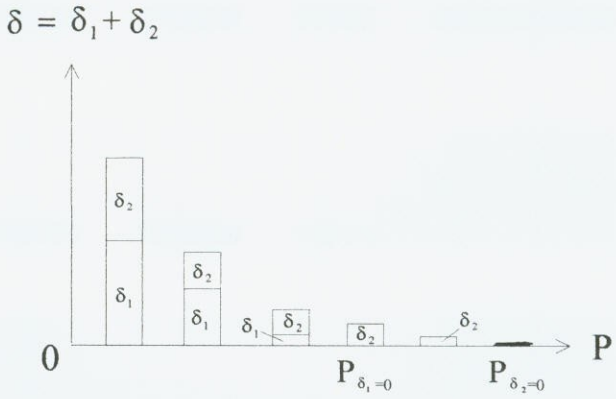



Fig. 7 Installed Load vs. Total Separation Under Low Horizontal Stress Conditions

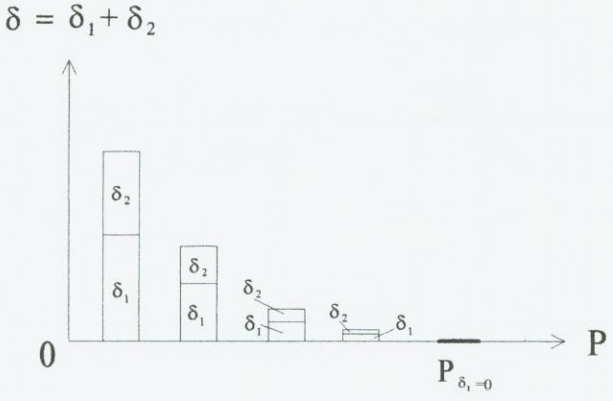



Fig. 6 Installed Load vs. Total Separation Under High Horizontal Stress Conditions

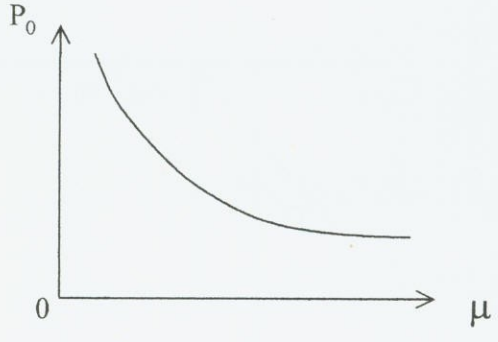



Fig. 8 Relationship Between Optimum Installed Load and Frictional Coefficient at Bedding Plane

16th CONFERENCE ON GROUND CONTROL IN MINING

# A Study of the Performance of Glass Fibre Rock Reinforcement Components

*Jonathan P. Furniss,* Postgraduate Student
*David J. Reddish,* Lecturer
Department of Mineral Resources Engineering
University of Nottingham
Nottingham, UNITED KINGDOM

*Graham Adkins,* Managing Director
MAI Systems UK Ltd.
Tuxford, Nottinghamshire
UNITED KINGDOM

## ABSTRACT

The paper describes a range of laboratory tests undertaken on full column resin anchored glass fibre rockbolt systems, to assess all aspects of their performance. Laboratory instrumentation has been developed for the accurate study of strain transferral from the Glass Fibre Reinforced Plastic (GRP) bolt, through the surrounding resin annulus, and into the rock.

Experience in laboratory testing to the new British Standard on glass fibre rockbolting is discussed. A critical comparison is made of the influencing parameters affecting underground rockbolted roadway performance to the parameters assessed by BS 7861: Part 1.

The work has been co-funded by MAI Systems UK Ltd. who supply GRP rockbolt components to the British coal mining industry, mainly for the reinforcement of coal ribsides. In rockbolting, glass fibre has a number of useful qualities which are discussed in the paper. These properties make the product more suitable than steel in certain applications, both in mines, and other engineering structures such as tunnels, soil stabilisation, and coastal defences.

## INTRODUCTION

GRP is a composite material and has two major components: continuous glass fibres held in a polyester resin matrix. Individual glass fibres are wound in bundles onto large rovings, which are all placed on a racking system. The ends of all the bundles are brought together through a bath of catalysed resin and are directed into a heated die. Excess resin is squeezed off the fibres as they enter the die. They are pulled through the die by a machine at the opposite end to the stack of fibre rovings. The speed of pulling, or pultrusion, is controlled to allow enough time for the composite to cure inside the die by an exothermic reaction. A continuous circular bar is produced, which is then cut to length and a threaded end system put on the bar to form a rockbolt.

In Australian longwall mining, resin anchored wooden dowels were first used as cuttable ribside reinforcement. These dowels had very limited effectiveness in controlling rib stability due to the low strength of the wood, and the poor bond strength between the dowel and the encapsulating resin. The next stage of development was an untensioned GRP dowel which suffered from the same basic problems as the wooden dowel. Next, came a tensionable plastic rockbolt to attempt to improve rib support confinement and reduce coal spalling. Tensionable GRP rockbolts followed which had much higher tensile and shear strengths. These were designed to tackle high shear stress environments. Finally, and more recently, in Australia, a tensionable mechanically anchored GRP rockbolt has enjoyed great success. This bolt, the RIMA dowel, is yieldable to cope with large rib movements[1].

Development of the surface texture of the bolt has been of major importance to the success of GRP rockbolts. Initially, attempts were made to roughen the surface of the very smooth bar which emerged from the pultrusion process. This was attempted by abrasion and/or the bonding of sand to the surface. These surface treatments resulted in a bolt which de-bonded from its encapsulating resin at a load far below its tensile capacity. Later, fabric tapes were used in the pultrusion process to give the bar a rough surface finish. Novel surface textures are investigated here, with the aim of developing a flexible rockbolt manufacturing process to cater for the exact requirements of the end user.

GRP has some advantages over the commonly used steel rockbolts. These are: longevity and corrosion resistance - a review is made of the important aspect of corrosion in rockbolting, and to what extent this can be overcome with the use of GRP components; also, cuttability, lower density and ease of handling, and cost effectiveness when compared to other specialised materials such as galvanised steel. Another useful aspect of GRP rockbolt components is their flexibility. They can be supplied with couplers and in tube form for deeper reinforcement where space is limited.

Various properties have been determined for the MAI GRP rockbolt, and are summarised in table 1. An AT steel rockbolt, commonly used in UK coal mines, has been tested and results from these tests are provided for comparison.

Table 1. Properties of MAI GRP and steel rockbolts

| Property | GRP | Steel |
|---|---|---|
| Mass (kg/m) | 0.79 | 2.93 |
| Tensile Strength (MPa) | 920[a] | 826 |
| Modulus of Elasticity (GPa) | 48.8 | 217 |
| Shear Strength (MPa) | 326 | 643 |
| Torsional Strength (Nm) | 54 | nd |
| Max. Bond Load (kN) | 330[b] | 280[c] |
| Max. Load on End System (kN) | 86 | 303 |
| Max. Load on Couplers (kN) | 60 | nd |
| System Creep (mm) | 0.74[d] | nd |

nd Not determined
a Theoretical
b On an embedment length of 450 mm
c On an embedment length of 125 mm
d On an embedment length of 300 mm, with a 2.25 tonne mass attached to the bolt

## BASIC PHYSICAL AND MECHANICAL PROPERTIES OF THE DOWEL

Due to the nature of the material, difficulties can arise in determining basic properties for a GRP rockbolt, such as its tensile strength. Different methods of testing have been reviewed, and compared where possible, to gain an appreciation of the ease and accuracy of the test method. Because GRP is a composite material, the quantity of glass fibres in the bar needs to be accurately determined and checked. A consequence of the unidirectional nature of the fibres is that the torsional strength becomes important. Problems also arise when attempts are made to fix a threaded end to the rockbolt, development of these systems is also discussed.

### Density

The relatively low density of GRP, compared to steel, means that GRP rockbolts are easier to handle in underground situations. A 22 mm diameter GRP bolt has a mass of 0.79 kg/m, for steel this value is 2.93 kg/m. The obvious advantage is that a GRP rockbolt weighs a quarter of that of a comparable steel one. It is therefore much easier to install when the bolt length becomes very long, especially in difficult locations.

### Fibre Volume Ratio

This is the fraction of the total volume of the composite which is taken up by glass, and was determined by a Loss on Ignition Test[2]. Small disc samples were cut from the rockbolt. These were conditioned in a drying oven, for 24 hours at 50°C, these were weighed and their density determined. The samples were placed in an ashing furnace, set to 625°C, until all the polyester matrix was burned off (after roughly 2 hours). The remaining fibres were weighed, their density was taken as 2.54 g/cm$^3$[3]. The fibre volume ratio, $V_f$, was calculated from equation 1, and found to be 0.661. In general, the strength of the composite increases with increased glass content, until a point where not enough matrix is present to bond the fibres together. Increasing $V_f$ much above its current value would probably not increase the strength of the rockbolt.

$$V_f = \frac{M_f / \rho_f}{M_c / \rho_c} \qquad (1)$$

where

$M_f$, $\rho_f$ = mass and density of fibres, respectively
$M_c$, $\rho_c$ = mass and density of composite, respectively

### Tensile Strength

The theoretical uniaxial tensile strength, UTS, of the GRP bolt is 920 MPa, calculated on a volume fraction basis. Knowing the tensile strength of both the glass fibres and polyester resin constituents. The UTS can be measured in the laboratory, from tests on specially prepared and machined specimens; or from double embedment pull tests, where the rockbolt is embedded inside two thick walled steel tubes. The double embedment test is discussed in more detail later. Problems always arise when GRP is gripped in tensile tests. The sample ends are crushed during the test by the jaws of the test machine as the clamping force increases when the tensile load is increased.

Using machined, dumbbell shaped, specimens[4], where the bolt is machined to 60% of its original diameter and then subjected to a tensile force. The average UTS was found to be 576 MPa for the MAI bolt. This relates to a failure load of 219 kN for a bolt of 22 mm in diameter. In a double embedment pull test, loads of up to 330 kN have been applied to the MAI "rough textured" bolt (see fig. 4a). At which point a bond failure occurred between the encapsulating resin and the bolt surface, see section on surface properties. Hence, it is felt that the use of machine specimens can lead to low estimates of UTS, this is probably affected by the crushing phenomenon. In a double embedment pull test, if the embedded length of the bolt was long enough, the true tensile strength of the bolt could be reached.

A method for the determination of in-plane tensile properties of polymer matrix composite materials, reinforced by high-modulus fibres, exists[5]. This method calls for the use of specially produced coupons of 1 mm thickness. These could conceivably be machined from the original rockbolt material. However, in polyester resin based GRP rods shrinkage cracks always exist in the core, due to cooling of the bar on emergence from the die in the pultrusion process. These cracks do not cause a problem when confined by the surrounding composite material. But, by wasting the rockbolt to a millimetre thickness in the centre of the bar, the effect of these cracks on the measured UTS may be distinct.

Another method of estimating the UTS of the GRP rockbolt is by the measuring its Flexural Strength[6], (fig. 1). Although this method is intended for inspection and quality control of the glass fibre rovings, a good estimate for UTS, of 810 MPa, was given by this relatively simple method.

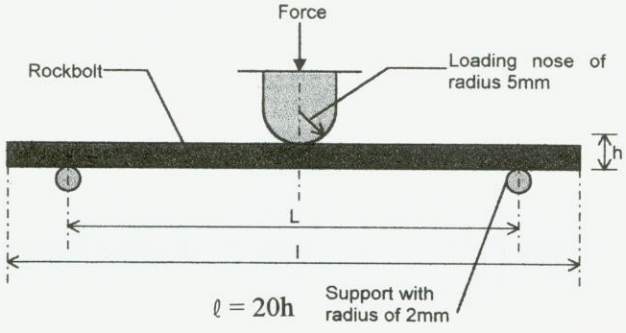



Figure 1. Detail of flexural test method.

Here, the Three Point Bend Test Method[7] is employed. This involves the application of a force to the rockbolt until failure occurs. The rockbolt, of diameter $h$, and length $l$=20$h$, is placed on two supports at a distance $L$=16$h$ apart. The rod is bent to fracture and the maximum force is used to calculate the flexural strength.

Modulus of Elasticity

The modulus of elasticity, E, of a GRP rockbolt can be measured in either of two ways - in tension[4,5], or in flexure[7]. Both methods have been used to evaluate this property. Machined (dumbbell) samples have been used. An average of 48.8 GPa can be achieved for E using this method. Unmachined samples have also been used as a bench test incorporating a hollow cylinder ram. Through which the bolt is inserted, and a clamp at either end of the bolt. This method has given a value of 49.2 GPa.

Alternatively, the Three Point Method has been used to evaluate $E_b$, the Modulus of Elasticity in Flexure (fig. 1). The average value derived using this method was 48.6 GPa, very close to that derived from the tensile test. Again, this is a relatively simple test compared to that outlined above, and involves no machining of the sample.

Shear Strength

One of the most useful properties of GRP in rockbolting is its relatively low shear strength (compared to steel). This allows it to be used in applications where subsequent cutting of the bolt will occur, such as in coal ribsides in longwall mining, and in forepoling in tunnel drivages. The use of standard steel rockbolts here would incur damage to any mechanised cutting head used for subsequent cutting of the reinforced strata.

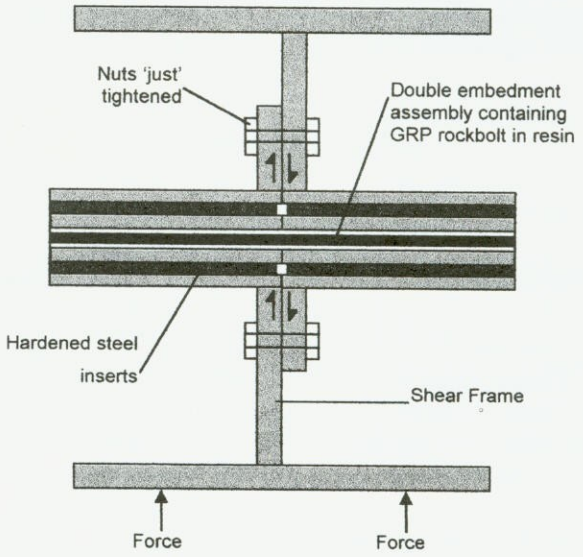



Figure 2. Section through the shear test apparatus.

The shear strength of the product has been measured in a double embedment shear test (fig. 2). This test is covered

by BS 7861[8], the recent standard covering rockbolt components used in coal mines, and is referred to throughout the paper. The average value derived from this single, sharp edged test is 326 MPa, this relates to a maximum shear force applied to a 22 mm bolt of 124 kN, the BS requirement is 120 kN.

Torsional Strength

Due to the unidirectional nature of the pultruded GRP rockbolt, it has a low resistance to torsional loads. These loads typically occur during installation of the bolt. As the rockbolt is spun through the resin cartridge, which is used to secure the bolt in the borehole, applied torque levels are low. Here the bolt remains intact. However, problems can occur during any pretensioning stage. If the fast setting resin at the back of the hole has cured, pretension can be applied to the bolt. This is applied as the slow setting resin along the full column of the rockbolt cures, by applying a torque to the end system. If the torque setting on the installation machine is set too high, the bolt can be twisted until the fibres dislocate.

The strength of the rockbolt in torsion has been measured in the lab. The plain end of the rockbolt was clamped in the 3 jaw chuck of a lathe, on the opposite (threaded end) a locknut was positioned. A socket over the nut was connected to a shaft, fixed in the centreline by clamping it to the tool post on the lathe. A torque wrench with a dial indicator was attached to the shaft As the chuck of the lathe was steadily turned it was possible to monitor the torsional load applied to the rockbolt. The torque required to break the bolt was 40 ft-lbs (54 Nm). This value relates to a pultruded rod with minimal shrinkage cracks, and no clearly visible separations in the fibre structure.

## SURFACE PROPERTIES

Safety

Flame retardancy and anti-static properties are important in coal mining applications. GRP rockbolts have been used for a number of years in UK coal mines, having gained acceptance in terms of the rockbolt's electrical resistance and flame retardancy. A 'carbon black' additive in the resin matrix decreases the electrical resistance, over a 100 mm length, to a value of $8.5 \times 10^6\ \Omega$. This is to ensure that a static charge can not build up on the bolt surface. The composite material is not readily combustible. After being subjected to a flame for 60 s, the persistence of flame or glow is less than a second. Both of these properties are covered by BS 7861. The requirements are a resistance of less than $10^9\ \Omega$, and a persistence of flame less than 10 s.

Bond Strength Between Rockbolt and Resin

Currently, the GRP rockbolts on the market mostly incorporate a rough surface texture, which is imparted on the bolt by the use of a fabric tape. This tape wraps around the bolt as the resin coated fibres are pulled into the die, and subsequently peels off as the cured bolt comes out of the die. The pattern on the inside surface of the tape ends up being the opposite of that on the surface of the rockbolt This finish is similar to the knurled one put on round steel components in order that they may be gripped by hand and twisted (fig. 4a). This type of rockbolt has gained wide acceptance for use in UK coal mines.

The tapes used in the manufacture of the bolt slow down the pultrusion process, faster rates of production could be realised without them. This means if they were omitted, a cost saving could be made in the manufacture of the rockbolt which could be passed on to the end user. However, this would lead back to the initial problem of having a completely smooth bolt which does not bond well to the encapsulating resin. Hence, a different approach to the problem of generating a good surface texture is required where the cost of the bolt is an issue or peak performance is not required. For this purpose, an investigation was made into a smooth bolt which had subsequently been machined with a scrolling groove along its full length (fig. 4b). The requirement here is that the cost of machining the bolt is lower than the cost saving by omission of the fabric tapes.

Double Embedment Pull Testing This test is covered in BS 7861. It involves the use of two thick walled steel tubes which are threaded on the internal surface with a ½ mm deep, 2 mm pitch thread. The internal diameter is 27 mm for a 22 mm rockbolt. The steel tubes are firmly joined together and one end is capped. A slow set resin is poured in and the rockbolt is inserted, whilst twisting it, to form a full column resin annulus along the whole length of the bolt (fig. 3). The embedment length is 450 mm.

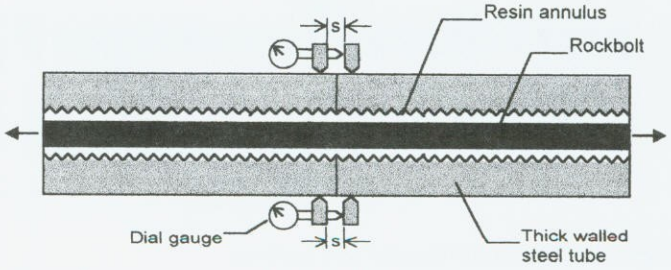



Figure 3. Arrangement for the double embedment pull test.

After the encapsulating resin has been allowed to cure for 24 hours, the two steel tubes are pulled apart in a tensile testing machine. The load is increased at 3 kN/s, whilst monitoring tube separation, s, with two dial gauges. An

attempt was made to investigate whether voids were formed in the resin column as it rose up the annulus between the rockbolt and the steel tube. If so, low bond strength values would be measured. A smooth bolt was inserted in the above manner, and then pulled out. After the bolt was completely free of the steel tube, a bright light was shone up the hole left behind. The resulting internal surface of the resin column was found to be perfect along the whole length. It is accepted that the rapidly rising resin column (on insertion of the bolt) is more likely to be void free when using a smooth bolt rather than a textured one. In order to analyse the latter arrangement the steel tube would have to be cut along its length, and the resin annulus examined.

Three different types of bolt have been tested. The traditional 'rough textured' bolt (fig 4a); the machined bolt (fig. 4b); and an 'overwound' bolt (fig 4c). This last rockbolt is manufactured by another company, and is one which has been overwound, in a scrolling fashion, during the pultrusion process, with a bundle of glass fibres. This overwind pinches the bolt where it makes contact, and thus, a ribbed effect is produced with peaks and troughs along the bolt. Bolt texture in fig. 4a is slightly exaggerated.

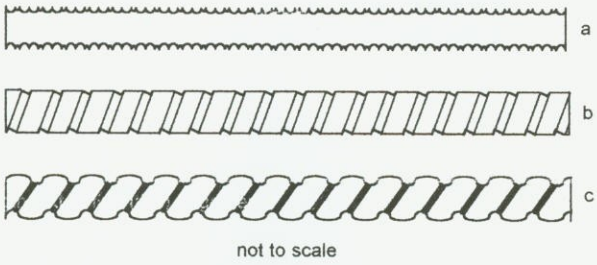



Figure 4. Different styles of rockbolt tested for bond strength.

Results

MAI ROUGH TEXTURE A maximum pull out load of 330 kN was achieved with this rockbolt. The texture imparted by the fabric tape in the pultrusion process bonds well to the encapsulating resin. The outer fibres are continuous and undisturbed, the surface texture is composed of ridges of polyester resin matrix. Failure occurs along the interface between rockbolt and resin.

MACHINED WITH GROOVE This rockbolt is less strong than the roughly textured one. This is due to the fact that the outer fibres along the bolt have been cut with a scrolling groove (fig. 5). It is these outer fibres which transfer load to the surrounding resin. When the fibres are interrupted in this way, stripping of the outermost ones can be observed. The notch depth, $d_n$; notch width, $w$; and the notch separation, $s$, can all be varied in the manufacturing process. The width is determined by the width of the tool used to cut the notch. The notch separation is controlled by the pitch of the groove cut along the length of the rockbolt. Various different styles of machined rockbolt have been tested for maximum pull out load. The effect of changing the notch shape, width, depth and separation have all been investigated.

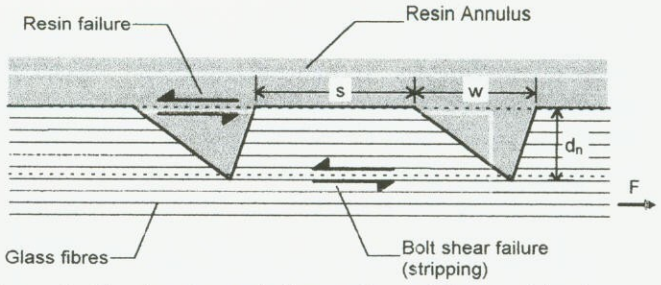



Figure 5. Section through the surface of the machined rockbolt.

The following conclusions have been drawn. Increasing notch depth, $d_n$, does not necessarily increase the maximum pull out load of the rockbolt for depths greater than about 1.5 mm. By increasing $d_n$, the area of the central 'undisturbed' core of the rockbolt is decreased. Hence, the maximum load which the rockbolt can carry is reduced. In terms of maximum load, the notch shape (square cut, 'U' shape, or 'V' shape) is not so important a factor as the ratio of notch separation to notch width, $s$:$w$. The shape of groove easiest to manufacture was a 'V' shape, giving a sawtooth effect (fig. 5).

The effect of varying $s$:$w$, with all shapes of groove, is illustrated in fig. 6. It can be seen that the optimum ratio of separation to width of the notch occurs at around 1.8, giving a failure load of around 280 kN. This translates to a 'V' shaped groove, 5 mm wide at its top, cut at an 8.5 mm pitch. Similarly, a square cut groove could be made 6 mm wide, at 11 mm pitch. With these configurations, a useful post-failure characteristic can be observed. Usually, two residual peaks occur which are nearly as large as the initial peak.

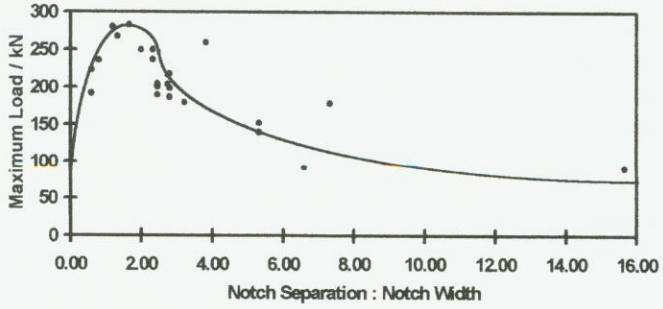



Figure 6. Variation of maximum pull out load with notch configuration on machined bolt.

When *s:w* is roughly greater than three, the failure mode is by shear in the resin annulus along the surface of the bolt. When *s:w* is less than three, the failure mode is by stripping of the outer fibres of the rockbolt; as these have become dislodged from the central core. Direction of failure slightly favours the shallow side of a 'V' notched rockbolt.

The stiffness' of three different 'V' notched rockbolts are compared in fig. 7. It can be seen that the notched rockbolts all have a similar stiffness, but it has been shown that the maximum load on pull out depends on the value of *s:w*. Maximum loads are not shown in fig. 7.

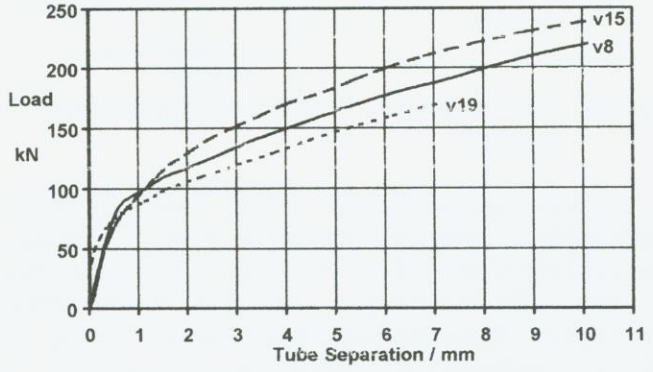



Figure 7. Tube Separation vs. load for an 8, 15 and 19 mm pitch 'V' notched rockbolt.

OVERWOUND (fig 4c) The highest maximum load was achieved with this rockbolt, in fact, with a 450 mm embedment the tensile strength of the bolt was reached. The load attained here was 378 kN for a nominal 22 mm diameter, this translates to a tensile strength of 994 MPa. This is higher than the 920 MPa theoretical strength of the MAI rockbolt. The reason why such a high pull out load is achieved with this type of rockbolt is that the surface is very coarsely textured, whilst outer fibres remain undisturbed. The continuous unidirectional nature of the fibres is preserved along the full length of the rockbolt and it is the fibres themselves which compose the surface texture.

Interlaminar Shear Strength

With the machined rockbolt, the highest pull out loads are obtained when stripping of the outer fibres occurs. The load at which failure occurs should be linked to the interlaminar shear strength of the composite. There is no method available for exact determination of this property for plastics[3]. A method for measurement of shear properties on plastics is the punch tool test. The rockbolt is cut into discs, which are sheared through by a punch and die arrangement (fig. 8). The nearer the internal diameter of the die and the external diameter of the punch are, the closer is the approximation to pure shear.

ASTM D 732-90[9] assumes a specimen which is drilled centrally to take a guide pin on the punch. A larger (50 mm) diameter disc is required with a thickness of 0.13 - 12.7 mm. Only 22 mm diameter rod was available for testing. Method 305A of BS 2782: 1970[10] allows the use of a disc which is 1.59±0.13 mm thick. Both methods require that the edges of the disc are clamped in place. This was not the case for the tests done here.

The interlaminar shear strength, $\tau_{il}$ was found from equation 2. The value ranged from 35 MPa for a disc thickness, T, of 3 mm; to 49 MPa for T = 10 mm. Although there was a fair amount of scatter in the results, shear strength variation in this region appeared to be linear. The reason for the scatter might be due to the disc not being clamped in place during the test.

$$\tau_{il} = \frac{W}{\pi dT} \qquad (2)$$

where W = force at fracture
$\pi$dT = shearing surface area if
d = diameter of punch
T = thickness of specimen

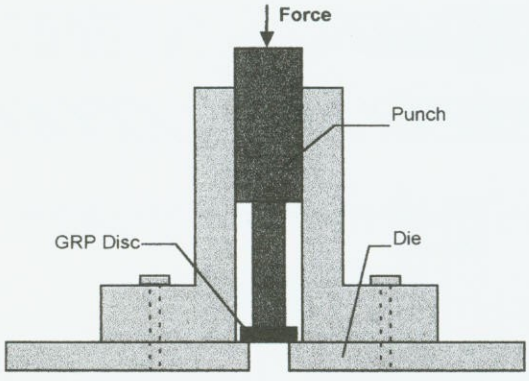



Figure 8. Section through Punch Tool apparatus to determine interlaminar shear strength of GRP material.

A more accurate value may be determined by following ASTM D 3914-80, this involves the compression of a cylindrical specimen. The specimen is made to shear between two centrally located notches, diametrically opposed and machined halfway through its diameter[11].

The mode of failure of the disc in the punch tool test is similar to that of the rockbolt in-situ. However, when the effective area of the shearing surface along the length of the embedment is taken into account, the calculated shear stress at failure ≈ 10 MPa. This value was calculated where $d_n$ = 2 mm, $w$ = 4.5 mm, and $s$ = 13.5 mm. Maximum force was

203 kN for an embedment length of 450 mm. The simplified shear strength was calculated from equation 2 by using 20 mm as the diameter of the sheared surface. And substituting 'separation÷pitch' x 'embedment length' for the thickness. However, it has to be considered that the continuous central core of bolt (18 mm) could carry a maximum of 234 kN, given its UTS of 920 MPa.

$$\tau = \frac{203 \times 10^3}{20\pi\left(\frac{13.5}{19}\right)450} = 10MPa$$

This analysis attempts to take into consideration the effect of the scrolling groove in the rockbolt. It may be that its effect is too complex for this simplified analysis. More vigorous methods of elemental analysis may give a better understanding of stress transferral from bolt to resin. The problem is exacerbated by the anisotropic nature of the GRP composite material.

## PROPERTIES OF THE GRP ROCKBOLTING SYSTEM

### End System Strength

The strength of the thread and plastic nut system on the end of the rockbolt is an important aspect of rockbolts made from GRP. It has been thought of by some as being the weak link in the system, especially in the Civil Engineering industry. With conventional steel bolts, it is possible to machine a threaded end onto the bolt which can carry a load equal to the tensile strength of the bolt itself. As discussed earlier, with unidirectional fibre composite materials, when the bolt is machined to produce a thread, as in the MAI product, the outer fibres are disrupted. So the UTS of the composite can not be utilised on the end system.

Much work has been done to maximise the end load capacity of the system, using a specially designed 'reversing cage' (fig. 9). The thread geometry (½" pitch) and the nut's characteristics have been optimised to give a system which not only has an end load capacity of 86 kN, but also exhibits residual peaks and troughs after the first peak load has been achieved (fig. 10) [12]. The BS requirement is 60 kN. More elaborate, larger, plastic nuts have also been developed which give an end load capacity of up to 150 kN. The resulting system has a continued strength after the peak load has been passed, unlike the moulded threads which are used by other manufacturers. These end systems are composed of a moulded plastic sleeve, which is bonded to the surface, a thread is cut into its outside surface. Other products exist incorporating very large nuts fitting onto moulded threads, having an end load capacity of up to 160 kN.

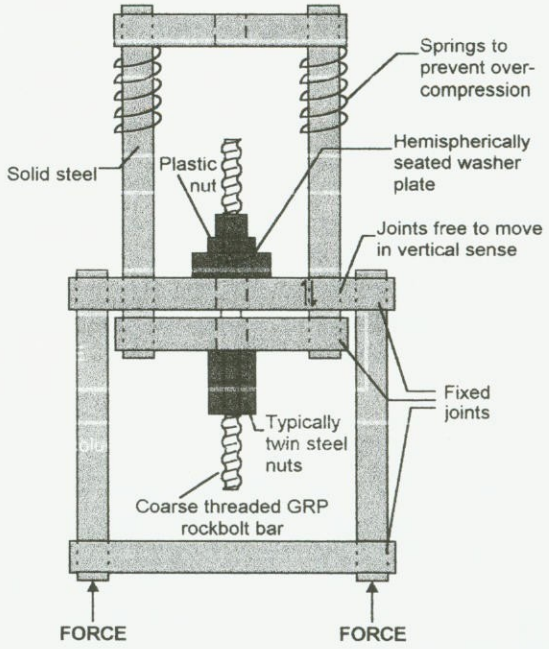



Figure 9. Side elevation of reversing cage used for the testing of rockbolt end systems.

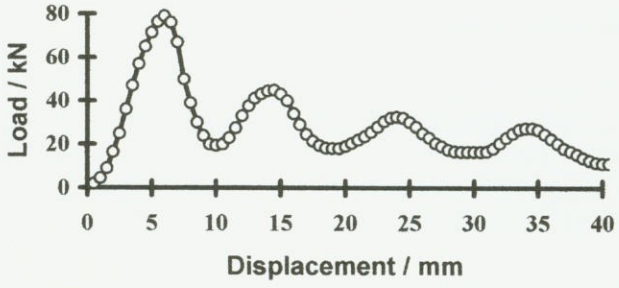



Figure 10. Typical Force Displacement graph as a plastic nut pulls over a MAI GRP machined thread.

Tests have also been undertaken to optimise the load at which the nut will 'pull through' a plastic patch plate to fulfil UK mining requirements. These tests were conducted on the bench using a calibrated, hollow cylinder, hydraulic ram. Ram pressure was gradually increased, using a pump, whilst monitoring the pressure gauge. The maximum load on pull through; which has been achieved with a large diameter plastic plate, incorporating a small plastic insert, is 67 kN. The BS requirement is 50 kN.

### Tubular Injection Rockbolts

GRP rockbolts can be supplied in tube form for deeper reinforcement, where required. These tubes can be coupled

together to form a longer (stiff) bolt than is possible to install - given the height or width limitations of the tunnel. Tube forms are used for injecting resin or grout to the back of the hole, rather than spinning through a resin capsule - over a very long length this becomes impractical. Tests have been undertaken to measure the end loading capacity of a tube which has been filled with grout and allowed to cure. The objective being to provide resistance to implosion of the tubular shaped rockbolt during the test. Results do not differ from those involving solid sections. In terms of the UTS of the rockbolt, this is a function of the effective cross sectional area. With a nominal hole diameter of 10 mm, the cross sectional area is reduced by 21%, when compared with a solid rockbolt. Hence, the theoretical UTS of the tube form is 730 MPa.

Tests have been undertaken to mimic injection of grout through the rockbolt and evaluate the maximum injection pressure achievable. The rockbolt was filled with oil, and the open end attached to a hydraulic ram. Ram pressure was slowly increase, the pressure gauge on the pump was monitored whilst observing the rockbolt for leakage. These always occur where the bolt is thinnest, i.e. where the rockbolt has been machined to form the threaded end. The average maximum injection pressure applied before leakage occurred was 433 psi.

### Rockbolt Couplings

A variety of rockbolt coupling devices have been tested in a straight tensile test. Couplers machined from metals have yielded a maximum tensile load resistance of around 60 kN. A prototype hand-woven Kevlar coupler has proven to be stronger, carrying an average tensile load of 88 kN.

### Long Term Creep

Creep in the system has been measured for a rockbolt, resin bonded into a block of limestone. The bonded length was 300 mm, the hole diameter was 35 mm. A 2¼ tonne block of steel was hung from the rockbolt via a hook system attached to the nut on the end of the rockbolt. Fig. 11 shows the movement of the free length of the rockbolt (measured with a dial gauges) relative to the rock face. This was limited to 0.74 mm in over 6 months.

### Installation

Tests have been done to evaluate the effectiveness of resin mixing during 'spinning in' of the rockbolt. This was done by installing the bolt inside a clear perspex tube, using a fast-set and a slow-set resin cartridge. As the fast set resin cured, the tube began to spin with the bolt. This was partly due to the hole diameter being slightly too small (26, not 27 mm) and that the tube was not fixed to the bench firmly enough. On observation of the complete installation though, it became apparent that the short fast-set resin at the back of the hole did not get a good mixing. This was due to the fact that the bolt was too short for the hole it was put in, even though the guidelines for installation of this system had been followed. This draws attention to the need to drill holes accurately to the correct length, taking into full considering the length of the threaded portion.

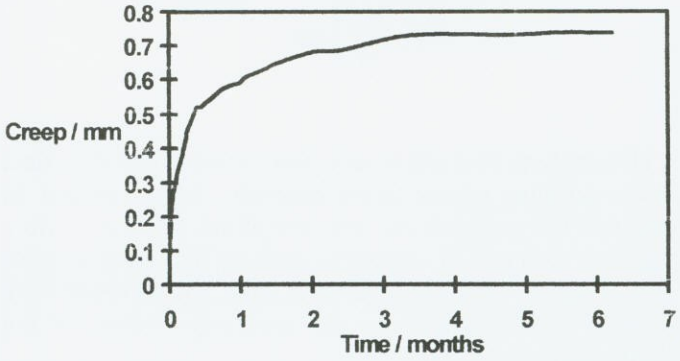



Figure 11. Long term creep test of a GRP bolt, resin bonded into a block of rock.

## ANALYSIS OF STRAIN TRANSFERRAL FROM BOLT TO ROCK

### The Different Methods of Measurement

For the accurate measurement of strain transferral from bolt, through the resin and into the rock; a series of tests are being conducted. The first is by a fully strain gauged pull out test in a sandstone block, this test has already been conducted. The second test, again, is a fully instrumented pull test in the lab, but using a tensile testing machine.

### Rock Block

A 1.4 m long GRP rockbolt was strain gauged, a resin layer was placed over each gauge, machined flat and another gauge placed on top. A corresponding gauge was bonded

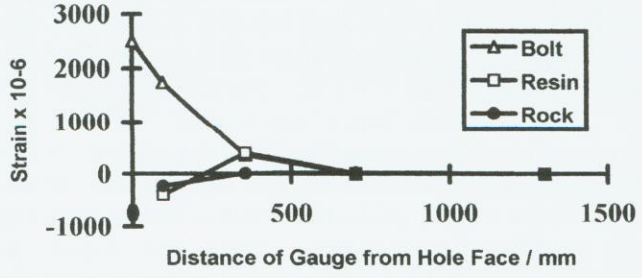



Figure 12. Relative strains on the bolt, inside the resin annulus and on the rock surface

to the internal surface of the borehole. The end system was loaded with a hydraulic ram up to 44 kN. The results are summarised in fig. 12. It can be seen that any load applied to the end system has limited effect down the hole at this low value.

Laboratory Instrumentation

In order to get by the awkward problem of loading the bolt to failure (this cannot be done using a threaded end system on a GRP rockbolt) a new test has been devised (fig. 13). This involves the embedment of the rockbolt inside a core of rock; which is, in turn, embedded inside a steel tube. Again, strain gauges are bonded onto the bolt, rock and inside the resin annulus to analyse strain transferral. The steel tube is pulled apart inside a servo-hydraulic stiff testing machine. Hence, the load applied can be very accurately controlled and held at values reaching the point of either bond failure, or tensile rupture of the bolt.

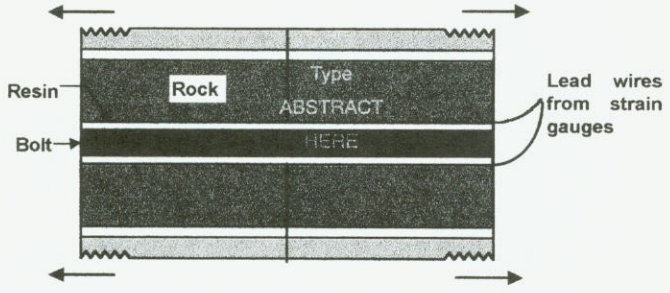



Figure 13. Fully instrumented pull test apparatus for measurement of strain transferral up to failure.

## CORROSION IN ROCKBOLTING

It has long been understood that GRP can offer excellent resistance to corrosive environments. This property can be of use in the underground environment. Where aggressive waters flow into tunnels, carrying high concentrations of sulphur dioxide and chlorides. Or where highly acid, or alkaline, waters are encountered, problems can occur with corrosion of steel rockbolts. Theoretically, the full column of resin grout surrounding the rockbolt should offer protection to the rockbolt from inflowing water. However, this assumes that the bolt has been installed in the centre of the borehole; that the resin encapsulation is watertight and has no breaks in it; also that all the resin has remained in the borehole during installation. Where the borehole has been drilled through fissures and voids, grout leakage into these holes can occur. Where any, or a combination, of these factors occurs there is the possibility for corrosive water to attack the surface of the rockbolt, turning the steel into iron oxide over a period of time. Subjected to water, of pH 4 to 7, the corrosion rate for steel is 0.1mm per year.

The currently available solutions to corrosion include galvanisation and epoxy coatings on standard steel rockbolts. Stainless steel is available for friction stabilizers. Integral polyethylene sleeves are supplied for mechanically anchored rockbolts. In civil engineering, corrugated plastic pipes are used as a barrier between the surface of the borehole and the steel rockbolt surface. Hence, borehole diameters are much larger. These processes all increase the cost of the rockbolt installation. With GRP, no additional measures should need to be taken in such circumstances.

A program of long term, accelerated, corrosion susceptability testing has been embarked upon to test the corrosion resistance of GRP rockbolts. There exists in composite materials a phenomenon called 'Environmental Stress Cracking'[13]. This can occur under conditions of attack from an aggresive environment, whilst the bolt is placed under a constant tensile stress. The effect of variation of both the chemical environment and the applied bolt stress is being investigated.

## BS7861: Part 1: 1996

Experience has been gained in testing to the new British Standard covering rock reinforcement components in coal mines. Section 5 of this standard covers features of GRP rockbolts and components. This standard was built around a number of tests applied to components which had previously been accepted for use in UK coal mines. It is of no surprise then, that the MAI product has properties closely matching the requirements of the standard, since it has been used for a number of years in UK coal mines. Some of the test methods in this standard deserve comment here though.

The standard requires that there be an installation feature, allowing the rockbolt to be installed prior to torqueing. This usually takes the form of a positive drive by means of a steel adapter to the thread form or a breakout facility on the nut, where the plastic nut is fitted with a blank end. In the UK at present approximately half the bolts are installed by each of these methods. The thickness of the end piece is set to allow spinning in of the rockbolt through the resin capsules. At a predetermined torque setting (40-125 Nm), the nut breaks out the end piece and is driven against the face plate. Torque is then applied to the drill to generate a small pretension in the bolt. Care must be taken here to avoid damage to the rockbolt by application of high torsional loads (see torsional strength). It has been found that the laboratory determination of nut breakout torque (following the BS) can give misleading results. Even though breakout nuts may work perfectly in the lab, installation failures have been observed underground. This



could be due to elevated temperatures in mine environments causing alteration of the plastic nut's properties, or, torque settings on installation equipment being inaccurate.

Bond strength, as defined by the standard, is the point at which the system stiffness falls to 20 kN/mm. This is determined from the load/extension graph for a pull out test at 450 mm embedment length, and should be greater than 245 kN. It is not understood why this stiffness limit has been chosen, and in fact, maximum pull out load is not addressed by the standard. This requirement is aimed to generate a coal rib which is reinforced to become as stiff as possible given the current cuttable rockbolt materials technology. At some mines however, very low levels of rib dilation can be observed. In these situations, the operator is forced to purchase a higher cost product than is necessary, in order to comply with the BS. The other scenario is where very high levels of rib dilation can occur, mobilising the UTS of the bolt very quickly. A rockbolt could be manufactured to comply with the standard, but however, exhibit no residual load bearing characteristic. Hence, when the maximum load of the bolt has been achieved, the bolt would break and would have to be replaced with another alongside.

The suggested method of determining the UTS of the rockbolt has been found to be completely impractical. The BS suggests the use of clamps on the ends of the bolt. A force is applied between these, and the requirement is a minimum failure load of 300 kN. It has been found that such clamps always slip at a load of around 80 kN, the estimated maximum load carried by the bolt is 350 kN. As mentioned earlier, the flexural test[6] may be the easiest way to estimate UTS.

## CONCLUSIONS

Standard and novel test methods have been applied to GRP rockbolt components in order to identify all aspects of their performance. It has been shown that some properties of GRP rockbolts are difficult to determine and care is needed when testing for these values, such as UTS. A flexible system of bolt manufacture has been developed to supply operators with a more cost effective solution to their particular problems. The new BS for rockbolt components in coal mines has affirmed the current performance of existing products, however, problems have occurred in testing to this standard. GRP components can provide an effective solution to rockbolting in aggressive or corrosive environments and long term structures.

## ACKNOWLEDGEMENTS

This work could not have been undertaken without the co-operation and aid offered by MAI Systems UK Ltd.

## REFERENCES

1. Skybey, G., "Continuous Improvement in Cuttable Coal Rib Support in Australian Coal Mines", Proc. of the 14th International Conference on Ground Control in Mining, August 1-3, 1995, pp. 189-193.
2. "Glass Reinforced Plastics: Determination of Loss on Ignition", BS 2782: Part 10: Method 1002: 1977, British Standards Institute, 5 pp.
3. Daniel, I.M., Ishai, O. "Engineering Mechanics of Composite Materials", Oxford University Press, 1994, 28, 306-307, 331.
4. "Standard Test Method for Tensile Properties of Plastics", ASTM Designation D 638-95, 1995, *Annual Book of ASTM Standards*, Vol. 08.01, American Society for Testing and Materials, pp. 45-56.
5. "Standard Test Method for Tensile Properties of Polymer Matrix Composite Materials", ASTM Designation D 3039-95, 1995, *Annual Book of ASTM Standards*, Vol. 15.03, American Society for Testing and Materials, pp. 114-123.
6. "Glass Reinforced Plastics: Determination of Flexural Strength of Rods Made of Roving-Reinforced Resin", BS 2782: Part 10: Method 1008B: 1996, British Standards Institute, 7 pp.
7. "Glass Reinforced Plastics: Determination of Flexural Properties. Three Point Method", BS 2782: Part 10: Method 1005: 1977, British Standards Institute, 5 pp.
8. "Strata Reinforcement Support System Components Used in Coal Mines: Part 1. Specification for Rockbolting", BS 7861: Part 1: 1996, British Standards Institute, 27 pp.
9. "Standard Test Method for Shear Strength of Plastics by Punch Tool", ASTM Designation D 732-90, *Annual Book of ASTM Standards*, American Society for Testing and Materials.
10. Ives, G.C., Mead, J.A., Riley, M.M. "Handbook of Plastics Test Methods", Iliffe Books, 1971, 143-145.
11. "Standard Test Method for In-Plane Shear Strength of Pultruded Glass-Reinforced Plastic Rod", ASTM Designation D 3914-80, *Annual Book of ASTM Standards*, American Society for Testing and Materials.
12. Reddish, D.J., Adkins, G.A., Dunham, R.K. "Glass Fibre Rock Reinforcement", Proc. of Roofbolting in Mining, Aachen, March 27-28, 1995, pp 133-153.
13. "Determination of ESC by the constant tensile stress method", BS 2782: Part 8: Methods 833A-C: 1993, British Standards Institute, 8 pp.

16th CONFERENCE ON GROUND CONTROL IN MINING

# A Method for the Selection of Rock Support Based on Bolt Loading Measurements

*Stephen P. Signer,* Mining Engineer
*Dennis Cox,* Engineering Technician
*Joanne Johnston,* Engineering Technician
National Institute for Occupational Safety and Health
Spokane Research Center
Spokane, WA

## ABSTRACT

A method to assist in the evaluation and selection of roof bolts using in situ measurements of roof bolt loading has been developed by researchers of the Spokane Research Center, National Institute of Occupational Safety and Health. Both axial and bending forces are measured by strain gauges at many locations along the length of fully grouted bolts during various stages of mining. This information is then used to (1) predict bolt loading for variations in bolt spacing, grade, and diameter, (2) calculate the design changes necessary in zones where bending loads are high, and (3) determine if bolt length is adequate. Results from several case studies of full-column bolt loading in coal mine gate roads are used to illustrate the design method. This knowledge will give design engineers a tool for the selection of roof support systems that will improve underground safety by reducing roof bolt failures.

## INTRODUCTION

In this paper, a method is described for selecting roof bolt diameter, spacing, and length based on in situ measurements of bolt loading. It is not meant to be used to the exclusion of other design methods and means of analysis. Rather, it should be used as another tool in a well-rounded approach to rock support selection and design. An excellent discussion of rock support design methods is available in Choquet and Hadjigeorgiou *(1)*.

Selection of rock reinforcement depends on many factors that require engineering judgment, such as geology, stress field, geometry, factor of safety, standup time, and estimated risk of roof failure. The intended use of the underground opening will dictate the selection of design loads. In mines, some areas are expected to remain open only for a matter of months, while other areas must remain open for many years. Therefore, more support must be installed where safety or economic interests require greater roof stability.

Civil engineering design approaches include a factor of safety to ensure stability for the life of the project. This is done by limiting the allowable stresses to a percentage of the yield strength or ultimate strength of the material. Mining often allows for the yielding of structures so that the material can be extracted at a minimum cost. This often results in a minimum amount of support installed, and previous research has shown that roof bolts are often loaded well past yield loads *(2-4)*.

The use of strain gauges to measure loading on fully grouted roof bolts has been used successfully to study support-rock interaction mechanics *(5-11)*. Effective use of strain gauges for long-term underground monitoring requires proper installation to eliminate moisture and long-term creep of the glue line *(12)*. Instrumented bolts should be calibrated and cycled many times to check that the gauge has been properly installed. During field investigations, rock deflections should be measured to detect separations in the horizon above the roof bolts.

## DESIGN METHOD

The following assumptions and generalizations are made as part of this design method. The amount of roof bolt loading required to stabilize the immediate roof can vary with respect to distance from ribs and into the roof. This relationship will be referred to as "support load profile." The bolt load depends on amount of area of roof exposed per bolt and the support load profile required for stability. This means that a change in bolt spacing will change bolt load as a function of support load profile. The support load profile consists of both axial and bending loads.

A support load profile can show various aspects of roof behavior. The amount of rock loading that roof bolts are required to support is a function of geology, geometry, and in situ stress fields. In some applications, the skin needs to be controlled while in other areas, roof bolts alone may not be adequate to maintain entry stability. Timing of support installation and distance from the face can also change support loading and roof behavior.

Factors that contribute to bolt loading can be complex and variable. This makes analytical and numerical approaches difficult. A method based on bolt load measurements can be useful to sup-

plement these methods to obtain a better understanding of particular support and rock interactions. Because loading patterns can vary significantly with respect to location, the selection of design loads requires that enough sites be tested to develop confidence in the relationship between bolt load profiles and mining location, geology, geometry, and stress fields. These load profiles can then be extrapolated to an entire area or separate design load profiles can be used when mining conditions vary.

Engineering design typically limits stress to either a percentage of the yield strength or a percentage of the ultimate strength. This safety factor is then applied to prevent material failure. Bolt loads can be axial, bending, and/or shear. Total fiber stress will be a combination of axial loading and bending moments. Axial loading is generally the primary force on a steel bolt. The nature of loading mechanisms and the uncertainties of determining just where loading is taking place makes it impossible to estimate shear loads. When movement takes place along joints, shear loading could be critical in the design of bolt systems, and additional research is required to develop a better understanding of this loading mechanism.

The development of bolt loading profiles requires the installation of instrumented roof bolts during mine development to allow normal rock movement and stress redistribution to load the bolts. The measured bolt locations and axial and bending loads are used to create bolt load profiles. Axial loads cause fiber stress in the bolts according to the formula—

$$\sigma_a = \frac{P}{A} \tag{1}$$

where $\sigma_a$ = axial stress, Pa,
$P$ = load, N,
and $A$ = steel area.

Bending moments measured by the instrumented bolts involve several factors that a design engineer should consider. Maximum bending moments can be localized and may not be accurately measured with an instrumented bolt. Bending is measured in only one orientation because of the limitations of the instrument. If possible, the bolts should be rotated so that they measure the highest estimated bending moment. Bending moments can be caused by joint movement, rotation of large blocks, and/or differential loading in mats and meshes. Considering the source and prevalence of bending loads when using the design formulas is important. Bending loads cause fiber stress in the bolts according to the formula—

$$\sigma_b = \frac{M}{S_x} \tag{2}$$

where $\sigma_b$ = bending stress, Pa,
$M$ = moment, N-m,
and $S_x$ = section modulus, $m^3$.

Total fiber stress then becomes—

$$\sigma_t = \sigma_a \pm \sigma_b \leq \sigma_{max} \tag{3}$$

where $\sigma_t$ = total fiber stress
and $\sigma_{max}$ = allowable fiber stress.

Bolt spacing is the primary variable manipulated in the design process. Both axial and bending loads measured with instrumented bolts can be estimated when using a new bolt spacing based on the following equations—

$$\frac{P}{S_1 S_2} = \frac{P_d}{S_{1_d} S_{2_d}} \tag{4}$$

and

$$\frac{M}{S_1 S_2} = \frac{M_d}{S_{1_d} S_{2_d}} \tag{5}$$

where $S_1$ = bolt spacing across the opening of instrumented bolts,
$S_2$ = bolt spacing down the entry of instrumented bolts,
$S_{1d}$ = new bolt spacing across the opening,
$S_{2d}$ = new bolt spacing down the entry,
and $P_d M_d$ = new load and moment values.

By solving for $P_d$ and $M_d$ and substituting equations 4 and 5 for 1 and 2, and solving for equation 3, then—

$$\sigma_t = \frac{S_{1_d} S_{2_d}}{S_1 S_2}\frac{P}{A} + \frac{S_{1_d} S_{2_d}}{S_1 S_2}\frac{M}{S_x} \leq \sigma_{max} \tag{6}$$

Both $P$ and $M$ are measured axial forces and bending moments derived from the instrumented bolts. The values of $A$ and $S_x$ are derived from the member selected for design considerations. $\sigma_t$ must be less than or equal to the selected maximum stress. Total stresses should be calculated for each bolt location to determine the highest value and must be less than or equal to a design stress based on the factor of safety selected. Safety, engineering judgment, and cost considerations will result in a design selection based on variations in bolt diameter, strength, and spacing.

Bolt diameter and bolt length are two of the major variables changed in the design process. These factors can have a significant effect on roof stability. Adequate anchorage length is also critical to ensuring the stability of the bolted horizon *(13)*. Anchorage length can be evaluated by examining load distribution with respect to the distance from the embedded end of the roof bolt and comparing to estimates of rock anchorage in that type of stratum.

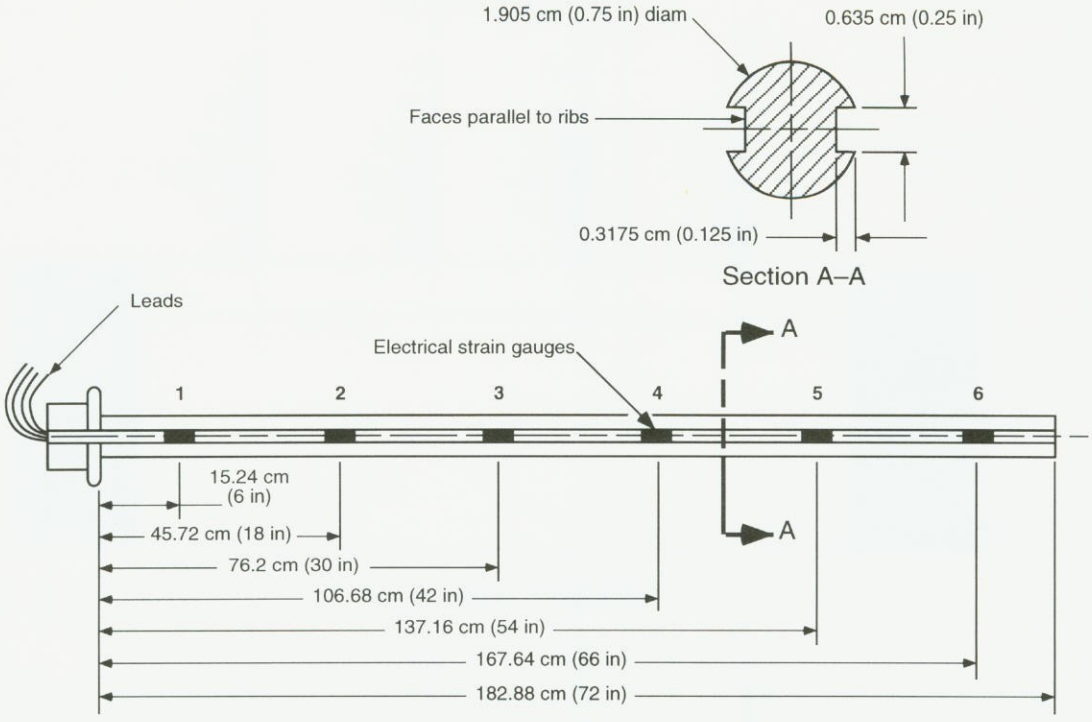



**Figure 1.—Instrumented roof bolt**

## CASE HISTORIES

To illustrate the use of this method, three sets of data from different coal mines were evaluated. Bolts used in these tests were standard grade 60, No. 6 rebar bolts milled with a 6.4-mm-wide by 3.2-mm-deep slot along each side. Strain gauges were installed as shown in figure 1. After milling, the cross-sectional area was 2.39 $cm^2$ and the section modulus was 0.338 $cm^3$. The instrumented bolts were calibrated in a uniaxial test machine to correlate voltage change to load change. During installation, the bolts were oriented with the strain gauges parallel to the ribs to measure localized bending effects in the mine roof. The data collection system was an Omnidata Polyrecorder 516-C. A completion box was made that provided 5-V excitation and completion resistors for the Wheatstone bridge circuits used to measure strain gauge voltage changes.

Five grade 60 bolts were tested to failure to determine the strength and yield point of the bolt after the slots had been milled. The slotting process reduced bolt strength by approximately 10%. A typical load strain curve from one of these tests is shown in figure 2. When the data from the instrumented bolts were reduced, the correlation coefficients from the axial calibrations were used to convert voltage changes to load changes. This process was accurate to ±0.4 kN. When bolt load levels exceeded the yield point of the steel, voltage readings were converted to strain readings, and these values were used in figure 2 to estimate bolt loading. However, converting voltage to strain is not as accurate as converting voltage to load.

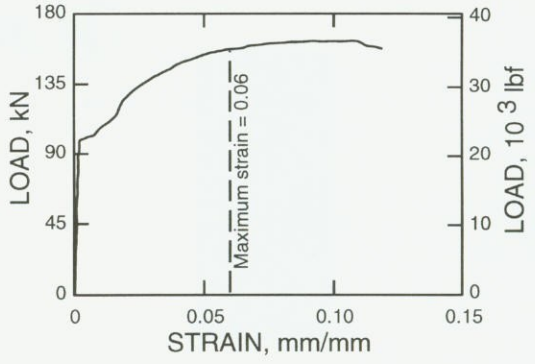



**Figure 2.—Stress-strain curve of slotted roof bolt**

### Site 1

The first test site was located in a two-entry gate road where the coal seam is approximately 2.5 m thick, and overburden is between 210 and 240 m deep. The mine roof is a competent mudstone interspersed with very fine grained sandstone and siltstone. Grouted bolts 1.8 m long, spaced in a square pattern approximately 1.2 by 1.2 m were used as the main roof support. Axial and bending loads shown in figure 3 form the load profile after the pass of the second longwall panel. Bending moments measured were primarily caused by rock loading in the mesh. Maximum fiber stresses are shown in table 1.

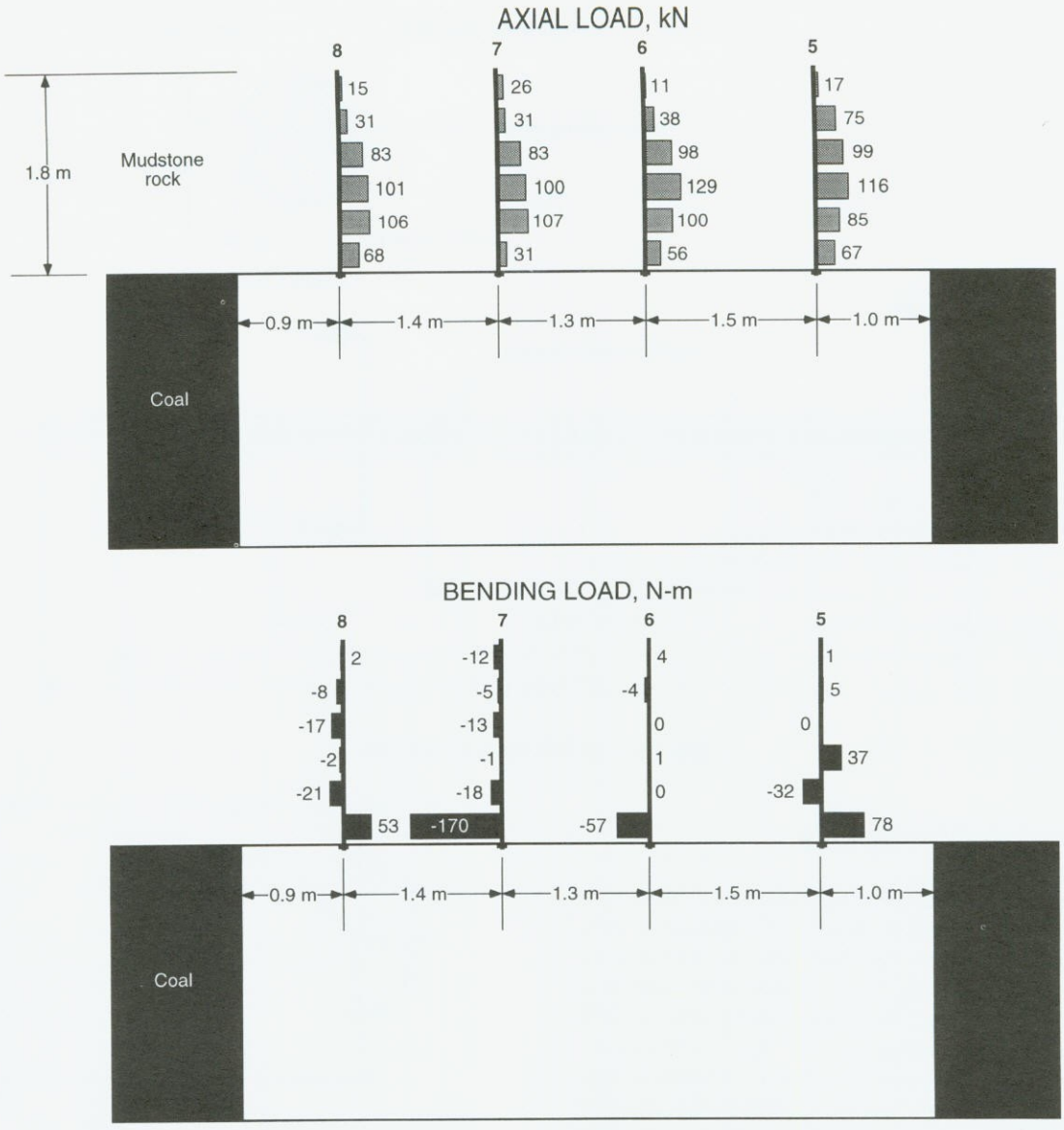



**Figure 3.—Load profiles for test site 1**

**Table 1.—Maximum fiber stress for test site 1, megapascals**

| Bolt | Strain gauge station | | | | | |
|---|---|---|---|---|---|---|
| | 1 | 2 | 3 | 4 | 5 | 6 |
| 5 ..... | 300 | 365 | 493 | 415 | 316 | 70 |
| 6 ..... | 250 | 418 | 539 | 410 | 161 | 46 |
| 7 ..... | 172 | 451 | 420 | 352 | 129 | 110 |
| 8 ..... | 298 | 451 | 422 | 352 | 132 | 66 |

The selected design stress for this test site was 414 MPa. Every roof bolt exceeded this value. Reducing the spacing between bolt rows, increasing the number of bolts per row, and increasing the diameter of the bolt are three ways to reduce fiber stress. Using these methods and equation 6 produced the figures shown in table 2.

**Table 2.—Roof bolt design alternatives**

| Number of bolts | $S_{d1}$, m | $S_{d2}$, m | Bolt diameter, mm |
|---|---|---|---|
| 4 ..... | 1.22 | 0.90 | 18, No. 6 rebar |
| 5 ..... | 1.02 | 1.08 | 18, No. 6 rebar |
| 4 ..... | 1.22 | 1.32 | 22, No. 7 rebar |

These selections assume an equal spacing of roof bolts. If there were sufficient data to suggest a consistent pattern of bolt load profiles, then irregular bolt spacings could be used. In this case, the safety factors should be increased to provide for variations that might overload the roof bolts. Each of these options would limit bolt stress to less than 414 MPa. The stress distribution along the bolt length indicates that there would be adequate anchorage length if a 1.5-m-long bolt were used in place of the 1.8-m-long bolt.

### Site 2

The second test site was located in a four-entry gate road with yield abutment pillars. Overburden at the test site is approximately 670 m. A 30-cm-thick layer of incompetent drawrock overlies the coal seam. The immediate mine roof is formed by a fossiliferous shale that grades into thinly interbedded shales and coals. This seam is overlain by a 30-cm-thick coal seam. Where the drawrock is thin, it falls during extraction of the coal together with the coal rider seam. The main roof above the rider seam consists of 30 to 60 cm of competent siltstone overlain by massive sandstone. Instrumented bolts were installed in areas where the rider seams remained intact. Row spacings were approximately 1.22 m.

Axial and bending loads (figure 4) show the load profile after entry development. Bending moments were significantly higher at this test site. High horizontal stresses produced lateral movements at the rider seam locations, which contributed to these bending stresses. Maximum fiber stress was 513 MPa on bolt 3 at 46 cm from the mine roof.

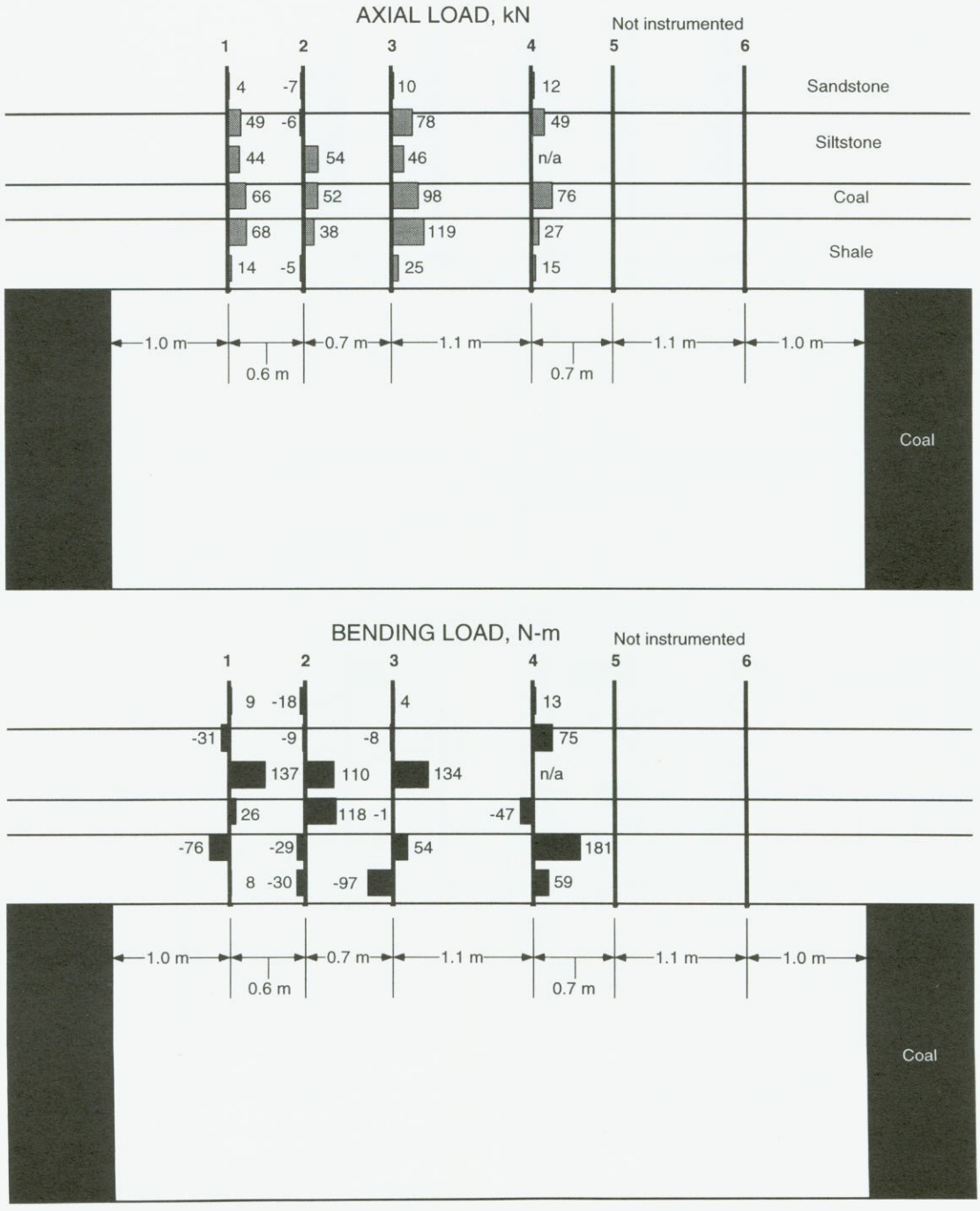



**Figure 4.—Load profiles for test site 2**

The selected design stress for this test site was 331 MPa. A lower stress limit was selected because maximum bending loads may be reached between strain gauges. Also, the amount of data at this test location was not extensive. Using six No. 6 bolts per row, the spacing between the rows was reduced to 0.83 m, and the spacing between the bolts in the row was 0.86 m. If five No. 7 bolts were used per row, then the bolt spacing would be 1 by 1 m.

### Site 3

The third test site was in a two-entry gate road. The coal seam is approximately 4.3 m thick and has a 16° pitch. Overburden at the test site is approximately 335 m deep. The entry was cut approximately 3 m high, and top coal was left on the roof and the floor. The top coal was approximately 0.5 m thick on the downdip side of the entry and 1.5 m on the updip side. Above the top coal, the immediate roof was a very low strength carbonaceous mudstone.

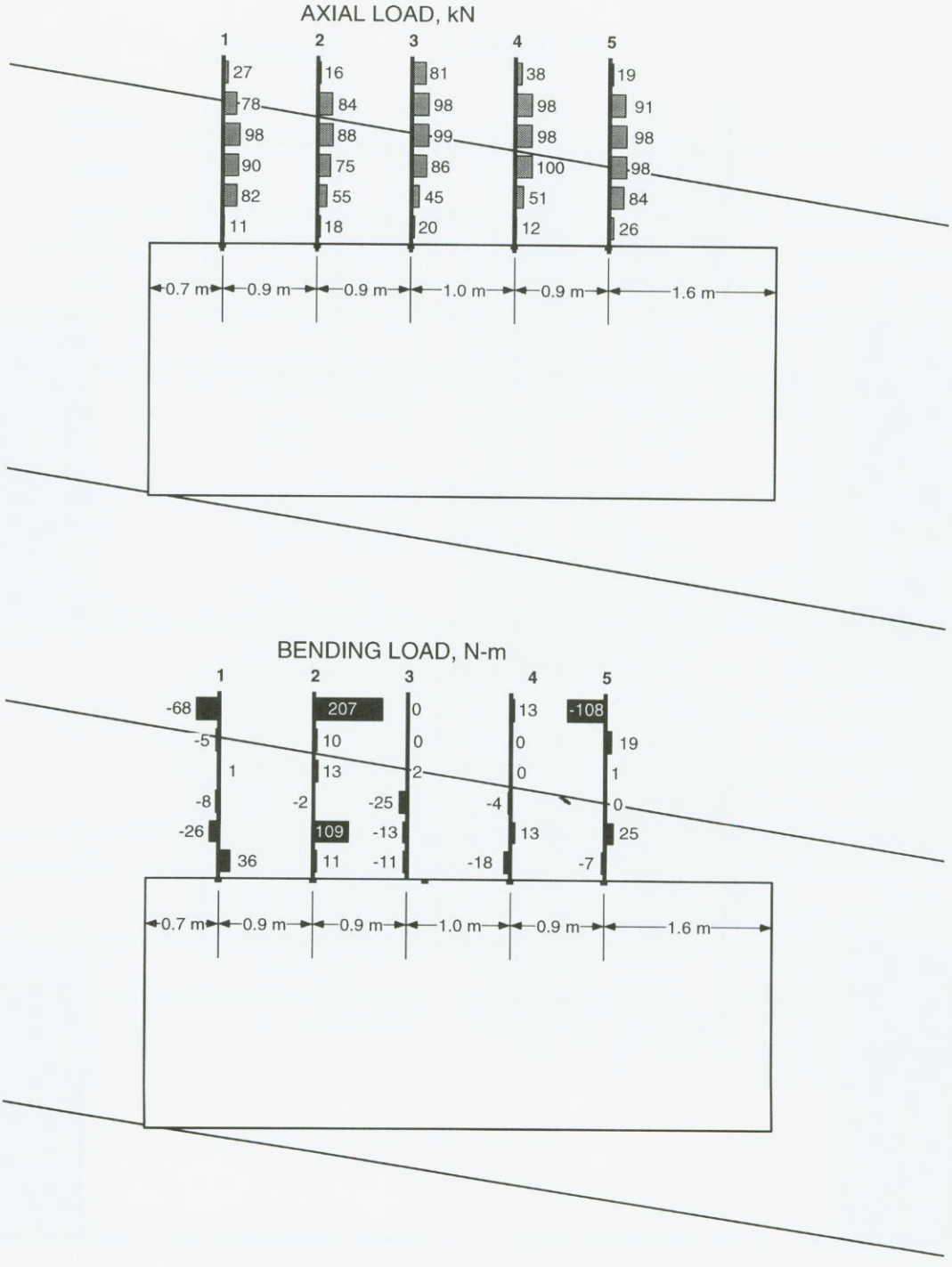



**Figure 5.—Load profiles for test site 3**

Row spacing of the roof bolts was approximately 1.2 m. Axial and bending loads (figure 5) form the load profile after the pass of the first longwall panel. Maximum fiber stresses are shown in table 3.

**Table 3.—Maximum fiber stress for test site 3, megapascals**

| Bolt | Strain gauge station | | | | | |
|---|---|---|---|---|---|---|
| | 1 | 2 | 3 | 4 | 5 | 6 |
| 1 .... | 156 | 423 | 402 | 411 | 343 | 315 |
| 2 .... | 108 | 554 | 319 | 406 | 382 | 682 |
| 3 .... | 117 | 225 | 434 | 420 | 413 | 339 |
| 4 .... | 104 | 252 | 432 | 412 | 410 | 196 |
| 5 .... | 130 | 426 | 411 | 416 | 435 | 400 |

The selected design stress for this test site was 414 MPa. The ultimate strength of the instrumented bolts was approximately 684 MPa. Station 6 on bolt 2 showed a combined stress that was very close to failure. It should be noted that the accuracy of the strain gauges decreased considerably at greater elongations, so the high stress readings should be taken as estimates.

The main concern at this test site was the lack of adequate anchorage length at the ends of the roof bolts. Cutters would form on the downdip side of the entry, and the bolts would appear to loose anchorage in the weak mudstone. The bolt load profile shows that high stresses were too close to the end of the bolts. Increasing bolt diameter, reducing bolt spacing, and/or increasing the number of bolts probably would not be enough to prevent this type of roof failure. A longer bolt that is angled over the ribs could solve the anchorage problem.

Every roof bolt exceeded the design stress value so other corrective action is required. Reducing the spacing between bolt rows, increasing the number of bolts per row, and increasing the diameter of the bolt are three ways to reduce fiber stress. Using these methods and equation 6 produced the results shown in table 4.

**Table 4.—Roof bolt design alternatives for test site 3**

| Number of bolts | $S_{d1}$, m | $S_{d2}$, m | Bolt diameter, mm |
|---|---|---|---|
| 5 ..... | 1.02 | 1.07 | 18, No. 6 rebar |
| 4 ..... | 1.22 | 0.89 | 18, No. 6 rebar |
| 4 ..... | 1.22 | 1.28 | 22, No. 7 rebar |

## SUMMARY

All of the design selections incorporated an evenly spaced bolting pattern. The design loads combined maximum axial and bending loads. Additional refinements could be made by allowing uneven spacings across the entry and using the exact load profile for the design loads. If this approach is used, the factor of safety should be increased to allow for variations and anomalies. After redesigning the bolting pattern, the pattern should be measured to see how close estimated loads compare with actual loads. In situ tests should also be conducted to establish anchorage capacities in the roof rock. This method could be used effectively for the development of an engineered solution having a selected factor of safety for selecting bolt diameter, spacing, and length. The end result will be fewer roof falls and safer conditions underground.

## REFERENCES

1. Choquet, P., and Hadjigeorgiou, J. "The Design of Support for Underground Excavations." *Comprehensive Rock Engineering: Principles, Practice, and Projects.* V. 4, Pergamon, 1993, pp. 313-345.

2. Signer, S. P., and S. D. Jones. "A Case Study of Grouted Roof Bolt Loading in A Two-Entry Gate Road." *9th International Conference on Ground Control in Mining: Proceedings*, ed. by Syd S. Peng (Morgantown, WV, June 4-10, 1990). Dept. Min. Eng., WV Univ., 1990, pp. 35-41.

3. Signer, S. P., C. Mark, G. Franklin, and G. Hendon. "Comparisons of Active Versus Passive Bolts in a Bedded Mine Roof." *Proceedings of 12th Conference on Ground Control in Mining*, ed. by S. S. Peng (Morgantown, WV, Aug. 3-5, 1993). Dept. Min. Eng., WV Univ., 1993, pp. 16-23.

4. Signer, S. P. "Field Evaluations of Grouted Roof Bolts." *New Technology for Longwall Ground Control. Proceedings: U.S. Bureau of Mines Technology Transfer Seminar*, comp. by C. Mark, R. J. Tuchman, R. C. Repshar, and C. L. Simon. U.S. Bur. Mines Spec. Pub. 01-94, 1994, pp. 91-101.

5. Serbousek, M. O., and S. P. Signer. "Load Transfer Mechanics in Fully Grouted Roof Bolts." *Fourth Conference on Ground Control in Mining* (Morgantown, WV, July 22-24, 1985). Dept. Min. Eng., WV Univ., 1985, pp. 32-40.

6. Serbousek, M. O., and S. P. Signer. Linear Load Transfer Mechanics of Fully Grouted Bolts. U.S. Bur. Mines Rep. Invest. 9135, 1987, 17 pp.

7. Maleki, H., S. P. Signer, M. E. King, and P. A. Edminster. "Evaluation of Support Performance in a Highly Stressed Mine." *Proceedings of 13th International Conference on Ground Control in Mining*, ed. by S. S. Peng (Morgantown, WV, Aug. 2-4, 1994). Dept. Min. Eng., WV Univ., 1994, pp. 9-17.

8. Larson, M., C. Stewart, M. Stevenson, M. King, and S. Signer. "A Case Study of a Deformation Mechanism Around a Two-Entry Gateroad System Involving Probable Time-Dependent Deformation." *Proceedings of 14th International Conference on Ground Control in Mining*, ed. by S. S. Peng (Morgantown, WV, Aug. 1-3, 1995). Dept. Min. Eng., WV Univ., 1995, pp. 295-304.

9. Farmer, I. W. "Stress Distribution Along a Resin Grouted Anchor." *Int. J. Rock Mech. Min. Sci. & Geomech*, v. 12, 1975, pp. 347-351

10. Dunham, R. K. "Anchorage Tests on Strain-Gaged Resin Bonded Bolts." *Tunnels and Tunneling*, v. 8, No. 6, Sept. 1974, pp. 73-76.

11. Gale, W. J, and M. W. Fabjanczyk. "Application of Field Measurement Techniques to the Design of Roof Reinforcement Systems in Underground Coal Mines." Proc., 13th Cong. of Council of Instit. Min. and Metal., Singapore, May 1986, pp. 135-141.



12. Johnston, J. L., and D. J. Cox. Instrumentation Procedures for Fully Grouted Rock Bolts. U.S. Bur. Mines Inform. Cir. 9341, 1993, 10 pp.

13. Littlejohn, S. "Overview of Rock Anchorages." *Comprehensive Rock Engineering: Principles, Practice, and Projects.* V. 4, Pergamon, 1993, pp. 413-450.

# Strategies for the Application of Rockbolting Technology to Longwall Gateroads in Chinese Coal Mines

*Zuoliang Xiu,* Senior Engineer
*Xingku Wang,* Engineer
Beijing Research Institute of Coal Mining, CCRI
Beijing, P. R. CHINA

*An Wang,* General Manager
Daliuta Coal Mine
Shenfu, Shaanxi Province, P. R. CHINA

## ABSTRACT

Experience indicates that rockbolting is the most efficient and cost effective means of supporting gateroads of retreating longwalls. However, gateroads supported solely by rockbolting currently accounts for less than 16% of the 4500km of annual gateroad drivage in China. According to a stated target of the Ministry of Coal Industry, this percentage should be at least 50% by the year 2000. Since the learning stage of the technology which is indicated by low drivage rates and frequent roof falls in rockbolted gateroads must be overcome , strategies for the application of rockbolting to gateroads have become the focus of discussions on this topic .

This paper presents the recent developments on longwall gateroad rockbolting technology in China. The development work has concentrated on understanding the mechanism of rockbolting; establishing new design procedures of bolting parameters for gateroad support; upgrading the consumable; optimizing bolt installation procedures; adopting better roofbolting machines; and developing adequate secondary reinforcement technique. The authors believe that this development work together with the on-going work in other aspects of gateroad rockbolting, as discussed in this paper , represent the rational strategies for the application of rockbolting technology to a wider range of longwall gateroads in Chinese coal mines .

## INTRODUCTION

Rockbolting is not something new in China and its first industrial utilization in Chinese coal mines can be traced back to the early 60's. Benefit gained from its application is so great that nowadays people hardly give any consideration to other types of supporting method for development roadways driven in either roof strata or floor strata. However, up until the middle 80's rockbolting was used only in main development roadways and, almost with no exception, in conjuction with shotcreting.

In the middle 80's, rockbolting in longwall gateroads was tried as a "nice to have" in a few collieries with favorable conditions. Although the results were reasonable, rockbolting in longwall gateroads was not widely accepted. At that time it was considered that rockbolting was effective only in roadways driven in rock. In longwall gateroads driven in coal seam and badly influenced by the abutment pressure of a longwall face, it will be ineffective and certainly not as reliable as standing steel supports. Moreover at that time, collieries were able to get steel supply from the government at very low price to make standing supports. This situation was changed with the introduction of market economy in the late 80's when collieries began to seek ways to reduce cost and to raise efficiency. It was under such an atmosphere that rockbolting in longwall gateroads was accepted as a "have to have". Initial use of gateroad rockbolting showed its outstanding advantages as compared with conventional support methods — low material cost; reduced physical labor; less injury in material handling and what is more, excellent longwall face ends which means more tonnage per shift. Only by this time was due enthusiasm given to the application of rockbolting to longwalls gateroads. In the early 90's, more than 200km of longwall gateroads were driven annually with rockbolting being the sole support. Yet this figure accounted for only 12%~15% of the 4500km annual drivage of longwall gateroads. According to a stated target of the Ministry of Coal Industry, this percentage should be at least 50% by the year 2000. While the future for gateroad rockbolting looks quite encouraging, efforts are needed to overcome the learning stage of the technology indicated by the following factors:

. low drivage rate. The average is 10m/day for fully mechanized heading and 6m/day for conventional heading (i.e. drilling/blasting);

. frequent roof falls. The total number of roof falls in rockbolted gateroads since the initial use is approaching 100, some of these resulting in fatality or injury.

So, strategies for the application of gateroad rockbolting to

Chinese coal mines have become the focus of attention of the whole industrial sector. Efforts made so far have yielded progress in upgrading gateroad rockbolting technology, yet further endeavor is needed on some specific aspects, as discussed in the paper.

## EFFORTS MADE SO FAR

### Research Programs

During the 8th "Five Year Plan " period, several research programs on gateroad rockbolting were funded by the Ministry of Coal Industry. These programs covered the main aspects of gateroad rockbolting technology including gateroad stability classification, mechanism of rockbolting, bolting parameters and design methods, rockbolting consumable and equipment, measurement and monitoring techniques and secondary reinforcement techniques to supplement rockbolting. Achievements of these programs have laid a good base for the development of gateroad rockbolting technology in China.

### Technical Exchange

Rockbolting delegations were sent to USA, Australia, UK and Russia and came back with new ideas and knowledge about gateroad rockbolting. Deep impressions left on the members during their visiting abroad was instrumental in reviving the interest of the coal mining industry in gateroad rockbolting and making it widely accepted. Moreover, the backwardness of the technology in China was realized and potential ways to improve it were founded. As well as these visits abroad, professionals from foreign universities, technical consultant agencies, and equipment manufacturers were invited to China to give lectures or presentations. All these have proved to be very helpful.

### Australian Rockbolting Technology Demonstration

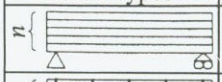
In December 1995, an agreement on a demonstration program of Advanced Technology of rockbolting was signed between the Ministry of Coal Industry of China and an Australian consultant company named SCT (Strata Control Technology Pty Ltd). This program included in-situ stress measurement, coring and testing of rock samples, computer modeling, field trial of gateroad rockbolting, and comprehensive monitoring. The field trial site was intentionally selected by the ministry in the tailgate of a retreating longwall which mines a 4.5m thick coal seam in one pass. The tailgate was driven along the goaf of the neighboring longwall panel mined out 11 months ago, with only a 3~4m wide barrier pillar being left. In the field trial stage, high strength full column resin encapsulated bolts domestically made according to specifications proposed by SCT were installed with pneumatic roofbolters imported from Australia. As compared with the old rockbolting system, drivage rate was increased by approximately 35% and roadway conditions were obviously improved during longwall retreating.

## ACHIEVEMENTS SO FAR

### Understanding the Mechanism of Bolting in Gateroads

During the initial use of gateroad rockbolting in China, few people really understood how bolts work in a specific roadway. Conventional explanation of the mechanism of rockbolting such as suspension effect, beam-building effect, arching effect etc. are cited in nearly every paper on this topic. But in fact these explanations are all subject to deliberation to a certain extent. For example, the author(i.e. the first author) of this paper has pointed out that the beam-building effect is of dual nature [1]. As shown in Table 1, while the bending strength is

**Table1 The Dual Nature of Beam Building Effect**

| Beam Types | *Bending Strength* | *Bending Stiffness* |
|---|---|---|
|  | $W_1 = n\ \frac{1}{6}bh$ | $[EI]_1 = \frac{E}{12}bh^3 n$ |
|  | $W_2 = \frac{1}{6}b(nh)^2$ | $[EI]_2 = \frac{E}{12}b(nh)^3$ |
| *Comparison* | $W_2 = nW_1$ | $[EI]_2 = n^2\ [EI]_1$ |

increased by $n$ times, which is always good for roof stability, the bending stiffness is increased by $n^2$ times. It is easy to work out that increasing bending stiffness will, under certain conditions, cause extra load from the overlying strata acting on the beam. The beam may not fail in tension because of the increased bending strength, but will fail in shear at the two ends This type of failure mode (Fig. 1) is quite common and features:

. a high angle or even vertical fracture plane at the two ends of the beam;

. a flat failure plane exactly at the bolted horizon where pretension of the bolts causes a tensile stress area around the top of each bolt;

. using longer bolts somehow just increase the height of roof fall [2].

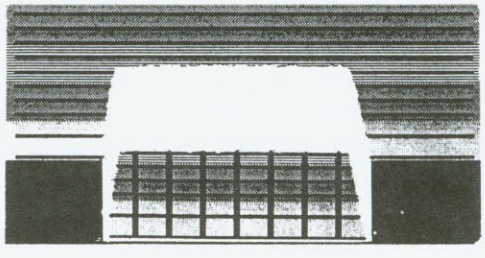


Fig.1 Failure Mode of Bolted Beam

Research work (including physical modeling and in-situ monitoring) and accumulation of practical experience have contributed to the new explanation of the mechanism of rockbolting in gateroads [3], of which the major points are:

. a bolt properly installed provides confinement in its axial and radial directions to the surrounding rock. This confining

effect, either active or passive depending on bolt type, is the basis of but not necessarily equals the function of bolting;

. only when the confining effect of bolts corresponds to the failure mode of the surrounding rock (not samples tested but the roof or the rib as a whole) does it turn into the actual function of bolting; so

. it is essential to know not only what bolts can do, but also what the rock needs the bolts to do to maintain stability. In other words, it is meaningless to talk about the mechanism of bolting without relating it to the failure mode of surrounding rock;

. the function of bolting is to reinforce certain area of the surrounding rock where stress may surpass the strength of the rock in the earlier stages of the deformation process and/or to balance the loads acting on failed or detached zone isolated by fractures to prevent it from falling in either the final stage (for intact rock) or sometimes the earlier stage (for broken rock);

. only when installed in a properly designed pattern can the confining effect of bolts completely correspond to the failure mode of the surrounding rock and be sufficient to control the failure; and so

. it is essential to correctly identify the failure mode of surrounding rock in order to know what the surrounding rock needs the bolts to do, because the failure mode of the roof and of the ribs may be manifold and may change from one to another.

## New Design Method

Several design methods of bolting parameters have been tried since the initial use of gateroads rockbokting in China. These methods include trials & errors, empirical approach based on rock classification, physical or numerical modeling, analytical equations, and most recently rockbolting expert system for gateroads. With the application of rockbolting to more and more difficult conditions, shortcomings of these methods gradually exposed. For example, since engineering experiences are generalized too far in the inference engines, inappropriate or even ridiculous designs often come out from some of the expert systems. Roof falls have been caused by incorrect designs from time to time.

A systematic design method (Fig.2) based on measurement and monitoring has been established most recently[3]. The development of this design method which follows roughly the same concept of NATM in tunnel engineering, has benefited a great deal from the experiences in Australia and UK. However, with a wide variation of geological conditions in different mining areas in China, more emphasis is placed on the initial design. The idea is that a better initial design means that the final design can be reached sooner and at lower cost of monitoring. The initial design is based on a newly developed failure mode identification system for surrounding rock of gateroads rather than any kind of rockmass calcification system.

In practice, this design method can be used in two ways. For gateroads with unfavorable conditions, initial design will be done after a full scope of measurement and site investigation; for gateroads with favorable conditions, initial design will be based mainly on information currently available, with only a few or even no measurements being needed. This makes the new design method more workable. This new design method, though not completely mature, is receiving more and more acceptance in China. A book written by the author to introduce this method will be published by the Publication House of Coal Industry by the end of this year.

## Upgrading of the Consumables

At the early stage of the application of rockbolting to longwall gateroads, the consumable used were apparently inferior to those used in Australia, UK, and USA. The story of cement cartridge may explain how awful the situation was. In the middle 80's, a DuPont production line of resin cartridge was imported from the US. But since at that time rockbolting were used mainly in roadways driven in rock with split sets being the dominate bolt type, the market for resin cartridge was very small and resin cartridges were quite expensive then. Coal mines that were leading the usage of gateroad rockbolting began to seek substitution for resin cartridge and therefore cement cartridges were developed. Being only 1/10 the price of resin cartridges, cement cartridges were very popular and if installed properly can give anchorage capacity as high as resin cartridges do. They are also as convenient to use as resin cartridges. However, a fatal shortcoming is that the performance of cement cartridges is significantly affected by variation in infiltration quality as a result of human judgment factors. Sometimes the anchorage was so poor that the bolt could be pulled out by hand. The first roof fall accident in rockbolted gateroad, which caused 6 fatalities and 4 injuries, was concluded to be caused mainly by poor anchorage of cement cartridges. Now in Chinese coal mines cement cartridges are no longer allowed to be used in the roof, hence resin cartridges have become the only choice. In Oct.1992, full column resin encapsulation was first tried. However, it is not until 1996 when the AT demonstration program was undertaken that full column resin encapsulation began to increase quickly.

During the AT demonstration, it was realized that correct annulus size as well as bolt profile is very important to obtaining good load transferring in full column resin encapsulation. Hence high strength bolts and low viscosity resin cartridges have been developed according to the specifications proposed by SCT for the AT demonstration program. With new heat treating technique which is both efficient and cost effective, the actual bolt specifications shown in Table 2 are very constant. When apparent improvement in

**Table 2 Specifications of High Strength Bolts**

| *Nominal Diameter (mm)* | *∅18* | *∅20* | *∅22* |
|---|---|---|---|
| *Yielding Load (kN)* | *175* | *206* | *254* |
| *Breaking Load (kN)* | *206* | *257* | *314* |
| *Elongation (%)* | *17* | *17* | *17.7* |

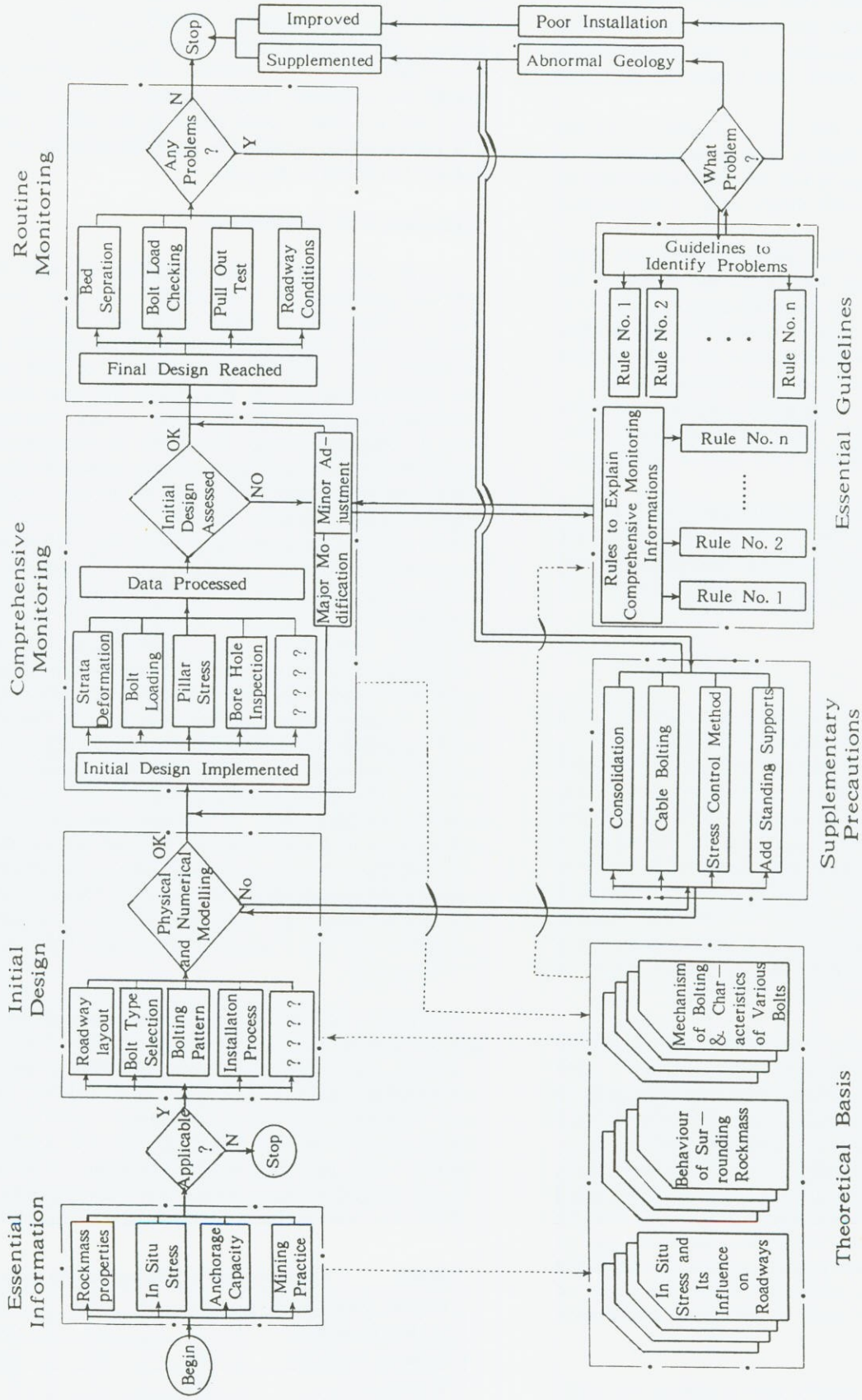



Fig. 2 Scheme of The Systematic Design Method of Bolting Parameters for Longwall Gateroads Based on Measurement And Monitoring

roadway conditions is noticed, the necessity of using high strength fully encapsulated bolts is not doubted any more but accepted immediately. Meanwhile, a kind of reinforced fiberglass bolts for ribbolting has also been developed and now is undergoing field trial in several coal mines.

Nowadays in China, roofbolts in gateroads are usually installed with straps or in a form of roof truss. There are two types of straps:W-strap made of steel plate and ladder- strap made of steel rebar. Several types of roof truss have been tried. In a research project funded by the Central Government, a brand new type of roof truss (Fig.3) was designed by the author and was proven to be successful during field trials. It features:

- active touching with the roof along the whole length of the horizontal member which serves as both a tie rod and a strap;
- high pretension of the horizontal member is achieved with low tightening torque;
- bigger tolerance for the positioning of inclined bolts;
- a minimum number of components to be assembled underground.

More than 7km of gate road with unfavorable strata conditions have been supported solely by this new type of roof truss since its introduction two years ago, with satisfactory roadway conditions.

**Adoption of Better Equipment**

The process of the development of rockbolting equipment for gateroads has been painful in China. When the performance of one type of roofbolter (say hydraulically powered) was not entirely satisfactory, interest was then shifted to the development of another type of roofbolter (say pneumatically powered) instead of trying to improve the former. So finally because of the dispersed input, there are altogether 3 types and12 models of roofbolters, but none of them proved to be successful. Should the input had been concentrated on one correct type of roofbolter, the situation would be different. To overcome this headache, many roofbolters have been imported in the past few years. Now pneumatically powered roofbolters from Australia account for more than 90% of the market in China. These imported roofbolters have proved to be both powerful and easy to operate, and have certainly made their due contribution to the increasing application of rockbolting in gateroads. Yet there is a concern that the inappropriate after sale service provided to the coal mines by the distributing agency instead of the manufacturers themselves will soon show its effect on the actual performance of the imported roofbolters. In fact, this is something now happening and resulting in problems for the coal mines. It seems that these imported roofbolters will soon have to be replaced by new ones either from abroad or from domestic manufacturers if suitable.

**Optimization of Bolt Installation Process**

In the early stage, bolts were installed 10~15 m away from the heading face, with props and wooden beams being used as temporary support for that distance. The normal practice was to cut to advance the roadway face for two 8-hr shifts and then stop for one 8-hr shift for roof bolting. This arrangement was considered to be more efficient and less

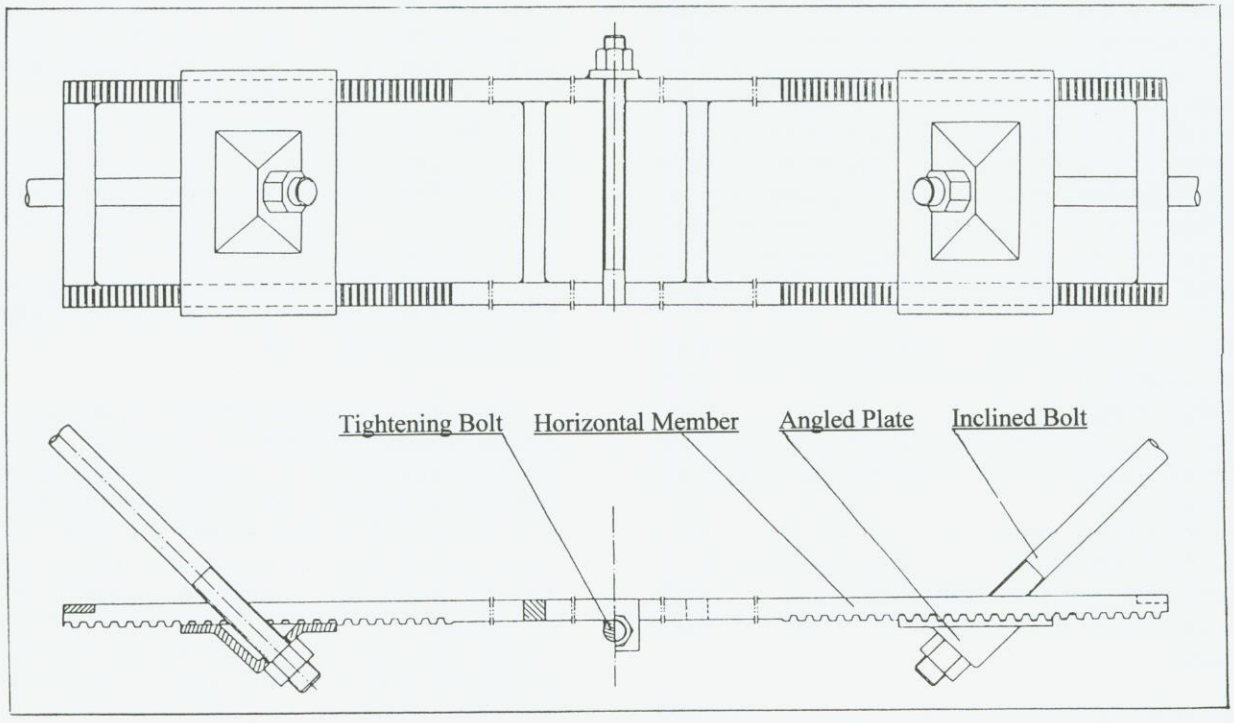



Fig.3 Structure of The New Type of Roof Truss

confusing. It is now gradually being realized that bed separation often occurs before bolt installation despite the resistance provided by the temporary support. So it is required that bolts be installed every two cutting cycles instead of two cutting shifts. Monitoring results indicate that roof lowering and bed separation is well controlled with this new arrangement.

With a shear pin configuration for full column resin encapsulated bolts and a special adapter for point anchor bolts, it is now able to install a roof bolt immediately after a hole is drilled, with mixing the resin and tightening the nut being accomplished in one pass. As a result, efficiency can be increased significantly.

**Secondary Reinforcement Techniques**

Rockbolting also have its effective bandwidth[4]. Under severe conditions ordinary rockbolting has to be supplemented with secondary reinforcement techniques. Consolidation with polyurethane injection is the first sort of secondary reinforcement for gateroad rockbolting and has been used in at least 22 coal mines in China. It is effective but also expensive, hence the acceptance is somewhat limited.

Cable bolting which features long tendon and high capacity has been scarcely used in longwall gateroads in China though it is used from time to time as one of the remedial or "firefighting "means for relatively important roadways such as underground transformer house or pump house. But now it is gaining more and more attention as an effective secondary reinforcement to ordinary rockbolting in gateroads. In an on-going research program conducted by the author, a new cable bolting system has been developed. Cables up to 7m long are partially encapsulated in 27mm diam. holes with resin cartridges. Two 23mm diam.×330mm fast setting and one 23mm diam.×880mm slow setting resin cartridges which give approximately 1.5m of encapsulation are used in each hole. The resin is mixed with the cable driven by a pneumatic roofbolter through a specially designed adapter and a guiding tube, just like installing a full column encapsulated bolt. This new cable bolting system has some outstanding advantages over conventional grouted (cement or resin) cable bolting systems, such as;

. The installation process is dramatically simplified and equipment cleaning is no longer needed, hence efficiency is significantly increased;

. There is no need for grout mixer and pump, so less equipment cost and lower labor intensiveness in handling this equipment result;

. No grout tube or breath tube is needed. Grout wasting problem is eliminated entirely. So it is more cost effective;

. Resin cures much faster than cement grout, so the cable can take load in 10 minutes instead of 3 days for cement grouted cable.

During field trial, more than 200 of the new cable bolts have been installed in the tailgate and the setting-up entry of a retreating longwall with no failed installation at all. On average, it takes two men using a pneumatic hand-held roofbolter 35 minutes to install a 6.5~7m long cable bolt, including drilling the hole, inserting resin cartridges and cable, mixing, putting on the plate and anchor, pretensioning the cable and cutting off the tail.

The nominal minimum breaking load of the 15.24mm diam. high strength low relaxation cable is 260.7 kN. In situ pull-out tests show the capacity of the new cable bolting system varies between 23.5 tons(with one or two of the 7 wires being broken) and 27.5 tons (with all the 7 wires being broken). In all the cases, the ultimate anchorage capacity proved to be sufficient.

## FUTURE DEVELOPMENT

**Rockbolting In Gateroads with Thick Top Coal**

Reserves of coal in seams thicker than 4.5 m accounts for 48% of the total reserves of all the state-owned coal mines in operation. Longwall slicing used to be the only mining method for thick coal seams. But it is disappearing very quickly with the successful introduction of sub-level caving method. There are now at least 32 sub-level caving longwall faces mining coal seams from 4.8m to up to 10 m thick in China.

Gateroads of sub-level caving longwall faces feature thick top coal which is both soft and less intact as compared with rock of the immediate roof. So they are technically difficult to be supported solely by rockbolting. However, for the following reasons rockbolting is a preferred supporting method:

. higher production of sub-level caving method requires a larger air quantity for ventilation, hence wider gateroads are needed. If steel girder is chosen, longer cross member means lower capacity and higher labor intensiveness;

. steel girders are passive supports. When they begin to take load, the top coal sitting on them has already become loosed. Fissures and fractures serve as air conduits for and spontaneous combustion is induced. Several fire accidents have happened in this manner in the past few years.

. Gateroads supported by steel girders or steel arches have proved to be inconvenient at the two ends of sub-level caving longwall faces during retreating.

Since 1995, the author has been conducting a research program proposed and funded by the Ministry of Coal Industry to explore the possibility of using rockbolting in gateroads with thick top coal. An initial field trial has been accomplished in a small section (2.8 × 2.6m) tailgate of a light duty sub-level caving longwall face, with the new cable bolting system being used. The second stage of field trial is currently underway in the maingate (4.6 × 3 m) of a standard sub-level caving longwall face. Since it was found that the anchorage of resin encapsulated bolts in the roof tends to deteriorate with the deformation of top coal, it is planned that the field trial will move into a third stage during which the installation of a new

type of bolt will be tried with a specially designed installation equipment. The new bolts will stab into the coal under the thrust of the installation equipment as a nail being punched into a wall.

**Rockbolting in Gateroads Driven along Goaf Side**

Driving gateroads (usually the tailgate) of longwall faces along the adjacent goaf sides with small barrier pillars 3~5m wide being left is something unique in China. This is required by the reserve management legislation and there is no sign that this will be changed in the near future. A lot of gateroads of this sort have been supported solely by rockbolting. The problem at this moment is that the rib on the small pillar side squeezes out badly during longwall retreating. It has also been advised by the Australian consultant during the AT demonstration that bolting can reinforce the strata within a certain area around the roadway but can not stop the large caving blocks potentially formed by goaf fractures extending over the gateroads from collapsing (Fig.4). The general stability

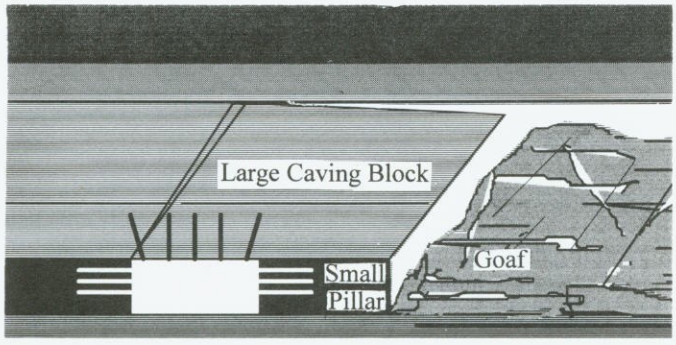



Fig. 4 Large Caving Block Supported by Small Pillar

of a gateroad in close vicinity of the goaf will depend on the fracture geometry of the adjacent goaf and the strength of the small pillar. The Australian consultant has recommended the use of larger pillars to get rid of the risk. Yet due to perceived logistical reasons, only two choices are available: one is to supplement the ordinary roofbolting with cable bolting and the other is to have a further strengthened small pillar at least as wide as the roadway so to prevent the caving blocks from rotating into the roadway. The effectiveness of the two choices is to be approved with future research work.

**Development of Adequate Techniques**

Though several kinds of instrument have been developed domestically in the past few years, there is still an urgent need of sophisticated monitoring instruments for the application of rockbolting to gateroads. For example, when using the new design method, it is essential to have good extensometers to measure the strata deformation, but unfortunately, none of the products available on the domestic market can meet the need in terms of accuracy and efficiency in data collection. Devices such as optical stratascopes and underground borehole TV cameras are all domestically unavailable. These are preferred to be imported from abroad.

On the other hand, though computer modeling is developing very fast and widely used in the application of gateroad rockbolting all over the world, the author believes that this technique is still quite backward in China, and at this stage it can do little for the development of gateroad rockbolting but prints or plots what is imagined by the person doing the modeling. Great effort is needed to change this situation.

**Innovation of New Equipment for Gateroad Drivage**

Currently, more than 80% of gateroads in China are developed by drilling and blasting method. Roadways driven with this conventional method suffer from loose ribs and poor profiling, and this is certainly not good for rockbolting. Mechanized drivage using roadheaders is much better than conventional drivage but far from perfect, because the roadheader system is not ideally designed to go with rockbolting in terms of cycled operation, especially when the roadway is not so wide and access on each side of the roadheader to the face is restricted. Hence the future of gateroad rockbolting in China will depend not only on its own development but also on the innovation of new equipment for in-seam roadway drivage. The author believes that something like a bolter/miner in-seam roadway development machine which features simultaneous cutting and bolting, but less sophisticated and smaller in size than those currently used in Australia and USA, is what should be developed domestically, with cooperation with foreign manufacturers being preferred.

## CONCLUSIONS

It is now widely accepted in China that rockbolting represents the most efficient and cost effective means of supporting gateroads of retreating longwalls. Strategies for the application of gateroad rockbolting have been the focus of the attention of the whole industrial sector because the learning stage of the technology must be overcome. Efforts made in the past few years, including domestic research work and international corporation, have achieved significant progress in understanding the mechanism of rockbolting in gateroads; establishing new design methods of bolting parameters; upgrading the consumable; adopting better equipment and developing secondary reinforcement to supplement ordinary rockbolting. However, in order to fully benefit from the application of gateroad rockbolting, further efforts are needed on some specific aspects such as rockbolting in gateroads of sub-level caving longwall faces and gateroads driven along the adjacent goaf sides; monitoring instruments; computer modeling technique; and innovation of new equipment for in-seam roadway drivage. Progress made so far and the on-going development work represent the rational strategies for the application of rockbolting technology to a wider range of longwall gateroads in Chinese coal mines.

## REFERENCE

1. Xiu Zuoliang, Study on The Mechanism of Rockbolting in

Gateroads of Retreating Longwalls (in Chinese), M.S. Thesis, Central Coal Research Institute, 1990

2. Virgil W. Snyder, Analysis of Beam Building Using Fully Grouted Roof Bolts, Proceedings of the International Symposium on Rockbolting, Abisko, August 28 ~ September 2 1983
3. Xiu Zuoliang, Wang Xingku, Systematic Design Method of Rockbolting Parameters for Longwall Gateroads Based on Measurement and Monitoring(in Chinese), the Chinese Coal Society Report 94-20214, Dec. 1996
4. Siddal, R G and Gale, W J, Strata Control — A New Science for an Old Problem, Colliery Guardian, June 1992

# A Troubleshooting Guide for Roof Support Systems

*Raymond A. Mazzoni,* Mechanical Engineer
*John E. Carpetta,* Engineering Technician
Mine Safety and Health Administration
Pittsburgh S & H Technology Center
Roof Control Division
Pittsburgh, PA

ABSTRACT

Over the last twenty years, roof support technology has made numerous advances since the original wedge and slotted bolts of the 1950's. By comparison, the roof supports used today are more complex and specialized than the supports used in the past, providing mines with a varied selection of supports from which to choose. As a result, when problems with supports are encountered, it is more difficult to determine whether it is the result of geological changes, poor installation practices, or malfunctioning supports. Recognizing this problem, MSHA's Roof Control Division of the Pittsburgh Safety and Health Technology Center, has undertaken the task of publishing a guide for troubleshooting problems encountered with roof support systems. The purpose of this guide is to provide a logical sequence to resolving the most common problems encountered with roof supports.

The objective of this paper is to introduce this guide to the mining industry as well as provide insight into the evolution of the guide from its beginnings as rudimentary charts to its more comprehensive present format as a practical guide for use by the mining community.

## INTRODUCTION

Roof falls continue to be a significant problem in both the Coal and Metal-Non Metal industries. In 1982, 55 miners killed by roof and rib falls in the nations mines. However, in 1996 that number fell to 11. At least a part of this reduction can be attributed to the use of new and/or more reliable roof support systems. A primary function of the Roof Control Division is the evaluation of roof support technology, both underground and in the laboratory. Since 1970, the Mine Safety and Health Administration, Roof Control Division (RCD) of the Pittsburgh Safety and Health Technology Center, personnel have advised manufacturers on the merits of new concepts, worked with industry groups to develop effective roof support component specifications and conducted hundreds of in-mine and over 1,000 laboratory investigations to enhance the application and insure the performance of various roof support systems. The supports in use today, while more effective in controlling adverse roof conditions, are also more complex. As a result, when problems with these supports are encountered, it is difficult to determine whether the problem is the result of geological changes, poor installation practices, or malfunctioning supports. Realizing this problem, the RCD has developed a guide to troubleshoot problems encountered with roof support systems. A manual titled "A Troubleshooting Guide for Roof Support Systems" was published in 1996 as MSHA Informational Report 1237. This guide provides a logical sequence to resolving the most common problems encountered with roof supports.

## TROUBLESHOOTING CHARTS

The Roof Control Division has routinely been involved in the design and testing of roof supports. Because of this involvement, the Division's knowledge of the associated problems that could occur with these supports is extensive. This information was acquired from hands on experience troubleshooting support problems both in the lab and in actual use underground, and also from feedback from the industry. While this information was always available within the division, it had never been compiled for easy reference. An effort to collect and catalog this information led to the formation of the first troubleshooting chart (Figure 1) in the early 80's. Initially, a chart was created for mechanical bolts, since they were the predominant roof support at the time. This chart was formulated by polling the industry regarding problems that had occurred with mechanical bolts, e.g. springy bolt, excessive bleed off, etc. After the problems had been tabulated, the most likely reasons that would cause the problem to occur were then listed. In most cases, there were several possible reasons that would cause a problem to occur, so they were categorized as most likely, secondary, and potential causes. As an example, with a springy bolt, the most likely cause would be that the hole was drilled too short. Secondary

causes could be from a bolt or anchor threads that have jammed, or galled threads during installation.

Some potential causes are defective threads or anchors, or a bail or pal nut that is too strong.

After the mechanical bolt chart was completed, another was made for fully grouted bolts which were also widely used at the time. As new supports were subsequently introduced, additional charts were introduced, following the same format as the original chart, for tensioned rebar, combination/point anchored bolts and mechanically anchored resin assisted bolts.

## TROUBLESHOOTING GUIDE

In 1992 the troubleshooting format was changed to make it more user friendly. The original charts were a very valuable tool for analyzing bolt problems, but they had limitations. They did not provide the user with a logical procedure for troubleshooting supports, nor did they list any methods for determining which probable causes actually resulted in the problem. The thinking at the time was to transform this information from its basic chart format to a more comprehensive guide in the mold of an automotive repair manual. A guide of this type would not only give the user a logical procedure for evaluating a particular support problem, it would also provide the user with methods to determine the cause of the problem as well as ways to correct the problem.

In order to simplify the troubleshooting procedure, the manual was divided into the following five sections:

**Mechanical Bolts** - Bolts using an expansion anchor without resin.
**Fully Grouted Bolts** - Non-tensioned, headed rebar.
**Tensioned Rebar Bolts** - Threaded deformed bar using a grout anchor and tension nut.
**Point/Combination Anchored Bolts** - Two-piece bolts using a grout anchor and a tensioning coupler without an expansion anchor.
**Mechanically Anchored Resin Assisted Bolts** - Tensioned grouted bolts using expansion anchors.

The guide contains a listing of problems for each support type, a diagnostic flow chart for each problem, a series of Appendices that outline troubleshooting methods, and the five troubleshooting charts for easy reference.

The flow charts (Figure 2) give the user a step by step procedure listing each probable cause in sequence, in the order that they are most likely to occur. Classifying the supports makes it easier to emphasize problems that are unique to a particular support type. Some components are common to all supports, e.g. washers and plates, and related problems associated with that particular component could occur with any support that uses the component. So, in order to simplify the guide, only one chart is listed for problems that are common to more than one type of support, and the user is then referred to that chart. The biggest improvement over the original charts is the appendix section which lists the procedures for evaluating the probable causes listed in the problem charts (Figure 3). These checks give a practical guide for evaluating the support to determine if the probable cause listed was indeed responsible for the problem. In this way, by following along the flow chart and performing the checks listed in the Appendices, the user can systematically troubleshoot a particular support problem.

## CONCLUSION

Over the years the RCD has fielded many questions regarding roof support performance. These questions came from MSHA inspectors, manufacturers, and mine personnel. The troubleshooting guide discussed in this paper (and published as MSHA Informational Report 1237) provides roof control specialists, both government and industry, a clear and concise format for analyzing roof support problems. This guide has been arranged to enable the user to approach the troubleshooting process in a logical progression. The problems and probable causes listed in each section are the result of data accumulated from years of laboratory and field investigations. The troubleshooting charts are quite comprehensive; however, due to the diversity of variables affecting strata control, they are not intended to solve every conceivable problem that might be encountered. Instructions for using the guide are included which utilize a sample case to instruct the user in the correct procedure.

The initial reaction to the guide to date has been very favorable, especially from the MSHA roof control specialists, who are often called upon to analyze roof supports on the spot. A copy of Informational Report 1237 can be obtained by contacting MSHA's National Mine Health and Safety Academy, P.O. Box 1166, Beckley, WV 25802.

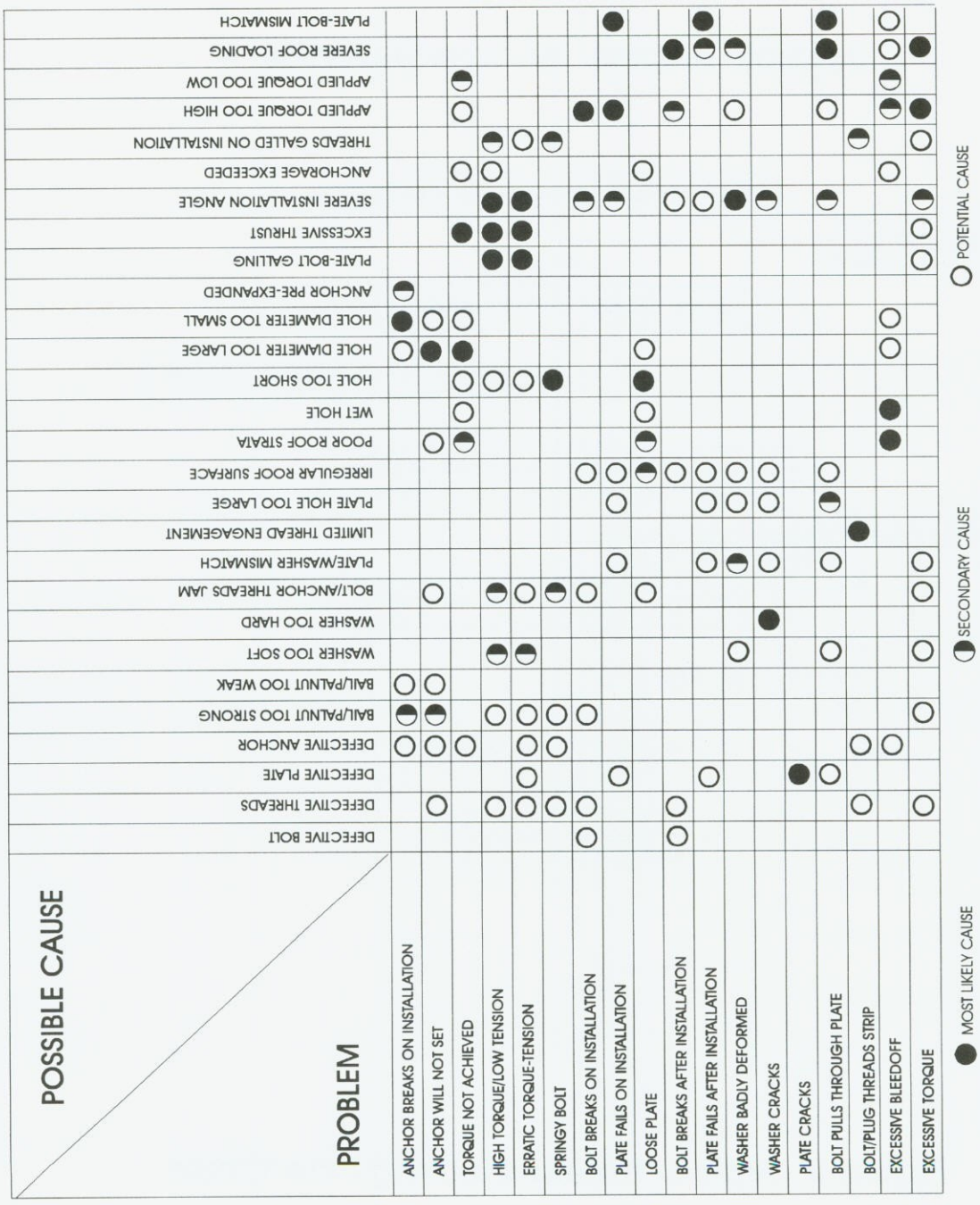



Figure 1. Mechanical Bolt Troubleshooting Chart

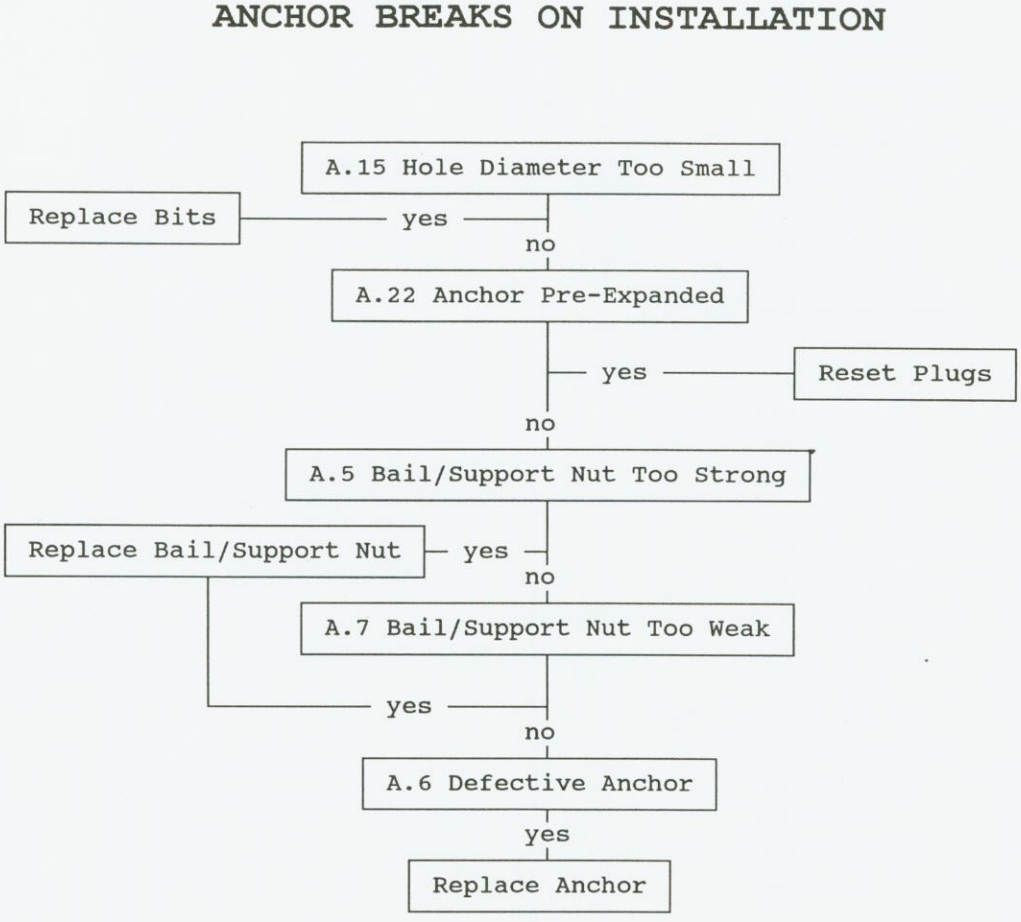



Figure 2. Typical Troubleshooting Flow Chart



### A.1 EXCESSIVE THRUST

Excessive thrust affects the installation by introducing additional friction which effectively increases the torque requirements for proper installation.
Some of the indications of excessive thrust are:

1. Smoke around the bolt head or tension nut after installation.
2. Sparking during installation.
3. The bolt head or tension nut is hot after installation.
4. Installed bolt torque substantially lower than bolter output.
5. Bolt head and/or washer welded to plate, or severe galling.

A simple check to determine if excessive thrust is causing the problem is to have the operator install several bolts in the following procedure:

1. Insert the bolt into the hole until the plate just contacts the roof.
2. Tighten the bolt.
3. Check the installation for the indications listed above. if none are evident, then excessive thrust should be ruled out.

### A.2 SEVERE INSTALLATION ANGLE

A severe installation angle will place eccentric loads on the roof bolt components which can result in premature failure. If you suspect severe installation angle is causing the problem install several bolts in an area where the roof is relatively flat and see if the problem has been eliminated.

### A.3 APPLIED TORQUE TOO HIGH/LOW

Torque variations can cause supports to be installed improperly which could result in component failure. Check the installed torque of several bolts immediately after installation. If the torque is too high or low check the bolter with an in-line torque meter or similar device.

### A.4 PLATE/BOLT MISMATCH

For an effective support it is important that the strength of the plates matches the strength of the bolts they are used with. Check the grade rating of the plate to determine if it is capable of supporting the ultimate load of the bolt or the installed load.
EXAMPLE: A grade 2 plate has a minimum ultimate load of 20,000 lbs. when tested over a 4" diameter hole as described in ASTM F432-88. The minimum ASTM ultimate load of a 3/4" dia. grade 75 bolt is 33,400 lbs. In this example you can expect the plate to fail before the bolt breaks.

## Figure 3. Typical Appendix Section

# A Statistical Overview of Retreat Mining of Coal Pillars in the United States

*Christopher Mark,* Mining Engineer
*Frank E. McCall,* Mining Engineer
*Deno M. Pappas,* Research Civil Engineer
National Institute for Occupational Safety and Health
Pittsburgh Research Center
Pittsburgh, PA

## ABSTRACT

The demographics and safety record of the pillar retreat segment of the U.S. coal industry was analyzed using statistics collected by the Mine Safety and Health Administration. Pillar recovery is practiced primarily by mines in Appalachia and the Midwest. Using 1993 data, the accident rates and productivity of a large sample of pillar retreat mines were found to be similar to other room-and-pillar mines in the same geographic areas. Pillar recovery apparently accounts for about 10% of all U.S. underground production, but has been associated with about 25% of the roof and rib fatalities during 1989-96. However, of the 28 fatalities that were analyzed, only 4 occurred for which no citations were issued for violations of mining law. Nearly one-half of the fatal incidents occurred during the mining of the last lift or pushout. All four no-citation incidents occurred during the removal of the last lift during a "Christmas tree" extraction sequence.

## INTRODUCTION

Pillar recovery has always been an integral part of U.S. underground coal mining. It can be a less capital-intensive, more flexible alternative to longwall mining for small, irregular reserves [Blaiklock 1992]. It is often employed in deeper, high-value seams where recovery rates would be unacceptably low if only development room-and-pillar mining was conducted.

The process of pillar recovery removes the main support to the overburden and allows the ground to cave. As a result, the pillar line is an extremely complex and high-stress rock mechanics environment. Historically, retreat mining has accounted for a large number of fatal roof fall accidents. During 1978-86, 67 roof fall fatalities were attributed to retreat mining, representing 29% of the total. Of the pillaring fatalities, 49% occurred during the mining of the final stump [Montague 1988]. Nevertheless, there has apparently never been a detailed study of the demographics and safety record of pillar retreat mining. This study attempts to fill the gap.

The overview presented here is based almost entirely on information collected by the Mine Safety and Health Administration (MSHA). Three primary sources were used:

- *MSHA Accident and Employment Data Base:* This data base contains information on the employment and production of all U.S. operating coal mines. It also contains information on all accidents reported to MSHA.

- *Data Base of Retreat Mines:* In 1993, MSHA formed the Mine Ventilation Bleeder and Gob Training Committee. Part of the committee's work was to survey the nine bituminous coal MSHA health and safety districts about the practices of their mines. The survey identified 186 nonlongwall mines that were maintaining an active gob and that produced more than 4,500 tons (5,000 st) in 1993 [Urosek et al. 1995]. These mines were approximately evenly divided between those that practiced full-pillar recovery and those that were limited to partial pillar extraction. An additional 181 mines had ventilated, inactive gobs. Some had permanently ceased retreat mining, others were developing for pillar recovery operations when they were surveyed. Therefore, the 186 active gob mines represent a large sample of the total retreat mine population. The identification numbers of these mines were the key to making comparisons using the MSHA Accident and Employment Data Base.

- *Fatal Accident Reports:* Since 1988, a total of 25 accidents resulting in 33 fatalities have occurred during pillar recovery operations. MSHA prepared detailed Reports of Investigation on all but the most recent of these fatal incidents, and the reports were subjected to in-depth analyses.

## DEMOGRAPHICS AND ACCIDENT RATES

Table 1 compares basic statistics for 1993 for three segments of the U.S. underground coal industry: (1) longwall mines, (2) all room-and-pillar mines, and (3) the sample of 186 room-and-pillar retreat mines.

**Table 1.— Demographics and accident statistics for U.S. underground coal mines by mine type[1]**

| Mine type | No. of mines | No. of employees | Average mine size (employees) | Tons, thousand st | Productivity, st/h | Total accident rate [2] | Roof/rib accident rate [2] | Total days lost rate [3] | Roof/rib days lost rate [3] |
|---|---|---|---|---|---|---|---|---|---|
| Room-and-pillar [4] | 1,014 | 33,073 | 33 | 214,299 | 3.45 | 15.92 | 1.44 | 451 | 41 |
| Retreat [5] | 186 | 9,129 | 49 | 61,701 | 3.27 | 15.58 | 1.14 | 432 | 29 |
| Longwall | 69 | 15,419 | 223 | 133,132 | 4.16 | 13.39 | 1.00 | 410 | 29 |
| Entire industry | 1,083 | 48,491 | 45 | 347,430 | 3.69 | 15.06 | 1.29 | 437 | 37 |

[1]Excludes anthracite mines and mines producing less than 5,000 st.
[2]Accident rates are calculated as the total number of injury accidents (severity 1-6) per 200,000 hours worked.
[3]Days lost rates are calculated as the total number of days lost due to injury per 200,000 hours worked.
[4]Room-and-pillar mines include all nonlongwall mines.
[5]Retreat mines are the 186 nonlongwall mines with active gobs identified by Urosek et al. [1995].

Source: MSHA Accident and Employment Data Base for 1993.

**Table 2.—Demographics and accident statistics for U.S. underground coal mines by MSHA district[1]**

| MSHA District No. | No. of mines | No. of employees | Average mine size (employees) | Tons, thousand st | Productivity, st/h | Total accident rate [2] | Roof/rib accident rate [2] | Total days lost rate [3] | Roof/rib days lost rate [3] |
|---|---|---|---|---|---|---|---|---|---|
| RETREAT [4] | | | | | | | | | |
| 2 | 13 | 1,029 | 79 | 4,495 | 2.10 | 27.40 | 1.31 | 942 | 24 |
| 3 | 7 | 240 | 34 | 1,702 | 3.46 | 10.15 | 0.41 | 145 | 11 |
| 4 | 57 | 2,184 | 38 | 15,260 | 3.60 | 15.91 | 1.37 | 592 | 47 |
| 5 | 37 | 1,215 | 33 | 7,504 | 2.91 | 11.64 | 0.78 | 230 | 13 |
| 6 | 28 | 948 | 34 | 7,525 | 3.74 | 15.22 | 1.49 | 302 | 21 |
| 7 | 34 | 1,878 | 55 | 12,069 | 2.99 | 13.31 | 0.84 | 271 | 15 |
| 8 | 8 | 1,323 | 165 | 9,755 | 3.64 | 16.48 | 1.42 | 387 | 38 |
| 9 | 7 | 314 | 45 | 3,388 | 4.83 | 6.56 | 0.86 | 330 | 78 |
| 10 | 0 | 0 | 0 | 0 | 0 | 0 | 0 | 0 | 0 |
| ROOM-AND-PILLAR [5] | | | | | | | | | |
| 2 | 52 | 2,122 | 41 | 11,134 | 2.66 | 26.34 | 1.15 | 785 | 31 |
| 3 | 60 | 1,720 | 29 | 11,093 | 3.38 | 11.50 | 0.85 | 306 | 33 |
| 4 | 256 | 7,490 | 29 | 49,797 | 3.80 | 16.31 | 1.64 | 564 | 56 |
| 5 | 164 | 4,090 | 25 | 21,465 | 2.82 | 12.97 | 1.24 | 456 | 37 |
| 6 | 228 | 5,447 | 24 | 34,356 | 3.65 | 16.42 | 1.82 | 400 | 50 |
| 7 | 192 | 6,069 | 32 | 37,087 | 3.08 | 14.34 | 1.11 | 309 | 20 |
| 8 | 23 | 3,443 | 150 | 25,435 | 3.75 | 17.27 | 1.41 | 466 | 37 |
| 9 | 20 | 836 | 42 | 8,061 | 4.37 | 10.30 | 1.08 | 317 | 36 |
| 10 | 19 | 1,856 | 98 | 15,685 | 4.07 | 16.88 | 2.29 | 413 | 65 |

[1]Excludes anthracite mines and mines producing less than 5,000 st.
[2]Accident rates are calculated as the total number of injury accidents (severity 1-6) per 200,000 hours worked.
[3]Days lost rates are calculated as the total number of days lost due to injury per 200,000 hours worked.
[4]Retreat mines are the 186 nonlongwall mines with active gobs identified by Urosek et al. [1995].
[5]Room-and-pillar mines include all nonlongwall mines.

Source: MSHA Accident and Employment Data Base for 1993.

Table 1 and figures 1-2 show that the sample of retreat mines employed 9,129 miners and produced 56 million t (61.7 million st) in 1993, representing 18% of the total underground production. The 56 million t (61.7 million st) includes both development and retreat tonnage. A reasonable estimate is that pillar recovery operations account for about one-third of coal

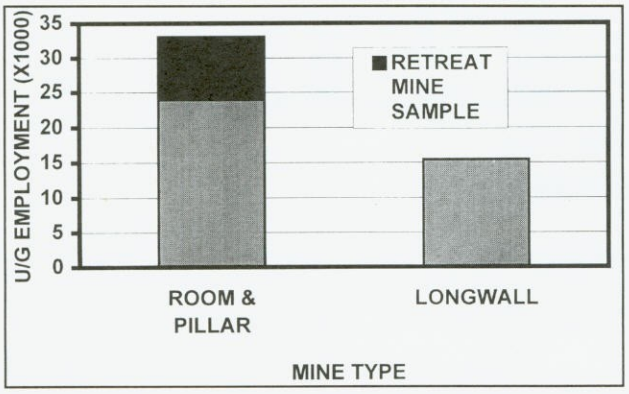



Figure 1. Employment at U.S. underground coal mines in 1993, by mine type.

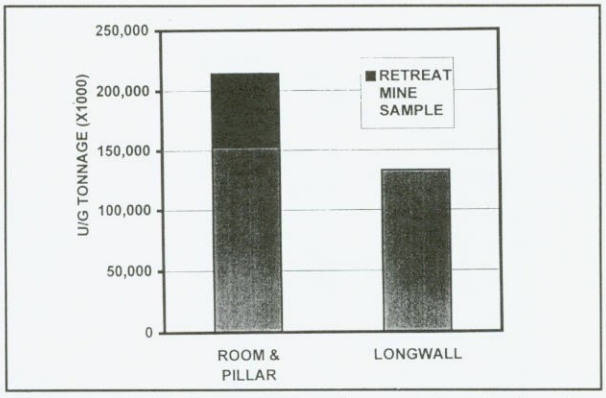



Figure 2. Production at U.S. underground coal mines in 1993, by mine type.

production from retreat mines [Reese et al. 1978]. Including some contribution from the mines with inactive ventilated gobs, it appears that pillar recovery may have accounted for about 10% of the 315 million t (347 million st) mined underground in 1993.

An average of 49 miners were employed at each pillar retreat mine, slightly more than at the typical room-and-pillar mine, but much less than at a longwall mine. The accident statistics in figure 3 show that, overall, the injury record of retreat mines was similar to that of other mining methods. Surprisingly, roof and rib accident rates in figure 4 were 21% *lower* at retreat mines than at other room-and-pillar mines. One possible explanation is that roof bolting, which is a significant source of roof fall injuries, is seldom employed during retreat mining. The rates for days lost from all accidents closely paralleled the overall accident rates.

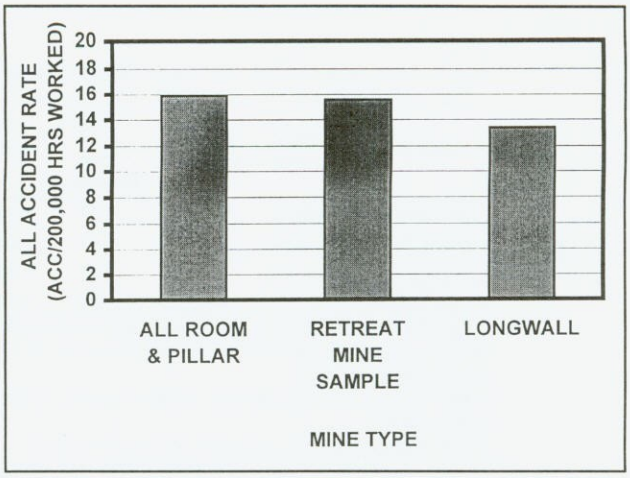



Figure 3. Accident rate at U.S. underground coal mines in 1993, by mine type.

Some regional trends are shown in table 2 and figures 5-6. It appears that retreat mining was widely practiced throughout the Appalachian and midwestern U.S. coal mining areas. The only MSHA districts with few active pillar recovery operations were District 3 (northern West Virginia), District 9 (primarily Colorado, Wyoming, and Utah), and District 10 (western Kentucky).

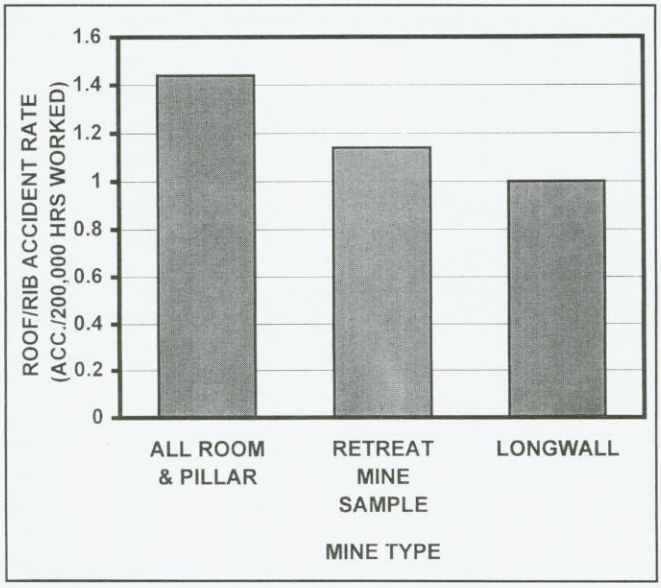



Figure 4. Roof/rib accident rates at U.S. underground coal mines in 1993, by mine type.

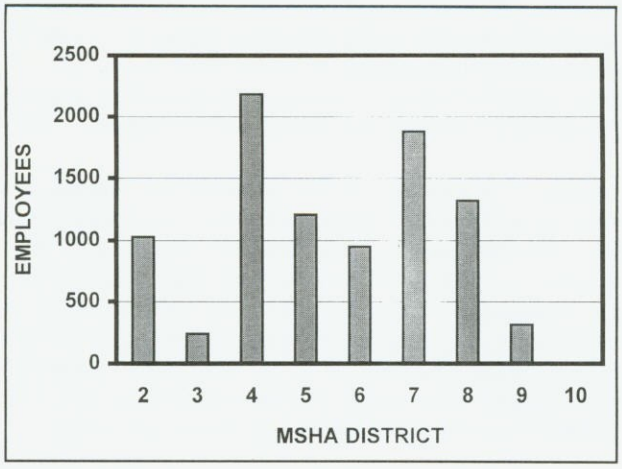



Figure 5. Employment at sample retreat mines, by MSHA district.

The largest number of retreat mines were found in the southern Appalachian coalfields (MSHA District 4 in southern West Virginia; District 5 in Virginia; District 6 in eastern Kentucky; and District 7 in eastern Kentucky and Alabama). These four MSHA districts accounted for 156 mines, or 85% of the sample. The retreat mines in this region were typically smaller than those in other districts, averaging 40 employees each, compared with 83 in the average mine outside the region.

Accident rates vary from MSHA district to district, as shown in figure 7. Within each district, they tend to be similar between the retreat mine sample and all room-and-pillar mines. Roof and rib accident rates were lower in 1993 at the retreat mines in six of the eight districts.

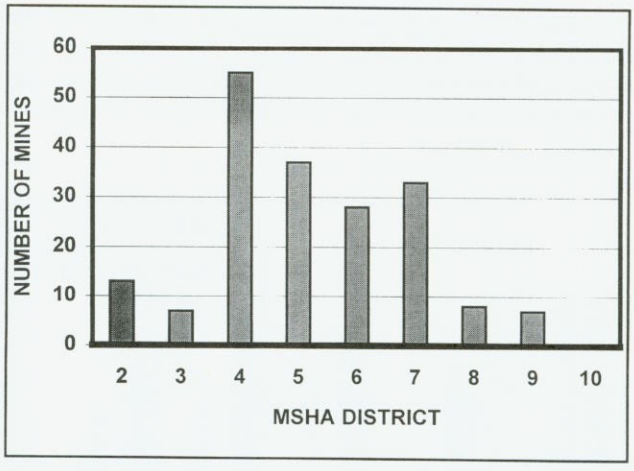



Figure 6. Number of sample retreat mines, by MSHA district.

Table 3 and figure 8 show that retreat mines tended to be larger than the average room-and-pillar mines. Only 15% of all small mines were conducting active pillar recovery operations, whereas about 40% of all medium and large mines were

**Table 3.— Demographics and accident statistics for U.S. underground coal mines by mine size[1]**

| Mine size | No. of mines | No. of employees | Average mine size (employees) | Tons, thousand st | Productivity, st/h | Total accident rate [2] | Roof/rib accident rate [2] | Total days lost rate [3] | Roof/rib days lost rate [3] |
|---|---|---|---|---|---|---|---|---|---|
| RETREAT [4] | | | | | | | | | |
| Small [5] | 133 | 2,892 | 22 | 20,376 | 3.50 | 13.18 | 1.20 | 305 | 27 |
| Medium [6] | 41 | 3,481 | 85 | 23,785 | 3.25 | 17.30 | 1.04 | 466 | 26 |
| Large [7] | 12 | 2,756 | 230 | 17,539 | 3.06 | 15.83 | 1.22 | 519 | 35 |
| ROOM-AND-PILLAR [8] | | | | | | | | | |
| Small [5] | 873 | 17,253 | 20 | 103,912 | 3.50 | 14.76 | 1.44 | 353 | 37 |
| Medium [6] | 113 | 9,166 | 81 | 67,299 | 3.57 | 17.07 | 1.45 | 541 | 46 |
| Large [7] | 28 | 6,653 | 238 | 43,087 | 3.17 | 16.84 | 1.43 | 539 | 41 |

[1]Excludes anthracite mines and mines producing less than 5,000 st.
[2]Accident rates are calculated as the total number of injury accidents (severity 1-6) per 200,000 hours worked.
[3]Days lost rates are calculated as the total number of days lost due to injury per 200,000 hours worked.
[4]Retreat mines are the 186 nonlongwall mines with active gobs identified by Urosek et al. [1995].
[5]Small mines are those employing fewer than 50 workers.
[6]Medium mines are those employing 50 to 150 workers
[7]Large mines are those employing more than 150 workers.
[8]Room-and-pillar mines include all nonlongwall mines.

Source: MSHA Accident and Employment Data Base for 1993.

recovering pillars.[1] Accident rates did not show any significant trends with regard to mine size.

## ANALYSIS OF FATAL INCIDENTS

A total of 25 fatal incidents, resulting in 33 deaths, have been attributed to retreat mining during 1989-96. Four of the retreat mining fatal incidents (comprising five fatalities) occurred during room development with no apparent influence of a gob. The remaining 28 fatalities represent 25% of the 111 roof and rib fatalities that occurred during this period (figure 9). A report by MSHA has not been completed on the most recent incident, a double fatality in Kentucky. A detailed analysis of the remaining 20 incidents is available elsewhere (Mark & Tuchman, 1997).

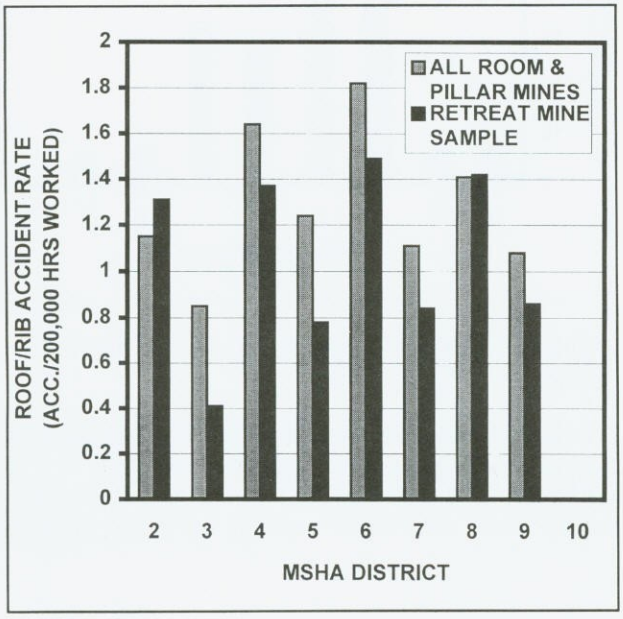



Figure 7. Roof/rib accident rates at retreat and all room-and-pillar mines, by MSHA district.

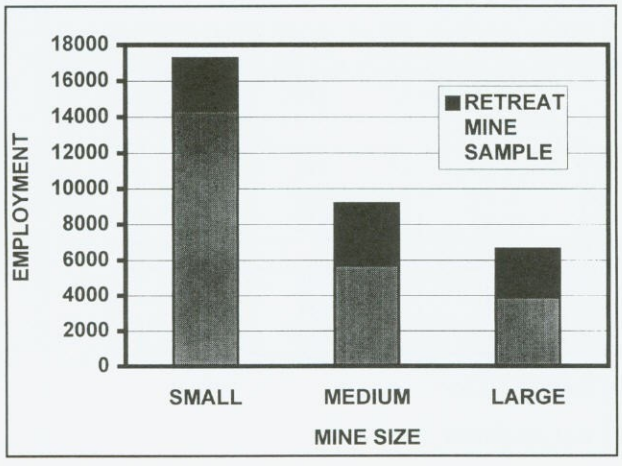



Figure 8. Employment at retreat and all room-and-pillar mines, by mine size.

[1]Small mines are those employing fewer than 50 workers; medium mines employ 50 to 150 workers; large mines employ more than 150 workers.

Figure 10 shows that, in four incidents, no citations were issued for violations of mining law or the mine's roof control plan. The remaining 16 fatal incidents were divided into 2 categories, or classes. Class 1 includes eight incidents where gross violation of mining law (and often common sense) was deemed to be the chief factor. Class 2 incidents were those where a violation contributed to the fatality, but where other factors appeared to have played an important role as well. Class 3 incidents were those for which no citations were issued.

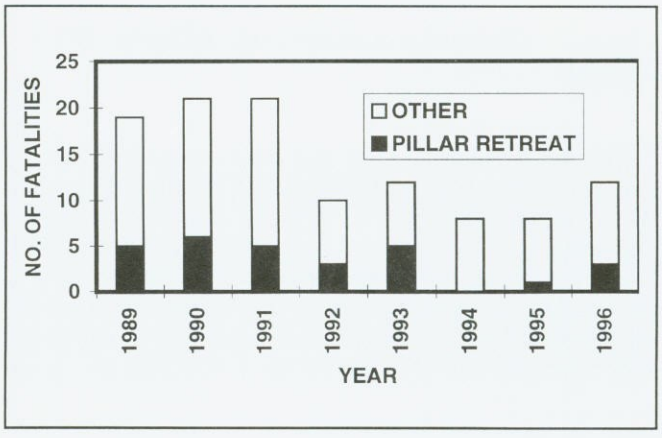



Figure 9. Fatal roof/rib fatalities 1989-1996.

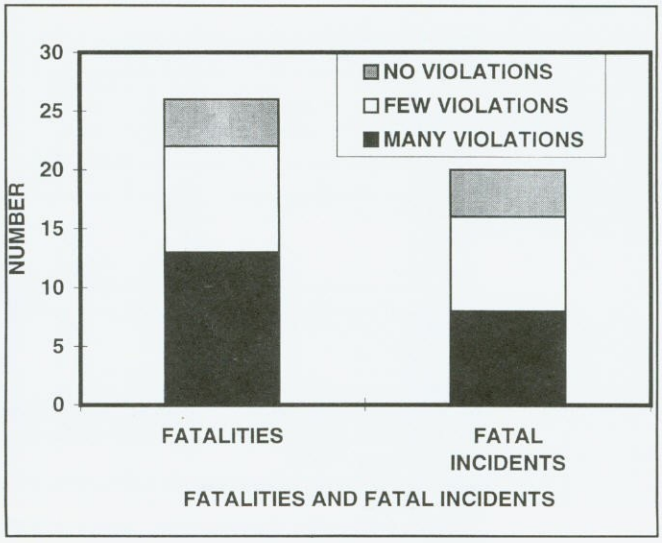



Figure 10. Fatal roof/rib incidents and fatalities associated with retreat mining 1989-1996.

Figure 11 shows that the States of Kentucky, Tennessee, and West Virginia have accounted for 92% of all pillaring fatalities. Every incident in Kentucky and Tennessee involved a violation. All four of the no-citation incidents occurred in West Virginia.

Geologic factors were cited in eight instances as contributing to the fatal incidents. Roof slips and slickensides were the most common features. The no-citation incidents also involved a first fall, high stress, and a multiple-seam interaction (figure 12). High vertical stress was a factor in three of the class 2 fatal incidents. The types of violations cited in the other incidents are shown in figure 13. Mining sequence violations were most frequently cited in the class 2 fatal incidents.

The mining techniques employed to extract pillars are shown in figure 14. All five fatalities during slabbing operations occurred on conventional mining sections. Partial pillaring or "Christmas tree" methods were used in 82% of the incidents where continuous miners were employed.

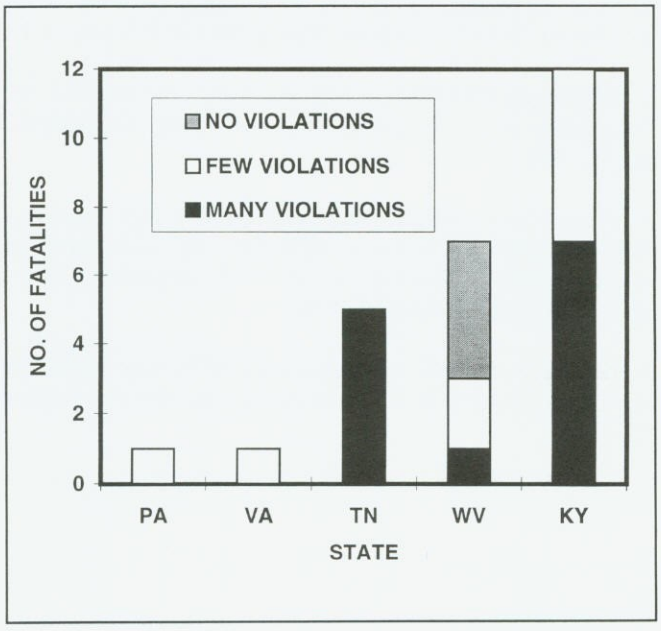



Figure 11. Location of the retreat mining fatal accidents.

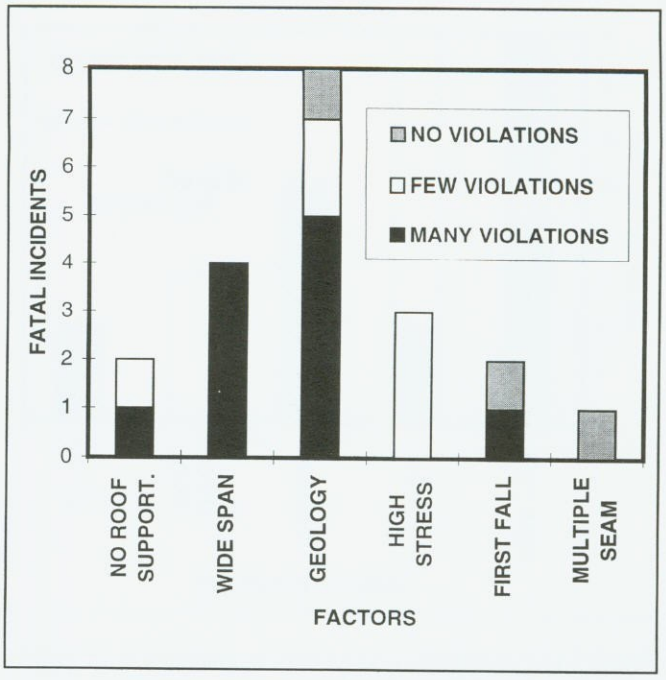



Figure 12. Contributing factors cited in the retreat mining fatal roof/rib incidents.

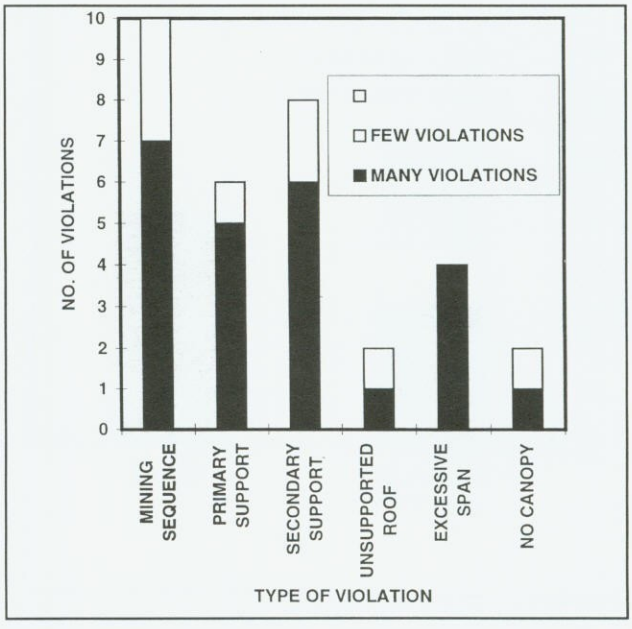



Figure 13. Types of violations cited in the retreat mining fatal roof/rib accidents.

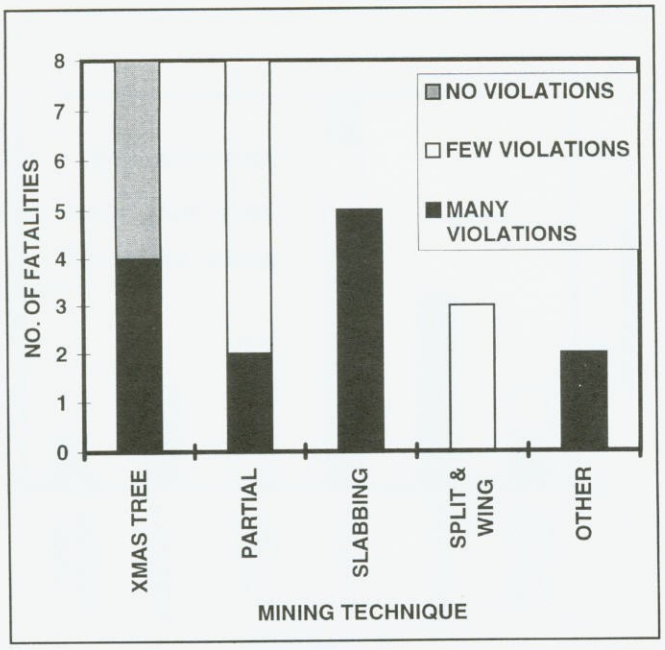



Figure 14. Pillar extraction techniques employed in the retreat mining fatal roof/rib accidents.

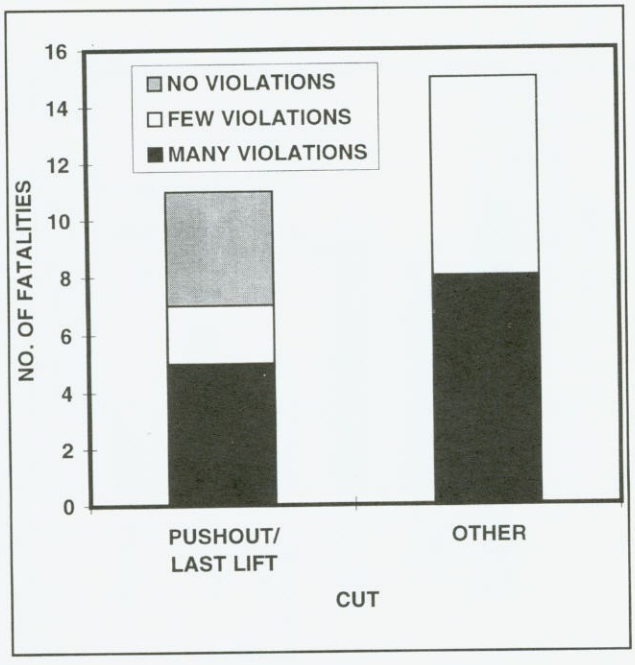



Figure 15. Lift being extracted when fatal roof fall occurred.

## CONCLUSIONS

Pillar recovery is employed in many U.S. coal regions. It is practiced primarily at many medium and some small mines. The overall accident rates for retreat mines appear to be similar to those of other room-and-pillar mines. The number of fatalities that have occurred during pillar recovery operations seems disproportionately high relative to coal production. Many fatalities that have occurred during retreat operations can be largely attributed to violations of existing mining law. Nearly 50% of fatal incidents have occurred during the recovery of the final lift (or pushout). Other potential problem areas include high stress/deep cover, first falls, geologic factors, mining sequence, and multiple-seam interactions.

## REFERENCES

1. Blaiklock J [1992]. A Kentuckian vote for continuous mining. Mining Magazine *June*:365-366.

2. Mark, C, Tuchman RJ [1997]. Proceedings: New Tecnology for Ground Control, in Retreate Mining, NIOSH IC 9446, 14-16.

3. Montague PG [1988]. Pillar recovery—the lost art? In: Proceedings of the American Mining Congress. Chicago, IL: pp. 531-548.

4. Reese RG, Dash BB, Hamilton PA [1978]. Coal recovery from underground bituminous coal mines in the United States, by mining method. Washington, DC: U.S. Department of the Interior, Bureau of Mines, IC 8785.

5. Urosek JE, Zuchelli DR, Beiter DA [1995]. Gob ventilation and bleeder systems in U.S. coal mines. Soc Min Eng preprint 95-78.

# Full-Scale Performance Evaluation of Mobile Roof Supports

*Thomas M. Barczak,* Research Physicist
National Institute for Occupational Safety and Health
Pittsburgh Research Center
Pittsburgh, PA

*David F. Gearhart,* Research Physicist
SSI Services, Inc.
Pittsburgh, PA

## ABSTRACT

The performance characteristics of Mobile Roof Supports (MRS's) were evaluated through full-scale testing in the Strategic Structures Testing Laboratory at the National Institute for Occupational Safety and Health, Pittsburgh Research Center. Safety issues pertaining to the operation and design of these supports for pillar extraction during retreat mining are examined. A unique load frame, called the mine roof simulator, provided a realistic simulation of mining conditions by inducing vertical, horizontal, and lateral loading on the support. The purpose of these experiments was to determine the capabilities and limitations of the supports and to investigate factors that influence the measurement of loading and loading rate. An evaluation of the support design and load conditions that can cause support failure or loss of support capacity are discussed relative to the laboratory tests. In general, lateral loading perpendicular to the longitudinal axis of the canopy is most severe, although horizontal loading in the direction of the long axis of the canopy can also produce critical loading in some cases. The experiments indicate that both setting force and leg pressure measurements are influenced by the staging of the leg cylinders. The implications of these factors on load rate measurement are evaluated. A comparison of MRS capacity and stiffness characteristics is made to conventional timber supports.

## INTRODUCTION

Mobile Roof Supports (MRS's) have improved the safety of pillar extraction during secondary mining by providing superior roof control and significantly reducing the materials handling associated with timber posts in pillaring operations. The superior capabilities of the MRS's have promoted pillar extractions in conditions such as weak roof and floor geologies prone to unpredictable caving that were previously too dangerous when using timber posts.

Since the introduction of MRS's in the United States in 1988, MRS technology has matured, with installations in more than 40 coal mines. Overall, MRS's have experienced widespread success. Few failures have been reported; these are typically attributed to lack of operating experience or severe conditions, such as those associated with the first or large areas of caving strata. Only one fatality has occurred on a mobile section; however, the fatality was not attributed to failure of the mobile supports. Nevertheless, some questions arose during the fatality investigation in 1995 regarding the performance capabilities of MRS's and the capability to assess ground instabilities from MRS loading.

In an effort to evaluate their support design, a support from J.H. Fletcher and Company (Fletcher) and Voest Alpine Mining and Tunneling (VAMT) was evaluated at the Pittsburgh Research Center's Strategic Structures Testing Laboratory through full-scale testing in the unique *mine roof simulator* load frame. Although the supports that were tested are similar in operating range and capacity, the Fletcher support utilized three-stage leg cylinders, whereas the VAMT support utilized two-stage leg cylinders. This difference in leg design should be considered when making comparisons of support performance, particularly the stiffness of the support.

A series of tests was conducted under controlled load conditions, which provides a better understanding of the performance capabilities and limitations of MRS's and factors that influence the measurement of loading and loading rate. This paper presents the results of these laboratory studies and compares differences in design philosophies and evaluates their impact on support performance. The supporting capabilities of MRS's is compared with those of conventional timber posts and cribs. Safety issues relative to support maintenance and operation are also discussed.

## STRATEGIC STRUCTURES TESTING LABORATORY

The Strategic Structures Testing Laboratory is a unique laboratory where full-scale mining equipment and roof support

structures can be tested in a controlled environment. Figure 1 shows an MRS in the laboratory's mine roof simulator load frame. This unique load frame is designed to simulate the loading induced on support structures due to the behavior of rock masses during mining. The load frame can provide controlled roof and floor movements to simulate the closure of the mine opening while generating up to 13,334 kN (3 million lb) of vertical force and 7,117 kN (1.6 million lb) of horizontal (shear) force.

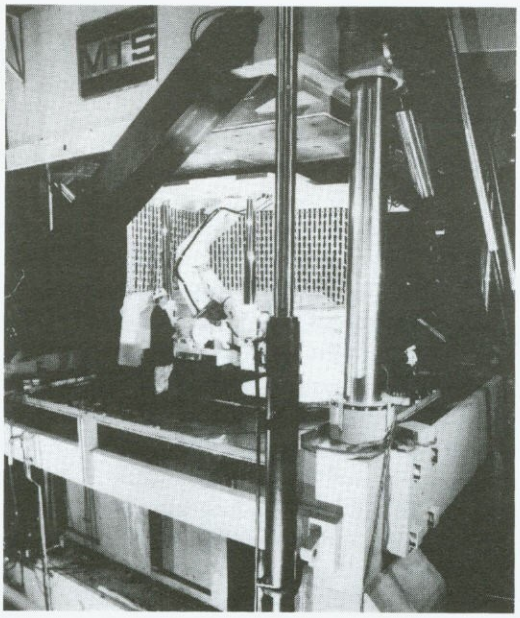


**Figure 1**. Full-scale testing of a mobile roof support in the unique mine roof simulator load frame.

The MRS was positioned in the proper orientation to allow the load frame to induce vertical, horizontal, or lateral loading on the support, as depicted in figure 2. Parameters investigated included; (1) setting pressure, (2) support height, (3) load vector (direction of loading), and (4) canopy contact configuration. Additionally, a variety of eccentric crawler frame contact configurations were evaluated with the Fletcher support. The testing effort focused on the following studies:

1. *Rated support capacity:* Determination of maximum support capacity in relation to the support's rated design capacity.
2. *Stiffness characteristics:* Measurement of support resistance and component responses to roof movements in the vertical, horizontal, and lateral directions.
3. *Setting force:* Evaluation of setting force as a function of leg staging and hydraulic pump pressure.
4. *Load and load rate measurement:* Evaluation of factors that affect the measurement of roof load and loading rate.
5. *Conditions that reduce support capacity:* Identification of load conditions that reduce support capacity.
6. *Critical load conditions:* Identification of load conditions that maximize component loading and those that produce critical loading where the structural integrity of the support is jeopardized.

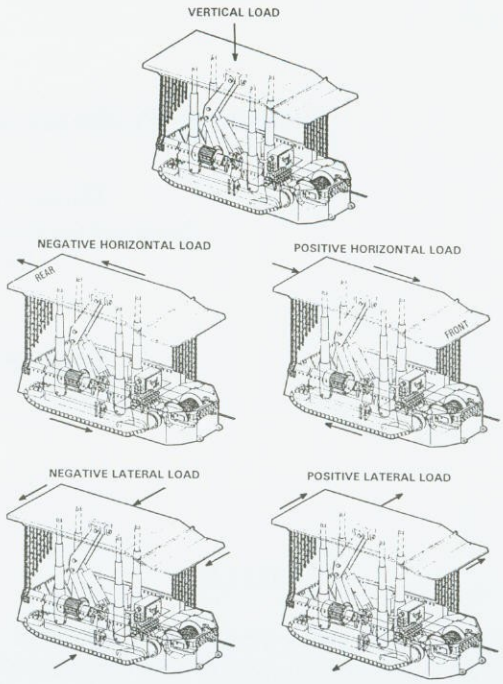



**Figure 2**. Vertical, horizontal, and lateral loading applied to the mobile roof supports by the mine roof simulator.

## MOBILE ROOF SUPPORT DESCRIPTION AND BASIC DESIGN PHILOSOPHIES

The VAMT support tested during this study was a model 185/380-540. The Fletcher support was a model MRS-13 with 1.45 m (57 in) to 3.71 m (146 in) operating height. Both supports were rated at 5,338 kN (600 tons) of support capacity. These support designs are representative of the support philosophies of the two manufacturers, although both manufacturers offer a variety of machines and designs to operate in mining heights ranging from 1.17 m (46 in) to 3.96 m (13 ft).

There are four significant differences in design philosophy between the two supports tested: (1) a flat-plate canopy construction versus a sloped-edge canopy construction, (2) a tilt-frame lemniscate assembly versus a rigid link lemniscate assembly, (3) internal versus exposed lemniscate assembly, and (4) a two- versus a three-stage leg cylinder design.

The Fletcher support utilized a canopy construction that is sloped at the edges, whereas the VAMT support utilized a flat-plate canopy design. The rationale for Fletcher's sloped-edge design is to accommodate edge and point loading with reduced deflection and stress at full load. The sloped edges are also intended to facilitate moving the support in uneven or jagged roof strata. A consequence of this design is increased canopy stiffness as the edge plates reduce the size and significantly stiffen the top canopy plate. Deflections as great as 7.6 cm (3 in) were observed over the length of the VAMT canopy when the support was loaded with a single contact placed near the canopy tip. The flat-plate concept typically provides greater roof coverage due to roof contact across the full width and length of the canopy structure. However, the greater roof contact will not necessarily translate into

larger support loads, since the roof typically behaves as some sort of beam with support loading controlled by roof displacements and not the dead weight of the rock mass.

Another major design difference pertained to the lemniscate assembly. The VAMT support utilized a lemniscate assembly connected to a tilt frame that permits single degree-of-freedom rotation of the lemniscate assembly due to lateral loading (see figure 3). The rotation is controlled by hydraulic cylinders called tilt cylinders. This design limits lateral load development in the

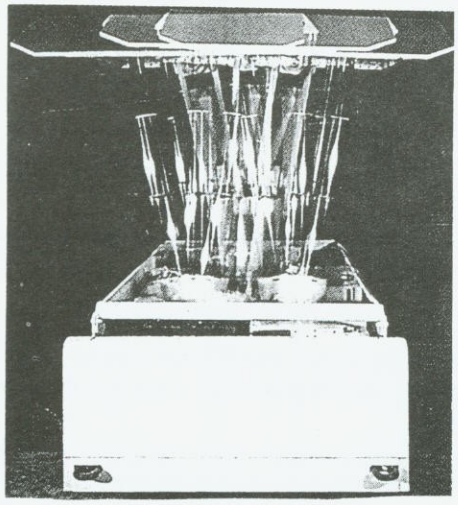


**Figure 3**. Tilt-frame lemniscate assembly utilized on the VAMT support

lemniscate assembly, but allows lateral translation of the canopy once the yield pressure of the tilt cylinders is reached. The Fletcher MRS, as tested, did not incorporate a tilt frame for the lemniscate assembly and relies on the strength of the lemniscate structure and connecting joints to resist lateral loading. The consequence of this design is significantly larger stress development in the lemniscate assembly due to lateral loading; however, the lateral translation of the canopy as a function of applied load is less than that of the VAMT tilt-frame design, particularly when the yield pressure of the tilt cylinders is reached.

The VAMT support also utilized a hydraulic cylinder, called an aligning cylinder (see figure 4), for the top lemniscate link, versus a rigid steel link in the Fletcher support. The aligning cylinder limits horizontal load development, thereby minimizing stress development in the lemniscate assembly due to horizontal loading.

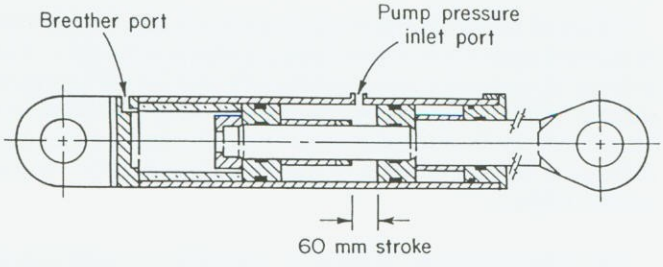



**Figure 4**. Aligning cylinder designed to control horizontal loading on the VAMT support.

When yield pressure is reached, the aligning cylinder yields through a 60 mm (2.4-in) stroke, permitting an equivalent horizontal displacement of the canopy relative to the base. When the rear legs are retracted, the aligning cylinder returns to its initial stroke and restores the canopy to its initial horizontal position.

The position of the lemniscate assembly also differed for the two supports tested. The caving shield protruded beyond the rear of the canopy in the Fletcher support, whereas the entire lemniscate assembly was internal (within the confines of the canopy) on the VAMT support. The VAMT support utilized a chain curtain to resist gob flushing into the support. Fletcher contends that the external position of the caving shield provides increased protection to machine components from gob material and can act as a wedge to help to push the support from heavily caved areas. The exposed caving shield can also cause additional loading on the lemniscate assembly due to gob loading.

The Fletcher support that was tested utilized three-stage leg cylinders, as opposed to two-stage leg cylinders in the VAMT support. The rationale for the three-stage design is to enhance operating range. A consequence of the three-stage design is larger diameter leg cylinders, which impacts the operating pressure and several performance parameters, as described later in this paper.

## ASSESSMENT OF LABORATORY TEST RESULTS

### Maximum Support Capacity

The maximum support capacity is controlled by hydraulic yielding of the leg cylinders, with a yield valve controlling the maximum pressure in the *bottom* stage of the leg cylinders. Normally, the left and right legs in the front and rear set are hydraulically connected together. As a result, the yield valve with the lowest operating pressure will control both legs in the set. The yield pressure required to provide a designated support capacity is a function of the effective area of the bottom stage of the leg cylinder. For example, the required yield pressure to produce 5,338 kN (600 tons) of support capacity was 26.3 MPa (3,820 psi) for the Fletcher support and 36.3 MPa (5,263 psi) for the VAMT support. This difference is due to the difference in leg diameters: 25.4 cm (10 in) for the Fletcher and 21.8 cm (8.6 in) for the VAMT support.

## STIFFNESS CHARACTERISTICS

A comparison of the vertical, horizontal, and lateral stiffness at a 2.4-m (96-in) operating height is presented in table 1. As seen in the table, both supports are much stiffer vertically than horizontally or laterally; this means that much more roof movement is required to produce equivalent support resistance to the applied displacement in the horizontal or lateral direction than for roof-to-floor convergence. It should also be noted that the initial horizontal and lateral stiffness of the support is sensitive to translational freedom in the various joints of the lemniscate assembly and the gear train of the crawler drive assembly. The stiffnesses shown in table 1 represent the support response once this translational freedom has been removed.

Table 1.—Comparison of support stiffness at a 2.4-m (96-in) operating height

| Load vector | Support stiffness, kN/cm (kips/in)[1] | |
|---|---|---|
| | VAMT support[2] | Fletcher support[3] |
| Vert. displ. | 3,002 (1,714) | 2,140 (1,222) |
| Hor. displ.[4] | 271 (155)[5];137 (78)[6] | 315 (180) |
| Lat. displ. | 91 (52)[7] | 137 (78)[8]; 39 (22)[9] |

[1]Stiffness measured when no leg stage is fully extended.
[2]Two-stage leg cylinder support design.
[3]Three-stage leg cylinder support design.
[4]Horizontal stiffness shown for horizontal displacement toward the plow of the support.
[5]Initial stiffness prior to pressure development in the aligning cylinder.
[6]Stiffness after aligning cylinder begins to develop pressure.
[7]Initial stiffness prior to yield of tilt cylinders. Load applications that would produce yielding of the tilt cylinders were not evaluated.
[8]Initial stiffness during first 1.3 cm (0.5 in) of lateral movement.
[9]Stiffness beyond initial 1.3 cm (0.5 in) of lateral movement.

## Vertical Stiffness

Vertical stiffness is controlled almost entirely by the stiffness of the hydraulic leg cylinders. It depends on the height of the support and decreases with increasing height. Therefore, the supporting force at a high operating height will be less than at a lower operating height for the same roof-to-floor convergence. Using the VAMT support as an example, the supporting force at a height of 3.8 m (148 in) is only 38% of the supporting force at a height of 2.4 m (96 in) for the same roof-to-floor convergence.

When none of the leg stages are fully extended, the support stiffness is constant from set to yield, and the setting pressure does not have a significant effect on the support stiffness. When the support is set with the bottom stage fully extended, the (vertical) support capacity as a function of displacement is bilinear. The initial stiffness is high, since the effective column length is now reduced to that of the upper stage of the leg cylinders, and decreases once the upper stage force exceeds that of the lower stage *setting* force.

As expected, the VAMT support was stiffer in response to vertical loading than the Fletcher support (see table 1). This is primarily due to the two-stage leg cylinder design in the VAMT support, compared with the three-stage leg cylinder design in the Fletcher support. All other things being equal, a three-stage leg cylinder will *always* be less stiff than a two-stage leg cylinder, because the stages act in series with the equivalent stiffness reduced as the number of stages increases. The stiffness of individual stages is governed primarily by the area and stroke of the cylinder, decreasing in stiffness as the area decreases or the stroke increases. Thus, the stage with the smallest diameter will be the least stiff stage and is likely to control the equivalent stiffness of the entire leg.

When both supports are set at the same *pressure*, they will reach yield load at nearly the same displacement. For example, with a setting pressure of 17.3 MPa (2,500 psi) at the 2.4-m (96-in) operating height, the VAMT support will reach yield load (5,338 kN (1,200 kips)) after 0.94 cm (0.37 in) of roof-to-floor convergence, compared with 0.86 cm (0.34 in) for the Fletcher support (see figure 5). However, when set to the same setting *force*, the Fletcher support will require 40% more displacement to reach yield load (see figure 6).

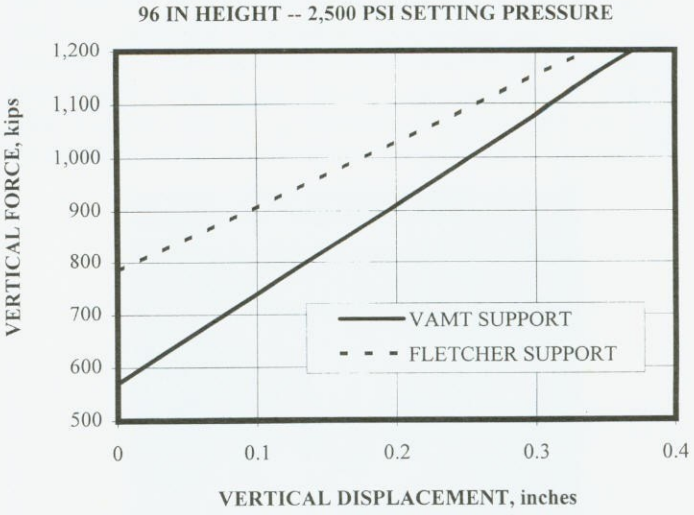



**Figure 5**. Both the VAMT and Fletcher support reach yield load at nearly the same displacement when set to the same setting pressure.

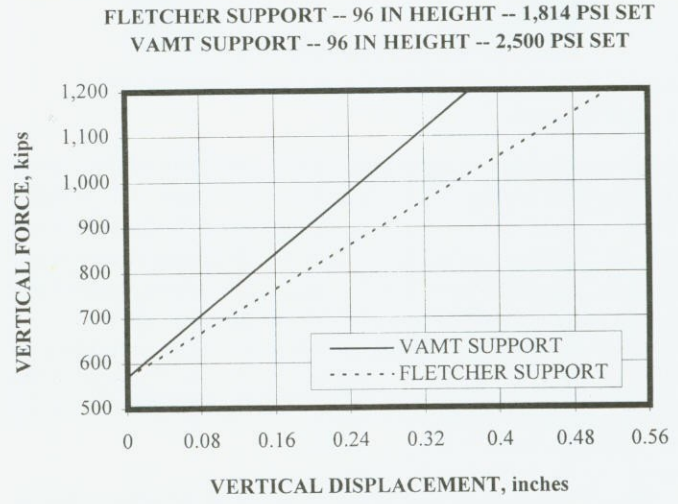



**Figure 6**. Roof to floor convergence required to produce yield load in Fletcher and VAMT support when both set to same setting force.

## Horizontal Stiffness

Horizontal stiffness is a measure of support resistance to forward or rearward displacements of the canopy relative to the base. The action of the lemniscate assembly primarily controls the horizontal stiffness of MRS's, since the leg cylinders are nearly vertical and do not provide much resistance to horizontal loading. Horizontal stiffness is at least an order of magnitude less than the vertical support stiffness.

The initial horizontal stiffness is controlled by translational freedom in the connecting joints of the lemniscate assembly and gear train of the drive motors. For example, up to 1.91 cm (0.75 in) of horizontal displacement of the canopy relative to the

base was required in the VAMT support before any significant load resistance was generated. The horizontal stiffness of the support is also height-dependent, decreasing at increasing heights.

Unlike the Fletcher support, which utilizes rigid lemniscate links, the horizontal force in the VAMT support, which utilizes a hydraulic aligning cylinder to limit the maximum horizontal loading, is a bilinear function of horizontal displacement. The horizontal stiffness at a particular height is reduced by as much as 50% when the aligning cylinder begins to develop load (see figure 7). The horizontal stiffness of the Fletcher support is 2.3 times that of the VAMT support when the aligning cylinder is controlling horizontal load development.

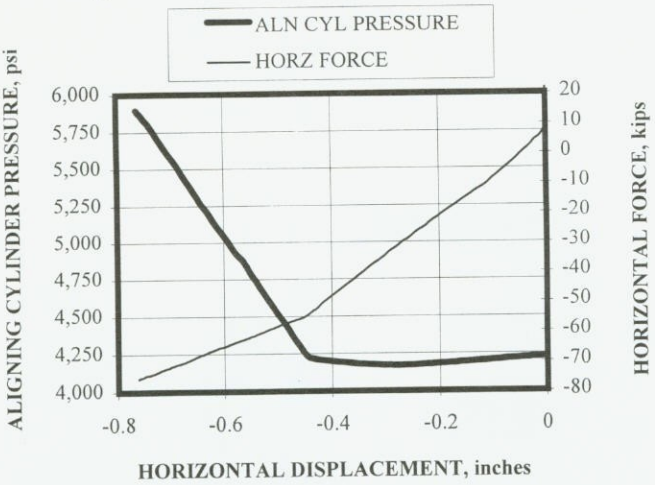



**Figure 7**. Reduction in horizontal stiffness when pressure develops in the aligning cylinder.

### Lateral Stiffness

Lateral stiffness is a measure of support resistance to applied left or right displacements of the canopy relative to the base. Thus, the direction of loading is across the width of the canopy versus along its length in horizontal stiffness evaluations. Lateral stiffness is also height-dependent.

For supports equipped with a tilt-frame lemniscate assembly such as the VAMT support, lateral stiffness is controlled primarily by the tilt cylinders, which control rotation of the lemniscate tilt assembly. The lateral stiffness of the Fletcher support tended to be bilinear with a high initial stiffness during the first 1.3 cm (0.5 in) of lateral movement, followed by a reduced stiffness for lateral movements beyond this, as shown in figure 8. The bilinear nature of the lateral stiffness is probably due to the interaction of the leg cylinders and the lemniscate assembly. This bilinear behavior was not observed in the VAMT support. As shown in table 1, the Fletcher support is stiffer than the VAMT support initially, whereas the VAMT support is stiffer than the Fletcher support when the lateral movement exceeds 1.3 cm (0.5 in).

The lateral stiffness is less than the horizontal stiffness by a factor of 3 for the VAMT support and a factor of 3.8 (initial stiffness) or a factor of 8 (final stiffness) for the Fletcher support at a 2.4-m (96-in) operating height.

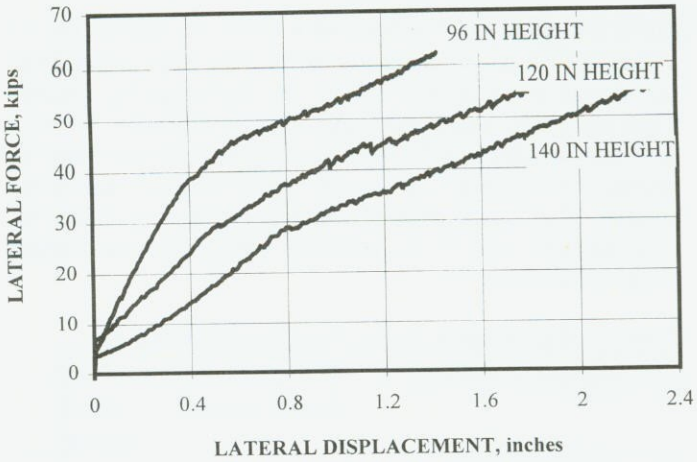



**Figure 8**. Bilinear stiffness response to lateral loading.

## ASSESSMENT OF SETTING FORCE

Setting force is defined as the force exerted against the mine roof and floor by actively setting the support using the internal hydraulic power. The setting force is determined by the effective leg area times the hydraulic pressure with the total setting force equal to the sum of all four leg cylinder forces. The effective leg area depends on the staging of the leg cylinders. Figure 9 compares the setting force as a function of hydraulic leg pressure with no stages fully extended for the Fletcher and VAMT supports. Because the VAMT support has smaller diameter leg cylinders, 21.8 cm (8.6 in) compared with 25.4 cm (10 in) for the Fletcher support, greater pressures are required to produce equivalent setting forces. For example, approximately 17.4 MPa (2,530 psi) of pressure is required to produce 3,558 kN (800 kips) of setting force with the Fletcher support, whereas 24.1 MPa (3,500 psi) would be required to produce an equal setting force with the VAMT support.

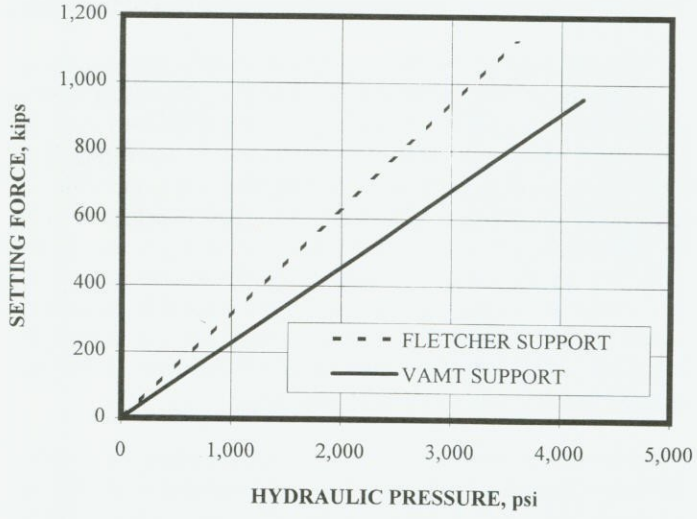



**Figure 9**. Comparison of setting forces with no stages fully extended for Fletcher and VAMT support.

The VAMT support utilized a two-stage leg cylinder, whereas the Fletcher support utilized a three-stage leg cylinder. Table 2

shows the reduction in setting force due to leg staging for the VAMT and Fletcher supports. As shown in the table, setting force can be reduced by as much as 70% for three-stage leg cylinders when the bottom and middle stages are fully extended. Because variances can also exist in each leg of the support with regard to staging, setting forces between the values shown in table 2 are possible. Thus, a wide range of setting forces can be provided for both supports even if the hydraulic setting pressures remain constant from set to set.

Table 2.—Reductions in setting force due to leg staging

| Leg stage condition | Reduction in setting force, % | |
|---|---|---|
| | Fletcher support[1] | VAMT support[2] |
| No stages fully extended | 0 | 0 |
| Bottom stage fully extended | 45 | 42 |
| Bottom and middle stage fully extended | 70 | NAp |

[NAp]Not applicable.
[1]Three-stage leg cylinder design.
[2]Two-stage leg cylinder design.

The effect of leg staging on setting force development can be explained by examining the operation of the leg during setting and the associated leg mechanics, as depicted in figure 10 for a three-stage leg cylinder. Operationally, when the support is raised, the bottom stage is designed to extend to full extension first, followed by the middle and top stages. Likewise, when the support is lowered, the bottom stage retracts first, followed by the middle and top stages. The setting force will always equal the force developed in the stage with the largest diameter that is *not* fully extended, equaling the pump pressure times the area of that stage.

When the support is initially raised from a collapsed position to a height greater than the bottom leg extension, the setting force is diminished in proportion to the area reduction of the next stage, as depicted in table 2. On subsequent setting events, the setting force depends on whether full extension of leg stages is required due to changes in operating height. Once a support is extended to an operational height with a diminished setting force due to the bottom or middle stage being fully extended, the setting force will be restored to its maximum capability if the support is reset at *any* lower height, provided the bottom stage has not been fully retracted, and the setting force again will be diminished if the support is reset at an equal or greater height.

An example is shown in figure 11 for a three-stage leg cylinder. Behavior of a two-stage leg cylinder can be deduced by elimination of the middle stage. Initially, the support is set at a height ($H_{INT}$) that causes the bottom stage to be fully extended, providing a diminished setting force. In preparation for the next cycle, the support is lowered, during which the bottom stage is partially retracted while the upper stages remain extended. When the support is reset (second cycle) at a lower operating height, full extension of the bottom stage is not required since the upper stages remain extended from the previous cycle. As a result, the setting force is restored to its maximum capability, equaling the setting pressure times the area of the bottom stage. Two scenarios are

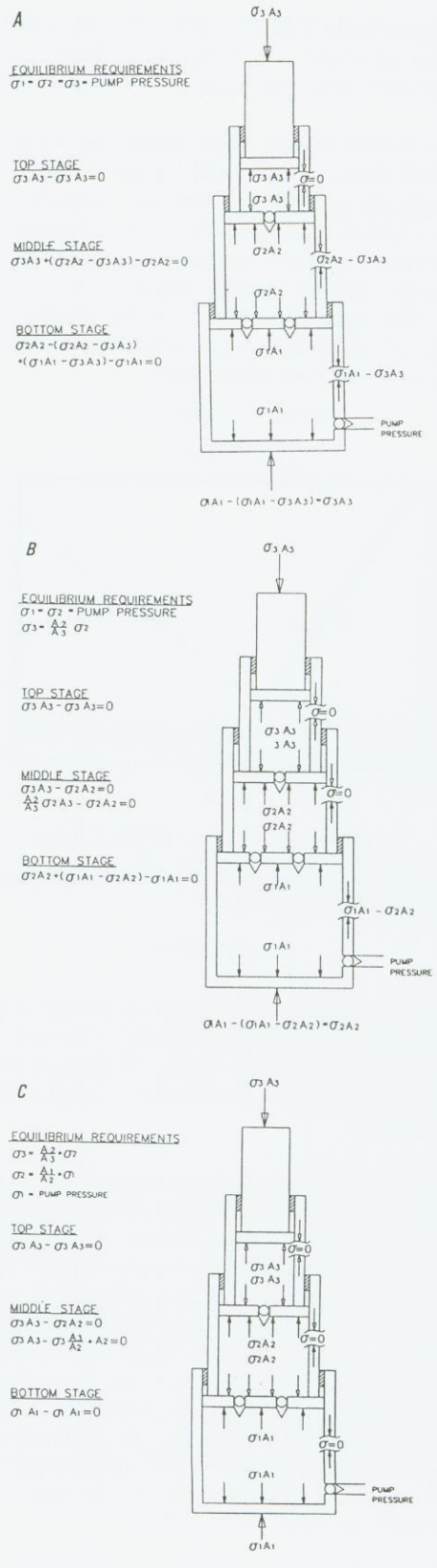



**Figure 10**. Leg mechanics. A, bottom and middle stages fully extended; B, bottom stage fully extended; C, no stage fully extended.

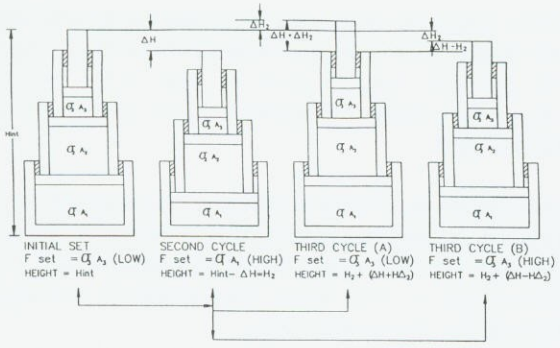



**Figure 11**. Conditions that produce diminished setting force and unrecorded roof loads.

examined for the third cycle. In both cases, the support is reset at a higher operating height than the second cycle. In the first case, the support is raised to a height greater than the initial height. In this case, the bottom stage is fully extended once again and the setting force is once again diminished. However, if the support is raised to a height on the third cycle that is less than the initial height, full extension of the bottom stage is not required and full setting capacity is maintained.

In summary, during an underground operation, the setting force will *always* be reduced on the mining cycle that establishes a *new maximum operating height* after an initial operating height that causes full extension of the bottom stage. All other cycles should provide full setting capability because extension of the bottom stage will not be required. Operationally, the probability of achieving maximum setting forces can be enhanced by establishing a maximum operating height as soon as possible. Ideally, when the support is initially taken underground, it can be brought to a location that is higher than where it will be placed into operation during pillar extraction, and fully extended. This will ensure full setting forces for all load cycles, provided the support is not lowered to the point where the bottom stage is fully collapsed, which would then cause retraction of the upper stages. In this case, a new maximum operating height would have to be established to prevent reductions in setting force.

## FACTORS AFFECTING LOAD AND LOAD RATE MEASUREMENTS

Since the dial gauges on the support measure pressure in only the bottom stage of the leg cylinder, an assessment of load and loading rates can only be determined through the full load cycle when none of the stages are fully extended. If the bottom stage or bottom and middle stages (three-stage cylinder design) are fully extended, the dial gauges will not record changes in pressure until the setting forces in the extended stages are overcome by additional load development in the upper stages. When this condition occurs, roof loading during the beginning of the loading cycle will go undetected by the dial pressure gauges. The period of undetected roof loading depends on the setting pressure and will increase with increasing setting pressure in a particular support.

Figure 12 shows the magnitude of roof loading that is not recorded by the dial pressure gauges when one or more leg stages

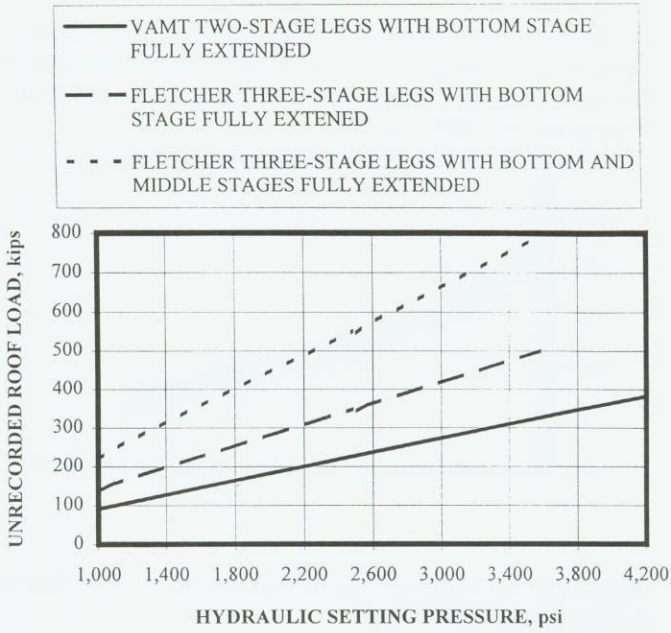



**Figure 12**. Unmeasured roof load when one or more of the stages are fully extended as a function of setting pressure.

are fully extended as a function of the setting pressure. As seen in the figure, the unrecorded roof loads increase linearly with increasing setting pressure. As expected, the magnitude of unrecorded roof loading is much greater for the Fletcher three-stage leg cylinders than for VAMT two-stage leg cylinders because the bottom stage area is 35% larger in the Fletcher support, creating a higher setting force in the bottom stage compared with the VAMT support at the same hydraulic setting pressure. Additionally, when the bottom and middle stages are fully extended, the load difference between the top and bottom stages governs the unrecorded roof load. As shown in figure 12, unrecorded roof load ranged from approximately 445 kN (100 kips) at 6.9 MPa (1,000 psi) of setting pressure to as high as 1,690 kN (380 kips) at full pump pressure for the VAMT support and 609 kN (137 kips) at 6.9 MPa (1,000 psi) of setting pressure to 2,202 kN (495 kips) at full pump pressure when the bottom stage of the Fletcher support is fully extended. When both the bottom and middle stages are fully extended, 3,509 kN (789 kips) of roof loading can go undetected by the dial gauges when the Fletcher support is set to full pump pressure.

Therefore, a false sense of loading and loading rate can be interpreted from the pressure gauges when the bottom leg stage is fully extended. This can result in unreliable information regarding roof stability and impending roof caving. However, the inaccurate information occurs only when a new maximum operating height is attained; therefore, the probability of inaccurate information depends on the mining conditions.

## CONDITIONS THAT REDUCE SUPPORT CAPACITY

One cause of reduced support capacity is the bleed-off of hydraulic pressure from the leg cylinders under static loading conditions. Bleed-off rates of 69 kPa (10 psi) to 138 kPa (20 psi)

per minute were common to both supports tested. As shown in figure 13, approximately 356 kN (80 kips) of load resistance was lost in 30 minutes because of loss of leg pressure under static loading for the VAMT support.

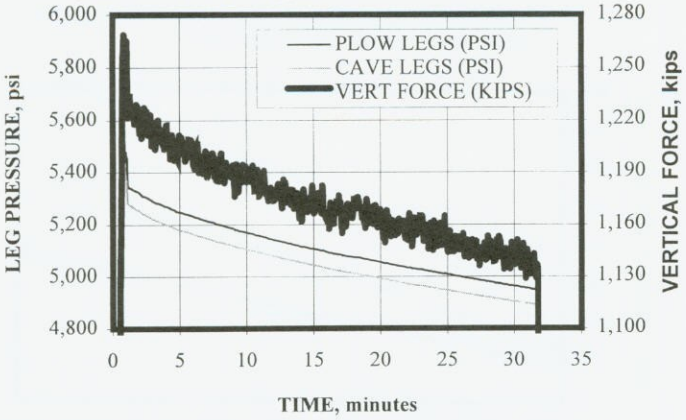



**Figure 13**. Reduction in support capacity due to bleedoff of leg pressures after leg yielding.

Horizontal loading can either increase or decrease support capacity depending on the change in leg pressures between the front and rear set of legs and the reaction of lemniscate assembly. Leg cylinders that are inclined toward the direction of the horizontal displacement will generally increase in pressure; those inclined away from the direction of the horizontal displacement will generally lose pressure. The net pressure change between the front and rear set of legs will generally determine whether the support capacity will be reduced or increased. However, the reaction of the lemniscate assembly must also be considered. For horizontal displacement of the roof toward the rear of the canopy, the lemniscate assembly develops an upward reaction at the canopy connection, which increases support capacity. Likewise, when the horizontal displacement is toward the plow, a downward reaction is developed at the canopy connection, which reduces support capacity.

For the two supports tested, horizontal displacement produced the most change in support capacity at the lower heights because of the greater leg inclination. Support capacity was reduced for horizontal roof displacement toward the rear of the canopy, and support capacity was increased when the horizontal canopy displacement was toward the plow. A maximum reduction in support capacity of 334 kN (75 kips) was observed for the VAMT support as a result of 2.0 cm (0.78 in) of horizontal roof displacement toward the rear of the canopy.

Lateral displacements of the canopy in both directions tended to produce a loss of leg pressure that resulted in loss of support capacity. Reductions in support capacity were typically less than 222 kN (50 kips) with less than 5 cm (2 in) of lateral displacement.

## CRITICAL LOAD CONDITIONS

In general, the worst-case load condition for MRS's is lateral loading. All of the rotational joints within the support are designed with a single rotational degree of freedom. Because lateral loading produces rotations along axes perpendicular to this rotational degree of freedom, it is the most severe load condition. As pin and clevis tolerances grow because of wear in the joints, stress development is likely to intensify because of eccentric loading within the joint.

Depending on the stiffness of the lemniscate assembly, horizontal loading can also produce critical loads in the lemniscate assembly components. VAMT uses a hydraulic cylinder in lieu of a rigid lemniscate link to limit stress development in the lemniscate assembly due to horizontal loading.

The worst-case load conditions for canopy and base structures are partial contact configurations that induce bending. The associated stress development will be a function of the stiffness of the structure in relation to the applied loading.

### VAMT Support

Highly loaded components on the VAMT support were the aligning cylinder and the canopy. The amount of horizontal force acting on the support required to produce pressure development in the aligning cylinder varied from 178 to 467 kN (40 to 105 kips) for support heights ranging from 2.4 to 3.8 m (96 to 148 in). Once pressure development begins, only another 67 to 89 kN (15 to 20 kips) is required to produce yield pressures of 40 MPa (5,800 psi) in the aligning cylinder.

A malfunction of the aligning cylinder occurred during a test in which the cylinder was yielded in compression under the application of horizontal displacement of the canopy toward the plow. At the completion of the test when the pump pressure was applied to the cylinder during the retraction of the rear legs, hydraulic fluid under considerable pressure blew out of the breather port on the base of the cylinder, indicating that the lower piston seals had been damaged. Strain data were recorded during the test from two strain gauges located on the clevis that connects the cylinder to the tilt-frame assembly. The strain responses are displayed in figure 14. An examination of the strain data suggests that the damage occurred at approximately 13 cm (5.1 in) of horizontal displacement of the canopy relative to the base. The sharp increase in strain that occurred just prior to this suggests that the cylinder was fully stroked. However, an analysis of the lemniscate geometry indicates that approximately 23 cm (9 in) of horizontal canopy movement is required to compress the aligning cylinder through its full 60 mm (2.4 in) of stroke. An examination of the damaged cylinder by VAMT revealed that the cylinder was radially deformed (ballooned), suggesting that the failure was caused by excessive hydraulic pressure. However, the strain data indicate that there were not sufficient forces acting to generate hydraulic pressure that would damage the cylinder. Therefore, the cause of the failure has not been satisfactorily determined. A new aligning cylinder was installed, and testing resumed. Subsequent tests at less-than-yield pressure were successfully conducted with no malfunctions of the aligning cylinder. However, at the discretion of VAMT, the new aligning cylinder was *not* tested under conditions that caused full compression or extension of the cylinder.

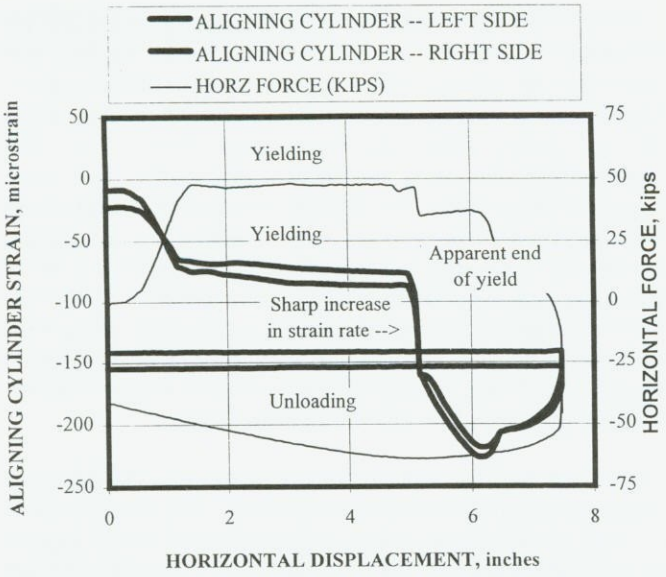



**Figure 14**. Failure of aligning cylinder during horizontal displacement toward the plow.

The worst load case for the canopy was concentrated loading at the center or at one end of the canopy. An assessment of stress at full support capacity can be made by extrapolating the measured canopy strains to 5,338 kN (1,200 kips) of support loading with a modulus of elasticity of 206,850 MPa ($30 \times 10^6$ psi) for steel. The "contact at center" configuration produces a stress of 625 MPa (90,600 psi) at 5,338 kN (1,200 kips) of support capacity. Assuming a yield strength of 690 MPa (100,000 psi) for the steel, this configuration is close to producing permanent deformation in the canopy. A contact located 15.2 cm (6 in) from the canopy tip is projected to produce a stress of 393 MPa (57,000 psi) at the measured strain locations at full support capacity. However, the maximum bending moment is located farther back toward the rear leg in this loading condition, and the maximum stress is known to be greater than that measured in this test.

### Fletcher Support

The most highly stressed components in the Fletcher support were the bottom lemniscate link and sections of the base (crawler) frame. An objective of the testing was to determine loading limitations for these components. The following limitations are based on extrapolation of test data, where a margin of safety was maintained during load application. No failures of any component were observed under the test conditions.

Lateral loading of 267 kN (60 kips) produced a stress of 207 MPa (30,000 psi) in the bottom lemniscate link. Assuming a 690 MPa (100,000 psi) yield strength, extrapolation of the test data indicates that permanent deformation of the link would occur if the lateral load exceeded 556 kN (125 kips).

Horizontal loading of 400 kN (90 kips) produced stresses as high as 310 MPa (45,000 psi) in the base cross frame member at a 3.1-m (120-in) support operating height. Extrapolation of these data suggests that the maximum horizontal loading capability for the base cross frame member at the 3.1-m (120-in) operating height is approximately 934 kN (210 kips), assuming a 690-MPa (100,000-psi) yield strength. At the 3.6-m (140-in) height, horizontal loading of 445 kN (100 kips) produced stresses as high as 393 MPa (57,000 psi). Extrapolation of these data suggests that the maximum horizontal loading capability for the cross frame member at the 3.6-m (140-in) operating height is approximately 778 kN (175 kips).

This analysis is conducted for full canopy and base contact. Eccentric load conditions on the crawler frame or canopy did not dramatically increase measured component strains.

## OTHER SAFETY CONSIDERATIONS

Any MRS will become unstable if any of the lemniscate pins fail. Since critical stresses can be developed within the range of possible horizontal and lateral loading, these pins should be periodically inspected. Additionally, before any of the lemniscate pins are removed, the canopy and lemniscate assembly should be supported to prevent both vertical and *horizontal* movement. Unrestrained movement of the canopy can result in serious injury or death.

Caution should be used when working around the support while it is pressurized. Oil leaking at these pressures can cause serious bodily damage. Likewise, pressure should be relieved before any hydraulic component is removed.

## COMPARISON TO TIMBER POSTS

The most obvious difference between MRS's and conventional timber posts is their size and effective roof coverage. Roof coverage depends on the manufacturer and support model, ranging from 3.3 to 7.9 $m^2$ (35 to 85 $ft^2$). In comparison, a wood post will provide less than 0.1 $m^2$ (1 $ft^2$) of roof coverage.

MRS's can provide an active load of up to 4,448 kN (500 tons) to the mine roof; wood posts are strictly passive supports. The load-bearing capacity of one MRS is about the same as six, 20-cm (8-in) diameter hardwood posts. The stiffness of an MRS varies by support design and is height-dependent for a specific support. In general, an MRS operating at less than 75% of its maximum height is stiffer than a single 20-cm (8-in) diameter post with no headboard or two 20-cm (8-in) diameter posts with headboards.

Another significant advantage of an MRS is that it will continue to provide close to its full rated capacity after reaching yield load and can maintain this load capacity until the full leg stroke is exhausted. Thus, whereas MRS's can provide support through several meters of closure, timber posts can fail at less than 2.5 cm (1 in) of convergence and have no residual strength after failure.

MRS's are also much better suited to handle eccentric load conditions caused by horizontal and lateral roof or floor movements, gob loading, and rib rolls, which are common during pillar extraction and often kick out breaker and turn posts. In

general, timber posts suffer reduced stability for anything but pure vertical loads.

## CONCLUSIONS

Full-scale testing of MRS's at the Strategic Structures Testing Laboratory provided a wealth of information pertaining to their performance capabilities and limitations. The tests were conducted in the unique mine roof simulator load frame under controlled conditions that simulate in-service load conditions.

The basic design of the VAMT breaker line support and the Fletcher MRS tested in this study is similar. Design differences that impacted support performance included the lemniscate assembly, the canopy construction, and the leg cylinder design.

The VAMT support incorporated a tilt frame with hydraulic cylinders to control horizontal and lateral loading; the Fletcher support utilized rigid lemniscate links to resist horizontal and lateral loading. The tilt concept limits stress development in the support structure, but permits greater translation of the canopy relative to the base, thereby allowing greater roof movements to occur, particularly when the hydraulic tilt cylinders have yielded. The advantages and disadvantages of these designs from a ground control perspective have not been evaluated.

Differences in the leg cylinder design caused most of the differences in support performance. The Fletcher support utilized a three-stage leg cylinder; the VAMT support, a two-stage leg cylinder. Consequences of the three-stage leg design were; (1) reduced support stiffness, (2) greater reductions in setting force when both the bottom *and* middle stages are fully extended, and (3) larger unrecorded roof movements, particularly when both stages are fully extended. The advantage of the three-stage leg design is greater operating range, providing a lower support profile for transporting and tramming underground.

A critical issue pertaining to the measurement of support loading and loading rate is the effect of the staging of the leg cylinders. When the bottom stage of the leg cylinders is fully extended, the dial pressure gauges do not respond to increases in support load until the setting force established in the bottom stage is overcome by pressure development in the upper stages. The unrecorded roof load is greater at high setting pressures and is minimized at low setting pressures. Operationally, the bottom stage will be fully extended when the support is first raised to a height that exceeds the bottom stage stroke and, on subsequent cycles, whenever a new maximum operating height is established. Therefore, when possible, it is recommended that the support be taken initially to a location with a height greater than the expected operating height during pillar extraction, and fully raised. This will eliminate the problem of unrecorded roof loading. However, if this practice is followed, the support should be lowered as little as possible when moving the support to the section and during cycle changes. If the support is lowered sufficiently to cause the bottom stage to fully collapse, the probability of unrecorded roof loading will increase.

Setting forces also greatly depend on leg cylinder staging and are diminished by as much as 70% for the Fletcher support with three-stage leg cylinders when the bottom and middle stages are fully extended. Setting pressure as measured by the dial gauges will not always reflect the true setting force. The same circumstances that cause unrecorded roof loading also cause diminished setting forces. It is desirable to avoid diminished setting forces because the effectiveness of the support to act as a breaker line for roof caving may be reduced for low setting forces. When comparing supports of different design, it is important to remember that the smaller diameter leg cylinder will provide less setting force for the same hydraulic pressure than supports with larger diameter leg cylinders. This is one reason that the VAMT support operates at higher pump pressure than the Fletcher support.

Both the Fletcher and VAMT supports were found to be structurally sound for *typical* load conditions. The canopy is likely to be the most highly stressed component on the VAMT support for most load conditions. Partial contact can cause stresses as high as 690 MPa (100,000 psi).

When horizontal or lateral loading is present, the lemniscate assembly and cross frame between the base crawler frames are likely to be the most highly stressed parts of the Fletcher support. Lateral loads in excess of 556 kN (125 kips) can cause damage to the bottom lemniscate link, and horizontal loads in excess of 778 kN (175 kips) can cause damage to the cross frame member. Unfortunately, there is no way to assess the magnitude of horizontal and lateral loads underground without installing additional instrumentation on the support.

The aligning cylinder on the VAMT support was damaged when it was yielded in compression by approximately 13 cm (5 in) of horizontal displacement of the canopy relative to the base. The probability of such large horizontal displacements during underground use is not known, but it is likely that this is an extreme load condition that will *not* occur during *normal* mining cycles. The cause of the failure was not satisfactorily determined. The damaged cylinder was replaced, and subsequent tests at less-than-yield pressure were conducted without any failures.

Because any support is unstable if the lemniscate link pins fail, all supports should be periodically inspected for damage or excessive deformation in the pin clevises. Furthermore, the canopy should be supported to prevent vertical and horizontal movement prior to removal or repair of an any lemniscate pin.

MRS's provide superior supporting capabilities compared with conventional timber posts. Each mobile support has a load-bearing capacity of approximately six timber posts and equivalent stiffness to two or more posts. MRS's provide significantly greater roof coverage and are much more stable for the types of eccentric loading that is common during pillar extraction. Furthermore, the active loading capability provides a more effective breaker line by minimizing initial roof movements that can lead to roof instability or caving inby the supports.



# Effect of the Interchamber Pillar Yield on the Surface Strains in the Movement Trough Edges

*Mikhail P. Nesterov,* Expert and Researcher
*N. F. Anikin,* Mine Surveying Engineer and Researcher
Institution of Halurgy
RUSSIA

## ABSTRACT

The paper presents the results of the research that can forecast the development of subsidences and deformations of the earth surface with time in the permanent marginal areas of the movement troughs arising when mining sylvinite beds in the Upper Kama deposit of potash ores where the rock formation support is made by means of interchamber (rib) pillars of various yieldability.

## THE PROBLEM IN QUESTION AND ITS TIMELINESS

In contrast to coal beds, mining of potash beds in a saliferous rock formations is usually made with the usage of supporting interchamber pillars. They are mainly used to avoid the appearances of water-conductive disturbances in the continuity of aquiclude formation. Weak rocks occurring in the immediate roof of beds requires, for operation safety, the reduction of room width from 16 m (with the most stable roof) down to 3 m (with the least stable one). However, in order to maintain the same rate of recovery of the beds, the width of pillars also has to be reduced in proportion to the width of rooms. This practice, under condition of constant productivity of the beds, makes the pillars unstable.

It is known that maximum deformations in the aquiclude formation and on the earth surface appear near the permanent and long time-abandoned boundaries of the mined-out gob (in the so-called Marginal Areas of Movement Troughs - MAMT). Therefore the following problems are urgent and pressing:

1. Determination of factors that affect deformations.
2. Determination of how these factors work.
3. Development of methods to take into account these factors and use them to forecast deformations within the MAMT limits.

## PECULIARITIES OF MINING SYLVINITE BEDS AT THE UPPER KAMA DEPOSIT

There are two commercial sylvinite beds in the Upper Kama deposit, namely, AB and Red 2 (Fig. 1). Their thickness varies from 2.4 to 4.5 m and from 3.5 and 9 m, respectively. These beds are divided by saliferous interburden with a thickness from 2 m to 11 m. One or both of these beds are mined depending on the allowable deformations in the aquiclude formations and structures on the earth surface.

When both sylvinite beds are mined with narrow rooms, the interburden dividing these beds is such that the deformation and interaction of pillars with floor and roof rocks in one bed is independent of the other. However, when the same beds are mined with wide rooms, the interburden dividing these beds start, as the time goes, to extrude into the rooms, becomes laminated and loses stability. Therefore, the originally rigid and wide pillars left in mined-out beds become high, yielding and intensively deformed.

Figure 2 illustrates the variety of changes in earth surface subsidences that take place in the areas of complete mining in the mines of the Upper Kama potash deposit under the current dimensions of rooms and interchamber pillars of various yieldability.

This paper illustrates how the above listed problems can be solved in the regions where only one of the two sylvinite beds were mined with pillars of various yieldability. This mining was performed under conditions where stowing rooms with salt wastes were not used, and

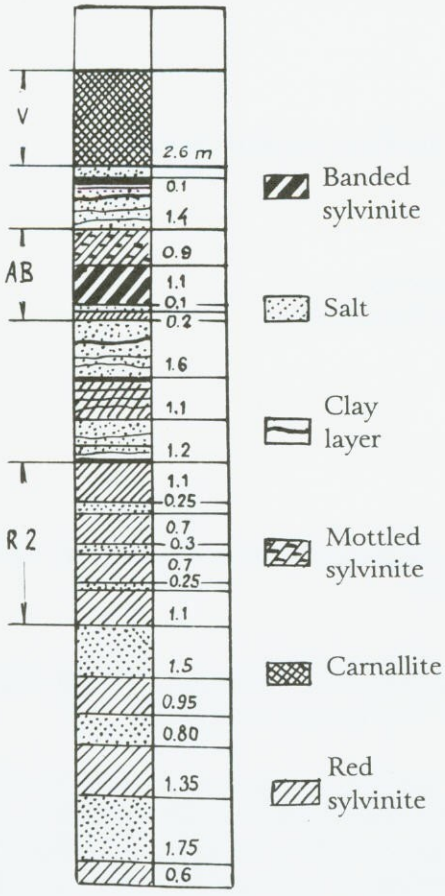



Figure 1. Structure of the formation enclosing recoverable sylvinite beds $K_2$ and AB and carnallite bed V.

with the front wide enough to provide complete undermining of the earth surface.

Note that there were three reasons to mining only one of the two sylvinite beds:

- when the second bed has been replaced with salt;
- when mining of both beds would not allow to reduce subsidences by backfilling of rooms with salt wastes;
- in the areas where overlying carnallite beds is to be mined has been separated from the upper sylvinite by a thin (2-3 m) interburden.

## EFFECT OF PILLARS' YIELDABILITY ON DISTRIBUTION OF SUBSIDENCES AND DEFORMATIONS OF THE EARTH SURFACE IN PERMANENT MARGINAL AREAS OF MOVEMENT TROUGHS (MAMT)

Results of multiannual systematic instrumental observations of the earth surface subsidences when using yield pillars has shown:

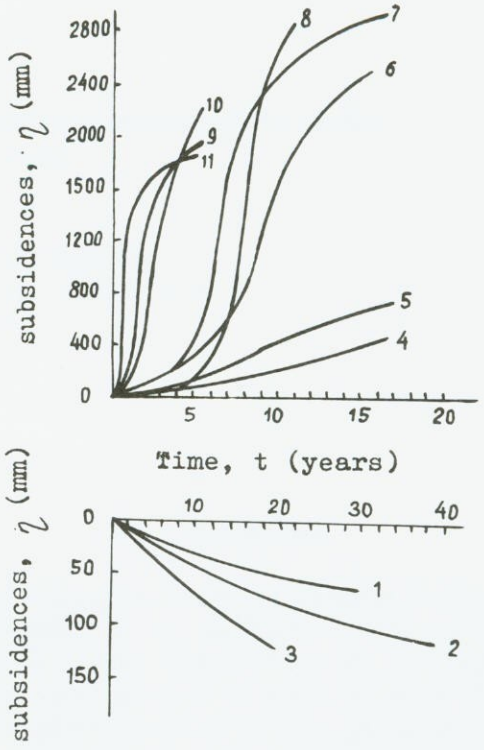



Figure 2. Examples of the earth surface subsidence developments in time under its complete undermining, with pillars of various yieldability.

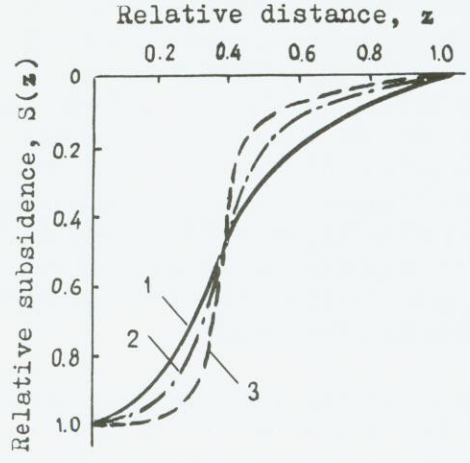



Figure 3. Distribution of relative subsidences, S(z), in the marginal area of a movement trough on the earth surface, with pillars of various yieldability. 1 - $\dot{\eta}$ = 5 mm/month; 2 - $\dot{\eta}$ = 20-60 mm/month; 3 - $\dot{\eta}$ = 150-300 mm/month.

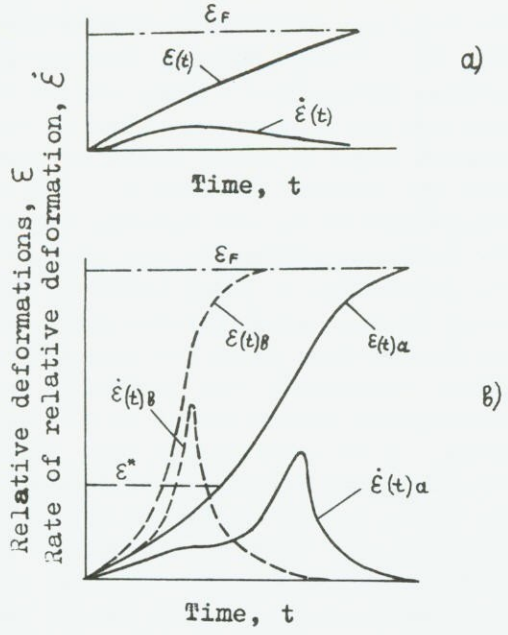



Figure 4. First (a) and second (b) types of regularities for variations in time of pillars' relative deformation, ε(t), and rates of these deformations, ε̇(t), with characteristic points.

- firstly, with equal subsidences on inner boundaries of MAMT the distribution of subsidences within MAMTs itself, at various yieldability of pillars and other equal conditions turns out to be unequal (Fig. 3).
- secondly, at any yieldability of pillars the distribution of subsidences within MAMT, expressed in terms of fractions of that in the zones of complete mining, changes with time.
- thirdly, when the overlying formation is supported by yield pillars, there are two types of time patterns in surface subsidences , η(t), and pillars' deformations, ϵ(t). They significantly differ in the values of maximum rate of surface subsidence η'(t) (Fig. 4).

Detailed analysis of conditions where these events took place enabled us to establish that distribution of relative subsidences of the earth surface S(z) in the MAMT with any yield pillars changed with η', the maximum attained rates of subsidence on the inner boundaries of MAMT. After the growth of these rates has stopped, changes in relative subsidences within MAMT are not observed.

Figure 5 shows the relationship between maximum rate of subsidence and relative subsidence S(z) and its 1st and 2nd derivative, where z in step of 0.1 is the ratio of the distance from the inner boundary of MAMT to the

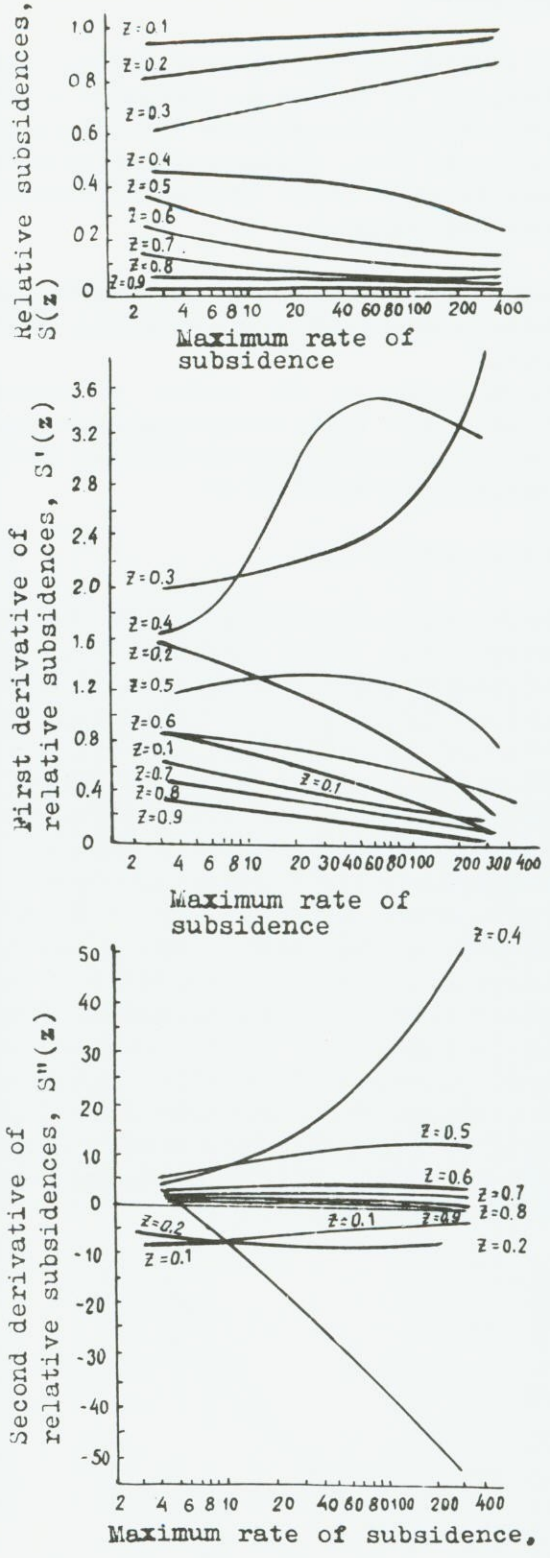



Figure 5. Relationship of relative subsidences, S(z) and their first, S'(z) and second, S"(z) derivatives in the marginal area of a movement trough vs. maximum attained rate of subsidence on the inner boundary of this area of the trough, $\dot{\eta}_{max}$ (mm/month).

width of MAMT.

To establish the type of time-dependent surface subsidence $\eta(t)$, we modeled the deformation of pillars that consisted of ore-bearing rocks and having various width to height ratios. Various time-dependent loads were applied to these models. The results obtained have been compared to those of:

- in-situ instrumentation of interchamber pillar deformations and earth surface subsidences resulting from it
- measurements, by the method of unloading (Nesterov et al., 1978), of the changes in loads that affect pillars as pillars are located farther from the boundary of the mined-out area.

It was established that:

- the first type of relationship, $\eta(t)$ (see Fig. 4a) is brought about under conditions where time-increasing loading of pillars C(t) does not reach the value at which the growth of pillar damage begins. For sylvinites of the Upper Kama deposit C(t) = 0.3 (Titov, 1983). Growth of pillars' loading to the maximum level occurs in two cases: i) either they are loaded by the increasing weight of rocks from the overlying formation as a result of cleansing work and growth in size of mined-out gob or, ii) due to reduction in their bearing capacity stipulated through increase in room heights because of loss in stability of rocks in the immediate roof. In the latter case the maximum rate of earth surface subsidence on the maximum height of pillars, M(t), increases with time and the maximum value of their loading C(t) at this height. The degree of pillars' loading is related to the rate of their relative deformations by the relation presented in Fig. 6.

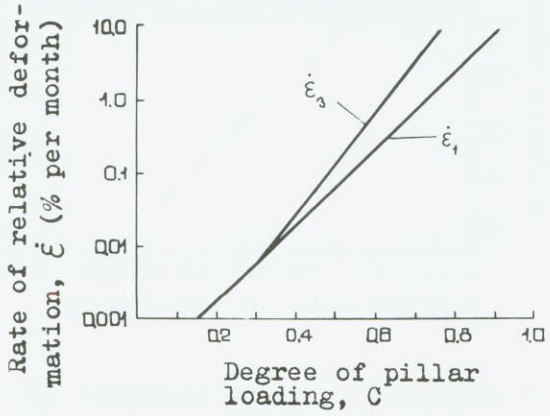



Figure 6. Relation of pillars' loading degree, C vs. their deforming rate, at the stage of established creep, $\dot{\varepsilon}_1$, and at the stage of progressive creep, $\dot{\varepsilon}_3$ - with their residual minimal strength, $P_{min}$.

- the second type of relationships of pillar deformation (Fig. 4b) is brought about in situations when the ultimate deformations in pillars turn out to be less than their final values $\epsilon^* \leq \epsilon_F$ whereas the maximum attained degree of pillars' loading becomes more than the ultimate one, C>/C(t). This type of relationships involves two variables, $\epsilon$ (t) and $\eta(t)$. For the first variable there is a time interval in which the deformations of pillars loaded by the whole weight of an overlying formation still do not reach the ultimate values. In this time interval the rates of pillars' deformation stay practically the same provided that there are no cave-ins from the roof of rooms. If these cave-ins do occur, then pillars deformation rate increases to certain extent because the bearing capacity of pillars is reduced with the growth of pillar height (curves with a in Fig. 4b). For the second variable $\epsilon(t)=\eta(t)/M(t)$, there is no such time interval (curves with b in Fig. 4b). This relationship, $\epsilon(t)$ and $\eta(t)$, is a characteristic of rather yieldable pillars for which the ultimate deformation is not great and is reached prior to the full loading of pillars by the overburden weight.

To reveal the relations between the maximum subsidence rate for the earth surface, $\eta'$, and factors that determine it for the second variable, $\eta(t)$, the analysis of the following results has been made:

- the results of multiannual survey of the development of surface subsidence under conditions of complete mining with pillars of various yieldability;
- the results of investigation of the mechanism of interaction between the pillars of various yieldability and roof and floor rocks, obtained by reentering the old mined-gobs (Nesterov and Marakov, 1995);
- the testing of pillar models installed into metal matrices imitating the mined-out gobs in rooms

It has been established that:

- the maximum subsidence rate corresponds, in this case, to the lowering in bearing capacity of pillars down to a minimal residual strength, $P_{min}$,
- the maximum rate of pillars deformation at their minimal residual strength can be described by curve $\dot{\varepsilon}$, in Fig. 6.

It is known that maximal absolute values for subsidences, tilts and curvature of the earth surface in the MAMT mainly depend on two factors: i) final subsidence on its (MAMT) internal boundary, which is easy to determine; and ii) the patterns of distribution, in this part of trough, of relative subsidence and their derivatives.

Therefore, the above results allow to determine the maximum (earth surface deformations expected in permanent marginal areas of movement troughs which arise when sylvinite beds with interchamber pillars of various yieldability are mined.

## CONCLUSION

The investigations performed have established that during sylvinite beds mining, when the rock formation is supported by the yieldable interchamber pillars, the distribution of the earth surface subsidences in permanent marginal areas of movement troughs, significantly depends on the maximal - already attained subsidence rate in the areas of complete mining.

The relationships have been established that relate the relative subsidences and their first and second derivatives in the marginal areas of the movement troughs to the rate of maximum subsidence of the earth surface.

The main relationships determining the development of relative time-dependent deformations in yieldable sylvinite pillars as well as conditions to which they correspond have been established. Also, the patterns have been found that allow the prediction of the maximum subsidence rates of the earth surface for each of these relationships.

Finally, it becomes possible to determine the maximum expected subsidences, inclinations and curvature in the permanent marginal areas of the movement trough under conditions when sylvinite beds with the rock formation supported by interchamber pillars of various yieldability are mined.

## REFERENCES:

1. Nesterov, M.P., Marakov, V.Y., and Neprimerov, A.F., Sylvinite pillars stress distribution variation as function of their age and spacing in the worked-out area. Collected transactions: Rock mass under stress. Novosibirsk. 1978, pp. 3-5.
2. Titov, B.V., Study of prolonged strength in saline rocks under various stressed states in relation to solving geomechanical problems. Thesis. VNINI Library. 1983. 250 pp.
3. Nesterov, M.P. and Marakov V.Y., Technogenic potash seams and their mining prospects. Mine Planning and Equipment Selection. Proceedings of the Fourth International Symposium. Balkema/Rotterdam, Brookfield. November 1995.

16th CONFERENCE ON GROUND CONTROL IN MINING

# Salt Pillar Design Equation

*Leo L. Van Sambeek,* Manager, Field and Services
RE/SPEC Inc.
Rapid City, SD

## ABSTRACT

Specification of properly sized pillars to support the overburden is one of the most challenging aspects of salt mine design. Interest in salt pillar design is heightened by the recent flooding of the Retsof salt mine, water inflows to the K2 potash mine, and closing of the Belle Isle salt mine because of ground control problems. A series of numerical modeling analyses show that a simple pillar design equation for salt pillars adequately reproduces results of extensive modeling efforts. The paper describes (1) the basis for the pillar design equation, (2) equation verification by comparison with numerical modeling results, and (3) equation validation by comparison with measurements and observations of salt pillar behavior.

## INTRODUCTION

Because ore left in pillars detracts from utilization of the mineral resource, the size of pillars can influence the viability of an underground mine. Even for salt (and potash) mines, where the mineral resource is often extensive, pillar design is still important. Deformation by creep is the dominant behavior in salt mines; creep rates are primarily controlled by stresses in the pillars. Therefore, pillar design influences rates of closure underground (equipment clearance and headroom), rates of subsidence on the surface, and life of the mine. Laboratory creep testing of salt specimens to obtain sophisticated creep laws and recent developments in numerical modeling allow rock mechanics practitioners to examine expected deformation patterns and deformation rates in salt pillars. In particular, numerical modeling provides insight on time-dependent stress states in pillars and the surrounding rock, as the process of creep redistributes stresses. While elegant in its purpose, numerical modeling can, however, be cumbersome in practice. A series of numerical modeling analyses demonstrate that a simple pillar design equation for salt pillars is capable of reproducing the results of extensive modeling efforts. This equation simplifies comparisons of different pillar sizes and shapes, and provides a tool for estimating stress conditions in salt pillars when deformation data are available. The pillar design equation may also have application for pillars in rocks other than salt and potash, when the rocks have a propensity to creep (even very slowly) and the mine life is long.

## BACKGROUND

### Average Vertical Pillar Stress

The removal of rock from an underground mine causes a redistribution of the stresses onto pillars or adjacent unmined areas. Stress redistribution (concentration) can be defined by the tributary loading theory with modification to account for special geometrical conditions (e.g., arching across narrow panels). According to tributary loading theory and for competent pillars, the average vertical stress in pillars is equal to the weight of the overburden borne by the pillar divided by the load-bearing area of the pillar. Hence, the average vertical stress $(\overline{\sigma}_v)$ is:

$$\overline{\sigma}_v = W_{OB}/A_P = \gamma z/(1 - E) \qquad (1)$$

where:

$W_{OB}$ = weight of overburden

$A_p$ = pillar area

$E$ = areal extraction ratio

$z$ = overburden thickness (i.e., depth)

$\gamma$ = average stress gradient for the overburden.

For mines with a wide expanse, $\overline{\sigma}_v$ is applicable for most pillars. For narrow mines, or narrow panels within a mine, $\overline{\sigma}_v$ may be reduced by a geometrical factor, but an average vertical stress still exists; i.e.,

$$\overline{\sigma}_v = \alpha \left[\gamma z/(1 - E)\right] \quad (2)$$

where $\alpha$ = geometrical factor $0 < \alpha \leq 1$. The geometrical factor is not used further in this paper; for the remainder of the paper, $\alpha = 1$, which implies full overburden loading as occurs in wide mines and panels.

According to tributary loading (Equation 1), the average vertical stress depends on neither the size nor the shape of pillars (assuming pillars are competent). The stresses acting normal to the vertical stress — the horizontal stresses — are known to have significant pillar-shape dependencies, however.

Average Horizontal Stresses

Van Sambeek [1984] proposes that the average horizontal stresses in a rectangular-shaped salt pillar after stress-relief creep (at steady-state stress conditions) are:

$$\begin{aligned} \overline{\sigma}_h &= \overline{\sigma}_v \left(0.1\ W_h{:}H\right) \\ \overline{\sigma}_H &= \overline{\sigma}_v \left(0.1\ W_H{:}H\right) \end{aligned} \quad (3)$$

where:

$\overline{\sigma}_h, \overline{\sigma}_H$ = average horizontal stresses parallel to the shortest and longest pillar dimensions

$W_h, W_H$ = shortest and longest horizontal pillar dimensions

$H$ = pillar height (vertical dimension).

A logical limit on the magnitude of the average horizontal stresses is that they do not exceed the average vertical stress. Therefore, application of Equation 3 is restricted to W:H < 10; later it will be shown that W:H < 5 is a better limit.

Average Effective Stress

The von Mises effective stress measure is commonly used to determine the creep rate for salt. The von Mises effective stress, when expressed in terms of the principal stresses, is:

$$\sigma_{ef} = \sqrt{3J_2} = \sqrt{\left\{(\sigma_1 - \sigma_2)^2 + (\sigma_2 - \sigma_3)^2 + (\sigma_3 - \sigma_1)^2\right\}/2} \quad (4)$$

Assuming (1) the average effective stress for rectangular-shaped pillars can be calculated from average vertical and horizontal stresses and (2) the vertical and horizontal stresses are principal stresses, and for simplification, $W_H = \beta W_h$ and $W = W_h$, then:

$$\overline{\sigma}_h = \overline{\sigma}_v \left(0.1\ W{:}H\right) \quad \text{and} \quad \overline{\sigma}_H = \overline{\sigma}_v \left(0.1\beta\ W{:}H\right) \quad (5)$$

and:

$$\left(\overline{\sigma}_{ef}\right)_\beta = \overline{\sigma}_v \sqrt{(0.1\ W{:}H)^2 (1 - \beta + \beta^2) - 0.1\ W{:}H(1 + \beta) + 1} \quad (6)$$

If the pillar is square, $\beta = 1$, and Equation 6 reduces to:

$$\left(\overline{\sigma}_{ef}\right)_{square} = \overline{\sigma}_v \left[1 - 0.1\ W{:}H\right] \quad (7)$$

As pillars become long in one dimension; i.e., as $\beta$ increases, a condition approaching plane strain is achieved. Based on stationary-stress creep considerations (e.g., Van Sambeek [1986]), no creep strain parallel to the long dimension occurs when the deviatoric stress component in that direction is zero; i.e., $\overline{S}_H = 0$ when:

$$\overline{\sigma}_H = \left(\overline{\sigma}_v + \overline{\sigma}_h\right)/2 \quad (8)$$

Using Equation 3 and the relationship $\overline{\sigma}_H = \beta\, \overline{\sigma}_h$, $\beta$ can be calculated for an effective plane-strain situation ($\beta_{max}$):

$$\begin{aligned} \beta\, \overline{\sigma}_h &= \left(\overline{\sigma}_v + \overline{\sigma}_h\right) \\ \beta_{max} &= \frac{\overline{\sigma}_v + \overline{\sigma}_h}{2\overline{\sigma}_h} = \frac{1 + 0.1\ W{:}H}{0.2\ W{:}H} \end{aligned} \quad (9)$$

Therefore, the average effective stress for long pillars ($W_H \geq \beta_{max}\ W_h$) is:

$$\left(\overline{\sigma}_{ef}\right)_{\beta max} = \frac{\sqrt{3}}{2}\, \overline{\sigma}_v \left[1 - 0.1\ W{:}H\right] \quad (10)$$

Equations 7 and 10 reveal that as W:H becomes large, the effective stress rapidly approaches zero. An alternative approach is shown in the appendix where nonlinear relationships are suggested for W:H > 5.

Pillar Creep Rates

For salt, steady-state creep rates are exponential functions of effective stress, such as:

$$\dot{\varepsilon}^c = A\, (\sigma_{ef})^n \quad (11)$$

where $A$ and $n$ are creep law parameters obtained from laboratory testing: $3 \leq n \leq 6$ and $A$ is site specific and temperature sensitive. The creep-strain rate in a particular direction is defined by generalizing Equation 11 (e.g., Fossum et al. [1988]):

$$\dot{\varepsilon}_x^c = A \left(\overline{\sigma}_{ef}\right)^{n-1} \left(\frac{3}{2}\ \overline{S}_x\right) \quad (12)$$

where:

$\dot{\varepsilon}_x^c$ = creep strain rate in the x-direction

$\overline{S}_x$ = average deviatoric stress for the x-direction.

The pillar shortening rate (vertical direction) is therefore:

$$\dot{\varepsilon}_v^c = \left(\frac{\Delta \dot{H}}{H}\right) = A\left(\overline{\sigma}_{ef}\right)^{n-1}\left(\frac{3}{2}\ \overline{S}_v\right) \tag{13}$$

and the pillar lateral expansion rates are:

$$\dot{\varepsilon}_h^c = \left(\frac{\Delta \dot{W}_h}{W_h}\right) = A\left(\overline{\sigma}_{ef}\right)^{n-1}\left(\frac{3}{2}\ \overline{S}_h\right)$$
$$\dot{\varepsilon}_H^c = \left(\frac{\Delta \dot{W}_H}{W_H}\right) = A\left(\overline{\sigma}_{ef}\right)^{n-1}\left(\frac{3}{2}\ \overline{S}_H\right) \tag{14}$$

where $\Delta \dot{H}$, $\Delta \dot{W}_h$, and $\Delta \dot{W}_H$ are rates of change in the respective pillar dimensions. The deviatoric stresses acting in the vertical, $\overline{S}_v$, and horizontal directions, $\overline{S}_h$ and $\overline{S}_H$, are:

$$\overline{S}_v = \overline{\sigma}_v\left(2 - (0.1\ \text{W:H})\,(1 + \beta)\right)/3$$
$$\overline{S}_h = \overline{\sigma}_v\left((0.1\ \text{W:H})\,(2 - \beta) - 1\right)/3 \tag{15}$$
$$\overline{S}_H = \overline{\sigma}_v\left((0.1\ \text{W:H})\,(2\beta - 1) - 1\right)/3$$

Equations 13 through 15 can be used to estimate the effect of changes in pillar size or shape. For example, changing the W:H from 3 to 2 will cause almost a doubling of the pillar shortening rate for the same average vertical stress. Another example is the comparison of square pillars and long pillars for the same minimum pillar width, pillar height, and extraction ratio; the pillar shortening rate for long pillars is less than 50 percent of that for square pillars of the same minimum width.

Pillar Strength

The approach of using average stresses (particularly effective stress) can also be used to inspect the potential for the stress states in pillars to be damaging. Van Sambeek et al. [1993] show the aptness of a simple dilation limit for salt as:

$$\zeta = \frac{\sqrt{J_2}}{I_1} \begin{cases} \geq 0.27 \text{ dilation-causing stress condition} \\ < 0.27 \text{ nondilating stress condition} \end{cases} \tag{16}$$

where $I_1$ is the first invariant of the total stress tensor ($I_1 = 3\sigma_m$) and $\sqrt{J_2}$ is the second invariant of the deviatoric stress tensor. (Recall $\overline{\sigma}_{ef} = \sqrt{3J_2}$, so $\sqrt{J_2} = \overline{\sigma}_{ef}/\sqrt{3}$.) The first invariant of the stress tensor, $I_1$ is:

$$I_1 = \overline{\sigma}_v + \overline{\sigma}_h + \overline{\sigma}_H = \overline{\sigma}_v\left(1 + 0.1\ \text{W:H} + 0.1\ \beta\ \text{W:H}\right) \tag{17}$$

where $\beta = W_H{:}W_h$ and $1 \leq \beta \leq \beta_{max}$, as before. Equations 16 and 17 lead to:

$$\zeta = \frac{\sqrt{(0.1\ \text{W:H})^2\left(1 - \beta + \beta^2\right) - 0.1\ \text{W:H}\left(1 + \beta\right) + 1}}{\sqrt{3}\left[1 + 0.1\ \text{W:H}\left(1 + \beta\right)\right]} \tag{18}$$

For square pillars ($\beta = 1$):

$$\zeta_{(\beta=1)} = \frac{1 - 0.1\ \text{W:H}}{\sqrt{3}\ (1 + 0.2\ \text{W:H})} \tag{19}$$

and for long rectangular pillars ($\beta = \beta_{max}$):

$$\zeta_{(\beta=\beta_{max})} = \frac{1 - 0.1\ \text{W:H}}{\sqrt{3}\ (1 + 0.1\ \text{W:H})} \tag{20}$$

Based on a limiting value of $\zeta = 0.27$, dilation is avoided when W:H > 2.75 for square pillars and W:H > 1.05 for long rectangular pillars.

## EQUATION VALIDATION

Obviously, any pillar design equation must provide results in agreement with results calculated by other accepted or empirical methods. For this paper, comparison will not be made with other salt pillar design equations in the literature (e.g., those reviewed by Beddoes and Mackintosh [1993]); instead, comparisons will be made to finite-element method (FEM) analyses to demonstrate whether or not the equation oversimplifies the situation.

Two series of finite-element analyses were performed to determine the pillar strain rates and room closure rates for various pillar W:H with constant extraction ratio and pillar height. Figures 1 and 2 show plots of the calculated stresses for the various shaped pillars (axisymmetric and plane strain). Comparisons of normalized average stress values from FEM analyses and the pillar design equation are shown in Figure 3. The values are also shown in Tables 1 and 2. The average vertical, horizontal, and effective stresses within the pillar are integrated average values along the midheight of the pillar. The agreement is excellent, which lends confidence to the use of average pillar stresses for design purposes.

The numerical modeling results were also evaluated in terms of the salt dilatancy criterion ($\sqrt{J_2}:I_1$) for comparison with Equations 19 and 20. The calculated dilatancy factor for axisymmetric and plane-strain pillars for various H:W is shown in Figure 4. In Figure 4, the dilatancy factor is the volume average across the entire pillar width (plane strain) or 85 percent of the pillar area (axisymmetry).

## EQUATION VERIFICATION

Before a pillar design equation can be used, it must be compared to actual pillar behavior. Closure information in terms of $\left(\Delta \dot{H}/H\right)$ and pillar geometries from nine salt mines, both bedded and domal, were used in the comparison. Average

vertical stresses were calculated based on tributary loading. The expected effective stress was then calculated according to the pillar geometries using Equation 6. The measured closure rates are plotted versus the calculated effective stress in Figure 5. A representative model based on a stress exponent of $n = 5$ is also shown. Scatter exists, and is expected, because no adjustments were made for salt type, age of the pillars, location of pillars within the mines, etc. The only factors considered were the reported extraction ratio, depth, and pillar W:H.

## CONCLUSIONS

Pillar design equations were presented which can be applied to comparisons of pillar behavior either from measured or calculated behavior. The equations are obviously approximate; however, they have application when numerical modeling is not practicable. The pillar design equations have limitations; for example, they are not applicable to very slender pillars (W:H < 1), and the linear equations are not suitable for very squat pillars (W:H > 5). While the easiest application is for uniformly sized pillars in a regular pattern over a wide area, the equations can be used in situations involving unequal pillars (such as yield and barrier (bearing) pillars) if proper attention is paid to equilibrating the strain rates by adjusting the average loads on the unequal sized pillars.

Additional data for actual pillars are required to further validate the approach to pillar design. The author would appreciate any information the salt and potash mining industries can provide.

## REFERENCES

**Beddoes, R. J. and A.D. Mackintosh, 1993.** *A Review and Evaluation of Design Criteria for Use in Evaporite Mines*, prepared under Canada/Nova Scotia Mineral Development Agreement by Golder Associates, Ltd., Calgary, Alberta, Canada, 53 p.

**Fossum, A. F., G. D. Callahan, L. L. Van Sambeek, and P. E. Senseny, 1988.** "How Should One-Dimensional Laboratory Equations be Cast Into Three-Dimensional Form?," *Proceedings, 29th U.S. Symposium on Rock Mechanics*, University of Minnesota, Minneapolis, MN, June, pp. 33–41.

**Van Sambeek, L. L., 1984.** *Potential Reduction in Surface Subsidence by Backfilling or Flooding the Belle Isle Mine*, RSI–0247, proprietary report prepared by RE/SPEC Inc., Rapid City, SD, for Cargill/Salt Division, Minneapolis, MN, 23 p.

**Van Sambeek, L. L., 1986.** *Creep of Rock Salt Under Inhomogeneous Stress Conditions*, Ph.D. Dissertation, T-3207, Colorado School of Mines, Golden, CO, 311 p.

**Van Sambeek, L. L., J. L. Ratigan, and F. D. Hansen, 1993.** "Dilatancy of Rock Salt in Laboratory Tests," *International Journal of Rock Mechanics and Mining Sciences & Geomechanics Abstracts*, Vol. 30, No. 7. pp. 735–738.

## APPENDIX A

Linear equations are developed in the main paper to describe the stresses in salt pillars according to their shape. Linear equations are adequate for pillars whose W:H < 5, but severely underestimate the effective stress situation for larger W:H. Nonlinear equations were fitted to the calculated stresses to better approximate the stresses in squat pillars. The nonlinear equations use the reciprocal of W:H such that conditions are defined at large W; e.g., H:W = 0 as W approaches infinity. The nonlinear equations for the axisymmetric and plane-strain situations are as follows:

Axisymmetric

$$\begin{aligned} \bar{\sigma}_r/\bar{\sigma}_v &= \exp\left(-3.418\,\mathrm{H{:}W}\right) \\ \bar{\sigma}_\theta/\bar{\sigma}_v &= -1.024 + \exp\left(-3.934\,\mathrm{H{:}W}\right) \\ \bar{\sigma}_{ef}/\bar{\sigma}_v &= 1 - \exp\left(-3.914\,\mathrm{H{:}W}\right) \\ I_1/\bar{\sigma}_v &= 1 + 2\exp\left(-3.83\ \mathrm{H{:}W}\right) \end{aligned} \qquad \text{(A-1)}$$

Plane Strain

$$\begin{aligned} \bar{\sigma}_h/\bar{\sigma}_v &= \exp\left(-2.931\,\mathrm{H{:}W}\right) \\ \bar{\sigma}_H/\bar{\sigma}_v &= \frac{1}{2}\left(1 + \exp\left(-3.042\,\mathrm{H{:}W}\right)\right) \\ \bar{\sigma}_{ef}/\bar{\sigma}_v &= \frac{\sqrt{3}}{2}\left(1 - \exp\left(-2.940\,\mathrm{H{:}W}\right)\right) \\ I_1/\bar{\sigma}_v &= \frac{3}{2}\left(1 + \exp\left(-2.970\,\mathrm{H{:}W}\right)\right) \end{aligned} \qquad \text{(A-2)}$$

**Table 1. Average Pillar Stresses in Axisymmetric Pillars**

| Pillar Shape | | Average Stresses From FEM Modeling | | | Average Stresses From Equations | | | |
|---|---|---|---|---|---|---|---|---|
| | | | | | Linear | | Exponential | |
| W:H | H:W | $\bar{\sigma}_{ef}/\bar{\sigma}_v$ | $\bar{\sigma}_r/\bar{\sigma}_v$ | $\bar{\sigma}_\theta/\bar{\sigma}_v$ | $\bar{\sigma}_{eff}/\bar{\sigma}_v$ | $\bar{\sigma}_h/\bar{\sigma}_v$ | $\bar{\sigma}_{eff}/\bar{\sigma}_v$ | $\bar{\sigma}_h/\bar{\sigma}_v$ |
| 1 | 1 | 0.99 | 0.08 | –0.05 | 0.90 | 0.10 | 0.98 | 0.02 |
| 1.5 | 0.67 | 0.92 | 0.17 | 0.02 | 0.85 | 0.15 | 0.93 | 0.07 |
| 2 | 0.5 | 0.84 | 0.23 | 0.11 | 0.80 | 0.20 | 0.86 | 0.14 |
| 3 | 0.33 | 0.72 | 0.33 | 0.26 | 0.70 | 0.30 | 0.72 | 0.28 |
| 4 | 0.25 | 0.63 | 0.39 | 0.36 | 0.60 | 0.40 | 0.62 | 0.38 |
| 5 | 0.2 | 0.56 | 0.45 | 0.44 | 0.50 | 0.50 | 0.54 | 0.46 |

**Table 2. Average Pillar Stresses in Plane-Strain Pillars**

| Pillar Shape | | Average Stresses From FEM Modeling | | | Average Stresses From Equations[a] | | | |
|---|---|---|---|---|---|---|---|---|
| | | | | | Linear | | Exponential | |
| W:H | H:W | $\bar{\sigma}_{ef}/\bar{\sigma}_v$ | $\bar{\sigma}_h/\bar{\sigma}_v$ | $\bar{\sigma}_H/\bar{\sigma}_v$ | $\bar{\sigma}_{eff}/\bar{\sigma}_v$ | $\bar{\sigma}_h/\bar{\sigma}_v$ | $\bar{\sigma}_{eff}/\bar{\sigma}_v$ | $\bar{\sigma}_h/\bar{\sigma}_v$ |
| 1 | 1 | 0.81 | 0.06 | 0.53 | 0.78 | 0.10 | 0.89 | 0.11 |
| 1.5 | 0.67 | 0.72 | 0.17 | 0.59 | 0.74 | 0.15 | 0.77 | 0.23 |
| 2 | 0.5 | 0.65 | 0.25 | 0.63 | 0.69 | 0.20 | 0.66 | 0.34 |
| 3 | 0.33 | 0.54 | 0.38 | 0.69 | 0.61 | 0.30 | 0.52 | 0.48 |
| 4 | 0.25 | 0.47 | 0.46 | 0.73 | 0.52 | 0.40 | 0.42 | 0.58 |
| 5 | 0.2 | 0.42 | 0.52 | 0.74 | 0.43 | 0.50 | 0.35 | 0.65 |

(a) NOTE: $\bar{\sigma}_H = (\bar{\sigma}_v + \bar{\sigma}_h)/2$.

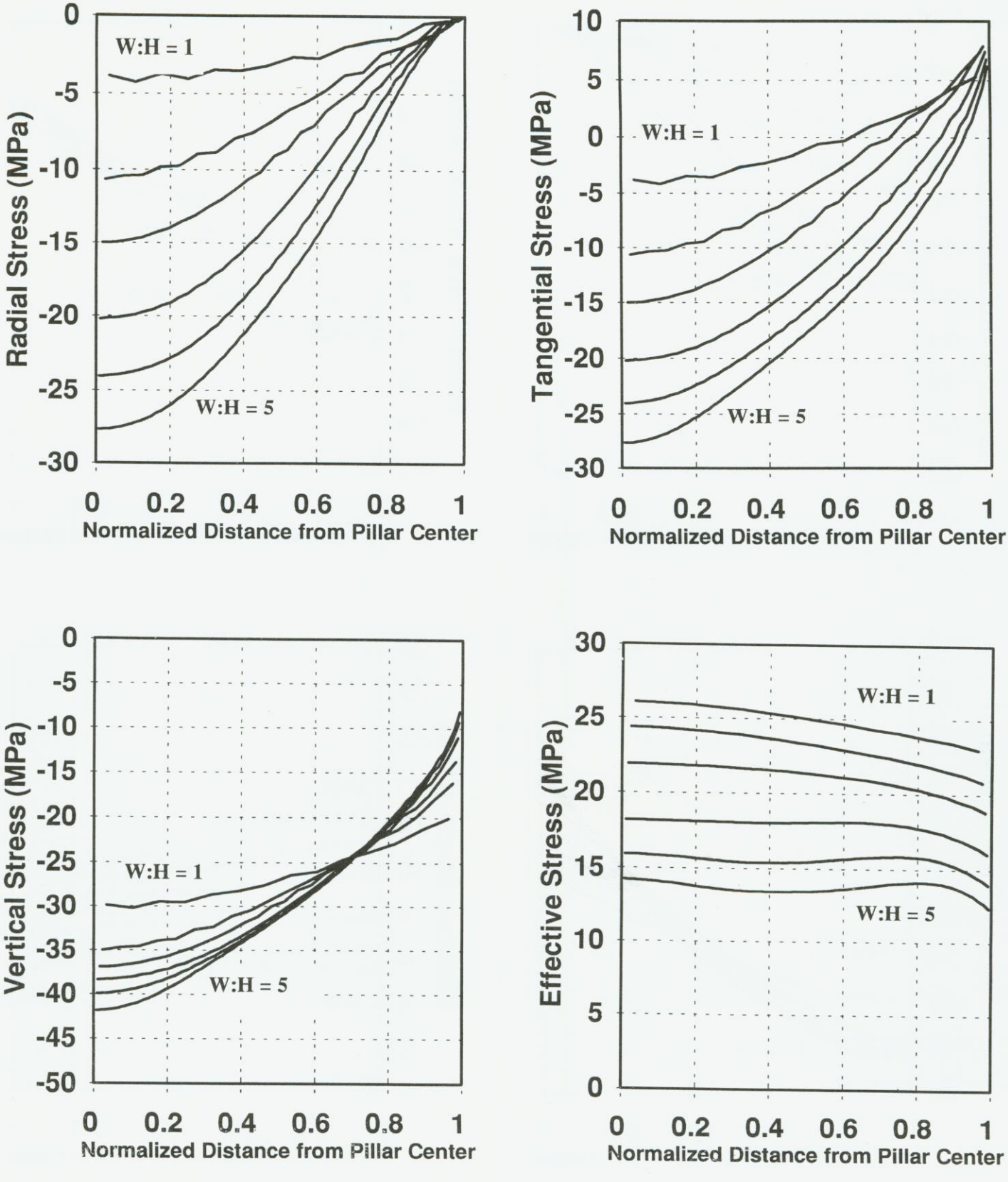
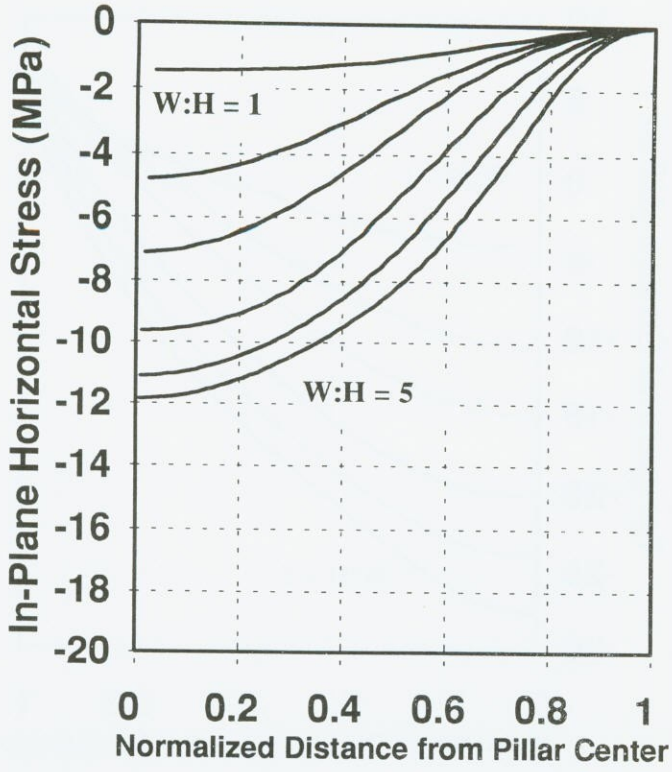
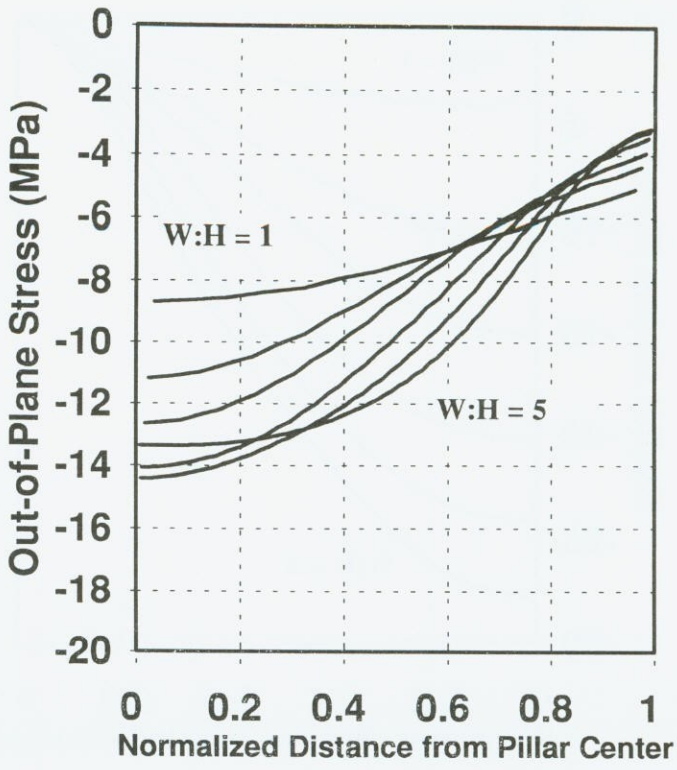
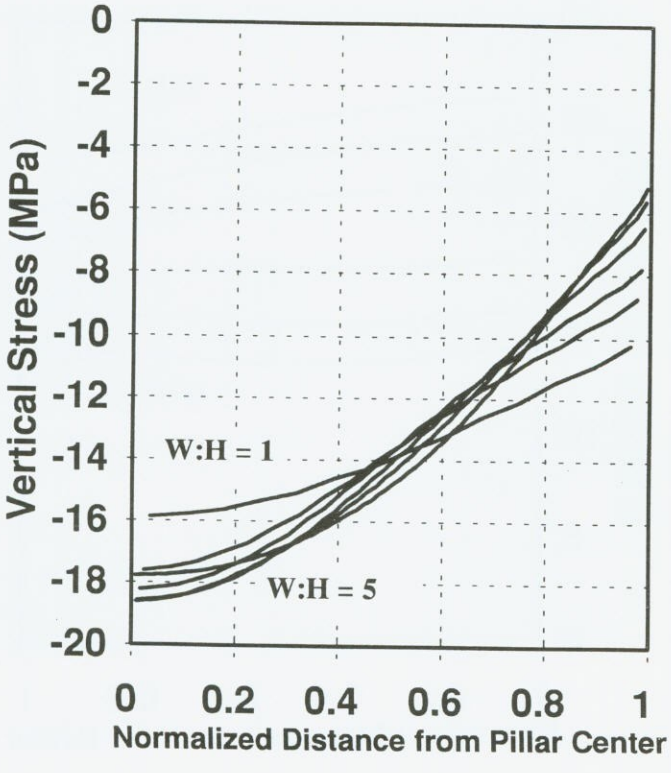



**Figure 1.** Radial, Tangential, Vertical, and Effective Stress Profiles for Axisymmetric Pillars.



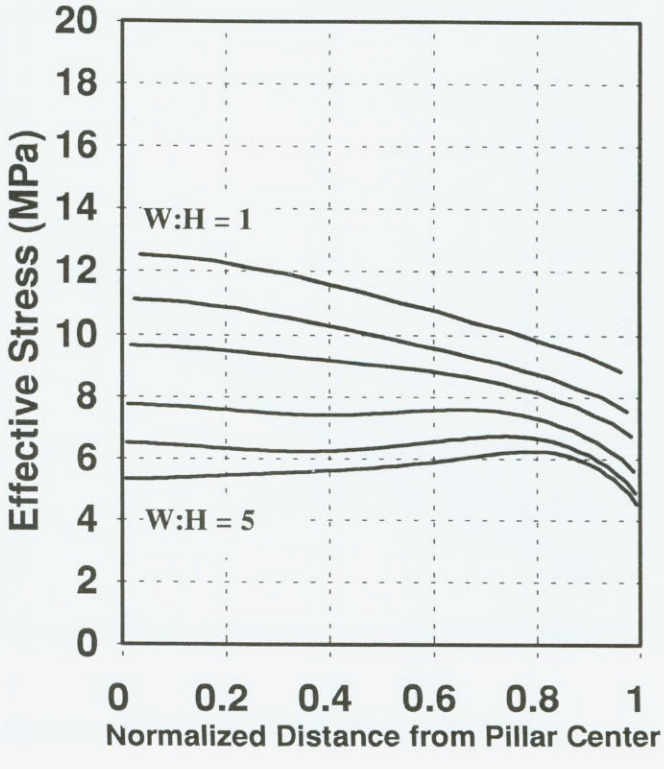




**Figure 2.** In-Plane and Out-of-Plane Horizontal, Vertical, and Effective Stress Profiles for Plane-Strain Pillars.

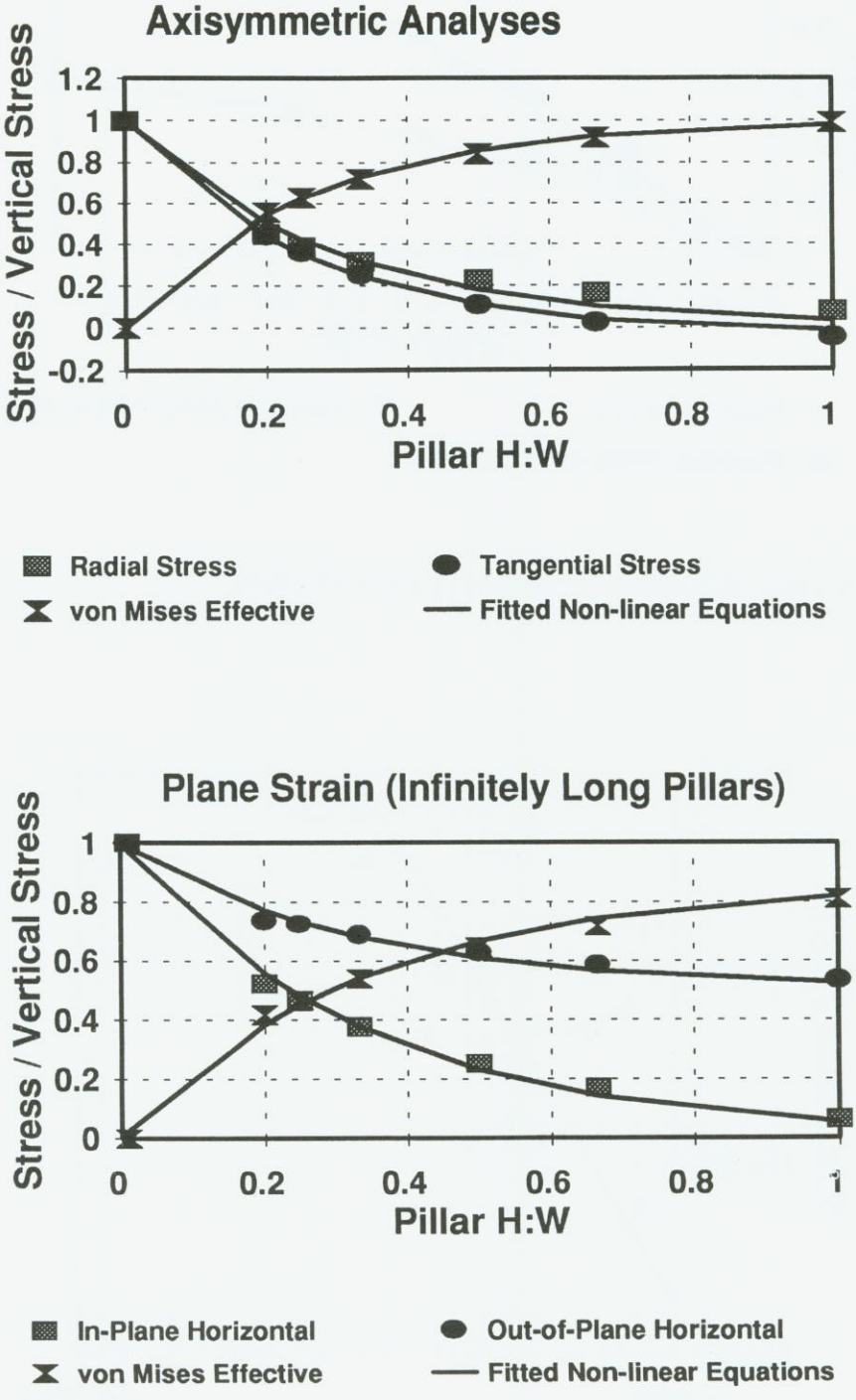



**Figure 3.** Normalized Average Stress Values for Axisymmetric and Plane-Strain Pillars of Various H:W.

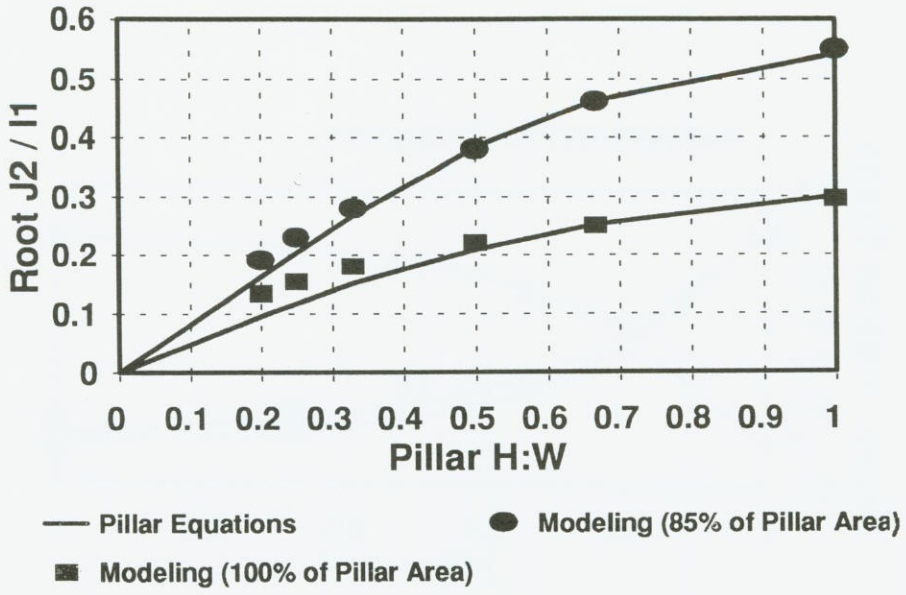



**Figure 4.** Dilatancy Factor Versus H:W for Axisymmetric and Plane-Strain Pillars.

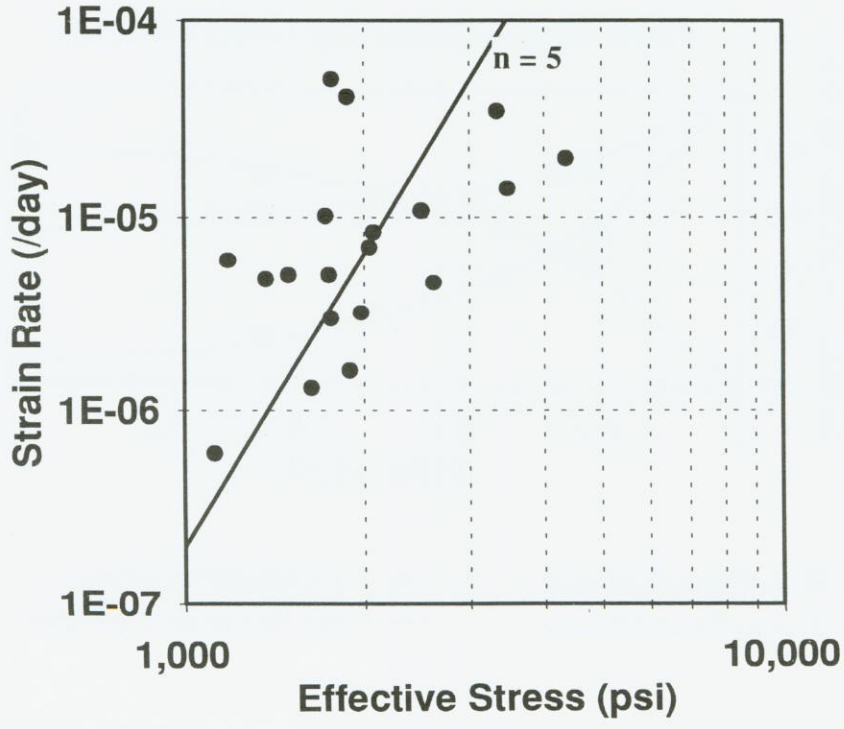



**Figure 5.** Measured Strain Rates for Pillars in Bedded and Domal Salt Mines Compared to Effective Stress Based on Pillar Equation.

# Case Study of Conditions Observed During the Removal of a Highly Fractured Roof Beam in Bedded Halite

*Liane J. Terrill*, Associate Engineer
*John D. VandeKraats*, Principal Engineer
Westinghouse Electric Corporation
Waste Isolation Division
Carlsbad, NM

## ABSTRACT

A 900 ft (275 meter) section of a highly fractured beam of halite was mined from the roof of a supported thirteen year old drift at the Waste Isolation Pilot Plant (WIPP). The operation was conducted with a continuous miner and allowed the unique opportunity to collect spatial information on roof beam geology and to observe ground support conditions during the mining advance. Photographs and fracture maps of the mining face document the progress of the operation and the deteriorated condition of the strata. This case study details the drift's excavation and support sequences, the geomechanical response, and the conditions found in the exposed roof beam.

## INTRODUCTION

The Waste Isolation Pilot Plant (WIPP) is located in southeastern New Mexico, 26 miles (42 km) east of Carlsbad, and is designed for permanent disposal of transuranic radioactive wastes left from the research and production of nuclear weapons. Project facilities include disposal rooms excavated approximately 2,150 ft. (655 m) underground in an ancient, stable salt formation. Transuranic waste consists of clothing, tools, rags, and other such items contaminated with trace amounts of radioactive elements, mostly plutonium.

The WIPP underground facility lies near the center of the Permian Salado Formation (Figure 1). The Salado is approximately 2000 ft (610 m) thick and is composed predominantly of bedded halite which dips gently southeast. The halite contains minor amounts of clay, anhydrite, and polyhalite with persistent layers of anhydrite and polyhalite serving as marker beds within the formation. Most excavations lie within a horizon that contains three particular anhydrite beds which are underlain by clay seams.

The layers of clay and anhydrite surrounding the excavations (Figure 2) have a significant impact on the mechanical performance of the excavations. Clay seams provide surfaces along which slip and separation can occur, whereas anhydrite layers act as a brittle units. Clay E, at the base of MB139, usually lies about 8 ft. (2.4 m) below the floor of the typically rectangular excavations. Clay G, at the base of Anhydrite "b", usually lies about 7 ft. (2 m) above the roof. The uppermost bed, Anhydrite "a", has Clay H at its base and usually lies about 13 ft. (4 m) above the roof. The immediate roof beam is that unit of rock between the roof and the overlying clay seam.

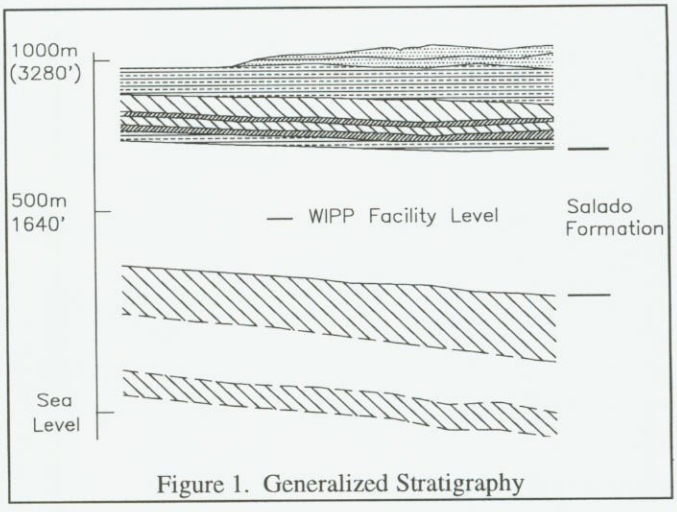



Figure 1. Generalized Stratigraphy

Excavations are predominantly oriented north-south or east-west. One of the primary north-south drifts is the East 140 (E140) drift (Figure 3). The roof beam, approximately 7 ft. (1.2 m) thick, extended over the length of the drift. Removal of a 900 ft. (275 m) section of this beam was the fourth major excavation sequence to occur in the southern portion of E140. Each sequence increased the height of the excavation without affecting width. Initial drift dimensions were 8 ft. (2.4 m) high by 25 ft. (7.6 m) wide. Two years after initial excavation, 4 ft. (1.2 m) were mined out of the floor. At five years, 3 ft. (1 m) were mined out of the roof. Excavation of the remaining roof beam brought the total excavation height to near 20 ft (6.1 m).

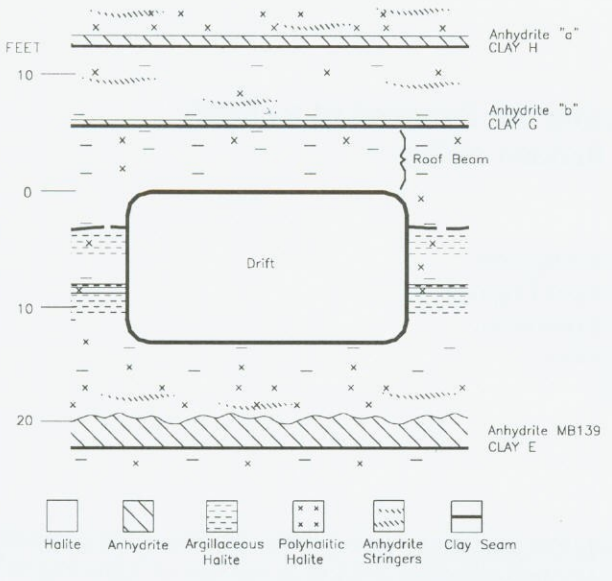



Figure 2. Horizon Stratigraphy

## ROOF BEAM STRATIGRAPHY

Numerous wetting and drying cycles that occurred during Salado deposition are reflected in depositional cycles present in the formation. A typical cycle consists of a basal claystone layer, followed by a layer of sulfate, followed by a layer of relatively pure halite that grades into relatively argillaceous halite. Before its removal, the E140 roof beam contained approximately 3 ft. (1 m) of relatively pure halite overlain by approximately 2 ft. (0.6 m) of relatively argillaceous halite, and terminated at the Clay G/Anhydrite "b" interface. Removal of the roof beam was made through Anhydrite "b" and the new beam formed by the new roof and the Clay H/Anhydrite "a" interface is approximately 7 ft. (2 m) thick and contains an almost complete depositional cycle.

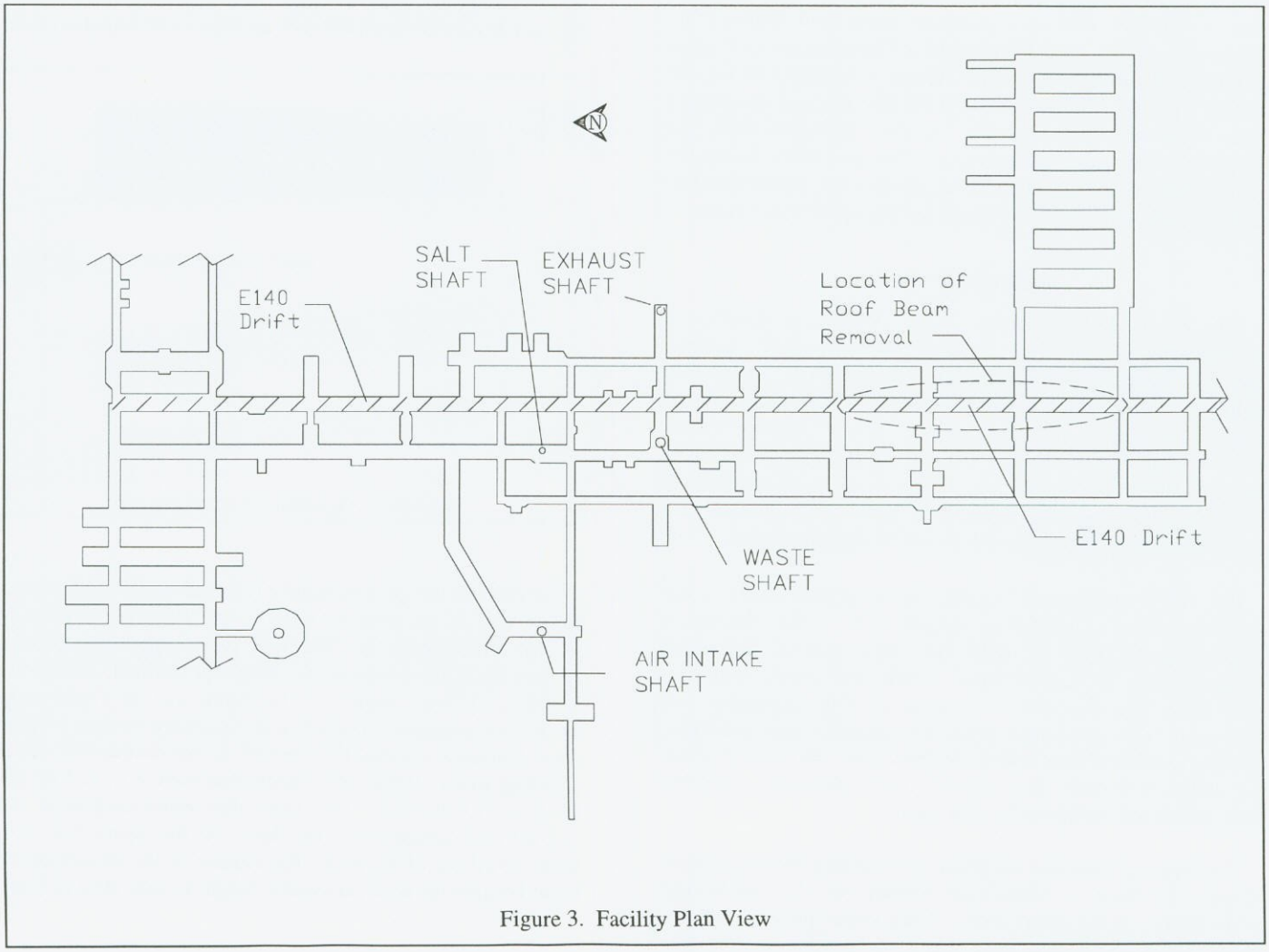



Figure 3. Facility Plan View

## ROOF BEAM DEFORMATION

Deformation and fracturing of the salt occurs throughout the mine as a result of continuous creep deformation. The geomechanical responses of the underground openings are monitored using a variety of geotechnical methods. In E140, convergence and roof expansion have been routinely monitored since initial excavation, and visual observations are made of excavation surfaces as part of ongoing assessments. Inspections of boreholes provide information on fracturing and offsetting of the subsurface strata.

Compression of the roof beam is evident by lateral movement of strata observed in inspection borehole arrays (consisting of three evenly spaced holes centered transverse in the roof) located throughout the area. The direction of offset along Clay G is observed as the movement of the roof beam relative to the overlying strata. Offsetting at Clay G is usually first observed in the side holes and is typically toward roof center (Figure 4).

Differential displacements along Clay G are commonly observed within individual arrays and are also indicated by the offset and failure of installed roof bolts at Clay G. Initial failures at a given location typically occur near the ribs with subsequent failures progressing toward drift centerline.

Convergence and roof expansion is monitored at regular intervals along the drift using geomechanical instrumentation. The data indicate uniform geomechanical responses at the monitored locations. Bowing of the roof toward the center of the drift is often evident with "hairline" vertical fracturing of the roof surface occasionally visible.

Significant low-angle fracturing in the area was first observed in a 50 ft. (15.3 m) section on the west side of the roof in 1991. Low-angle fracturing is the term commonly applied to fractures occurring in the roofs near the ribs which typically slant upward at about 20 to 25 degrees from horizontal towards the centerline. Subsurface expressions of these fractures are observable in intersecting observation boreholes.

In subsequent years, fracturing was increasingly observed in many areas of the drift. Low-angle fracturing tended to propagate along one rib for a distance, stop relatively abruptly, and begin to propagate along the opposite rib in a similar fashion. These transitions often occurred in less than 10 ft. (3 m) and in one location actually overlapped by about 4 ft. (1.2 m). Vertical fractures, when noted, typically occurred in or near these transition areas. Fewer fractures were observed in the vicinity of existing cross drifts and were often absent within the intersections.

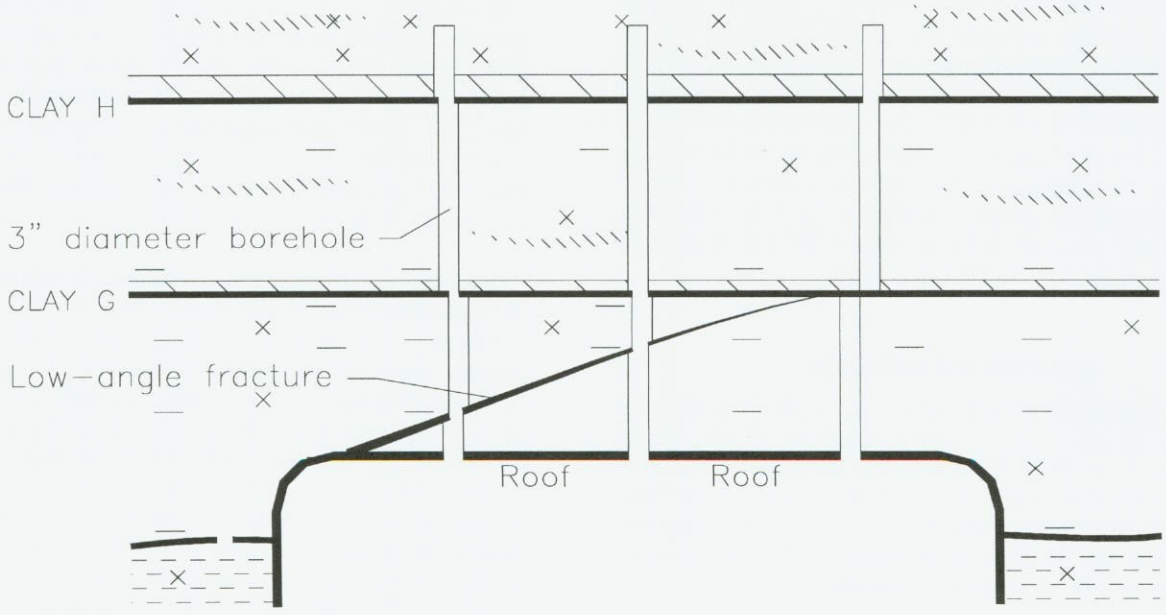



Figure 4. Typical Roof Beam Deformation

## GROUND CONTROL

The E140 drift was first pattern-bolted in early 1988 with 8 ft. long, 3/4 in. diameter mechanically anchored bolts. The pattern installed was a 12 ft. by 3 ft. (3.7 m x 0.9 m) offset pattern (i.e. transverse rows of bolts spaced 3 ft. apart with rows alternatively having 2 or 3 bolts per row on a 12 ft. spacing).

The area was frequently inspected for spalls or loose rock, which, when identified, were scaled either by hand or with a mechanical scaler. Typically, any loose ground developing in the vicinity of low-angle fractures was supported with chain-link mesh pinned with short, mechanically anchored bolts.

Over time, supplemental support was installed in areas containing zones of well developed low-angle fracturing. Types of support ranged from the simple installation of additional mechanical bolts to installation of a heavy support "blanket". This blanket consisted of welded wire mesh held in place with a wire rope lacing. The lacing was pinned with point-anchored 7/8 inch diameter threaded bar in a 4 ft. by 4 ft. pattern.

Because of the high level of maintenance required in parts of the East 140 drift, the possibility of "taking down" or removing the roof beam was evaluated as a means of ground control. Although a number of options were evaluated, only two received serious consideration: the use of explosives to shoot the ground down or the use of a continuous miner to mine the beam down.

The presence of advanced fracturing and penetrations by rock bolts throughout the roof beam made the results of using explosives somewhat unpredictable. Of prime concern was the possibility of inducing fracturing in the strata above Clay G, which would affect long-term stability and permeability, both of prime importance at the WIPP. The installed ground support systems also posed a concern for mining the beam down. This concern was concentrated on the ability of a continuous miner to handle the amount of steel installed in the roof. However, after some trial runs with a Dosco MD-1100 road header, the decision was made to mine the beam down.

## ROOF BEAM REMOVAL

Prior to commencing excavation, rock bolt supports were installed at locations where brows would be created by the mining. Brows would be located at the north and south ends of the section slated for removal and at intersecting cross-drifts. To reach the roof beam mining face, a 5 ft. (1.5 m) ramp was constructed at the northern brow location. Personnel access was prohibited in the areas to be excavated.

Mining progressed southward in a step-wise manner. A mechanical scaler equipped with a flat-edged spade bit was used to reach out under the face in order to cut the heads off of rock bolts and to peel back any mesh or wire rope installed as ground support. Then the Dosco miner was used to mine the roof beam by sweeping horizontally then upward, cutting through any ground support not removed by the scaler. Typically, the miner would advance 10-15 ft. (3-5 m), cutting one side of the beam, pull back, and then flush up the second half. Then the scaler would advance and the process was repeated. The ramp was extended by muck created by the mining process. Subsequent to mining, the newly created beam was supported with mechanically anchored bolts anchored slightly below the overlying clay seam (Clay H).

## E140 ROOF BEAM FRACTURE OBSERVATIONS

During the project, the advancing face was mapped and photographed approximately every 10-15 feet (3-5 m) to document the characteristics of the exposed roof beam, including its shape, geology, and deformation features (Figure 5).

In all areas, the mapped face of the roof beam exhibited readily observable sagging, or bowing, with respect to the horizontal cuts made by the road-header across the face. Cutting began where Clay G met the rib and proceeded laterally across the drift to where Clay G met the opposing rib. The bowing of the roof beam was reflected by increasing distance (toward excavation center) of the newly cut roof to Clay G. At drift centerline this distance was typically estimated to be about 8 inches.

The exposed geology below Clay G was consistent with the WIPP facility stratigraphy. The lower part of the beam consisted of relatively pure, coarsely- to medium-crystalline halite while the upper part consisted of relatively argillaceous, medium- to finely-crystalline halite that terminated at Clay G. The contact between the halite layers was diffuse and subhorizontal to occasionally undulatory across the mining face. This contact was undulatory along the length of the drift as well, sometimes lying within 1 ft. (0.3 m) of Clay G to 3 or 4 feet (1.0-1.2 m) below the clay. The contact between the upper argillaceous layer and Clay G was sharp.

En echelon fractures were a notable deformation feature observed in the exposed roof beam. These fractures occur in an overlapping or staggered arrangement where individual fractures are relatively short but collectively form a linear zone in which the strike of the individual fractures is oblique to that of the zone as a whole. The en echelon fractures typically lay horizontally or sub-horizontally within the face, ranged from several inches up to a few feet long, and had observed apertures as large as 1/2 in. (13 mm). Typically, the lowest fracture (nearest the original roof surface) was located near one rib and subsequent fractures were staggered upward and toward drift centerline. The angle of the zone of fracturing was estimated with a pocket transit and found to average about 20°.

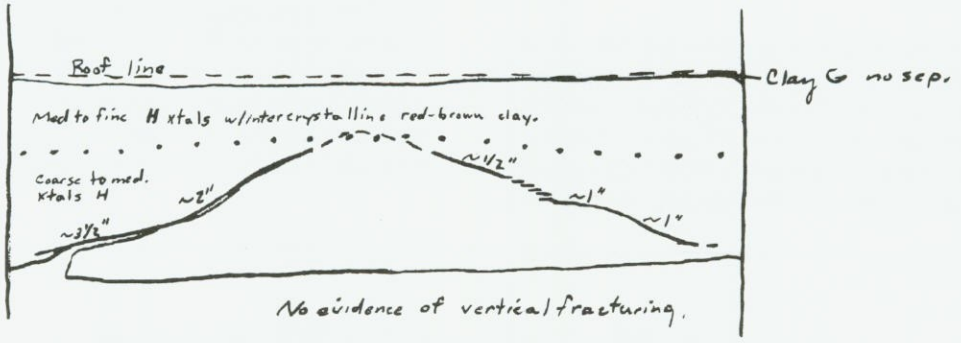
Although the effects of changes in halite crystal size and clay content do not seem to have much, if any, effect on the development of the en echelon fracturing, the linear zone surrounding the fractures appeared disturbed by the fracturing process. The halite immediately surrounding the fractures had a brittle appearance, often displaying a crushed or sugary texture.

Low-angle fractures, previously observed on the roof surface and in observation boreholes, were readily visible in the face and appear to result from the linking up of individual en echelon fractures (Figure 6). Whereas the en echelon fractures lay oblique within the zone of fracturing, their connection typically resulted in longer fractures of greater aperture that lay parallel within the zone. Low-angle fractures in one location had observed apertures up to 1 ft. (0.3 m), however most typically ranged up to about 4 in. (10 cm).

Development of low-angle fractures typically predominated on one side of the roof beam, often crossing the full thickness of the beam and terminating at Clay G. This "side-swapping" was consistent with observations made prior to roof beam removal in which low-angle fracturing was found to propagate along opposite sides of the roof in a staggered fashion. Also consistent with previous observations was that fewer fractures were observed in the vicinity of existing cross drifts and were often absent within the intersections.

Separation along Clay G usually occurred at the point where the dominant fracture set approached the roof. The length of the separation was typically on the order of 2 to 5 feet (0.6-1.5 m). Separations were typically about 1/4 to 1/2 inch (6-13 mm) with some noted up to 2 inches (5 cm). Separations tended to decrease substantially in size and occurrence within 50 feet (15.1 m) of intersecting cross-drifts and were absent within the intersections.

Offsetting of strata, previously observed along low-angle fractures and Clay G in observation boreholes, was evident from deformations observed in rock bolts exposed by the mining. Up to about 1 in. (2.5 cm) of axial offset was observed in some intact bolts resulting from the effects of strata displacement along fractures or Clay G. The directions of bending observed in the bolts were consistent with strata offset directions observed in inspection boreholes.



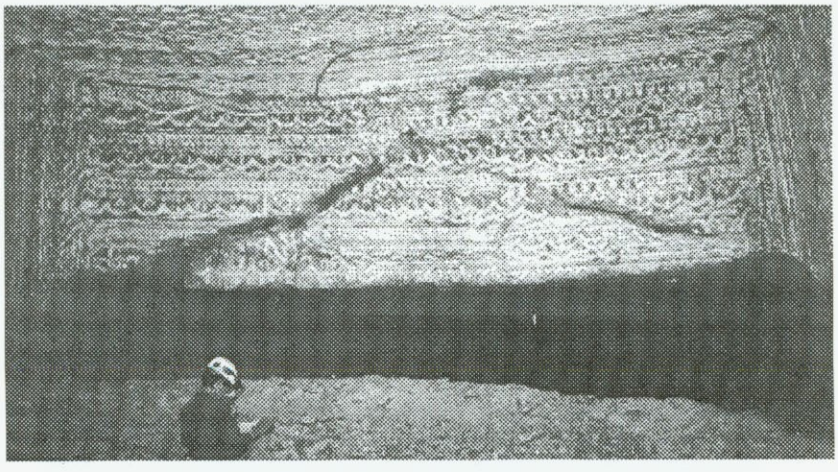



Figure 5. E140/S1368, View South

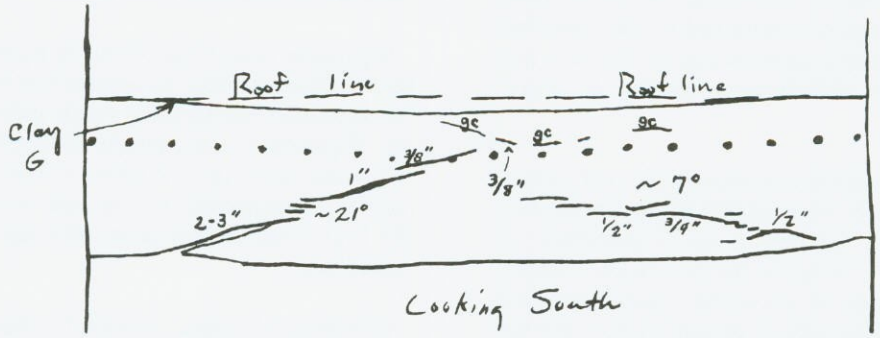



Figure 6. E140/S1095

The effects of stratigraphic offset on the bolts is more severe at Clay G than that along low-angle fractures. This is due in part to the Clay G plane being relatively normal to rock bolt axes (whereas low-angle fracture planes are oblique) and in part due to less confinement in the relatively wide apertures of low-angle fractures. In some cases, salt had apparently flowed around the bolts.

In most areas, installed support apparently had little or no effect on displacement along low-angle fractures. However, one location, which had been heavily supported, contained fractures with apertures up to 1 ft. (0.3 m) (Figure 7). This may be attributable to the support successfully resisting offset along the fracture, causing buckling of the hanging rock which resulted in large apertures between the buckled rock and the overlying strata.

In the area where significant low-angle fracturing was first observed in 1991 fracturing was most well-developed and vertical fractures were observed near the upper corner of the roof beam on the side opposite the low-angle fracture (Figure 8). These were apparently formed by tensile stresses resulting from the beam bending down along the low-angle fracture. In other areas, vertical fractures that had been observed in the roof surface prior to excavation were found to be limited to within the first few inches of the surface. These fractures are probably the result of tensile stress manifest due to beam bowing.

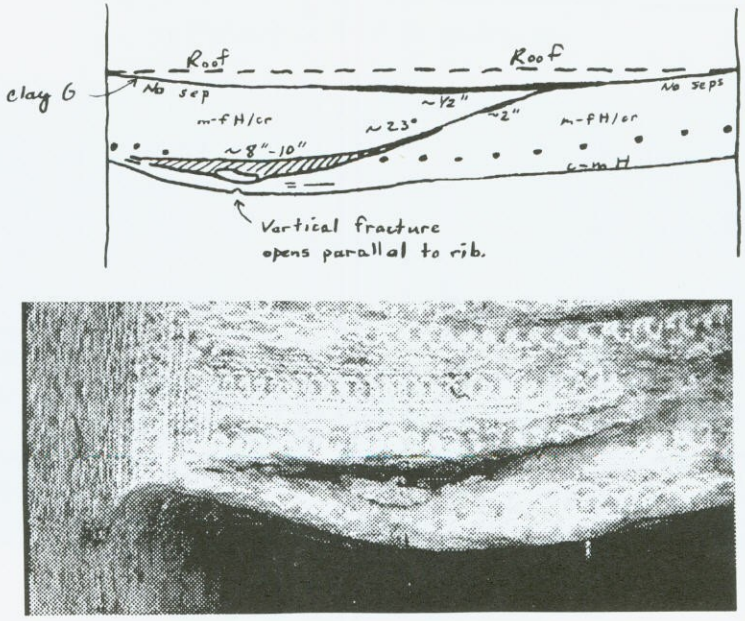
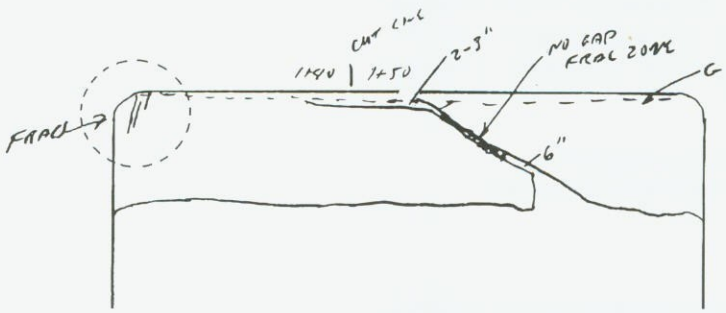



Figure 7. E140/S1508, View South



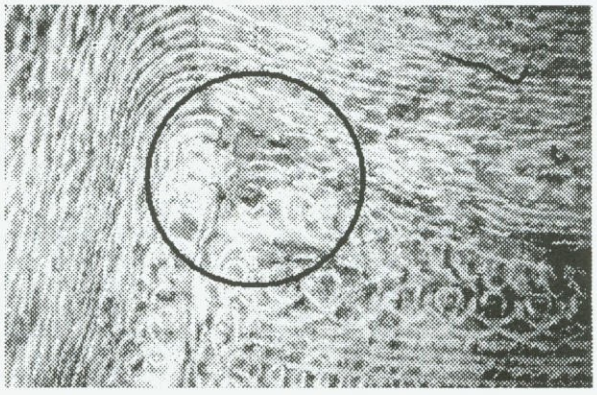



Figure 8. E140/S1468, View South

## POST-EXCAVATION CONDITIONS

Preliminary geomechanical data indicate decreased rates of convergence along with significant decreases in roof expansion rates. See Francke, et al, 1997, for a discussion of the geomechanical response.

No fracturing of the new roof surface is observed to date. A few observation boreholes contain shallow fractures at approximately 1 ft. (0.3 m) above the roof surface with apertures of 1/16" or less. One fracture was noted as being concomitant with a thin (approximately 1/8" thick) anhydrite drape. Small offsets are evident along two of these fractures, the directions of which suggest that the displacements occurred before roof beam removal.

Prior to roof beam removal, observations of conditions at the second clay seam, Clay H, showed displacements to be toward drift center at rates approximately one third of displacement rates at Clay G. Preliminary assessment of offset rates at Clay H (now the first clay seam) show little or no change.

## REFERENCES

1. U.S. Department of Energy (DOE), 1983, "Correlation of Drillhole and Shaft Logs", TME 3179.

2. Francke, C.T., and Terrill, L.J., 1991, "The Excavation Effects Program at the Waste Isolation Pilot Plant", Innovative Mine Design for the 21st Century, proceedings of the International Congress on Mine Design, Balkema.

3. U.S. Department of Energy (DOE), 1995, Geotechnical Analysis Report, DOE-WIPP 95-2100.

4. Westinghouse Electric Corporation, 1996, 1996 Long-Term Ground Control Plan for the Waste Isolation Pilot Plant, WIPP/WID-96-2180.

5. Terrill, L.J. and J.D. VandeKraats, 1995, "Analysis of Rockbolt Performance at the Waste Isolation Pilot Plant", proceedings of Fourteenth International Conference on Ground Control in Mining, West Virginia University.

6. Francke, C.T., L.J. Terrill, and J.D. VandeKraats, 1997, "Case Study of the Effects of Stratigraphic Location on Roof Stability in Rock Salt", proceedings of Sixteenth Conference on Ground Control in Mining, Morgantown, West Virginia.



Processing and final preparation of this report were performed by the Westinghouse Electric Corporation's Waste Isolation Division, the management and operating contractor for the Waste Isolation Pilot Plant, under U.S. Department of Energy contract DE-AC04-86AL31950.

This document has been submitted as required to
Office of Scientific and Technical Information
PO Box 62
Oak Ridge, TN 37831
(615)576-8401
Additional information about this document may be obtained by contacting the National Technical Information Service, U.S. Department of Commerce, 5285 Port Royal Road, Springfield, VA 22101.



# Case Study of the Effect of Stratigraphic Location on Roof Stability in Rock Salt

*Chris T. Francke,* Senior Engineer
*Liane J. Terrill,* Associate Engineer
*John D. VandeKraats,* Principal Engineer
Westinghouse Electric Corporation
Waste Isolation Division
Carlsbad, NM

## ABSTRACT

The Waste Isolation Pilot Plant is a deep underground facility mined in bedded salt interspersed with persistent clay interbeds. The clay seams delineate beams of salt above and below the excavations which strongly influence excavation performance. This paper reviews available rock mechanics information relevant to improving drift stability by removing the roof beam. Conceptual deformation mechanisms, relevant field data, and numerical analyses were used to investigate the effects of mining the roof of the excavations along a clay seam. Finally, a case study that applies the results of this investigation is presented.

## INTRODUCTION

The Waste Isolation Pilot Plant (WIPP) is located in southeastern New Mexico, 42 kilometers east of Carlsbad. WIPP is a U.S. Department of Energy facility designed for permanent disposal of transuranic radioactive wastes left from the research and production of nuclear weapons. Project facilities include disposal rooms excavated approximately 655 meters underground in an ancient, stable salt formation. Transuranic waste consists of clothing, tools, rags, and other such items contaminated with trace amounts of radioactive elements, mostly plutonium. The WIPP underground facility layout is shown in Figure 1.

The behavior of underground excavations WIPP has been intensely studied for over fifteen years. All excavations have performed their intended functions safely with normal maintenance and ground support. The deformation mechanisms are well understood. With many openings now twelve years old or older and a 35 year operational phase scheduled to begin in 1998, these drifts are required to be safe and usable for nearly fifty years. Because the performance standards at a nuclear waste repository are so demanding, the process of ground control and excavation design in such cases are particularly challenging, especially in a time dependent material such as the rock salt in which the WIPP repository is situated.

One method of extending the life of long-term excavations such as access drifts and shaft stations is the periodic removal of fractured rock and the re-mining of the excavation roof up to the nearest clay seam. Conceptual deformation mechanisms believed to be at work at WIPP are briefly discussed. Field data from excavations with a clay seam forming the roof are reviewed and compared to excavations with the roof beam delineated by the roof-line and the nearest clay seam. Numerical modeling results compare excavations with and without clay seams at the roof line, as well as the effect of removing the roof to the clay seam well after initial excavation.

## CONCEPTUAL DEFORMATION MODEL

The stability of excavations at WIPP is assessed by analysis of creep displacement and fracture formation. Fracturing and increasing displacement are closely related and in the absence of increased stress levels or increased temperature, displacement rate increases can only be caused by forming and opening fractures. Figure 2 shows a schematic of a typical WIPP excavation and the associated stratigraphy and fracture patterns.

Immediately after excavation, high displacement rates are observed which rapidly decrease. Localized shallow spalls associated with poor rock conditions are sometimes observed soon after excavation. This "primary creep" stage usually lasts less than two years. It is followed by a longer period of relatively low, steady displacement rates. During this period, low angle (less than 45 degrees from horizontal) shear fractures may form in the roof. These fractures generally begin at the roof-line near one or both ribs and terminate at the clay seam. The fractures shown in Figure 2 are

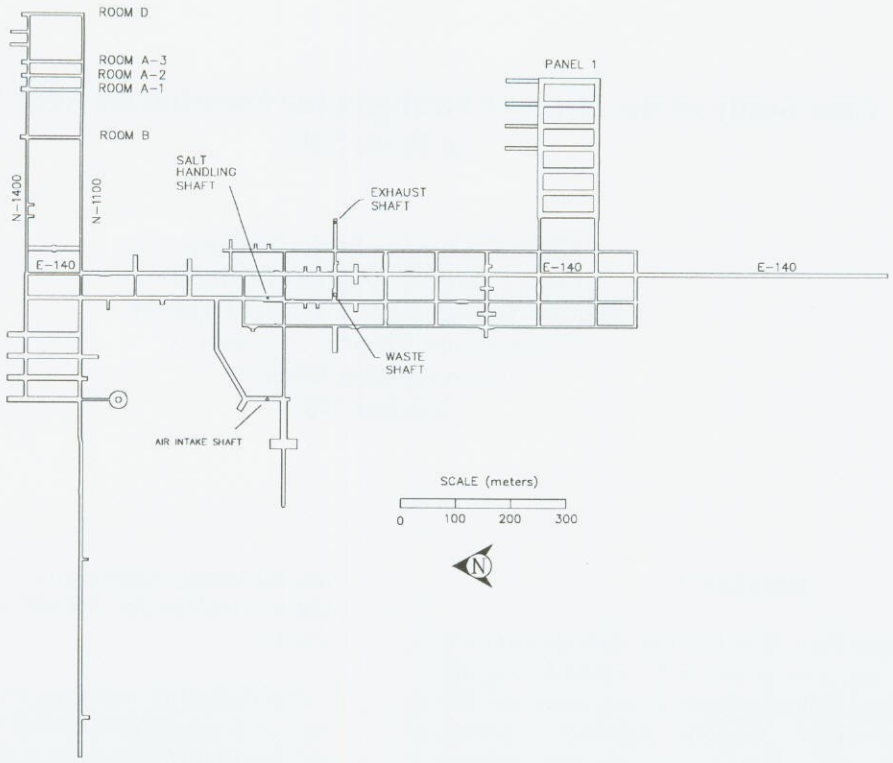



Figure 1. WIPP underground facility layout.

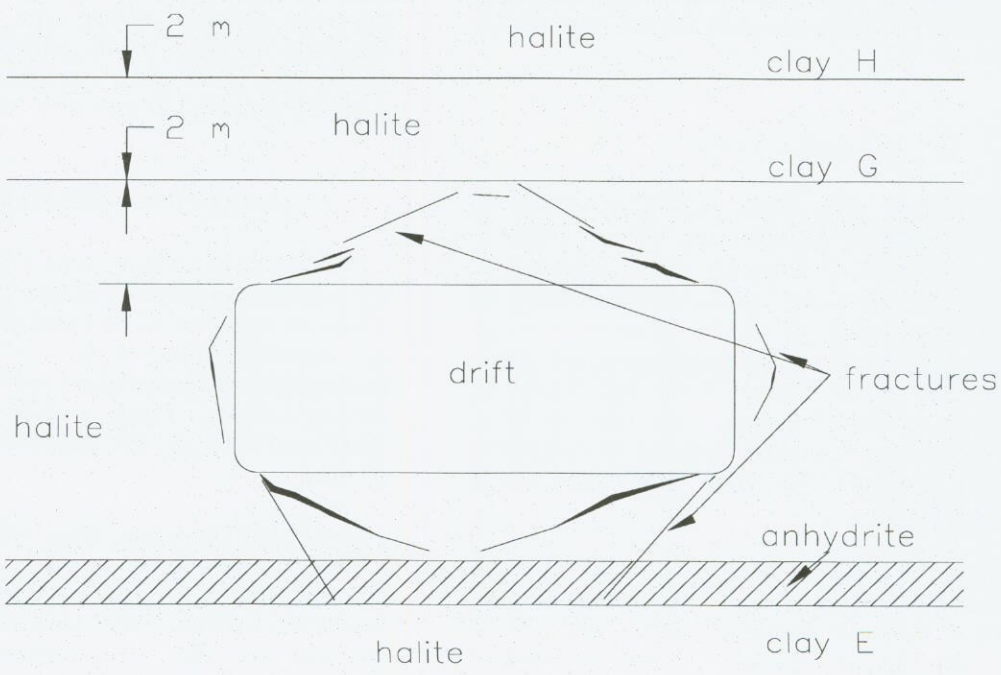



Figure 2. Generalized stratigraphy and fracture patterns surrounding a WIPP excavation.

a generalization. The actual fracture patterns are more complex but follow the same general pattern. See Terrill and VandeKraats, 1997, for an in-depth discussion of the fracturing. This "steady-state" deformation stage generally lasts at least two years but frequently much longer. A third deformation stage can begin if displacements due to fracture formation become significant. In this stage, deformation rates will increase until roof collapse occurs if adequate ground support is not installed. This "tertiary" creep stage has been seen to last as long as seven years in unsupported WIPP excavations. Two excavations at WIPP were allowed to progress through the tertiary stage up to collapse so that the failure process could be thoroughly understood (Francke, et al., 1994).

The geometry and intensity of fracture formation in the roof of WIPP excavations is primarily controlled by the geology and the excavation shape (DOE, 1993). Zones of high shear stress develop in the roof near the ribs immediately after excavation. These zones are weakened relative to the rest of the roof beam. At the same time, the pillars expand into the excavations. Horizontal offsetting of adjacent layers along clay seams under the horizontal displacement of the pillar is observed. This effectively concentrates the pillar expansion between the clay seam immediately above the roof and the clay seam immediately below the floor. The high horizontal load on the roof beam causes large displacements and ultimately causes fracture formation. The weak zones formed in the roof by the early high shear stress are the most probable locations for fracture concentration due to the high strain rate induced in the roof beam by the pillars. These fracture zones, usually first observed during the steady-state phase of deformation, usually consist of a series of smaller en-echelon sub-horizontal fractures that together form diagonal zones originating near each rib and terminating near the clay seam. The development of extensive fractures in the roof beam reduces the ability of the roof beam to resist the horizontal loading from the pillar, thus allowing higher beam compression rates and increasing fracture formation. If left unsupported, the fracturing will eventually increase to the point where the roof beam can no longer support its own weight, resulting in a roof fall.

Standard ground control systems such as rock bolts can prevent large scale ground falls even when the roof is highly fractured. However, the continuing creep movements drastically reduce the effective life of rockbolts and other fixtures that penetrate the roof. This can result in high maintenance requirements for older excavations. An excavation design that minimizes the roof fracturing will minimize ground control costs. The conceptual model proposed above suggests that an excavation with its roof mined along a clay seam would be more stable than one with a roof beam. The concept is that the rock below the clay seam along the roof-line would slip into the room, relatively unopposed, as the pillar expands, thus reducing to a minimum the transmission of horizontal load to the roof and therefore reducing the fracturing in the roof. Furthermore, the conceptual model suggests that an excavation with clay seams along both the roof and floor line would be optimal.

## FIELD DATA

In order to verify the conceptual model, field data from the WIPP underground facility was examined. The vast majority of excavations at WIPP were initially mined with the roof about two meters below the clay seam. However, there are several drifts that were mined with the roof at the clay seam or that were later enlarged so that the roof was brought up to the clay seam.

### Beam Removed After Initial Mining

Prior to the large scale field implementation that will be discussed later, the only excavation that has had the roof beam removed up to a clay seam well after initial mining is the Salt Shaft Station. This opening is unusual in several respects. It is the oldest drift in the facility (mined in 1982) as well as the largest in width (10.7 meters). Because it was the first facility level drift created at WIPP, the Salt Shaft Station is the only drift that was mined using standard drilling and blasting techniques. The roof of the excavation was initially mined to within about 0.7 to 2.0 meters below the persistent clay seam, clay G. By 1987, the roof had deteriorated to the point that it was decided to excavate the roof up to clay G.

Nearly ten years has passed since the roof beam was removed. In that period, the large scale fracturing that had developed in the original roof has not recurred. Only minor spalling easily handled with wire mesh has been noted to date. Other than mesh support, the roof remains largely unbolted.

The geomechanical instrumentation record also shows a dramatic change in behavior after roof beam removal. A number of roof-to-floor convergence meters and roof borehole extensometers were installed in the station before and after roof beam removal. The results shown in Figure 3 are typical of all of these instruments. This figure shows convergence rate data from a vertical convergence meter located in the shaft station. The rate before the roof beam was removed is about four inches per year. After the roof was moved to Clay G, the rate decreased to about 1.5 inches per year.

The fracture and instrument data from this opening show that conditions improved dramatically after the roof-line was moved to the nearest clay seam. In addition, it is clear that the poor ground conditions seen in the roof before beam removal have not reappeared in the decade since the roof beam was removed.

### Roof Originally Mined at Clay Seam

There are two groups of excavations at WIPP that fall into this category. One set consists of openings, designated rooms A, B, and D, that were mined for rock mechanics experiments conducted by Sandia National Laboratories. These openings were mined 5.5 meters high by 5.5 meters wide and were not rockbolted. Both the roof and the floor of these excavations were located along clay seams. These rooms were remarkably

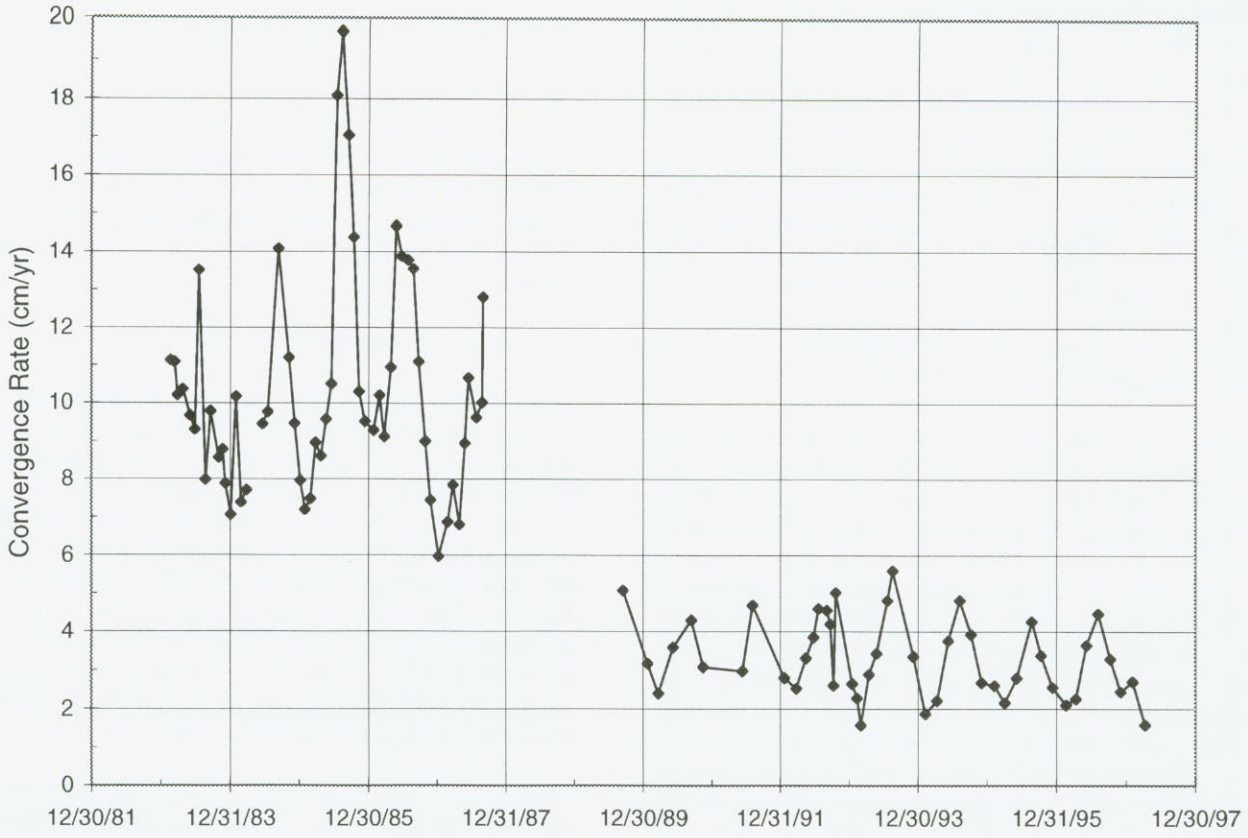



Figure 3. Typical Convergence Results for the Salt Shaft Station.

stable, especially considering the experimental conditions they were subjected to. Several of these rooms were heated to artificially accelerate closure rates. Air temperatures were raised to about 60 degrees Celsius for about three years. According to the accepted creep constitutive model used at WIPP, the temperature increase should cause displacement rates about five times the rates at in-situ temperatures. Despite this, the rooms performed well. Several had thin slabs (about 0.5 meters thick) break loose from the roof. However, these could have easily been controlled with standard rockbolts. The relatively good performance of these rooms, especially considering the extreme thermal loading, indicate that the location of clay seams at the roof and floor lines is an extremely stable configuration.

One other drift at WIPP has clay seams at the roof and floor lines. This drift, designated N1100, has the smallest cross-sectional area at WIPP ( 2.4 meters high, 4.3 meters wide). A drift running parallel to N1100, designated N1420, is configured identically to N1100 except that the roof-line is about 1.3 meters higher. The N1420 drift has a section of salt approximately 1.6 meters thick between the roof-line and the first clay seam, while N1100 has the roof-line located level with the clay seam. The two drifts were also mined simultaneously, so they are the same age allowing a good comparison between similar drifts with different roof beam configurations.

Roof fracturing is relatively intense in the N1420 drift. Large scale diagonal fractures developed along with vertical cracks in the roof. The N1100 drift has very little fracturing. In terms of fracture development, the N1100 drift, with the roof-line and floor-line at clay seams, is in much better condition than the N1420 drift, with the roof mined between clay seams and the floor located at a clay seam.

Geomechanical instrumentation data shows similar disparities between the two drifts. Figure 4 compares vertical convergence rates in the N1420 and the N1100 drifts. The rates in the N1420 drift are approximately 1.5 times the rates in the N1100 drift. This may be attributed to the fracture formation in the roof beam of the N1420 drift, which is absent from the N1100.

Summary of Field Data

Field observations in the form of geomechanical instrumentation and fracture mapping have been examined in all rooms without clay seams forming the roof or floor and in the only room that has had the roof removed to a clay seam. In all cases, the drifts with a clay seam forming the roof performed much better than their counterparts with a roof beam. Without exception, the field data demonstrate that initially mining drifts with a clay seam forming the roof makes

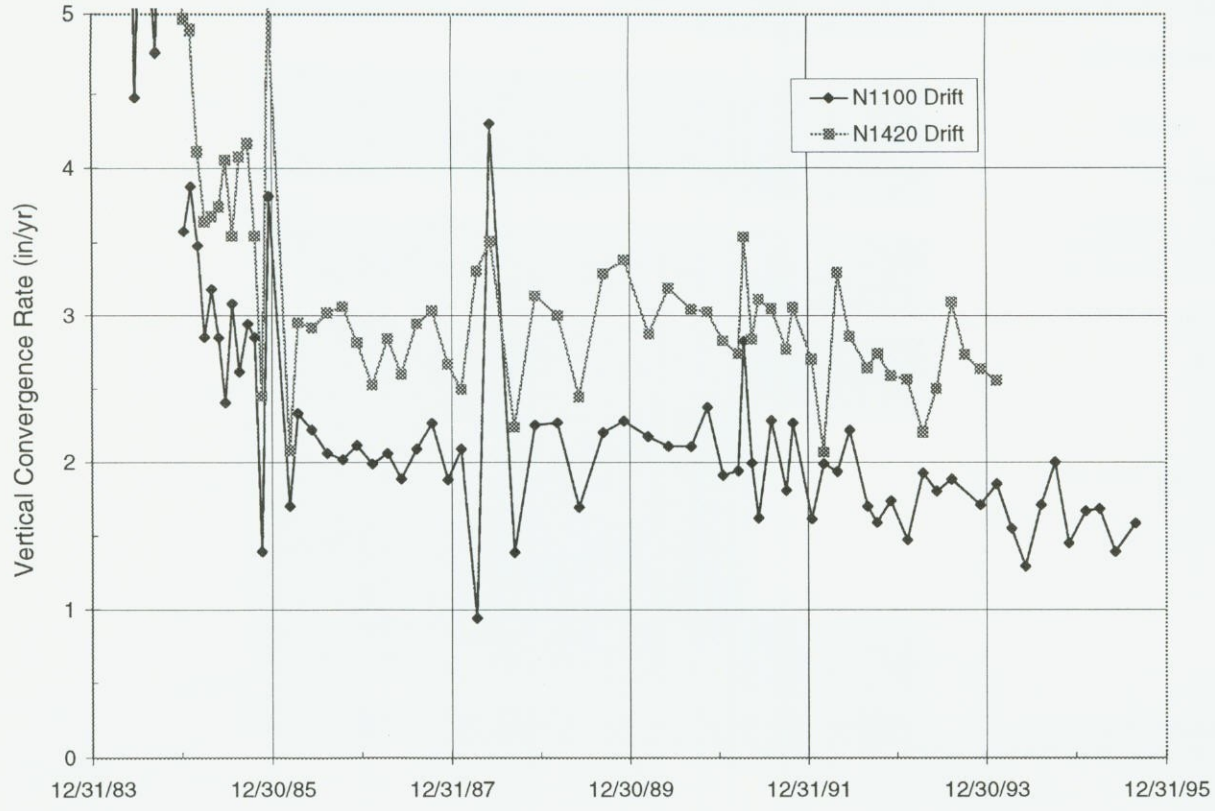



Figure 4. N1100 and N1420 Convergence Results.

for long-lasting, stable excavations. The field data also demonstrates that removing a roof beam well after excavation improves the stability of a drift.

## NUMERICAL MODELING

Although there is a preponderance of evidence in the field data supporting the decision to remove the roof beam from older excavations, numerical analyses, in the form of finite difference modeling, were also used to investigate the effect of roof beam removal and the advantages of mining drifts without roof beams. The finite difference code used was Fast Lagrangian Analysis of Continua (FLAC) (Itasca Consulting Group, 1993). For this study, the E140 drift was modeled. This drift is one of the main access routes in the WIPP underground facility. It also has one of the longest required useful lives of all the excavations. It was proposed to do the initial implementation of the roof beam removal technique in this drift. Two models of the E140 drift were developed. One model had the roof-line at its original location about 2 meters below the clay seam. A second model had the roof-line moved up to the clay seam ten years after the initial excavation. Although the models cannot simulate fracturing, the potential for fracturing can be related to zones of high strain concentration in the models.

Figures 5 and 6 show the strain distribution around the opening 20 years after initial excavation for the models without and with the roof beam removed, respectively. The strain is less in the roof after twenty years for the case with the roof beam removed than it is in the case with the roof beam left in place. This would presumably indicate that removing the roof beam would reduce maintenance requirements for the excavation.

## IMPLEMENTATION AND RESULTS

The first large scale implementation of the roof beam removal technique occurred in a 275 meter long section of the E140 drift. The roof was excavated up to the Clay G layer using a continuous mining machine. The re-mining of the roof took place approximately thirteen years after the initial excavation of the drift. Shortly after mining was completed, the new roof was supported with 1.2 meter mechanically anchored bolts. For a detailed description of the removal operation and the fracturing observed in the roof beam, see Terrill and VandeKraats, 1997.

Although long term data after the beam was removed is not yet available, early results indicate that the operation was a success. Figures 7 and 8 show vertical and horizontal convergence rate plots for a location in the E140 drift. The vertical convergence rate at this location clearly shows a reduction after the beam was removed. This is probably due to several factors. First, a certain amount of the pre-removal vertical convergence was undoubtedly due to the formation and extension of fractures. This was eliminated when the beam was

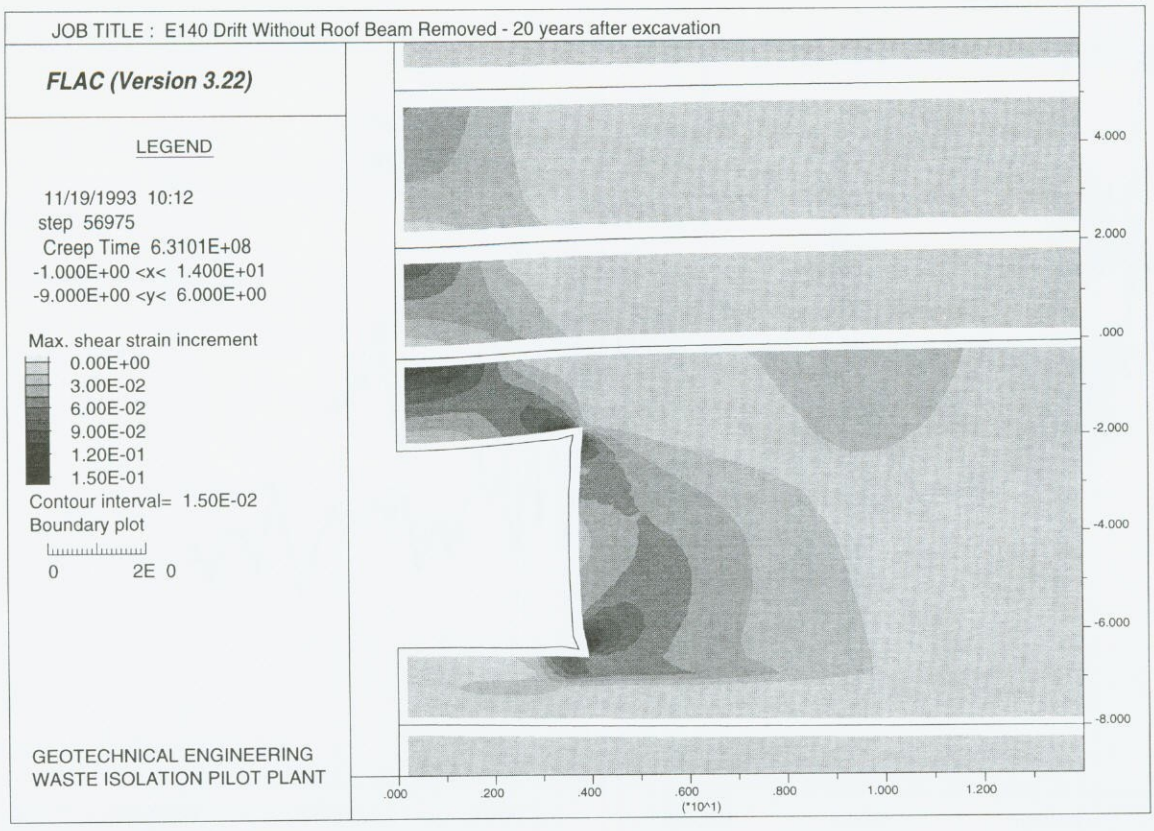



Figure 5. Model results for the E140 Drift without roof beam removed

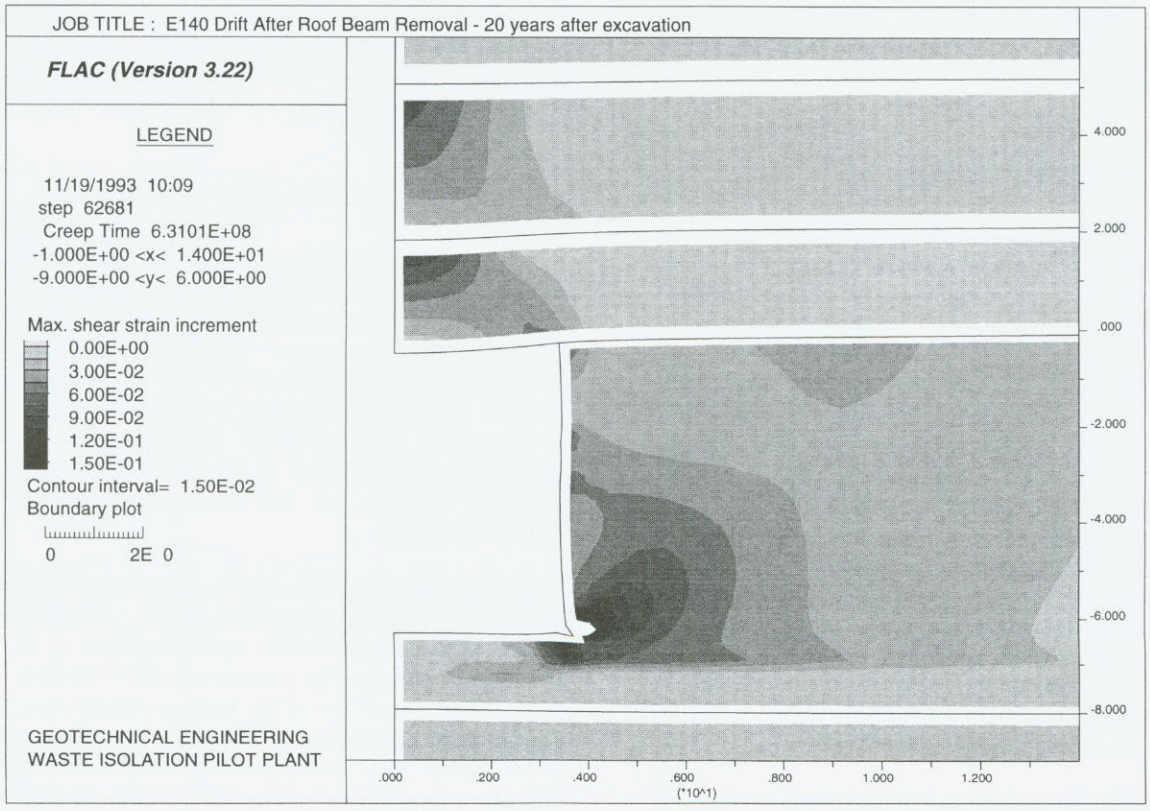



Figure 6. Model results for the E140 Drift with roof beam removed

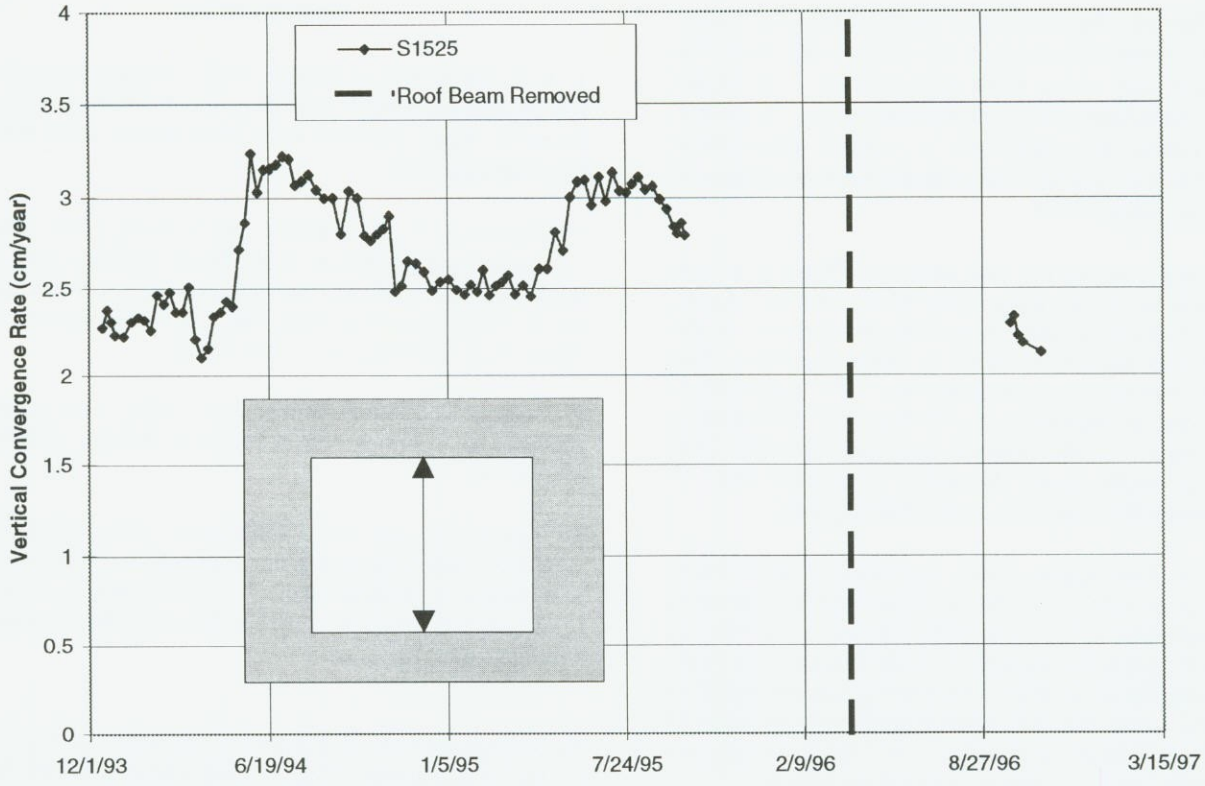



Figure 7. Vertical Convergence Results for the E140 Drift

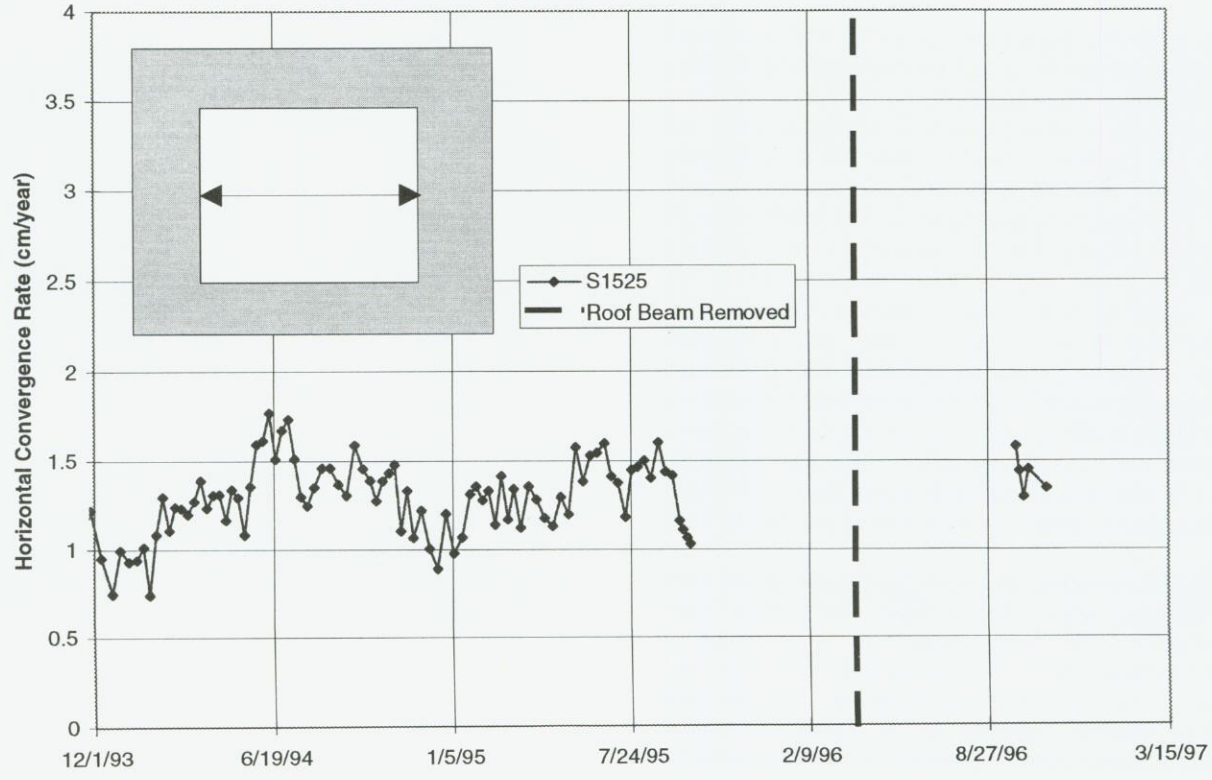



Figure 8. Horizontal Convergence Results for the E140 Drift



removed. Second, the conceptual model presented earlier suggests that the horizontal load in the original roof beam was probably higher than in the beam after removal. The higher load should lead to higher creep displacement rates. In general, one would expect the magnitude of vertical convergence decrease after beam removal to be proportional to the degree of fracturing in the original roof.

The horizontal convergence rate shown in Figure 8 is very nearly the same or slightly higher after beam removal. Again, the conceptual model would suggest that the removal of the roof beam would reduce resistance to pillar expansion, thus increasing the horizontal convergence rate. The magnitude of the increase may be dependent on the degree of fracturing in the original roof. If the original roof had relatively little fracturing, one would expect the ability of the roof beam to resist horizontal pillar expansion to be relatively high.

In terms of convergence rates immediately after beam removal, it can be safely said that the beam removal operation improved conditions in the E140 drift. However, the real test of success will be fracture formation. In the months after beam removal, no significant slabbing or fracturing has developed in the roof beam. If, as in the Salt Shaft Station roof, fracturing in the E140 drift roof does not develop to any significant degree, then the method can be considered a long-term success.

## CONCLUSIONS

The results show that the presence of a clay seam at the roof of an excavation extends the life of the excavation by reducing the degree and rate of fracturing in the roof material. The clay seams are very weak compared to the surrounding rocksalt, and therefore do not efficiently transfer stress and displacements from the laterally expanding pillars. The clay seams essentially concentrate stress and displacement in the rock intervals between the roof and the first clay seam above the excavation and between the floor and the first clay seam below the excavation. This leads to greater levels of fracturing and displacement than would be seen if the rock mass were homogenous. It is demonstrated through field observations and numerical modeling that the lowest-maintenance, longest-lived excavations at the WIPP repository level will have clay seams located at both the roof and the floor. The least favorable arrangement is seen in openings with a clay seam at the floor level with another clay seam several meters above the roof-line.

In the field demonstration, the horizontal convergence rates increased slightly, while the vertical convergence rates decreased slightly. This was attributed to the reduction of stress in the roof beam due to the location of the clay seam, and the elimination of a large amount of fracturing. The new roof is currently in excellent condition and is expected to require much less maintenance than the previous excavation geometry. The roof beam removal technique is under serious consideration for further application at WIPP, especially in excavations that will require long-term stability.

## REFERENCES

1. U.S. Department of Energy, 1993, "Current Bases for Roof Fall Prediction at WIPP and a Preliminary Prediction for SPDV Room 2," Waste Isolation Pilot Plant Report DOE/WIPP 92-024, Carlsbad, NM.

2. Francke, C.T., S.J. Patchet, and S. Saeb, 1994, "Roof fall monitoring and prediction at the Waste Isolation Pilot Plant," Rock Mechanics Models and Measurements, Proceedings of the 1st North American Rock Mechanics Symposium, Austin, Texas, A.A. Balkema, pp. 1041-1048.

3. Itasca Consulting Group, Inc., 1993, Fast Lagrangian Analysis of Continua (FLAC) User's Manual, Minneapolis, Minnesota.

4. Terrill, L.J., and J.D. VandeKraats, 1997, "Case study of conditions observed during the removal of a highly fractured roof beam in bedded halite," Proceedings of the 16th Conference on Ground Control in Mining, Morgantown, West Virginia, pp. 235-242.

Processing and final preparation of this report were performed by the Westinghouse Electric Corporation's Waste Isolation Division, the management and operating contractor for the Waste Isolation Pilot Plant, under U.S. Department of Energy contract DE-AC04-86AL31950.

16th CONFERENCE ON GROUND CONTROL IN MINING



# Ground Control and the Inundation of the Retsof Mine

*Vincent A. Scovazzo,* Senior Geomechanics Specialist
John T. Boyd Company
Pittsburgh, PA

## ABSTRACT

On March 12, 1994, the 1,100-foot deep 2 Yard South panel of the 110-year-old Retsof Mine collapsed. At the time of this occurrence, the Retsof Mine was characterized as the world's largest, most productive salt mine. The collapse produced a seismic event and resulted in a sinkhole and small lake forming on the surface. An existing highway bridge was rendered unusable. Water entered the mine and despite valiant efforts by the miners and the mining company, the entire mine was flooded and lost. John T. Boyd Company (BOYD) studied the incident to evaluate design procedures, and assess the short- and long-term environmental impacts of the collapse.

This paper presents our analysis of the cause of the collapse and our review of the rock mechanics design of 2 Yard South panel. Our review is, in part, based on a rock mechanics monitoring program of 2 Yard South. The monitoring program was established by the mining company as the panel was developed and continued even after the panel became unstable.

## INTRODUCTION

The Retsof Mine is located in Livingston County, New York, approximately 30 miles southwest of Rochester. Salt from the B6 Bed of the Silurian age Salina Group was produced from the mine which encompasses an approximate 6,500 acres. The mine lies at approximately 1,100 feet below the surface with intervening bedrock comprised of salt, shale, and limestones. Thick glacial deposits of Pleistocene age mantle the area.

Beginning on March 12, 1994, the 2 Yard South panel, near the mine's southeastern extent, collapsed allowing a large continuous flow of ground water into the mine. Subsequently, the adjacent 11 West panel collapsed. Sinkholes formed above both the 2 Yard South and 11 West panels. The 110-year-old mine was completely flooded and closed in 1995.

This study concluded that the 2 Yard South panel collapse occurred due to the use of yield pillars in an area where solid rock cover was insufficiently thick to accommodate the formation of an arch in the overburden.

## GEOMECHANICAL INVESTIGATION

BOYD studied the geomechanical and environmental aspects of the incident. These included an assessment of the design and installation of the yield pillars and determined the relationships among yield pillars, overburden thickness, mine collapse, subsidence, and dewatering. A projection of the environmental impacts following mine abandonment was also prepared.

In this presentation, only a review of pillar design procedures will be discussed. This review considers the question of whether procedures other than the commonly accepted method used would lead to different conclusions.

## PILLAR DESIGN

Similar to many mining operations, the new pillar design at the Retsof Mine likely progressed through the following logical steps:

- Establish the need for a new pillar design
- Design the pillar
- Construct and monitor test panels, and assess results
- Construct and monitor a production panel and assess results.

### Need for a New Pillar Design

The Retsof Mine experienced floor heaving or squeezes which appears to be caused by pillar foundation

failure of pillar spreading. Pillar foundation failure may be mitigated by:

- Strengthening the foundation, i.e., providing a larger pillar, or
- Lessening the load on the pillar foundation, i.e., providing smaller pillars which will yield at a predetermined load.

This predetermined load for the yield pillar is chosen to be less than the foundation strength. The use of yield pillars was likely motivated by the demonstrated ineffectiveness of large pillars to control foundation failure at the Retsof Mine and the reported success of yield pillars at a competing New York State salt mine.

Pillar Design

There are many acceptable methods for the design of pillars, each having advantages and disadvantages. The procedure employed at Retsof is widely used and involves the following basic steps:

- Identify pillar structures that have been successful at other mines in the local area with similar conditions and adopt these pillar dimensions.
- Construct a test panel having a smaller width than the final production panel.
- Monitor the behavior of the openings and pillars in the test section to assess stability in the narrower panel.
- Upon favorable test results, construct and monitor other wider test panels or a production panel.
- If monitoring and visual inspections of the production panels show the pillars to be stable, the design is accepted.

The disadvantages of this method are:

- Visual inspections and, to a lesser extent, instrumentation monitoring only indicate what is happening close to the mine opening and does not present a clear picture of mine-wide stability.
- The method cannot take into account the range of variables that may exist within a reserve and by its nature can only consider the conditions at the test sites.
- As the test panels are widened, loads are shifted higher into the overburden. Previous panels did not test these higher materials, thus each new wider panel has to be approached with caution.

To assess the design at the Retsof Mine, BOYD evaluated test panels and production panels using available monitoring data. One of the test panels and the 2 Yard South production panel will be used as examples to present our procedure. Mechanical strength test data was unavailable for review, thus mechanical properties were assumed based on data obtained from a literature review.

The normal procedure, upon deciding to evaluate the applicability of yield pillars for a mine, is to evaluate if these pillars have the potential to abruptly fail. As part of our assessment, we also determined if the yield pillars at Retsof can fail in this manner. Our assessment applies Wilson's[1] soft rock pillar equation. This equation was selected because it is readily applied and commonly available in the literature.

More rigorous salt pillar equations that takes into account the dilation limit for salt are also available to assess yield pillar strength and behavior. BOYD's parallel assessment used the dilation limit to develop a failure envelope which was placed into Wilson's equation. A cleaner and mechanically more appropriate approach is to use Van Sambeek's equation[2] published within these proceedings.

For a less rigorous approach, the rock strength in the form of cohesion and internal angle of friction was needed. Site specific rock strength data for the Retsof B6 Salt Bed was unavailable for this analysis, thus the strength parameters employed in this analysis were taken from literature with the most helpful reference being that of Abel[3].

$S$ = Uniaxial Compressive Strength = 4,157 psi
$\varphi$ = Internal Angle of Friction = 35°

Lomenick and Bradshaw[4] published some strength data for the Retsof B6 Bed, but this publication is too obscure for common usage.

These strength parameters were derived through laboratory testing. The unaxial laboratory strength for salt is normally reduced by a factor ranging from four to twelve to obtain in situ or rock mass strength. It has been BOYD's experience that a reduction factor of around ten is generally appropriate. The rock mass strength applied by BOYD in Wilson's equation was 416 psi.

The uniaxial compressive strength of rock salt is dependent on the length of time the load is applied. However, for the less rigorous analysis of pillar failure, we are only interested in very short-term strength. The other values assumed in the analysis were measured from supplied mine maps or taken from available geologic data. For the 2 Yard South area, these parameters are:

$H$ = Total Overburden Thickness = 1,100 ft
$H_G$ = Thickness of Glacial Till and Soil = 500 ft
$\gamma_G$ = Density of Glacial Till and Soil = 150/lb ft$^2$
$H_R$ = Thickness of Rock = 600 ft

$\gamma_R$ = Density of Rock = 160 lb/ft$^2$
$m$ = Extraction Thickness = 12 ft
$p$ = Pillar Width and Length = 21 ft

Wilson's equation for pillar strength can be used if the strength of the floor, roof, and pillar materials are known. Here we assumed that the floor and roof, as well as the pillar, are composed of salt. If we are analyzing yield pillars only, Wilson's equation can be simplified to:

$$P = \sigma_v \left( \frac{1}{3} p^2 \right) \quad (1)$$

Where:

$$\sigma_v = \frac{1}{S_m} \exp\left( \frac{(\tan\beta)^{0.5}(\tan\beta - 1)p}{2m} \right)$$

$$\tan\beta = \frac{1 + \sin\varphi}{1 - \sin\varphi}$$

$P$ = Pillar Strength, pounds
$\sigma_v$ = Maximum Vertical Stress, psf

The maximum overburden load, on these pillars is determined as:

$$L = (H_G\gamma_G + H_r\gamma_R) \text{ (Equal Area)} \quad (2)$$

The yield pillar safety factor is calculated to be just under one for supporting the maximum overburden load. This calculated safety factor assumes the entire overburden above the pillar is to be supported. However, yield pillars are designed to carry only a portion of this load, with the remainder transferred to larger pillars or to unmined areas. Since some transferring of load through arching of the overburden will decrease the load needed to be carried, it is appropriate to conclude that these pillars will not abruptly fail.

The more rigorous approach shows these pillars just exceed the dilation limit under full overburden load. This further shows it safe to assume these pillars would not abruptly fail.

Establish a Test Panel

With confidence that the yield pillars will not suddenly fail, a test panel is constructed and monitored. To aid in evaluating the information from the monitoring program, calculations and plots are prepared that predict possible closures. The monitoring information is plotted against the predicted values to aid in determining panel stability. These predictive calculations are often adjusted to fit a test panel that proves to be stable. BOYD used two curves to assess the closure behavior of the test panels—closure versus time and closure rate versus time.

9 Yard East data was selected for in-depth study because it is the widest panel among the test areas. Mining in 9 Yard East would affect more of the overburden which would result in more potential load being placed on the yield pillars. Closure stations C5, C6, and C8 were located within the yield pillar area. The closure data from these stations were plotted on Figure 1 to ascertain if the test area is stable and is closing at an acceptable rate. The lines on Figure 1, representing the closure stations, are smooth and nearly straight and the rate of closure is decreasing over time. A smooth line with a decrease in closure rate over time is indicative of a stable mining section. At this point, the yield pillars in 9 Yard East are indicated to be performing as designed.

The behavior of the pillars to overburden load was estimated using the Burgers Model. This model is chosen for the less rigorous analysis because it can be found in introductory rock mechanics text such as Goodman.[5] The Burgers Model can be represented by the equation;

$$\epsilon(t) = 2\frac{\sigma}{9K} + \frac{\sigma}{3G_2} + \frac{\sigma}{3G_1} + \frac{\sigma}{3G_1}\exp\left( \frac{-G_1 t}{\eta_1} \right) + \frac{\sigma}{3\eta_2} t \quad (3)$$

The following are the parameters applied, and due to the lack of material testing data, the values are based on Goodman[5];

$\epsilon(t)$ = Axial Strain at time t, in/in
$\sigma$ = Axial Stress, psi
$K$ = Bulk Modulus, 0.8 x 10$^6$ psi
$G_1$ = Parallel Shear Modulus, 0.3 x 10$^6$ psi
$G_2$ = Series Shear Modulus, 1.0 x 10$^6$
$\eta_1$ = Parallel Viscosity, 7.0 x 10$^6$ psi minute
$\eta_2$ = Series Viscosity, 8.3 x 10$^{10}$ psi minute
$t$ = Time, minute

The results of the Burgers Model are plotted with the results of the closure monitoring program. However, the original slope of the Burgers Model curves did not accurately predict the closure data of the stable 9 Yard East panel. The model was adjusted to the closure data by changing $\eta_2$ from 8.3 x 10$^{10}$ to 5.0 x 10$^9$ psi minutes while keeping all other parameters constant. These adjusted curves are also shown on Figure 1, as are the estimated closures at different supported overburden thicknesses.

The 600 ft overburden line represents the division in the overburden between bedrock and unconsolidated material. This appears to be an acceptable adjustment not only for the curve but because;

- The pillars appear to be supporting from 150 to 200 feet of overburden above the mine, and
- At all times, all closure rates can be explained by loads applied by just the rock overburden.

The more rigorous approach used the creep values as reported by Lomenick and Bradshaw[4] to develop the following equation;

$$\varepsilon(t) = 1.53 \times 10^{-13} \sigma^3 t^{0.162} \quad (4)$$

The data used to develop this equation was obtained from specimens tested at a 4,000 psi load. At that load, Lomenick and Bradshaw noted that the Retsof salt has a higher initial strain (smaller elastic modulus) and a lower deformation rate than all of the other six salts studied. Equation 4 at 4,000 psi predicts a higher initial strain and lower deformation rate than the more generalized Equation 3. At lower stress levels, these equations are closely matched with strain rate being nearly identical at stress near 2,000 psi. Below this point, Equation 3 predicts a higher rate of deformation than Equation 4.

Both equations diverge rapidly after one month of applied load. This is not surprising since Lomenick and Bradshaw's experiment length was just over one-half of a day. It appears that the less rigorous Burgers Model is more applicable to this analysis.

At this point curves can be developed that predict mine closure behavior. Having developed these curves and successfully completed several test areas, establishing a production panel is the logical next step.

## Establishing a Production Panel

Before committing to a panel wider than a test panel, it is appropriate to examine the arch that will form in the overburden to assess its stability. The 2 Yard South panel is 670 ft wide, and the rock overburden is approximately 600 ft thick. Therefore, the arch that forms must have a height-to-width ratio of less than 0.9, probably around 0.7. Experience has shown that stable arches can be achieved with ratios from 0.5 to 2.5. In general, stable arches form at a ratio of 0.5 in strong rock overburden comprised mostly of sandstones and limestones with very little dead load (glacial till, soil, and water), and/or the production pillars are strong enough to support most of the overburden. The opposite is true for stable arch ratios near 2.5. Clearly, a 670-foot wide panel at the Retsof Mine would be marginally stable.

## CLOSURE OF THE 2 YARD SOUTH PANEL

Floor, pillar, and roof expansion, roof sag, and room closure data for 2 Yard South panel were reviewed. Special attention was given to the closure data which were analyzed and compared to mine development in 2 Yard South and 11 West. To understand the results of this analysis, the closure data are presented here in two forms: as graphs of closure rate versus time for closure stations in room 58 (Figure 2) and as isopleths of closure rates for 2 Yard South (Figures 3 through 10).

As a point of reference, the closure rate caused by a load equal to the load of 600 ft of rock overburden has been placed on Figure 2. This closure rate was calculated using Equation 3 and is around 51 inches per year. The thickness of solid rock overburden is 600 ft and 500 ft of unconsolidated material, glacial till and soil, overlies this rock. Since the unconsolidated material is not self supporting, the rock arch above the panel must hold this material. Thus, BOYD concluded that a closure rate somewhere above 51 inches per year would represent instability in the arch. Since the term arch as used here represents the mechanism of overburden support and not a precise physical place within the overburden, the exact closure rate for instability is not accurately quantifiable. But it is reasonable to assume that a rate 60 inches per year represents overburden instability.

## Graphs of Closure Rates

Figure 2 show initial closure rates were generally below 40 inches per year and began to increase to 60 inches per year around August 26, 1993 (reading dates August 23 and 30, 1993). By September 3, 1993, closure station C30 was above a rate of 60 inches per year. A rate of 51 inches per year would require a load on the pillar equal to 600 ft of overburden (solid rock load). Normally this would be a significant concern but, as can be seen in Figure 5, a connection between 1 and 2 Yard South was being completed. This connection affected ground control by:

1. Reducing the confinement on the barrier pillar between 1 and 2 Yard South, allowing the barrier to yield at greater rate.
2. Forcing the barrier to bear some of the overburden load once supported by the solid salt block formerly located in the connection area.
3. Increasing panel width in the area of rooms 60A through 61A.

The increase in closure rates can be explained by this change in ground control conditions caused by mining the connection. If the mine were stable at that time, closure rates should start to return to normal after experiencing the effects of the connection. And indeed on September 10, 1993 (readings on September 7 and 13)

most closure rates in this and adjoining rooms were decreasing. However, on September 20 closure rates were again on the rise which indicated unstable conditions in 2 Yard South.

Isopleths of Closure Rates

The isopleths of closure rates are shown on Figures 3 through 10. Figures 3 and 4 show isopleths of a stable condition in 2 Yard South. The distribution of closure rates as shown on these figures can easily be explained by mining events and ground response. Even Figure 5, which shows a large area where closure rates are above 60 inches per year, can be explained by mine events. In this case, the area of 60 inches per year closure rate can be explained by mining the connection between 1 and 2 Yard South, as discussed previously.

Figure 6, which represents closure rates around September 3, 1993, shows one noteworthy closure rate of over 80 inches per year for closure station C34. This location is encircled by an area of 60-inch-per-year closure rates, suggesting the high reading over 80 inches per year completes a trend.

Problematic conditions are further indicated when the isopleth representing closure rates around September 20, 1993, is studied on Figure 7. This drawing shows two areas where closure rates are exceeding 60 inches per year. At the core of both of these areas are stations where closure rates are greater than 85 inches per year. These two areas are separated by an area where closure rates are lower than 60 inches per year, suggesting that two events are occurring that are causing these high closure rates. The more southern of these two areas is near active mining and closure rates are normally rapid, although 85 inches per year is significantly high. The other area is near the barrier pillar separating 1 and 2 Yard South, suggesting the mine may be unstable in that area.

These rates are shown to continually increase in Figures 8 through 10 ( September 30 through October 28). Figure 8 represents closure rates occurring around September 30, 1993. Again two areas of rapid closure are identified. In both areas, closure rates have advanced to over 120 inches per year. The last readings were taken on November 8, but so few closure stations were accessible or operating that no further isopleths could be constructed. Attempts were made to replace some closure stations in mid-December 1993 and these were read until March 3, 1994, when conditions had deteriorated to the point that no additional readings were attempted.

## CONCLUSION

Closure data recorded around September 20, 1993, indicated zones of instability were present in 2 Yard South panel. On March 12, 1994, 2 Yard South panel collapsed. Based on the information presented here, the likely sequence of collapse was as follows:

1. The arch above the 2 Yard South panel was so wide that it could not support the unconsolidated glacial till load resulting in fracturing of the solid rock strata.

2. This fracturing produced a seismic event and formed paths through the overburden for ground water to flow into the mine.

3. This flow was so rapid it flooded the mine and piped sand and other fine-grain materials into the fractures.

4. The soil-till structure collapsed due to piping of the soil material and formed the observed sinkholes.

## REFERENCES

[1]Wilson A.H. and Ashwin D.P., "Research into the Determination of Pillar Size," The Mining Engineer, Transactions of the Institution of Mining Engineers, 1972, Vol. 131, Part 9, pp. 409-416.

[2]Van Sambeek L.L., "Salt Pillar Design Equation," 16th International Conference on Ground Control in Mining, 1997.

[3]Abel J.F., "Soft Rock Pillars," International Journal of Mining and Geological Engineering, 1988, Vol. 6, pp. 215-248.

[4]Lomenick T.F. and Bradshaw R.L., "Deformation of Rock Salt in Openings Mined for the Disposal of Radioactive Wastes," Rock Mechanics, 1969, pp. 5-30.

[5]Goodman R.E., "Introduction to Rock Mechanics," 2nd Edition, John Wiley and Sons, 1989, p. 562.

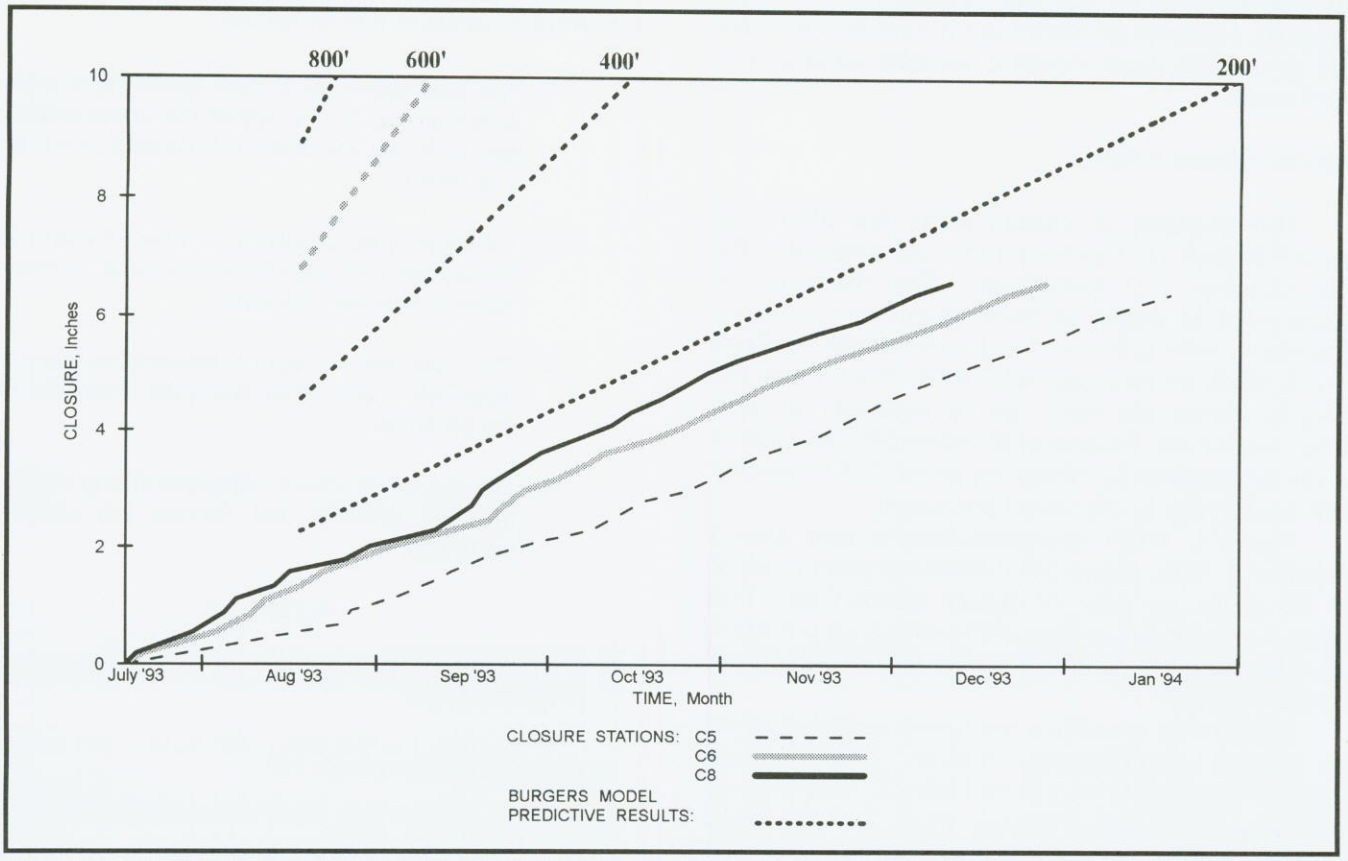



FIGURE 1. CLOSURE VERSUS TIME, 9 YARD EAST, RETSOF MINE

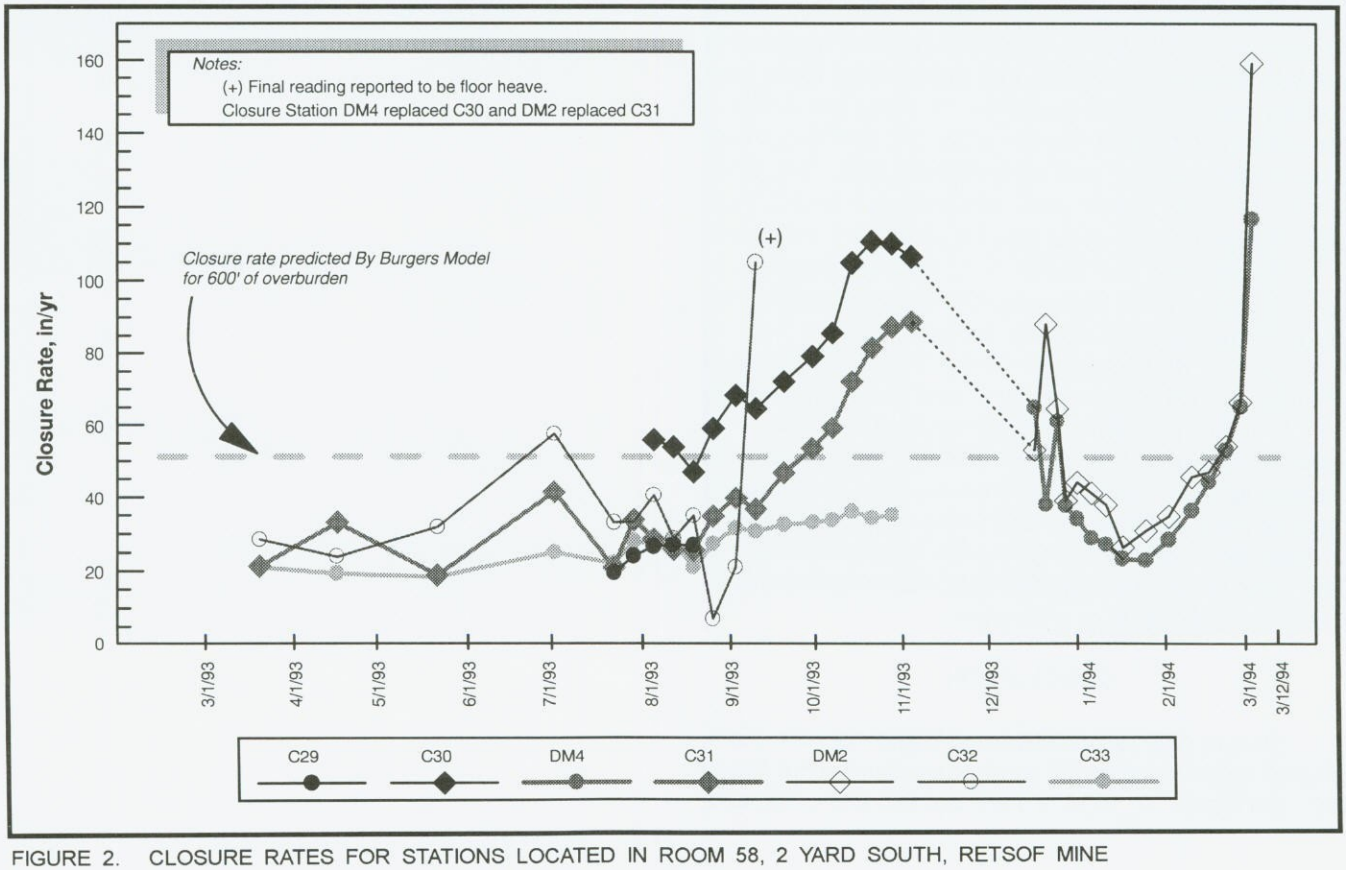



FIGURE 2. CLOSURE RATES FOR STATIONS LOCATED IN ROOM 58, 2 YARD SOUTH, RETSOF MINE

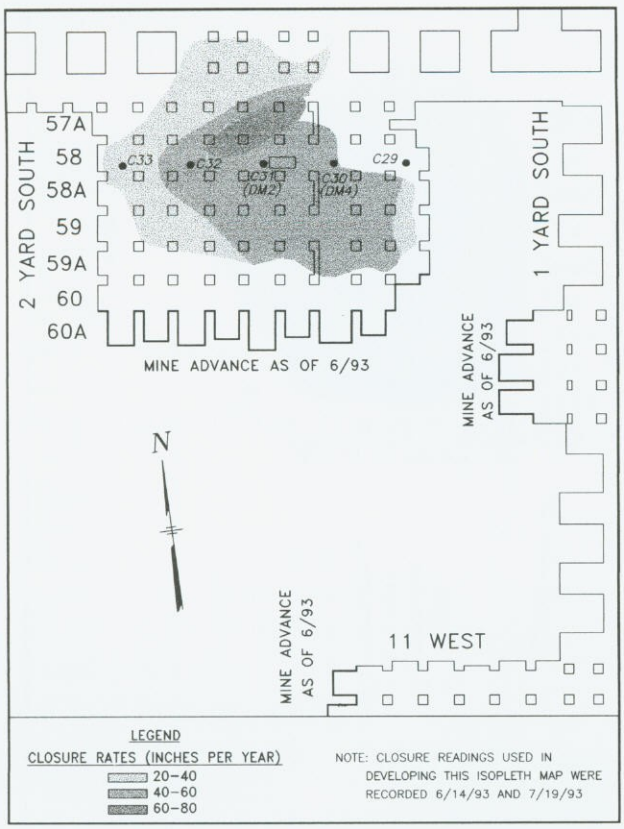



FIGURE 3. ISOPLETHS OF CLOSURE RATE AS OF 7/1/93 AND MINE ADVANCE AT END OF 6/93

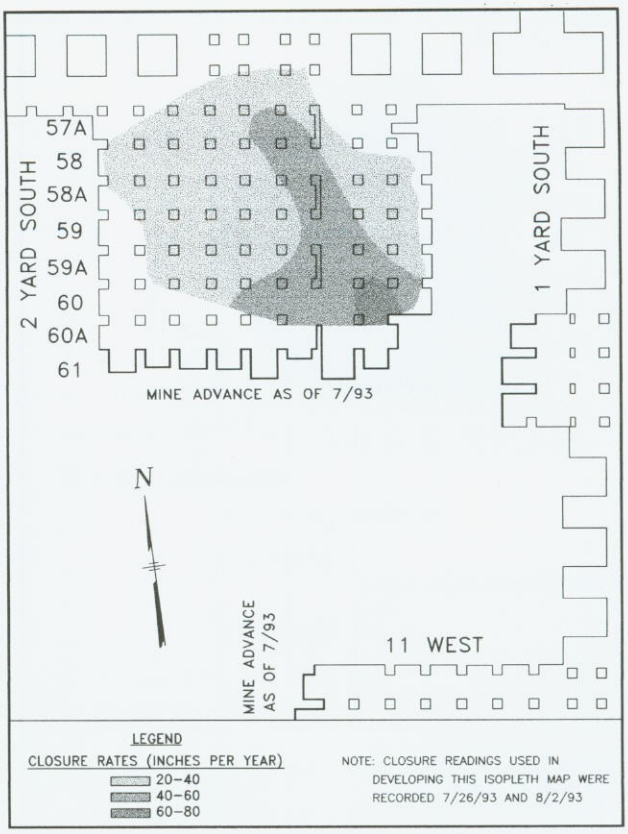



FIGURE 4. ISOPLETHS OF CLOSURE RATE AS OF 7/29/93 AND MINE ADVANCE AT END OF 7/93

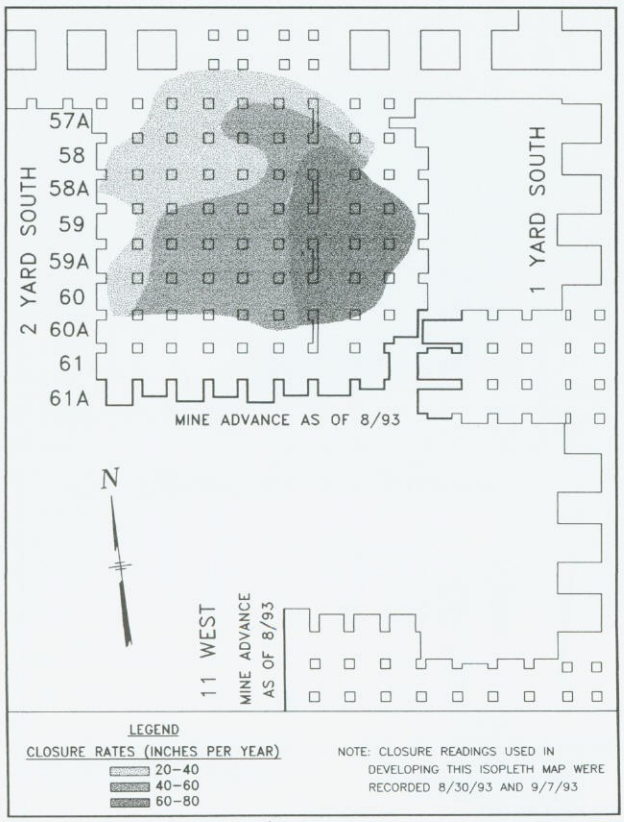



FIGURE 5. ISOPLETHS OF CLOSURE RATE AS OF 9/3/93 AND MINE ADVANCE AT END OF 8/93

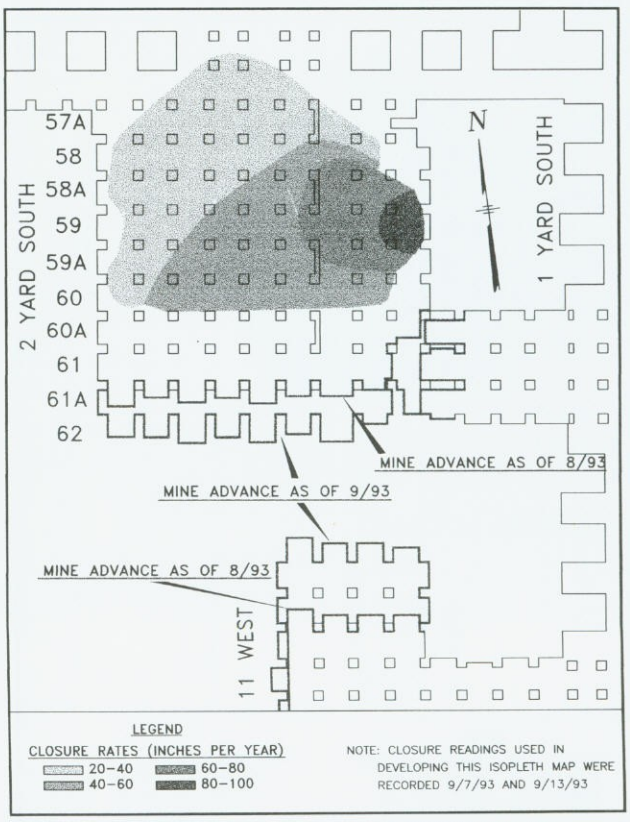



FIGURE 6. ISOPLETHS OF CLOSURE RATE AS OF 9/10/93 AND MINE ADVANCE AT END OF 8/93 AND 9/93

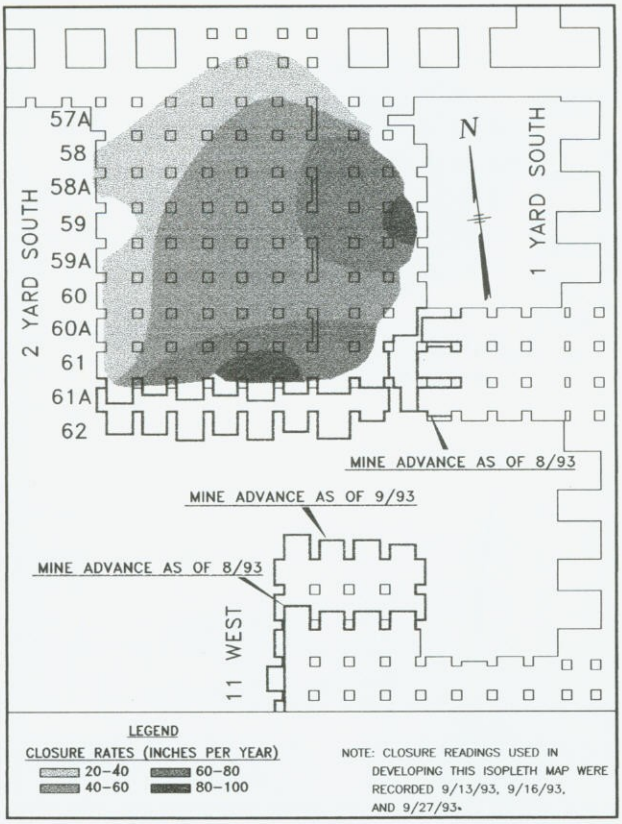



FIGURE 7. ISOPLETHS OF CLOSURE RATE AS OF 9/20/93 AND 9/21/93 AND MINE ADVANCE AT END OF 8/93 AND 9/93

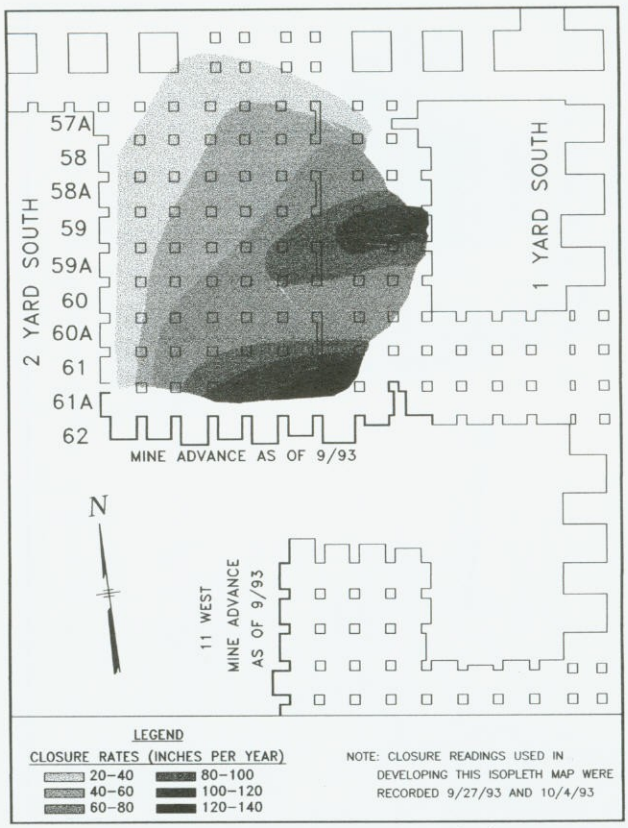



FIGURE 8. ISOPLETHS OF CLOSURE RATE AS OF 9/30/93 AND MINE ADVANCE AT END OF 9/93

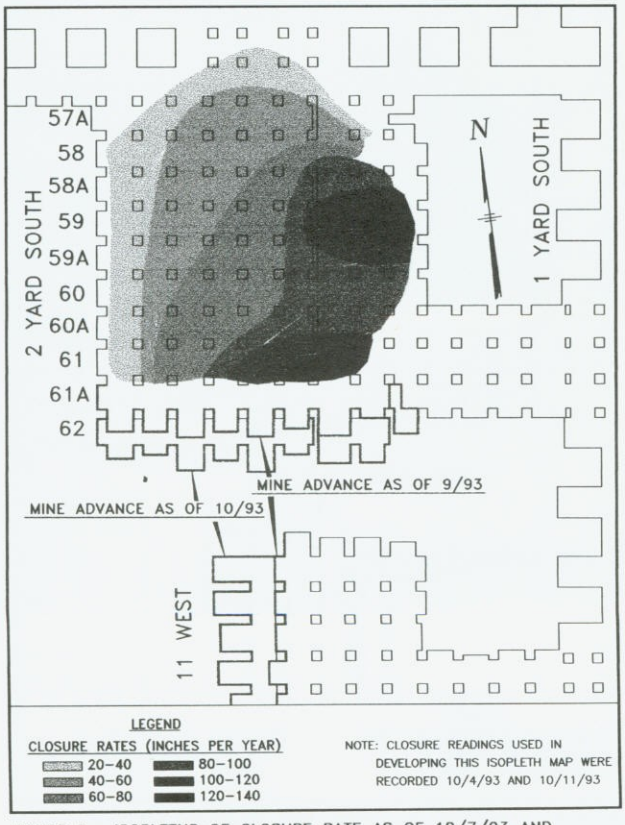



FIGURE 9. ISOPLETHS OF CLOSURE RATE AS OF 10/7/93 AND MINE ADVANCE AT END OF 9/93 AND 10/93

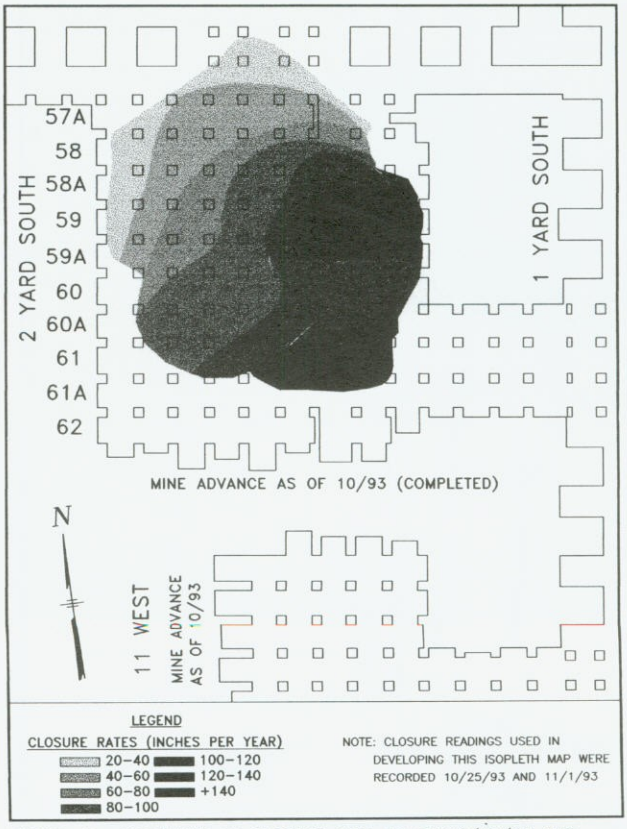



FIGURE 10. ISOPLETHS OF CLOSURE RATE AS OF 10/28/93 AND MINE ADVANCE AT END OF 10/93 (COMPLETED)



# Weatherability Test of Rocks for Underground Mines

*Kot F. Unrug*, Professor
Department of Mining Engineering
University of Kentucky
Lexington, KY

## ABSTRACT

The shale response to moisture changes and the major finding of the appropriate research concerning this subject are briefly reported in this paper. Also described are mine ambient atmospheric conditions which are responsible for moisture changes in mines. The need for a quantitative measure of the weathering potential of roof rock is demonstrated in relation to its influence on safety and the potential for increasing the cost of mine operations. The weatherability test presented in this paper has been developed and used in many mines. It imitates the natural process in a mine by subjecting the rock sample to alternating wet and dry cycles. The natural changes are thus accelerated, but are similar to the natural conditions to which the surrounding excavation rock will be exposed. The measure of the weatherability index is the percentage of the initial sample mass remaining after the test as the largest fragment of the sample. Thus, the index changes, from 100% for rock affected by moisture changes which disintegrates completely, to 0% for rock totally unaffected. In this paper, the apparatus and testing procedures are described. Also presented are examples of test results, with a discussion of the design implication to be considered by mine planners.

## INTRODUCTION

The majority of mines in the West Kentucky-Illinois and Appalachian coal fields are fairly shallow, and many operate above drainage. Consequently, the air that ventilates mines varies in temperature and moisture due to a broad range of seasonal changes. High production mines require large quantities of air to meet safety requirements. In the eastern part of the country where most coal mines are located, winters can be very cold with sub-freezing temperatures, and summers are usually hot and humid. The temperature of the rock mass remains constant, thus affecting relative humidity conditions in the mine through heat exchange between the rock and ambient mine atmosphere. As a result of these changes, there are two distinct periods--one, of moisture deposition during the summer, and two, a dry period during the winter, when moisture is evacuated from the mine by low humidity air. The other sources of water (moisture) in mines are technological, e.g., the dust control sprays from the mining machines, and natural, e.g., water percolating from underground and surface aquifers. Another source might be an old mine works nearby containing water. Those are usually localized and limited to certain areas of a mine. Long term excavation, such as mains and submains, are exposed to the fluctuation of moisture in the mine atmosphere over many years. Carboniferous rocks associated with coal measures, when exposed to changes in humidity, can drastically change their geotechnical parameters through the weathering process. During the mine design, it is essential that the weatherability of the immediate roof and the floor are known in advance. Thus, the appropriate decisions concerning strata control can be made, taking into account the true future rock behavior, which will exist over the prevailing period of mine life. In pre-mining conditions, cores from exploration holes are available. The cores should be used for geotechnical characterization of the mine roof, the seam, and the mine floor. Also, at that time, the weatherability test should be run on samples corresponding to the immediate roof and floor. In spite of the thorough research of shales and other rocks sensitive to weathering, there was not available a low cost practical test, allowing for characterization of the weathering potential of rocks. Such a test has been developed, answering the need for engineering characterization of rock required for the realistic design of roof control measures.

## INFLUENCE OF SURFACE ATMOSPHERIC CONDITIONS ON MINE AIR

Field investigations (Bruzewski & Augenbauch, 1977) and (Unrug & Nandy, 1988) have demonstrated that weather conditions at the surface will affect mine ambient atmosphere via the ventilation system. Through monitoring, it has been established that during the tempering of the air to the mine conditions, moisture is interchanged between the air and the exposed mine rock. Depending on the difference in air temperature and humidity, moisture can either condense and be absorbed by rock or can be

transferred from rock into the airflow of mine ventilation. Due to seasonal changes in temperature, there are two distinctive periods. In the first, summer, warm humid air enters the mine and cools down, reaches the dew point, and moisture is deposited on the excavation perimeter. The second period, during the winter, external temperatures are lower than those in mines, and thus, the trend is reversed. Cool dry air is warmed when entering a mine, and when flowing through, moisture is evacuated from a mine. Figure 1 shows an example of relative humidity and temperature distribution in the Eastern Kentucky mine, while Figures 2 through 6 present data gathered by Bruzewski & Aughenbauch in the Illinois mine. Figure 2 depicts daily temperature and humidity changes in both surface and underground air. Figure 3 shows the effect of distance required for the underground air to equalize with the mine temperature and establish a corresponding relative humidity. Figures 4 through 6 show changes recorded over a longer period of time in panel intake and exhaust, and absolute humidity distribution as well as gains and losses in moisture over a three-year period.

## WEATHERING CHARACTERISTICS OF SHALES

A large percentage of immediate roofs in coal mines are composed of shales and a similar type of rock with a high content of clay minerals. Some of those minerals expand when in contact with water, which is adsorbed on clay particles. Shale is hydrophilic and attracts water and because of that moisture can quickly penetrate along the bedding planes and fissures, affecting a considerable volume of rock. However, permeability of intact shale is low, particularly in the direction perpendicular to bedding. It is well known in mining practice that shale strata can effectively isolate the water level in the confined conditions of a rock mass. In unconfined conditions, the shale which absorbs moisture will expand. The volume increase causes a reduction in density, an increase in porosity, and a loss of strength, as shown in Figure 7. Under confined conditions, shale cannot flake and disintegrate, but rather will produce swelling pressures capable of breaking the shale itself as well as the surrounding rock. The swelling pressures (as measured by an oedometer test) can vary substantially due to the mineralogical composition of shale and have been reported to be within the range of 4,000 to 14,000 PSI

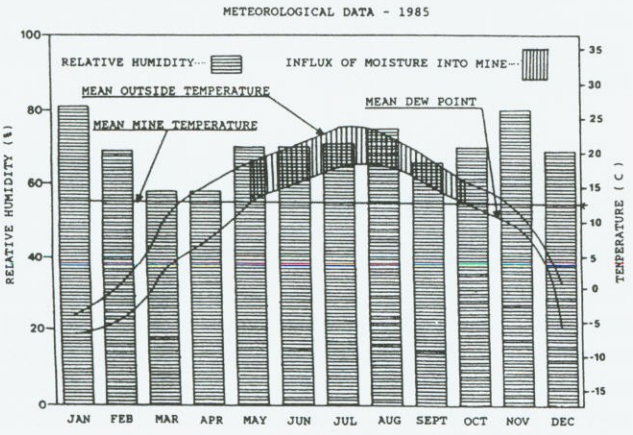



Figure 1. Relative humidity and temperature distribution at the mine site (Unrug and Nandy, 1988).

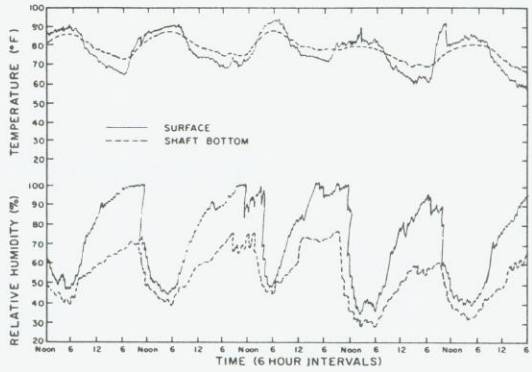



Figure 2. Comparison of temperature and humidity recordings of surface and measurement station close outby, (Bruzewski & Aughenbaugh 1977).

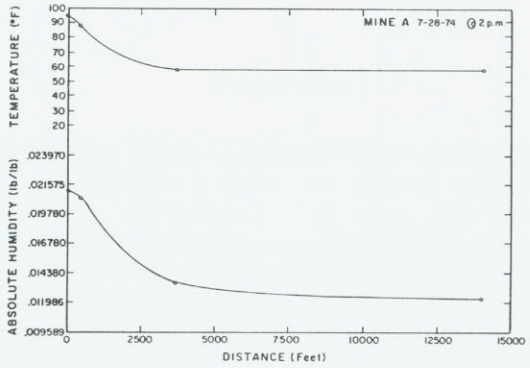



Figure 3. Tempering of air flow distance into mine A from surface intake (Bruzewski &Aughenbaugh 1977).

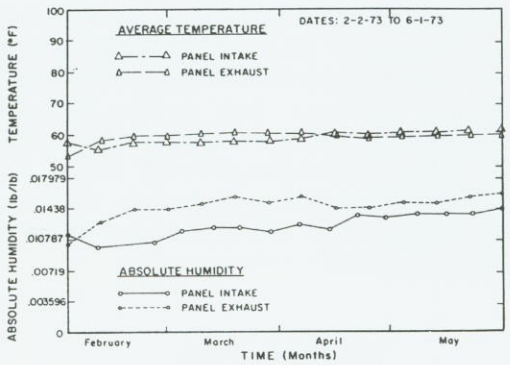



Figure 4. Comparison of temperature and humidity for intake and exhaust of an active mining panel (Bruzewski &Aughenbaugh 1977).

(Aughenbaugh & Adam, 1979).

In mining conditions, a combination of stress relief and physico-chemical effects of water usually causes changes in the mine roof. During the wetting period, the following can take place. Stress relief leads to a change of inter-particle stress, which in turn facilitates flow and adsorbtion of water. Stress relief causes the opening of fissures, facilitating more penetration of water. During the drying period, shales give up their water and reduce their volume. Subsequently, more fissures are created and

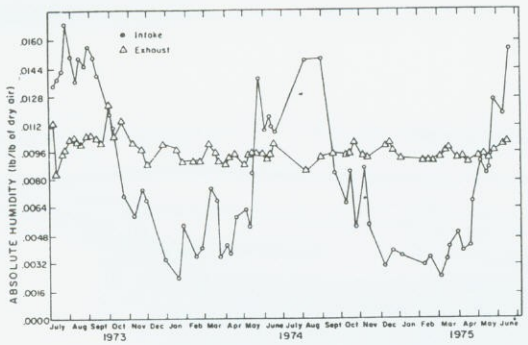



Figure 5. Seasonal plots comparing absolute humidity at Mine A intake and exhaust stations (Bruzewski Aughenbaugh 1977).

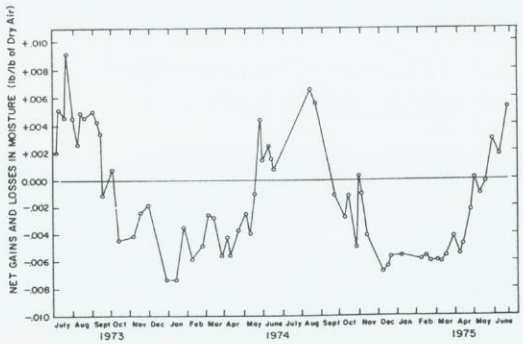



Figure 6. Seasonal gains and loses of moisture at Mine A, (Bruzewski Aughenbaugh 1977).

during the next wet cycle, water penetrates more deeply, increasing the affected volume of rock.

This moisture penetration mechanism negatively affects shaly roof rocks when supported with mechanical conventional roof bolts. Moisture penetrates into the annular space between the bolt rod and rock, altering the shale and decreasing its strength. Mine air penetrates into the roof bolt holes causing swelling of the rock column around the bolt, thus increasing the load on a bolt, sometimes above its anchorage capacity. This, together with a decrease of rock strength in the anchorage area, leads to slipping of an anchor and bleeding of tension (Unrug & Nandy, 1988). During the dry season, humidity is evacuated from the mine; then shale shrinks so the bolts completely lose their tension. Because of the described process in shaly roofs, it is better to use fully grouted resin bolts. In such a support system, moisture can only penetrate into the roof from the direction perpendicular to bedding at a much slower rate, and it affects only the exposed roof surface.

## STRATA CONTROL CONSIDERATIONS

The mining engineer responsible for the design of strata control makes his decisions based on stratigraphic information and strength parameters of rock strata. Past experience also plays an important role, because it indicates other time-dependent characteristics of roof rock. Typically, moisture sensitive shale roof falls from between the roof bolts, and after some time creates a roof line depicted in Figure 8. Such response of the roof causes operational difficulties and raises costs, because fallen roof rock has to be cleaned and disposed of, transport can be negatively affected, and resistance to air flow is increased. In the case of long term excavations such as mains and submains, rehabilitation with costly rebolting, might be required.

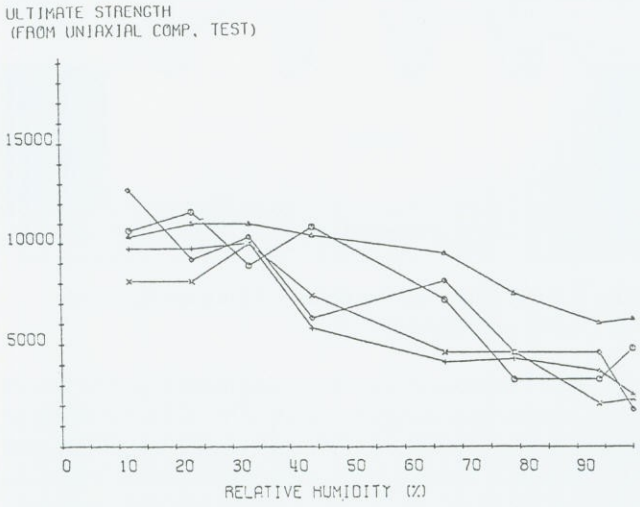



Figure 7. Decrease of uniaxial compressive strength with increase of humidity, (Aughenbaugh 1979).

Since the most intense temperature and relative humidity changes are within the intake ventilation ways close to portals, surface protection of excavation roofs in such areas is beneficial. Shaft and slope stations which remain in use for the life span of the mine should be protected against weathering. Similarly, belt ways and main transportation entries, functions vital for mine operations, should have stable roof conditions. Several ways to protect the roof can be applied. Shotcreting is probably the most durable but the most expensive method. There are also other coating mixtures, based on cementous materials, that are available for insulation purposes. The previously mentioned coatings are expensive and thus seldom used. The author developed a water based emulsion, which is inexpensive and easy to apply by spraying the freshly excavated roof during development. Such emulsion encapsulates shaly rock with film like coating, which is not penetrable for moisture, and thus preserves the natural, stable "in situ" moisture content of rock.

In some cases, the immediate roof weathers rapidly and completely loses its integrity, with some delay resulting in the effect of "draw rock," where the whole stratum falls. The author encountered such conditions in a shallow mine in Indiana. Rather than face the problem of excessive cleaning (Figures 9 and 10), a successful remedy was suggested--the application of roof screening, which held the roof material suspended by bolts.

The minimum cost of roof control depends on its effectiveness and time of installation during development. All later repairs and other remedial measures interfere with mining operations, are

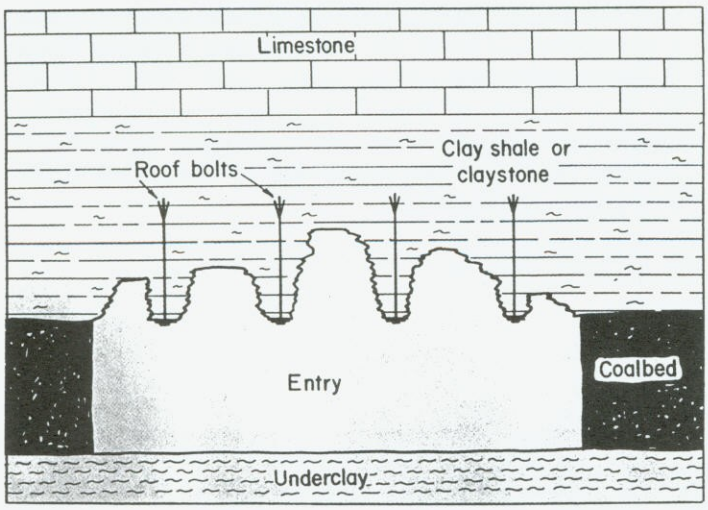



Figure 8. Roof failure attributed to moisture sensitive roof rock, (Moebs and Stateham, 1985).

usually labor intensive, and could be also hazardous. The cost of cleaning a ton of rock is approximately $70. Thus, the ability to predict the future response of rock to the weathering process is of great importance. The available testing techniques are either too complicated and costly or were developed for different conditions. For instance, mineralogic analysis can determine the presence of swelling clay minerals such as illite and montmorylonite; oedometer testing can determine swelling pressure; and a slake durability test gives slaking characteristics of rock, but none of these tests addresses directly the behavior of immediate roof and floor in the underground mine. This has led to development of a test which is directed specifically to prediction of weatherability of rock in the conditions of an underground coal mine.

## WEATHERABILITY TEST

Several prerequisites for the test have been established:

- It should be suitable for testing cores from the exploration drilling as well as samples collected in the mine,
- Samples should not require machining,
- Test procedure should be simple,
- Apparatus should be able to hold larger number of samples during the test, and
- Test conditions should simulate weathering cycles in mines, accelerating them in time.

The above prerequisites were taken into consideration when developing test procedures and testing apparatus. The testing procedure is as follows. Rock samples in the form of drill cores or of irregular shape (e.g., collected from the roof fall) with weights between 0.5 Kg to 2 Kg, are first dried to a constant weight in the laboratory oven at a low temperature setting (70-80 degrees Celsius - usually for 24 hours). After weighting, they are placed in the apparatus, numbered, and photographed. During the test, they are soaked with water for 1 hour. Then the water automatically drains below the level of a screen and the styrofoam plate, isolating the chamber with samples from the source of

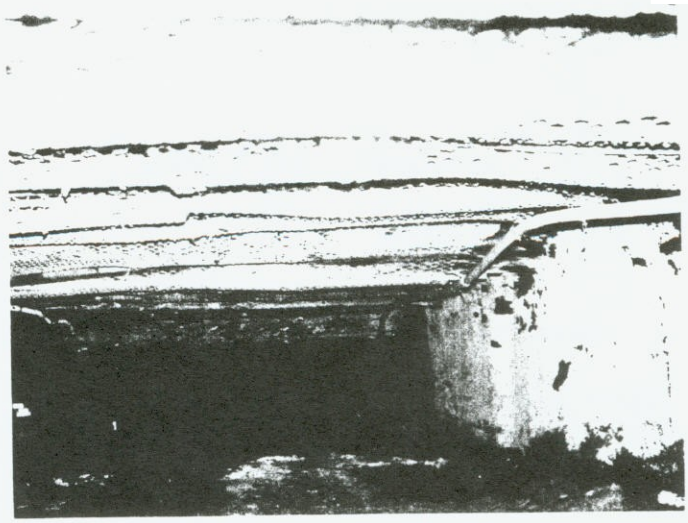


Figure 9. View of the entry with roof supported by fully grouted resin bolts, garden screen and straps.



Figure 10. Crosscut view from the intersection as in Figure 9, without screen and straps. (Pictures were taken 3 months after development).

moisture (lower part of the tank containing water). Then the dry cycle begins, when air flow is imposed over the samples for 6 hours. The wet cycle then starts again and the sequence is repeated. The appearance of the samples is checked, and a decision is made as to how many cycles should be run before terminating the test. Usually three to five cycles are sufficient to achieve meaningful changes. At the termination of the test (and during the test, if required), photographs are taken for comparison with the picture taken before the test. The largest elements of samples surviving the test are dried in a laboratory oven and weighted. The Weatherability Index, (WAI), is calculated as a weight percent loss from the initial weight of the sample.

$$WAI=(\frac{W_{ini}-W_{rem}}{W_{ini}})*100$$

where: WAI - Weatherability Index,%
$W_{ini}$ - Initial weight of sample, Gram
$W_{rem}$ - Weight of the largest remaining fragment of a sample, Gram

The results are presented in a table with corresponding photo documentation for visual representation of WAI numbers.

## WEATHERABILITY TESTING APPARATUS

The testing apparatus was built from readily available and inexpensive components. Its major part is a tank (drinking trough for farm animals) in which a grill with the screen is affixed and on which the samples are placed. The water level in the tank is adjusted by a float-controlled valve, which cuts off the water supply when water covers the samples. Another drain valve is controlled by a timer (activated after 1 hour). The water drains down, lowering the level below the grill. The styrofoam plate, cut to the shape of the tank, floats and shields the water table from the air above during the drying cycle. During the soak cycle, it is pressed by water against the grill. Another position of the float, through the action of electric relay, cuts off the drain valve when water in the tank reaches the prescribed low level (during the dry cycle). The chamber above the grill, where samples are placed, is created by two vertical walls (painted plywood or plastic sheets), slipped down in the guiding slots (rails), and from the top, is covered with a transparent lid (acrylic) with handles for lifting. The side walls do not completely reach grill level, leaving slots for air to move on both sides. In a side chamber of the tank (trough), a room fan is affixed with plastic wire ties in a horizontal position. This fan is controlled by a timer switch and switches on when water stops draining. The air is pushed by a fan from one side chamber to another, drying the samples. Looking through the lid or by lifting it, one can observe the changes in samples, as well as take pictures for the record. Figure 11 shows a schematic of the testing apparatus. It is recommended that samples are placed on a screen sideways and that the bedding planes are in a vertical direction. Such a system makes for easier observation of changes in samples, which tend to split along the bedding planes. During the test, samples disintegrate to a certain degree, and some completely turn to mud. For cleaning of the chamber after a test, one can use a vacuum cleaner to remove rock fragments from the screen. The smaller particles tend to fall through the screen and stay on the styrofoam plate. The dividers and grill are made to be easily removable, allowing for cleaning of the apparatus.

## EXAMPLES OF RESULTS OF THE WEATHERABILITY TESTS

The results of the weatherability test are presented as photographs, allowing for qualitative, visual, assessment of how the changing moisture conditions affect the rock. Quantitative results are in tabular form, where there is listed the initial and final weight of samples, and the corresponding values of the Weatherability Index (WAI) in percent.

In Figures 12 through 15, and in Table 1, results from an Appalachian (Tennessee) mine are presented. Ten samples were collected from the roof falls, and another five samples were from core drilling in the mine floor. The numbers obtained of WAI indicate that the shaly roof rock weathers considerably. Water penetration into the micro cracks is visible in the pictures (these cracks were not visible when examining dry sample). At the moment when rising water in the tank touches the bottom of the sample, capillary water moves quickly along the cracks, making them visible and showing as dark lines. Intensity of this phenomenon increases with the number of cycles, compare Figures 12 and Figures 13 and 14, showing how the wet-dry cycles cause deterioration of rock.

**The floor samples weather less than the roof rock, as is demonstrated by the corresponding WAI numbers. The most weathering prone stratum was 14 to 20 inches below the mine floor, with the corresponding WAI = 25.9%.**

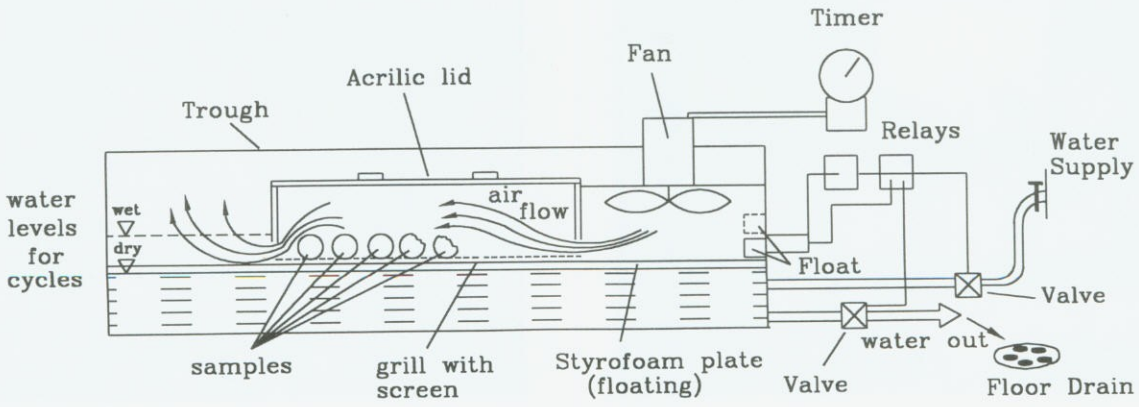



Figure 11. Schematic of the weatherability test apparatus.

**TABLE 1** WEATHERABILITY TEST OF ROOF AND FLOOR ROCK

TENNESSEE COAL MINE

TESTED NOVEMBERR 1995

| SAMPLE LOCATION | SAMPLE NUMBER | DRY WEIGHT BEFORE TEST Gram | DRY WEIGHT AFTER TEST Gram | WEATHERABILITY FACTOR % |
|---|---|---|---|---|
| IMMEDIATE ROOF Number | | | | |
| 1 | W1-ROOF FALL | 1040.30 | 580.20 | 44.23 |
| 2 | W2-ROOF FALL | 1573.10 | 1066.60 | 32.20 |
| 3 | W3-ROOF FALL | 1391.80 | 1086.80 | 21.91 |
| 4 | W4-ROOF FALL | 1443.60 | 1198.30 | 16.99 |
| 5 | W5-ROOF FALL | 1690.00 | 775.70 | 54.10 |
| 6 | W6-ROOF FALL | 1097.30 | 479.30 | 56.32 |
| 7 | W7-ROOF FALL | 1079.90 | 600.40 | 44.40 |
| 8 | W8-ROOF FALL | 1050.40 | 493.80 | 52.99 |
| 9 | W9-ROOF FALL | 1332.30 | 800.00 | 39.95 |
| 10 | W10-ROOF FALL | 1519.30 | 759.90 | 49.98 |
| SAMPLES | W11-IMMED. FLOOR | 1069.30 | 1069.30 | 0.00 |
| FROM FLOOR CORE | W12-IMMED. FLOOR | 568.40 | 567.10 | 0.23 |
| DRILLING | W13-15" BELOW SEAM | 477.60 | 450.80 | 5.61 |
| | W14-20" BELOW SEAM | 378.40 | 280.40 | 25.90 |
| | W15-25" BELOW SEAM | 364.60 | 363.80 | 0.22 |




Figure 12. Samples in weatherability test apparatus before test. Rising water touches sample's bottoms and rises through cracks.



Figure 13. Close up of lump sample 10 at the beginning of the 3-rd wet cycle. Note the water rising in micro-cracks.

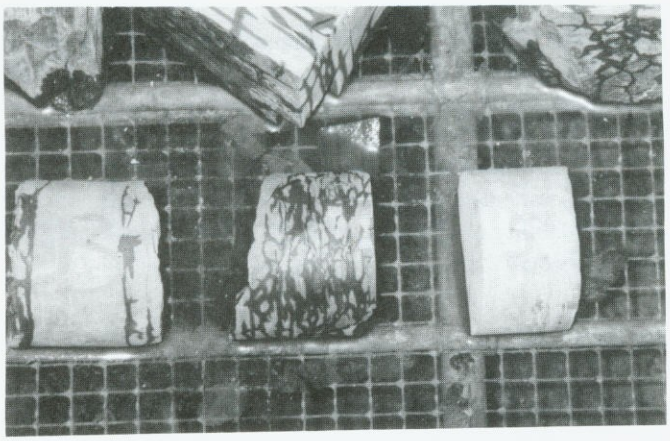


Figure 14. Close up of core sample 4 at the beginning of the 3-rd wet cycle. Note the water rising in micro-cracks.

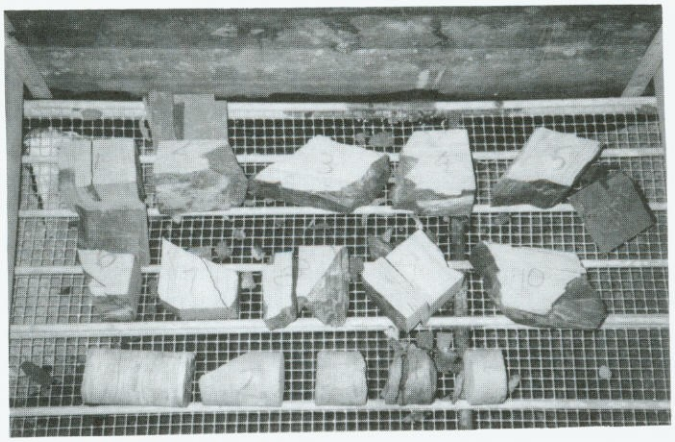


Figure 15. Samples in weatherability test apparatus after 3 cycle test, compare with Figure 12.

**TABLE 2** WEATHERABILITY TEST OF ROOF AND FLOOR ROCK

TESTED SEPTEMBER 1995

| SAMPLE LOCATION FROM THE COLLAR Inches | SAMPLE NUMBER | DRY WEIGHT BEFORE TEST Gram | DRY WEIGHT AFTER TEST Gram | WEATHERABILITY INDEX % |
|---|---|---|---|---|
| 3 | W1-ROOF CORE | 405.3 | 169.1 | 58.28 |
| 17 | W2-ROOF CORE | 599.4 | 67.3 | 88.77 |
| 30 | W3-ROOF CORE | 808.1 | 0 | 100 |
| 40 | W4-ROOF CORE | 574.3 | 0 | 100 |
| 47 | W5-ROOF CORE | 766.8 | 0 | 100 |
| SAMPLES FROM ROOF FALL. BREAK 58 | W6-IMMED. ROOF | 717.1 | 306.3 | 57.29 |
| | W7 " " | 678.5 | 297.6 | 56.14 |
| | W8 " " | 711.6 | 404.4 | 43.17 |
| SAMPLES FROM ROOF FALL. BREAK 18 | W9-IMMED. ROOF | 852.00 | 419.1 | 50.81 |
| | W10-IMMED. ROOF | 899.3 | 564 | 37.28 |
| | W11-IMMED. ROOF | 880.6 | 369.2 | 58.07 |
| SAMPLES FROM ROOF FALL BREAK 72 | W12-IMMED. ROOF | 512.30 | 280.20 | 45.31 |
| | W13-IMMED. ROOF | 512.70 | 345.10 | 32.69 |
| | W14-IMMED. ROOF | 614.20 | 613.20 | 0.16 |
| | W15-IMMED. ROOF | 464.30 | 463.80 | 0.11 |
| FROM 6" CO-RE DRILLED UNDER THE PILLAR | W16-IMMED.FLOOR | 1029.70 | 0.00 | 100.00 |
| | W17-IMMED.FLOOR | 455.30 | 0.00 | 100.00 |
| | W18-IMMED.FLOOR | 680.70 | 0.00 | 100.00 |
| | W19-IMMED.FLOOR | 490.00 | 0.00 | 100.00 |
| | W20-IMMED.FLOOR | 364.40 | 0.00 | 100.00 |

Another example is from a West Kentucky mine. The samples for testing were from the core drilling in the mine roof, rock fragments collected from the roof falls, and floor material originated from the horizontal 6 inch core drilling under the coal pillar. Since the floor core was used for the compressive strength tests, only the remainder of the core after machining of cube samples was available for the weatherability testing, resulting in inadequate sample size . The results of the testing are given in Figures 16&17, and in Table 2. The results show that the immediate roof rock, composed of black shale, is more durable than the upper roof strata composed of the gray shale. It is thus very important to maintain the insulating, immediate roof stratum in intact shape to prevent the deterioration of the above laying roof strata. Floor material is very sensitive to weathering. Therefore, very good management of water is required in the mine. Any water spills should not be tolerated, and if any water inflow occurs, it should be directed to the sump and pumped away. This is important, not only for maintaining good haulage conditions, but also for stability of coal ribs in pillars, which when standing on weak deformable rock, would break and roll.

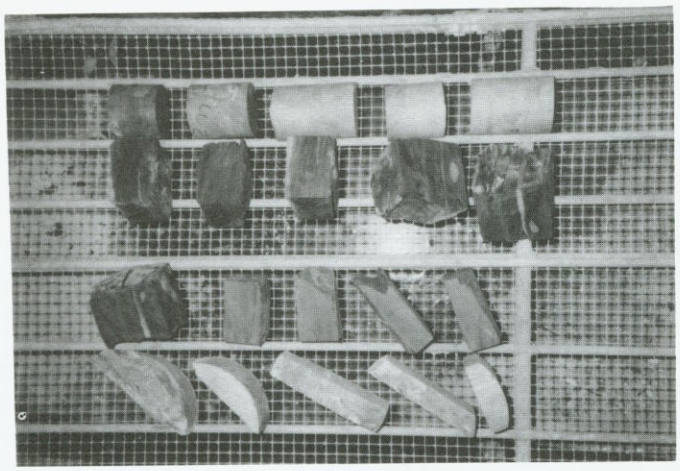


Figure 16. Samples in weatherability test apparatus before test, West Ky. mine.

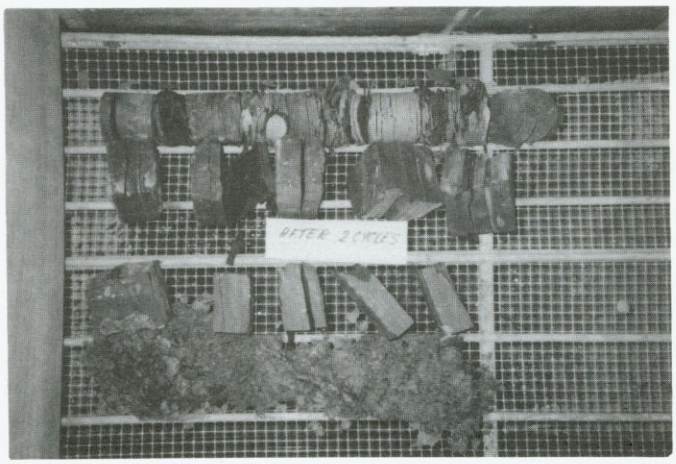


Figure 17. Samples in weatherability test apparatus after 3 Wet-dry cycles. Note disintegration of fireclay floor samples. West Ky. mine.

## CONCLUSION

The described weatherability test gives important information concerning behavior of rock, which has great influence on mining operations. It should be run on material obtained from the exploration drilling in the pre-mining stage so that the obtained data could be used for ground control in mine design and for preparing a feasibility study. If geologic conditions in the reserve vary, weatherability tests should be run on rocks characteristic for the particular locale.

## REFERENCES

1. Aughenbaugh, N.B. Effect of Moisture on Shale. 3rd Annual Soil Mechanics and Foundation Engineering Conference. University of Kansas. March 15, 1974.

2. Bruzewski, R.G. and. Aughenbaugh N.B, Effects of Weather on Mine Air. Mining Congress Journal, September 1977.

3. Aughenbaugh, N.B. and M.E. Adam. Interaction of Mechanical Rock Bolts with Shale Roofs in Coal Mines. First Conference on Ground control Problems in the Illinois Coal Basin. Sponsored by DOE and SIU. Carbondale, Il. 1979.

4. Einstein, H. H. Design and Construction of Tunnels in Swelling Rock. Society of Mining Engineers of AIME. Mini Symposium NO. 81-M&E-04. Effects of Moisture on Ground Control in Mining and Tunneling, 1981.

5. Aughenbaugh, N.B. Effects of Humidity on Ground Control in Mining and Tunneling. Society of Mining Engineers of AIME Mini Symposium NO. 81-M&E-04. Effects of Moisture on Ground Control in Mining and Tunneling, 1981.

6. Moebs, N.N. and R.M. Stateham. The Diagnosis and Reduction of Mine Roof Failure. Coal Mining. March 1985, pp. 42-48.

7. Unrug, K.F..and S.K. Nandy. Analysis of the Deterioration Process in a Shaly Roof Based on Field Monitoring, Mining Engineering, February 1988. pp.124 -126.

# Shear Strength Characteristics of Soft Rock Joints Based on Constant Normal Stiffness Testing

*B. Indraratna,* Senior Lecturer
*N. Aziz,* Associate Professor
*A. Haque,* Doctoral Candidate
Department of Civil & Mining Engineering
University of Wollongong, Northfields Avenue
Wollongong, NSW, AUSTRALIA

## ABSTRACT

Large-scale shear apparatus is designed to investigate the shear behaviour of simulated soft rock joints under constant normal stiffness condition. Regular saw-teeth profiles having inclinations between 9.5° and 26.5° have been tested. The strength envelope based on these test results indicates that predictions made by Patton (1966) are accurate for the lower asperity angles. However, for higher asperity angles, Patton's model overestimates the shear strength especially in the low to medium normal stress range. In contrast, while Barton's model (1973) is realistic for Constant Normal Load (CNL) condition, it seems to be inappropriate for modelling the shear behaviour of soft joints under Constant Normal Stiffness (CNS) condition. An empirical strength envelope for the prediction of peak shear strength of joints is proposed in this study to account for the change in normal stress and surface degradation during CNS shearing.

## INTRODUCTION

The laboratory investigation of shear behaviour of rock joints is generally conducted by the conventional direct shear test, where the normal stress acting on the shear plane is maintained constant during the test. Such testing is referred to as Constant Normal Load (CNL) condition in this paper. However, shearing of non-planar discontinuities causes considerable amount of dilation, and if some of this dilation is inhibited by the surrounding rock mass, then an inevitable increase in normal stress takes place. Therefore, the actual shearing of discontinuities is closer to Constant Normal Stiffness (CNS) condition, where the normal stress acting on the shear plane varies with the shear displacement. Shear behaviour of hard rock discontinuities under CNS has been investigated by several researchers [e.g. Benmokrane & Ballivy, 1989; Skinas et al., 1990; Ohnishi & Dharmaratne, 1990; Haberfield & Johnstone, 1994], and extended to the field of rock-socketed piles [e.g. Lam & Johnstone, 1989]. Nevertheless, very limited studies have been conducted on soft rock joints under CNS. In this study, a large-scale shear apparatus was designed by the authors to accommodate the change in normal stress with dilation during shearing to simulate the CNS condition. Soft rock joints have been simulated by joints made from gypsum plaster where dimensionless strength properties accurately represent a variety of soft rock joints (Indraratna, 1990).

## MODELLING OF SOFT ROCK

### Joint Preparation

Joints having saw-teeth surface profiles were cast inside the shear box itself to establish fully mated joints, where asperity inclinations of 9.5° (Type I), 18.5° (Type II) and 26.5° (Type III) were tested. Gypsum plaster was mixed with water in the ratio of 5:3 by weight and poured into a specially designed shear box containing the required surface profile. The moulds were stripped after one hour and left inside an oven for 14 days at a controlled temperature of 50° C. After air curing for one day, the specimens were tested at room temperature.

### Properties of Intact Model Material (Gyprock)

Several tests were conducted under uniaxial compression on cylindrical specimens of 50 mm diameter, cured for 14 days at 50° C. This gyprock was characterized by an uniaxial compressive strength ($\sigma_c$) of 11 to 13 MPa and a Young's modulus (E) of 1.9 to 2.3 GPa which was found suitable to simulate the behaviour of soft rocks such as coal and mudstone (Indraratna, 1990).

## LARGE-SCALE CNS SHEAR APPARATUS

The CNS shear apparatus consists of two steel boxes of size 250x75x150 mm at the top and of size 250x75x100 mm at the bottom. As shown in Figure 1, the top box can only move in the vertical direction. The bottom box is fixed on a rigid base through steel bearings and can move only in the shear (horizontal) direction. The desired initial normal stress ($\sigma_{no}$)

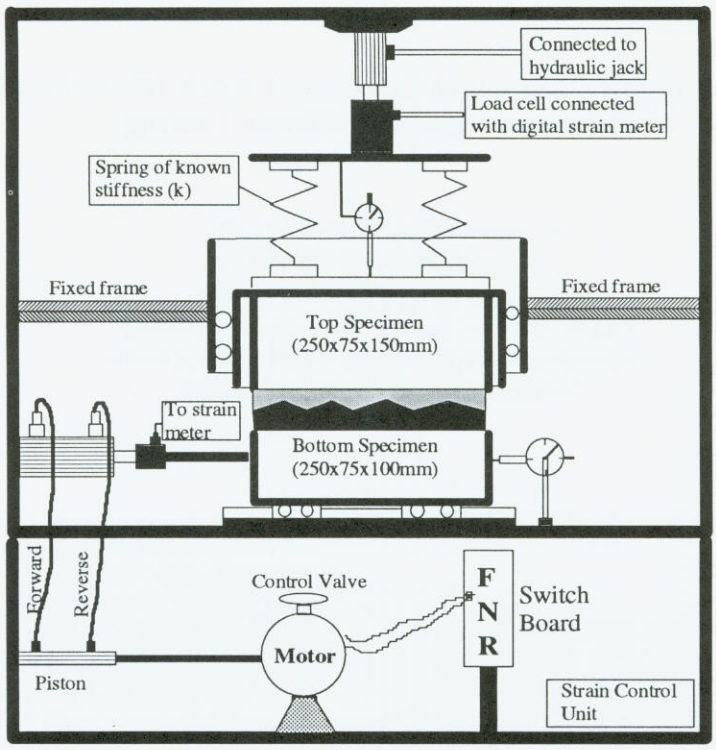



Figure 1. Schematic illustration of the CNS shear apparatus.

can be applied by a hydraulic jack, and the applied load can be measured by a calibrated load cell. The maximum normal load capacity of the apparatus is 120 kN. The shear load is applied via a transverse hydraulic jack which is connected to a strain controlled unit. The applied shear load can be recorded with the change in horizontal displacement through strain meters fitted to a load cell. The apparatus has a maximum shear load capacity of 180 kN and the rate of shear strain can be varied between 0.35 and 1.70 mm/min. A set of springs are used to simulate the normal stiffness of the surrounding rock mass as shown in Figure 1. The dilation and shear displacement of the joint are recorded by dial gauges or LVDT's mounted on the top of the specimen and in the shear direction, respectively.

## RESULTS AND DISCUSSIONS

Tests were performed on Type I, II and III joints under a constant normal stiffness (k) of 8.5 kN/mm. The initial normal stress was varied from 0.05 to 2.43 MPa, and the specimens were sheared at a strain rate of 0.50 mm/min. Normal load, shear load and dilation were recorded at every 0.50 mm of horizontal movement. A typical shear behaviour of Type II soft joints under CNS testing is shown in Figure 2. It is observed that the shear stress increases with the horizontal displacement until "peak to peak" contact of the asperities is reached. At higher initial normal stress, the peak shear strength is also greater, which is attained at a lower displacement. Compared to the shear stress, the change in normal stress is insignificant especially at higher $\sigma_{no}$ values. This is because of suppressed dilation at higher $\sigma_{no}$. The shape of the dilation-horizontal displacement curves represent clearly the effect of $\sigma_{no}$ and the degree of asperity degradation. It is evident that even at a very low normal stress of 0.05 MPa, the surface of the Type II asperity degrades considerably giving a slope much less than 18.5° for the dilation-displacement curve (Fig. 2c). Similar behaviour was observed for Type I and III joints also.

The stress paths representing the change in shear stress with normal stress for different initial normal stresses for Type I, II and III profiles are plotted in Figure 3 for comparison. It is evident from these test results that the peak shear stress increases with the increase in $\sigma_{no}$. The shear strength also increases with the increase in the asperity angle. However, some intesesting observations are noted under certain $\sigma_{no}$ values of 0.16, 0.56 and 1.63 MPa, where the peak stress observed for Type II profile is, in fact, greater than that of Type III profile. This may be attributed to the high stress concentration around the asperities of Type III joints, which cause enhanced surface degradation. In general, the current test results confirm that dilation of the joints increases with the incraese in asperity angle, and decreases with the increase in normal stress during shearing, where surface degradation of the asperities is inevitable.

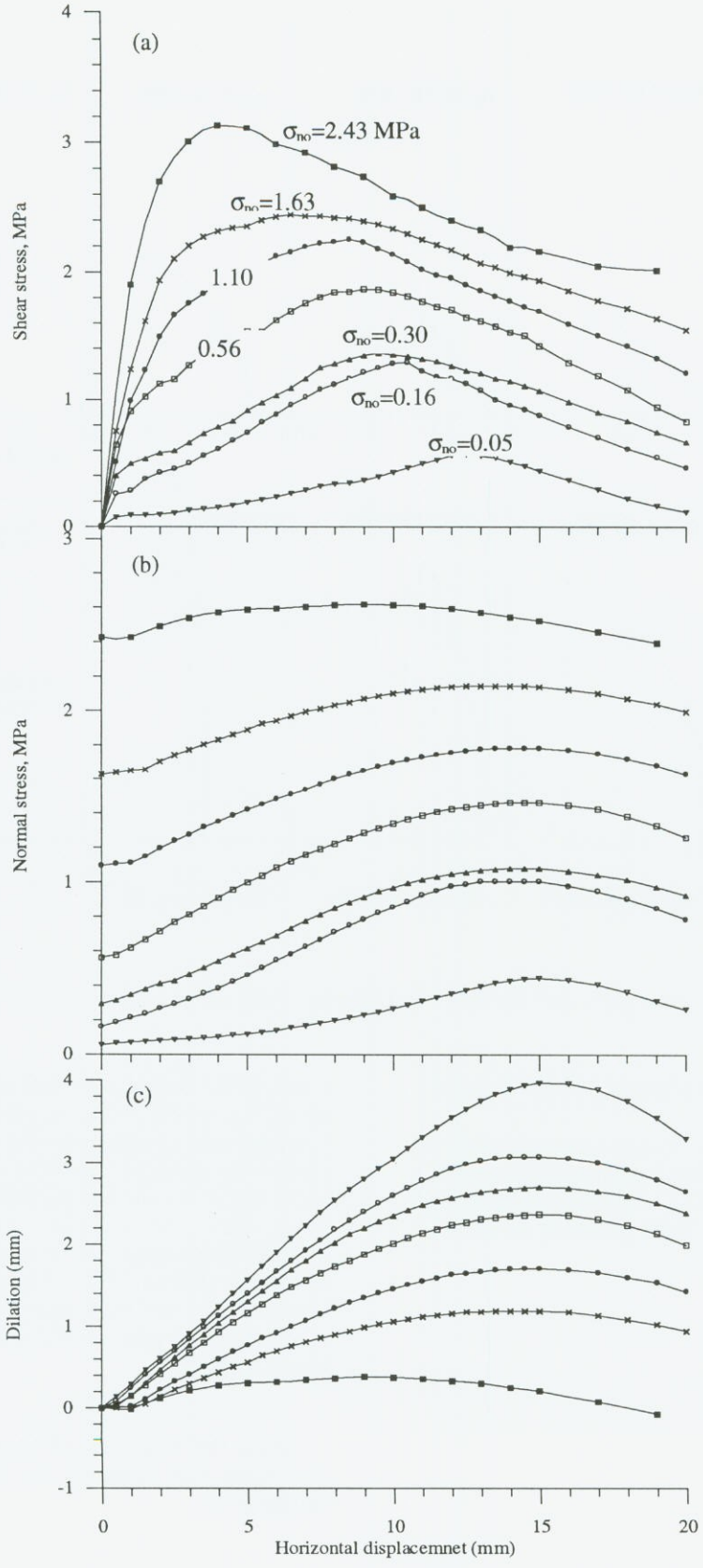



Figure 2. Shear behaviour of a typical profile Type II under CNS condition.

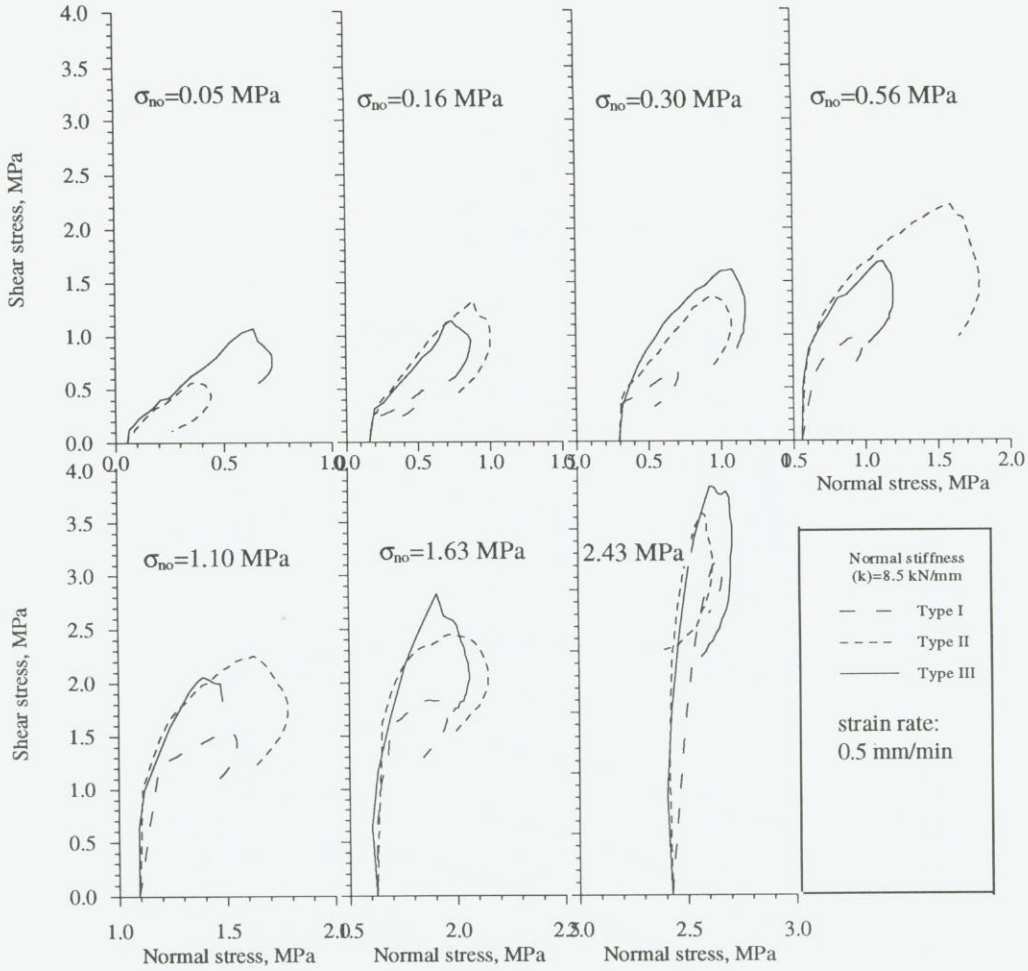



Figure 3. Stress paths for Type I, II and III profiles under various initial normal stress ($\sigma_{no}$).

## MODELS FOR PEAK SHEAR STRENGTH ENVELOPE

Patton (1966) conducted a series of tests on regular saw-teeth artificial joints under Constant Normal Load conditions (CNL). These test results fitted very well to a bilinear shear strength envelope which can be rewritten in the following forms:

For asperity sliding:

$$\tau_{p(CNL)} = \sigma_{n(CNL)} * \tan(\phi_b + i_o) \quad (1)$$

For asperity shearing:

$$\tau_{p(CNL)} = c + \sigma_{n(CNL)} * \tan(\phi_b) \quad (2)$$

where, CNL= constant normal load condition, $\tau_p$= peak shear stress, $\sigma_n$= normal stress, $\phi_b$=basic friction angle, c=cohesion intercept and $i_o$=initial asperity angle. According to Patton (1966), the sliding of asperities takes place under low normal stress, but after a certain magnitude, shearing through asperities takes palce. In contrast, other researchers considered simultaneous sliding and shearing to obtain different strength envelopes (Barton, 1973; Maksimovic, 1996). It has been observed that the peak shear strength predicted by Patton's model at low-medium normal stress generally overestimates the actual strength.

Barton (1973) introduced a non-linear strength envelope for non-planar rock joints for the Constant Normal Load (CNL) condition as:

$$\left(\frac{\tau_p}{\sigma_n}\right)_{CNL} = \tan\left[\phi_b + JRC * \log_{10}\left(\frac{\sigma_c}{\sigma_{n(CNL)}}\right)\right] \quad (3)$$

where,

$\phi_b = \phi - (d_n + s_n)$ ,

$d_n$ = peak dilation angle which decreases with the increase in normal stress,

$s_n$ = angle due to shearing of asperities which increases with the increase of the normal stress as more surface degradation occurs,

JRC= joint roughness coefficient, and

$\sigma_c$ = uniaxial compression strength.

The method suggested by Xie & Pariseau (1992) has been used to define the value of JRC for the Type I, II and III saw-teeth profiles in the current study, as explained below:

$$JRC = 85.2671 * (D-1)^{0.5679} \quad (4)$$

where, $D = \dfrac{\log(4)}{\log\left[2\left(1 + \cos\tan^{-1}\left(\dfrac{2h}{L}\right)\right)\right]}$

In the above, D=fractal dimension, h=average height of asperity and L=average base length of asperities. Accordingly, the JRC values of 4.2, 9.0 and 13.8 have been calculated for Type I, II and III joints, respectively.

Assuming that at the peak shear strength under CNS condition, normal stress momentarily remains constant, Eqn.3 (Barton, 1973) can then be employed to estimate the peak shear strength. The shear strength predicted in this manner for a range of normal stresses seems to underestimate the laboratory measurements (Table 1). Seidel & Haberfield (1995) reported similar conclusions when Barton's model was employed to predict the peak shear strength of hard concrete-rock joints.

In order to incorporate the effect of asperities on the extent of dilation, the behaviour of Type I, II and III joints could be represented by the following equations adopted from Jing et al. (1993) and modified to suit the CNS condition.

Type I: $$i_{\tau_p}/i_o = \left[1 - \sigma_{n(CNS)}/\sigma_c\right]^{0.19} \quad (5a)$$

Type II: $$i_{\tau_p}/i_o = \left[1 - \sigma_{n(CNS)}/\sigma_c\right]^{1.5} \quad (5b)$$

TypeIII: $$i_{\tau_p}/i_o = \left[1 - \sigma_{n(CNS)}/\sigma_c\right]^{3.0} \quad (5c)$$

where, $i_{\tau_p}$ = total dilation angle at peak shear stress under CNS condition, $\sigma_{n(CNS)}$ = normal stress corresponding to peak shear stress for a given $\sigma_{no}$, $\sigma_c$=uniaxial compression strength, $i_o$=initial angle of asperity and b=surface property which accounts the degradation of joints.

The normal stress $\sigma_{n(CNS)}$ corresponding to peak shear stress under Constant Normal Stiffness (CNS) condition can be computed by knowing the associated dilation and normal stiffness of the joints. Further details of quantifying dilation corresponding to peak shear stress and for known asperity height (a) and initial normal stress, $\sigma_{no}$ have been discussed by Indraratna et al. (1997).

Once the angle $i_{\tau_p}$ is known, the total friction angle ($\phi$) corresponding to the peak shear stress can be evaluated from ($\phi_b + i_{\tau_p}$). The peak shear strength can then be obtained by replacing $i_o$ in Eqn. 1 with the value of $i_{\tau_p}$ obtained from Eqn. 5. Based on this analysis, the authors propose the following strength envelope for CNS testing of soft joints:

$$\left(\frac{\tau_p}{\sigma_n}\right)_{CNS} = \tan\left[\phi_b + i_o\left(1 - \frac{\sigma_{n(CNS)}}{\sigma_c}\right)^{\beta}\right] \quad (6)$$

where,

$\sigma_{n(CNS)} = \left(\sigma_{no} + \dfrac{k * d_v}{A}\right)$ = normal stress corresponding to peak shear stress for a given $\sigma_{no}$ under constant normal stiffness condition,

k = normal stiffness (kN/mm),

$d_v$= dilation corresponding to peak shear stress (mm), and

A = joint surface area (sq.mm).

Eqn. 6 is employed to predict the peak shear strength for Type I, II and III profiles for the range of $\sigma_{no}$ from 0.05 to 2.43 MPa. It is verified that the proposed model predicts the shear strength more accurately, especially in the low to medium stress range than other models (Table 1). The stresses obtained from Eqn.1&2 (Patton, 1966) and Eqn.6 proposed by the authors are plotted together with the experimental results as shown in Figure 4. It is evident that the proposed non-linear equation describes the peak shear strength envelope more accurately than the bi-linear Patton's model, for constant normal stiffness condition.

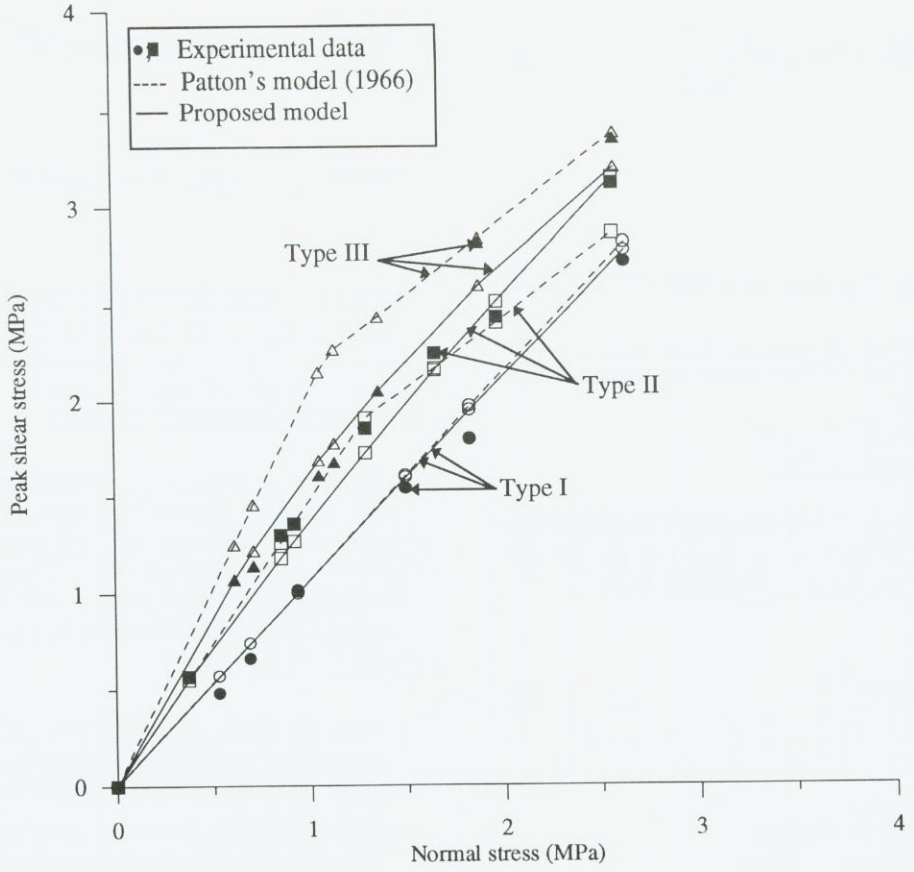



Figure 4. Peak shear strength envelopes for Profile Types I, II and III.

## CONCLUSIONS

This study was an attempt to compare and contrast the shear strength of soft joints under Constnat Normal Stiffness (CNS) condition with the conventional direct shear behaviour (Constant Normal Load condition). The cured gypsum represents an array of soft sedimentary rocks, and the behaviour of these soft joints under CNS condition is different to the direct shear or CNL behaviour as widely discussed in the past by many researchers in terms of shear strength envelopes. The laboratory results indicate that the peak shear stress increases as the initial normal stress is increased, and also that the peak shear stress occurs at a smaller shear displacement at higher levels of $\sigma_{no}$. In CNS testing, the joint behaviour is best illustrated in the form of stress paths, where both the shear and normal stresses change with horizontal displacement.

The observed shear behaviour of soft joints under CNS conditions is more realistic than the CNL condition. The CNS experimental results define a non-linear shear strength envelope for soft joints in comparison with linear or bi-linear envelopes often proposed for CNL test results. Patton (1966) theory overestimates the peak strength for higher asperity angles, where joint degradation is inevitable during sliding. In contrast, Barton (1973) model seems to underestmate the shear strength under CNS condition, although it is adequate for describing the shear behaviour under CNL condition. The non-linear empirical strength envelope proposed by the authors for soft simulated joints include the effect of asperity geometry and the extent of dilation during shearing.

## REFERENCES

1. Barton, N. Review of a new shear strength criterion for rock joints. Engineering Geology, 7, Elsevier, pp.287-332, 1973.

2. Benmokrane, B. and Ballivy, G. Laboratory study of shear behaviour of rock joints under constant normal stiffness conditions. Proc. 30th U.S. Symp. on Rock Mech., (Khair ed), Balkema Publishers, Rotterdam, pp.899-906, 1989.

3. Haberfield, C.M. and Johnstone, I.W. A mechanistically-based model for rough rock joints. Int. J. Rock Mech. Min. Sci. & Geomech. Abstr., Vol.31, No.4, pp.279-292, 1994.

4. Indraratna, B. Development and applications of synthetic material to simulate soft sedimentary rocks. Geotechnique, 40:2, pp.189-200, 1990.

5. Indraratna, B., Haque, A. and Aziz, N. Shear behaviour of soft joints using large-scale shear apparatus. 1st Asian Rock Mechanics Symposium (ARMS), Seoul, Korea (in press), 1997.

6. Jing, L., Stephansson, O., and Nordlund, E. Study of rock joints under cyclic loading conditions. Rock Mech. & Rock Engng., No. 26(3), pp. 215-232, 1993.

7. Lam, T.S.K. and Johnstone, I.W. Shear behaviour of regular triangular concrete/rock joints -- Evaluation. J. Geotech. Engrg., ASCE, Vol.115, No.5, pp.728-740, 1989.

8. Maksimovic, M. The shear strength components of a rough rock joint. Int. J. Rock Mech. Min. Sci. & Geomech. Abstr., Vol.33, No.8, pp.769-783, 1996.

9. Ohnishi, Y. and Dharmaratne, P.G.R. Shear behaviour of physical models of rock joints under constant normal stiffness conditions. Proc. Int. Conf. on Rock Joints, Leon, Norway, (Barton & Stephansson eds), Balkema Publishers, Rotterdam, pp.267-273, 1990.

10. Patton, F.D. (1966). Multiple modes of shear failure in rock and related materials. Ph.D. thesis. Univ. of Illinois, Urbana, 282p, 1966.

11. Seidel, J.P. and Haberfield, C.M. The application of energy principles to the determination of the sliding resistance of rock joints. Rock Mech. & Rock Engrg., Vol.28, No.4, pp.221-226, 1995.

12. Skinas, C.A., Bandis, S.C. and Demiris, C.A. Experimental investigations and modelling of rock joint behaviour under constant stiffness. Proc. Int. Conf. on Rock Joints, Leon, Norway, (Barton & Stephansson eds), Balkema Publishers, Rotterdam, pp. 301-308, 1990.

13. Xie, H. and Pariseau, W.G. Fractal estimation of joint roughness coefficients. Proc. Int. Conf. on Fractured and Jointed Rock Masses, Laketahoe, California, USA (Myer, L.R., Tsang, C.F., Cook, N.G.W. & Goodman, R.E. eds). Balkema Publishers, Rotterdam. 3-5 June 1992, pp.125-131, 1992.

Table 1. Experimental and model predicted results of peak shear stress.

| Asperity Type | Initial normal stress, $\sigma_{no}$ (MPa) | Experimental results | | Predicted Peak Shear Stress (MPa) | | |
|---|---|---|---|---|---|---|
| | | $\sigma_n$ (MPa) | $\tau_{peak}$ (MPa) | Barton (1973) | Patton (1966) | Proposed Model |
| Type I (i=9.5°) | 0.16 | 0.53 | 0.49 | 0.49 | 0.57 | 0.57 |
| | 0.30 | 0.69 | 0.66 | 0.64 | 0.74 | 0.74 |
| | 0.56 | 0.94 | 1.01 | 0.85 | 1.00 | 1.00 |
| | 1.10 | 1.50 | 1.54 | 1.32 | 1.61 | 1.60 |
| | 1.63 | 1.83 | 1.80 | 1.60 | 1.97 | 1.95 |
| | 2.43 | 2.54 | 2.72 | 2.24 | 2.82 | 2.78 |
| Type II (i=18.5°) | 0.05 | 0.37 | 0.57 | 0.46 | 0.55 | 0.55 |
| | 0.16 | 0.85 | 1.30 | 0.95 | 1.26 | 1.18 |
| | 0.30 | 0.92 | 1.36 | 1.02 | 1.36 | 1.27 |
| | 0.56 | 1.29 | 1.86 | 1.36 | 1.91 | 1.73 |
| | 1.10 | 1.65 | 2.25 | 1.68 | 2.17 | 2.16 |
| | 1.63 | 1.97 | 2.44 | 1.96 | 2.41 | 2.52 |
| | 2.43 | 2.57 | 3.12 | 2.47 | 2.87 | 3.15 |
| Type III (i=26.5°) | 0.05 | 0.61 | 1.07 | 0.90 | 1.25 | 1.07 |
| | 0.16 | 0.71 | 1.14 | 1.01 | 1.46 | 1.22 |
| | 0.30 | 1.05 | 1.61 | 1.37 | 2.15 | 1.69 |
| | 0.56 | 1.13 | 1.68 | 1.45 | 2.27 | 1.78 |
| | 1.10 | 1.36 | 2.05 | 1.68 | 2.44 | 2.05 |
| | 1.63 | 1.88 | 2.82 | 2.17 | 2.84 | 2.60 |
| | 2.43 | 2.58 | 3.35 | 2.79 | 3.38 | 3.20 |

# Comparison of Pillar Strengths Calculated Using Empirical Equations and Finite Elements

*Aarao de Andrade Lima,* Professor
*Tumkur Rajaro Gopinath,* Professor
*Marconi Edson de Alcantara,* Graduate Student
Department of Mining and Geology
Federal University of Paraiba
Campina Grande, PB, BRAZIL

## ABSTRACT

Mechanical properties typical of coal are used in the comparisons of pillar strengths based on finite elements and the empirical equations of Holland-Gaddy, Salamon-Munro, Obert-Duvall, and Bieniawski-PSU. A correlation among the strength parameters which are employed in the empirical equations, in Mohr-Coulomb and Hoek-Brown failure criteria is established. Emphasis is given to the important distinction between the mechanical properties of small rock specimens and those related to the rock mass. An elastoplastic version of Hoek-Brown criteria has been developed and implemented in a finite elements code. The strengths calculated using the empirical equations showed a good agreement when the ratio width by height of the pillars varied from 1 to 8, except for Holland-Gaddy equation which exhibited lower values. Under the hypothesis of associative perfect elastoplasticity used, pillar strength calculated using Mohr-Coulomb yield criterion became excessively high for all the models having a pillar width by height ratio above 2. The finite elements solution based on Hoek-Brown criterion predicted strengths around fifty percent larger than Bieniawski-PSU equation when the pillars width by height ration varied from 3 to 8, showing good agreement below that range. It has been concluded that, under the hypothesis of percfect plasticity, stress analysis techniques may overestimate the strength of rock structures subjected to high confining stresses.

## PURPOSE AND SCOPE

Using the finite element method (FEM) as the technique for stress analysis, and the classical empirical equations due to Holland-Gaddy, Salamon-Munro, Obert-Duvall,and Bieniawski-PSU, for calculating the strength of mine pillars, this research has the following objectives:

- development of a correlation among the mechanical properties used in the empirical equations, and in Mohr-Coulomb and Hoek-Brown failure/yield criteria;
- implementaion of Hoek-Brown criterion under elastoplastic regime in a FEM program;
- comparison of pillars strength predicted using empirical equations and the FEM, with both Mohr-Coulomb and Hoek-Brown criteria, according to the variation of the width-to-height ratio of the pillars.

Two-dimensional plane-strain has been used in the FEM models in order to decrease computer time. This restricts the FEM results to long pillars. As an additional simplification, isotropic elastic properties have been assumed for both pillars and country rock. In the elastoplastic range the perfect elastoplasticity model and the normality rule have been adopted. The material properties for the examples analyzed, using empirical equations and the FEM, are typical of coal mines, because of the widespread interest of the subject.

## ROCK MASS MECHANICAL PROPERTIES

The estimation of rock mass properties based on laboratory testing of small samples constitutes one of the most challenging and important topics of rock mechanics nowadays (1). Proceeding in a fairly basic way, the unconfined compressive strength of a cubic sample with a side measuring $D$ may be expressed as (2, p.156):

$$\sigma_D = \sigma_C \left( \frac{D_c}{D} \right)^{\alpha}, \qquad D < D_M \tag{1}$$

$$\sigma_D = \sigma_M, \qquad D \geq D_M \tag{2}$$

where $\sigma_C$ is the strength of a laboratory size sample measuring $D_C$; $D_M$ is the so called critical size for a given rock mass, beyond which the compressive strength may be assumed constant for practical mine problems; $\sigma_M$ is the strength for samples with edges larger than or equal to $D_M$; and $\alpha$ is a parameter depending on the rock type. Figure 1 depicts those concepts, using the coal properties adopted here. For rocks other than coal, $D_C$ is the diameter of cylindrical rock samples usually about 7.5 cm,

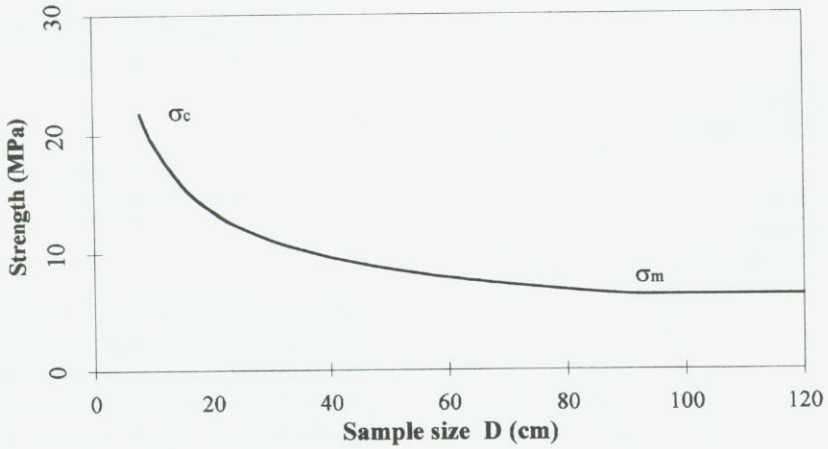



**Figure 1. Effect of sample size on the unconfined compressive strength of rock.**

according to the standards. For coal, $\alpha$ may be typically taken equal to 0.5, and $D_M$ varies from 3 to 5 feet (3, 4). For other classes of rock $\alpha$ is generally below 0.5 (2).

The scale effect of strength of the rock mass under confining stresses has not been so well studied (1). However, considering that the rock mass retains part of its resistance through the residual internal friction, one may anticipate a smaller effect of sample size in the frictional part of the rock mass strength. In this way, the rock mass angle of internal friction, and Hoek-Brown related parameter, has been considered equal to that of the laboratory value. This simplification should be further investigated, depending on the availability of data. Also, the modulus of elasticity of the intact rock (laboratory specimens) have been used directly in the FEM analysis, without any consideration of scale effect. This assumption will not affect significantly the results because the ratio between the modulii of the country rock and that of the coal should be close for both the rock mass and laboratory size samples.

## HOEK-BROWN FAILURE CRITERION

Based on extensive experimental data about rock failure under triaxial stresses, and using detailed statistical analysis, Hoek and Brown (2,5) have proposed a failure criterion for rock mass obeying the following equation:

$$\sigma_1 = \sigma_3 + \sqrt{m\sigma_c\sigma_3 + s\sigma_c^2} \qquad (3)$$

where $\sigma_1$ and $\sigma_3$ are the principal stresses in the stage of rupture; $\sigma_C$ is the compressive strength of the intact rock, $m$ and $s$ are parameters depending on fracturing and alteration of the rock mass, and also depending on the petrologic rock class.

Values of $m$ and $s$ are also correlated to rock mass classification systems, or to the mean spacing of discontinuities. The shape of the envelope depends on the value of $m\sigma_C$, while its distance to axis $\sigma_3$ depends on the value of $s\sigma_C^2$. Hoek-Brown envelope is shown in Figure 2 for the mechanical properties of coal used here.

## RELATIONSHIPS BETWEEN HOEK-BROWN AND MOHR-COULOMB CRITERIA

Because of its simplicity and long tradition, Mohr-Coulomb criteria is still quite used in the fields of soil and rock mechanics. Mohr-Coulomb criterion has a linear envelope expressed by the following equation (6, 7):

$$\tau = c + \sigma\tan\phi \qquad (4)$$

where $\sigma$ and $\tau$ are the normal and shear stresses, respectively, acting at the plane of rupture; $c$ is the cohesion; and $\phi$ is the angle of internal friction. One may also express the failure criterion in terms of principal stresses as:

$$\sigma_1 = \sigma_c + \sigma_3\tan\beta \qquad (5)$$

where

$$\tan\beta = \tan^2\left(45° + \frac{\phi}{2}\right) \qquad (6)$$

The following may also be derived:

$$\sigma_c = \frac{2c\cos\phi}{1-\sin\phi} \qquad (7)$$

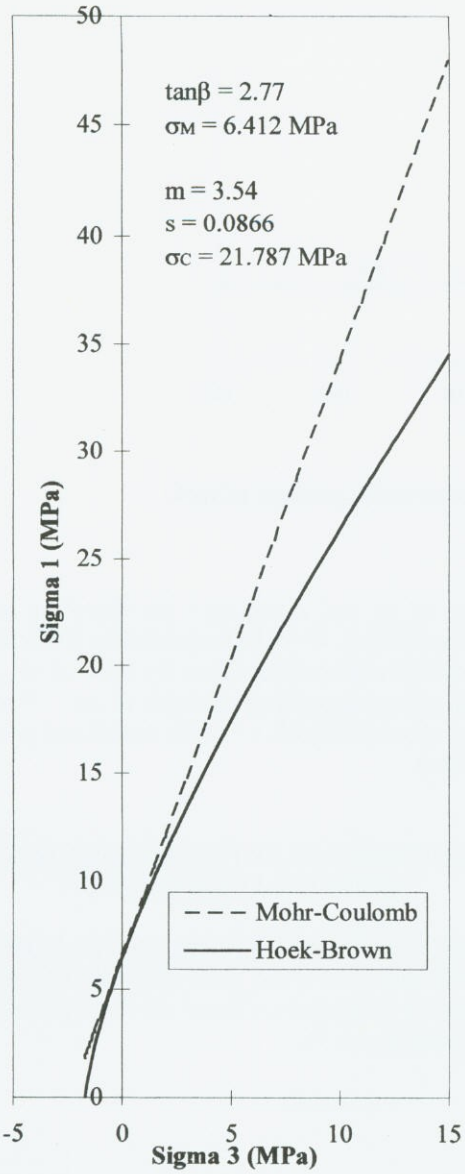



**Figure 2. Hoek-Brown and Mohr-Coulomb envelops.**

As shown in Figure 2, it is possible to correlate both Hoek-Brawn and Mohr-Coulomb criteria taking a tangent line at the point of intersection of both envelopes with the $\sigma_1$ axis. By differentiating equation (3) with respect to $\sigma_3$, at $\sigma_3 = 0$, one gets the following equations (8, 9):

$$\tan\beta_M = 1 + \frac{m}{2\sqrt{s}} \tag{8}$$

$$\sigma_{CM} = \sigma_C \sqrt{s} \tag{9}$$

$$\phi_M = 2\left[\arctan\left(\sqrt{1 + \frac{m}{2\sqrt{s}}} - 45°\right)\right] \tag{10}$$

$$c_M = \sigma_{CM} \frac{1 - \sin\phi_M}{2\cos\phi_M} \tag{11}$$

where the subscript $M$ in the variables stand for the fact that they are Mohr-Coulomb criterion parameters calculated from Hoek-Brown criterion, and are scaled down to rock mass properties. It should be pointed out that $\sigma_{CM}$ of equation (9) should have an equal value to $\sigma_M$ of equation (2), since both represent the compressive strength of the rock mass.

By substituting equations (8) and (9) into equation (3), one may rewrite Hoek-Brown criterion in terms of rock mass compressive strength as follows:

$$\sigma_1 = \sigma_3 + \sqrt{2(\tan\beta - 1)\sigma_3 + \sigma_M^2} \tag{12}$$

## USE OF EMPIRICAL EQUATIONS

### Calculation of Stresses by the Tributary Area Approach

The use of empirical equations involves the calculation of vertical stresses acting at the pillars due to overburden by means of the tributary area approach. In this method the mean vertical stress at the pillar is given by (6)

$$S_p = \gamma z \frac{A_t}{A_p} \tag{13}$$

where $\gamma$ is the mean specific weight of overburden rock, $z$ is the depth of the seam, $A_t$ is the total area of influence of the pillar, and $A_p$ is the area of the pillar. For long pillars the areas are calculated using a slice of unitary length (2). The hypothesis that the pillar must support the weight of the overburden up to the surface is valid only when the dimensions of the panel are large with respect to the depth of the seam. Otherwise, with the creation of a pressure arch, part of the overburden weight is transferred outside of the panel. Another simplifying assumption of this method is that the stresses are distributed uniformly across the pillar. That simplification becomes inaccurate if the ratio width-to-height ratio of the pillar is large.

### Empirical Equations Background

A large number of empirical equations have been proposed for coal pillars (3, 10, 11). However, all those equations take into

account the following factors affecting pillar strength: uniaxial compressive strength of the rock; dimensionless ratio between width and heigth of the pillar; and volume of the pillar, or scale effect. Also, each equation recommend the use a specific factor of safety, defined as:

$$F_s = \frac{C_p}{S_p} \tag{14}$$

where $C_p$ is the pillar strength calculated using a specific empirical equation. In addition, the empirical equations have their range of utilization for specific ranges of the width-to-height ratio of the pillar (generally more than 1, and always less than 12).

In Holland-Gaddy (12) equation the strength is given by:

$$C_p = k\frac{1}{\sqrt{H_p}}\sqrt{\frac{W_p}{H_p}} \tag{15}$$

where $H_p$ is the pillar height, $W_p$ is the pillar width, taken as its smaller dimension, and material parameter $k$ is given by (3):

$$k = \sigma_C\sqrt{D_C} \tag{16}$$

where $\sigma_C$ is the uniaxial compressive strength of a cubic sample with edge $D_C$. The factor of safety recommended for that equation varies from 1.8 to 2.2.

Salamon-Munro equation has the following form (13):

$$C_p = K\frac{1}{H_p^{0.20}}\left(\frac{W_p}{H_p}\right)^{0.46} \tag{17}$$

where $K$ is the uniaxial compressive strength of cubic samples of coal with edge of 1 foot. When the strength is measured from samples with edge different from 1 foot the following correction should be applied (3):

$$K = \sigma_c\sqrt{\frac{D_C}{D_1}} = \frac{k}{\sqrt{D_1}} \tag{18}$$

where $D_1$ is the value of 1 foot expressed in the same unit of length used for $D_C$. It is important to notice that equation (17) is not dimensionally correct. When other units different from feet are used, one should divide the results expressed by the equation by a factor equal to the number of feet in the unit used, affected by the power 0.2; for instance, using meters the factor for division is equal to $3.2008^{0.2}$. The factor of safety for Salamon-Munro equation is about 1.6.

Obert-Duvall equation (6) initially adopted a strength parameter related to the intact rock, together with a large factor of safety, about 4.0. It has been later modified for use with rock mass strength parameter (3, 11), requiring a factor of safety between 1.5 to 2.0. In its modified version Obert-Duvall equation is expressed as:

$$C_p = \sigma_M\left(0.778 + 0.222\frac{W_p}{H_p}\right) \tag{19}$$

Where $\sigma_M$ is the uniaxial compressive strength of the rock mass, calculated according to equations (1) taking $D$ equal to the critical size $D_M$.

Bieniawski-PSU equation (3) is similar to Obert-Duvall one, having the following form:

$$C_p = \sigma_M\left(0.64 + 0.36\frac{W_p}{H_p}\right) \tag{20}$$

and requiring a factor of safety between 1.5 to 2.0.

Empirical Equations Results

The study of the effect of the variation in the ratio $W_p/H_p$ is conducted by fixing $W_p$ at 12m, and varying $H_p$ from 12m to 1m, as shown in Figure 3. The calculations have been performed for the ratio $W_p/H_p$ equal to 1, 2, 3, 4, 5, 6, and 8, corresponding to $H_p$ equal to 12, 6, 4, 3, 2.4, 2, and 1.5m, respectively. Some of the unusually large values used for pillar height will not affect the calculations conducted here, having been maintained just for the convenience of constructing FEM meshes. The strength properties used for coal are typical of Pittsburgh seam (3), having the following values:

$\boldsymbol{k}$ = 6.132MPa.m$^{1/2}$
$\sigma_M$ = 6.412MPa
$\boldsymbol{K} = \boldsymbol{k} / (D1)^{1/2} = 6.132 / (0.3048)^{1/2} = 11.107$MPa.

Those data have been checked against values of $\sigma_C$ scaled down to $\sigma_M$, for the properties of other coal seams around the world (14).

Applying the material parameters of coal strength to the empirical equations, and varying $W_p/H_p$ from 1 to 8 one gets the curves shown in Figure 4. It can be observed the good agreement

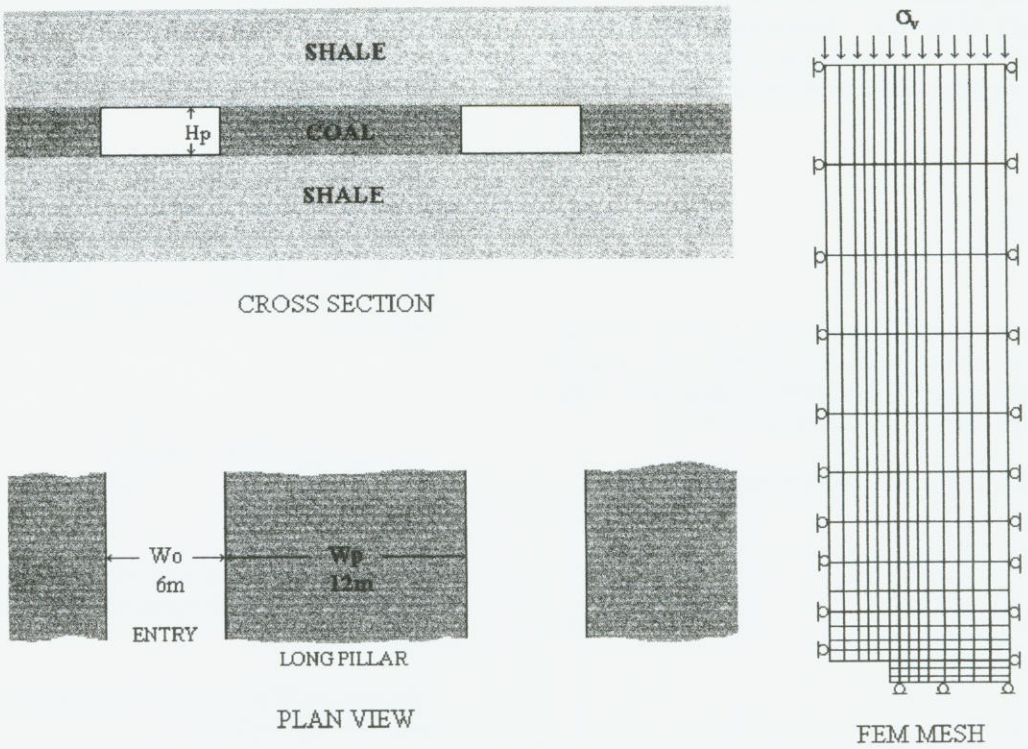



**Figure 3. Geometric definitions of pillar, and finite elements mesh.**

between Salamon-Munro and Bieniawski-PSU equations. On the other hand, Holland-Gaddy equation underestimates the pillar strengths, while Obert-Duvall equation yields an intermediate result. By dividing the equations by their recommended average factors of safety, that is, 2.0, 1.6, 1.75, and 1.75 respectively, one arrives at the results shown also in Figure 4. It can be seen that the division by the factors of safety did not affect the relative positions of the curves.

## USE OF FINITE ELEMENTS

### Input Data Used in the FEM Models

The FEM code due to Hinton and Owen (15) has been adopted in this research. The original code has been designed for elastoplasticity under Tresca, von Mieses, Mohr-Coulomb, and Drucker-Prager yield criteria. Hoek-Brown criterion has been implemented in the FORTRAN code for elastoplasticity material model (9).

The basic mesh used is made up of 209 linear elements and 240 nodes as shown in Figure 3. Different models have been constructed from the basic mesh by varying $H_p$ from 1.5 to 12m, such that the ratio $W_p/H_p$ was varied from 1 to 8. From the roof to the top of the mesh a 30 m layer has been placed in the model to provide a realistic stress distribution across the pillar. The mesh has been laterally restrained as shown in Figure 3. The overburden load $\sigma_V$ has been applied in 4 increments, with the load levels selected such that at the last load increment all elements accross the pillar mid-height have undergone plastic flow, or have exhibited factors of safety very close to 1. A global factor of safety of the pillar is also calculated automatically by the program using the equation:

$$\bar{\bar{f}}_s = \frac{\sum f_i \Delta x_i}{W_p/2} \qquad (21)$$

where $f_i$ and $\Delta x$ are the factors of safety and width of each element at the middle of the pillar. The collapse load is calculated by interpolation of over two load increments, such that the global factor of safety assumes value 1.

The material properties given in Table 1 for both coal and country rock have been taken from the literature (16-18.). The resistance properties have been scaled down to rock mass ones. Hoek-Brown parameters s and m have been calculated using equations (8) and (9).

### FEM Results

Principal stresses and Hoek-Brown factors of safety across the horizontal plane passing through the mid height of the pillar are shown in Figure 5, for the model $W_p/H_p = 3$.

The strength of long pillars (divided by 1.4) are shown in Figure 6 for both yield criteria. When $W_p/H_p$ is larger than 2, the collapse load predicted by Mohr-Coulomb yield criterion becomes very large, therefore these results are not plotted.

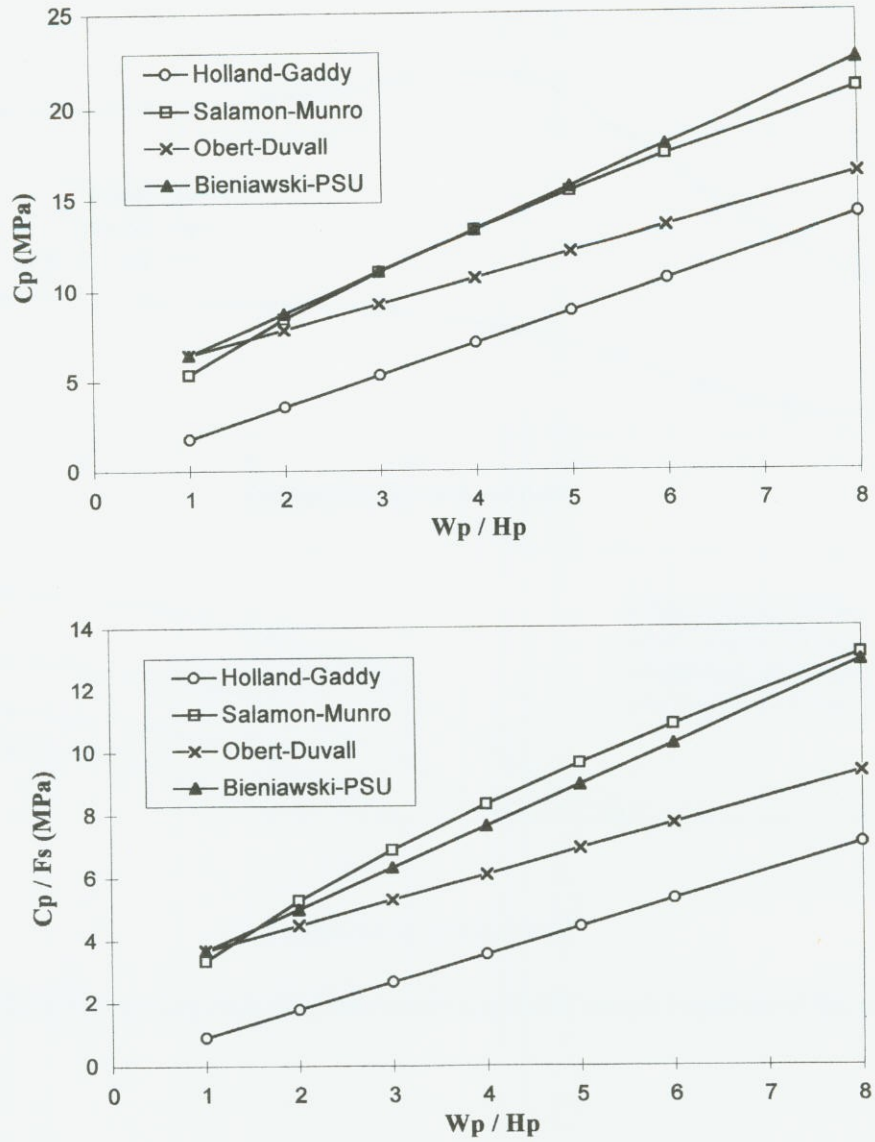



Figure 4. Pillar strengths calculated using empirical equations and strengths devided by factors of safety.

Table 1. Mechanical Properties Used in the FEM solutions

| Material Properties | Coal | Shale |
|---|---|---|
| Elastic modulus (GPa) | 2.8 | 9.7 |
| Poisson's ratio | 0.3 | 0.3 |
| Cohesion $c_M$ (MPa) | 1.93 | 4.00 |
| Angle of friction | 28 | 30 |
| Strength $\sigma_M$ (MPa) | 6.41 | 13.86 |

## COMPARISON OF RESULTS

Before comparing the strengths predicted using FEM and empirical equations one should be aware that the empirical equations heve been developed for rectangular pillars, with the length to width ratio generally less than 2. According to Jaegger and Cook ( 7, p. 486) long pillars exhibit a strength about 40 percent larger than rectangular pillars of equivalent sizes and rock properties. Therefore, for comparative purposes the strengths calculated using FEM have been divided by 1.4 before plotting in Figure 6.

Since Bieniawski-PSU equation showed a good agreement with the other ones, except for Holland-Gaddy equation, as previously discussed, it has been plotted together with the FEM strengths shown in Figure 6.

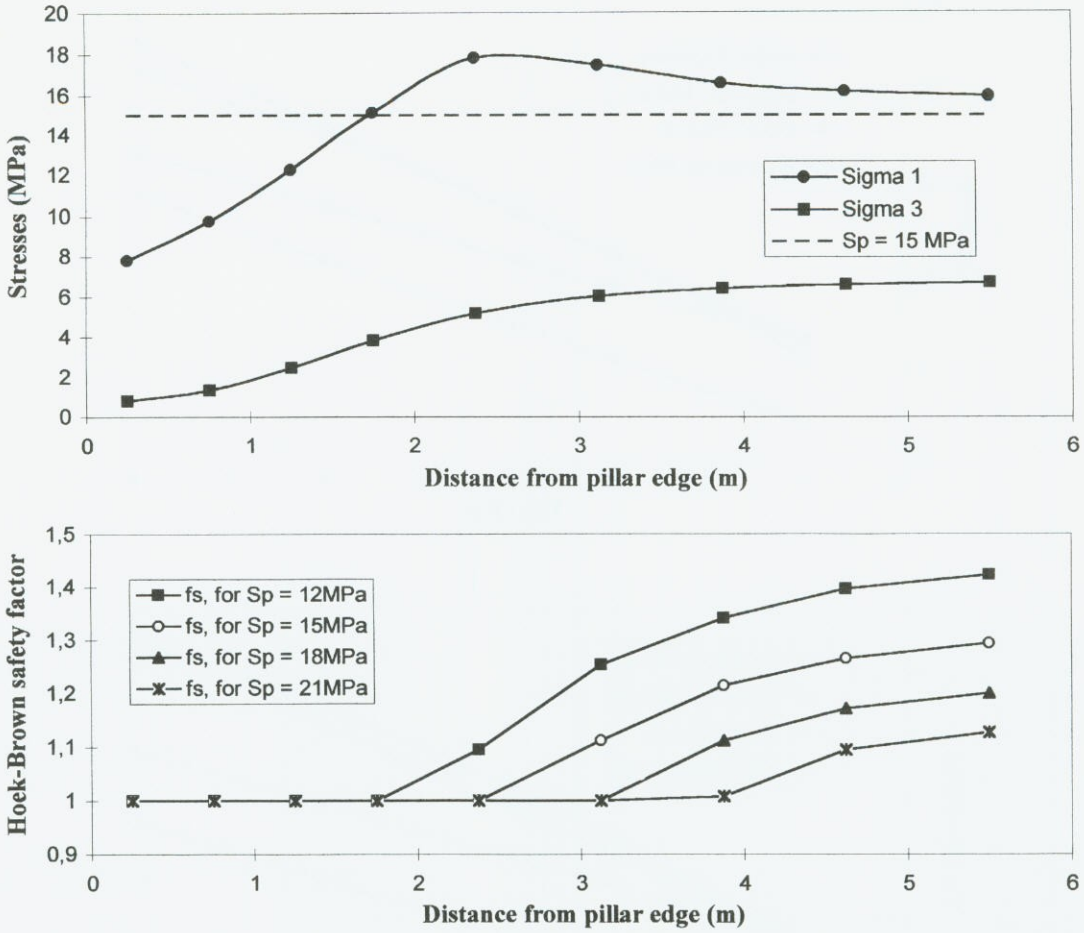



**Figure 5. Principal stresses and Hoek-Brown factors of safety across a horizontal plane passing through the pillar mid height.**

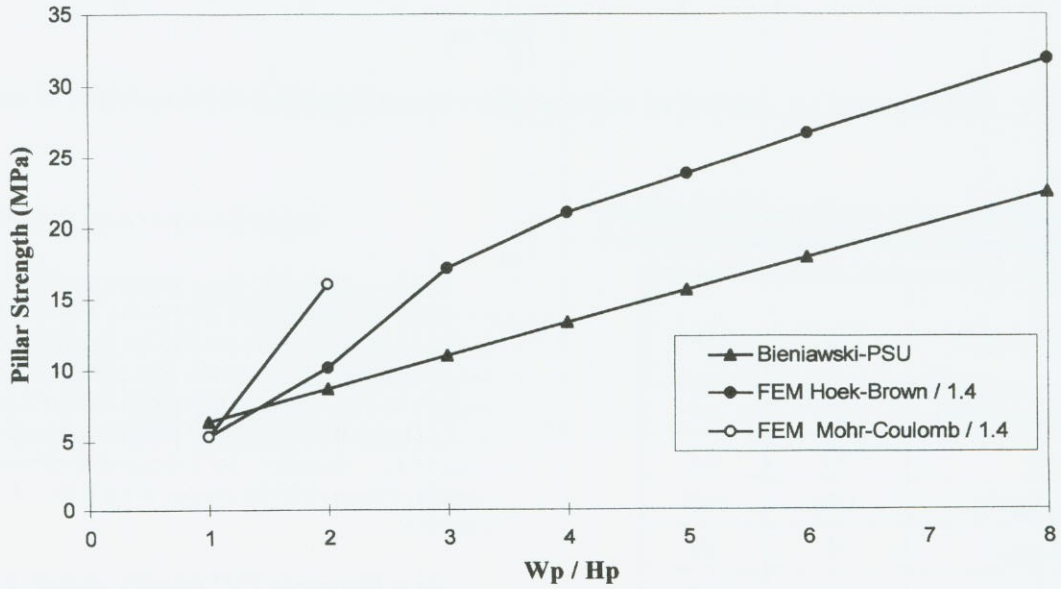



**Figure 6. Pillar strengths calculated using the FEM compared with Bieniawski-PSU equation strengths.**

## CONCLUSIONS

It has been observed that under the assumption of perfect elastoplasticity Mohr-Coulomb yield criterion grossly overestimates the strength when the height to width ratio of pillars becomes larger than 2. Hoek-Brown yield criterion gives more realistic results up to $W_p/H_p = 2$. When the width-to-height ratio varied from 3 to 8 the solutions based on Hoek-Brown criterion predicted strengths around fifty percent larger than Bieniawski-PSU, as it can be seen in Figure 6. It has been concluded that, under the hypothesis of percfect plasticity, stress analysis based techniques, such as finite elements or boundary elements, may overestimate the strength of rock structures subjected to high confining stresses.

The knowledge of post failure mechanical properties of rock mass (strain or work softening parameter) is required for a more realistic approach. These parameters should be determined independently for cohesion and friction related properties of the rock mass. Another factor that may be of importance is the existence of a discontinuity in the contact of coal with the rock of the roof and floor. That can be modeled using special joint elements, if the angle of friction and stiffness properties of the discontinuity are known.

As a final improvement for this study, 3-D geometry should be modeled even though the amount of computer time will require powerful machines, because of the many iterations required to reach the collapse load.

## REFERENCES


1. Pinto da Cunha A. (Editor) *Scale Effects in Rock Masses 93*, pp. 217-224, A. A. Balkema, Rotterdam (1993).

2. Hoek E. and Brown E T. *Underground Excavations in Rock*, IMM, London (1982).

3. Bieniawski Z. T. Improved design of room-and-pillar coal mines for U. S. conditions. In: Brawner C. O. (Editor) *Stability in Underground Mining*, pp. 19-51, SME/AIME, New York (1983).

4. Bieniawski Z. T. An overview of ground support considerations in room and pillar coal mining. In: Chuck Y. P. (Editor) *Ground Control in Room and Pillar Mining*. pp. 95-104, SME-AIME, NewYork (1982).

5. Hoek E. and Brown E. T. Empirical strength criterion for rock masses. *J. Geotechnical Eng. Div.* **106**, ASCE, 1013-1035 (1980).

6. Obert L. and Duvall W. I. *Rock Mechanics and the Design of Structures in Rock*, John Wiley, New York (1976).

7. Jaegger J. C. and Cook N. G. W. *Fundamentals of Rock Mechanics*, 2nd. edn. Chapman and Hall, London (1976).

8. Hoek E. Estimating Mohr-Coulomb friction and cohesion values from Hoek-Brown failure criterion, *Int. J. Rock Mech. Min. Sci. & Geomech. Abstr.*, **27**, 3, pp. 227-229 (1990).

9. Alcantara M. E. Elastoplasticity implementation of Hoek-Brown rock mass failure criterion. (in Portuguese) *M. S. Thesis*, Department of Mining and Geology, Federal University of Paraíba, Brazil (1997).

10. Tsur-Lavie Y. and Denekamp S. A. Size and shape effect in pillar design. In: Farmer I. W. (Editor) *Strata Mechanics*, pp. 245-248, Elsevier, Amsterdam (1982).

11. Logie C. V. and Matheson G. M. A critical review of the current state-of-the-art design of mine pillars. In: Brawner C. O. (Editor) *Proc. 1st Int. Conf. on Stability in Underground Mining*. pp. 359-382 (1982).

12. Holland C. T. Mine pillar design. In: Given I. A. (Editor) *SME Mining Engineering Handbook*, Vol. I, 13.8, SME-AIME, New York (1973).

13. Salamon M.D.G. and Munro A. H A study of the strength of coal pillars. *J. South African Inst. Min. Metall.* **68**, pp. 55-67 (1967).

14. Lama R. D. and Vutukuri V. S. *Handbook on Mechanical Properties of Rocks*, Vol. II, Transtech Publications, Clausthal, Germany (1978).

15. Owen D. R. J. and Hinton E. *Finite Elements in Plasticity*. Pineridge Press, Swansea, (1980).

16. Peng S. S. and Su W. H. The causes of cyclic excessive convergence at the longwall tailentry. *Int. J. Mining Eng.* **1**, pp. 27-41 (1983).

17. Peng S. S. and Su W. H. 3-D structural analysis of longwall panels. *Proc. 21st U. S. Symp. on Rock Mechanics*, Rolla - MO (1980).

18. Jeremic M. L. and Lutley H. J. Stress analysis in underground extraction of steeply dipping thick coal seams. *Proc. 21st U. S. Symp. on Rock Mechanics*, Rolla - MO (1980).



# Effects of In-seam and Near-seam Conditions and Asymmetric Pillar Loading on Coal Pillar Strength

*Daniel W.H. Su,* Senior Research Engineer
*Gregory J. Hasenfus,* Group Leader
CONSOL Inc.
Research and Development
Library, PA

ABSTRACT

The importance of incorporating fundamental principles of rock material response and failure mechanics into a pillar strength design model has been demonstrated. To accurately assess pillar strength, a model should account not only for the characteristics of the coal, but also for those of the surrounding strata. The interactions between the pillar and the surrounding roof and floor dictate ultimate pillar strength. Confinement, or the lack thereof, provided by roof and floor frictional end-constraint is one of the most significant factors in the strength of very wide pillars. The best conditions for end-constraint occur with ideally strong roof and floor. In this paper, it will be shown that weak roof and floor may decrease the ultimate pillar strength by as much as 30% compared to ideal conditions. Field observations confirm this pillar strength reduction in the presence of weak roof and floor. Furthermore, rock partings within the coal have a variable effect on pillar strength, depending on the parting strength. A competent shale parting within the coal reduces the effective pillar height, thus increasing the ultimate pillar strength; a weak claystone parting slightly decreases the strength. Imposed load distribution also has a significant effect on pillar strength, such that asymmetric pillar loading, similar to that observed in pillars adjacent to high extraction mining, reduces the ultimate pillar strength below that of equivalent pillars subject to uniform load distributions.

# Ground Control Worker Safety During Extended Cut Mining

*Roy H. Grau, III,* Mining Engineer
*Eric R. Bauer,* Mining Engineer
National Institute for Occupational Safety and Health
Pittsburgh Research Center
Pittsburgh, PA

## ABSTRACT

The trend in underground room-and-pillar coal mining is to employ remote-control continuous mining machines to take extended cuts of 40 ft or more. Roof fall safety hazards to the mine worker associated with extended cutting are not completely defined but are known to include removal of the miner operator from the protective canopy, noncompliance with approved cutting depth and CM operator positioning. This report summarizes ground control research performed by the National Institute for Occupational Safety and Health (NIOSH) researchers at the Pittsburgh Research Laboratory concerning extended cuts. A combination of statistical analysis and underground investigations have been conducted. Statistical analysis of extended cut use, along with roof fall accidents and fatalities data delineate the extent of the problem in U.S. coal mines. Additionally, an underground study is described where the long-term roof stability of extended cut areas are compared to standard cuts.

## INTRODUCTION

The accepted practice in the U.S. coal industry during room-and-pillar mining has been to advance the mine face 20 ft (6 m) until the continuous mining machine (CM) operator's compartment is just outby the last row of roof bolts. Then a roof bolting crew installs permanent roof supports to stabilize the mine roof. This sequence of 20 ft (6 m) cuts and roof supporting operation has, for many years, been the standard throughout the industry. The advantages of this methodology include minimization of both the amount of unsupported mine roof and the time between mine roof exposure and mine roof bolting (1). After the adaptation of remote-controlled CM, extended cuts, those longer than 20 ft (6 m), have become increasingly popular.

Like many other technological advancements, extended cut operations offer benefits (ergonomic and production factors), but also create problems. As with any mining method, concern is raised for the ultimate safety of the worker. For example, the miner operator is required by law to remain under supported roof. However, remote-control mining of extended cuts removes the operator from the protection of the CM canopy. In addition, many miner operators place themselves in a more hazardous position because they are free to move about and may inadvertently proceed in-by the permanent supports. Another potential disadvantage of extended cut mining is an increase in the mining to support time.

## APPLICATION OF EXTENDED CUTS

For clarity, the definition of the term "extended cutting" will be that used by the Mine Safety and Health Administration (MSHA). MSHA defines extended cut mining as "any cut in which the on-board manual controls of the CM are advanced inby the last row of permanent roof supports or any cut in which the mining machine is advanced more than 20 ft (6 m) inby the last row of permanent roof support."

The most recent available data show an increasing trend in extended cut approvals granted by MSHA (figure 1). Although in that period the total number of producing underground bituminous coal mines decreased from 1,596 to 942 (-40%), the number of extended cut approvals have increased from 206 to 399 (+94%). Extended cuts are being taken during room-and-pillar mining, retreat mining, and for longwall gate road development. In 1995, approximately 45% of the producing underground bituminous coal mines had approval to mine extended cuts. The approved extended cut depths range from 21 (6.4 m) to 65 ft (19.8 m), with 30 ft (9 m) and 40 ft (12 m) being approved most often. Cuts deeper than 40 ft (12 m) are allowed, primarily for crosscut mining, and constitute only 4.7% of the total for the time period 1988 to 1995 (2). It is presumed that extended cuts are becoming more popular due to the pressure mine operators have to develop longwall gate roads rapidly or to increase production.

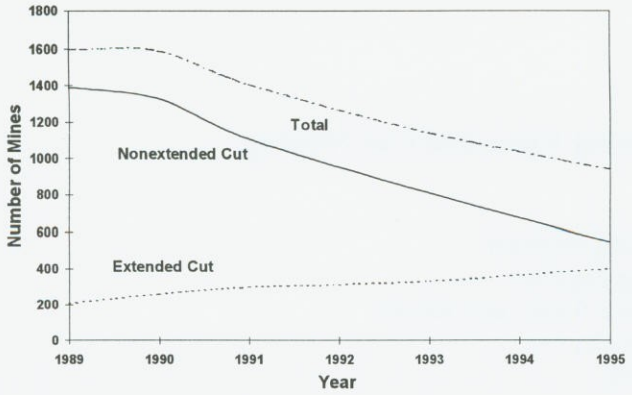



Figure 1. Underground bituminous coal mine plan approvals, 1989-1995.

The ground control concerns for extended cut include both roof stability issues and procedural methods. From a roof stability perspective, does extended cut mining increase the probability for roof falls? Short- and long-term roof stability has commonly been attributed to minimizing mine roof damage prior to the installation of permanent support. One factor believed to minimize roof damage is quick mining to roof bolting time. However, with extended cutting, this time horizon increases. Other concerns with extended cutting include when to take an extended cut and, if taken, the maximum safe depth-of-cut. Factors which complicate the application of extended cuts include geologic and physical characteristics of the mine roof. These concerns are currently answered qualitatively rather than quantitatively. CM operators make these decisions daily and respond using intuition and knowledge.

## ROOF FALL ACCIDENT ANALYSES

To determine if extended cut mining has led to an increase in roof failures and/or roof fall injuries and fatalities, the reported roof fall accidents and roof fall fatality reports were analyzed. The accidents investigated herein are defined in 30 CFR, Section 50.2. There are 12 definitions of roof falls listed. Four of the most common roof fall accidents involve fatality, life threatening injury, an unplanned roof fall at or above the bolt anchorage zones in active workings where roof bolts are used, or an unplanned roof or rib fall in active workings that impairs ventilation or impedes passage. MSHA underground coal-mine roof fall fatality reports for 1988 through 1995 were reviewed to determine the fatalities where extended cutting was a contributing factor. The reported roof falls were statistically analyzed and incidence rates calculated for mines with and without an extended cut approval.

### Roof Fall Fatalities

A review of the 97 roof fall fatalities that occurred in underground bituminous coal mines indicated that extended cutting may have been a contributing factor in 25 (25.8%) of the fatalities, while the remaining 72 (74.2%) occurred for reasons other than the mining of an extended cut. Figure 2 illustrates roof fall fatalities in extended cut and nonextended cut mines. Note that the number of fatalities for extended cut mines was lower for all years except 1995, when it was equal.

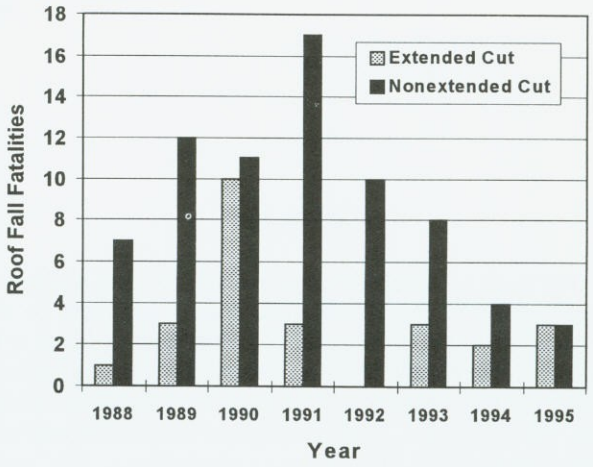



Figure 2. Roof fall fatalities for extended and nonextended cut, 1988-1995.

### Reported Roof Fall Accidents

All roof fall accidents reported to MSHA by mine operators for the years 1989, 1990, 1991, 1993, and 1995 were extracted from MSHA's Health and Safety Analysis Center (HSAC) Accident Database. Data from 1992 and 1994 were excluded because in those years an accurate list of mines with extended-cut approval was unavailable. The data includes roof falls resulting in no injuries, injuries, and fatalities.

Incidence rates, normalized with respect to hours worked underground, are used to analyze accident data. This approach gives a more concise measure of accidents, allowing comparison between different size mines, years, and populations. Table 1 contains reported roof fall accident incidence rates based on employee hours worked for extended and nonextended cut mines (these data include accidents that occur anywhere in the mine). The analysis shows that the incidence rate of reported roof fall accidents for extended cut mines is 4.74 versus 4.82 for nonextended cut mines. This indicates that, based solely on whether a mine had an extended cut approval or not, the difference in the incidence rate of reported roof fall accidents are negligible.

Table 1. Accident incidence rates based on underground employee hours worked, 1989-1991, 1993, and 1995

| Mine category | Total roof fall accidents | Total underground hours worked | Incidence rate[1] |
|---|---|---|---|
| All . . . . . | 13,655 | 571,701,998 | 4.78 |
| Extended cut . . . | 7,454 | 314,250,741 | 4.74 |
| Nonextended cut | 6,201 | 257,451,257 | 4.82 |

[1]Incidence rate = $\frac{\text{No. of reported roof fall accidents}}{\text{Total underground hours worked}}$ x 200,000

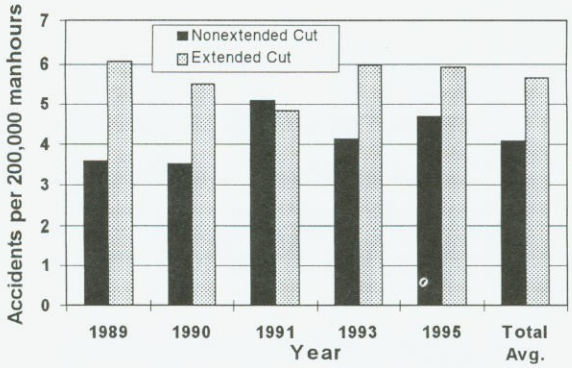



Figure 3. Accident incidence rate in continuous miner sections for extended and nonextended cut mines.

## Accidents in Continuous Miner Sections

Extended cuts are used only on continuous mining sections. Therefore, it is appropriate to examine accidents occurring where continuous mining was used. This would eliminate accidents occurring on longwall sections. Analysis of these data show that most accidents are non-injury type. For instance, in 1995 non-injury accidents on non-longwall sections accounted for 82% of all roof fall accidents. Most of the remaining accidents are classified as "hit by falling rock" (17.6%) with an additional less than 1% termed as "other".

More importantly, consideration must be given to the incidence rates based on man-hours. Continuous miner section accident data for the years 1989 through 1995 are shown in table 2 and figure 3. Note that, the incidence rate for mines using extended cuts was higher than the nonextended cut mines during four out of the five years presented. The average accident incidence rate (per 200,000 man-hours worked) for the five year period was 5.6 for extended cut and 4.1 for nonextended cut. This increase may be attributed to a combination of factors including removal of the miner operator from the protective canopy, noncompliance with approved cutting depth (3) and CM operator positioning (4).

## UNDERGROUND CASE STUDY

An underground, mine-site investigation was conducted to evaluate extended cut mining ground hazards. The study was conducted at an underground mine in Pennsylvania to evaluate the relationship between depth-of-cut and roof conditions during coal extraction. Subsequently, the long-term stability of extended and nonextended cut areas was evaluated. The authors acknowledge that this is one specific mine site and may not represent conditions for all underground coal mines. The study mine operated in the Lower Kittanning Coalbed with an approval to extract 40-ft-deep (12-m-deep) cuts.

## Ground Conditions - Initial Study

The investigation involved an initial study simultaneous with mining and a follow up study 10 months after mining. In-mine mapping included recording the depth-of-cut and roof conditions (figure 4). The immediate roof conditions were evaluated using a rating system modified for extended cuts from one previously used for detecting horizontal stress damage and general mine roof degradation (5, 6). In this study, the roof rating system used a subjective numerical rating of 0 to 5.0, with 0 being the most stable and 5.0 the least stable. A description of this system is shown in the legend on figure 4.

Table 2. Accidents in continuous miner sections for extended and nonextended cut mines

| Year | Nonextended Cut | | | Extended Cut | | |
|---|---|---|---|---|---|---|
| | Accidents | Man-hours | Incidence rate[1] | Accidents | Man-hours | Incidence rate[1] |
| 1989 | 891 | 49,909,654 | 3.6 | 1,043 | 34,454,004 | 6.1 |
| 1990 | 832 | 47,071,848 | 3.5 | 1,099 | 39,772,228 | 5.5 |
| 1991 | 990 | 38,887,806 | 5.1 | 937 | 38,732,580 | 4.8 |
| 1993 | 517 | 24,941,422 | 4.1 | 1,018 | 34,111,621 | 6.0 |
| 1995 | 384 | 16,345,123 | 4.7 | 1,215 | 41,227,482 | 5.9 |
| Total Avg. | 3,614 | 177,155,853 | 4.1 | 5,312 | 188,297,915 | 5.6 |

[1]Incidence rate = $\frac{\text{No. of reported roof fall accidents}}{\text{Total underground hours worked}}$ x 200,000

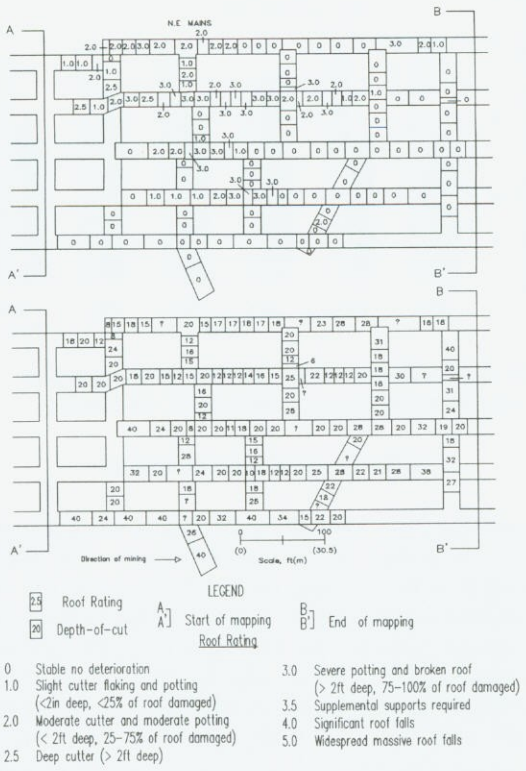



Figure 4. Depth-of-cut and roof conditions in study mine.

Some basic statistics for the depths-of-cut in the study area are shown in table 3. This data contradicts the common misconception that once a mine is granted an extended cut approval, all cuts thereafter will be extended cuts. For example, 69% of the cuts were nonextended, 31% were extended, while only 5.4% of the extended cuts were mined to the maximum allowable depth. From testimonies given by various miner operators and management personnel, almost all extended cuts were taken in stable mine roof. Our study verifies the fact that extended cuts are more likely taken in stable roof because 34 out of 40 extended cuts were mined where the roof was stable. There was a strong tendency for standard cuts to be taken where the mine roof was less stable. However, there were times when standard cuts were taken where the mine roof was stable. For instance, standard cuts were made in stable mine roof areas to keep the faces even, as a result of machine problems, end of shift, two cut rule, etc. Table 4 illustrates that when stable roof conditions were present, 50% of the cuts were nonextended. No extended cuts exceeding 25 ft were made in roof areas with a rating greater than zero. Figure 4 illustrates that, in general, the bad roof and shorter cuts were found on the left side of the section. Since the right side of the section experienced more stable roof conditions, the majority of the extended cuts were mined on that side.

Table 3. Summary mine statistics for underground study

| Statistic | Value |
|---|---|
| Total cuts | 129 |
| Range of depths, ft (m) | 6-40 (2-12) |
| Mean, ft (m) | 20.57 (6.27) |
| Standard deviation, ft (m) | 7.47 (2.28) |
| Percent < 20 ft (6 m) deep | 69.0 |
| Percent > 20 ft (6 m) deep | 31.0 |
| Percent max. 40 ft (12 m) deep | 5.4 |

Table 4. Frequencies for type of cuts in stable roof (Roof Rating = 0)

| Type of cut | Initial Rating | No. of cuts[1] | Percent |
|---|---|---|---|
| Extended | 0 | 34 | 50 |
| Nonextended | 0 | 34 | 50 |
| Total | 0 | 68 | 100 |

[1]Number of cuts includes only those of known depth.

## Ground Conditions - 10 Months After Mining

The study area was examined and remapped approximately 10 months after mining. Roof condition changes were noted and compared to the initial roof conditions, providing an estimate of the long-term stability (figure 5). The long-term stability was analyzed by comparing changes in category ratings in both extended and nonextended cut areas. Table 5 presents information within each rating category that experienced a change in roof conditions. Except for the areas with an original roof condition rating of 3.0, the percent of areas experiencing change was fairly similar. Table 6 compares the changing roof conditions in extended cuts and nonextended cuts. The table reveals that nearly twice as many extended cuts experienced changing roof conditions than nonextended cuts. Note, it is more difficult to evaluate change in areas of poor roof conditions as compared to changes in stable roof areas. This could explain some of the reasons for the larger percentage of observed changes in the extended cut areas.

Table 5. Areas of changing roof conditions based on original roof rating

| Original rating | No. of areas[1] | No. changed | Percent changed |
|---|---|---|---|
| 0.0 | 81 | 23 | 28.4 |
| 1.0 | 14 | 3 | 21.4 |
| 2.0 | 23 | 8 | 34.8 |
| 2.5 | 3 | 1 | 33.3 |
| 3.0 | 20 | 0 | 0.0 |

[1]Number of areas include the 129 cuts of known depth plus 12 areas of unknown depth.

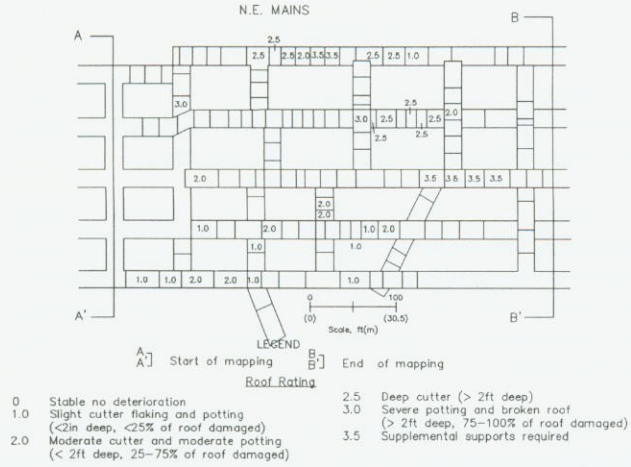



Figure 5. Roof condition changes in study mine.

Table 6. Comparison of changed roof conditions in Extended and nonextended cuts

| Type of cut | No. of cuts[1] | No. changed | Percent changed |
|---|---|---|---|
| Extended . . . . . | 40 | 16 | 40.0 |
| Nonextended . . . . . | 89 | 18 | 20.2 |

[1]Number of cuts includes only those of known depth.

In comparing the time effects of how roof conditions have changed in extended cut or standard cut areas, consideration must be given to the fact that extended cuts are generally taken where the mine roof is stable. Comparisons between the depth-of-cut should occur in areas that have been started in similar mine roof conditions. In this study, four areas were identified that met these conditions (figure 6). For the purpose of analysis, it was determined that the cuts within each area to be compared should be contiguous to ensure similar geologic conditions. Furthermore, only areas with an initial rating of zero were selected because changes in these areas were easily quantified.

The characteristics of the study areas are shown in table 7. There are a total of 37 cuts, three of which were discounted due to cut length uncertainty. Study areas 1-4 each had 6, 10, 7, and 11 cuts, respectively. The table shows cut length and the corresponding mine roof rating at the time of mining and 10 months later. After 10 months, the average mine roof deterioration of the standard cuts was 1.2 and for extended cuts was 1.3. Although fewer standard cuts experienced a change in roof condition, those cuts where the rating changed had nearly twice the rate of severe mine roof deterioration (rating = 3.5) (figure 7).

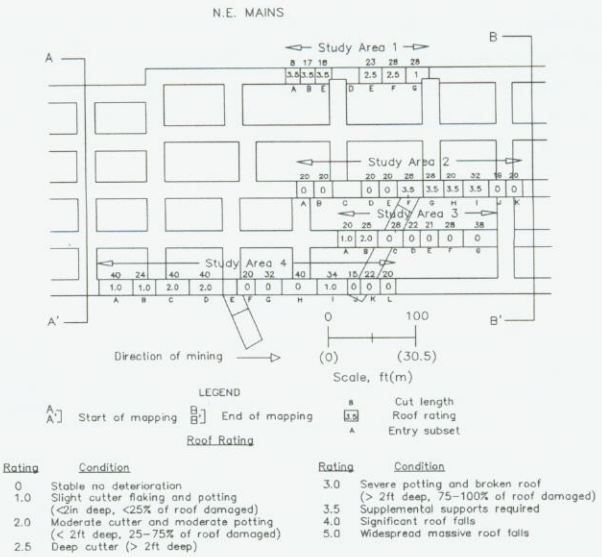



Figure 6. Four study areas.

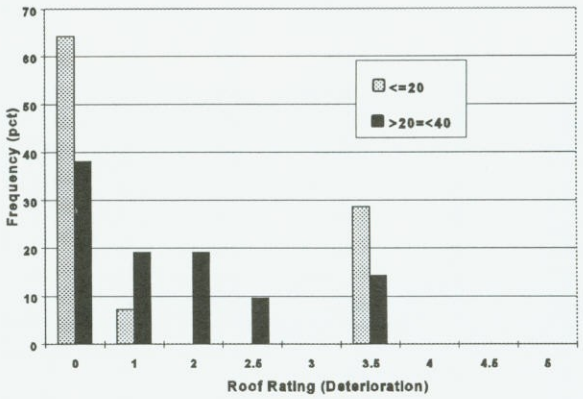



Figure 7. Roof rating 10 months after mining.

## SUMMARY & CONCLUSIONS

The most recent available data shows an increasing trend in extended cut approvals. There are no known reasons to suggest that the increasing trend of extended cut approvals will cease. Therefore, within the next 2 years, more mines may be operating under an extended cut permit than not. From a mine roof fall fatality perspective, the number of fatalities was lower for extended cut mines as compared to nonextended cut mines for all years except 1995 when it was equal. On a mine-wide basis, the accident incident rate between extended and nonextended cuts appears similar. However, when continuous miner accidents are analyzed, the incident rate from accidents due to mine roof falls was higher in mines with extended cuts. This increase may be attributed to a combination of factors including removal of the miner operator from the protective canopy, noncompliance with approval depth, and CM operator positioning.

The underground study revealed that most cuts were not extended but were the normal 20 ft or less. Almost all extended

cuts were taken in areas of stable mine roof. In areas showing initial stable mine roof conditions, a high percentage of extended cuts experienced mine roof damage over time, but in standard cut areas where change occurred it appeared that the change was more severe.

Table 7. Long-term stability of extended and nonextended cuts

| Cuts in Each Study Area | Entry Subset | Entry Type | Cut Length | Roof Rating Before | Roof Rating After |
|---|---|---|---|---|---|
| Area 1 | | | | | |
| 1 | B | Entry | 17 | 0 | 3.5 |
| 2 | A | Entry | 18 | 0 | 3.5 |
| 3 | C | Cross-cut | 18 | 0 | 3.5 |
| 4 | E | Entry | 23 | 0 | 2.5 |
| 5 | G | Entry | 28 | 0 | 1 |
| 6 | F | Entry | 28 | 0 | 2.5 |
| Area 2 | | | | | |
| 1 | J | Cross-cut | 19 | 0 | 0 |
| 2 | A | Entry | 20 | 0 | 0 |
| 3 | B | Cross-cut | 20 | 0 | 0 |
| 4 | D | Entry | 20 | 0 | 0 |
| 5 | E | Entry | 20 | 0 | 0 |
| 6 | K | Cross-cut | 20 | 0 | 0 |
| 7 | H | Entry | 20 | 0 | 3.5 |
| 8 | F | Entry | 28 | 0 | 3.5 |
| 9 | G | Cross-cut | 28 | 0 | 3.5 |
| 10 | I | Entry | 32 | 0 | 3.5 |
| Area 3 | | | | | |
| 1 | A | Entry | 20 | 0 | 1 |
| 2 | E | Entry | 21 | 0 | 0 |
| 3 | D | Entry | 22 | 0 | 0 |
| 4 | B | Entry | 25 | 0 | 2 |
| 5 | C | Cross-cut | 28 | 0 | 0 |
| 6 | F | Entry | 28 | 0 | 0 |
| 7 | G | Cross-cut | 38 | 0 | 0 |
| Area 4 | | | | | |
| 1 | J | Cross-cut | 15 | 0 | 0 |
| 2 | F | Entry | 20 | 0 | 0 |
| 3 | I | Entry | 20 | 0 | 0 |
| 4 | K | Entry | 22 | 0 | 0 |
| 5 | B | Cross-cut | 24 | 0 | 1 |
| 6 | G | Cross-cut | 32 | 0 | 0 |
| 7 | I | Cross-cut | 34 | 0 | 1 |
| 8 | H | Entry | 40 | 0 | 0 |
| 9 | A | Entry | 40 | 0 | 1 |
| 10 | C | Cross-cut | 40 | 0 | 2 |
| 11 | D | Entry | 40 | 0 | 2 |

## REFERENCES


1. Bauer, E. R., D. M. Pappas, and J. M. Listak. Ground Control Safety Analysis of Extended Cut Mining. U.S. Bureau of Mines' Information Circular 9372, 1993, 24 pp.

2. Bauer, E. R., G. J. Chekan, and L. J. Steiner. Stability Evaluation of Extended Cut Mining in Underground Coal Mines. Paper in Proceedings 36th U.S. Rock Mechanics Symposium. (NYRocks '97'), June 29-July 2, 1997, Columbia University., NY. International Journal Rock Mechanics & Mining Science 34:3-4, Paper 302, 1997.

3. Davis, A. Extended Cuts: An Accident Analysis and Inventory of Approvals. MSHA, Div. Saf., Coal Mine Safety and Health, Internal Report, April 15, 1991, 32 pp.

4. Steiner, L. J., F. C. Turin, and C. A. Hamrick. Ergonomic and Statistical Assessment of Safety in Deep-Cut Mining, U.S. Bureau of Mines' Special Publication 18-94, 1994, 174 pp.

5. Molinda, G. M. Personal communication, 1996.

6. Mucho, T. P. and C. Mark. Determining Horizontal Stress Direction Using the Stress Mapping Technique. Proc. 13th Int'l Conf. on Ground Control in Mining, WVU, Morgantown, WV, Aug. 2-4, 1994, pp. 277-289.

large deformations can be used to control the failed or failing roof. Further, cable bolt loads were below the ultimate strength of the cables. When considering the area of the room and the depth of the failure, the loads on the bolts should have been significantly higher, which indicates that a portion of the rock is self supporting with the cables being responsible for maintaining this condition. The postfailure material does not sustain high displacement rates and if properly supported, can form a stable roof. Therefore, if supplemental support such as vertical cables withstand the failure process, or are placed after the failure, the cables can provide a solution to roof control problems created by high horizontal stresses.

## CONCLUSIONS

The room widening experiment did produce a roof fall, as well as a recorded pattern of roof movement and displacement rates leading to the failure. However, much of the movement was related to the instantaneous and transient response of the roof to the mining activity. Although these two phases are important to the overall roof strain, the displacement rates measured during these phases are not pertinent to determining if the roof will fall. During the steady state displacement rate phase, the observed displacement rates were high. These high rates were the result of the substantial load developed in the roof from room widening. Because the rate led to a roof fall, the rate is higher than the critical rate though setting an upper limit for this parameter. An accelerated displacement rate caused by an additional small load placed on the roof from movement occurring at a deeper roof horizon developed just prior to the fall. This movement should not be considered the tertiary creep phase. Although a potential warning, this may not be a reliable indicator since this acceleration developed from an additional roof load.

Because one of the rooms was in postfailure due to horizontal stress damage prior to room widening, the two rooms responded differently. The roof in the postfailure room had larger movements and was sensitive to mining activities in the adjacent room. However, the supplemental support in the form of cable bolts was able to stabilize the roof and prevent a roof fall.

A continuous monitoring system for the extensometers was important in this experiment for the analysis of the complex roof movement, which is further highlighted by the roof movement data that was missed on the roof failure caused by the horizontal stress prior to room widening. Since this test site, other improvements have been made to the mechanical extensometer system that allows for up to five anchor positions connected through a single instrument box. Although a data logger was used in this experiment, the extensometers can be connected to a mine wide monitoring system. However, from a practical standpoint, the use of a continuously monitored extensometer may still be limited to critical areas such as along the beltline, headgate entry, or a test site.

## REFERENCES

1. MacDonald, R. J. and D. A. Payne. Changing Mining Methods at Cape Breton Development Corporation. CMI preprint #48, Presented at the 94th Annual Meeting, Montreal, 1992, 13 pp.

2. Stace, L. R. and P. W. Lloyd. Managing A New Technology-An Update of UK Rockbolting Story. Proceedings 15th International Conference on Ground Control in Mining. Aug. 13-15, 1996, Golden, CO, pp. 333-347.

3. Obert L. and W. I. Duvall. Rock Mechanics and The Design of Structures In Rock. John Wiley, NY, 1967, 650 pp.

4. Serbousek, M. O., H. N. Maleki, and J. R. M. Hill. Use of Ground Movements for Detection of Roof Stability Problems. Paper C4 in the Proceedings of the 8th International Strata Control Conference, Dusseldorf, 1989, 18 pp.

5. Maleki, H. N. and J. R. McVey. Detection of Roof Instability by Monitoring the Rate of Roof Movement. USBM RI 9170, 1988, 12 pp.

6. Mark, C., R. Watts, T. E. Marshall, M. O. Serbousek, and F. Carr. Using Computerized Mine-Wide Monitoring For Ground Control. Preprint 94-168, Presentation at the SME Annual Meeting, Albuquerque, NM, Feb. 14-17, 1994, 8 pp.

7. Pothini, B. R. and H. von Schonfeldt. Roof Fall Prediction at Island Creek Coal Company. Proc. 1st Intl. Symp. on Stability in Coal Mining, Vancouver, 1978, pp. 215-227.

8. Campoli, A. A., D. Rebuck, T. P. Mucho, and G. M. Molinda. State-Of-The-Art Room-And-Pillar Retreat Mining In The Kittanning Coalbed. Proceedings 15th International Conference on Ground Control in Mining. Aug. 13-15, 1996, Golden, CO, pp. 269-285.

The critical displacement rate has been used to identify the divide between those rates that result in failure and those rates where the roof remains stable (*4*). A number of investigations have determined the critical rates at specific coal mines though each investigation required a large number of extensometers. In the western U.S., critical displacement rates observed at two different coal mines were 0.06 to 0.08 cm/d (0.025 to 0.032 in/d) (*5*). For longwall entries in Alabama, the critical rate was found to be about 0.06 cm/d (0.025 in/d) though the dynamics of the mining, as well as changing geology, complicated the determination of the critical rate (*6*). Subsequent increases in loads not only increased the steady state displacement rate but also added new components of instantaneous strain and transient creep. For an investigation at a coal mine in Virginia, the rate was found to 0.25 cm/d (0.1 in/d) for 4 way intersections (*7*). There appears to be a definite range for the critical displacement rate although site specific mining and geologic conditions will affect and determine the critical rate, while the load will determine the displacement rate.

Because the location of roof falls is unpredictable, to obtain further information on displacement rates and patterns that result in a roof failure, the National Institute for Occupational Safety and Health, Pittsburgh Research Center, conducted a room widening experiment in cooperation with RoxCoal. In this investigation, two rooms were widened with one of the rooms containing supplemental support. A roof fall developed in the room without the supplemental support where extensometers recorded the displacement rates and patterns leading to the failure.

## MINE LOCATION AND GEOLOGY

The mine where the investigation was conducted is located in the lower Kittanning seam in Somerset County, Pennsylvania. At this site, the immediate mine roof consists of a moderate strength shale and sandy shale with a Coal Mine Roof Rating ranging from 50 to 60 (*8*). The coal seam which is 2.3 m (7.5 ft) thick is extracted by room-and-pillar mining with retreat pillar recovery. Development entry widths range from 4.9 to 5.5 m (16 to 18 ft).

## TEST ROOMS AND INSTRUMENTATION

Figure 1 shows the two test rooms, 5S1 and 5S2, that were mined as well as the instrumentation plan used to monitor roof movement. In the two rooms, the primary support consisted of 1.8 m (6 ft), 1.6 cm (5/8 in) diameter, fully grouted rebar installed on 1.2 m (4 ft) centers. Supplemental support in the form of 6 cable bolts were placed in 5S1 prior to room widening. The cable bolts were made from a 1.5 cm (0.6 in) in diameter, 7 strand steel cable with a rated ultimate capacity of 263 kN (58,800 lbf) and were 3.6 m (12 ft) long with a 1.2 m (4 ft) resin-grout anchor. No supplemental support was installed in room 5S2.

In each room, roof movements were measured by one sonic probe extensometer and two modified Miner's Helper[2]

[2]Reference to specific products does not imply endorsement by the National Institute for Occupational Safety and Health.

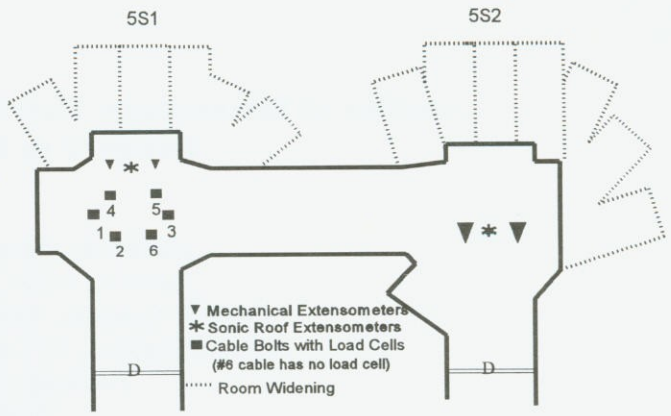



Figure 1. Plan view showing the two test rooms, 5S1 and 5S2, the instrumentation, cable bolts and room geometry after widening.

extensometers. For the sonic probe extensometer, magnetic anchors were placed in the borehole at a 0.3 to 0.45 m (1 to 1.5 ft) spacing, starting 10 cm (4 in) above the roof line. This provided 16 measuring points in the roof to a depth of 5.8 m ( 19 ft). The sonic probes remained in the roof throughout the duration of the experiment. The Miner's Helper extensometers, a mechanical rod type extensometer, were modified to allow for three positions to be monitored with the anchors placed at 1.2, 2.4, and 4.0 m (4, 8 and 13 ft) into the roof. The base reference for this extensometer was the roof line. In addition to the extensometers in room 5S1, hydraulic U-cells were installed on 5 of the cable bolts to monitor cable loads at the bearing plate. The extensometers were installed just after room development and 3 days prior to room widening, while the cable bolts and load cells were installed on the day the rooms were widened.

All the instrumentation was connected to data loggers which provided a continuous record of roof movements and cable loads. However, the data loggers were not connected to the instrumentation until just prior to room widening, so there was no continuous record of roof movement from development to room widening. To enable the mechanical extensometers to be read by the data logger, string potentiometers were attached to the rods. Monitoring of the instrumentation continued for a period of 21 days.

## ROOM WIDENING AND ROOF FALL

Three days after development, the test rooms were widened with table 1 showing the mining sequence. The room widening was started in 5S1 where figure 1 shows how the rooms were developed. During widening of 5S1, 0.3 to 0.6 m (1 to 2 ft) of the immediate roof fell in the newly developed cuts. Room widening took approximately 1.5 h in 5S1 with mining of room 5S2 starting 30 minutes after the completion of S51. Only in one of the cuts made on the right side of the room was there any instability noted in the lower portion of the roof of 5S2. During mining, timber posts had been set to protect the continuous miner. These posts were knocked down as each room was completed, leaving the newly developed areas unsupported. Both rooms were widened to

# Analysis of Extensometer Data from a Room Widening Experiment Designed to Induce a Roof Fall

*Dennis R. Dolinar,* Mining Engineer
*David C. Oyler,* Mechanical Engineer
*Craig S. Compton,* Mining Engineering Technician
National Institute for Occupational Safety and Health
Pittsburgh Research Center
Pittsburgh, PA

## ABSTRACT

Roof falls, even of supported roof, still constitute a major hazard in underground mines. However, associated with any fall or instability is a pattern of roof movement. Therefore, the National Institute for Occupational Safety and Health, Pittsburgh Research Center, has been conducting research into the development of practical extensometer systems that can be used to measure this displacement and to determine if a roof fall may occur, thus increasing miner safety. For extensometers to be used in the detection of potential roof falls in coal mines, an understanding of the movement and displacement rates that will lead to roof failure is required. Because roof falls are unpredictable, it is often very difficult to obtain this information. Therefore, in a coal mine in the lower Kittanning seam in Pennsylvania, a room widening experiment was conducted to intentionally cause a roof fall while roof movement data was collected.

In this experiment, two adjacent rooms 5.5 m (18 ft) wide supported with 1.5 m (5 ft) resin-grouted bolts and instrumented with extensometers were widened to 9 m (30 ft). In one of the rooms, 3.6 m (12 ft) cable bolts were installed as supplemental support. In the room with no additional support, a roof fall occurred 72 h after the room was widened. Much of the 3 cm (1.2 in) of movement in this room resulted from the instantaneous and transient response to mining with displacement rates up to 7.6 cm/d (3 in/d) being measured. This was followed by a steady state displacement phase with a rate of 0.43 cm/d (0.17 in/d). Just 12 h before the fall, movement deeper in the roof caused the rate to accelerate to 1.1 cm/d (0.44 in/d). The roof in the room with the supplemental cable support did not fall even though the total roof deformation was over 7.6 cm (3 in). Significant roof movements and strains in the cabled room were detected to a depth of 3 m (10 ft) while maximum cable loads were over 180 kN (40,000 lbf). Essentially, the roof was in postfailure with the cables maintaining the material, while roof stability was indicated by a steady state displacement rate of only 0.025 cm/d (0.01 in/d) at the end of the test.

## INTRODUCTION

Roof falls still represent a significant hazard to the safety of underground coal miners even when the roof is supported. Monitoring of roof movement with extensometers is a method that has been used to identify unstable roof conditions, and thus, extensometers have the potential to reduce accidents or trigger action, such as the placement of supplemental support (*1, 2*).[1] Both the total roof movement or strain and the roof displacement rate can provide information relevant to roof stability. For roof movement, the timing of the placement of the extensometer is important in determining the total strain, while the roof displacement rate is much less sensitive to this parameter. Therefore, the displacement rate has an advantage over using the total movement or strain as a method of determining instability. However, a displacement rate that leads to instability or a roof fall must be established, which can require a large number of measurements to develop.

Roof displacement rates are a function of the time dependent properties of the roof material and/or structure. Therefore, the displacement rates can be considered in terms of material creep parameters. In general, rock will exhibit an initial instantaneous movement to load or stress as well as a time dependent movement. The time dependent response is composed of a transient, steady-state and tertiary or failure phases (*3*). Following the instantaneous phase, the transient phase occurs whose affects diminish exponentially with time. The steady state phase is the long-term creep rate that is linear over time and is the displacement rate that is considered in evaluating the potential for a roof fall. The steady state creep level is dependent on and proportional to the roof load or stress. If the steady state creep rate is sufficient, a tertiary phase may develop where rate acceleration occurs leading to failure. However, the tertiary phase can not always be identified and, therefore, may not be a reliable indicator of failure. Further, roof failures also occur under both the instantaneous and the transient phases.

[1]Italic numbers in parentheses refer to items in the list of references at the end of this report.

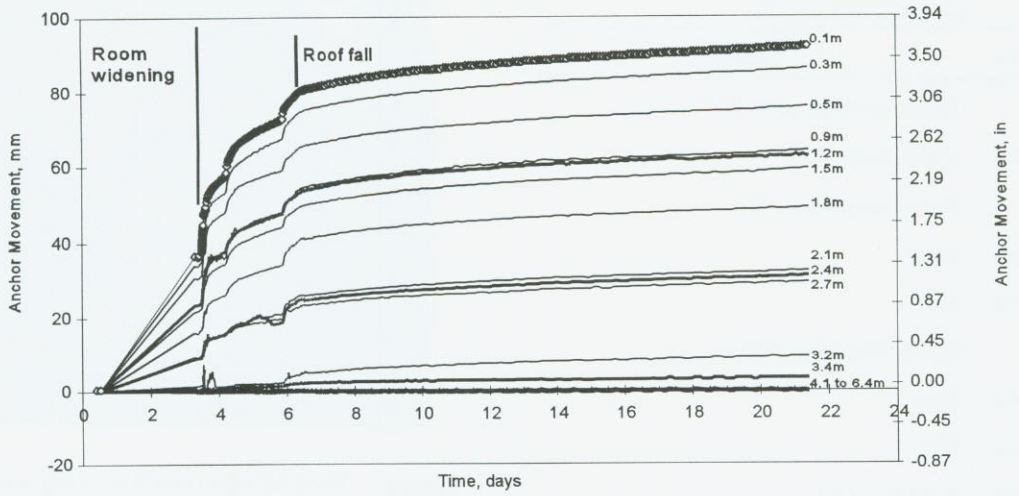



Figure 4. Roof displacement measured by the sonic extensometer in 5S1.

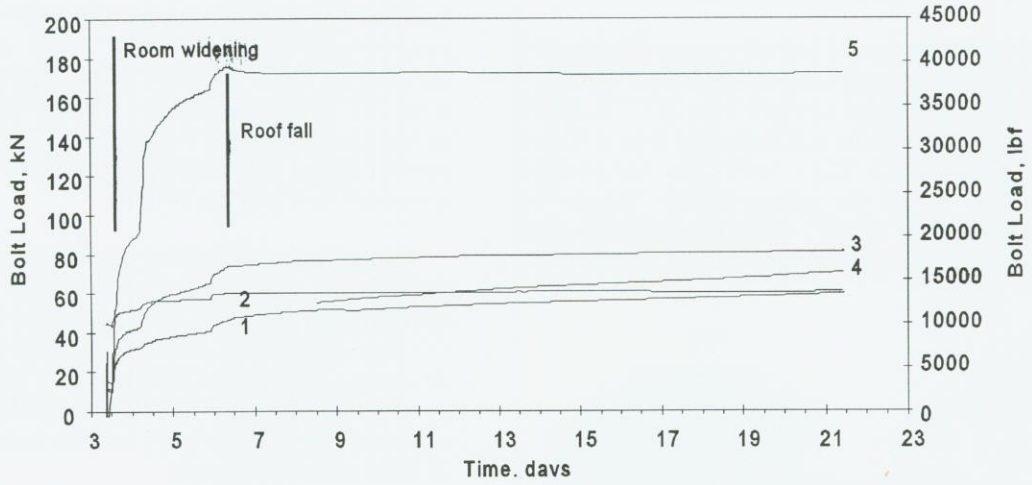



Figure 5. Cable bolt loads measured in 5S1.

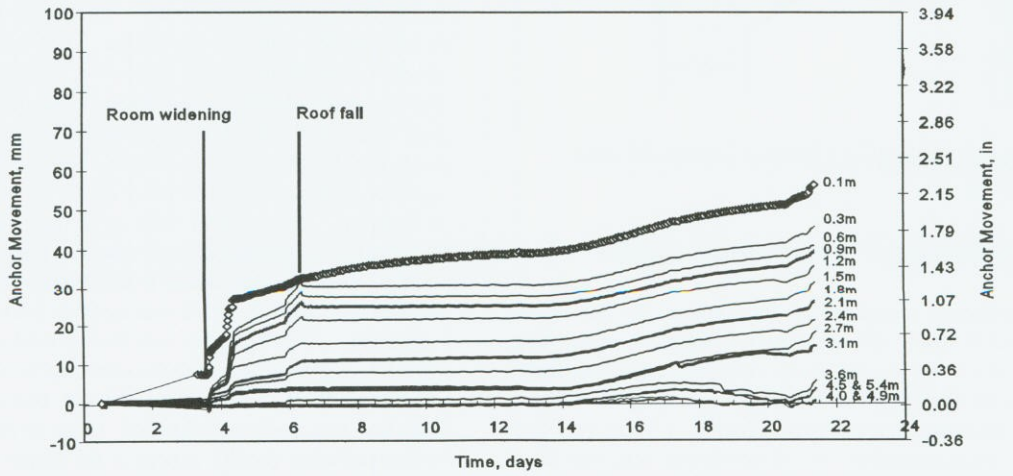



Figure 6. Roof displacement measured by the sonic extensometer in 5S2.

Table 1. Time when events occurred in room widening experiment.

| Day | Time | Event |
|---|---|---|
| 0 | - | Room development, 5S1 and 5S2 |
| 3 | 09:35 | Cable Bolts, 5S1 |
| | | Room Widening, 5S1 |
| 3 | 12:17 | Start |
| 3 | 13:25 | End |
| | | Room Widening, 5S2 |
| 3 | 13:52 | Start |
| 3 | 15:10 | End |
| 6 | 09:46 | Roof fall, 5S2 |

approximate 9 m (30 ft) and upon completion had the same approximate geometry and amount of coal support removed.

Six days after development and 3 days after room widening, the roof fell in room 5S2 and the interconnecting crosscut (figure 2). Only a small portion of the fall extended into room 5S1. The height of the fall was above the primary bolt horizon (1.8 m, 6 ft) and possibly up to 2.4 to 3.6 m (8 to 12 ft). In 5S2, the roof fall came to within 0.3 m (1 ft) of the instrumentation, though the instrumentation did survive. Figure 3 shows the roof fall in room 5S2. The instrumentation was monitored until 15 days after the roof fall.

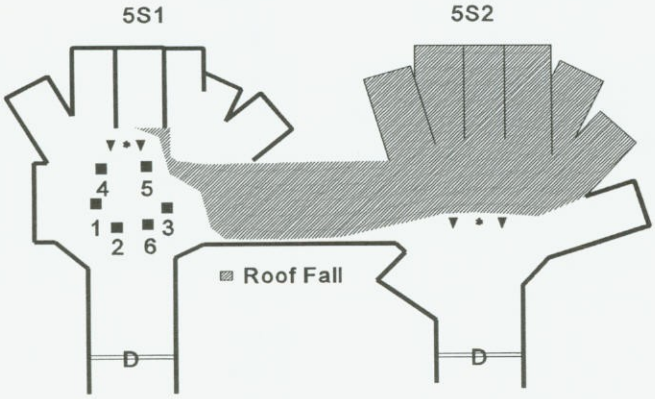



Figure 2. Plan view showing roof fall that occurred 3 days after room widening.

## ROOF MOVEMENT AND CABLE LOADS

The roof movements measured at each anchor by the sonic probe extensometer in room 5S1 are shown in figure 4, where the top anchor at 6.1 m (20 ft) is used as the reference (assumes little or no movement at this height in the roof). A total of 9.1 cm (3.6 in) of roof movement was recorded with 3.8 cm (1.5 in) occurring prior to room widening. Roof movement was seen to a depth between 3.0 and 3.5 m (10 and 11.5 ft). The roof responded immediately to the room widening of both 5S1 and 5S2, while

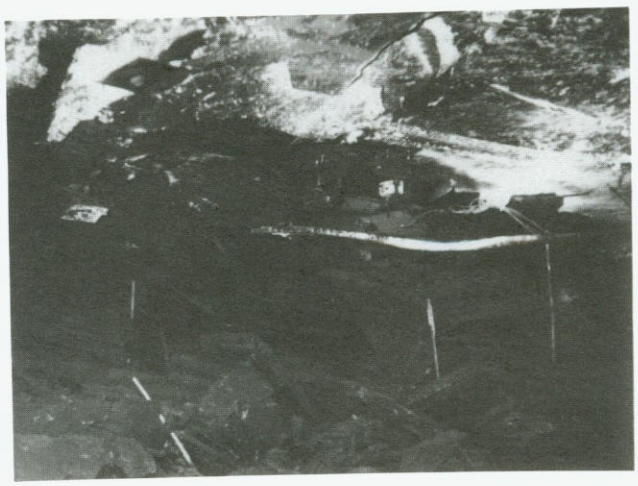


Figure 3. Roof fall observed from outby instrumentation, room 5S2.

there was an accelerated period of roof movement just prior to the roof fall. The stair step nature of the movement is caused by the sensitivity of the roof to changes in equilibrium conditions in the two rooms from mining. Most of the movement from room widening to the roof fall is the result of instantaneous and transient strain (85 to 90%) with only a small portion developed from the steady state or long-term displacement rate. Following the roof fall, the roof appears to have stabilized with less than 0.5 cm (0.2 in) of movement over a 14 day period.

Figure 5 shows the cable bolt loads measured by the load cells. Because the cables bolts were installed just prior to room widening, they did not see the displacement that occurred in room 5S1 after development. However, the cable loads still increased by an average of 89 kN (20,000 lbf) with a maximum load of nearly 179 kN (40,000 lbf) recorded on one cable just as the roof fall occurred. The cables did respond to the same roof movements that affected the extensometers.

In room 5S2, the roof movements measured by the sonic probe extensometer are shown on figure 6. During development and prior to room widening, little movement occurred except in the lower 0.3 m (1 ft) of the roof. This is the same part of the roof that fell in 5S1 and one lift in 5S2. This lower portion of the roof acted independent of the main roof throughout the experiment. Upon room widening, the instantaneous roof response resulted in only about 0.8 cm (0.3 in) of movement of the main part of the roof, much less than was seen in room 5S1. A second period of rapid roof movement occurred about 14 h after mining had been completed. Room 5S1 also saw this same delayed response through the interconnecting crosscut. There was then a period of continued roof movement at a decreased rate for about 36 h. Just prior to the roof fall, there was another period of accelerated roof movement. At failure, the roof had moved about 3.2 cm (1.25 in) with the depth of movement extending to between 3.5 and 4.0 m (11.5 and 13 ft). Following the fall, there was a small upward defection of a portion of the roof. Little or no movement was seen in the roof after the fall except in the lower roof until 7 days after the roof fall. Roof movement then appears to be taking place along the edge of the roof fall, starting about 7 days after the roof

failed. Even at this time, roof movement extended up to 3 m (10 ft) well above the length of the primary support. With room widening, as expected, there was an instantaneous response to the removal of the supporting coal. However, larger movements and displacement rates than in 5S2 were recorded. Over a period of 7 h, starting with room widening, the roof moved 2 cm (0.8 in) starting at a displacement rate of 17 cm/d (6.6 in/d) for the 1.5 h required to mine the room. This was followed by a rate between 3 to 4.3 cm/d (1.2 to 1.7 in/d) for the rest of the period. There was no delay in the response to room widening as was seen in 5S2, while the roof in 5S1 was sensitive to the activities occurring in 5S2. In response to the delayed movement in 5S2, there was another period of accelerated movement where for 6.5 h the average displacement rate was 2.1 cm/d (0.85 in/d). Finally, just before failure, another period of increased acceleration occurred with an average displacement rate of 1.1 cm/d (0.43 in/d) over a 11.5 h period. Again, both of these last movements show the sensitivity of the roof to equilibrium changes and strongly suggests that the roof was in postfailure.

When the fall occurred, the average strain in the supported section of the roof was 2.1% with a maximum strain of 8% and a total movement of 9.1 cm (3.6 in). After the fall, the roof did reach a more stable equilibrium. The displacement rate averaged 0.05 cm/d (0.02 in/d) until the end of the monitoring period and was decreasing. At the end, the displacement rate was only 0.03 cm/d (0.01 in/d). Obviously, there were very large displacement rates measured from room widening to the roof fall. However, these rates must be considered as instantaneous or transient displacement rates. Although a roof fall could have occurred during this phase with sufficient strain, the steady state displacement rate appears to indicate the roof has achieved equilibrium or stability.

## Room 5S2

Except for the lower one foot, the roof in the room behaved as a competent intact member through development. Upon room widening, total room response to the initial instability was not completed until 24 h after the event with the largest response occurring 14 h after mining was completed. Essentially, some time was required for the new roof loads to open separations in the supported roof of the room and crosscut. The total movement from the initial room widening was 1.8 cm (0.7 in) with maximum displacement rates during this period of 3.3 and 7.9 cm/d (1.3 and 3.1 in/d) for periods of from 1 to 2 h. Figure 10 shows the roof strains for selected times. The average roof strain over the bolted section after widening was 0.6%. Up to this point, the roof movement and strain are considered to be instantaneous and transient resulting from the creation of the wider opening.

The roof movement then slowed considerably for a period of 36 h approaching a steady state phase, where this is the displacement rate that is considered for determining a critical rate leading to a roof fall. The displacement rate averaged 0.43 cm/d (0.17 in/d) for this period. Although this is the rate that resulted in the roof fall, the critical rate would be lower.

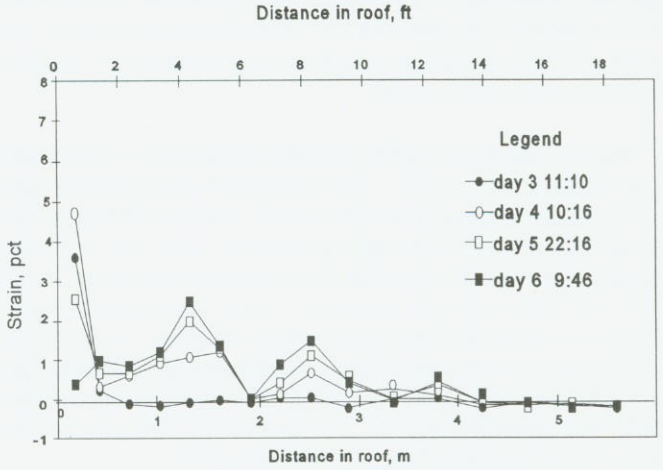



Figure 10. Strain levels measured in roof, 5S2.

Twelve hours before the roof fall, another accelerated period of roof movement occurred marked by movement at a deeper roof horizon. Essentially, this movement caused an additional load to be placed on the roof. The initial displacement rate was almost 5 cm/d (2 in/d), though for only a 30 minute interval followed by a rate of 1.1 cm/d (0.44 in/d) for an 11 h and 30 minute period. However, with a small increase in the load or strain, there was a substantial increase in the displacement rate. The roof strains are much lower than those for 5S1 and averaged only 0.8% at failure, but this is the strain at the edge of the fall where the strain toward the center would be higher. Also, significant roof movement had developed above the bolted horizon to depths of 2.1 to 2.4 m (7 to 8 ft).

The steady state displacement rates of 0.43 and 1.1 cm/d (0.17 and 0.44 in/d) are quite high, where the second rate shows how sensitive the system was to small load changes and how close the system was to failure. With widening, the roof was pushed close to failure by the substantial load or strain produced by the increased roof span. This resulted in a high steady state displacement rate that would lead to a roof fall. Though this rate is above the critical displacement rate, an upper limit is set for this parameter. The final period of accelerated roof movement, before failure, could be seen as another warning of the failure. However, this final period cannot be considered the tertiary creep phase, but the result of the additional load placed on the roof thus increasing the displacement rate.

## CABLE BOLTS

After room widening, even though the roof was in postfailure, the roof did not fall in 5S1. Essentially, the cable bolts prevented a roof fall. The cables were able to bring the postfailure material in the roof into equilibrium and allow for 5.1 cm (2.0 in) of displacement after installation. Significant roof deformations extended up to a depth of 3.5 m (11.5 ft), but did not go above the length of the cable. Roof displacement rates were only 0.025 cm/d (0.01 in/d) at the end of the test indicating a stable condition. This shows that cables and other similar types of support that can take

fall and continuing to the end of the experiment. Because the movement was not seen with the mechanical extensometers, it is not known whether this movement is real or the result of a problem with the sonic extensometer.

Figure 7 shows the roof movements measured by a mechanical rod extensometer in 5S1. The mechanical extensometers gave similar results as the sonic extensometers, except with less vertical detail because of wider spaced anchors. For 5S2, the total displacement measured by the deepest anchor was about 3.0 cm (1.2 in), close to that measured by the sonic extensometer. However, because of the loss of detail, the lower 1.2 m (4 ft) of roof appears to have moved during development instead of just the lower 0.3 m (1 ft). After the roof fall, the measurements indicate little roof movement in 5S2. Because of the large movements, some of the mechanical anchors slipped in 5S1.

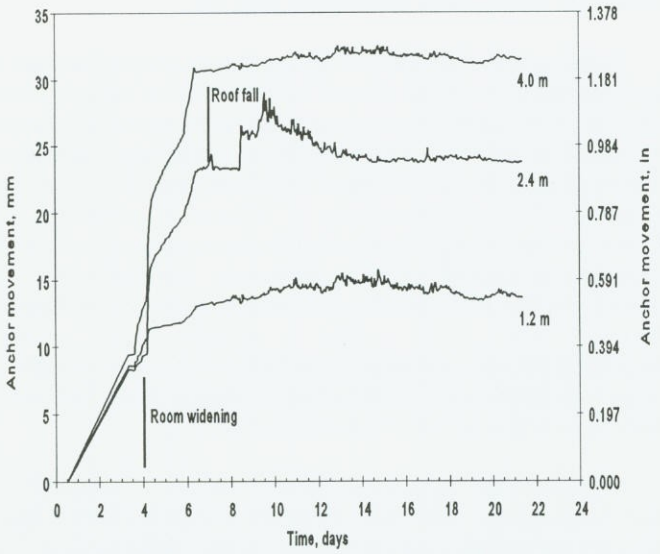



Figure 7. Roof displacement measured by mechanical extensometer in 5S2.

## DISPLACEMENT RATES AND ROOF FAILURE

### Room 5S1

The roof in 5S1 had already failed prior to room widening. Therefore, any subsequent movement must be interpreted as postfailure roof movement. Apparently, the roof was damaged from the horizontal stress. Previous stress mapping at the mine showed some evidence of stress damage but no definite failure direction was indicated thus, raising some doubt as to the nature and direction of the stress field. However, during the room widening experiment, roof cutters in the crosscuts just outby the test rooms (figure 8) gave clear evidence of damage caused by the horizontal stresses and from these cutters a stress direction could be determined. Room 5S1 was developed and widened first, apparently into the stress field thus creating a stress shadow for the entry leading to 5S2. This reduced the potential for stress damage to develop in the 5S2 test area. During room widening, the lower 0.3 and 0.6 m (1 to 2 ft) of the immediate roof fell in 5S1, while this only occurred in one lift driven in a near east-west direction in

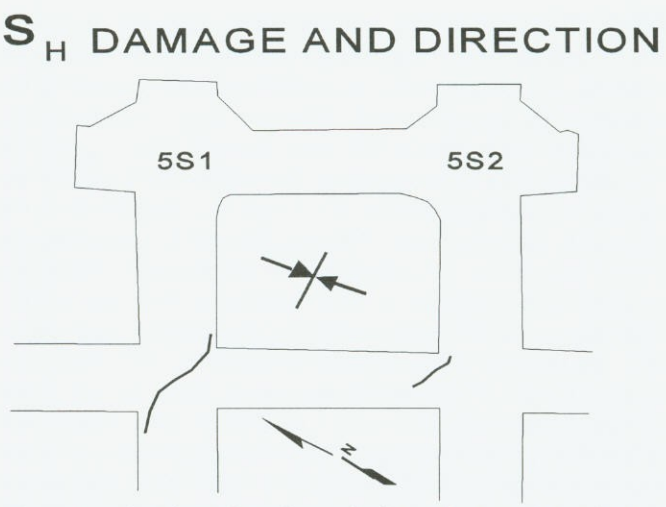



Figure 8. Direction of maximum horizontal stress determined from stress damage.

5S2. The roof failure in 5S1 may have created a stress concentration where the room was widened resulting in the failure of the lower roof. Because this roof failure and stress concentration did not occur in 5S2, only when the lift was taken perpendicular to the stress direction did the lower roof fall as the room was widened into the stress field. The stress damage indicates that the principal horizontal stress is in the north-south direction with the rooms driven in a northeast orientation. During the failure process, the roof had moved 3.8 cm (1.5 in) in less than 3 days or at an average rate of 1.3 cm/d (0.5 in/d). Unfortunately, the instrumentation was not connected to the data logger during this period. Therefore, the pattern of roof movements resulting in failure is not known. However, such fast displacement rates over a very short period of time is a good indicator of a roof failure caused by the horizontal stress. Essentially with this type of failure, little advanced warning will be seen from the displacement rate until the failure is well developed.

Figure 9 shows the calculated strains in the roof at specified times. Prior to room widening and the installation of cable bolts, the average roof strain through the bolted section was 1.1% with a maximum strain of 2%, an indication that the roof had probably

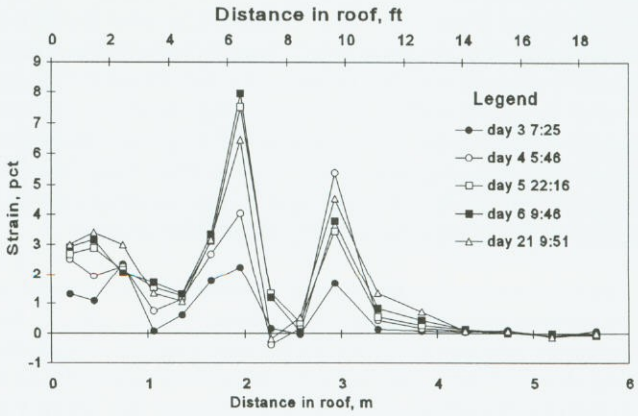



Figure 9. Strain levels measured in roof, 5S1.

# Airbag Support for Ground Control in Thin Seam Coal Mining

*Fan Shaogang,* Engineer
*Kang Lijun,* Senior Engineer
Central Coal Mining Research Institute
P.R. CHINA

*Yu Kaiqing,* Senior Engineer, Manager
Kekeng Colliery of Shangjing Coal Bureau
Yongan, P.R. CHINA

*Zhang Zhanggen*, Senior Engineer, Chief Engineer
Wangzhuang Colliery of Lu'an Coal Bureau
Changzhi, P.R. CHINA

## ABSTRACT

In this paper, the airbags' structure and technical characteristics and its applications in China are described. Based on the practice of the airbags in mining thin seams, the effects on ground control are discussed. This paper also analyzes the interaction mechanism between the airbag and surrounding rocks.

## INTRODUCTION

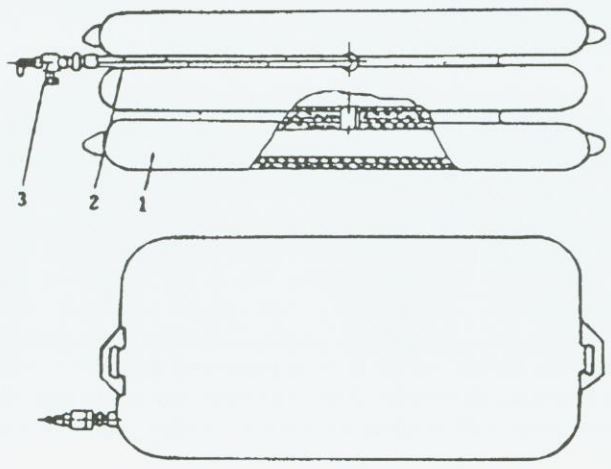
The thin seam reserves in China is very rich, the minable reserves of which accounts for 20% of the total recoverable reserves. However, the thin coal seam production only makes up 11% of the whole coal production in 1996, and this percentage is still decreasing. The main reason is that the mining conditions are poor and the mechanization level of mining in thin seams is low. The PS Series Airbags were successfully developed in 1991 by Beijing Research Institute of Coal Mining, together with the factories and mines concerned. In recent years, the airbags have been used in about 20 faces all over China, with good economic profits being achieved. In order to improve the performances of the airbags and optimize the structural parameters and mechanical characteristics, a further research on the control characteristics of the airbags to the surrounding rocks has been carried out.

## STRUCTURE AND FEATURES OF AIRBAGS

The airbag is a new kind of support for the faces in thin seams, using compressed air as its working medium. In the face, the airbag can be moved either by hand or by the driving mechanism. The airbag with driving mechanism is called self-advancing airbag.

### Structure of Airbag

The airbag is composed of a rubber bag, high pressure hoses and a cut-off valve. The rubber bag consists of two or three nylon cord bags, which are put into an integral unit after vulcanization. Meanwhile, the self-advancing airbag needs to have a flange connecting with the driving mechanism. The structure and technical parameters of the airbag are shown in Figure 1 and Table 1.




**1 - Rubber bag 2 - High pressure hose 3 - Valve**

**Fig. 1 Diagrammatic Sketch of Airbag**

**Table 1. Main technical parameters of airbags**

| Index | Type | | | |
|---|---|---|---|---|
| | PS0.8 | PS1.0 | PSZ1.0 | PS1.2 |
| Working Height | | | | |
| Hmax (mm) | 800 | 1000 | 1015 | 1200 |
| Hmin (mm) | 300 | 400 | 415 | 500 |
| Setting Load (kN) | | | | |
| Air Pressure 0.4MPa | 104~350 | 180~360 | 180~360 | 127~360 |
| Air Pressure 0.5PMa | 130~440 | 220~450 | 220~450 | 160~450 |
| Outside Dimensions | | | | |
| Length (mm) | 1,400 | 1,400 | 1,400 | 1,400 |
| Width (mm) | 800 | 800 | 900 | 800 |
| Height (mm) | 300 | 400 | 415 | 500 |

## Technical Features of Airebags

***Airbags have high setting load and working resistance.*** If pressurized with compressed air, the airbag will expand between the roof and floor. When the air pressure inside the airbag reaches the rated value, it also reaches its rated setting load. When the roof converges during mining, the airbag begins to bear the additional load of the rock strata. While the airbag's volume contracts, its inside pressure increases. In the meantime, the contacting area between the airbag and the roof or floor increases correspondingly, and its supporting resistance is raised. The compressed air inside the airbag follows the gaseous equation of the isothermal process. That is, the product of the volume and pressure keeps constant.

The working resistance of the airbag equals to the product of the inner pressure and the contacting area between the airbag and the surrounding rock. The theoretical calculation formula of the airbag's working resistance(F) is:

$$F=\left[L_a-\frac{\pi(H-\Sigma h)}{2K}\right]\left[L_b-\frac{\pi(H-\Sigma h)}{2K}\right]\left\{(P_o+P_\sigma)\frac{(H_o-\Sigma h)\left[L_aL_b-\frac{\pi(L_a+L_b)(H_o-\Sigma h)}{4K}+\frac{\pi(H_o-\Sigma h)^2}{6K^2}\right]}{(H-\Sigma h)\left[L_aL_b-\frac{\pi(L_a+L_b)(H-\Sigma h)}{4K}+\frac{\pi(H-\Sigma h)^2}{6K^2}\right]}\right\} \quad \text{-----(1)}$$

where $L_a$ -- longitudinal half-length of the airbag
$L_b$ -- transversal half-length of the airbag
$H_0$ -- primary supporting height of the airbag
$\Sigma h$ -- total thickness of the airbag's wall
$P_0$ -- primary inner pressure
$P_\sigma$ -- atmospheric pressure
K -- number of bags
H -- working height of the airbag

From equation (1), we know the working resistance of the airbag is mainly determined by the primary inner pressure, the primary supporting height and the working height. In fact, both contacting area and inner pressure will vary with roof convergence, mining height, etc.. Under the conditions of the primary height of the airbag $H_0$=1000mm, the primary inner pressure $P_0$=0.5MPa, the working characteristic curves of the laboratory measurement and theoretical calculation over Type PS1.0 -100/5 Airbag is shown in Figure 2.

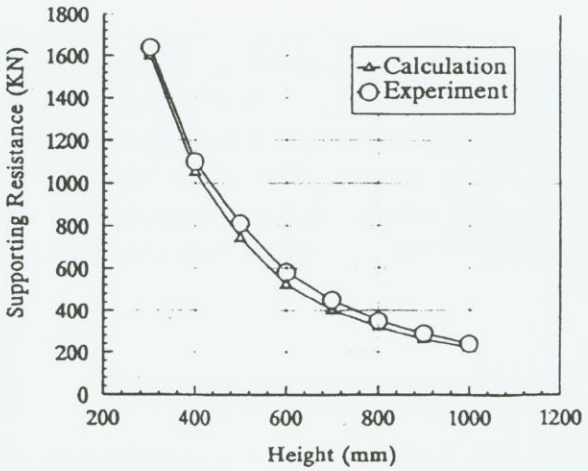



**Fig. 2 Working Characteristic Curves of Airbag**

***Airbags can effectively impede the roof's horizontal thrust.*** Since the airbag is flexible and has comparatively large supporting area, it can contact closely with the roof & floor pressurized with the compressed air. When the roof convergence and horizontal movement occur, the frictional resistance between the airbag and roof will reduce the horizontal movement of the roof (the frictional factor between the rubber and rock is up to 0.8~0.9).

***Airbags can resist a strong impact load.*** During roof weighting, the roof will produce an impact load on the supporting equipment. For the hydraulic supports and single props, the impact load can be mainly relieved by releasing liquids through the safety valve. For the airbag, its shape can be changed quickly because its rubber casing is flexible and its

working medium - air can be compressed several times over. Therefore, when the impact load hits, the airbag can rapidly contract to absorb the energy of the impact load. And the airbag's supporting resistance can be raised quickly to reach the equilibrium state of supporting.

***With small specific pressure, airbags are suitable for the loose floor.*** Since the airbag can contact with the rock flexibly and closely and the contacting area is large, a uniform resistance is imposed on the roof & floor, and the specific pressure is very small. No failure occurs in the rock surface, owing to low specific pressure-- not more than 1.2 MPa. The integrity and stability of the roof & floor are kept very well and the phenomenon of supports' punching into the floor will never occur.

In addition, the airbag has good performance features, such as simple structure, easy maintenance, high safety coefficient ( its working pressure is 5-6 bar and burst pressure is 20 bar, so its safety coefficient is 3.0-4.0), large magnification ratio, long life-span, strong capacity to resist stabbing(generally, the shape of the airbag's shell is changed with the shape of the roof).

## APPLICATION OF AIRBAGS

Since 1991 when they were successfully developed, the airbags have been applied in Zaozhuang Coal Bureau, Kailuan Coal Bureau, Tianfu Coal Bureau, Shangjing Coal Bureau, Zhongliangshan Coal Bureau, Yongrong Coal Bureau, Wangyang Coal Mine and Datai Coal Mine ,etc.. Under seam conditions featuring dip angle 0 ~ $90^0$, shear height less than 1.0 m and the roof medium-stable, the airbags have been successfully used. Table 2 introduces the comprehensive applications of the airbags and Figure 3~6 introduce airbags layouts in the faces. In figure 3~6, 1 refers to haulage roadways, 2 refers to airways, 3 refers to airbags, 4 refers to hydraulic (frictional or wooden) single props.

**Table 2 Applications of airbags in China**

| Name of Mine | Thick-ness (m) | Dip Angle (°) | Roof | Floor | Airbags Layout |
|---|---|---|---|---|---|
| Zhu zibu | 0.6~ 0.8 | 14~ 17 | lime-stone | mud-stone | Replace wooden chock |
| Kekeng | 0~ 1.17 | 25~ 35 | mud-stone | mud-stone | Replace close wooden prop |
| Wang yang | 0.7~ 1.25 | 2~ 3 | shale | shale | Replace close frictional prop |
| Datai | 0.97~ 1.3 | 67 | powder sand-stone | fine sand-stone | Replace close single hydra. prop |
| Yang liuba | 0.39~ 2.9 | 69~ 85 | powder sand-stone | bauxite shale | Replace close wooden prop |

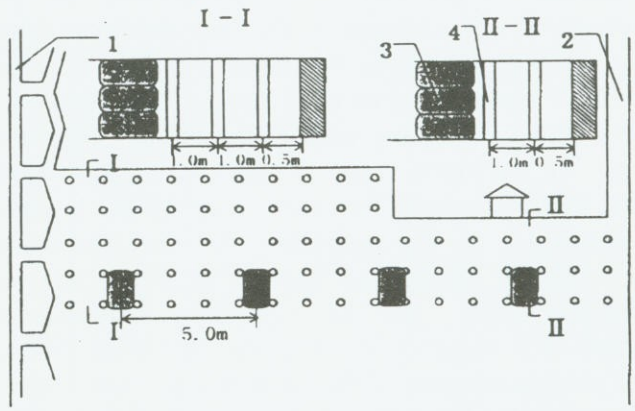



**Fig. 3 Diagrammatic Sketch of Airbag Layout in the Face of Kekeng Coal Mine**

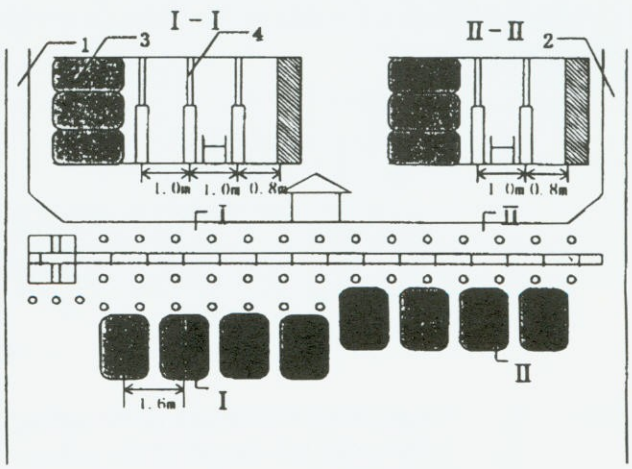



**Fig. 4 Diagrammatic Sketch of Airbag Layout in the Face of Wangyang Coal Mine**

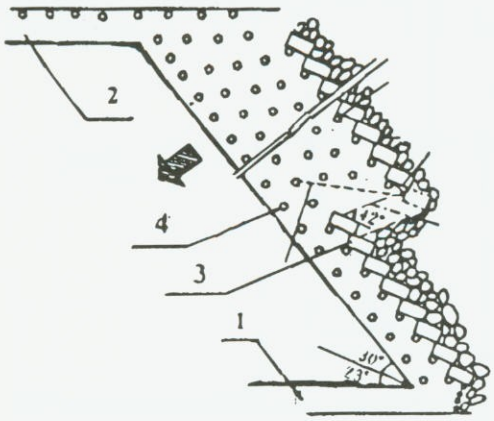



**Fig. 5 Diagrammatic Sketch of Airbag Layout in the Face of Datai Coal Mine**
(also see page 303)

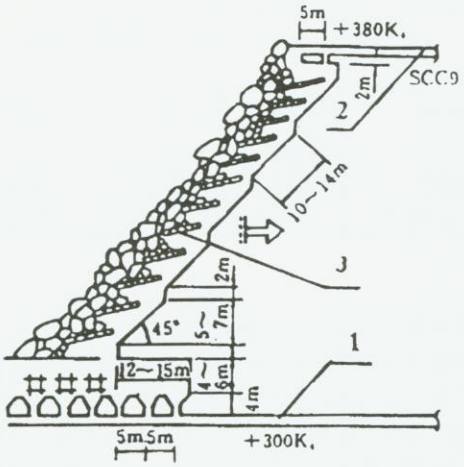



**Fig. 6 Diagrammatic Sketch of Airbag Layout in the Face of Yangliuba Coal Mine**

## Applications of Airbags in the Flatly Inclined and Inclined Coal Seams

***Application of airbags in KeKeng coal mine (Fig. 3).*** The airbags are used in the face, together with the wooden props. Both the row spacing of the prop and the prop spacing in the face are 1.0m. The airbags are placed at the end row of roof control area with the spacing of 5.0m. After the airbags replace the skin-to-skin props in the rear row, the ground behavior appears to be relaxed. The prop's broken rate is reduced, and the timber consumption decreases from 57.3M$^3$/10,000 tons to 29.3m$^3$/10,000 tons.

***Application of airbags in Wangyang coal mine (Fig. 4).*** The airbags are used in conjunction with the frictional props in the face. In front of the airbags, two rows of frictional props are erected , with the prop spacing of 0.8m and the row spacing of 1.0m. The airbags are placed at the end row of roof control area, with the spacing of 1.6m. After the airbags are used in the face, the phenomenon of roof's bench convergence is eliminated and the rate of roof convergence is reduced from the original 157mm/day to 74mm/day during weighting.

## Applications of Airbags in the Steeply Inclined Coal Seams

***Application of airbags in Datai coal mine (Fig. 5).*** The face is laid out along the false-inclined direction. The false-inclined angle is 30$^0$. In the meantime, the haulage roadway and airway are driven in the inclined slope with the angle of 23$^0$~25$^0$ to the strike. The airbags and hydraulic single props are mixedly used in the face. The close-set airbags are placed along the false-inclined direction of the face. Each time the face advances in three circulation, all the airbags of the face are moved and placed once in sequence from downward to upward. The airbags slow down the ground behavior of the face. The working efficiency and coal production are raised accordingly.

***Application of airbags in Yangliuba coal mine (Fig. 6).*** The face is laid out along the false-inclined direction. The false-inclined angle of the face is 45$^0$. The coal wall of the face is divided into 8-10 sections. The section along the false-inclined direction is called a bench in China, which is 10~14 m long. The section along the inclined direction is called a shortwall in China, which is 2.0m long. The bench and shortwall are necessary for mining by air picks. There are rows of close-set airbags in the face. There are 5~6 airbags in each row of close-set airbags. The close-set spacing is 2.5~3.5 m. Every time the face advances in a cycle, the last airbag of the close-set airbags is moved to the front of the first airbag of the next close-set airbags. After the close-standing wooden props are replaced by the close-set airbags, a better roof & floor control in the face is realized. The potential for sliding downward the floor is eliminated.

The accidents of gob's pushing over the close-set supports are avoided. The timber consumption is also reduced from 256m$^3$/10,000 tons to 84.6 m$^3$/10,000 tons.

## APPLIED FEATURES OF AIRBAGS TO ROOF & FLOOR

### Supporting Features of Airbags

The airbag with flexible shell can contact closely with the uneven roof & floor, thus a uniform resistance is produced. Generally, the airbag's contacting area with the floor can be up to 0.4 ~0.8m$^2$, which is 40 ~ 80 times of that of a single prop. The contacting specific pressure on floor is 0.25 ~ 0.75MPa, which is 1/27 ~ 1/80 of that of a single prop. For the loose floor, the airbag has significant advantages.

***Comparison of contacting stress on rock surface***

$$P(r) = \frac{P}{2\pi\alpha\sqrt{\alpha^2 - r^2}} \qquad \text{-----(2)}$$

where $P(r)$ -- contacting stress of rock surface
$\alpha$ -- radius of the stamp die
$r$ -- distance between point and central shaft
$P$ -- uniform pressure

With equation (2), the contacting stress between the die and the surface of the rock can be computed(a single prop or an airbag can be considered as a stamp die), and the stress inside the rock can also be calculated. Under the conditions that the equivalent diameter of a single prop is 6.5cm (its equivalent area is 33.16cm$^2$) and the equivalent radius of an airbag is 30cm (its equivalent area is 706.5cm$^2$) when Type PS1.0-100/5 Airbag is 1.0m high, the stress distribution of the contacting surface is shown in Figure 7, and Table 3. It is obvious that the contacting specific ratio of the single prop is higher than the airbag, the stress in the edges of the single props is much higher. On the contrary, the stress in the center or edges of the contacting area for the airbag is very small.

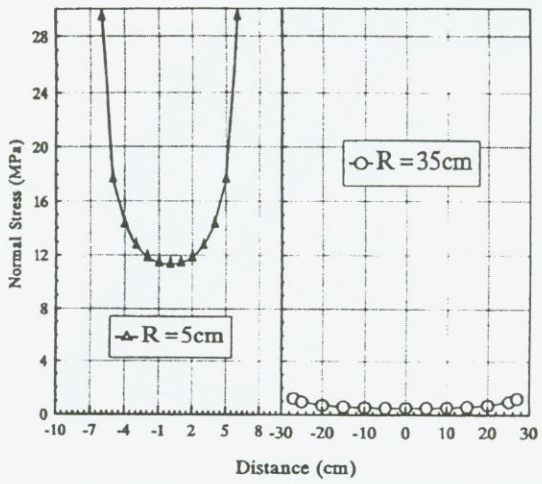



**Fig. 7 Comparison of Contacting Stress**

**Table 3 Comparison of contacting stress (according to rated load 300kN), MPa**

| position | Single Prop A | Airbag B | Ratio A/B |
|---|---|---|---|
| r=0.9R | 25.94 | 1.218 | 21.4 |
| Symmetric center | 11.31 | 0.53 | 21.32 |

***Comparison of vertical stress on surrounding rocks between airbags and single props***

The vertical stress inside the rock strata , caused by the airbags or single props, can be calculated with the mechanical model of a uniform load on the semi-infinite plane. The basic equation is:

$$\sigma = \frac{\sigma_{yo}}{2}\left[tg^{-1}\left(\frac{x}{y}\right) - tg^{-1}\left(\frac{x-a}{y}\right) + \frac{XY}{X^2+Y^2} - \frac{(X-a)Y}{(X-a)^2+Y^2}\right]$$

-----(3)

where

$$\sigma_{yo} = \frac{P_m}{\pi R^2} \qquad \text{-----(4)}$$

$P_m$ -- rated working resistance of the prop or airbag
R -- equivalent radius of the stamp die
a -- contact width of the airbag or single prop and the surrounding rock
X,Y -- coordinate of the point inside the strata
$\sigma$ -- vertical stress inside rock strata
$\sigma_{yo}$ -- contacting stress of rock surface

With equations (3) and (4), we can get the calculation results shown in Table 4 and Figure 8. In Table 4, $\sigma$(A) is corresponding to the single prop and $\sigma$ (B) is corresponding to the airbag. Compared the airbag with the single prop, the airbag creates a large area of compression stress inside the surrounding rock. The stress value is only 1/4 ~ 1/3 of that of the single prop. The attenuation of stress decreases from surface to depth.

**Table 4 Vertical stress of support inside surrounding rock, MPa**

| Spacing to Surface(Z) | (A) | (B) | A/B |
|---|---|---|---|
| **Z = 0.5m** | 7.406 | 1.327 | 5.58 |
| **Z = 1.0m** | 3.734 | 0.767 | 4.87 |
| **Z = 1.5m** | 2.494 | 0.527 | 4.73 |
| **Z = 2.0m** | 1.870 | 0.399 | 4.68 |

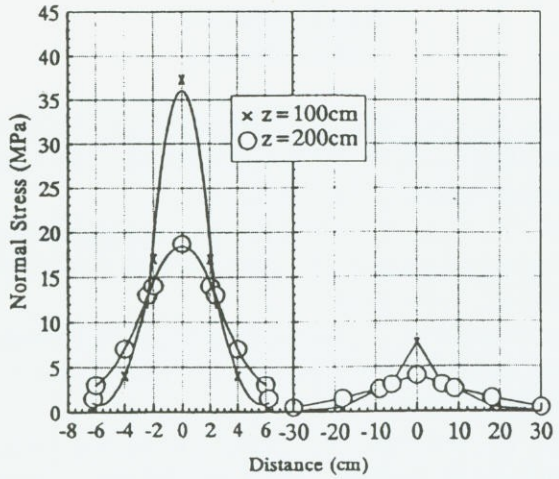



**Fig. 8 Comparison of Vertical Stress**

***Rigidity features of the airbag-surrounding rock interaction system*** According to the field measurements, the working characteristics of the airbag is determined by the initial pressure and the working height. The working characteristics of the airbag appears to be from the slightly incremental resistance to the rapidly incremental resistance. For the PS1.0~100/5 Airbag, its working process can be divided into three sections. The rigidity of the three sections are shown Table 5.

**Table 5 Working rigidity of airbag (kN/mm)**

| Inner Pressure MPa | 1000~800 mm | 800~600 mm | 600~400 mm |
|---|---|---|---|
| 0.28 | 0.265 | 0.435 | 1.135 |
| 0.39 | 0.35 | 0.65 | 1.465 |
| 0.48 | 0.367 | 0.70 | 1.60 |
| 0.59 | 0.50 | 0.75 | 1.80 |

From table 5 we can see that the rigidity increases quickly with the increase of the compression. In the meanwhile, the rigidity increases clearly with the increase of the primary pressure of the airbag. The influence of the primary pressure upon the rigidity is more remarkable with the increase of the compression. For PS1.0-100/5 Airbag with the initial height of 1.0m and the compression up to 0.4m, the rigidity is up to 1.135kN/mm when the primary inner pressure is 0.28MPa. And the rigidity is 1.80kN/mm when the inner pressure is 0.59MPa. The latter is 1.585 times of the former. That indicates the primary pressure not only influences the setting load ,but also influences the increment of the working resistance in the course of compression. Table 6 points out the rigidity of airbag , the hydraulic single prop and hydraulic support. The rigidity of the airbag at the primary stage is much lower than both the hydraulic single prop and hydraulic support. However, for thin seams of less than 1.0m thick, the low rigidity would not produce unfavorable results.

**Table 6 Comparison of Rigidity of Airbags and Single Hydraulic Props**

| Type of support | Single hydra. Prop | Hydraulic support | Airbag |
|---|---|---|---|
| **Rigidity at primary supporting stage** | 125 kN/m | 66.7 kN/mm | 1.885 kN/mm |
| **Rigidity at rapid incremental resistance stage** | 0 (constant resistance) | 0 (constant resistance) | 4.22 kN/mm |

***Interaction features of airbags and surrounding rock*** Figure 9 shows the relation-ship between the setting load of PS1.0-100/5 Airbag and the seam thickness . From Figure 9 we see that the setting load is directly proportional to the primary inner pressure and inversely proportional to the seam thickness. The smaller the seam thickness is, the better

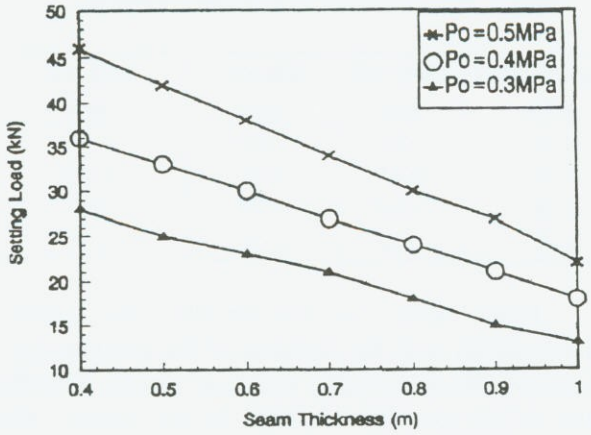



**Fig. 9 Relationship Between Setting Load of Airbag and Seam Thickness**

the mechanical performance of airbags. Figure 10 shows the relationship between the displacement of surrounding rock and the bearing capacity of PS1.0-100/5 Airbag with the primary pressure of 0.5MPa. From Figure 10 we can see that airbag's bearing capacity will reach 1100kN when the compression is up to 0.6m. Then the inner pressure is only 1.2MPa, which is far lower than the burst pressure. In other words, all these mentioned above indicate that the airbag has a larger excess supporting capacity.

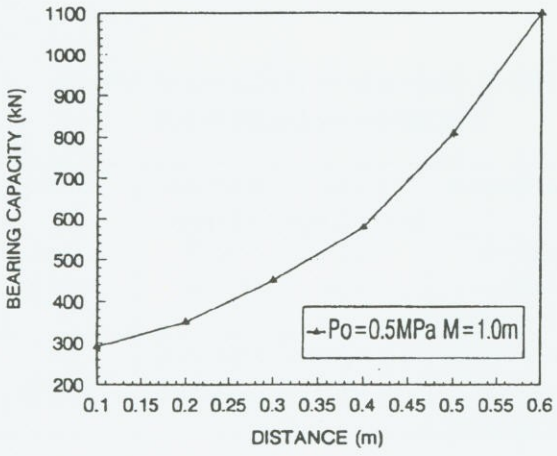



**Fig. 10 Relationship Between Bearing Capacity of Airbag and Displacement of Surrounding Rock**

## CONCLUSION

1. Airbags can apply a uniform pressure to the rock strata and maintain the vertical stress inside the surrounding rock in compression. Compared with single props ,airbags are more suitable for loose floor.

2. The airbag's layout depends on the seam conditions, characteristics of the roof, etc.. A reasonable layout will have good effects on the ground control; support will not punch into the floor; accidents of sliding down the floor and the gob material pushing over the close-set supports in the steeply seams will be avoided.

3. Disadvantages of the airbags are lower primary rigidity and low availability of supporting resistance. The higher rigidity can be rapidly realized if some emulsion or water is injected into the airbag. But the airbag can not be handled easily because the airbag with liquid is much heavier.

## REFERENCES

(all in Chinese)

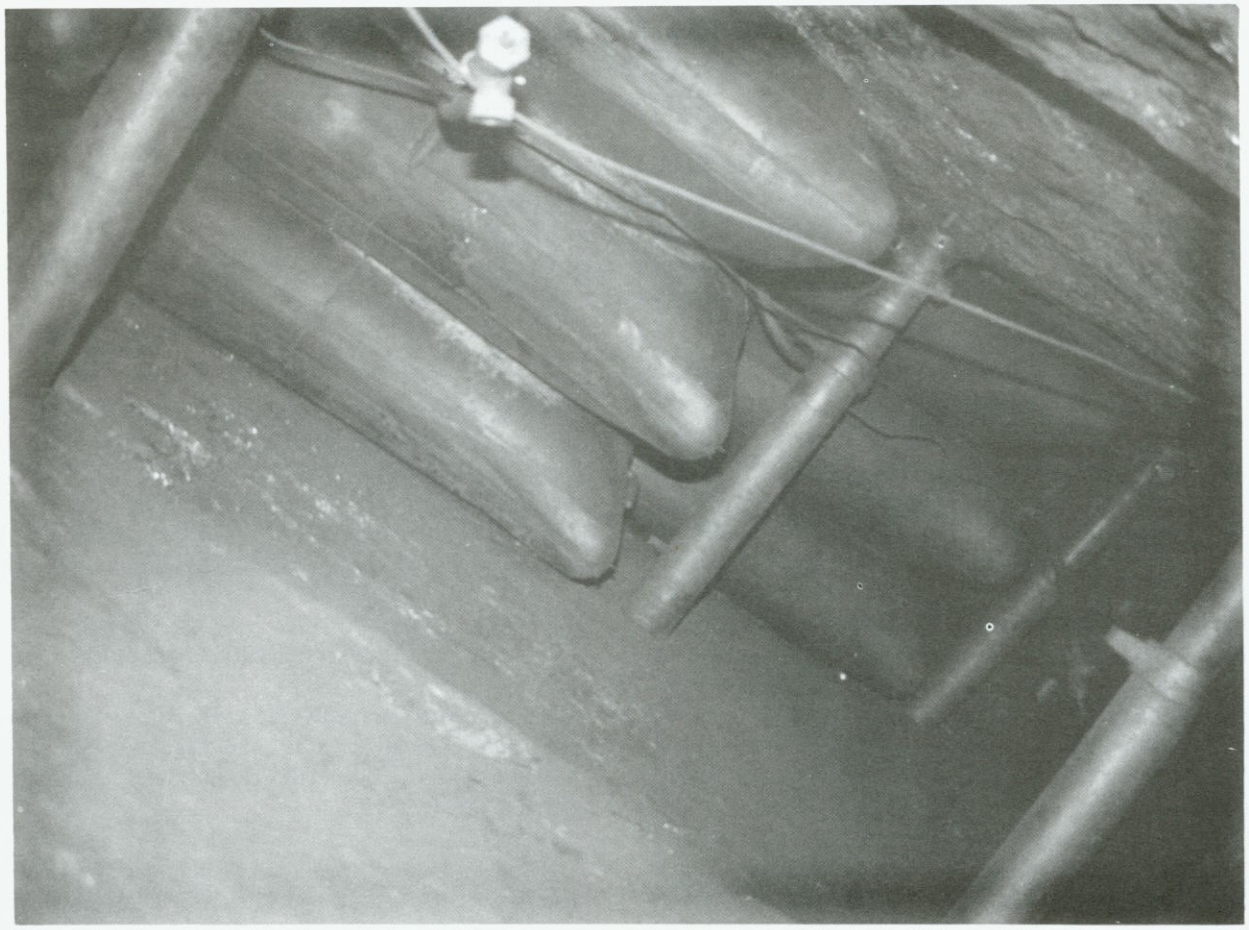
1. Shi, Y., and Sun, S., Adaptability of Airbags to Surrounding Rock in Thin Coal Seams , Journal of China Coal Society, Vol. 20, No. 4

2. Shi, Y., Sun, S., and Fan, S., Application and Development Prospect of Airbags in Thin Coal Seams, China Coal, June, 1995

3. Sun, S. and Fan, S., Application Study on Airbags in Steeply Inclined Thin Coal Seams, Coal Science and Technology , Sept. 1995

4. Yu, K. and Fan, S., Study on Airbag Support Technology in Inclined Thin Coal Seams, Ground Pressure and Strata Control, March, 1995

5. Sun, S. and Fan, S., Test Study on Self-advancing Airbags in Thin Coal Seams, China Coal, Dec. 1996



Airbags Installed in Datai Coal Mine (see Figure 5)

# Development of a Statistical-Analytical Approach for Assessing Coal Bump Potential

*Hamid Maleki,* President
Maleki Technologies, Inc.
Spokane, WA

*Eric Zahl,* Civil Engineer
*John Dunford,* Mining Engineer
National Institute for Occupational Safety and Health
Spokane Research Center
Spokane, WA

## ABSTRACT

Coal bumps are defined as sudden failures of rock and coal near entries that are of such a magnitude that they expel large amounts of material into a mine opening. Coal bumps are influenced by geologic conditions, the geometric design of coal mine excavations, and the sequence and rate of extraction. Researchers from private industry and the National Institute for Occupational Safety and Health have studied mechanisms of violent failure and have identified individual factors that contribute to coal bumps. In an attempt to develop tools for assessing coal bump potential, the authors initiated a comprehensive study using information from 25 case studies undertaken in U.S. mines. Multiple linear regression and numerical modeling analyses were used to identify the most significant variables contributing to coal bumps (excluding bumps related to fault-slip).

Twenty-five geological, geometrical, and geomechanical variables were considered initially. The most important of these variables were then identified as (1) energy as calculated using the mechanical properties of the strata, depth of overburden, and joint density, (2) mining method, (3) pillar factor of safety, and (4) stress gradient and yield characteristics.

## INTRODUCTION

Coal bumps are not only a safety concern in U.S. coal mines, but have also affected safety and resource recovery in other countries, including Germany, England, Poland, France, Mexico, China, India and South Africa. Gradual or progressive failure, which is commonly experienced in coal mines, has less effect on mining continuity and safety and is generally controlled by timely scaling, cleaning, and bolting.

Researchers from private industry, government, and academia have studied the mechanisms of coal bumps *(1-4)* and mine seismicity *(5-6)* and have identified individual factors that contribute to coal bump occurrence, including rapid changes in stress over a short distance or time, stiffness and strength of near-seam strata, and dynamic effects associated with failure of surrounding rocks. In an attempt to identify the most significant variables contributing to coal bumps, the authors analyzed information from 25 sites in mines in Colorado, Utah, Virginia, and Kentucky.

## RESEARCH RATIONALE

The need for an analytical methodology for assessing coal bumps has been indicated in conference proceedings *(4)* and by accident statistics gathered by the Mine Safety and Health Administration (MSHA).

Underground coal mines have a higher incidence of accidents relative to surface coal mines (figure 1). Of particular concern is the potential for an increased number of bumps in mines using the longwall mining method, especially because trends indicate more extensive use of this method. Energy Information Administration data show that longwall production has risen from 20% in 1983 to 45% in 1995 as a percentage of all underground coal production *(7)*. Although room-and-pillar operations are more prone to bumps, it is anticipated that as easily recovered reserves are mined, the trend will be toward deeper mines and those in less stable geologic settings. Both conditions are known to increase bump potential. In addition, new advances in longwall mining technology, such as longer panel length (up to 5,500 m in a mine in Colorado), are creating the need to better understand bump potential so that the problem may be addressed in new mine designs.

MSHA statistics for 1978 through 1995 were analyzed by National Institute for Occupational Safety and Health (NIOSH) personnel using the U.S. Bureau of Mines' Accident Data Analysis (ADA) program *(8)*. No field in the MSHA database specifically indicates injuries resulting from coal bumps, so ADA code categories designated as "fall of roof," "fall of rib-side-face," "falling material," or "entrapment" were compared to the remain-

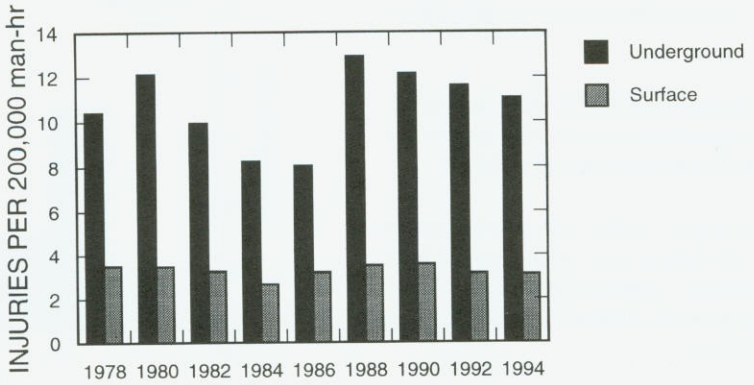



**Figure 1.—Accident incident rates in underground and surface coal mines in the United States, 1978-1994**

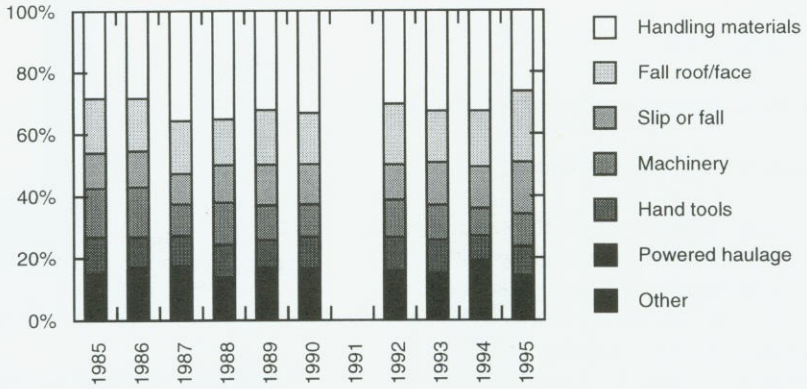



**Figure 2.—Accidents in U.S. longwall mines by category, 1985-1995**

ing accident injury categories (figure 2). "Materials handling" appeared as the largest contributor to accidents, but the great diversity of causes of these accidents would require a significantly larger research effort than would addressing the second largest contributor, "falls of roof and rib."

Coal bumps are of primary concern to miner safety in relation to falls of roof and rib. These categories do not specifically identify coal bumps, but provide a basis for understanding the level of problems associated with ground control that may be resolved with methods described in this paper.

## FACTORS INFLUENCING COAL BUMPS

In an attempt to identify the most significant factors that contribute to coal bumps, the authors analyzed geologic, geotechnical, and in-mine monitoring data from 25 sites in 6 room-and-pillar coal mines and 19 longwall mines in Colorado, Utah, Virginia, and Kentucky. Both computational and statistical techniques were used in the analyses. The first step involved the identification of 25 geologic, geometric, and geomechanical variables that might have had the potential to contribute to coal bump occurrence (tables 1, 2, and 3). Typical frequency histograms are presented in figures 3, 4, and 5 and show the range of coverage provided by the selected variables.

In situ strength was estimated in 12 coal seams where uniaxial compressive strength exceeded 14 MPa. Allowances were made for favorable local yielding characteristics of mine roof and floor in reducing damage severity. Pillar and face factors of safety were calculated using displacement-discontinuity methods for specific geometries.

Some of the variables used in the first step of the analysis are described below.

- *Mechanical property values.* Mechanical property values for

roof, floor, and coal seams were originally obtained through laboratory tests of samples of near-seam strata. The in situ strength of coal seams was estimated using procedures suggested by Maleki *(9)*.

- *Horizontal stresses.* Maximum and minimum secondary horizontal stresses were originally obtained using overcoring stress measurements from one to three boreholes *(10)*.

- *Pillar and face factors of safety.* Pillar and face factors of safety were obtained in individual case studies using both two- and three-dimensional, displacement-discontinuity techniques *(11-13)*. Results were compared with field data when such data were available.

- *Energy release.* Energy release from a potential seismic event was calculated using both boundary-element modeling and analytical formulations as suggested by Wu and Karafakis *(14)* to estimate energy accumulation in both roof and coal, and energy release *(6)* in terms of Richter magnitude ($M_l$) using the following formula:

$$1.5\ M_l = A \times \log (E) - 11.8,$$

where E = total accumulated energy in roof and seam, ergs,

and A = coefficient depending on joint density,

- *Damage rating.* A damage rating to assess the severity of coal bumps was developed by and based on the authors' observations of physical damage to face equipment and/or injury to personnel, as well as observations by other researchers as cited in the literature. Damage levels were assigned a ranking between 0 and 3. Level 1 signifies interruptions in mining operations while level 3 signifies damage to both face equipment and injuries to mine personnel.

- *Roof beam thickness.* Roof beam thicknesses varied between 1.5 and 12 m. The thickness chosen for evaluation was the strongest beam of the near-seam strata located between 1 and 4 times the total seam thickness in the immediate mine roof. Although there is some evidence that massive upper strata have contributed to coal bumps in some mines *(4)*, their influence was not directly evaluated in this study because of the lack of geological and mechanical property data.

- *Local yield characteristics.* Local yield characteristics of immediate roof and floor strata influence coal pillar failure and the severity of coal bumps. This factor varied from 0 to 2, where 0 indicates insignificant yielding in the roof and floor and 2 indicates favorable, gradual yielding.

- *Stress gradients.* Stress gradients varied from 0 to 2, depending on whether or not mining proceeded toward an area of high stress (resulting either from previous mining or rapid changes in topography) and/or abnormal geologic conditions such as occasionally found near faults or grabens.

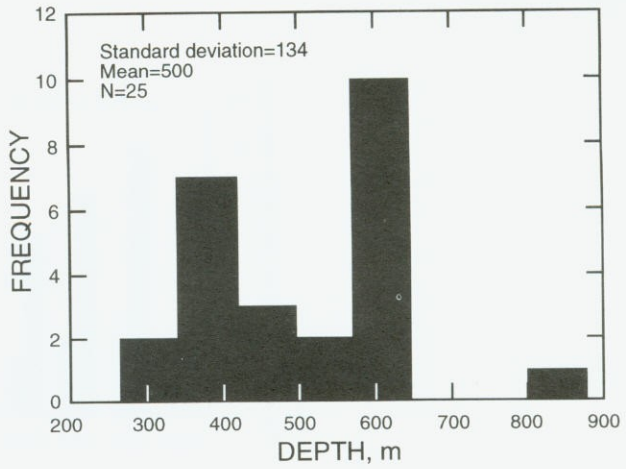



**Figure 3.—Frequency diagram for depth**

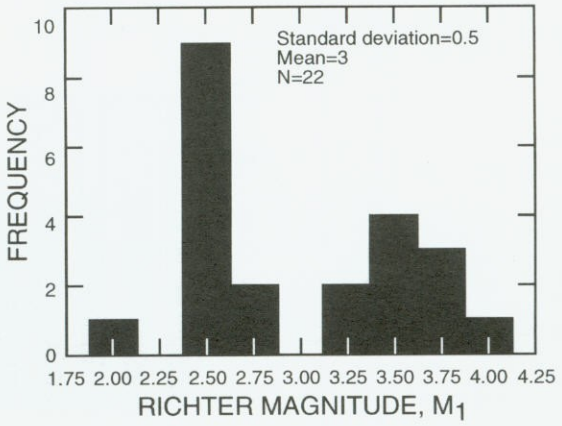



**Figure 4.—Frequency diagram for released energy**

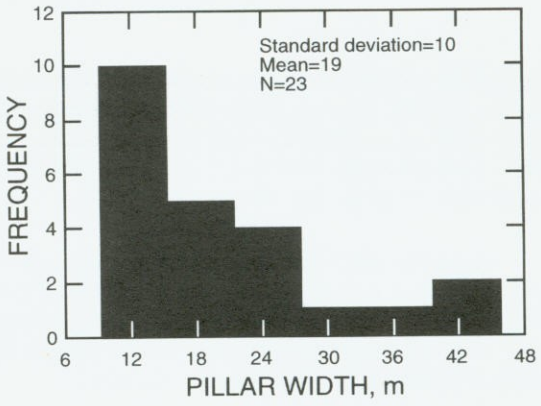



**Figure 5.—Frequency diagram for pillar width**



**Table 1.—Statistical summary of geologic variables.**

| Variable | Mean | Standard deviation | Range | No. of cases |
|---|---|---|---|---|
| Joint sets | 1.4 | 0.6 | 1-3 | 25 |
| Cleat sets | 1.8 | 0.4 | 1-2 | 25 |
| Inseam partings | 1 | 0.9 | 0-3 | 21 |
| Joint spacing, m | 6.7 | 5.5 | 1.5-15 | 24 |
| Rock Quality Designation | 77 | 18 | 50-100 | 15 |
| Depth, m | 500 | 134 | 275-820 | 25 |
| Roof beam thickness, m | 4.3 | 3.3 | 1.5-12.2 | 25 |
| Young's modulus, coal, MPa | 3310 | 830 | 2410-4620 | 25 |
| Young's modulus, roof and floor, MPa | 20,700 | 6900 | 6900-33,000 | 25 |
| Uniaxial strength, MPa | 22 | 5.2 | 13.8-32 | 25 |
| Uniaxial strength, roof and floor, MPa | 100 | 23.8 | 55-150 | 25 |
| Max. horizontal stress, MPa | 13 | 7.6 | 0.7-26 | 25 |
| Interacting seams | 1.2 | 0.4 | 1-3 | 25 |
| Local yield characteristics | 0.8 | | 0-2 | 25 |

**Table 2.—Statistical summary of geometric variables.**

| Variable | Mean | Standard deviation | Range | No. of cases |
|---|---|---|---|---|
| Pillar width, m | 19 | 0 | 9-42 | 23 |
| Pillar height, m | 2.5 | 0.3 | 1.7-3 | 25 |
| Entry span, m | 5.8 | 0.3 | 5.5-6 | 25 |
| Barrier pillar width, m | 50 | 27 | 15-73 | 6 |
| Face width, m | 167 | 40 | 61-244 | 25 |
| Mining method | 1.2 | 0.4 | 1-2 | 25 |
| Stress gradient | 0.9 | 0.6 | 0-2 | 25 |

**Table 3.—Statistical summary of geomechanical variables**

| Variable | Mean | Standard deviation | Range | No. of cases |
|---|---|---|---|---|
| Pillar factor of safety | 0.8 | 0.3 | 0.5-1.4 | 23 |
| Face factor of safety | 0.9 | 0.2 | 0.6-1.5 | 22 |
| Energy ($M_1$) | 3 | 0.5 | 2-4 | 22 |
| Damage | 1.4 | 1 | 0-3 | 25 |

## Bivariate Correlations and Data Reduction

In the next step of the analysis, "damage" was denoted as the dependent variable against which all other variables were tested to determine which of these variables were effective in deducing bump potential.

Based on preliminary bivariate correlations among all geologic, geometric, and geomechanical variables, the number of variables was reduced by combining some variables into new ones and eliminating those that were intrinsically interrelated. In addition, the cause-and-effect *(15)* structure in the data was identified, helping to tailor the procedures for multiple regression analysis using forward stepwise inclusion of variables. The new variables were as follows:

*Pqratio* Ratio of maximum principal horizontal stress (P) to minimum stress (Q).

*Strenrc* Ratio of uniaxial compressive strength of the roof to the coal.

*Jointrf* Joint spacing times roof beam thickness divided by mining height.

**Table 4.—Bivariate correlation coefficients between damage and selected other variables**

| Significant variables[1] | Coefficient | Insignificant variables | Coefficient |
|---|---|---|---|
| Damage | 1 | Pillar width | 0.1 |
| Energy | 0.65 | Ratio of P to Q | 0.1 |
| Gradyield | -0.57 | Young's modulus of roof to coal | 0.07 |
| Jointrf | 0.52 | | |
| Pillar factor of safety | -0.44 | | |
| Uniaxial strength of roof to coal | 0.36 | | |
| Face factor of safety | -0.33 | | |
| No. interacting seams | 0.33 | | |
| Panel width to depth | -0.31 | | |
| Mining method | 0.26 | | |

[1] Two-tailed tests

*Gradyield* Ratio of roof and floor yield characteristics to stress gradient.

*Panelwd* Ratio of panel width to depth.

*Youngrc* Ratio of Young's modulus of the roof to the seam.

Table 4 presents the bivariate correlation coefficients between the damage variable and selected geologic and geometric variables. Energy ($M_l$), face factor of safety, stress gradient, pillar factor of safety, joint spacing, and uniaxial compressive strength of roof to coal were the most significant. Other variables were poorly correlated with damage, including the ratio of P to Q, pillar width, and Young's modulus of roof to coal.

**Multiple Linear Regression Analysis**

There are two methods used by engineers and researchers as tools to help predict conditions in the future: statistical and computational. Starfield and Cundall *(16)* identify rock mechanics problems as "data-limited," that is, one seldom knows enough about a rock mass to use computational models unambiguously. Statistical methods, on the other hand, are uniquely capable of being applied where there are good data but a limited understanding of certain natural phenomena, such as coal bumps.

In this study, the authors combined the strength of both methods to identify important variables and to develop predictive capabilities. Computational methods have been used to assess the influence of a combination of geometric variables into single variables, such as pillar factor of safety and released energy. This was very useful for increasing goodness-of-fit and enhancing multiple regression coefficients. Statistical methods were used to identify significant variables, to build confidence intervals, and so forth.

In the final step in the analysis, a multilinear regression procedure was used, which involved entering the independent variables one at a time (table 4) into an equation using a forward selection methodology *(15)*. In this method, the variable having the largest correlation with the dependant variable is entered into the equation. If a variable fails to meet entry requirements, it is not included in the equation. If it does meet the criteria, the second variable with the highest partial correlation will be selected and tested for entering into the equation. This procedure is very desirable when there is a cause-and-effect structure among the variables. An example of the cause-and-effect relationship is shown when a greater depth reduces pillar factor of safety, contributes to an accumulation of energy, and ultimately results in greater damage. Using the above procedures, any hidden relationship between depth and pillar factor of safety, energy, and damage is evaluated and taken into account during each step of the analysis.

Several geomechanical variables (table 3) were initially used as dependent variables. The multiple correlation coefficient (R), which is a measure of goodness-of-fit, for the last step was 0.87.

The assumptions of linear regression analysis were tested and found to be valid by an analysis of variance, F-statistics, and a plot of standardized residuals (figure 6) *(15)*. Residual plots did not indicate the need for inclusion of nonlinear terms because there was no special pattern in the residuals.

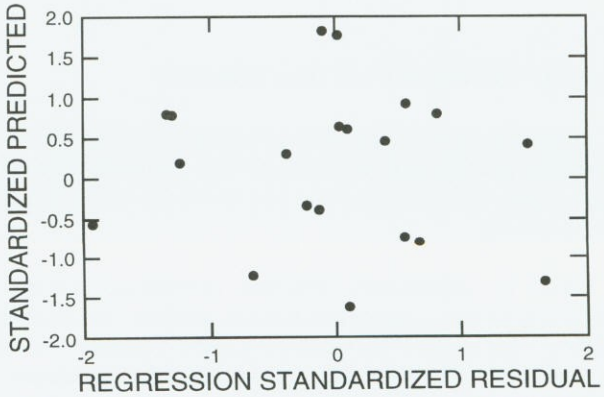



**Figure 6.—Standardized scatterplot for dependent variable, "damage"**

**Table 5.—Standardized regression coefficients and statistical significance**

| Variable | Standardized coefficient | T-significance |
|---|---|---|
| Energy | 0.28 | 0.049 |
| Pillar factor of safety | -0.34 | 0.011 |
| Mining method | 0.26 | 0.064 |
| Gradyield | -0.55 | 0.0004 |
| Constant | NA | 0.234 |

NA Not applicable.

### Important Variables Contributing to Bump-Prone Conditions

Based on an examination of standardized regression coefficients (table 5), the following variables best explain variations in damage and thus statistically have the most significant influence on coal bump potential.

- *Energy.* This variable includes the effects of the mechanical properties of the roof and coal, depth, stress field, and joint density, and thus directly relates to damage.

- *Mining method.* Mining method has a bearing on coal bump potential. The room-and-pillar method is associated with a higher degree of damage than is longwall mining.

- *Pillar factor of safety.* Gate pillar geometry contributes directly to the severity of damage.

- *Stress gradient and yield characteristics.* Mining toward areas of high stress creates a potential for coal bumps, while localized yielding roof and floor conditions encourage gradual failure, which reduces the amount of damage.

## CONCLUSIONS

A statistical-analytical approach was used to identify the most significant factors contributing to coal bumps. Twenty-five variables were initially considered (mechanical properties of strata, stress fields, face and pillar factors of safety, joint spacings, mining methods, and stress gradients, among others). Pillar and face factors of safety were calculated using displacement-discontinuity methods for specific geometries. The most important variables contributing to coal bumps were identified as (1) energy as calculated using the mechanical properties of the strata, depth of overburden, and joint density, (2) mining method, (3) pillar factor of safety, and (4) stress gradient and yield characteristics.

By combining the strength of both computational and statistical methods, the authors are making significant progress in predicting coal bump potential and for building confidence intervals. Since the method relies on an extensive amount of geotechnical data from 25 case studies in U.S. coal mines, it will be helpful to mine planners in selecting relevant variables for assessing bump-prone conditions, which in turn will result in safer designs for coal mines.

## REFERENCES


1. Crouch, S. L., and C. Fairhurst. The Mechanics of Coal Mine Bumps and the Interaction Between Coal Pillars, Mine Roof, and Floor. U.S. Bur. Mines contract H0101778, Feb. 1973, pp. 25-26.
2. Babcock, C. O., and D. L. Bickel. Constraint—The Missing Variable in the Coal Burst Problem. Paper in *Rock Mechanics in Productivity and Protection. Proceedings, 25th Symposium on Rock Mechanics*, ed. by C. H. Dowding and M. M. Singh (Northwestern Univ., Evanston, IL, June 25-27, 1984). Soc. Min. Eng., 1984, pp. 639-647.
3. Iannachione, T., and J. C. Zelanko. Pillar Mechanics of Coal Mine Bursts: A Control Strategy. Paper in *Proceedings of the 16th World Mining Congress* (Sofia, Bulgaria, Sept. 12-16, 1994). Bulgarian Nat. Organ. Comm., v. 5, 1994, pp. 15-23.
4. Maleki, H. An Analysis of Violent Failure in U.S. Coal Mines: Case Studies. Paper in *Proceedings: Mechanics and Mitigation of Violent Failure in Coal and Hard-Rock Mines,* ed. by H. Maleki, P. F. Wopat, R. C. Repshar, and R. J. Tuchman. U.S. Bur. Mines Spec. Publ. 01-95, 1995, pp. 5-25.
5. Arabasz, W. J., S. J. Nava, and W. T. Phelps. Mining Seismicity in the Wasatch Plateau and Book Cliffs Coal Mining District, Utah, USA: Overview and Update. Presented at 15th International Conference on Ground Control in Mining,Golden, CO, Aug. 13-15, 1996.
6. McGarr, A. Some Applications of Seismic Source Mechanism Studies to Assessing Underground Hazard. Paper in *Rockbursts and Seismicity in Mines*, ed. by N. C. Gay and E. H. Wainwright (Proc. of Symp. on Seismicity in Mines, Johannesburg, S. Afr., 1982). S. Afr. Inst. Min. Metall., Symp. Series 6, 1984, pp. 199-208.
7. National Mining Association. Facts About Coal. 1996, p. 23.
8. Cullen, E. B. Accident Data Analysis: A Users Guide. Spokane Research Center, U.S. Bur. Mines, 1988, 97 pp.




9. Maleki, H. In Situ Pillar Strength and Failure Mechanisms for U.S. Coal Seams. Paper in *Proceedings of the Workshop on Coal Pillar Mechanics and Design*, comp. by A. T. Iannacchione, C. Mark, R. C. Repsher, R. J. Tuchman, and C. C. Jones (Santa Fe, NM, June 7, 1992). U.S. Bur. Mines Inform. Cir. 9315, 1992, pp. 73-77.
10. Bickel, D. Rock Stress Determinations from Overcoring: An Overview. U.S. Bur. Mines Bull. 694, 1993, 146 pp.
11. Maleki, H. Development of Modeling Procedures for Coal Mine Stability Evaluation. Paper in *Rock Mechanics Contributions and Challenges: Proceedings of the 31st U.S. Symposium*, ed. by W. A. Hustrulid and G. A. Johnson (CO School of Mines, Golden, CO, June 18-20, 1990). Balkema, 1990, pp. 85-92.
12. Crouch, S. L. Analysis of Stresses and Displacements Around Underground Excavations: An Application of Displacement Discontinuity Method. Univ. MN Geomechan. Rep., 1976.
13. Zipf, R. K., Jr. Stress Analysis in Coal Mines with MULSIM/NL. Paper in *Proceedings of the 89th Meeting of the Rocky Mountain Coal Mining Institute* (Beaver Creek, CO, 1993). Rocky Mt. Coal Min. Instit., Lakewood, CO, 1993, pp. 38-43.
14. Wu, X., and M. G. Karfakis. An Analysis of Strain Energy Accumulation Around Long- wall Panels Under Strong Roofs. Paper in *Proceedings, 5th Conference on Ground Control for Midwestern U.S. Coal Mines*, ed. by Y. P. Chugh and G. A. Beasley (Collinsville, IL, June 1994). Dept. of Min. Eng., S. IL Univ., 1994, pp. 230-253.
15. SPSS. *Statistical Packages for the Social Sciences*, Chicago, IL, 1995.
16. Starfield, A. M., and P. A. Cundall. Toward a Methodology for Rock Mechanics Modeling. *Inter. J. Rock Mech. Min. Sci. & Geomech. Abst.*, v. 25, no. 3, 1988, pp. 99-106.

# Ground Control Criteria for Coal Reserve Optimization in Multiple-Seam Mines

*Eric Westman,* Research Assistant
*J. Luo,* Research Assistant
*Chris Haycocks,* Charles T. Holland Professor
*Mike Karmis,* Head
Department of Mining and Minerals Engineering
Virginia Polytechnic Institute and State University
Blacksburg, VA

## ABSTRACT

Ground control problems caused by multiple-seam interaction frequently sterilize coal reserves. Interaction mechanisms differ for overmining and undermining and are controlled by mining, spatial, and geologic conditions at each site. A multiple-seam interaction analysis software program, UGLY (Upperseam Gateroad Longwall Stability), has been used to evaluate sterilization of coal reserves due to overmining at three locations. Four case histories were reviewed to determine the effectiveness of improved ground control in mitigating interaction effects.

## INTRODUCTION

Sterilization of reserves due to interaction continues to be a major problem for many U.S. coal seams. In Appalachia, coal recovery from longwalls that overlie or underlie mined-out seams may be impossible or may be significantly reduced because of multiple-seam conditions. Determining which areas have not been sterilized is an essential precursor to long-range planning and for conservation of resources. Current techniques used in reserve calculation underestimate and oversimplify sterilization due to seam interaction. By understanding the mechanisms involved in multiple-seam interaction and the tools available for assessing and mitigating the effects of interaction, the most efficient use of remaining resources can be achieved.

Interaction has been demonstrated to have a major effect on reserve estimation (Sellami et al., 1994). Current standards for estimating reserves assume complete sterilization if the seams are within 40 ft (12 m) and no interaction effects if the innerburden is more than 40 ft (12 m) thick (Wood et al., 1983, Rohrbacher et al., 1993). Prior work has produced computerized evaluation methods to determine coal reserves influenced by multiple-seam mining (Zhou et al., 1990). To evaluate multiple-seam effects, hazard maps have also been used with significant success and permit the user to determine the degree of damage that is acceptable during the mining process (Fraher et al., 1992). In evaluating a property, the cost of mining through areas adversely impacted by interaction must be determined. Based on the severity of the interaction, costs can range from increased support needs to abandonment of the property. The relationship between damage due to interaction and mining cost is likely similar to Figure 1. This paper evaluates potential ground control problems due to interaction and their effect on reserve determination.




Figure 1: Hypothetical relationship between damage due to multiple-seam interaction and mining cost.

## GROUND CONTROL PROBLEMS CAUSED BY INTERACTION

The primary interactions associated with overmining are due to subsidence or pressure arching (Holland, 1951). Zones of horizontal compression and tension are created by trough subsidence of the upper seam. A tensile zone results in fractured, reduced strength coal, floor, and roof, causing in increased potential for roof falls. The zone of horizontal tension can also be influenced by increased vertical stresses due to bending of the beds, resulting in potential entry convergence. Stiffer geologic strata (such as sandstones or limestones) tend to bridge the voids of the lower mine,

reducing the effect of subsidence in the upper seam. Additionally, greater lower seam mining height and extraction ratio yield higher subsidence. Results of case studies show that as time increases between mining of the two seams, conditions generally improve (Figure 2). Interseam shearing, a massive block subsidence resulting in a roof fall extending from the lower seam to the upper seam, can also be a problem with overmining if the seams are within approximately 50 ft (15 m) of each other.

The transfer of stresses beneath remnant structures, resulting in concentrated areas of increased vertical stress, is the primary interaction encountered in undermining. The effects of workings in overlying seams can extend to depths of 110 ft (35 m) for room and pillar mining, and up to 700 ft (210 m) for an active longwall (Scurfield, 1970). Stiffer materials, such as sandstone and limestone, tend to reduce the distance of stress transfer, while softer materials, such as shales, tend to transfer stress greater distances.

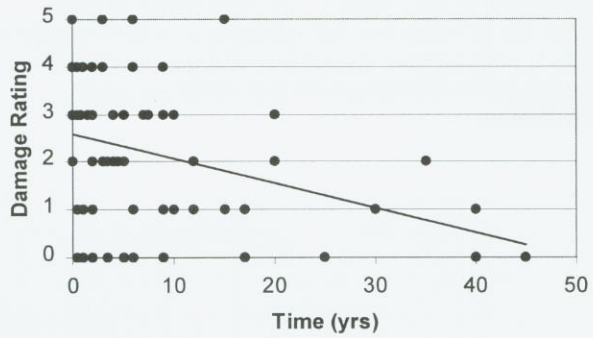



Figure 2: Relationship between Damage Rating and Time

The stresses considered with undermining result from the abutment stresses developed in the upper seam. Development, forward, side, and rear abutment stresses all transfer to lower strata. Room and pillar mining only results in development stresses. In longwall mining and pillaring, forward, side, and rear abutment stresses are also produced, resulting in transfer of much higher stresses than room and pillar. Typical distribution of these stresses around a longwall panel is shown in Figure 3. High vertical stresses can cause face weighting, floor heave, and excessive rib spalling.

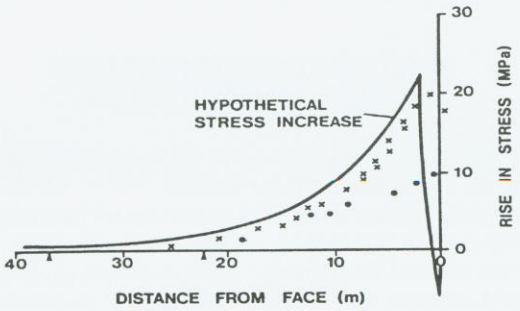



Figure 3: Typical distribution of forward abutment stresses in a longwall panel (Wilson, 1981)

## EVALUATION OF INTERACTION FROM OVERMINING

A rating system has been established (Zhou and Haycocks, 1986) for quantifying the damage developed by multiple-seam interaction (Table 1). A lower rating (0-1) indicates negligible damage due to interaction, while a higher rating (4-5) indicates severe damage resulting in the likelihood of abandonment of mining. A middle rating (2-3) indicates moderate to considerable levels of damage, with potential for causing abandonment.

Table 1. Rating scale for quantifying damage due to multiple-seam interaction

| Rating | Damage |
|---|---|
| 0 | No Damage |
| 1 | Fractures present, no roof problems |
| 2 | Fractures present, visible movement |
| 3 | Roof problems encountered |
| 4 | Major roof problems encountered, entire entries caved |
| 5 | Coal abandoned due to roof control problems |

UGLY (Upperseam Gateroad Longwall Stability), a multiple-seam interaction analysis software program (Luo et al., 1997), was used to determine the amount of sterilization caused by interaction from overmining. UGLY is a Windows-based program that can either analyze an existing pillar system or design a system for expected interaction. It can be used for both room and pillar and longwall analyses. The following equation is used for determining the damage rating in overmining:

$$DR = \left[ 3.84 \left( \frac{T_l^3 H T_o}{T_i} \right)^{0.05} E_l^{1.16} T^{-0.07} \right] - 2.25$$

Where DR = Damage Rating
$T_l$ = Lower seam mining thickness (ft),
$T_o$ = Thickness of overburden (ft),
$T_i$ = Thickness of innerburden (ft),
H = Hardrock in innerburden (%),
$E_l$ = Extraction ratio of lower seam, and
T = Time delay between mining of upper and lower seams (years).

It can be seen that the most important factors are lower seam mining height and extraction ratio. A plot of predicted versus measured damage ratings for 54 case studies (Figure 4) shows a good correlation.

Using the UGLY package, an analysis was conducted for three mines operating in southwestern Virginia during 1996. Three of the most productive seams in southwestern Virginia were

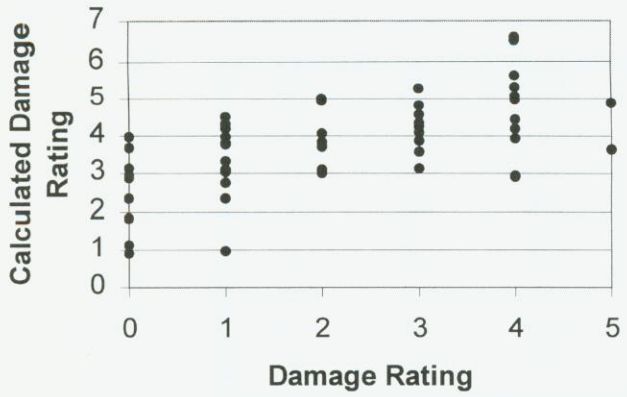



Figure 4: Predicted vs. measured Damage Ratings for 54 overmining case studies

the Dorchester, Norton, and Upper Banner. A currently operating underground mine was chosen from each of these seams to examine the effect of multiple-seam interaction on adjacent seams. As an example of the input data used in the analysis, Table 2 shows the input data used in the analysis of the Dorchester seam. The required input parameters for the Norton and Upper Banner seams were the same.

The analysis showed that mining in the Dorchester seam results in moderate damage and potential sterilization of the Lyons, Blair, and Clintwood seams above it and the Norton formation below it. Mining in both the Norton and Upper Banner formations did not result in sterilization of the adjacent seams. If the mining heights in the Upper Banner had been closer to the 72-in. (180-cm) height of the Dorchester, the Splash Dam seam would have been sterilized, but the 48-in. (120-cm) mining height did not sterilize the Splash Dam. These results are significant because they show that the current standard for reserve estimation, assuming any seams within 40 ft (12 m) are sterilized, is not always accurate. In the case of the Upper Banner mine, the Splash Dam seam is only 30 ft (9 m) above, but the Splash Dam could still be mined. In the case of the Dorchester mine, even though the Lyons, Blair, and Clintwood seams are up to 150 ft (45 m) above, they all were sterilized by the mining in the Dorchester.

## REVIEW OF OVERMINING CASE STUDIES

Four overmining case studies were reviewed to analyze ground conditions encountered and methods used to alleviate interaction effects. Physical parameters of these studies are shown in Table 3. Case study number one was a five-entry room and pillar mine in Tennessee extracting over remnant pillars (Engineers International, 1981). The damage incurred was severe but did not require abandonment of mining. Entry development in the upper seam caused floor cracks along the pillar ribs and side support was needed to prevent sloughing. The failure mechanism was likely pillar load transfer and innerburden shearing with bed separation. The techniques used to mitigate the situation included pillar columnization and mining the upper seam prior to the lower seam.

The second case study was a West Virginia longwall mine (Su et al., 1984). The problem developed as mining progressed over the gob/solid coal interface of a sub-adjacent longwall. Cracks as high as 20 ft (6 m) opened in the roof resulting in roof falls. The face was finally halted due to convergence of the roof and floor, resulting in abandonment. The failure was due to mining through a zone of increased horizontal tension and vertical compression due to trough subsidence. Possible support techniques that could have been used to forestall abandonment of mining include increased secondary support and incorporating additional bolts and trusses.

The third case study was a West Virginia room and pillar mine (Su et al, 1984). Very severe damage was incurred by mining over remnant pillars left between two gob areas in the lower seam. Four out of the five upperseam development entries were completely filled with roof fall material for several hundred feet. Similar to the second case study, the probable cause of failure was mining through a zone of high horizontal tension. Techniques that could have possibly helped mine through the area successfully include increasing time between mining of the two seams and adding supplemental roof support.

The final case study was a Pennsylvania room and pillar mine extracting over the gob/solid interface of a lower seam pillaring mine (Chekan et al., 1985). Pillar load increase was not significant, but roof falls of 10-12 ft (3-4 m) height and entry convergence were encountered, especially over the area of the gob/solid interface. Considerable damage was encountered, but did not result in abandonment of mining. Techniques used

Table 2. Input to UGLY for overmining analysis. Sample shows data used for Dorchester seam analysis.

| | | | | |
|---|---|---|---|---|
| Lower seam mining height (in) | 72 | | | |
| Lower seam extraction ratio (%) | 65 | | | |
| Overlying bed | Lyons | Blair | Clintwood | Addington |
| Innerburden thickness (ft) | 50 | 100 | 150 | 200 |
| Percent hardrock in innerburden (%) | 30 | 40 | 40 | 40 |
| Overburden thickness (ft) | 450 | 400 | 350 | 300 |
| Time between mining (yrs) | 3 | 3 | 3 | 3 |
| Calculated damage | Moderate | Moderate | Moderate | Negligible |

Table 3. Parameters of overmining case studies

| Location | TN | WV | WV | PA |
|---|---|---|---|---|
| Lower seam thickness (in) | 36 | 84 | 27 | 29 |
| Mining technique | R/P | LW | R/P | R/P |
| Extraction ratio (%) | 80 | >90 | 75 | 75 |
| Innerburden thickness (ft) | 65 | 188 | 80 | 95 |
| Percent hardrock (%) | 75 | 60 | 25 | 25 |
| Upperseam thickness (in) | 60 | 77 | 53 | 62 |
| Mining technique | R/P | LW | R/P | R/P |
| Overburden thickness (ft) | 230 | 1120 | 170 | 500 |
| Time between mining (yrs) | 3 | NA | 3 | 4 |
| Damage Rating | 4 | 5 | 5 | 3 |

to control the damage and allow continuation of mining included: additional roof support (longer bolts) for mining over pillar-supported areas, and 5-in. by 7-in. by 16-ft (12-cm by 18-cm by 5-m) timbers bolted on 2-ft (0.6 m) centers for mining over the gob/solid interface areas. Although the conditions were similar to the third case study, effective use of ground support allowed the continuation of mining.

## MINIMIZING INTERACTION EFFECTS ON RESERVES

Effects of interaction can be aggravated by geology but mitigated by design and support. Interaction effects are magnified by increased cover and soft, thin, multiple-layer innerburdens. Prior to mining, an understanding of the effects of interaction can be used in the design stage to minimize multiple-seam interaction effects. For overmining, critical areas such as mains and panel entries for longwall mines should be located in a destressed area. If the pressure arch and subsidence trough analyses indicate a sufficient width for the entries, this would be the optimal location for them. Gob/solid coal interfaces should be avoided for critical areas of the mine. When mining sequence dictates mining through an area stressed by pressure arching or trough subsidence, rate of face advance can be varied in an attempt to minimize complications. Experience has shown that increasing or decreasing rate of face advance can have a significant effect on ground conditions.

The final criteria which can be incorporated into mine design for either over or undermining are the selection of mining method and the amount of time between mining of the two seams. Selection of mining method will likely be determined by factors other than expected multiple-seam interaction, however mining method may have significant impact on ability to control interaction effects. Room and pillar mining is more flexible than longwall in terms of the ability to place structure where necessary to offset interaction effects and so may allow improved ground control conditions. If conditions permit, it has been shown that increasing the length of time between mining of adjacent seams generally decreases the level of damage experienced.

When interaction effects are encountered during mining, support can be used to help alleviate the effects and allow continuation of mining. If excessive rib spalling develops, the ribs should be supported with bolts and either discrete boards or continuous pans. If rib spalling is allowed to become excessive, the strength of the pillar can be compromised, resulting in aggravation of interaction effects. Zones of high horizontal tension and/or vertical compression should have the roof adequately supported. Prior to mining, primary support can be designed for areas that are expected to be problematic. When unexpected problem areas are encountered, secondary support can be increased. Typically, the primary and secondary support used in problematic areas can include longer bolts, continuous pans or mats between the bolts, and trusses. The purpose of these supports is to reinforce the beam behavior of the roof by keeping the roof strata intact.

## CONCLUSIONS

Ground control problems caused by multiple seam interaction can sterilize otherwise economically mineable coal properties. By understanding the mechanisms involved and the costs necessary to mitigate potential damage from interaction, coal reserves can be optimized. Three underground mines operating in multiple seam environments were analyzed with UGLY, a multiple-seam interaction analysis software program. Results showed that the currently used rule of interaction if the seams are within 40 ft (12 m) is inaccurate. In one case, a seam 30 ft (9 m) above the currently mined seam was not damaged significantly, allowing future mining. In another case, three overlying seams, up to 150 ft (45 m) above the current seam, were subjected to interaction effects that could result in moderate damage and sterilization. Analysis of four additional case histories showed that effective mine design and support use may allow mining to continue in areas affected by seam interaction.

## ACKNOWLEDGEMENTS

This work was supported by the Powell River Authority under the project entitled: "Estimation of Mineable Coal Reserves in Central Appalachia With Special Reference to Southwest Virginia."



## REFERENCES


Sellami, M., J. Tissaoui, C. Haycocks, and M. Karmis, 1994, "Computer Evaluation of Reserve Losses due to Multi-Seam Interaction," Proc., 8th International Conf. of the Assoc. for Computer Methods and Advances in Geomechanics, West Virginia Univ., Morgantown, WV., pp. 1889-1894.

Wood, G.H., T.M. Kehn, M.D. Carter, and W.C. Culbertson, 1983, "Coal Resource Classification System of the U.S. Geological Survey," U.S. Geological Survey Circular 891, 65 pp.

Rohrbacher, T.J., D.D. Teeters, G.L. Sullivan, and L.M. Osmonson, 1993, "Coal Resource Recoverability," U.S. Bureau of Mines IC 9368, 48 pp.

Zhou, Y., R. Milici, and E. Campbell, 1990, "Computer-Aided Evaluation of Coal Reserves Influenced by Multiple-Seam Mining," Proc., 4th Conf. on Use of Computers in the Coal Industry, West Virginia Univ., Morgantown, WV., pp. 211-219.

Fraher, R., C. Haycocks, M. Karmis, and Y. Zhou, 1992, "Ground Control Hazard Analysis in Multi-Seam Mining," Proc., 11th Int'l. Conf. on Ground Control in Mining, Univ. of Wollongong, N.S.W., pp. 302-307.

Holland, C.T., 1951, "Multiple-Seam Mining," Coal Age, August, pp.89-93.

Scurfield, R.W., 1970, "Staffordshire Mining Layout for the Mid-1970's," Mining Engineer, Vol. 130, pp. 73-84.

Wilson, A.H., 1981, "Stress and Stability in Coal Ribsides and Pillars," Proc., 1st Conf. on Ground Control in Mining, West Virginia Univ., Morgantown, WV, pp. 1-12.

Zhou, Y. and C. Haycocks, 1986, "Geologic and Spatial Factors in Multi-Seam Mining," Proc., 4th Annual Workshop, Generic Mineral Technology Center, Moscow, ID, pp. 115-126.

Luo, J., C. Haycocks, and M. Karmis, 1997, "Gate Road Design in Overlying Multiple Seam Mines," Preprint 97-107, SME Annual Meeting, Denver, CO, 4 pp.

Engineers International, Inc., 1981, "Investigation of Problems and Benefits of Underground Multiple Seam Coal Mining," Final Technical Report, Dept. of Energy Contract DE-AC01-70ET14242, 292 pp.

Su, W.H., S.S. Peng, and S.M. Hsiung, 1984, "Optimum Mining Plan for Multiple Seam Mining," Interim Report, Department of Mining Eng., College of Mineral and Energy Resources, West Virginia Univ., Morgantown, WV, 71 pp.

Chekan, G.J., R.J. Matetic, and J.A. Galek, 1985, "A Case Study of Ground Control Problems Related to Multiple Seam Mining in the Pittsburgh and Sewickly Coalbeds," SME-AIME Preprint, Albuquerque, NM, October, pp. 16-18.

Chekan, G.J., and J.M. Listak, 1993, "Design Practices for Multiple-Seam Mine Longwall Mines," U.S. Bureau of Mines, IC 9360, 29 pp.

# Calcium Aluminate Binders in Hard Rock and Coal Mining

*Bernard Woolley,* Market Development Manager
Lafarge Calcium Aluminates
Chesapeake, VA

## Abstract

The history of the use of calcium aluminates in mining is discussed including a review of very rapid hardening concretes, anchoring using cement capsules and pumped ground control systems. Specific reference is made to the long term performance of highly abrasion resistant orepass lining in South Africa and the use of rapid hardening materials for a range of applications in Australian coal mine where water infiltration creates difficulties or where rapid repair or return to service is required.

The topics covered in detail are, high strength abrasion resistant concretes with a 20 year, 30 million ton ore pass life. Rapid reinstatement of wet and worn roadways using mineral dewatering and rapid roadway rebuild solutions, all in 1 maintenance shift. The different applications are illustrated using examples from operating mines.

## Introduction

Calcium aluminates are a group of synthetic minerals, which react with water when ground to cement fineness and so have found applications in construction, as well as in other applications, heat resisting refractory concretes, and abrasion resistant materials. They are also used in blended formulations for building needs and for the treatment of aqueous effluents, including in mines. When used for making concrete industrial calcium aluminate cements set normally between 2-4 hours after mixing and gain strength very quickly, giving strong concretes within 6 hours 20 MPa (4,200 psi). They are resistant to acids as unlike Portland cements they do not contain free CaO and are stable after firing to high temperatures (up to 1,800°/3,200°F).

Calcium aluminates are usually described using the cement notation which avoids cumbersome formulas and equations. The oxides are represented by a single letter for example C stands for CaO, A for $Al_2O_3$, H for $H_2O$ and so on. Tricalcium aluminate hydrate $3CaO:Al_2O_3:6H_2O$ one of the hydrates formed when $CaO:Al_2O_3$ hydrates would be written C3A6H. Ferric oxide, $Fe_2O_3$ is written F, Silica $SiO_2$ as S and so on, this notation is used in some of the references quoted. A typical oxide analysis of the most widely used calcium aluminate cement is given below.

**Table 1 Oxide Analysis**

| $CaO$ | $Al_2O_3$ | $Fe_2O_3$ | $SiO_2$ | $TiO_2$ |
|---|---|---|---|---|
| 38-48% | 37-39% | 16-18% | 2-4% | 2-3% |

## Mining applications of Calcium Aluminates

The development of calcium aluminates began more than a century ago in the same period that Portland cements first appeared. The original purpose was for sulfate resistance (including gypsum mines) and it has proved eminently successful for this application. Very rapid hardening is another property for which it has become renowned. Calcium aluminates are now made worldwide by a number of companies. A more extensive account of the chemistry and wider use of calcium aluminates can be found in papers by George and others (1-3). The information in this paper is based on data from the Lafarge Aluminates S.S. Company.

Calcium aluminate cements were first shotcreted in the 1920's in the USA. In general they were mainly used for their sulfate resistance properties and speed of

hardening. The earliest record of them being used in mining are in Tunisian phosphate mine. In the 1950's in the United Kingdom calcium aluminates were used for sinking shafts for coal mines for speed and sulphate resistance and it is probable they were used in Zambia in the copper mines for acid resistance and rapid hardening applications in the 1960's. South African gold mines have a long history of use due to their rapid hardening and abrasion resistance.

Modern mine usage of these cements has expanded significantly since the 1970's when they were first used for rapid hardening cement based cartridges for rapid installation of roof bolts in the hot environment of South African gold mines, where resin based materials were too sensitive to the high ambient temperatures. Subsequently they were used as a component in mine packing, pumped roof support systems developed originally by the British Coal Board in the early 1980's (6), and as orepass lining materials in South Africa (4). Today the use of calcium aluminates is widespread in South African and Australian mines for a variety of uses and since the early 1990's they have been used in Canadian mines for shotcrete acceleration or abrasion resistance. In the USA, calcium aluminates are used in proprietary roof packing systems, as shotcrete accelerators and as rapid hardening cements for diamond drill holes (5) and cable bolting.

## Applications in Ground Control

Ore Pass Linings

In particularly onerous conditions of sliding abrasion and impact such as orepasses many solutions are used or have been tried, such as high abrasion resistant steels or ceramic liners. These solutions are usually extremely costly and not always easy to install in deep ore pass conditions.

In 1983 mine engineers designing orepasses some 1,830m (6000 ft) deep for the then new Freddies No. 5 mine had to look at new lining solutions to the orepasses because of problems encountered due to erosion of the footwall of the first orepass immediately after it was bored. This was due to the presence of altered quartzite rock. This disintegrated after wetting and drying cycles.

The design criteria for the lining material were as follows:

1. Maximum orepass operating life preferably without repair or down time during 20 year life of mines.
2. The rock had to be sealed off from any running water so it did not degrade.
3. It had to support subsequent mining stresses.
4. It had to support the abrasion of impact to protect the rock walls.
5. The lining had too be installed quickly because of scheduling.
6. Installation had to be as easy as possible.

**Possible solutions**

1. Steel tube liners
2. Welded steel railway line mats
3. Concretes

It was quickly decided that only a concrete solution offered a relatively low cost and easy to install system. Although ceramic systems in particular also offered very long wear resistance.

A variety of concrete solutions were examined, including the use of armored steel balls embedded in concrete but the choice was narrowed down to shotcretes based on Portland cements and Calcium Aluminates because of the ease of installation.

A series of tests were carried out on possible concrete solutions which are shown in Figures 1 and 2. The test clearly showed that the Fondag material consisting of Ciment Fondu Lafarge, calcium aluminate cement, Alag calcium aluminate aggregate and natural corundum was the most effective material. After the mine engineers had seen some practical examples of the material in high wear and impact conditions, it was chosen to line the orepass.

The Fondag was shotcreted onto mesh welded to 10 cm (4 in) anchors, spaced at 1 m (39 in) centers. The lining thickness varied between 35 cm (14 in) on the foot wall side where the abrasion and impact was most severe and 15 cm (6 in) on the hanging wall side. The 7 day cube strengths were 77 MPa (11,200 psi). Cubes taken during construction were crushed in 1995 and the strengths was 90 MPa (13,100 psi). The ore pass has had only one minor repair up to June 1997, in the Y-leg impact section. Over 30 million tons of ore being passed to date.

This application has been discussed in more detail by van Heerden (4). Many similar installations have been carried out in South Africa. In 1996 two more major orepass liners have been installed with this material in South Africa in preference to Portland cement silica fume concretes. This solution has also been recently used in Canada.

### Roadway reinstatement

The strata underlying the coal seam is often relatively weak and this was the case at Exxon Ulan Colliery in Australia and in addition there was considerable amounts of water entering the mine workings. The mine used a lot of tracked vehicles, which has led to the rapid breakdown of the roadway surface at intersections due to the braking and acceleration of the vehicles. Mud accumulations in the swillies could be up to 1 m (3 ft) deep. When the roadways were restored and reprofiled with scrapers, they degraded again quickly.

The engineers at Exxon Ulan Colliery in Australia were faced with the following problems:

1. Keep roadways open at all times, particularly intersections.
2. Reduce maintenance costs on roadways and vehicles.
3. Maintain roadways in operating shifts, so that the maintenance shift could be more effectively used.
4. Avoid any problems with cleaning the coal.
5. Find a one man or maximum two man solution.
6. Safe to use, at minimum cost.

No obvious solution was apparent at the time apart from concreting all the roadways which would have been too expensive.

The first problem was to stabilise the roadways which were permanently under repair. Ulan approached Lafarge Aluminates as a specialist cementing company. After various trials a product Flashfill was developed which packed in supersacks or in bags could be applied to the wet roadway by a front end loader and then worked into the surface ballast using a scraper. The top 15 cm (6 in) of surface was sufficiently hard in about one hour for traffic to be resumed.

The next problem was how to remove the mud collected in the swillies. In some areas it could be pumped, in others it could be scraped out but there still remained areas where it was too viscous to pump easily but too wet to scrape out within the time constraints. Another powered product Mineralsponge was developed, which met most of the criteria demanded. It was applied with a front loader over the surface and worked into the mud and left to react. The mud becomes lumpy and "cakey". The presence of some coal fines or pieces of coal does not affect the process. It is hard enough to muck out in one hour and taken out on the coal conveyor with mined coal. It is then separated from the coal easily without contamination. The roadway can then be reprofiled with ballast aggregate.

The final problem was to ensure a more permanent solution at intersections. With the same criteria in mind around product Minexpress was developed which can be pumped with a grout pump into the profiled ballast. The very high fluidity grout penetrates into the aggregate and the consolidated mass is hard enough in 4-6 hours for the heaviest traffic. The strengths of laboratory specimens at 6 hours are around 35 MPa (5,100 psi). This type of product is also used for establishing flat surfaces such as longwall pads or workshop floors very quickly in areas which are difficult to access or require long transport times of wet concrete.

These solutions allow safe, dry, rapid movement in a wet mine with low labour costs and virtually no inconvenience to mine traffic. Maintenance costs of mine vehicles has also been considerably reduced.

### Conclusions

Calcium aluminates offer a variety of properties in mining, rapid hardening using conventional techniques without admixtures and high strengths in 6 hours, up to 30 MPa (4,200 psi) or more depending on the water content and aggregate used. They offer chemical resistance where saline ground water conditions exist. Calcium aluminate grouts have much higher fluidities than Portland cements allowing a number of pumping and grouting applications which are more difficult with Portland based materials. Blended with other materials they can act as water absorbent systems, compressible roof support products and ground stabilization cements for temporary or permanent roadways or surfaces. They are also used as rapid hardening shotcrete systems and as accelerators for Portland based systems. Used with hard aggregates it produces highly abrasion resistant concretes and used in addition as an aggregate, exceptional abrasion resistance can be obtained.

### Acknowledgments

I have drawn on advice and assistance from numerous people in preparing this paper but particularly Mike George - Lafarge Aluminates, Richard Hardwick - Lafarge Aluminates Australia, Dennis van Heerden - Lafarge Aluminates Southern Africa, and Edouard Lastennet - Lafarge Calcium Aluminates Canada.

### References

1. George, C.M., 1983, Industrial Aluminous Cement, Structure and Performance of Cement, edited by Barnes, P., Applied Science, London.
2. Robson, T.D., 1962, High alumina cements and concretes, Contractors Record, London.
3. George, C.M., 1980, Aluminous cements, A synthesis of recent publications, Proc. 7th International Congress Chemistry of Cement, Vol. 1, Septima, Paris, France, pp. V-1/3-V-1/26.
4. Van Heerden, D, 1966, The use of Ciment Fondu based linings in ore passes, GFSA Ore Pass Engineering Workshop, GFTS, Johannesburg, South Africa.
5. Beauchemin, J., 1976, The difference between Ciment Fondu and a hole in the ground, 33rd Canadian Diamond Drilling Association, Sudbury, Canada.
6. Brooks, S.A. and Sharp, J.H., 1990, Ettringite-based Cements, Chap. 24 in Calcium Aluminate Cements, edited by R.J. Mangabhai, E. & F.N. Spon, London, pp. 335-349.

**Fig 1 Abrasion in dry conditions**

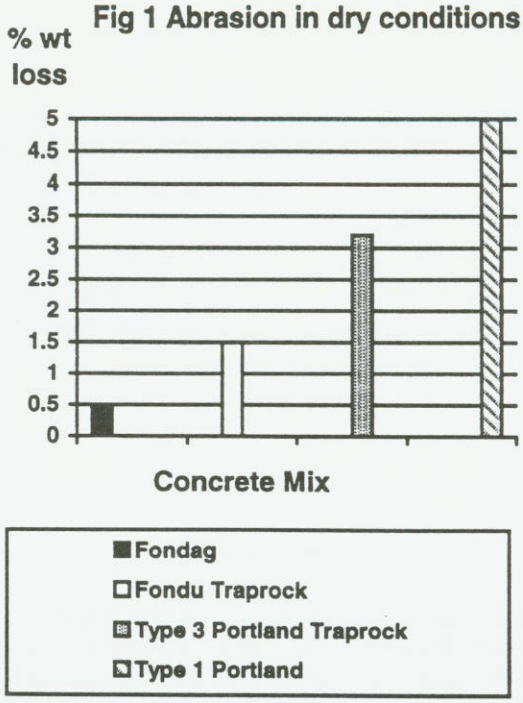
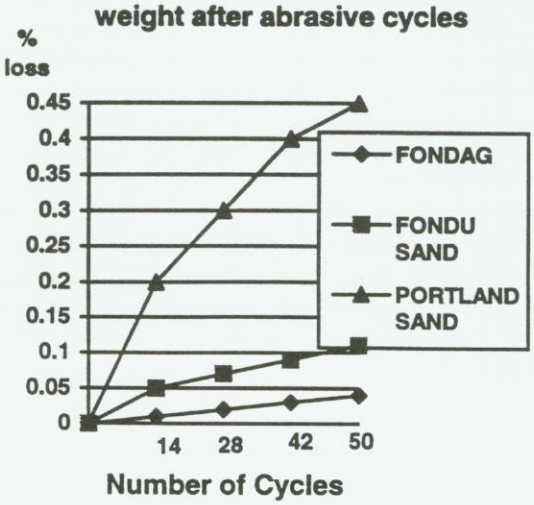



**Fig 2 Comparison of % loss in weight after abrasive cycles**





# Simplified Pre- and Post-processing Technique for Performing Finite-element Analyses of Deep Underground Mines

*Marc T. Filigenzi,* Mechanical Engineer
National Institute for Occupational Safety and Health
Spokane Research Center
Spokane, WA

## ABSTRACT

Two of the major ground control safety issues confronting underground mine operations today are shaft pillar stability and the failure of rock around active mine openings. Failure of a mine shaft can lead to the entrapment of workers. Failure of rock around active underground mine openings can lead to roof falls, which in turn can result in worker injuries and fatalities.

Finite-element analysis has proven to be a reliable method for predicting stresses and displacements around underground mine openings. However, this is a complex and time-consuming technique and is not used as often as it could be in mine planning. The purpose of this paper is to demonstrate one technique developed at the Spokane Research Center that allows the user to create a finite-element model of a two-dimensional section of an underground mine in a relatively straightforward manner. This model is then used to calculate stresses, displacements, and safety factors around mine openings. With this information, mine planners can evaluate the stability of mine openings as well as the stability of pillars and mine shafts. This analysis will help develop mining sequences and layouts that minimize stresses in that section of the mine. This, in turn, should minimize the occurrence of shaft failure, roof falls, and other hazards associated with underground mining.

## INTRODUCTION

The prediction of stresses and displacements around underground mine openings has proven to be a difficult challenge. However, the rewards of such predictions can be substantial. If a mine planner knows that a particular sequence or configuration of excavations will lead to unacceptably large displacements in the rock mass, and that these displacements may affect shaft stability, the planner can modify that sequence or configuration in order to maintain the integrity of the shaft. Such modifications can also minimize stresses in and around mine openings, which, in turn, can reduce the occurrence of roof falls and other hazards associated with the failure of rock.

Finite-element analysis has proven to be an effective method for predicting stresses in rock mass caused by underground mining *(1)*. These earlier studies relied upon the UTAH2PC finite-element program for the analysis of underground mining near a mine shaft. The UTAH2PC code can analyze a two-dimensional section of an underground mine in which there are several formations having anisotropic material properties. The program can also analyze multiple cut-and-fill operations.

However, UTAH2PC does not have an automatic finite-element mesh generator. Each node of the finite-element mesh must be manually located, and each element must be explicitly defined. This leads to a tremendous amount of labor and bookkeeping for an analyst using this program, as well as a reduction in the flexibility of the analysis. If the analyst wishes to modify the geometry of the mine openings or geology, the nodes and elements of the finite-element mesh must be manually relocated and redefined, or the mesh must be regenerated.

Many finite-element analysis programs are available today that include automatic mesh generators and intuitive, user-friendly interfaces (ANSYS, COSMOS/M, PATRAN, etc.). These programs will automatically create a finite-element mesh with all the necessary nodes and elements. However, many of these programs are intended for mechanical engineering design and are not suitable for models possessing the anisotropic material properties or brittle-failure criteria associated with rock.

As a solution to these problems, researchers at the Spokane Research Center, Spokane, WA, have developed a finite-element pre- and postprocessing procedure that takes advantage of the automatic mesh-generating capabilities of ANSYS, a commercially available, finite-element analysis program, while at the same time utilizing the analytical capabilities of the UTAH2PC finite-element code. With this procedure, a user can model two-dimensional sections of underground hard-rock mines, even those with multiple formations and anisotropic materials. These models can be used to plan mining sequences and layouts that will avoid the creation of regions of unacceptably high displacements or stress concentrations.

## REQUIREMENTS FOR SOFTWARE

1. Computer-aided design (CAD) software capable of saving drawing files in IGES format. Third-party programs are available that will convert other drawing formats (such as DXF) into an ANSYS format.

2. ANSYS version 5.0 or later (pre- and postprocessor only). This program is used to create the finite-element mesh and view the results of the analysis.

3. ANS2UT2.EXE. This program is used to convert ANSYS output files into UTAH2PC input files and create a UTAH2PC runstream file.

4. UTAH2PC.EXE.[1] This program is used to perform the finite-element analysis.

5. CONVERT.EXE.[2] This program is used to convert UTAH2PC results files into ANSYS input files.

## REQUIREMENTS FOR ANALYSIS

1. Vertical section map of the area of the mine to be analyzed. This map should illustrate the major geologic features of that section.

2. The location of all existing and proposed mine openings.

3. Material property data along each axis of anisotropy for each of the important geologic features of the section map. These data should include–

A. Elastic modulus.
B. Shear modulus.
C. Poisson's ratio.
D. Compressive strength.
E. Tensile strength.
F. Shear strength.
G. Angle of inclination of the axis of anisotropy with the x-axis.
H. Specific gravity, if gravity loading is to be applied to the model.

4. In situ stress. This stress can be caused solely by gravitational loading or it can be input as a formula where vertical, horizontal, and shear stresses are functions of depth.

5. Measurements of displacement of the rock mass as mining progresses. This information is required to calibrate the finite-element model.

## SYMBOLS

$\sigma_v$ = Vertical stress.

$\sigma_h$ = Horizontal stress.

X = Depth in feet.

## EXAMPLE PROBLEM

An example analysis has been provided to illustrate the technique. Figure 1 shows the geometry of the geology and proposed mine openings used in this example. The mine consists of three major formations. In situ stress is given by the following formula.

$$\sigma_v = 0.1X + 1000$$

and $$\sigma_h = 0.01X + 1000.$$

The model used to illustrate this technique contained 11,955 nodes and 11,952 elements and took approximately 6 hours to create and analyze on a 66 MHZ Pentium PC with 64 megabytes of RAM. Text appearing inside square brackets [ ] is a command issued to ANSYS.

## PROCEDURE

### Step 1: Create Data for Analysis

1-1. Begin by digitizing mine drawings using a CAD program. Either horizontal or vertical sections may be digitized and modeled. If vertical sections are to be analyzed, then the drawing should be digitized so that mine depth increases along the positive x-axis, as shown in figure 1. This is necessary to accommodate UTAH2PC's coordinate system, which defines positive x as pointing down. The drawing should include only major geologic formations. Note that in the example, an extra line segment was added to break formation 1 into two sections. This was done to isolate the area of formation 1 in which mining is to occur. The purpose for this isolation will be explained later. Avoid overlapping and concurrent line segments (figure 2). ANSYS will not generate a finite-element mesh if these conditions are present.

### Step 2: Create Finite-Element Mesh

2-1. Export the final drawing in an IGES format. If the CAD program does not have IGES export capabilities, then contact your ANSYS distributor for other available translators.

---

[1]UTAH2PC was written by William Pariseau of the University of Utah under contract with the U.S. Bureau of Mines and is available at no cost from the Spokane Research Center, NIOSH, Spokane, WA 99207.

[2]ANS2UT.EXE and CONVERT.EXE were both written by researchers at the Spokane Research Center of the U.S. Bureau of Mines and are available at no cost from the Spokane Research Center, NIOSH, Spokane, WA 99207.

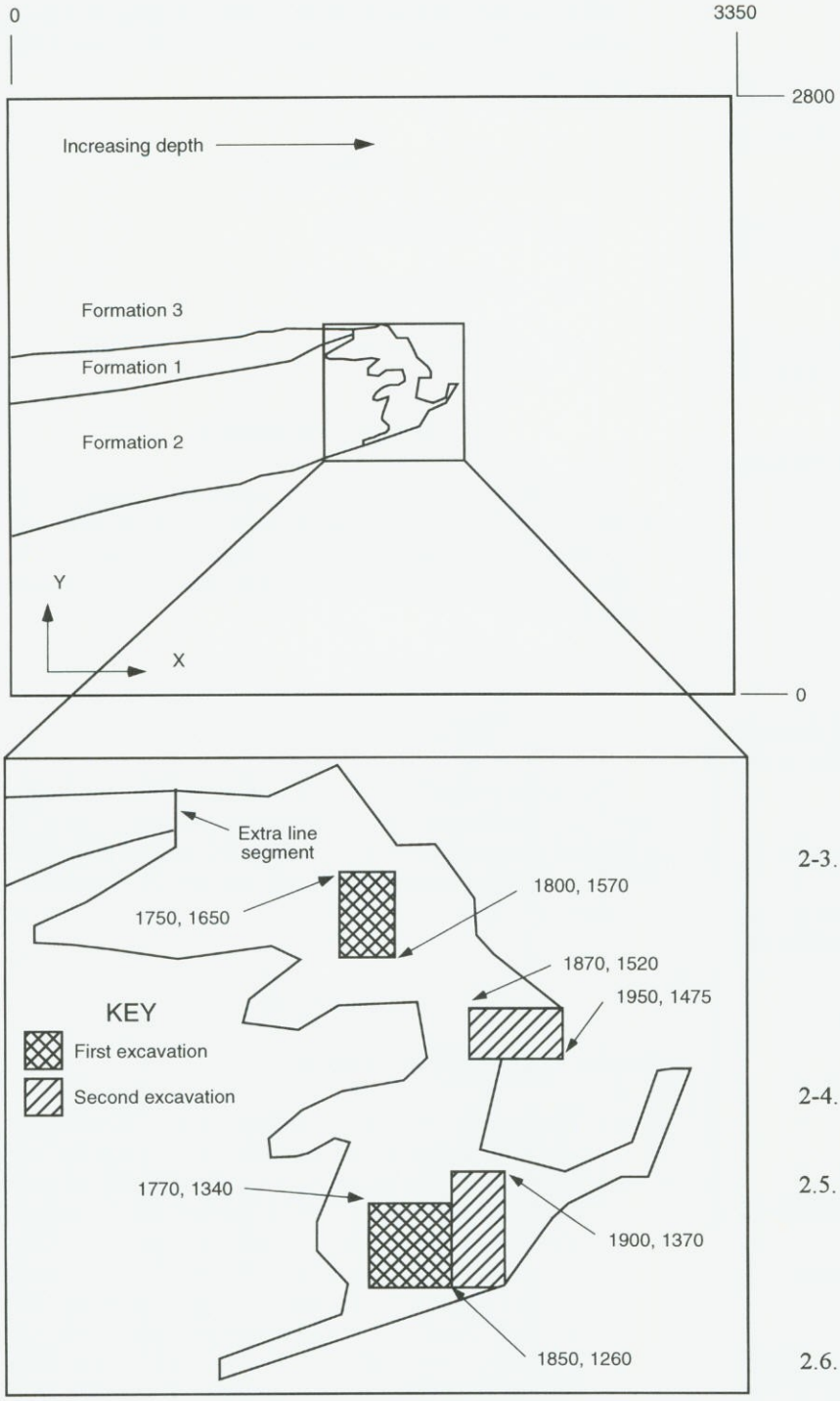



**Figure 1.—Mine plan**

2-2. Run ANSYS from the directory that contains the IGES format file created in step 1.

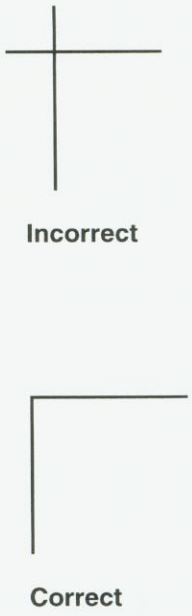



**Figure 2.—Line configuration**

2-3. Input the IGES format file. This step will read in all of the line segments created by the digitizing process in step 1.
[/aux15]
[iges,*fname,ext*] (*filename,ext* is the name and extension of the IGES file created in step 2-1.)
[finish]

2-4. Enter the ANSYS preprocessor.
[/prep7]

2.5. Define element types to be used. This step will tell ANSYS to use three- and four-node, two-dimensional elements when creating the finite-element mesh.
[et,1,plane42]

2.6. View line segments. The plot should look identical to the digitized mine elevation drawing created in step 1-1.
[lplot]

2.7. Merge coincident keypoints. Keypoints are the points that define the ends of each line segment. By issuing the following command, any keypoints which are within a radius of 1 unit from each other will be merged together into one keypoint. This step will eliminate extraneous keypoints that might have been created during the digitizing process.
[nummerge,kp,1]

2-8. Create areas using the lines created in the previous steps. This is done by selecting the lines that bound a region of the model. In this example, formation 1 was divided into two areas: area 1, where mining is to occur, and area 2, which is located in the same formation as area 1, but which will not be mined. Formation 2 was defined as area 3, and formation 3 was defined as area 4 (figure 3).
[al,p]

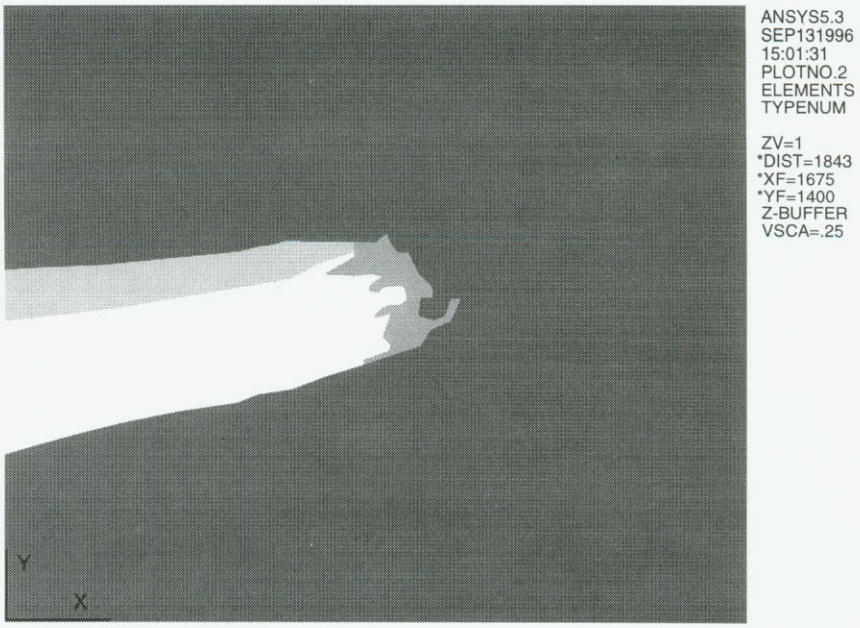



**Figure 3.—Line plot**

2-9. Mesh the model.

A. Define element size. There are several factors to consider when setting the element size. The smaller the element size, the greater the number of elements generated for a given area. The more elements, the more accurate the results, but the greater the demand on computer resources. Another consideration when setting element size is that stresses will concentrate in the region of mine openings and diminish away from mine openings. Therefore, the elements near mine openings should be of a relatively small size (for greater accuracy), while elements away from mine openings can be kept large (to reduce demand on computer resources). It is up to operator experience to determine exactly how to size elements throughout the model. Note that an analysis can be run with a relatively course mesh (larger element size) and then rerun with a finer mesh (smaller element size). If there is no appreciable change in the results, then there is likely no need to further refine the element size. However, if the results do change appreciably, then the model should be recreated with smaller elements and the analysis repeated. In the example, mining will take place in area 1. Therefore, this is the area in which stresses will concentrate, and smaller elements will be required. In addition, smaller elements will be used to better define the mine openings. In the example, elements were given an edge length of 5 feet.
[esize,5]

B. Assign proper material numbers to the areas where a finite-element mesh is to be created. At this point, only area 1 is to be meshed, and area 1 is in formation 1, so each element generated should be assigned material number 1. The material properties associated with material number 1, as well as all other materials used in the model, will be listed in a file that will be used later in the analysis (see step 4-3).
[mat,1]

C. Select and create a mesh for area 1. During this phase, ANSYS will create a finite- element mesh for the area selected.
[amesh,p]

D. Create a finite-element mesh for each of the outer areas. These areas do not require the small element size that was used for area 1. Therefore, a different meshing strategy is used. In addition to specifying the element size, as was done in step 2-9-A, the user can also force ANSYS to create a mesh with a set number of elements along each line segment. This technique allows the user to vary the size of elements throughout the model. There is no rule to specify how many elements should be placed along each line segment. The operator must use judgment and experience to make this determination. Again, because stresses will concentrate around mine openings, smaller elements should be used around the area of mining, and larger elements may be used away from the area of mining. In the example, ANSYS was told to place 20 elements along the outsides of the model. Ten-foot elements were placed along the lines closer to area 1 (figure 4).
[lesize,p]

E. Specify the number of element faces to be placed along each line division as 1.
[esize,1]

F. Complete the mesh of areas in formation 1 by generating a mesh of area 2.
[amesh,p]

G. Set the material number to 2 (for formation 2) and generate a mesh of area 3.
[mat,2]
[amesh,p]

H. Set the material number to 3 (for formation 3) and generate a mesh of area 4.
[mat,3]
[amesh,p]

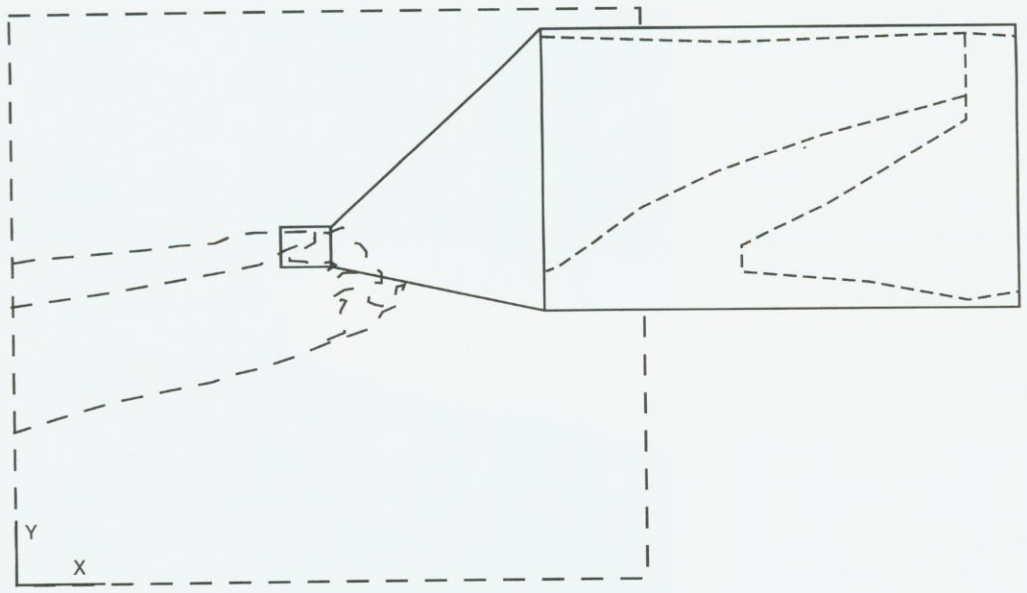



**Figure 4.—Area plot**

I. View all elements.
[eplot]

J. If the element sizes were not properly determined, then ANSYS will warn that poorly shaped elements were created. UTAH2PC will not run an analysis if the model contains poorly shaped elements. This problem may occur if the element size changes too rapidly near the area of mining. To correct this problem, the operator must first delete the elements generated in the areas outside the mining regions. Second, the operator must force ANSYS to slow the rate at which the elements size increases as the elements radiate away from the area of mining. Finally, the areas outside the mining regions must be re-meshed.
[aclear,p] Deletes elements from selected areas.
[mopt,trans,1] Slows rate of element growth.
[amesh,p] Re-meshes areas.

**Step 3: Output Data**

3-1. Copy a list of the elements to a file named ELIST.DAT.
[ewrite,elist,dat,,0]

3-2. Copy a list of nodes to a file named NLIST.DAT.
[nwrite,nlist,dat,,0]

3-3. Select the nodes to be constrained only in the x-direction. In this example, these are the nodes lying along line x = 3350 (the "bottom" of the model). Do not include the two nodes at the corners of the model. These nodes are constrained in the x- and y-directions. Copy a list of these nodes to a file named UX.DAT.
[nsel,s,p]
[nwrite,ux,dat,,0]

3-4. Select the nodes to be constrained only in the y-direction. In this example, these are the nodes lying along lines y = 0 and y = 2800. Again, do not include the two nodes at the bottom corners of the model. Copy a list of these nodes to a file named UY.DAT.
[nsel,s,p]
[nwrite,uy,dat,,0]

3-5. Select the nodes that are to be constrained only in the x- and y-directions. In this example, these are the two nodes at (3350,0) and (3350,2800). Copy a list of these nodes to a file named UXUY.DAT.
[nsel,s,p]
[nwrite,uxuy,dat,,0]

3-6. Select the elements to be cut during the first excavation. In the example, the cut elements are contained within two rectangles, the first with coordinates (1850,1260), (1900,1370), and the second with coordinates (1950,1775), (1870,1520) (figure 1). There are several steps involved in selecting these cut elements.

A. Select nodes within the first set of coordinates. First, select all nodes between x = 1850 and x = 1900. Then, from these nodes, reselect the nodes lying between y = 1260 and y = 1370.
[nsel,s,loc,x,1850,1900]
[nsel,r,loc,y,1260,1370]

B. Select all elements in contact with these nodes.
[esln,s,0]

C. Group these elements into a component named "ekill1a."
[cm,ekill1a,elem]

D. Select the nodes within the second set of coordinates. First, select the nodes between x = 1950 and x = 1870.

Then, from these nodes, reselect the nodes lying between y = 1475 and y = 1520.
[nsel,s,loc,x,1950,1870]
[nsel,r,loc,y,1475,1520]

E. Select all elements in contact with these nodes.
[esln,s,0]

F. Group these elements into a component named "ekill1b."
[cm,ekill1b,elem]

G. Group the two components into an assembly called "ekill1."
[cmgrp,ekill1,ekill1a,ekill1b]

H. Select all nodes and elements in the model.
[allsel]

I. Select the elements stored in the assembly "ekill1." These are the elements to be excavated in the second step of the analysis.
[cmsel,s,ekill1]

J. Copy a list of these elements to a file named EKILL1.DAT.
[ewrite,ekill1,dat,,0]

3-7. Repeat this process for the elements to be cut for the third step of the analysis, saving the element listing as EKILL2.DAT.

3-8. Save ANSYS database and exit the program.
[save]
[finish]
[/exit]

**Step 4: Prepare Data for Analysis**

Run ANS2UT2 from the directory that contains the files created in step 3. This program will convert the ANSYS output files into UTAH2PC input files. The program also creates the master runstream file for UTAH2PC. Consult the UTAH2PC documentation for more information on UTAH2PC files. ANS2UT2 will request the following information:

4-1. Job title. This is an arbitrary title for the UTAH2 runstream file and can be up to 80 characters long.

4-2. Master runstream file name. This is the user-supplied name of the master runstream file to be created by ANS2UT2 and provides the input for the UTAH2PC analysis. Three master runstream files were created for the example, one for each of the three load steps. The first (L1.DAT) contains all the data necessary for UTAH2PC to calculate the state of stress of the model prior to any excavation. The second (L2.DAT) contains all the data necessary for UTAH2PC to calculate the state of stress of the model after the first excavation. The third (L3.DAT) contains all the data necessary for UTAH2PC to calculate the state of stress of the model after the second excavation.

4-3. Material properties file name. This file is provided by the user and contains material properties for each of the materials used in the analysis.

4-4. Number of different material types. The user is to define the number of different material types used in the analysis. Note that each of the different material types should be defined in the material properties file. Three material types were used in the example analysis, one for each of the three geologic formations.

4-5. ANSYS element connection filename. This is the element listing generated by ANSYS (see step 3-2 above). The default is ELIST.DAT. ANS2UT2 will convert this file into a UTAH2PC formatted file named ELIST.UT2.

4-6. ANSYS node location filename. This is the node listing generated by ANSYS (see step 3-1 above). The default is NLIST.DAT. ANS2UT2 will convert this file into a UTAH2PC formatted file named NLIST.UT2

4-7. ANSYS cut or fill element listing. This is the list of elements to be cut or filled (see step 3-6-A above). In this example, the first load step has no cut or fill element listing. The elements cut in the second load step are listed in the file EKILL1.DAT. The elements cut in the third load step are listed in the file EKILL2.DAT. ANS2UT2 will convert these files into UTAH2PC formatted files. The name of the UTAH2PC format file is supplied by the user. ANS2UT2 will also prompt the user for the name of a file that UTAH2PC will create and store the number of each node that is attached to the cut elements.

4-8. Gravity loading. Select this option if the first load step is used to calculate loading by gravity. If gravity loading is selected, then the material properties file must include the specific gravity for each of the materials listed.

4-9. Initial stress. As an alternative to gravity loading, initial stress can be provided either from a file (such as the results from a previous load step) or calculated from known stress gradients. If the stress gradient is known, then ANS2UT2 will prompt the user for the following information.

A. Name of the initial stress file to be created.

B. Depth to top of model.

C. Slope and constant defining stress gradients. Stress is defined by the formula–

$$y = mx + b,$$

where $y$ = stress gradient,
$m$ = slope of gradient,

x = depth in feet,
and b = constant.

In the example, the initial stress for load step 1 was defined by the following formulae.

$$\sigma_v = 0.1X + 1000$$

and $$\sigma_h = 0.01X + 1000.$$

These formulas were provided to ANS2UT2, which applied these values to all of the elements in the model and saved the results in the file STRESS.UT2.

4-10. Boundary node listing. The boundary node listing is generated by ANSYS (see steps 3-3, 3-4, and 3-5 above). The default is UX.DAT, UY.DAT, UXUY.DAT. ANS2UT2 will convert these three files into a single UTAH2PC formatted file named BOUND.UT2.

4-11. Screen output filename. This is a file that will contain the UTAH2PC runstream output. This file name does not require an extension. The first four characters of this file name will be used as the first four characters for UTAH2PC stress and displacement output files.

4-12. Number of load steps. This is the number of increments to reach final load. Usually 10 increments are sufficient.

4-13. Maximum number of iterations per load. This is the number of iterations allowed per load step. A value of 80 was used in the example analyses.

4-14. Iteration interval. This is the number of iterations between printing of residuals and should be less than the maximum number of iterations. A value of 20 was used in the example analysis.

4-15. Type of analysis. Analyses include plane stress, plane strain, axially symmetric, elastic, or elastic-plastic. The type of analysis used in the example problem was an elastic-plastic analysis with a quadratic yield condition.

4-16. Caving. An elastic-brittle analysis can be pursued by selecting the caving analysis. This program option is somewhat experimental and should be used with care.

4-17. Batch runstream. Some data files can be skipped during a sequential batch run consisting of several back-to-back program passes. Select this option if this action is desired.

4-18. UTAH2PC to write output files. Select this option if UTAH2PC is to save output files (recommended).

4-19. Input units. If metric units are used in the model, then "yes" should be selected. Otherwise, the default is "no."

4-20. Error value. The program will exit the equation solver when the residuals are reduced to a value less than the error value. A value of 1 is recommended.

4-21. Orf value. An over-relaxation factor is used to accelerate the equation-solving procedure. Orf should be between 1 and 2 (1.86 recommended).

4-22. Xfac and Yfac. These are the scale factors used to convert the measurement units in the mine plans into inches or millimeters, as appropriate.

4-23. Efac and Sfac. These are scale factors used to change elastic properties (efac) or strength properties (sfac).

Load step 1 consists of applying the initial stress field to the model. During load step 2, the resultant stresses from load step 1 are applied to the model, and the first excavation takes place. During load step 3, the resultant stresses from load step 2 are applied to the model, and the second excavation takes place.

**Step 5: Analyze Data**

Run UTAH2PC from the directory containing the files created in step 4. UTAH2PC will prompt the user for the name of a runstream file (as created in step 4-2) and will then perform the analysis. Output includes cartesian stresses and element safety factors, element principal stresses and strains, and node force and displacements. For the example analysis, UTAH2PC was executed three times, once for each of the three load steps.

**Step 6: Prepare Results of Analysis**

Run CONVERT from the directory that contains the files created in step 5. This program converts Cartesian stresses, element safety factors, and node displacement files generated by UTAH2PC into a format ANSYS can read. CONVERT will prompt the user for the name of the UTAH2PC output file to be converted and the name of the ANSYS input file to be created.

**Step 7: Review Results of Analysis**

7-1. Run ANSYS from the directory that contains the ANSYS files created in step 6.

7-2. Resume the original model database.
[resume,*filename,db*] *filename,db* is the file name and extension of the ANSYS database. The default is file.db.

7-3. Enter the ANSYS postprocessor.
[/post1]

7-4. Create element tables that are to contain the stresses and safety factors generated by UTAH2PC in step 5 and converted into ANSYS format in step 6.
[etable,Sxx]
[etable,Syy]
[etable,Szz]
[etable,Txy]
[etable,Fac]




**Figure 5.—Safety factors around openings**

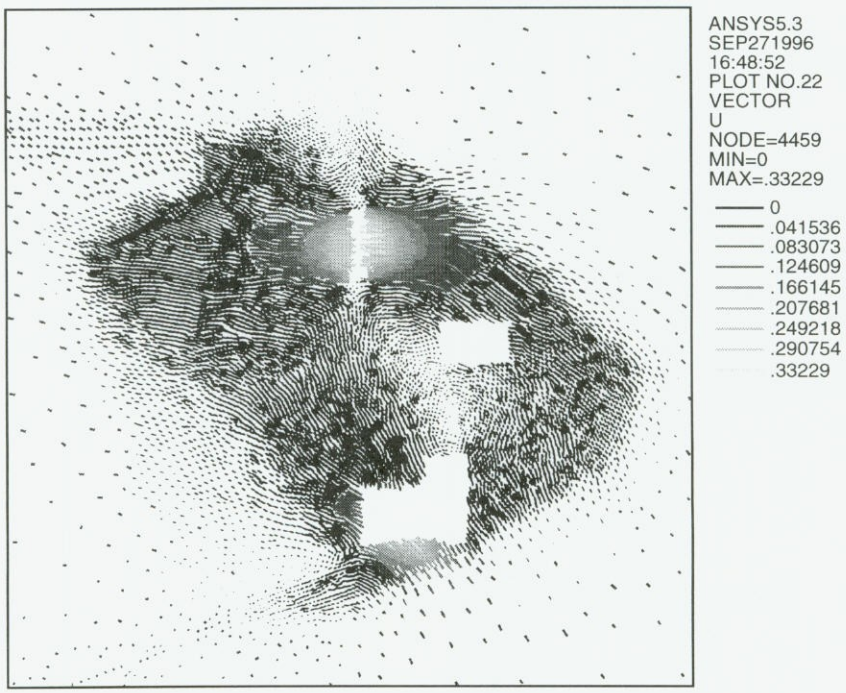



**Figure 6.—Displacements around mine openings**

7-5. Enter the converted stress and displacement files from load step 1 into the element tables.
[/input,*filename,ext*]

7-6. View analysis results. The following commands will cause ANSYS to plot the results of the analysis.
[pletab,sxx] Generate a plot of vertical stresses.
[pletab,syy] Generate a plot of horizontal stresses.
[pletab,txy] Generate a plot of shear stresses.
[pletab,fac] Generate a plot of safety factors.
[plvect,u,,,,vect] Generate a plot of displacements.

7-7. Repeat steps 7-5 and 7-6 to review the results from load steps 2 and 3. Figures 5 and 6 illustrate the resultant safety factors and displacements around the mine opening.



## SUMMARY AND CONCLUSIONS

The technique explained above is one method that will allow mine planners to generate a two-dimensional, finite-element model of an underground section of a mine in a relatively straightforward manner. This model can be analyzed, and resultant stresses, displacements, and safety factors around mine openings can be viewed. This information allows a mine planner to develop mine plans that reduce the potential for rock failure around mine openings.

Cross sections consisting of several formations of anisotropic materials can be modeled, but many variables can affect the accuracy of the model, including the number and location of joints and fractures, the presence of water, the accuracy of measurements of material properties and in situ stress, and the actual geometry of the various formations and openings. It is therefore critical that a mine planner validate the results of the analysis by comparing the predicted response of the mine with the actual response of the mine. The elastic material properties may be validated by comparing predicted displacements with actual displacements. Strength properties may be validated by comparing predicted yield zones with observed yield zones *(2)*. These comparisons will allow a planner to determine if the material properties used in the model should be modified in order to create a more accurate model.

## REFERENCES

1. Pariseau, W. G., J. C. Johnson, M. M. McDonald, and M. E. Poad. Rock Mechanics Study of Shaft Stability and Pillar Mining, Homestake Mine, Lead, SD. (In Three Parts). U.S. Bur. Mines RI 9531, 1995, 20 pp.

2. Pariseau, W. G. Research Study on Pillar Design for Vertical Crater Retreat (VCR) Mining (contract JO215043, Univ. UT). U.S. Bur. Mines OFR 44-86, 1986, 232 pp.; NTIS PB 86-210960.

# PRACTICAL COAL PILLAR DESIGN CONSIDERATIONS BASED ON NUMERICAL MODELING

Daniel W. H. Su
Gregory J. Hasenfus

CONSOL Inc.
Research & Development
4000 Brownsville Road
Library, Pennsylvania 15129

## ABSTRACT

This paper demonstrates that finite element modeling can be used to predict in situ coal pillar strength, even under non-ideal conditions where interface friction and roof and floor deformation are the primary controlling factors. A practical coal pillar strength consideration is presented which incorporates the results of numerical modeling and field measurements. Nonlinear pillar strength curves are presented to relate pillar strength to width-to-height ratio under both simulated steel platen loading and strong roof and floor in-mine conditions. Confinement generated by the frictional effect at coal/steel or coal/rock interfaces is demonstrated to accelerate pillar strength increase at a width-to-height ratio of about 3 for a simulated in situ coal pillar and about 5 for simulated steel platen loading. Frictional constraint limitations and coal plasticity decelerate pillar strength increase at width-to-height ratios of about 6 for the simulated in situ condition and about 10 for the simulated steel platen loading conditions. The simulated strong roof and floor in situ strength curve compares favorably with the measured peak strengths of five failed pillars in two southwestern Virginia mines, and is in general agreement with many existing coal pillar design formulas at width-to-height ratios less than 5. However, for wide pillars the curve presented in this paper predicts a higher in situ coal pillar strength than most accepted formulas. As the coal market becomes increasingly competitive, and more efficient room and pillar and longwall development designs are evaluated, additional focus will be placed on pillar design optimization. Optimum pillar design must account for variable mine geology, geometry, and stress states. While safety is paramount, overestimation of large pillar sizes for premining design using existing formulas and subsequent trial and error optimization are costly alternatives to accurate pillar design methodologies.

## BACKGROUND

The strength of coal and coal pillars have been the subject of considerable research, especially for the past 40 years. Because of the highly variable and anisotropic nature of coal, the seemingly simple task of defining in situ coal strength is often very difficult and complex. Coal strengths measured in the laboratory are known to increase with increasing width-to-height ratio and to decrease with increasing specimen height and size. Based on the shape and size effect determined

in the laboratory, a number of empirical pillar strength formulas (Gaddy, 1956, Holland, 1964, Obert and Durall, 1967, Salamon and Munro, 1967, Bieniawski, 1968, and Hustrulid and Swanson, 1981) and closed form analytical solutions for pillar strength (Wilson, 1972 and Barron, 1984) were proposed and used with some success during the past three decades. The empirical pillar strength formulas were validated through many years of actual use, typically with pillars exhibiting low width-to-height ratios. In the past, regulatory authorities and many coal operators gravitated towards these empirical formulas because of their simplicity and ease of application. However, these formulas have at least two major drawbacks: 1) their predictions may not be extrapolated with confidence beyond the data they were derived from, typically from pillars with width-to-height ratios of 5 or less (Mark and Iannacchione, 1992), and 2) they treat the entire coal pillar as a single structural element to obtain an average pillar strength, often without consideration for roof and floor end constraint and subsequent interactions.

The importance of friction and end constraint on laboratory coal strength has been demonstrated by many researchers, including Khair (1968) and Babcock (1994). Brady and Blake (1968) reported that during a uniaxial compression test, the state of stress within the specimen is triaxial and is biaxial at the free surface. In spite of this, the compressive strength obtained by testing a specimen with a diameter-to-length ratio (D/L) of 0.5 is approximately the correct uniaxial stress strength. However, this is not true for test specimens having a D/L ratio greater than 0.5. Babcock (1990) also demonstrated that the state of stress, not the geometry, was responsible for the change in strength with the D/L ratio. Specimens of coal, limestone, marble, and sandstone, with D/L ratios of 1, 2, 3.5, 5, and 8.5, were made to fail in compression at about the same stress for each rock type by removing end frictional effects with layers of PTFE of selected thicknesses. Panek (1994) also reported that lateral confinement generated by the end frictional effect may transform rock samples from a brittle to ductile state at width-to-height ratios between 1.5 and 3.5. Bieniawski (1981) and Salamon and Wagner (1985) suggested that confinement generated by the end constraint of coal may increase more rapidly for width-to-height ratios greater than 5.

Practitioners and researchers alike, including Conroy (1977), Mark and Bieniawski (1986), Hasenfus and Su (1992), Maleki (1992), and Parker (1993) have noted the significance of roof and/or floor interactions on in situ pillar strength. Maleki (1992) illustrated four types of in situ coal pillar failure mechanisms under excessive vertical stress commonly observed in the U.S. In addition to the structurally controlled progressive failure of the coal rib, these mechanisms include failure in the roof, failure at seam contacts (partings), and failure within the floor; all of which in turn may lead to progressive pillar core failures.

To account for the apparent increase of pillar strength due to confinement at high W/H ratios, Bieniawski (1981) modified his original empirical formula for pillars with width-to-height ratios of 5 or more. Salamon and Wagner (1985) also proposed a squat pillar formula for use in South African coal mines to account for the rapid increase in pillar strengths at high width-to-height ratios. The squat pillar formula has been employed in South Africa (Madden, 1988). Wagner (1974) demonstrated that pillar stress within even a relatively small pillar near the peak load was highly nonuniform and that pillar failure was progressive (Figure 1). This progressive failure mechanism was utilized in the confined core concept of pillar strength proposed by Wilson (1972), which started

with the assumption that coal follows a linear Mohr-Coulomb failure criterion. Barron (1984) later modified Wilson's assumption of exponential increase of horizontal confining stress by introducing the nonlinear Hoek-Brown criterion. This exponential increase is also implied in the modified Bieniawski and the squat pillar strength formulas. Salamon (1992) suggested the many shortcomings of Wilson's basic idea can be removed by the introduction of a layered model of the stratified rocks in the roof and floor.

With the increasingly powerful computing capabilities, and the increased commercial availability of sophisticated numerical modeling software, computer models of varying sophistication have been used since the earlier 1980's to study pillar strength and failure mechanisms. Kripakov (1981) and Hsiung and Peng (1985) used the finite element modeling technique to evaluate pillar strength. However, their results showed, what is believed to be, unrealistic exponential strength increases at high width-to-height ratios. Interface friction was not simulated in either case. Iannacchione (1990) used the FLAC code to study the effects of roof and floor interface slip on coal pillar strength. His results indicated that interface slip is the primary factor controlling the strength of in situ pillars, although the use of the linear Mohr-Coulomb failure criterion still led to very high peak stresses.

## MODELING OF IN SITU COAL PILLAR BEHAVIOR BY ABAQUS

The ABAQUS finite element code was employed in an attempt to simulate complex in situ coal pillar failure mechanisms and to estimate in situ coal pillar strength. The ABAQUS code has been used previously (Hasenfus and Su, 1992) for subsidence prediction and for evaluating longwall chain pillar response. Field data were obtained to verify ABAQUS predictions.

In this paper, two-dimensional coal pillar models were simulated to examine the effect of end constraint and frictional slip on pillar strength. Two groups of models, one representing steel platen loading and the other simulating in situ pillar loading, were examined to illustrate the fundamental difference between laboratory testing using steel platens and in-mine loading of pillars under strong roof and floor conditions. In the steel platen loading simulation, coal specimens were assumed to be 5-feet high and the width-to-height ratio was varied from 1 to 16. The frictional coefficient between the coal and steel platens was assumed to be 0.20. Two-dimensional interface elements were used to model the coal/steel interfaces. An extended Drucker-Prager yield criterion with strain softening was used to model the deformation of coal and the steel platens were assumed to be of the same width as the coal specimens. Figures 2 and 3 show the vertical and lateral stress distributions at peak stress for a sample having a width-to-height ratio of 7. Due to symmetry, only the right-hand side of the model needed to be simulated. The large-scale coal strength was assumed to be 1,000 psi, which represents the average in situ coal strength of the Pittsburgh No. 8, Pocahontas No. 3, and Illinois No. 6 seams. Mark (1990) reported that meaningful results can be achieved with empirical strength formulas if an average value of the in situ strength of 900 psi is used for the U.S. coal seams.

Figures 4 to 8 show the development and distribution of plastic strain for five successive load states for a simulated steel platen loading example. At a pressure of 1,000 psi, shear planes start to develop at angles of about 45° to the axis. For a 5-foot-wide pillar (W/H = 1), these planes would intersect at the center of the pillar and the pillar would fail. For the hypothetical 35-foot-wide pillar, however, there was nearly 30 feet of pillar core beyond the intersection of the shear planes. As the pressure continued to increase, the shear planes and plastic zones progressed towards the center of the pillar until the peak load was reached. Peak strengths for hypothetical coal pillars under steel platen loading conditions are plotted in Figure 9 against width-to-height ratio. In addition to the 1000 psi large-scale coal strength, a low 740 psi coal strength was also simulated to evaluate the effect of coal strength on pillar strength at high width-to-height ratios. It is seen that for the cases simulated, the effect of large-scale coal strength on the peak pillar strength gradually diminishes at very high width-to-height ratios.

In the simulation of in-mine pillar failure mechanisms, the entries adjacent to the pillars were assumed to be 18 feet wide and the roof and floor were assumed to be comprised of very competent rocks. The coal/rock interfaces were assumed to possess nearly zero cohesion, to have a 0.25 frictional coefficient, and to exhibit softened surface behavior. The softened surface behavior simulates the existence of a thin, slickensided clayey layer between the coal and the stiff roof and floor rocks. The estimated peak strengths of the simulated mine pillars are also plotted in Figure 9 against width-to-height ratio. As expected, with very competent roof and floor extending over and beyond the pillars to provide extra confinement, the estimated peak pillar strengths are slightly higher than those calculated for simulated steel platen loading. An apparent acceleration of strength increase is noted at a width-to-height ratio of about 3.0. This is consistent with intuition and observations by Panek (1994), Bieniawski (1981), and Salamon and Wagner (1985) which suggest that confinement due to frictional end constraint will enhance the strength performance as a pillar or specimen becomes squat.

It should be noted that, if the coefficient of friction is reduced due to the presence of moisture or slickensided interfaces, lower ultimate pillar strengths are expected for the respective width-to-height ratios. In addition, it is anticipated that under such conditions the effect of constraint will be muted producing a strength curve more readily approximated by a straight line. The presence of weak partings like clay veins may also weaken the pillar (Maleki, 1994 and Biswas et al., 1995), whereas, the presence of strong shale partings may strengthen the pillar by reducing the effective height. Future efforts will evaluate the effect of these and other typical geological and end constraint variations, including poor roof and floor conditions, on the pillar strength response.

## COMPARISON WITH OTHER PILLAR DESIGN FORMULAS

Figure 10 shows the comparison of in situ coal pillar strength increases predicted by the ABAQUS model using strong roof and floor conditions with those predicted by the Holland-Gaddy formula, the Bieniawski formula, the Barron curve, the modified Bieniawski formula, and the squat pillar formula proposed by Salamon and Wagner. The Holland-Gaddy formula, which is used widely in the U.S. coal industry and by state and federal regulatory agencies, at best estimates a lower bound

pillar strength at width-to-height ratios greater than 5. The Holland-Gaddy equation and the original Bieniawski formula do not show the intuitively obvious strength increases with the onset of pillar confinement, and predict much lower pillar strengths than those illustrated herein for width-to-height ratios greater than 4.0. The strength increase relationship suggested by the ABAQUS modeling most closely resembles that proposed by Barron, for width-to-height ratios of 10 or greater. This is because both models predict a decelerating strength increase for width-to-height ratios greater than 6. This deceleration results from end constraint limitations and the ultimate plastic response of coal under high triaxial stress states. The Barron equation, however, does not predict the onset of pillar strength acceleration, again intuitively obvious as a result of pillar core confinement. Bieniawski recognized this as is reflected in his modified formula, but failed to account for ultimate strength deceleration at higher width-to-height ratios.

## COMPARISON WITH FIELD PILLAR PRESSURE MEASUREMENTS

Pillar pressure measurements from five failed pillars in two southwestern Virginia coal mines were compared to the ABAQUS in situ model pillar strength curve. The first three pillars were part of a four-entry longwall development design that employed pillar widths of 30, 80, and 30 feet across the development (Campoli et al., 1990). The 30-foot pillar adjacent to the headgate entry failed as soon as the longwall face retreated past the pillar. Similarly, the tailgate 30-foot pillar failed as soon as the subsequent longwall face retreated past the pillar. The average measured pressure increase in both pillars was approximately 3,000 psi. Since the pre-longwall average pillar pressure in the 30-foot pillar was about 3,500 psi, the peak pillar strength was approximately 6,500 psi. The 80-foot abutment pillar failed as the subsequent longwall face approached and the average measured pillar pressure increase was about 5,600 psi. With a pre-longwall average pillar pressure of about 3,300 psi, the peak strength for the 80-foot abutment pillar was about 8,900 psi.

The other two pillars were part of a four-entry longwall development that employed pillar widths of 78, 82, and 32 feet across the development (Hasenfus and Su, 1992). The 32-foot tailgate pillar failed at a peak average stress of 4,300 psi before the tailgate-phase longwall face approached. The 82-foot pillar failed in the tailgate phase at an average pressure of 8,500 psi as the face approached to within 100 feet. In the above two cases, the coal seam thickness was about 5 feet. Figure 11 shows that the peak strength of the five failed pillars are in good agreement with the ABAQUS model pillar strength.

## DISCUSSION

The finite element model results, as presented, are not intended to suggest a new pillar design relationship with width-to-height ratio. However, they are presented to illustrate the significance of incorporating the well-documented, fundamental principles of rock material response and failure

mechanics into a design model capable of handling the complex interactions occurring not only within the coal seam, but also in the surrounding roof and floor. Although the effects of weak roof and/or floor on pillar strength are not discussed, preliminary model simulations indicate that with a weak roof or floor, ultimate pillar strength may decrease by as much as 30%.

While the "in situ" uniaxial coal strength is observed to have some effect on pillar strength (Figure 9), its significance is often overrated. As was demonstrated in this study, a small change in interface frictional constraint can be just as significant to peak pillar strength. In fact, for coal pillars with high width-to-height ratios, the ultimate pillar strength is more dependent on end constraints than the uniaxial compressive strength of coal. In addition, at large width-to-height ratios, the variability of pillar strength estimates by current design formulas (Figure 10) is significantly greater than suggested variations in uniaxial compressive strength. This reduces the significance of laboratory coal compressive strength determination for such conditions. For practical purposes, the authors believe that a coal strength of about 950 psi ± 150 psi will suffice for most U.S. bituminous coal seams.

While it may be tempting to use the model results to estimate pillar strength, the authors do not advocate this approach due to the extremely complex interactions among the variable and complex geology, geometry, and stress distribution encountered in the mining environment. Instead, the use of site specific model formulation and subsequent pillar design analysis is recommended. This recommendation, however, is not an attempt to diminish the practice of pillar design via empirical models and/or practical mine experience as long as the limitations of the empirical model and/or experience are considered.

Future modeling with ABAQUS will be conducted to simulate variable roof and floor properties and the subsequent effect on pillar design. It is anticipated that such study will lead to a better understanding of the mechanisms of pillar failure and their relative influence on peak pillar strength and surrounding mine design.

## CONCLUSIONS

A practical coal pillar strength consideration is discussed which considers the complex failure mechanisms of in situ coal pillars. With the capability of modeling interface friction and various boundary conditions, the ABAQUS finite element code is an effective tool for site specific evaluation of in situ coal pillar strength. The modeling technique will be most useful for conditions where interface friction and roof and floor deformation are the primary controlling factors. An in situ coal strength of 1,000 psi was assumed.

Nonlinear pillar strength curves are illustrated to relate the increase of pillar strength to the width-to-height ratio. Confinement generated by frictional effects at the coal/steel or coal/rock interface was shown to increase the pillar strength more rapidly at width-to-height ratios of about 3 for simulated in situ coal pillars and about 5 for simulated steel platen loading of coal pillars. The ABAQUS modeled in situ pillar strength curve for strong roof and floor conditions compares favorably with the measured peak strengths of five failed pillars in two southwestern Virginia coal mines, and is



in general agreement with many existing coal pillar design formulas at width-to-height ratios less than 5. However, for wide pillars the curve predicts a higher in situ coal pillar strength than most accepted formulas. Consequently, use of more conservative empirical formulas may lead to the employment of unnecessarily wide pillars.

## REFERENCES


Babcock, C. O., "Critique of Pillar Design Equations From 1833 to 1990," BuMines IC 9398, 1994, 98 pp.

Babcock, C. O., "True Uniaxial Compressive Strength of Rock or Coal Specimen are Independent of Diameter-to-Length Ratios," BuMines RI 9316, 1990, 31 pp.

Barron, K., "An Analytical Approach to the Design of Coal Pillars," CIM Bulletin, Vol. 77, No. 868, 1984, pp. 37-44.

Bieniawski, Z. T., "Improved Design of Coal Pillars for U.S. Mining Conditions," First Annual Conference on Ground Control in Coal, 1981, pp. 13-22.

Bieniawski, Z. T., "The Effects of Specimen Size on the Compressive Strength of Coal," International Journal of Rock Mechanics Mineral Science, Vol. 5, 1968, pp. 325-335.

Biswas, K., Peng, S. S., and Tsang, P., "Influence of Partings in a Coal Seam on Long-Term Pillar Stability," Proceedings of the Fourteenth Conference on Ground Control in Mining, West Virginia University, 1995, pp. 80-93.

Brady, B. T. and Blake, W., "An Elastic Solution of the Laterally Constrained Circular Cylinder Under Uniaxial Loading," Tenth U.S. Symposium on Rock Mechanics, 1968, pp. 199-214.

Campoli, A. A., Barton, T. M., Van Dyke, F. C., and Gauna, M., "Optimizing Longwall Gate Entry System Design in Bump Prone Coal Mines," BuMines RI 9342, 1990.

Conroy, P., "Rock Mechanics Studies, USBM Demonstration, Old Ben No. 24," Preliminary Report Panel 1, USBM Contract No. J0333949, 1977, 39 pp.

Gaddy, F. L., "A Study of the Ultimate Strength of Coal as Related to the Absolute Size of the Cubical Specimens Tested," Bulletin VpI, Vol. 49, No. 10, 1956, Tables 6-10.

Hasenfus, G. J. and Su, D. W. H., "A Comprehensive Integrated Approach for Longwall Development Design," BuMines IC9315, 1992, pp. 225-237.

Holland, C. T., "The Strength of Coal in Mine Pillars," Proceedings Sixth Symposium on Rock Mechanics, 1964, pp. 450-456.

Hustrulid, W. A. and Swanson, S. R.," Field Verification of Coal Pillar Strength Prediction Formulas," Bureau of Mines Contract Ho 242059, 1981.

Hsiung, S. M. and Peng, S. S., "Chain Pillar Design for U.S. Longwall Panels," Mining Sciences and Technology, Vol. 2, 1985, pp. 279-305.

Iannacchione, A. T., "The Effect of Roof and Floor Interface Slip on Coal Pillar Behavior," Proceedings of the 31st U.S. Symposium on Rock Mechanics, Golden, Colorado, 1990, pp. 156-160.

Khair, A. W., "The Effects of Coefficient of Friction on Strength of Model Coal Pillar," Master Thesis, Department of Mining Engineering, West Virginia University, 1968, 63 pp.

Kripakov, N. P., "Analysis of Pillar Stability on Steeply Pitching Seams Using the Finite Element Method, BuMines RI8579, 1981, 33 pp.

Madden, B. J., "The Performance of Coal Pillars Designed to the Squat Pillar Formula," Twenty-Ninth U.S. Symposium on Rock Mechanics, 1988, pp. 699-708.

Maleki, H., "In Situ Pillar Strength and Failure Mechanisms for U.S. Coal Seams," Proceedings of the Workshop on Coal Pillar Mechanics and Design, BuMines IC9315, 1992, pp. 73-77.

Mark, C. and Iannacchione, A. T., "Coal Pillar Mechanics: Theoretical Models and Field Measurements Compared," Proceedings of the Workshop on Coal Pillar Mechanics and Design, BuMines IC 9315, 1992, pp. 78-93.

Mark, C. and Bieniawski, Z. T., "Field Measurements of Chain Pillar Response to Longwall Abutment Loads," Proceedings, Fifth Conference on Ground Control in Mining, June 1986, pp. 114-122.

Mark, C., "Pillar Design Methods for Longwall Mining," BuMines IC9247, 1990, 53 pp.

Obert, L. and Duvall, W. I., "Rock Mechanics and the Design of Structures in Rock," John Wiley and Sons, New York, 1967, pp. 542-545.

Panek, L., "Sealing Mine Pillar Size and Slope With the $\psi$ Function," SME Annual Meeting, Preprint 94-52, February 1994, 4 p.

Parker, J., "Mine Pillar Design in 1993: Computers Have Become the Opiate of Mining Engineering, Parts I and II," Mining Engineering, July 1993, pp. 714-717, and August 1993, pp. 1047-1050.

Salamon, M. D. G. and Monro, A. H., "A Study of the Strength of Coal Pillars," Journal of South Africa Institute of Mining and Metallurgy, Vol. 68, 1967, pp. 55-67.

Salamon, M. D. G. and Wagner, H., "Practical Experiences in the Design on Coal Pillars," Proceeding of the Twenty-First International Conference of Safety in Mines Research Institute, Sydney, Australia, 1985, pp. 3-10.

Salamon, M. D. G., "Strength and Stability of Coal Pillars," Proceedings of the Workshop on Coal Pillar Mechanics and Design, BuMines IC 9315, 1992, pp. 94-121.

Wagner, H., "Determination of Complete Load-Deformation Characteristics of Coal Pillars," Proceeding of the 3rd International Conference on Rock Mechanics, Denver, Colorado, 1974, pp. 1076-1081.

Wilson, A. H., "Research Into the Determination of Pillar Size, Part I, An Hypothesis Concerning Pillar Stability," The Mining Engineer, Vol. 131, 1972.

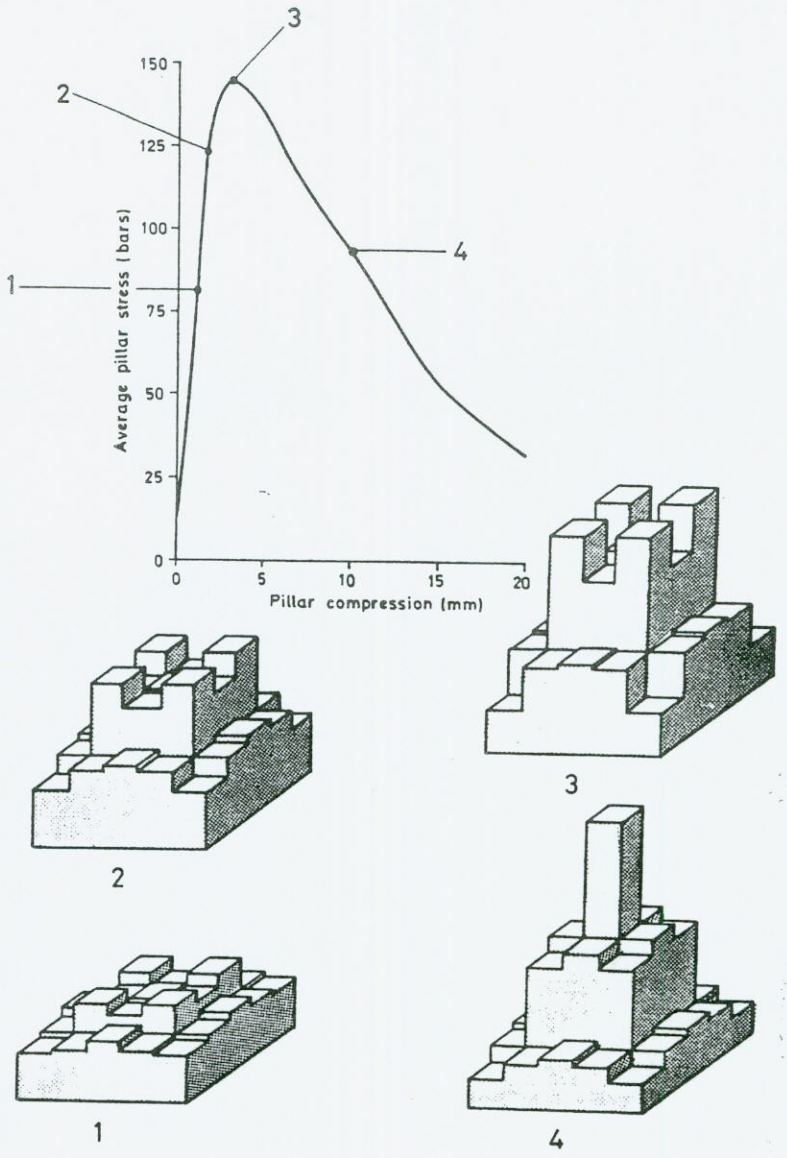



FIGURE 1. A COMPLETE AVERAGE STRESS-COMPRESSION CURVE FOR A COAL PILLAR WITH A WIDTH-TO-HEIGHT RATIO OF 2 AND ISOMETRIC HISTOGRAMS SHOWING THE VERTICAL STRESS DISTRIBUTION AT VARIOUS STAGES OF COMPRESSION.

(AFTER WAGNER, 1974)

FIGURE 2.

VERTICAL STRESS DISTRIBUTION NEAR PEAK STRENGTH (3200 PSI)

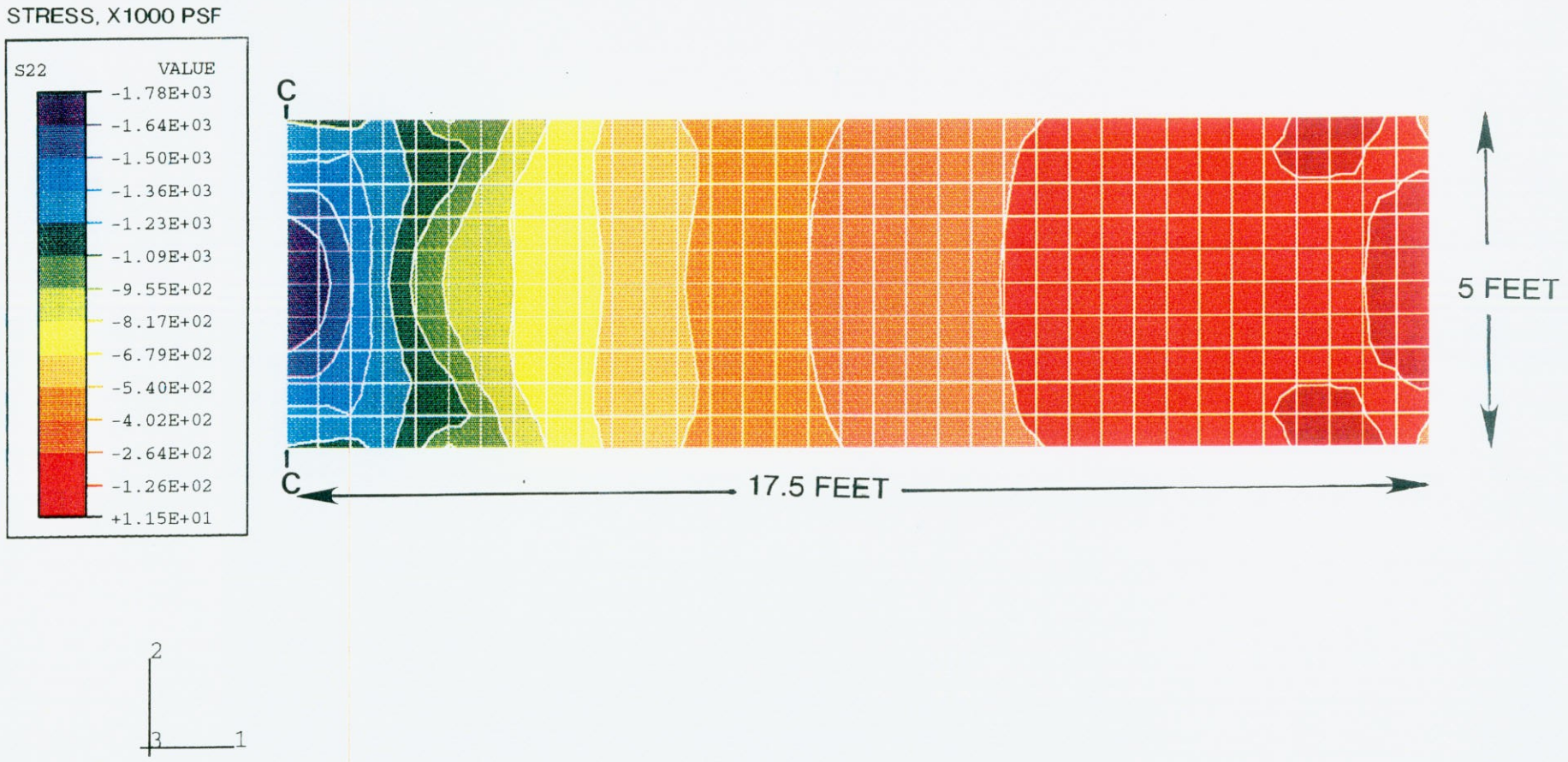


FIGURE 3.

HORIZONTAL STRESS DISTRIBUTION NEAR PEAK STRENGTH

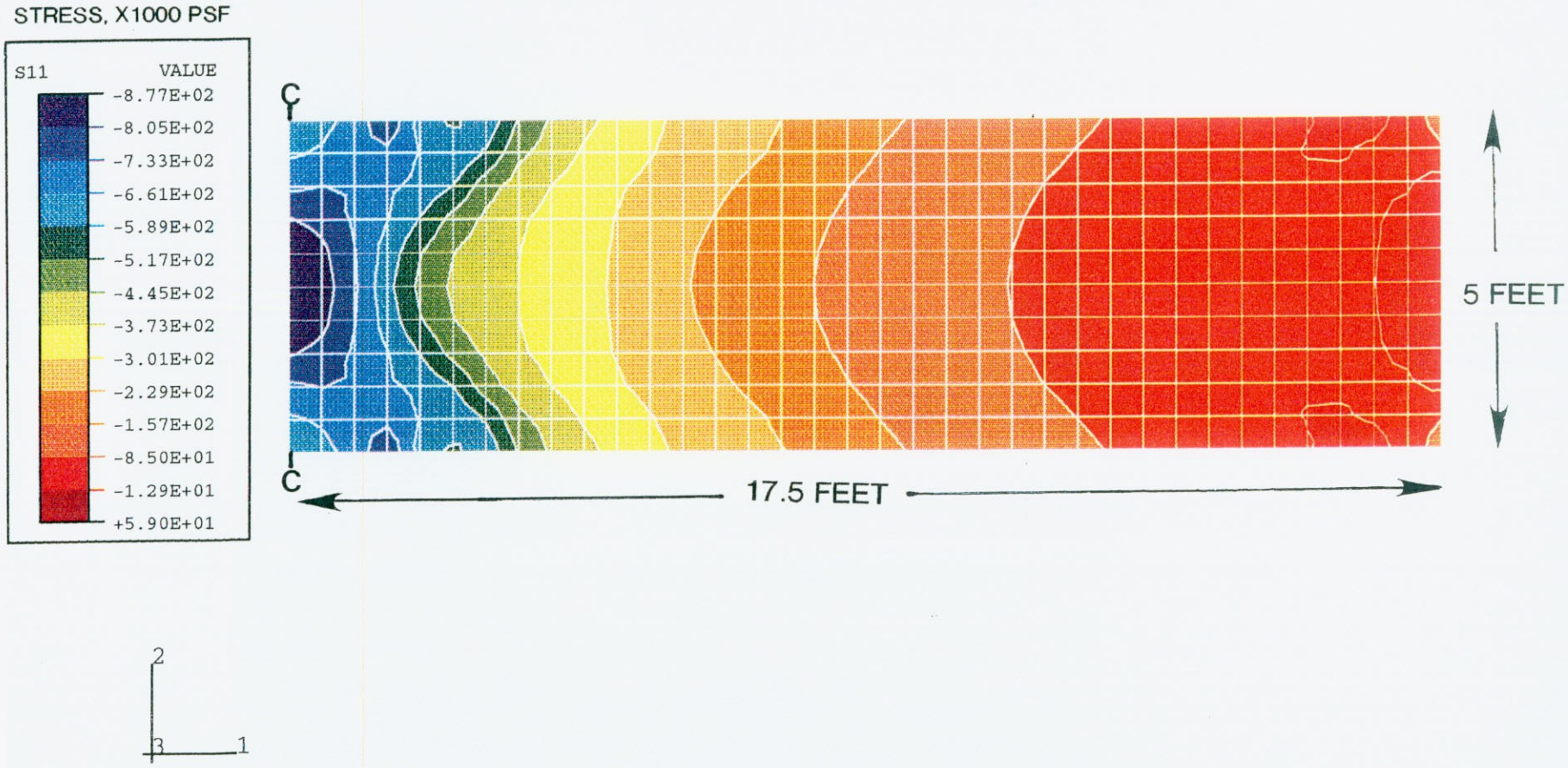


FIGURE 4.

# PLASTIC STRAIN DISTRIBUTION AT 1000 PSI

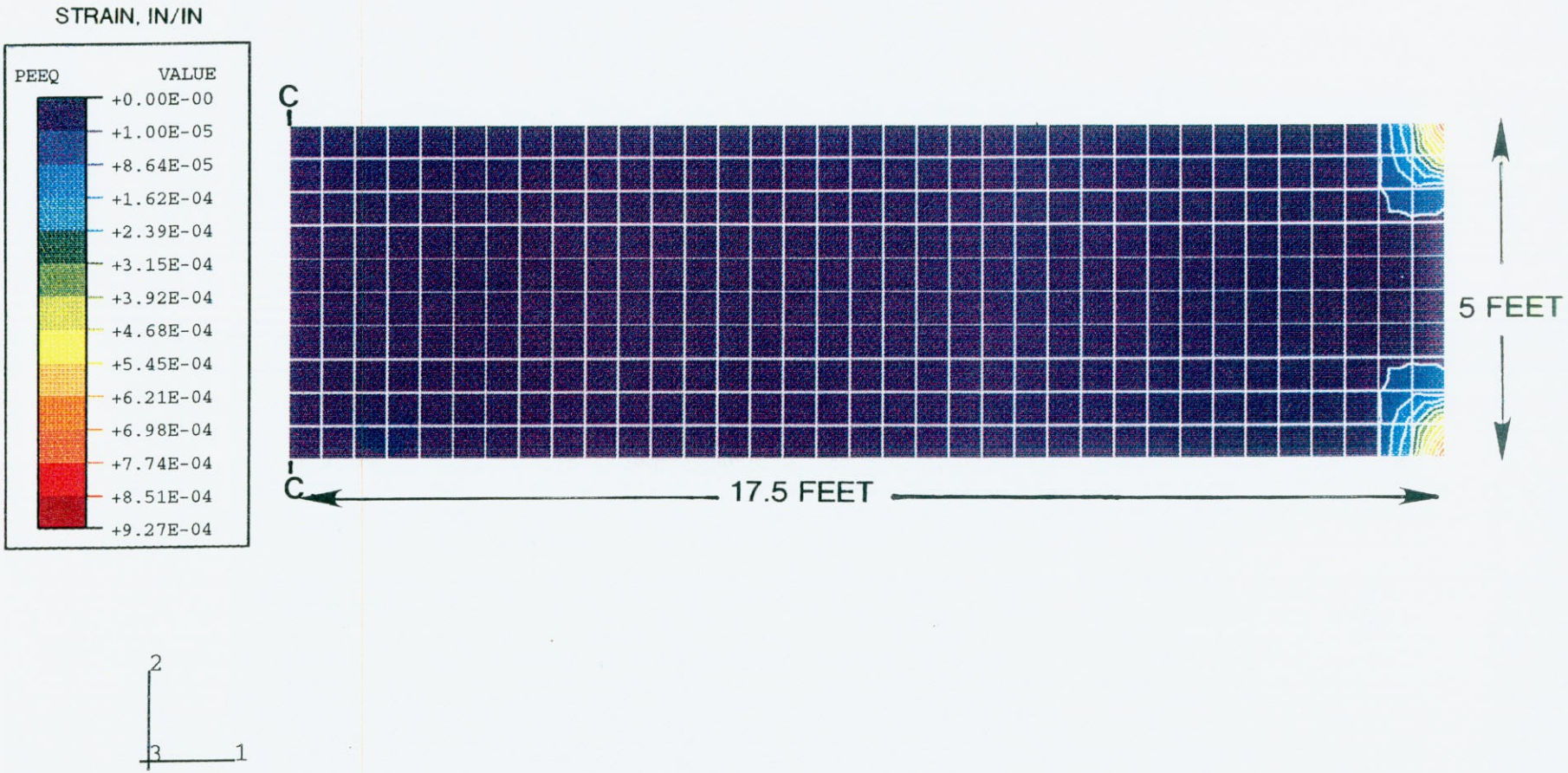


FIGURE 5.

# PLASTIC STRAIN DISTRIBUTION AT 1200 PSI

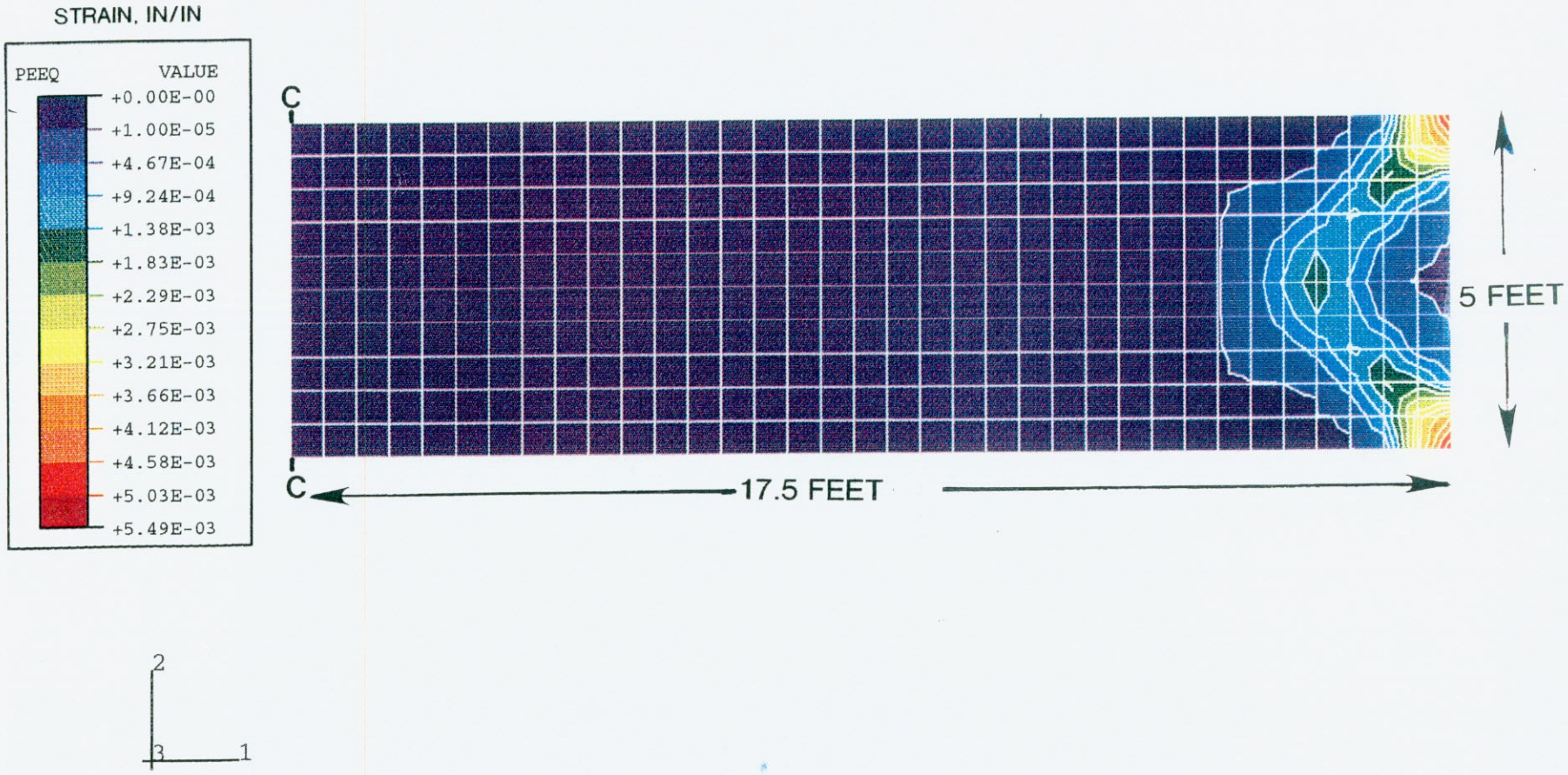


FIGURE 6.

# PLASTIC STRAIN DISTRIBUTION AT 1600 PSI

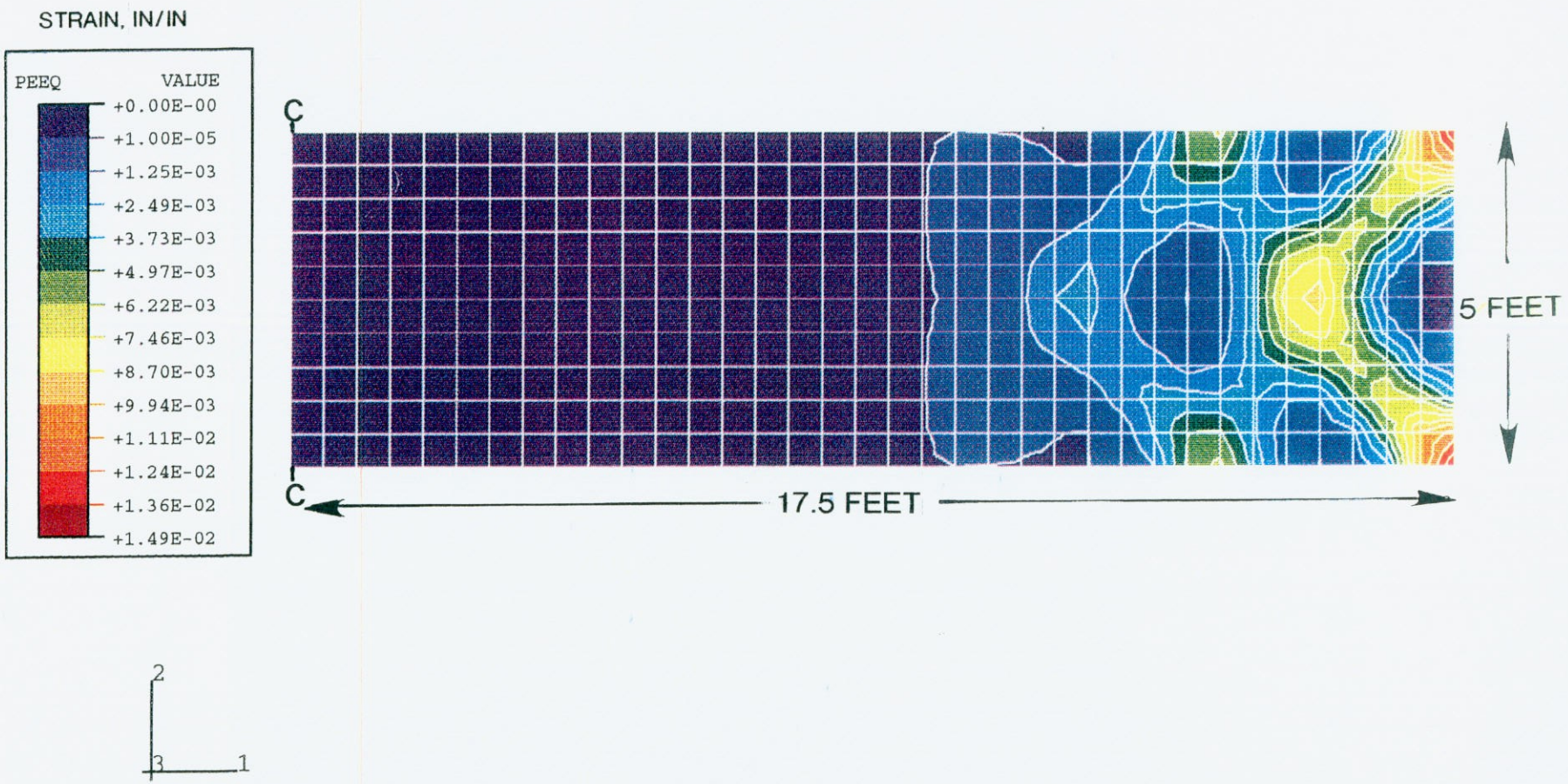


FIGURE 7.

# PLASTIC STRAIN DISTRIBUTION AT 2200 PSI

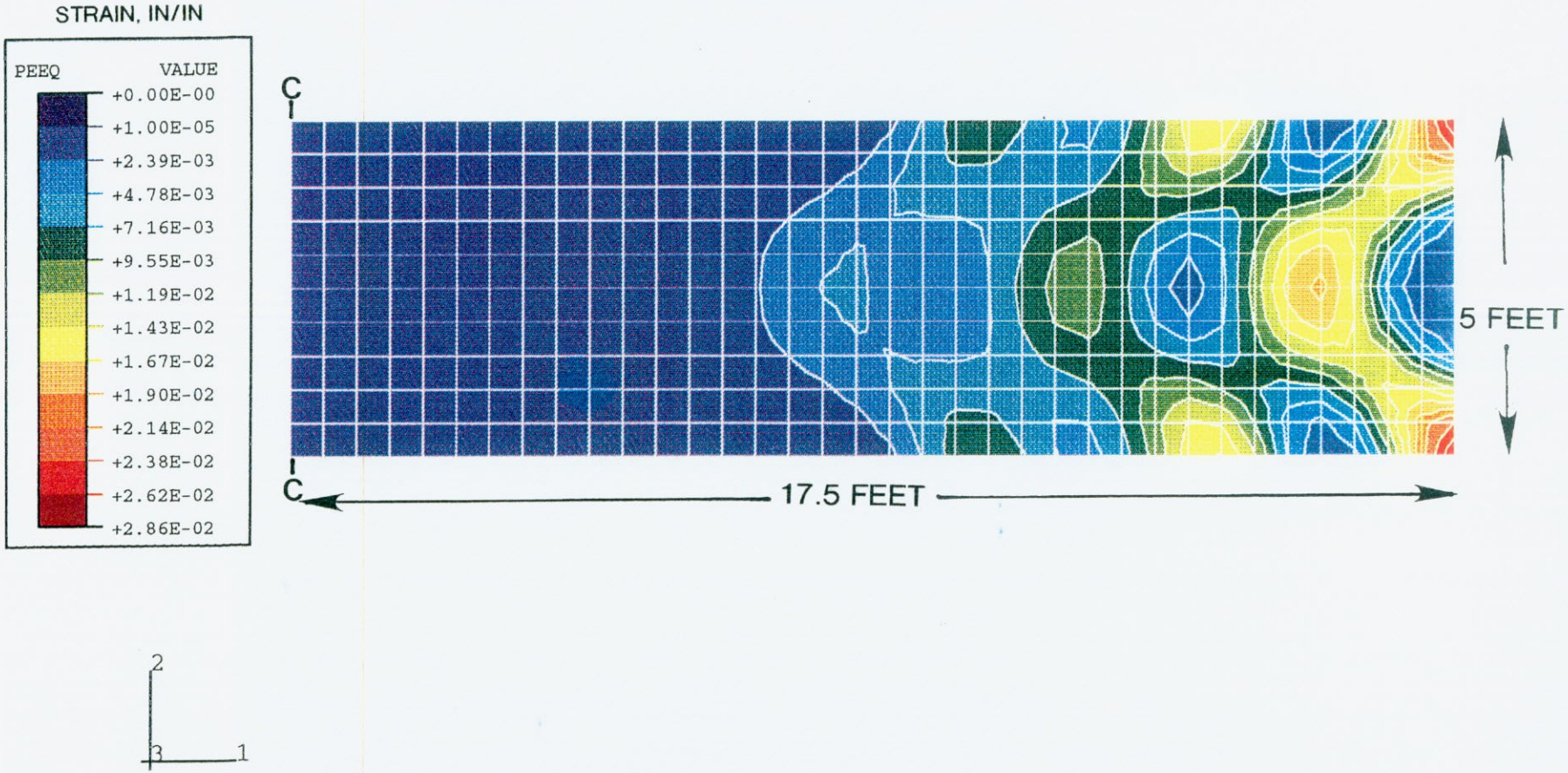
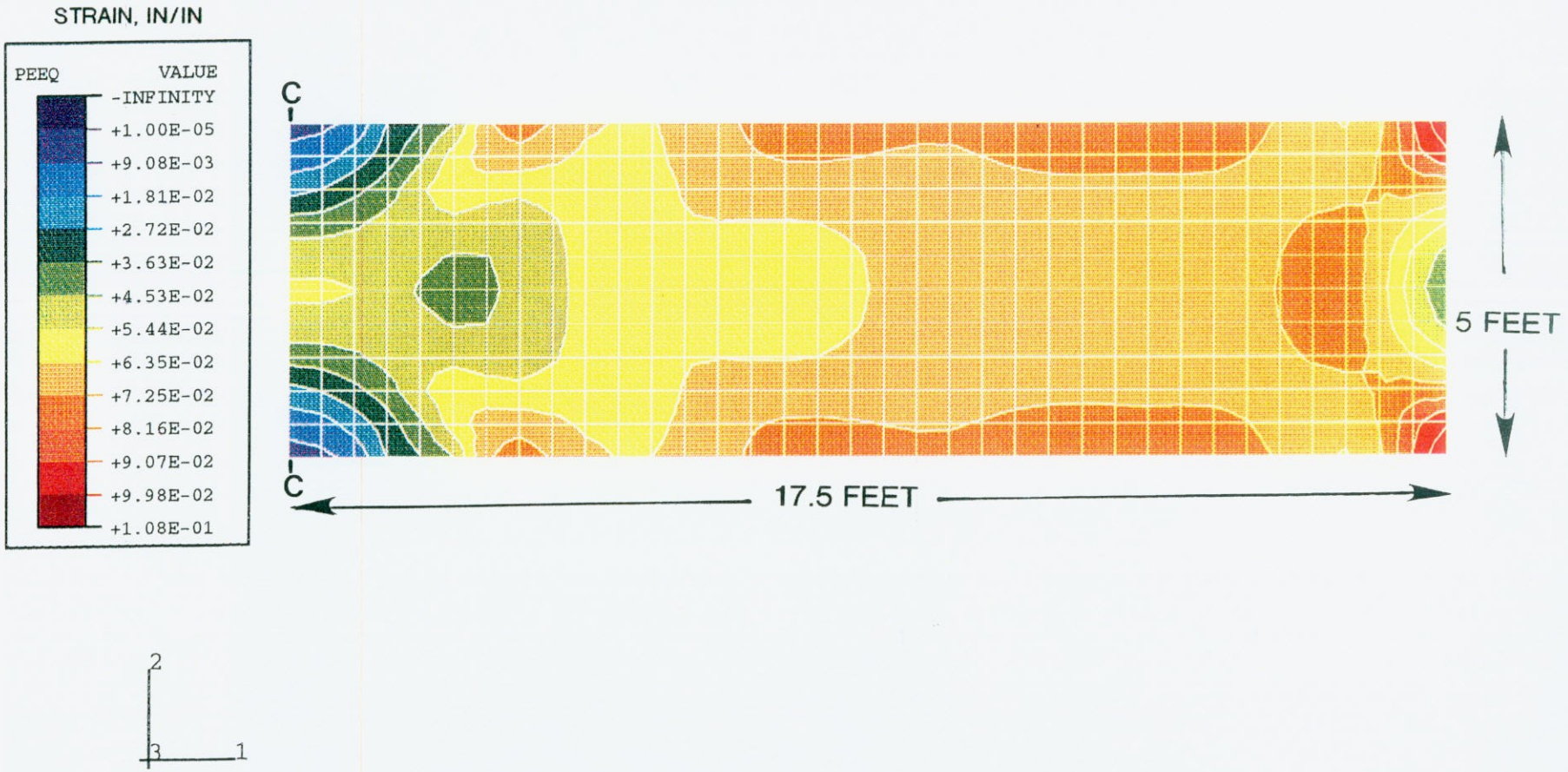


FIGURE 8.

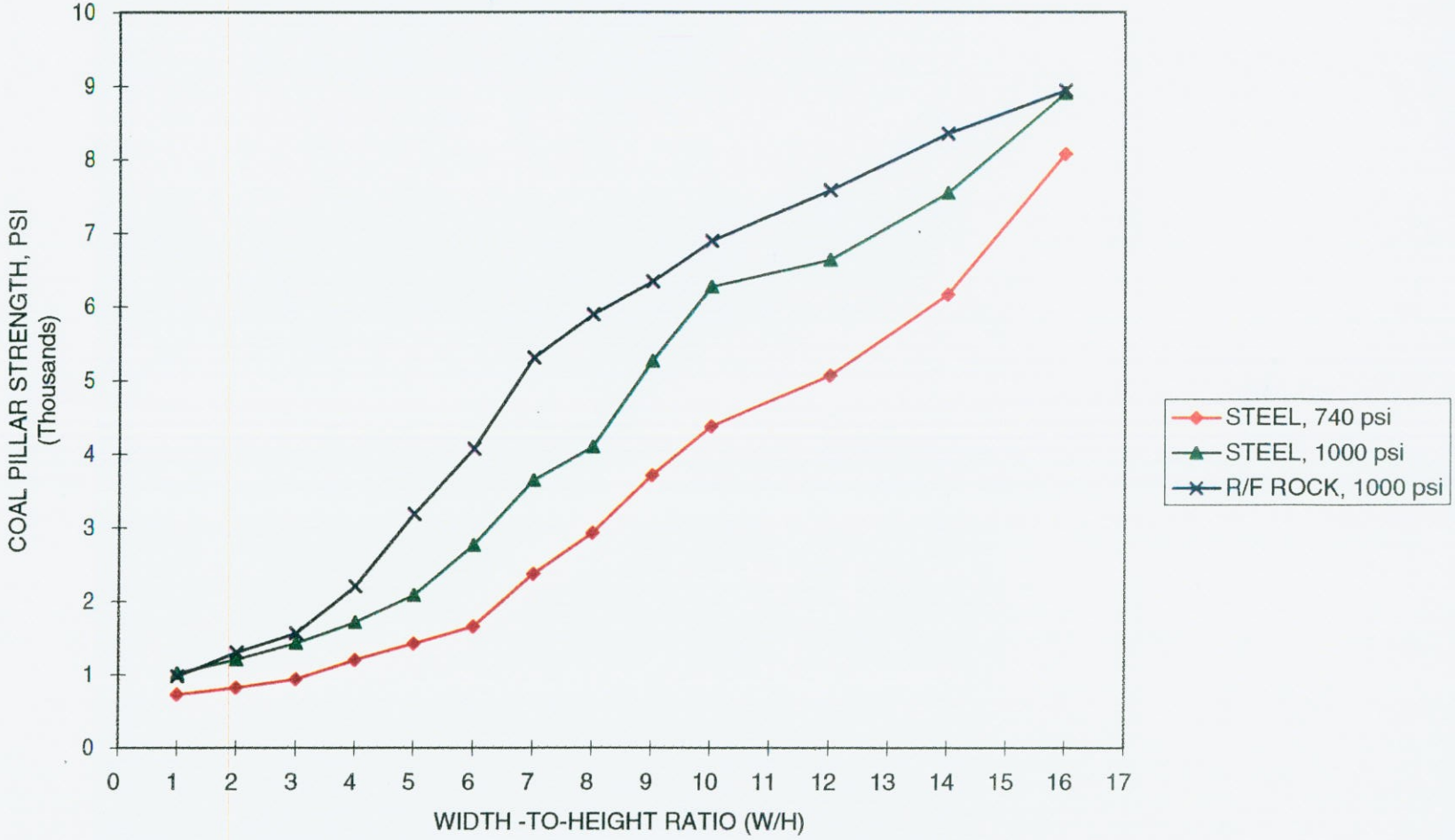
# PLASTIC STRAIN DISTRIBUTION NEAR PEAK STRENGTH (3200 PSI)



# FIGURE 9.

## COAL PILLAR STRENGTH VS. W/H

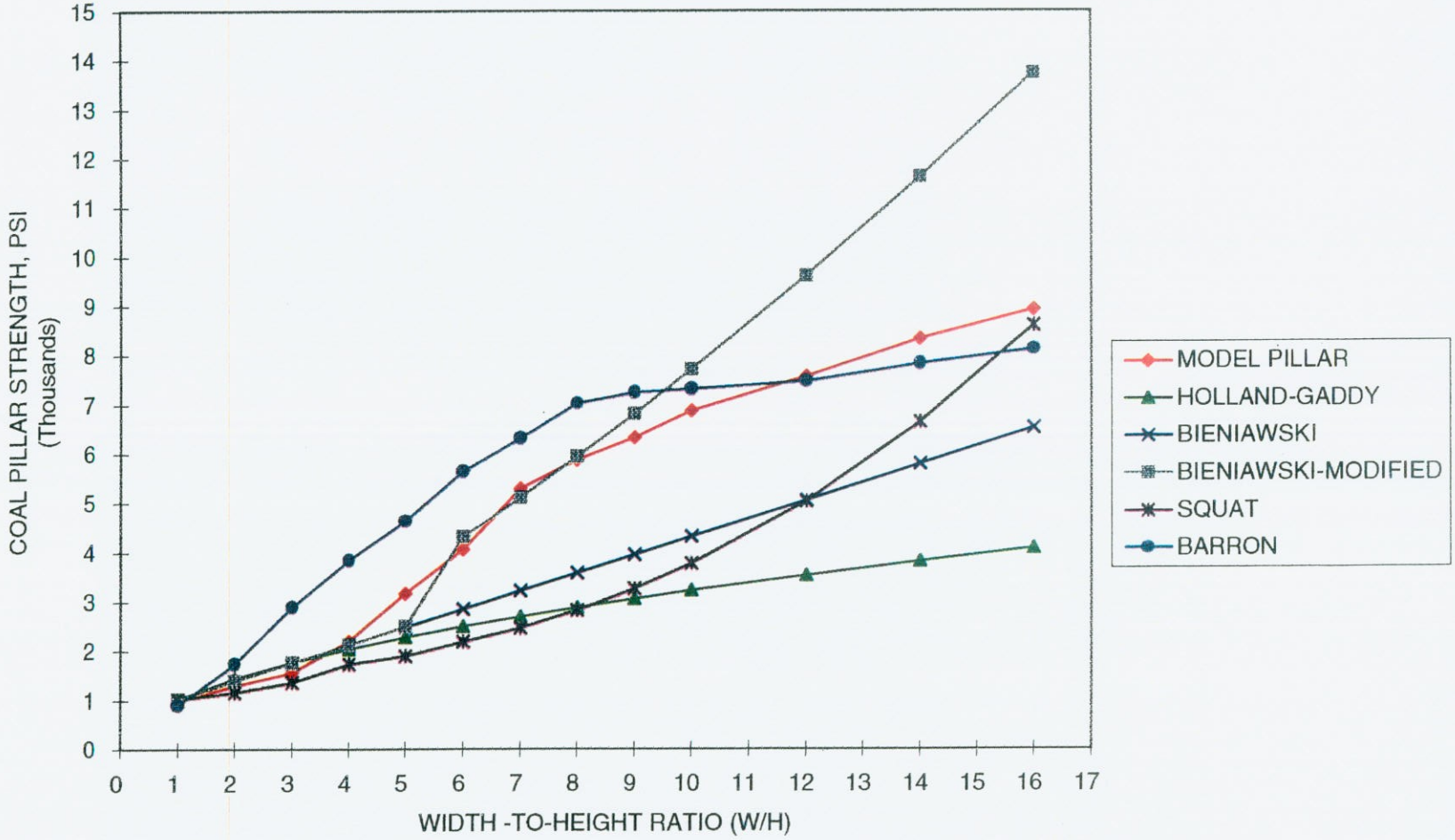
### COAL PILLAR HEIGHT=5 FEET



# FIGURE 10.

## PILLAR STRENGTH COMPARISON

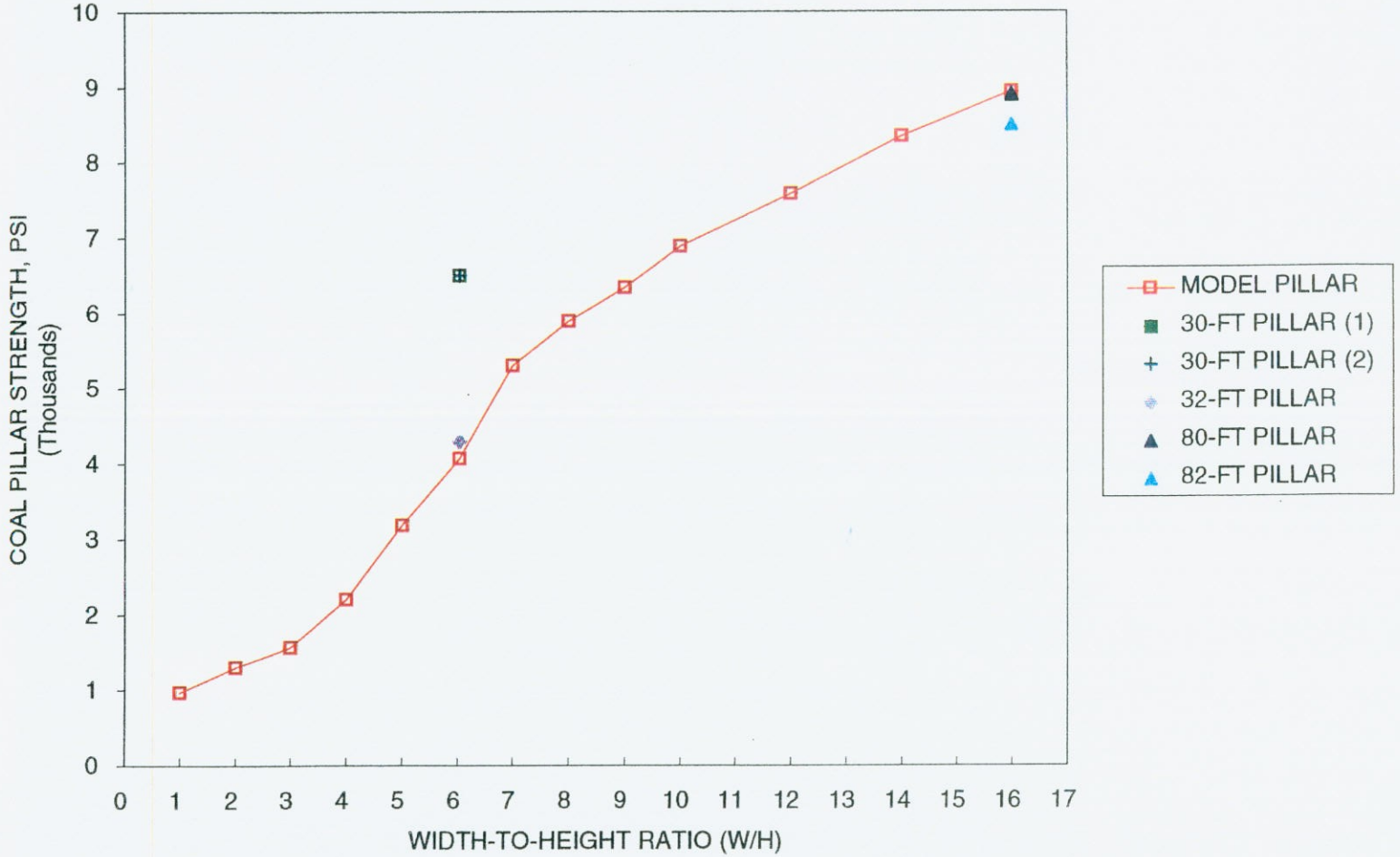
### MODEL PILLAR VS. EXISTING FORMULAS



# FIGURE 11.

## PEAK STRENGTH COMPARISON

### MODEL PILLAR VS. FAILED PILLARS





# EFFECTS OF IN-SEAM AND NEAR-SEAM CONDITIONS ON COAL PILLAR STRENGTH

Daniel W. H. Su
Gregory J. Hasenfus

CONSOL Inc.
Research & Development
4000 Brownsville Road
Library, Pennsylvania 15129

## ABSTRACT

The importance of incorporating fundamental principles of rock material response and failure mechanics into a pillar strength design model has been demonstrated. To accurately assess pillar strength, a model should account not only for the characteristics of the coal, but also for those of the surrounding strata. The interactions between the pillar and the surrounding roof and floor dictate ultimate pillar strength. Confinement, or the lack thereof, provided by roof and floor frictional end-constraint is one of the most significant factors in the strength of very wide pillars. The best conditions for end-constraint occur with ideally strong roof and floor. In this paper, it will be shown that rock partings within the coal have a variable effect on pillar strength, depending on the parting strength. A competent shale parting within the coal reduces the effective pillar height, thus increasing the ultimate pillar strength; a weak claystone parting slightly decreases pillar strength. Seam strength has negligible effect on the peak strength for pillars at high width-to-height ratios. For practical coal pillar design, determination of intact coal strength thus becomes unnecessary and for wide pillars an average seam strength of 950 psi may suffice for most U.S. bituminous coal seams. Furthermore, very weak floor may decrease the ultimate pillar strength by as much as 50% compared to ideal conditions. Field observations confirm pillar strength reduction in the presence of weak floor. Due to the site-specific nature of coal pillar design, no single pillar design formula or model will apply in all instances. Understanding the site-specific parameters is important for successful coal pillar design. A rigid pillar design guideline may lead to impractical coal pillar design.

## INTRODUCTION

The strength of coal and coal pillars has been the subject of considerable research during the past 40 years. Coal strengths determined in the laboratory typically increase with increasing specimen width-to-height ratio and decrease with increasing height and size. Based on the shape and size effect derived from testing of cubical specimens, during the past three decades, a number of empirical pillar strength formulas (Gaddy, 1956, Holland, 1964, Obert and Durall, 1967, Salamon and Munro, 1967, Bieniawski, 1968, and Hustrulid and Swanson, 1981) and closed-form analytical solutions for pillar strength (Wilson, 1972 and Barron, 1984) were proposed and used by coal operators and regulatory authorities with varying degrees of success. However, empirical formulas may not be extrapolated

with confidence beyond the data from which they were derived, typically from pillars with width-to-height ratios of five or less (Mark and Iannacchione, 1992), and these formulas inherently ignore roof and floor end constraint and subsequent interactions.

The importance of friction and end constraint on laboratory coal strength has been demonstrated by many researchers, including Khair (1968), Brady and Blake (1968), Bieniawski (1981), Salamon and Wagner (1985), Babcock (1990, 1994), and Panek (1994). Practitioners and researchers alike, including Conroy (1977), Mark and Bieniawski (1986), Hasenfus and Su (1992), Maleki (1992), and Parker (1993) have noted the significance of roof and floor interactions on in situ pillar strength.

The importance of incorporating fundamental principles of rock material response and failure mechanics into a pillar strength design model has been demonstrated (Su and Hasenfus, 1996). To accurately assess pillar strength, a model should account not only for the characteristics of the coal, but also for those of the surrounding strata. The interactions between the pillar and the surrounding roof and floor frictional end-constraint is one of the most significant factors in the strength of very wide pillars. The best conditions for end-constraint occur with ideally strong roof and floor. Under such ideal conditions, a nonlinear relationship between pillar strength and pillar width-to-height ratio is likely. Confinement provided by friction at the coal/rock interfaces begins to accelerate pillar strength increase at a width-to-height ratio of about 3. Frictional constraint limitations and coal plasticity begin to decelerate the strength increase at a width-to-height ratio of about 7. In this paper, the effects of rock partings and weak floor rock on in situ coal pillar strength are examined through a series of finite element simulations. The effect of in situ seam strength on the ultimate coal pillar strength is evaluated as is the validity of two most popular empirical formulas.

## EFFECTS OF ROCK PARTINGS ON COAL PILLAR STRENGTH

Rock partings or binders are found in many coal seams in the United States. However, most pillar design concepts consider the coal seam as a uniform structure for the sake of simplicity. Biswas et al., (1995) studied the time-dependent penetration of moisture into binders and subsequent weakening of the coal pillar structure. In this paper, ABAQUS (Hibbitt et al., 1996) finite element simulation is employed to study the effect of soft and hard rock partings on the static loading of in situ coal pillars.

To illustrate the effect of rock partings on coal pillar strength at various width-to-height ratios, two series of finite element models were constructed to simulate the effect of both strong and soft partings. The models included not only the pillar in question, but also the effect of adjacent pillars and entries. A total pillar height of 5 feet was employed in the models, which included a mid-pillar parting thickness of 1 foot. The roof and floor were simulated to be very competent rocks. The coal/rock and coal/parting interfaces were assumed to possess zero cohesion, to have a 14° frictional angle, and to exhibit softened surface behavior. The softened surface behavior was used to simulate the existence of a thin slickensided clayey layer along the interfaces. A coal seam strength of 1,000 psi was used for the models. Parting rocks were simulated to be a weak claystone and a medium-

strength shale. Representative properties of the coal, roof, floor, and parting rocks employed in this study are provided in Table 1. Figure 1 illustrates the near-seam finite element mesh layout for a 30-foot wide pillar containing a 1-foot mid-pillar parting, and the resulting Mises stress distribution around and within the pillar near its peak strength.

The estimated peak strengths of the simulated mine pillars with rock partings are plotted in Figure 2 against the width-to-height ratios. Also included in Figure 2 is the peak strength of the same pillar without rock partings (Su and Hasenfus, 1996). These results indicate that rock partings within the coal can significantly affect pillar strength, the nature of the change depending on the parting strength. A weak parting rock, such as the simulated claystone, can fail prematurely, thus increasing the depth of pillar yield and subsequently reducing the peak pillar strength. Conversely, a more competent shale parting effectively reduces pillar height, thus increasing the width-to-height ratio and subsequently the peak pillar strength. Note that in the simulated strong parting scenario, the pillar strengths gradually begin to approach those for pillars without parting with increasing width-to-height ratios (in this situation, beyond a width-to-height ratio of 6) due to failure of the shale rock. It thus becomes evident that both the parting strength and the interaction between the parting and coal will affect peak pillar loading and that the ability to predict this effect without site specific considerations of parting strength and thickness may lead to erroneous pillar strength results.

## EFFECT OF SEAM STRENGTH ON ULTIMATE PILLAR STRENGTH

For coal pillar design, many pillar strength formulas have been used in the United States. However, for subsidence control plans, most state regulatory guidelines recommend the use of the Bieniawski and/or the Holland-Gaddy formulas for sizing of pillars. Besides the width-to-height ratio, the most critical parameter for these and other empirical formulas is the seam strength, which is considered to be equivalent to the laboratory coal strength divided by an appropriate size effect. The most common approach for estimating seam strength is to scale the intact coal strength using the equation,

$$\sigma_s = \frac{K}{36^a} = \frac{\sigma_c D^a}{36^a}, \qquad (1)$$

where $\sigma_s$ is the in situ seam strength in psi, $\sigma_c$ is the laboratory-derived uniaxial compressive strength of coal samples in psi, D is the cubical dimension of the laboratory specimen in inches, and $a$ is a seam-specific constant ranging from 0.15 to 0.60. This equation typically assumes that a critical size of 3 feet exists beyond which no significant decrease in sample strength will occur. Experimental data indicate that such a statement is true for Pittsburgh and Pocahontas No. 3 seams. The question arises whether or not the seam strength derived from Equation (1) is a realistic estimate for all seams that may possess different fracture frequencies and geological conditions.

A significant problem in using Equation (1) for determining the seam strength is the choice of the uniaxial compressive strength, $\sigma_c$. Compressive tests on coal specimens, even from the same location, show a wide scatter of uniaxial compressive strength (Newman and Hoelle, 1993). Typically, a mean compressive strength is obtained from such tests which, due to the sampling procedure and presence of discontinuities, may not necessarily exhibit normal distribution. Therefore, a fairly large number of compressive tests may be needed to determine a meaningful compressive strength. For practical purposes in coal pillar design, particularly in the case of new reserves where only exploratory drill core is available for testing, the number of tests required is unrealistically high and determination of intact coal strength data becomes a difficult or futile exercise. In recent years, however, Mark (1990) and Mark and Barton (1996) reported that meaningful results can be achieved with empirical strength formulas if an average seam strength value of 900 psi is used for U.S. bituminous coal seams. They also suggested that pillar stability design is more reliable when a uniform seam strength is used to evaluate all cases.

To further investigate this issue, a series of finite element models was constructed to examine the effect of seam strength on ultimate pillar strength at various width-to-height ratios. Prior numerical study of simulated pillars compressed between steel platens had suggested that the seam strength has a significant effect on pillar strength but diminishes with increasing width-to-height ratios (Su and Hasenfus, 1996). In Case 1 of this study, the coal was modeled with a seam strength of 1,000 psi and a pronounced post-yield strain softening property to represent seams with widely spaced cleats. In Case 2, the seam strength was modeled to be 900 psi with the coal exhibiting a nearly elastoplastic behavior to represent seams with closely spaced cleats. The dependence of post-yield behavior on cleat spacing has been documented by Ko and Gerstle (1976) for a number of U.S. bituminous coal seams. Generally speaking, coal seams with widely spaced cleats have higher strength and pronounced post-yield strain softening, while coal seams with closely spaced cleats have lower strength and no post-yield strain softening. For most U.S. bituminous coal seams, the seam strength falls within the 900 to 1000 psi range. Therefore, Cases 1 and 2 represent two extremes of coal behavior commonly observed in the U.S. coal fields. Figure 3 illustrates the resulting estimated peak strengths at various width-to-height ratios for Cases 1 and 2. From the results, it appears that the in situ strength of coal has only a small effect on the peak pillar strength. On a percentage basis, the seam strength affects the peak pillar strength more at low width-to-height ratios. This effect diminishes at higher width-to-height ratios. Therefore, for practical finite element model simulation of pillars with high width-to-height ratios, a uniform seam strength averaging about 950 psi is adequate for most U.S. bituminous coal seams. These results are in good agreement with the findings reported by Mark (1990) and Mark and Barton (1996). Note that the post-failure behavior of the coal is slightly more influential than the seam strength for width-to-height ratios between 4 and 10.

## EFFECT OF WEAK FLOOR STRATA ON PILLAR STRENGTH

Many researchers in the past decade have noted the significance of weak floor strata on in situ coal pillar strength (Conroy, 1977; Chugh, 1986; Hasenfus and Su, 1992; Maleki, 1992; and Parker,

1993). The most common weak floor stratum beneath U.S. coal seams is claystone (fireclay), which is inherently weak, often slickensided, and highly susceptible to water degradation. Severe floor bearing problems for mine equipment and for coal pillars may occur within localized coal seam structural depressions, especially when one or more near-seam water source is present.

In this paper, the effect of weak floor strata on ultimate coal pillar strength is examined via a series of finite element simulations and subsequent comparisons with available field data. The claystone floor strata were modeled to be weaker than coal to represent strength degradation due to water saturation. The resulting peak pillar strengths versus width-to-height ratios, shown in Figure 4, indicate that, compared to a strong floor, **a weak claystone floor may significantly reduce the ultimate peak pillar strength as a result of reduced pillar confinement near the floor interface**. In this series of simulations, the differences in peak pillar strength increases with increasing pillar width-to-height ratios. In addition, beyond the width-to-height ratio of 8, the peak strength asymptotes toward a maximum value, apparently limited by the plastic-flow of the very weak claystone beneath. At high width-to-height ratios, the peak strength reduction is nearly 50%.

Also plotted in Figure 4 are measured peak pillar strength data for two 32-foot, one 78-foot, and one 82-foot pillars in a southwestern Virginia coal mine that exhibited site-specific thick and weak floor claystone. The model results are in good agreement with the field measurements.

## COMPARISON OF PILLAR DESIGN FORMULAS

Many empirical and analytical pillar design formulas as well as numerical pillar design models have been proposed and used with varying degrees of success during the past three decades. However, it is the opinion of the authors that the use of pillar design formulas is extremely site-specific, strongly dependent on local geological conditions, and primarily dictated by the coal/rock interaction and the resulting confinement (Su and Hasenfus, 1996). Currently, there exists no simple pillar design formula that can account for all in situ conditions that affect pillar strength.

**Figure 5 shows a comparison of the popular** Bieniawski and Holland-Gaddy formulas with the ABAQUS modeled peak pillar strengths for three conditions: pillars confined by very competent roof and floor rocks; pillars confined by competent roof and weak floor rocks; and pillars with a weak claystone binder. Compared to the ABAQUS model, for competent roof and floor strata, the Bieniawski and Holland-Gaddy formulas can underpredict the peak pillar strength by as much as 30% to 60% for width-to-height ratios greater than 5. On the other hand, the Bieniawski formula compares more favorably with the ABAQUS weak parting simulation and the weak floor simulation for pillar width-to-height ratios less than 10. Similarly, the Holland-Gaddy formula compares favorably with both the weak parting and weak floor ABAQUS results for width-to-height ratios less than 5, and at very large width-to-height ratios it compares better with the ABAQUS weak floor

results than does the Bieniawski formula. It is apparent that weak roof, floor, and seam parting conditions will each serve to comparatively reduce the effects of confinement provided by strong, competent roof and floor. In addition, for limited width-to-height ratios, simple linear empirical pillar strength models are in general agreement with the detailed ABAQUS finite element models for certain weak roof, floor, or parting conditions.

## CONCLUSIONS

The importance of incorporating fundamental principles of rock material response and failure mechanics into a pillar strength design model or formula has been demonstrated. To accurately assess pillar strength, a model or formula should account not only for the characteristics of coal, but also for those of the surrounding strata. When necessary material data are available, numerical models are ideal tools for handling complex interactions occurring not only within the coal seam, but also in the surrounding roof and floor.

While the seam strength is observed to have some effect on pillar strength, its significance is often overrated. In fact, for coal pillars with large width-to-height ratios, the ultimate pillar strength is more dependent on end constraints than on seam strength. This reduces the significance of laboratory coal compressive strength determination for such conditions. For practical purposes, a uniform seam strength averaging about 950 psi is adequate for most U.S. bituminous coal seams, when employing finite element models to simulate pillars with high width-to-height ratios.

The finite element model results, as presented, are not intended to suggest new pillar design relationships with width-to-height ratios. The primary objective of this paper is to emphasize the site-specific nature of coal pillar design and the value of using modeling procedures to account for such site-specific conditions. Understanding the site-specific parameters is an important ingredient for successful coal pillar design. Due to the variability of in situ properties, no currently available empirical or analytical pillar design formula is applicable in all cases. Utilization or imposition of pillar design formulas that do not, or cannot, account for site-specific variations in roof, floor, and parting conditions may lead to incorrect assessments of pillar strengths, whether high or low, and incorrect estimates of pillar design safety factors. Empirical, analytical, or numerical design procedures should be validated by mine or site-specific measurements or observational field studies whenever possible.

## REFERENCES


Babcock, C. O., "Critique of Pillar Design Equations From 1833 to 1990," USBM IC 9398, 1994, 98 pp.

Babcock, C. O., "True Uniaxial Compressive Strength of Rock or Coal Specimen are Independent of Diameter-to-Length Ratios," USBM RI 9316, 1990, 31 pp.

Barron, K., "An Analytical Approach to the Design of Coal Pillars," CIM Bulletin, Vol. 77, No. 868, 1984, pp. 37-44.

Bieniawski, Z. T., "Improved Design of Coal Pillars for U.S. Mining Conditions," First Annual Conference on Ground Control in Coal, 1981, pp. 13-22.

Bieniawski, Z. T., "The Effects of Specimen Size on the Compressive Strength of Coal," International Journal of Rock Mechanics Mineral Science, Vol. 5, 1968, pp. 325-335.

Biswas, K., Peng, S. S., and Tsang, P., "Influence of Partings in a Coal Seam on Long-Term Pillar Stability," Proceedings of the Fourteenth Conference on Ground Control in Mining, West Virginia University, 1995, pp. 80-93.

Brady, B. T. and Blake, W., "An Elastic Solution of the Laterally Constrained Circular Cylinder Under Uniaxial Loading," Tenth U.S. Symposium on Rock Mechanics, 1968, pp. 199-214.

Campoli, A. A., Barton, T. M., Van Dyke, F. C., and Gauna, M., "Optimizing Longwall Gate Entry System Design in Bump Prone Coal Mines," USBM RI 9342, 1990.

Chugh, Y. P., "In Situ Strength Characteristics of Coal Mine Floor Strata in Illinois," USBM Open File Report 16-87, 1986, 160 pp.

Conroy, P., "Rock Mechanics Studies, USBM Demonstration, Old Ben No. 24," Preliminary Report Panel 1, USBM Contract No. J0333949, 1977, 39 pp.

Gaddy, F. L., "A Study of the Ultimate Strength of Coal as Related to the Absolute Size of the Cubical Specimens Tested," Bulletin VPI, Vol. 49, No. 10, 1956, Tables 6-10.

Hasenfus, G. J. and Su, D. W. H., "A Comprehensive Integrated Approach for Longwall Development Design," USBM IC9315, 1992, pp. 225-237.

Hibbitt, D., Karlsson, B., and Sorensen, P., ABAQUS Version 5.6, Hibbitt, Karlsson & Sorensen, Inc., Pawtucket, RI, 1996.

Holland, C. T., "The Strength of Coal in Mine Pillars," Proceedings Sixth Symposium on Rock Mechanics, 1964, pp. 450-456.

Hustrulid, W. A. and Swanson, S. R., "Field Verification of Coal Pillar Strength Prediction Formulas," USBM Contract Ho 242059, 1981.

Khair, A. W., "The Effects of Coefficient of Friction on Strength of Model Coal Pillar," Master Thesis, Department of Mining Engineering, West Virginia University, 1968, 63 pp.

Ko, H. Y. and Gerstle, K. H., "Constitutive Relations of Coal and Coal Measure Rocks," Interim Report, USBM Contract G01550156, 1976.

Maleki, H., "In Situ Pillar Strength and Failure Mechanisms for U.S. Coal Seams," Proceedings of the Workshop on Coal Pillar Mechanics and Design, USBM IC9315, 1992, pp. 73-77.

Mark, C. and Barton, T., "The Uniaxial Compressive Strength of Coal: Should it be Used to Design Pillars ?," Proceedings of the 15th International Conference on Ground Control in Mining, Golden, Colorado, 1996, pp. 61-78.

Mark, C. and Iannacchione, A. T., "Coal Pillar Mechanics: Theoretical Models and Field Measurements Compared," Proceedings of the Workshop on Coal Pillar Mechanics and Design, USBM IC 9315, 1992, pp. 78-93.

Mark, C. and Bieniawski, Z. T., "Field Measurements of Chain Pillar Response to Longwall Abutment Loads," Proceedings, Fifth Conference on Ground Control in Mining, June 1986, pp. 114-122.

Mark, C., "Pillar Design Methods for Longwall Mining," BuMines IC9247, 1990, 53 pp.

Newman, D. A. and Hoelle, J. L., "The Impact of Variability in Coal Strength on Mine Planning and Design - A Case History," Proceedings of the 12th International Conference on Ground Control in Mining, Morgantown, West Virginia, 1993, pp. 237-243.

Obert, L. and Duvall, W. I., "Rock Mechanics and the Design of Structures in Rock," John Wiley and Sons, New York, 1967, pp. 542-545.

Panek, L., "Sealing Mine Pillar Size and Slope With the $\psi$ Function," SME Annual Meeting, Preprint 94-52, February 1994.

Parker, J., "Mine Pillar Design in 1993: Computers Have Become the Opiate of Mining Engineering, Parts I and II," Mining Engineering, July 1993, pp. 714-717, and August 1993, pp. 1047-1050.

Salamon, M. D. G. and Monro, A. H., "A Study of the Strength of Coal Pillars," Journal of South Africa Institute of Mining and Metallurgy, Vol. 68, 1967, pp. 55-67.

Salamon, M. D. G. and Wagner, H., "Practical Experiences in the Design on Coal Pillars," Proceeding of the Twenty-First International Conference of Safety in Mines Research Institute, Sydney, Australia, 1985, pp. 3-10.

Su, D. W. H. and Hasenfus, G. J., "Practical Coal Pillar Design Considerations Based on Numerical Modeling," Proceedings of the 15th International Conference on Ground Control in Mining, Golden, Colorado, 1996.

Wilson, A. H., "Research Into the Determination of Pillar Size, Part I, An Hypothesis Concerning Pillar Stability," The Mining Engineer, Vol. 131, 1972.

**Table 1**

**In-Situ Mechanical Properties of Coal, Rock, and Interfaces Used in the Finite Element Models**

| | Young's Modulus, x $10^6$ psi | Poisson's Ratio | Uniaxial Compressive Strength, psi | Cohesion, psi | Frictional Angle, degree |
|---|---|---|---|---|---|
| Coal | 0.28 | 0.30 | 900/1,000 | - | 30 |
| Strong Roof/ Floor Rocks | 4.50 | 0.20 | 15,000 | - | 42 |
| Weak Floor Rock | 0.21 | 0.38 | 300 | - | 24 |
| Weak Rock Parting | 0.21 | 0.38 | 300 | - | 24 |
| Strong Rock Parting | 0.42 | 0.28 | 1,750 | - | 30 |
| Coal/Rock Interface | - | - | - | 0 | 14 |

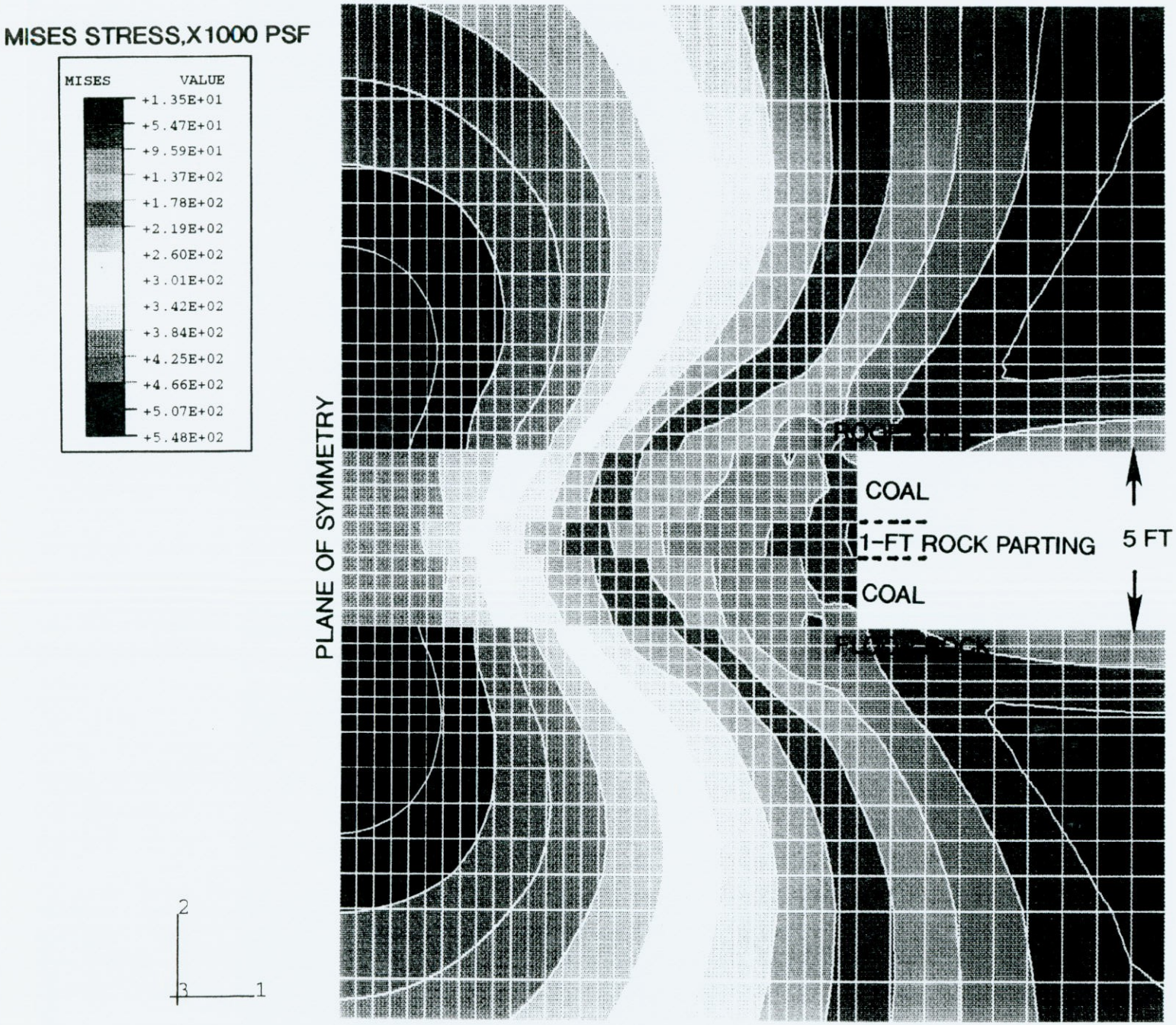



**Figure 1. Mises Stress Distribution in the Roof, Coal Pillar, and Floor.**

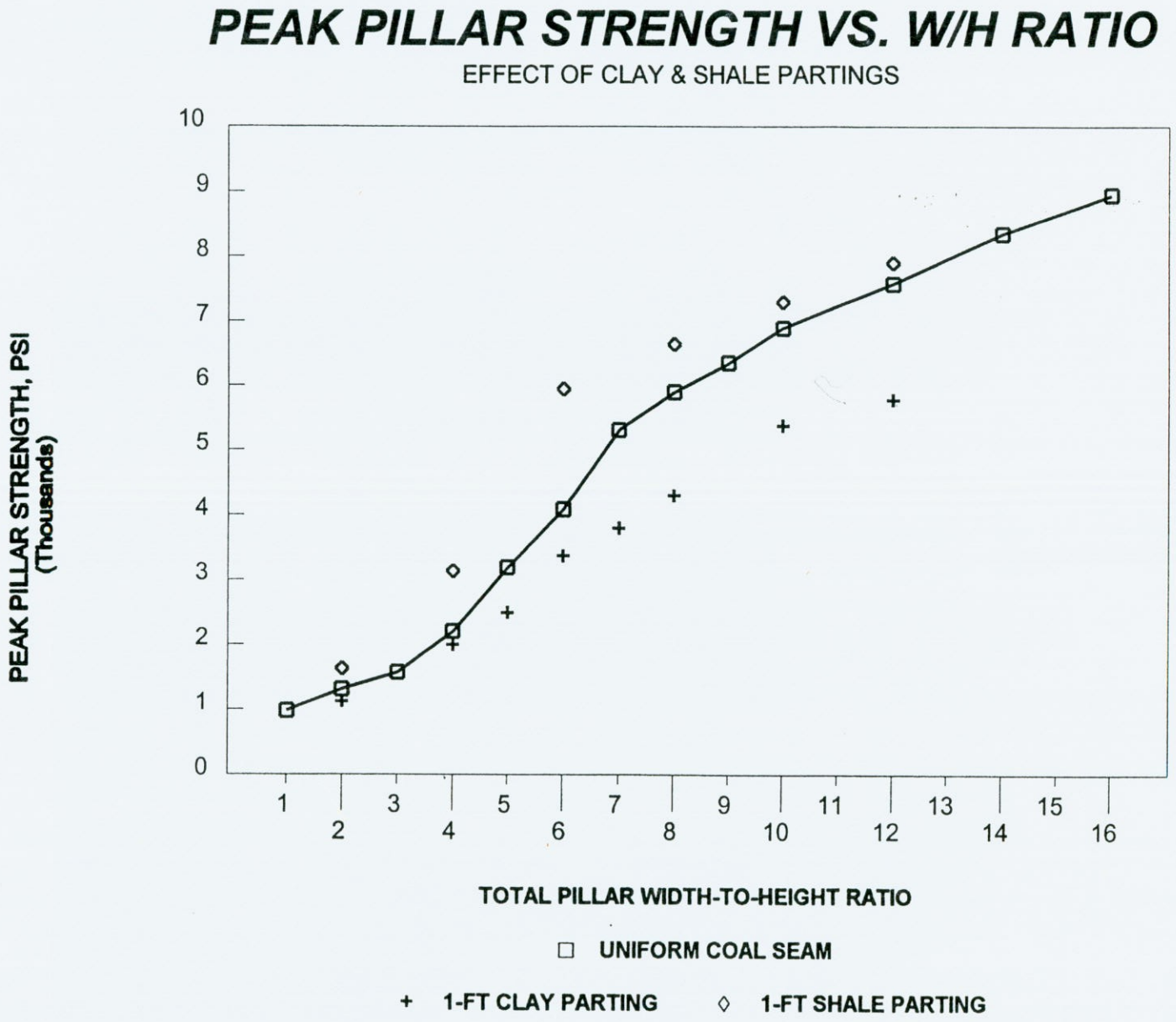



Figure 2. Effect of Clay and Shale Parting on the Ultimate Strength of Coal Pillars.

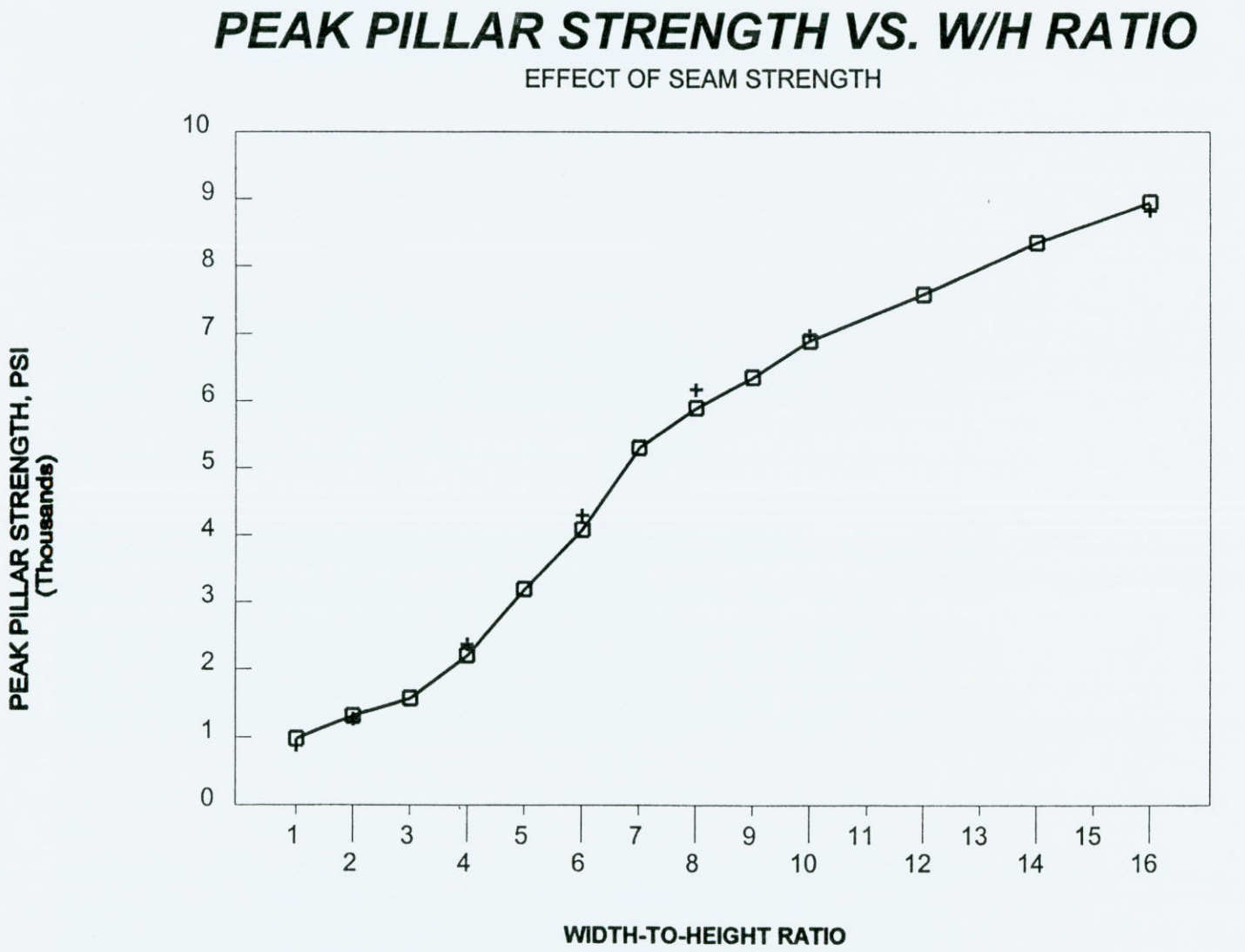



**Figure 3. Effect of Seam Strength on the Ultimate Strength of Coal Pillars.**

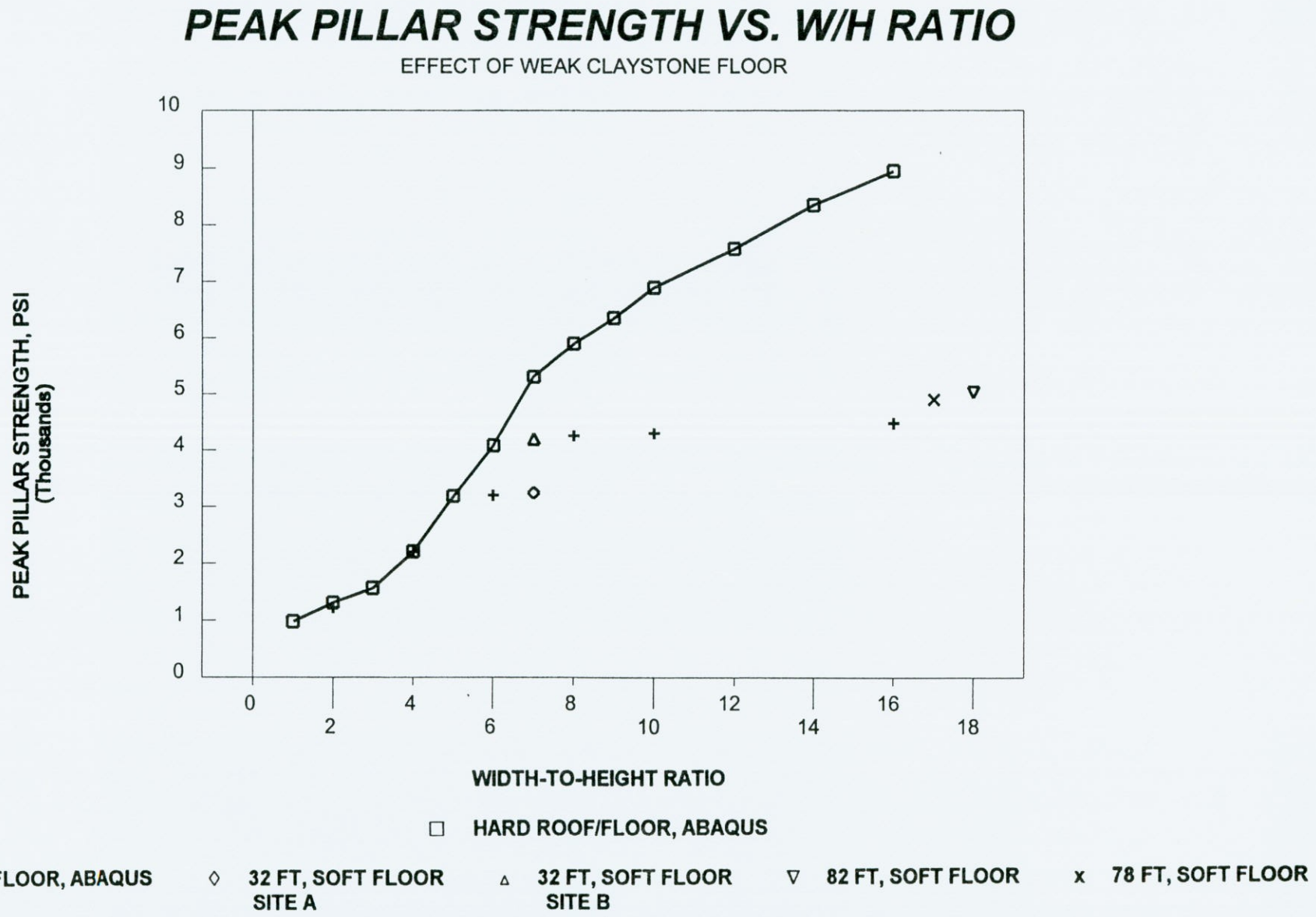



**Figure 4. Effect of Weak Claystone Floor on the Ultimate Strength of Coal Pillars.**

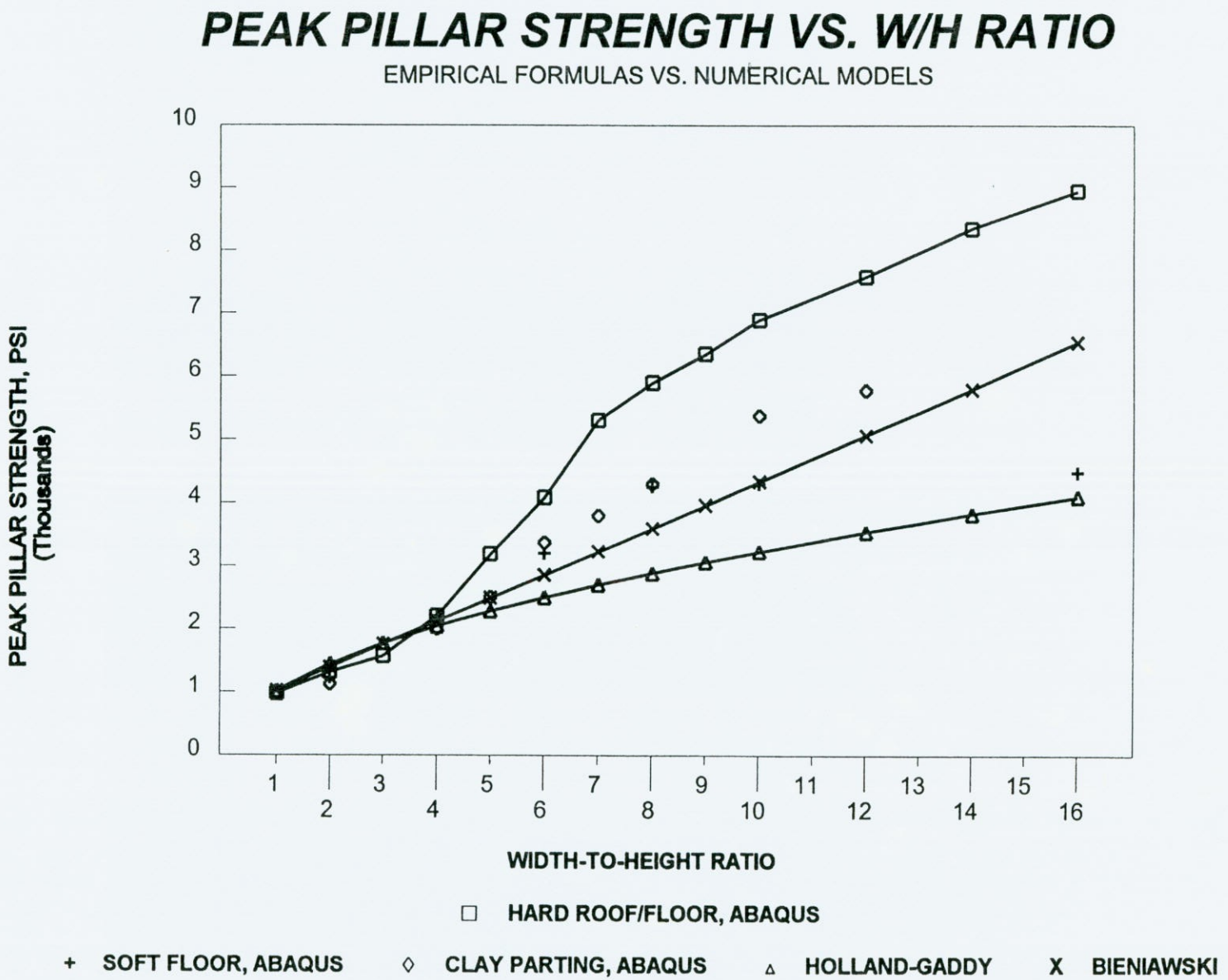



**Figure 5. Comparison of Bieniawski and Holland-Gaddy Formulas With Numerical Models.**



# AUTHOR'S INDEX


Adkins, G., 173
Amick, M.R., 105
Anikin, N.F., 221
Aziz, N., 267

Barratt, D.R., 130
Barczak, T.M., 9, 211
Bauer, E.R., 283

Campoli, A.A., 105
Cario, S., 1
Carpetta, J.E., 199
Cassie, J., 58
Chen, H. J., 43
Chen, J., 1
Cheng, H., 79
Compton, C.S., 289
Cox, D., 183

de Alcantara, M.E., 274
DeMichiei, J., 1
Dolinar, D.R., 9, 289
Dunford, J., 304

Fan, S., 296
Filigenzi, M.T., 320
Francke, C.T., 243
Furniss, J.P., 173

Gearhart, D.F., 211
Gopinath, T.R., 274
Grau III, R.H., 283
Gu, Q., 85
Guo, S., 117, 158, 167

Haque, A., 267
Hasenfus, G., 282
Haycocks, C., 311
Hustus, J., 9

Indraratna, B., 267

Johnson, K.L., 25
Johnston, J., 183

Kang, L., 296
Karmis, M., 311
Kelley, J.H., 98
Khair, A.W., 117
Klishin, V.I., 110

Li, J., 85
Lima, A.d.A., 274
Lloyd, P.W., 33
Luo, J., 311
Luo, Y., 43, 50

MacDonald, R.J., 68
Maleki, H., 304
Mark, C., 204
Matsui, K., 91
Mazzoni, R.A., 199
McLennan, A., 58
McCall, F.E., 204
Mendoza L., R., 139
Mills, P.S., 105
Mishra, M., 1
Mohammad, N., 33
Molinda, G.M., 9

Nesterov, M.P., 221

Oldsen, J.G., 117
Oram, J.S., 16
Orea R., R., 139
Oyler, D.C., 289

Pappas, D.M., 204
Peng, S.S., 43, 50, 79
Ponder, C.G., 16

Rataj, M., 149
Reddish, D.J., 33, 173
Rico, G.H., 139
Rohaly, A.J., 105

Scovazzo, V.A., 251
Shi, S., 85
Shimada, H., 91
Signer, S.P., 183
Stankus, J.C., 117, 158, 167
Su, D.W.H., 282

Tadolini, S.C., 139
Terrill, L.J., 235, 243
Thomas, R., 149

Unrug, K.F., 259

VandeKraats, J.D., 235, 243
Van Sambeek, L.L., 226

Wang, A., 191
Wang, X., 191
Westman, E., 311
Woolley, B., 316

Xiu, Z., 191

Yu, K., 296

Zahl, E., 304
Zhang, C., 85
Zhang, Z., 296

